ONR Grant N00014-96-1-0433: Final Scientific Report - 2001

1. **Title of Grant:** Coherent Control of Chemical Reactions

2. **Principal Investigator:** P. Brumer, University Professor and Roel Buck Professor of Chemical Physics,, Chemical Physics Theory Group, University of Toronto, Toronto, Canada M5S 3H6

Subcontractor: M. Shapiro, Jacques Mimran Professor of Chemical Physics, The Weizmann Institute of Science, Rehovot, Israel

3. **Grant No:** N00014-96-1-0433; **PR No.:** 00PR01683-00

DISTRIBUTION STATEMENT A
Approved for Public Release
Distribution Unlimited

20011126 127

ONR Grant N00014-96-1-0433: Final Scientific Report - 2001

1. **Title of Grant:** Coherent Control of Chemical Reactions

2. **Principal Investigator:** P. Brumer, University Professor and Roel Buck Professor of Chemical Physics,, Chemical Physics Theory Group, University of Toronto, Toronto, Canada M5S 3H6

Subcontractor: M. Shapiro, Jacques Mimran Professor of Chemical Physics, The Weizmann Institute of Science, Rehovot, Israel

3. **Grant No:** N00014-96-1-0433; **PR No.:** 00PR01683-00

SUMMARY OF RESEARCH ACTIVITIES, 1998-2001

Over the past three years we have made significant contributions to the ongoing development of the coherent control of atomic and molecular processes. Specifically, we have contributed to (1) bimolecular reaction dynamics and controlled collision phenomena; (2) control of molecular chirality and asymmetric synthesis; (3) theory, and practical considerations, in the control of the photodissociation of real systems; (4) control in large molecular systems; (5) the continued development of semiclassical mechanics specifically for coherent control applications; and (6) control of molecular nanoscale deposition on surfaces.

Appendix A contains a summary of publications over the past three years. A brief description of results follows below. Research in each of these areas is continuing in our laboratories.

1. *Bimolecular Reactions:* Most of the coherent control work done over the past decade, barring one of our earliest papers, has focused on unimolecular dynamics. However, a large number of processes of chemical interest result from bimolecular collisions. Over the past three years we have made great progress in understanding conditions under which bimolecular collisional control is possible. Specifically, we derived the kinematic requirements for bimolecular control which ensure quantum interference from terms which are of the same energy in the center of mass system, and of the same center of mass momentum [1]. In addition, we demonstrated [2] that such conditions were automatically satisfied in collisions between identical particles, e.g. the rearrangement AB + AB $--> $ A_2 + B_2. As an initial step towards understanding these processes, we undertook a detailed study of a simple collision – rotational excitation in H_2 + H_2, and demonstrated [3] that control arose from entangled rotational-translational states, and that extensive control was achievable at cold temperatures. We also showed that reactions such as F + HD [4] show considerable control. The latter result is significant since F + HD is a

resonance-mediated reaction, earlier thought to be uncontrollable.

2. *Control of Asymmetric Synthesis—Right vs. Left Handed Molecules:*

The existence of enantiomers, i.e. two molecules that are mirror images but are not superimposable, is one of the fundamental broken symmetries of nature [5]. Chemistry has long been challenged by the need to selectively enhance the production of particular enantiomers. This need stems primarily from the specific bio-activity of enantiomers, i.e. some enantiomers will be active biologically whereas the other enantiomer will either be inactive or harmful. Unfortunately, enantiomers are indistinguishable chemically unless one of the reagents, or the system environment, is chiral. For this reason asymmetric synthesis (i.e. techniques for the separation, enhancement or interconversion of enantiomers) is a central research field in modern chemistry. Indeed, this year's Nobel Prize in Chemistry was awarded for work on chiral synthesis using catalysts and other non-optical techniques.

Recently, we demonstrated [6] that the strong dipole-electric field interaction can be used to control the interconversion of right and left handed molecules. This original scenario, which we have submitted for patent protection [7], requires that we selectively excite M_J states (where M_J is the projection of the total angular momentum along the z-axis), as distinct from $-|M_J|$ states. This is feasible experimentally if we use appropriately applied external magnetic fields.

We applied this scenario to the enantiomeric interconversion of gas phase dimethylallene [8] a molecule which we showed, through molecular structure computations [9], to display the necessary structural features for enantiomeric control. Control was outstanding (with over 92% conversion obtained) for a realistic model using reliable Franck-Condon factors and exact asymmetric rotor wavefunctions.

In order to bypass the M_J requirement we considered the formalism [10] associated with excitation of an enantiomeric mixture with three perpendicular linearly polarized

lasers. Preliminary results show that this scenario should allow for the desired enhancement and control of the enantiomeric excess without the need for M_J selection.

In addition, we proved a theorem [11] that provides the general conditions under which enantiomeric control via the dipole-electric field interaction is possible. This result will serve to guide the future development of light-based asymmetric synthesis schemes. Specifically, this theorem states that any light-matter scenario that is sensitive to a change in sign of the electric field [i.e. $E(t)$ goes to $-E(t)$] allows for control.

In separate work, the STIRAP approach was extended to formally design a "Cyclic Population Transfer" Scheme for the controlled interconversion of enantiomers [12]. This approach also requires selection of M_J levels, but allows us to bypass possible competitive processes (e.g. internal conversion) associated with the electronic excitation step in the method described above.

3. *Control in Large Molecules:* One of the major issues in coherent control is the nature and extent of control for large molecules. Our general theory [13] shows that control is indeed possible under a wide variety of circumstances and recent experimental optimal control studies on large molecules support this expectation [14]. During the past three years we obtained two new results that are relevant to this issue. First, we showed that chaotic dynamics, anticipated to occur more readily with increasingly large systems, does not diminish control [15,16]. Second, we demonstrated [17] the possibility of controlling Hydrogen atom transfer in [2-(2' hydroxyphenyl)-oxazole], a molecule containing 35 coupled degrees of freedom! This work is intimately linked to that described in the section "Semiclassical Mechanics", below.

4. *Multiproduct Chemical Reactions:* Crucial to the continuing development of coherent control is the demonstration of successful control over a multiproduct chemical reaction. To this end we completed the initial phase of studies on the A band photodissociation of CH_2IBr at 248 nm where two products, CH_2I + Br and CH_2Br + I, are

obtained. (CH_2IBr is amongst a class of widely studied substituted methane molecules, all of which are of considerable interest to experimentalists.)

Specifically, we developed a potential surface [16] for a collinear model of CH_2IBr that reproduces the uncontrolled photodissociation results of Butler et al [18] and carried out bichromatic control calculations on this system. The results made clear that considerable control is possible and that such control can occur upon excitation from either regular or chaotic Hamiltonian eigenstates. Additional studies were carried out on model CH_2IBr potential surfaces to examine the relationship between the molecular phase [19] and the system dynamics. Doing these computations required that we design and implement a new method [20] for carrying out energy-resolved photodissociation calculations on systems that dissociate to more than one product state. The method, involving the use of a negative imaginary potential [21] in conjunction with the well established Artificial Channel Approach [22], was highly successful.

5. *Semiclassical methods:* Since quantum mechanics will, in the foreseeable future, be limited to small molecules, we have been developing semiclassical approaches to treating laser controlled photodissociation and control. Over the past three years we have several significant contributions to this area. In particular, we considered control of adiabatic CH_2IBr [23] and non-adiabatic ICN [24] photodissociation. In both cases the Herman-Kluk propagator successfully reproduced the correct amplitude and phases of the quantum interference term responsible for control. Further, the former computation introduced a new approach to computing the cumulative matrix elements [13] that is applicable both quantum mechanically as well as classically.

These results motivated the extension of bichromatic control to the case of proton exchange in the excited electronic state of HPO [17], a molecule with 35 degrees of freedom. In this case the background serves to decohere the proton dynamics. Hence, the fact that we can control this motion in the presence of all of these degrees of freedom, as we have

demonstrated, clearly implies that control in large molecules is both feasible, and can be readily accomplished.

We also carried out a number of studies in semiclassical methodology. Our recent work [25] indicates that the filters, such as the Filinov filter [26] do not significantly improve convergence rates. This suggests further studies to identify methods of improving semiclassical methodology, currently under consideration. For example, we have designed a method based upon the correspondence [27] between the classical object $\delta(E-H)$, where H is the Hamiltonian, and the quantum continuum projector $|\psi^- >< \psi^-|$. Our initial studies gave results [28] in excellent agreement with the quantum result for the test case of diatom dissociation to a single product state. As a consequence, we extended these studies [29] to the collinear photodissociation of CH_2IBr. Comparisons with our quantum results showed very good agreement, both for the cross sections as well as for the complex interference contributions. As a consequence, this approach, which entails no oscillatory integrands, gave very good results for the coherently controlled photodissociation of CH_2BrI. Extensions of this method are under consideration.

6. *Focusing molecules:* In earlier work [30] we showed that coherent control can be used to alter the polarizability of molecules. In particular, by preparing a molecule in an initial coherent superposition state and subjecting the system to a pair of lasers that lifts each of these levels to a fixed energy, one can produce an effective polarizability that is much larger or much smaller than the natural value. Indeed, one may even produce a polarizability of opposite sign. We have now shown [31,32] that this modified polarizability can be used to optically focus molecules on the nanometer scale.. In particular, by exposing the molecule in the superposition state to two standing wave laser fields we can produce a force on the molecule that is comprised of three terms, two natural terms due to the presence of two independent fields plus an additional term that depends upon quantum interference. The latter term allows for the focusing or defocusing of molecules depending on the phase between the two fields. We have applied the method to focus N_2 [31] as well as Ar [32]. In

the Ar case, the atom was excited to Rydberg levels so that the required incident electric field intensities are quite small (e.g. 20 W/cm^2). Control over the deposition was found to be extensive, leading to narrow lines (on the order of 5 nanometers in the case of zero transverse velocity) with controllable intensities. The resultant technique was submitted for patent protection [33].

Note that a number of related projects are ongoing in the research groups of Brumer and of Shapiro, computational and theoretical studies of decoherence free subspaces, studies of fundamentals in chaotic dynamics and in isolated molecule dynamics [?], studies of decoherence [35], studies of the complete suppression of spontaneous emission and other spontaneous decay processes using optimal control and photon echo techniques [36], experimental studies on the control of the branching ratio in Na_2 photodissociation [37] etc. that serve to enhance, through synergism, our coherent control work.

Finally, we have done much to bring coherent control to the scientific fore. For example, Brumer was the co-chair of the First Gordon Research Conference on Quantum Control in 1999, and Shapiro was the chair of the Second Gordon Conference on Quantum Control held in 2001 (both partially sponsored by ONR). Further, we have completed the vast majority of our monograph "Principles of the Coherent Control of Molecular Processes", a manuscript that sheds light on the essence of control in a large numbers of areas including Chemistry, Device Physics, Quantum Optics, etc. and provides a basis for further innovative work.

REFERENCES

[1] P. Brumer, A. Abrashkevich and M. Shapiro, Faraday Discussions 113, 291 (1999)

[2] P. Brumer, K. Bergmann and M. Shapiro, J. Chem. Phys. 113, 2053 (2000)

[3] B. McQuarrie and P. Brumer, "Entanglement and Coherent Control in Diatom-Diatom Scattering" (manuscript in preparation)

[4] R.T. Skodje, D. Skouteris, D.E. Manalopoulos, S.H. Lee, F. Dong and K. Liu, J. Chem. Phys. 112, 4536 (2000); Phys. Rev. Lett. 85, 1206 (2000).

[5] J.J. Sakurai, Modern Quantum Mechanics, (Benjamin, Menlo PArk, 1985)

[6] M. Shapiro, E. Frishman and P. Brumer, Phys. Rev. Letters 84, 1669 (2000)

[7] "Coherently Controlled Laser Distillation of Chiral Enantiomers", U.S. Patent Application 09/628,681

[8] D. Gerbasi, M. Shapiro, and P. Brumer, J. Chem. Phys. 115, 5349 (2001)

[9] E. Deretey, M. Shapiro and P. Brumer, "Chiral Molecules With Achiral Excited States: A Computational Study of 1,3-Dimethylallene", J. Phys. Chem. (in press)

[10] M. Shapiro, E. Frishman and P. Brumer, "Controlled Asymmetric Synthesis via the Dipole-Electric Field Interaction: Three Perpendicular Lasers" (manuscript in preparation)

[11] "Principles of Light-Induced Achiral Asymmetric Synthesis", P. Brumer, E. Frishman and M. Shapiro, Phys. Rev. A (in press)

[12] P. Král and M. Shapiro, Phys. Rev. Lett. 87, 183002 (2001)

[13] M. Shapiro and P. Brumer, Adv. Atom. Mol. and Opt. Physics, 42, 287 (2000)

[14] A. Assion, T. Baumert, M. Bergt, T. Brixner, B. Keifer, V. Seyfried, M. Strhle and

G. Gerber, Science 282, 919 (1998); T.C. Weinacht, J.L. White and P.H. Bucksbaum, J. Phys. Chem A103, 10166 (1999); R.J. Levis, G.M. Menker and H. Rabitz, Science 292, 709 (2001)

[15] J. Gong and P. Brumer, Phys. Rev. Lett. 86, 1741 (2001)

[16] D.G. Abrashkevich, M. Shapiro and P. Brumer, "Coherent Control of the CH_2Br + I $\leftarrow$ CH_2BrI $\rightarrow$ CH_2I + Br Branching Photodissociation Reaction, J. Chem. Phys. (submitted)

[17] V. Batista and P. Brumer, "Control of Reaction Dynamics in a Large Molecular System" (manuscript in preparation)

[18] L.J. Butler, E.J. Hintsa, and Y.T. Lee, J. Chem. Phys. 84, 4104 (1986); L.J. Butler, E.J. Hintsa, S.F. Shane, and Y.T. Lee, J. Chem. Phys. 86, 2051 (1987).

[19] The molecular phase α_{ij} of the product matrix elements $\langle E, n, q^-|\mu|E_i\rangle\langle E_j|\mu|E, n, q^-\rangle$ that affects control was originally introduced in P. Brumer and M. Shapiro, Chem. Phys. Lett. 126, 541 (1986). The relationship between the phase and the underlying dynamics has been explored extensively by Seideman, Gordon and coworkers—see, e.g., R.J. Gordon, L. Zhu and T. Seideman, J. Phys. Chem 105A, 4387 (2001)

[20] D. Abrashkevich, P. Brumer and M. Shapiro, J. Chem. Phys. 114, 54 (2001)

[21] D. Neuhauser and M. Baer, J. Phys. Chem. 90, 4351 (1989); *ibid.*, 91, 4651 (1989); D. Neuhauser, R. S. Judson, R. E. Jaffe, M. Baer, and D. J. Kouri, Chem. Phys. Lett. 176, 546 (1991).

[22] This approach was first introduced in M. Shapiro, J. Chem. Phys. 56, 2582 (1972).

[23] V. Batista and P. Brumer, J. Chem. Phys. 114, 10321 (2001)

[24] V.S. Batista and P. Brumer, J. Phys. Chem. [Miller Honor Issue] 105, 2591 (2001)

[25] M. Spanner, V. Batista and P. Brumer, "The Effectiveness of the Filinov Filter in Semiclassical IVR Computations" (manuscript in preparation)

[26] See, e.g., N. Makri and W.H. Miller, Chem. Phys. Lett. 130, 10 (1988)

[27] J. Wilkie and P. Brumer, Phys. Rev. A 55, 27, (1997); *ibid.* A 55, 43, (1997).

[28] D. Abrashkevich and P. Brumer, "A Correspondence Approach to Semiclassical Matrix Elements for Coherent Control; Na_2 Photodissociation", (manuscript in preparation).

[29] B. McQuarrie and P. Brumer, "A Correspondence Approach to Coherently Controlled Photodissociation", (manuscript in preparation)

[30] E. McCullough, M. Shapiro and P. Brumer, Phys. Rev A 61, 041801-1 to 041801-4 (2000)

[31] B. Dey, M. Shapiro and P. Brumer, Phys. Rev. Lett. 85, 3125 (2000)

[32] B. Dey, M. Shapiro and P. Brumer,"Coherently Controlled Nanoscale Deposition: Rydberg States of Ar" (manuscript in preparation)

[33] "Nanometric Scale Coherently Controlled Molecular Deposition", U.S. Patent Applications 09/531,036 and (CIP) 09/684,203

[34] For a thorough discussion see S.A. Rice and M. Zhao, "Optical Control of Molecular Dynamics", (Wiley, N.Y., 2000)

[35] H. Han and P. Brumer (work in progress)

[36] E. Frishman and M. Shapiro (work in progress)

[37] Z. Qun, M. Keil and M. Shapiro (work in progress)

APPENDIX A: Coherent Control Activities Over Past Three Years

Publications:

A. Refereed Publications:

1. "Coherent Control of the $CH_2Br + I \leftarrow CH_2BrI \rightarrow CH_2I + Br$ Branching Photodissociation Reaction", D. G. Abrashkevich, M. Shapiro and P. Brumer, J. Chem. Phys. (submitted)

2. "Phase Control of Nonadiabatically-induced Quantum Chaos in An Optical Lattice", J. Gong and P. Brumer (submitted)

3. "Cyclic Population Transfer in Quantum Systems with Broken Symmetry", P. Král and M. Shapiro, Phys. Rev. Lett. (in press)

4. "Coherent Control of Quantum Chaotic Diffusion: Diatomic Molecules in a Pulsed Microwave Field", J. Gong and P. Brumer, J. Chem. Phys. (in press)

5. "Principles of Light-Induced Achiral Asymmetric Synthesis", P. Brumer, E. Frishman and M. Shapiro, Phys. Rev. A (in press)

6. "Chiral Molecules With Achiral Excited States: A Computational Study of 1,3-Dimethylallene", E. Deretey, M. Shapiro and P. Brumer, J. Phys. Chem. (in press)

7. "Theory of Enantiomeric Control of Dimethylallene Using Achiral Light", D. Gerbasi, M. Shapiro, and P. Brumer, J. Chem. Phys. 115, 5349-5352 (2001)

8. "A Direct Approach to One Photon Interference Contributions in the Coherent Control of Photodissociation", V. Batista and P. Brumer, J. Chem. Phys. 114, 10321-10331 (2001)

9. "On the Origin of Pulse Shaping Control of Molecular Dynamics", M. Shapiro and P. Brumer, J. Phys. Chem. [Miller Honor Issue] 105, 2897-2902 (2001)

10. "Coherent Control of Quantum Chaotic Diffusion", J. Gong and P. Brumer, Phys. Rev. Lett. 86, 1741-1744 (2001)

11. "Semiclassical Dynamics in the Coherent Control of Nonadiabatic ICN Photodissociation", V.S. Batista and P. Brumer, J. Phys. Chem. [Miller Honor Issue] 105, 2591-2598 (2001)

12. "Coherent Control of Atom-Diatom Reactive Scattering: $H+H_2$ in Three Dimensions", A. Abrashkevich, M. Shapiro and P. Brumer, Chem. Phys. 267, 81-92 (2001)

13. "Multi-Arrangement Photodissociation Calculations Utilizing Negative Imaginary Potentials", D. Abrashkevich, P. Brumer and M. Shapiro, J. Chem. Phys. 114, 54-60 (2001)

14. "Coherently Controlled Nanoscale Molecular Deposition", B. Dey, M. Shapiro and P. Brumer, Phys. Rev. Lett. 85, 3125-3128 (2000)

15. "Identical Collision Partners in the Coherent Control of Bimolecular Reactions", P. Brumer, K. Bergmann and M. Shapiro, J. Chem. Phys. 113, 2053-2055 (2000)

16. "Semiclassical Initial Value Representation Techniques for Chaotic Systems", B. McQuarrie and P. Brumer, Chem. Phys. Lett. 319, 27-44 (2000)

17. "Coherently Controlled Asymmetric Synthesis with Achiral Light", M. Shapiro, E. Frishman and P. Brumer, Phys. Rev. Letters 84, 1669-1672 (2000)

18. "Coherent Control of Refractive Indices", E. McCullough, M. Shapiro and P. Brumer, Phys. Rev A 61, 041801-1 to 041801-4 (2000)

19. "Coherent Control of Atomic, Molecular and Electronic Processes", M. Shapiro and P. Brumer, Advances in Atomic, Molecular and Optical Physics, 42, 287-343 (2000)

20. "Optimized Imploding Waves in the Coherent Control of Bimolecular Processes: Atom-Rotor Scattering", E. Frishman, M. Shapiro and P. Brumer, J. Phys. Chem (Wilson Honor Issue), J. Phys. Chem A103, 10333-10342 (1999)

21. "Laboratory Conditions in the Coherent Control of Reactive Scattering", P. Brumer, A. Abrashkevich and M. Shapiro, Faraday Discussions 113, 291-302 (1999)

22. "Decoherence and Correspondence in Chaotic Hamiltonian Systems", J. Gong and P. Brumer, Phys. Rev. E 60, 1643-1647 (1999)

23. "Coherent Enhancement and Suppression of Reactive Scattering and Tunneling", E. Frishman, M. Shapiro and P. Brumer, J. Chem. Phys. 110, 9 (1999)

24. "Coherent Control of Reactive Scattering", A. Abrashkevich, M. Shapiro and P. Brumer, Phys. Rev. Lett. 81, 3789-3792 (1998); Erratum: Phys. Rev. Lett. 82, 3002 (1999)

25. "Semiclassical Initial Value Approach for Chaotic Long-lived Dynamics", G. Campolieti and P. Brumer, J. Chem. Phys. 109, 2999-3003 (1998)

B. Conference Proceedings

26. "Coherent Control of Molecular Dynamics", in *Structure and Dynamics of Electronic Excited States*, P. Brumer and M. Shapiro, ed. J. Laane, K. Takahashi and A.D. Bandrauk (Springer, N.Y., 1999)

27. "Scenarios in Coherent Control", in *Coherent Control in Atoms, Molecules and Semiconductors*, P. Brumer and M. Shapiro, ed. W. Potz and W. A. Schroeder, (Kluwer Academic Publishers, Dordrecht, 1999)

28. "Quantum Coherence in the Control of Molecular Processes", P. Brumer and M. Shapiro, Laser and Particle Beams, 16, 599-603 (1998)

C. Patents

29. "Nanometric Scale Coherently Controlled Molecular Deposition", U.S. Patent Application 09/531,036 and 09/684,203,

30. "Coherently Controlled Laser Distillation of Chiral Enantiomers", U.S. Patent Application 09/628,681. (Not ONR supported)

D. Manuscripts in Preparation (Preliminary draft versions of a number of these manuscripts have been provided in the Three Year Review)

31. Comment on "Reaction Imaging With Interferometry", J. Gong, V. Zeman and P. Brumer, for Phys. Rev. Lett.

32. "Coherent Control of Resonance-Mediated Reactions: F+HD", V. Zeman, P. Brumer and M. Shapiro

33. "Entanglement and Coherent Control in Diatom-Diatom Scattering", J. Gong, M. Shapiro and P. Brumer

34. "Decoherence Effects in Reactive Scattering", H. Han and P. Brumer

35. "Controlled Nanoscale Deposition and Controlled Polarization in Ar", B. Dey, M. Shapiro and P. Brumer

36. "Chiral Molecules With Achiral Excited States: A Computational Study of the structure of Ketone-Alcohol Complexes", Y. Brumer, K. Baldridge, P. Brumer and M. Shapiro

37. "The Effectiveness of the Filinov Filter in Semiclassical IVR Computations", M. Spanner, V. Batista and P. Brumer,

38. "A Correspondence Approach to Semiclassical Matrix Elements for Coherent Control; Na_2 Photodissociation", D. Abrashkevich and P. Brumer

39. "A Correspondence Approach to Coherently Controlled Photodissociation: Multiple Product Channels", B. McQuarrie and P. Brumer

40. "Control of Reaction Dynamics in a Large Molecular System", V. Batista and P. Brumer

41. "Principles of the Coherent Control of Molecular Processes", (monograph), M. Shapiro and P. Brumer

Coherent Control of the $CH_2Br+I \leftarrow CH_2BrI \rightarrow CH_2I+Br$ Branching Photodissociation Reaction

Dmitri G. Abrashkevich, Moshe Shapiro* and Paul Brumer

Chemical Physics Theory Group, Department of Chemistry

and Photonics Research Ontario,

University of Toronto,

Toronto M5S 3H6, Canada

Abstract

Coherent control over branching in the photodissociation of collinear CH_2BrI to yield either CH_2Br+I or CH_2I+Br is examined computationally. Quantum photodissociation calculations, using two excited potentials surfaces, are carried out using a new method incorporating negative imaginary absorbing potentials within the artificial channel method. Extensive control over the I/Br branching ratio is shown to result as experimentally controllable laser amplitudes and phases are varied. Such control is observed for excitation from either initial superpositions of chaotic or regular CH_2BrI bound states.

---

*Permanent Address: Chemical Physics Department, The Weizmann Institute of Science, Rehovot, 76100, Israel

I. INTRODUCTION

Considerable experimental and theoretical effort has been directed over the past few years towards the goal of laser control over molecular dynamics. A most promising and successful approach is Coherent Control (CC) [1–5], in which different coherently interfering pathways combine constructively or destructively in order to enhance or suppress the production of a given product.

Computational studies of coherent control play an important role in providing detailed insight into control mechanisms and in laying the groundwork for experiments on particular systems. Thus far, studies of this kind on unimolecular processes have essentially been limited to photodissociation into different electronic states [4,5]. However, from the viewpoint of Chemistry, there is greater interest in the control of chemical reactions that produce different chemical products. The only quantum computations on control of photodissociation in a realistic system of this type were done by us [6] on HOD $\rightarrow$ HO +D or DO + H. However, our computations were not completely general insofar as they took advantage of the similar potentials in the product HO +D and DO +H channels. Here we present the first fully quantum computation of coherent control in a realistic branching reaction that leads to different chemical products [7]. 10 In particular, in this paper we apply the bichromatic CC scenario [1] in conjunction with our recently developed ACM-NIP photodissociation approach [8] to test the possibility of controlling the photodissociation of collinear CH_2BrI. In this scenario one uses a coherent bichromatic laser field to excite a coherent superposition of two bound eigenstates, $|E_1\rangle$ and $|E_2\rangle$, of energies E_1 and E_2, to a single continuum eigenstate leading to the desired products [1]. The two ω_1 and ω_2 frequencies that comprise the bichromatic field are tuned to satisfy the condition that $\omega_1 - \omega_2 = (E_2 - E_1)/\hbar$.

The computation presented in this papers take advantage of the most recent developments in computational techniques in energy resolved photodissociation studies, which allow for the treatment of branching reactions. Specifically, we use our recently developed method [8] in which a negative imaginary potential (NIP) method [9,10] is used to transform a multi-arrangement-channels system into a collection of single-arrangement-channel problems. The

desired dipole transition amplitudes are then calculated directly using the artificial channel method (ACM) [11,12] with the efficient log-derivative propagator [13]. The method has been successfully tested for the rather complicated VUV photodissociation of CO_2 [8] in the collinear approximation.

We focus on the photodissociation of CH_2BrI. Excitation of this molecule in the A and B absorption bands has been experimentally shown to lead to bond selective photodissociation [14–20]. It would therefore be interesting to see whether CC methods control these branching ratios and even reverse the natural branching ratios, which are now known in detail at several wavelengths [16]. Further, CH_2BrI is part of the dihalomethane family, whose natural UV photodissociation produces reactive halogens harmful to the troposphere and to the marine boundary layer [19,20].

We restrict attention to CH_2BrI treated as a pseudo-linear-triatomic molecule, composed of the I, the CH_2 group and the Br atom arranged in space in this order. The full nine-dimensional rotating CH_2BrI calculation is conceptually possible but computationally intractable at this time. Moreover, we believe that essential aspects of the physics are captured by our present model. Within the framework of this model we have constructed three empirical potential energy surfaces (PES), whose parameters are determined by fitting the results of our calculations to all the available experimental data. These include, the A and the B bands absorption spectra and the I/Br branching ratios at 193.3 and 248.5 nm as measured by Butler et al. [16]. We have also studied the degree of control as a function of some freely varying potential parameters. Finally, phase coherent control, originating from a superposition of highly excited vibrational states in the "chaotic regime" of the ground electronic PES is also demonstrated.

The paper is organized as follows. In Section II we review the bichromatic CC scenario. In Section III, the kinematic model of CH_2BrI system and the associated parameterization of the potential energy surfaces used are explained. The results of our calculations are presented and discussed in Section IV, and the paper is summarized in the last Section.

II. THE BICHROMATIC COHERENT CONTROL SCENARIO

Consider the photodissociation of a CH_2BrI molecule prepared in a superposition of bound states $|E_j\rangle$ of H_g, the nuclear Hamiltonian in the ground electronic state $|\,g\,\rangle$:

$$\Psi_g(t) = |\,g\,\rangle \sum_j c_j |E_j\rangle \exp(-iE_j t/\hbar), \tag{1}$$

where E_j are the energies of the bound eigenstates $|E_j\rangle$. The molecule is subjected to the following light field:

$$\varepsilon(t) = \int d\omega\, \varepsilon(\omega)\, \cos(\omega t + \phi_\omega). \tag{2}$$

Here $\varepsilon(\omega)$ is the electric field amplitude at frequency ω.

Assuming the Born-Oppenheimer approximation, we obtain the probability of photodissociation to yield fragments in the q (chemical) arrangement and internal state f, at total energy E, i.e. in the product state $|\,E, f, q\,\rangle$ by expanding the system wave function in the bound and continuum electronic×nuclear eigenstates:

$$\Psi(t) = |\,g\,\rangle \sum_j c_j |E_j\rangle \exp(-iE_j t/\hbar) + \sum_e |\,e\,\rangle \sum_{f,q} \int dE\, B(E, f, q|t) |E, f, q^-\rangle \exp(-iEt/\hbar), \tag{3}$$

where $|E, f, q^-\rangle$ is an eigenstate of H_e, the nuclear Hamiltonian in an excited electronic state $|\,e\,\rangle$ with total energy E. The "-" notation indicates that this state represents an (infinitesimally narrow) wavepacket, correlating as $t \to \infty$ with the fragments in the state $|\,E, f, q\,\rangle$.

Since only the continuum eigenfunctions pertain to the dissociation process, the energy-resolved overall probability to produce fragments in arrangement-channel q is given in terms of the continuum expansion coefficients as,

$$P(E, q) = \sum_f |B(E, f, q|t \to \infty)|^2. \tag{4}$$

The $B(E, f, q|t)$ coefficients are obtained by substituting Eq. (3) into the time-dependent Schrödinger equation:

$$i\hbar\frac{\partial\Psi(t)}{\partial t} = H\Psi(t). \tag{5}$$

Here H is the total Hamiltonian given in the dipole approximation as $H = H_{\rm M} - {\rm d}\varepsilon(t)$, where d is the projection of the electric dipole operator on the direction of the polarization of the electric field and H_M is the (nuclear+electronic) material Hamiltonian.

After making the substitution of Eq. (3) into Eq. (5), we obtain, using first-order perturbation theory and the rotating wave approximation [12,21], that,

$$B(E,f,q|t) = \frac{i}{2\hbar}\sum_j c_j\langle E,f,q^-|{\rm d}_{e,g}|E_j\rangle \int d\omega\,\varepsilon(\omega)\exp(-i\phi_\omega)\int_{-\infty}^{t} dt'\,\exp\left[i(\omega_{EE_j}-\omega)t'\right], \tag{6}$$

where ${\rm d}_{e,g} \equiv \langle\,{\rm e}\,|{\rm d}|\,{\rm g}\,\rangle$ and $\omega_{EE_j} = (E-E_j)/\hbar$.

Denoting $\varepsilon(\omega)\exp(-i\phi_\omega)$ by $\bar{\epsilon}(\omega)$ and using the fact that at $t\to\infty$ the time integral is reduced to a delta function, we have that,

$$B(E,f,q|\infty) = \frac{\pi i}{\hbar}\sum_j c_j\langle E,f,q^-|{\rm d}_{e,g}|E_j\rangle\,\bar{\epsilon}(\omega_{EE_j}). \tag{7}$$

Hence that,

$$P(E,q) = \left(\frac{\pi}{\hbar}\right)^2\sum_f\left|\sum_j c_j\langle E,f,q^-|{\rm d}_{e,g}|E_j\rangle\,\bar{\epsilon}(\omega_{EE_j})\right|^2. \tag{8}$$

Expanding the square in Eq. (8) gives

$$P(E,q) = \left(\frac{\pi}{\hbar}\right)^2\sum_{i,j}F_{i,j}\mu_{i,j}^{(q)}, \tag{9}$$

where

$$F_{i,j} = c_i\bar{\epsilon}(\omega_{EE_i})c_j^*\bar{\epsilon}^*(\omega_{EE_j}), \quad \mu_{i,j}^{(q)} = \sum_f\langle E_i|{\rm d}_{e,g}|E,f,q^-\rangle\,\langle E,f,q^-|{\rm d}_{e,g}|E_j\rangle. \tag{10}$$

Note that all molecular attributes are contained in $\mu_{i,j}^{(q)}$ and that control over the branching ratios results from changing the experimentally-controlled parameters in the $F_{i,j}$ terms, e.g. the magnitudes and phases of the laser and the coefficients describing the initially prepared superposition state [Eq. (1)]. Equation (9) provides a particularly convenient form

for guiding CC experiments because it allows for the extraction of the $\mu_{i,j}^{(q)}$ numbers from experimental data, thereby providing the entire "control map", i.e., $P(E,q)$ as a function of $F_{i,j}$. For example, in the bichromatic case, $P(E,q)$ is given as a bilinear form in $c_i\bar{\epsilon}(\omega_{EE_i})$, determined by three independent complex parameters $\mu_{i,j}^{(q)}$, $i=1,2; j<i$. In this case the control map may be determined experimentally by performing six measurements of the product yield at six independent values of the $F_{i,j}$ variables. Inversion of Eq. (9) then allows for the extraction of the three complex $\mu_{i,j}^{(q)}$ numbers which allow the experimentalist to tune the fields to get any desired value of $P(E,q)$ between $P_{min}(E,q)$ and $P_{max}(E,q)$. The latter extrema can also be determined analytically from Eq. (9).

III. THE PSEUDO LINEAR TRIATOMIC MODEL OF CH_2IBr

To simplify the calculations, we treat CH_2BrI as a pseudo linear triatomic, composed of the I, CH_2 and Br groups arranged on a line in this order. The model implicitly assumes that the higher frequency C-H motions are frozen. Accordingly, the dissociating process is described by just two coordinates: $r_{\mathrm{C-Br}}$, the separation between the center-of-mass of the CH_2 group and Br, and $r_{\mathrm{C-I}}$, the separation between CH_2 and I.

In order to compute the dipole transition amplitudes $\langle E,f,q^-|\mathrm{d}_{e,g}|E_i\rangle$ which make up the $\mu_{i,j}^{(q)}$ matrix elements of Eq. (9), we need to solve the nuclear Schrödinger equations in the ground and excited electronic states,

$$\left[-\frac{\hbar^2}{2\mu}\frac{\partial^2}{\partial R^2}-\frac{\hbar^2}{2m}\frac{\partial^2}{\partial r^2}+W_{\mathrm{g}}(R,r)-E_i\right]\langle R,r|E_i\rangle=0, \tag{11}$$

$$\left[-\frac{\hbar^2}{2\mu}\frac{\partial^2}{\partial R^2}-\frac{\hbar^2}{2m}\frac{\partial^2}{\partial r^2}+W_{\mathrm{e}}(R,r)-E\right]\langle R,r|E,f,q^-\rangle=0. \tag{12}$$

These two equations are expressed in two Jacobi coordinates, r and R, defined for each arrangement as,

$$r=r_{\mathrm{C-X}},\quad R=r_{\mathrm{C-Y}}+\gamma_X r_{\mathrm{C-X}},\quad \gamma_X=\frac{m_{\mathrm{X}}}{(m_{\mathrm{X}}+m_{\mathrm{CH_2}})}, \tag{13}$$

where, X = Br, Y = I for the CH_2Br+I arrangement and X = I, Y = Br for the CH_2I+Br arrangement. The masses appearing in Eq. (11) and Eq. (12) are defined for each CH_2X+Y arrangement as,

$$\mu = \frac{m_Y m_{CH_2X}}{(m_I + m_{CH_2} + m_{Br})}, \quad m = \frac{m_X m_{CH_2}}{(m_X + m_{CH_2})}, \tag{14}$$

$$m_{CH_2X} = m_{CH_2} + m_X, \quad m_{CH_2} = m_C + 2m_H, \tag{15}$$

with m_a, $a = \mathrm{H, C, Br, I}$, is the mass of the indicated atom.

The ground state potential $W_g(R, r)$ is constructed as a sum of the two Morse potential functions:

$$W_g(R, r) \equiv W_g(r_{C-I}, r_{C-Br}) = V^I_{Morse}(r_{C-I}) + V^{Br}_{Morse}(r_{C-Br}), \tag{16}$$

where the CH_2-I part of the potential is taken from Ref. [22]:

$$V^I_{Morse} = D^I \exp[-\alpha^I(r_{C-I} - r^I)] \left\{\exp[-\alpha^I(r_{C-I} - r^I)] - 2\right\}, \tag{17}$$

with, $D^I = 0.0874$, $\alpha^I = 0.87094$, $r^I = 4.04326$, all expressed in atomic units (au). The Morse potential for CH_2-Br stretch is parameterized following the ground potential of CH_3Br molecule [23–25], as,

$$V^{Br}_{Morse} = D^{Br} \exp[-\alpha^{Br}(r_{C-Br} - r^{Br})] \left\{\exp[-\alpha^{Br}(r_{C-Br} - r^{Br})] - 2\right\}, \tag{18}$$

with, $D^{Br} = 0.10694$, $\alpha^{Br} = 0.9154$, and $r^{Br} = 3.6849$, all in au. The ground electronic state PES of CH_2BrI obtained in this way is shown in Fig. 1.

In order to obtain a form capable of describing the two continuum absorption bands of CH_2BrI, a flexible parameterization of the excited PES was adopted. Experimentally, the CH_2BrI spectrum [16] consists of two broad bands, one (the A-band), peaking near 270 nm, corresponds to the promotion of a non-bonding iodine electron to a C-I antibonding orbital, and the other (the B-band), peaking near 215 nm, corresponds to the promotion of a non-bonding Br electron to a C-Br antibonding orbital.

We have chosen to represent the A-band and B-band excited PES, denoted as W_a and W_b, respectively, as,

$$W_e(r_{C-Br}, r_{C-I}) = \left[V^I_e(r_{C-I}) + V^{Br}_{Morse}(r_{C-Br})\right] f(x) +$$

$$\left[V_{\rm e}^{\rm Br}(r_{\rm C-Br}) + V_{\rm Morse}^{\rm I}(r_{\rm C-I})\right]\left[1 - f(x)\right], \quad {\rm e} = {\rm a, b}. \tag{19}$$

The $V_{\rm e}^{\rm I}$ and $V_{\rm e}^{\rm Br}$ (e=a,b) functions are purely repulsive terms, given as,

$$V_{\rm e}^{\rm I}(r_{\rm C-I}) = C_{\rm e}^{\rm I}\exp\{-\beta_{\rm e}^{\rm I} r_{\rm C-I}\}, \quad V_{\rm e}^{\rm Br}(r_{\rm C-Br}) = C_{\rm e}^{\rm Br}\exp\{-\beta_{\rm e}^{\rm Br} r_{\rm C-Br}\}. \tag{20}$$

$f(x)$ of the above is a "bond-switching" function,

$$f(x) = \frac{1}{1+\exp\{\alpha_h(x-x_h)\}}, \quad x = \frac{r_{\rm C-Br}}{(r_{\rm C-I}+r_{\rm C-Br})}, \quad x_h = 0.5, \quad \alpha_h = 30. \tag{21}$$

The switching of the Morse potentials ensures that the excited state potentials asymptotically approach the correct fragment potentials [8],

$$v_s^{\rm X}(r) \equiv \lim_{R_{\rm Y}\to\infty} W_s(R_{\rm Y}, r_{\rm C-X}) = V_{\rm Morse}^{\rm X}(r_{\rm C-X}),$$

$$s = {\rm g, e};\ {\rm X = I},\ {\rm Y = Br\ or\ X = Br},\ {\rm Y = I}. \tag{22}$$

The absolute values and nuclear coordinates dependence of the $\rm d_{e,g}$ transition-dipole matrix elements are not yet known for this system. Since we are interested only in the ratios of products, for which the absolute magnitudes of the dipole matrix elements are not important in the weak field limit, we have assumed the transition dipoles to be constant, their ratio being fixed according to the absorption maximum of the A-band relative to that of the B-band as, $\rm d_{A,g}/d_{B,g} = 0.48783$.

As shown below, the relative value of the dipole moments and the excited PES's chosen here account well for the observed absorption spectra in the A and the B bands. The features that are not treated are the sharp structures near 190 nm [16], which are due to transition to Rydberg states, and the three body dissociation channel $CH_2BrI \rightarrow CH_2 + I + Br$. In addition, the calculations presented below assume the validity of the Born-Oppenheimer approximation. The non-Born-Oppenheimer coupling terms between the excited PES of Eq. (19) were neglected because there was not enough experimental information to warrant their inclusion.

Despite the neglect of the non-Born-Oppenheimer coupling terms, the most important interference effect between the two PES, that of the interference between transitions leading to

the same final product state, arising mainly at wavelengths where the A and B bands overlap, was taken into account. This was done by computing the photodissociation cross-sections as the square of the absolute-value of the sum of the two photodissociation amplitudes leading, via each (A or B) excited electronic state, to the same final $\mid E, f, q \rangle$ fragment state.

The $C_{\rm e}^{\rm X}$, $\beta_{\rm e}^{\rm X}$, $X = {\rm I}, {\rm Br}$, ${\rm e} = {\rm a}, {\rm b}$, parameters in the potentials were chosen to reproduce the experimental I/Br branching ratios at two wavelengths, 193.3 nm and 248.5 nm, i.e. experimental [16] ratios of 1.2:1 and 1:3.5, respectively. The values we adopted (in au) are, $C_{\rm a}^{\rm I} = 1.25$, $\beta_{\rm a}^{\rm I} = 0.75$, $C_{\rm a}^{\rm Br} = 0.25$, $\beta_{\rm a}^{\rm Br} = 0.25$, $C_{\rm b}^{\rm I} = 0.23$, $\beta_{\rm b}^{\rm I} = 0.08$, $C_{\rm b}^{\rm Br} = 0.729$, $\beta_{\rm b}^{\rm Br} = 0.9$. We found, in contrast to the absorption peak positions and band widths, that the I/Br ratios at 248.5 and 193.3 nm are very sensitive to these potential parameters. Contour plots of the $W_{\rm e}$ PES's as functions of the C-I and C-Br distances are shown in Fig. 2. We also provide, in Figure 3, a cut through the three surfaces and the associated frequencies, in order to clarify the control scenario.

The degree of overlap with the ground state wavefunction, which to a large extent determines which dissociation channel dominates each band, is greatly influenced by the $\beta^{\rm I}$ and $\beta^{\rm Br}$ parameters. Thus $W_{\rm a}$, which determines the dynamics in the A-band region, is parameterized by $\beta_{\rm a}^{\rm I} = 0.75$, which is much larger than $\beta_{\rm a}^{\rm Br}$ (=0.25). In contrast, in $W_{\rm b}$, $\beta_{\rm b}^{\rm I}$ (=0.08) is much smaller than $\beta_{\rm b}^{\rm Br}$ (=0.9). As a result, the dissociation on the $W_{\rm a}$ PES produces more iodine (peaking at 274.5 nm) than bromine (peaking at 247.2 nm), while dissociation on the $W_{\rm b}$ surface produces more bromine (which peaks at 213.5 nm) than iodine (peaking at 194.4 nm).

Given these potentials, we solved the nuclear Schrödinger equations in the excited states [Eq. (12)] numerically using a method that we recently introduced [11,12]. Specifically, the computation is complicated because of the existence of two (q =CH_2Br +I and q'=CH_2I+Br) arrangement channels. In order to treat such a problem we have employed the Negative Imaginary Potential (NIP) method [9,10], in conjunction with the Artificial Channel Method (ACM) [11,12], the latter allowing for the direct calculation of the photodissociation transition amplitudes without the explicit solution of the wavefunctions of Eq. (11) or Eq. (12).

The combined NIP-ACM is described in detail in Ref. [8]. In essence, the NIP method re-

duces a multi-arrangements system to a set of single-arrangement problems. This is achieved by adding short-range NIPs, $U_{\rm e}^{\rm Im}(R,r)$, e = a, b, at the entrance regions of all the product channels $q' \neq q$, where q is the arrangement we wish to study. In this way the flux to all $q' \neq q$ arrangements is absorbed, while leaving the solutions in the q arrangement intact. This allows for the use of the appropriate q specific Jacobi coordinate system of Eq. (11) and Eq. (12) for each arrangement. By repeating this procedure for each of the q arrangement channels we can compute the detailed state-to-state $\langle E, f, q^- | {\rm d}_{e,g} | E_j \rangle$ photodissociation amplitudes of Eq. (6) for all the arrangements.

The linear ramp potential of Ref. [9] was chosen as the form of the NIP, i.e.

$$U_{\rm e}^{\rm Im}(R,r) = \begin{cases} -iU_{\rm e}^{(0)} \dfrac{r - r_{\rm e}^{(1)}}{r_{\rm e}^{(2)} - r_{\rm e}^{(1)}}, & r_{\rm e}^{(1)} \leq r \leq r_{\rm e}^{(2)} \\ 0, & \text{otherwise} \end{cases}, \quad {\rm e} = {\rm a, b}. \tag{23}$$

Having chosen the $U_{\rm e}^{\rm Im}(R,r)$ NIP, Eq. (12) is now solved for the complex potential $\tilde{W}_{\rm e}(R,r)$ defined as,

$$\tilde{W}_{\rm e}(R,r) = W_{\rm e}(R,r) + U_{\rm e}^{\rm Im}(R,r), \qquad {\rm e} = {\rm a, b}. \tag{24}$$

In order to solve the nuclear Schrödinger equations [Eq. (11) and Eq. (12)], which are partial differential equations in two (R and r) variables, we expand the nuclear wavefunction in the usual manner in a vibrational basis $\langle r | \varepsilon_v \rangle$ which is the solution of the Schrödinger equation,

$$\left[\varepsilon_v + \frac{\hbar^2}{2m} \frac{d^2}{dr^2} - v_{\rm g}(r) \right] \langle r | \varepsilon_v \rangle = 0, \tag{25}$$

of either the CH_2-I or the CH_2-Br fragment (assumed to be in their ground electronic state). By inserting this expansion into Eq. (11) and Eq. (12) we obtain a set of (Coupled Channels) ordinary second order differential equations which are solved by the log-derivative method [13].

In order to converge the bound state calculation [Eq. (11)], a basis set composed of $N_{\rm g} = 15$ vibrational states ($v = 0, 1, ..., 14$) was used. A much larger basis had to be used for the excited states calculations, especially at high excitation frequencies. While the results were fully convergent with $N_{\rm a,b} = 40$ basis functions for the major arrangements, i.e., the CH_2Br+I arrangement in the A-band and the CH_2I+Br arrangement in the B-band, 95 basis

functions had to be used to attain convergence for CH_2Br+I arrangement in the B-band and the CH_2I+Br arrangement in the A-band .

We have chosen the $U_e^{(0)}$ constant of Eq. (23) to be equal to 0.05 au. This value ensures that all the flux perpendicular to the $r = r_e^{(1)}$ line in the (R, r) plane is completely absorbed before the propagation reaches the $r = r_e^{(2)}$ line. The values of the $r_e^{(1)}$ and $r_e^{(2)}$ variables were chosen as the smallest for which converged results (i.e. converged in the number of vibrational channels) were insensitive to changes in these r values. As the photon energy is raised, the number of vibrational channels, N_e, in the wavefunction expansion has to be increased in order to attain convergence [8]. This also affects the value of $r_e^{(1)}$. Thus, at 248.5 nm convergence is attained for $r_e^{(1)} = 5.0$ and N_e=40, while $r_e^{(1)} = 8.0$ and N_e=95 must be chosen in order to attain converged results at 190.0 nm.

The $\langle E, f, q^- | \mathrm{d}_{e,g} | E_j \rangle$ transition amplitudes were obtained directly using the ACM [11,12] coupled to the log-derivative propagator [13]. The $\langle \varepsilon_{v'} | \left[\tilde{W}_e(R, r) - v_g(r) \right] | \varepsilon_v \rangle$ potential matrix elements (which serve as input to the Coupled Channels equations) were calculated using the Discrete Position Operator Representation (DPOR) method [26] (see also [8]). In the Born-Oppenheimer approximation the photodissociation amplitudes can be calculated separately for each electronic transition. The total cross section was therefore obtained by squaring the absolute value of the sum of the e=a and e=b photodissociation amplitudes.

The natural ("un-controlled") continuum absorption spectrum of CH_2BrI calculated in this manner, assuming that the ground vibrational state $|E_1\rangle$ is initially populated, is shown in Fig.3. The computed spectrum is in good agreement with the experimental result, peaking at 213.5 nm for the B-band and at 274.5 nm for the A-band, as compared with the experimental values of 215 nm and 270 nm, respectively. Other properties such as the I/Br ratio at two wavelengths, at 193.3 nm and at 248.5 nm were also computed and found to be in good agreement with the experimental results [16]. The branching ratios at other wavelengths have so far not been measured.

IV. COHERENT CONTROL OF THE BRANCHING PHOTODISSOCIATION OF CH_2IBr

Consider then the application of bichromatic control to the $CH_2Br + I$ ($q = 1$) $\leftarrow$ $CH_2BrI \rightarrow CH_2I + Br$ ($q = 2$) photodissociation process. The initial superposition state of Eq. (1) is accordingly chosen as,

$$\Psi_g(t = 0) = |\, g\,\rangle \{c_k|E_k\rangle + c_l|E_l\rangle\}\,. \tag{26}$$

The dissociation laser electric field $\varepsilon(\omega)$ is comprised of two sharp lines, at frequencies $\omega_k = (E - E_k)/\hbar$ and $\omega_l = (E - E_l)/\hbar$. The ratio of product yield in the two arrangements at energy E is $R(E) = \frac{P(E,q=1)}{P(E,q=2)}$, written [1], using Eq. (9), as,

$$R(E) = \frac{|\mu^{(1)}_{k,k}| + x^2|\mu^{(1)}_{l,l}| + 2x\cos(\theta_k - \theta_l + \alpha^{(1)}_{k,l})|\mu^{(1)}_{k,l}|}{|\mu^{(2)}_{k,k}| + x^2|\mu^{(2)}_{l,l}| + 2x\cos(\theta_k - \theta_l + \alpha^{(2)}_{k,l})|\mu^{(2)}_{k,l}|}. \tag{27}$$

The $\alpha_{i,j}$ in this equation are the so-called "molecular" phases, defined as,

$$\mu^{(q)}_{i,j} = |\mu^{(q)}_{i,j}|\exp(i\alpha^{(q)}_{i,j}), \tag{28}$$

x is given by $x = f_l/f_k$, where f_j is defined as,

$$\bar{\epsilon}(\omega_{EE_j})c_j = f_j\exp(i\theta_j), \quad j = k, l. \tag{29}$$

The x and $\theta \equiv \theta_l - \theta_k$ serve as the experimental knobs for bichromatic control.

In addition to the two interfering pathways (see Eq. (7) or Eq. (27)), which contribute to photodissociation at energy $E = E_k + \hbar\omega_k = E_l + \hbar\omega_l$, there are two additional pathways ("satellites") causing dissociation at energies $E' = E_k + \hbar\omega_l$ and $E'' = E_l + \hbar\omega_k$. Because each satellite occurs at a different energy, the interference term between the two satellites averages out to zero over time. Hence the satellites do not interfere with each other, neither do they interfere with the two ("main") pathways at energy E. The non-interfering (and therefore uncontrollable) contributions of the two satellites must nevertheless be included in the yield calculations.

A. Control over the A-band and the B-band dissociation of CH_2BrI

We first present results of our calculations for two excitation wavelengths, $\lambda_1 = 248.5$ nm and $\lambda_1 = 193.3$ nm, for which experimental I/Br branching ratios are available [16]. In the CC calculations the quoted value of λ_1 serves to indicate the total energy E, given as, $E = E_k + hc/\lambda_1$ where $E_k < E_l$. The second CW source is therefore at a wavelength λ_2 satisfying $E = E_k + hc/\lambda_1 = E_l + hc/\lambda_2$.

The calculated I/Br branching ratios for excitation from a superposition of the $|E_1\rangle$ and the $|E_2\rangle$ vibrational states at an energy corresponding to $\lambda_1 = 248.5$ nm, are shown in Fig. 3 as a function of the dimensionless amplitude $s = 1/\left\{1 + |\frac{f_1}{f_2}|^2\right\} = 1/\left\{1 + \frac{1}{x^2}\right\}$ where $x = |f_2/f_1|$, and the $\theta = \theta_1 - \theta_2$ phase. Varying s from zero to one corresponds to changing the initial superposition state from the pure $|\,E_1\,\rangle$ state to a state made up entirely of state $|\,E_2\,\rangle$.

The results presented in Fig. 5, at $\lambda_1 = 248.5$ nm, clearly demonstrate the broad range of control over the I/Br branching ratio. The I/Br branching ratio can be varied from 0.39, at $s = 0.24$, $\theta = 0°$, to 6.22, at $s = 0.7$, $\theta = 187.2°$. This corresponds to a variation in the CH_2Br+I yield of 26.1% to 85.1 %. By contrast, the uncontrolled I/Br ratio attained with only one laser is 1.2 for $s = 0$ and 3.73 for $s = 1$, in accord with experiment.

A smaller range of control is attainable in the presence of a strong natural bias. For example, in Fig. 6 we present results at an energy corresponding to $\lambda_1 = 193.3$ nm. At this energy the I/ Br branching ratio, though varying substantially between 0.007, at $s = 0.86$, $\theta = 331.2°$, and 0.26, at $s = 0.08$, $\theta = 21.6°$, is always smaller than 1. This limitation is due to the fact that $\lambda_1 = 193.3$ nm lies at the tail of the B-band where the natural dynamics is heavily biased towards the dissociation of the C-Br bond.

In fact the wide range of control demonstrated in Fig. 5 is due to the substantial overlap between the A and the B bands at $\lambda_1 = 248.5$ nm. As we move closer to the absorption maxima of either band, the degree of control is reduced. For example, at $\lambda_1 = 251$ nm, the I/Br branching ratio, though varying substantially (from 2.57 to 28.5), never dips below the value of 1. In a similar fashion, closer to the B-band maximum, at $\lambda_1 = 245$ nm, the I/Br branching ratio varies from 0.02 to 0.43, but never exceeds unity.

The nature of the initial superposition state significantly affects the attainable range of control. For example, the most striking results were obtained by using a superposition of the $|E_1\rangle$ and the $|E_5\rangle$ states at $\lambda_1 = 248.5$ nm. As shown in Fig. 7, the I/Br branching ratio can be varied in this case from 0.06 at $s = 0.06$, $\theta = 180°$ to 297.71 at $s = 0.1$, $\theta = 0°$.

As noted above, the degree of control is diminished by the existence of the uncontrollable "satellites" [3], not included in the computations reported above. Figure 8 shows contour plot of I/Br branching ratio which includes the satellite contributions. Results for the excitation with $\lambda_1 = 248.5$ from a superposition of $|E_1\rangle$ and $|E_2\rangle$ states are presented. Since the satellite contributions cannot be expressed in terms of the x or s parameters, we assumed that both laser field amplitudes are equal to 1, $|\varepsilon_1| = |\varepsilon_2| = 1$. As expected, the addition of the uncontrolled satellite terms reduces the range of control (compare to Fig. 4), which now extends from 0.99 at $s = 0.44$, $\theta = 0°$ to 5.03 at $s = 0.88$, $\theta = 187.2°$. Similarly, for example, control for excitation with $\lambda_1 = 248.5$ from a superposition of $|E_3\rangle$ and $|E_4\rangle$ states extends over the range 0.94 at $s = 0.54$, $\theta = 180°$ to 6.87 at $s = 0.76$, $\theta = 0°$ when the satellites are included, as compared to the control ratios cited above.

B. Control in a single excited state dissociation model

In many of the examples in the previous section we found a strong correspondence between the excited PES and the preferred product arrangement. Thus at $\lambda_1 = 248.5$ nm, there exists a heavy bias for the W_a PES to yield the CH_2Br+I arrangement and the W_b PES to yield the CH_2I+Br arrangement. It is therefore important to investigate a model system in which the dynamics on a single PES bifurcates into the two arrangements more democratically. Further, such a structure is expected to be characteristic of many systems. In order to study this type of control we have devised a model excited PES, W_h, which has single absorption band whose minimum and maximum in the I/Br yield occur at not-too-distant excitation wavelengths.

The model PES chosen, shown in Fig. 9 as a cut through the surfaces and as a contour plot in Fig. 10a, has the same form as the PES of Eq. (17) with the following parameters: $C_h^I =$

0.37, $\beta_h^I = 0.3$, $C_h^{Br} = 0.27$, $\beta_h^{Br} = 0.35$. The feature allowing for the more even bifurcation pattern is the almost symmetrical location of the saddle point region near $r_{C-Br} \approx r^{Br}$ and $r_{C-I} \approx r^I$. This location brings about a good overlap between the ground wavefunction and the excited wavefunctions leading to both product channels. In order to best choose the NIP in this case, special care had to be taken with respect to the choice of the $r_e^{(1)}$ parameter. This variable was assigned the value of 4.9 *au* after performing an extensive set of convergence tests. Convergence was achieved when the same value of $r_e^{(1)}$ could be used for a variety of values for the total number of channels. Here, the convergence issues were similar to those discussed for the CO_2 dissociation [8] where the two product channels, corresponding to CO +O and O + CO, both have large overlap with the excited ground state. The photodissociation probabilities for both arrangements obtained using the above model PES are shown in Fig. 10b. The CH_2Br+I channel (solid line) is seen to peak at 239.4 nm while the CH_2I+Br channel (dashed line) peaks at 238.4 nm.

Figure 11 shows the coherently controlled I/Br branching ratios at the maximum ($\lambda_1 =$ 239 nm) of the total absorption spectrum. Clearly in evidence is the extensive range of attainable control in this model: The I/Br branching ratio varies from 0.85 at $s = 0.94$, $\theta = 43.2^o$ to the maximum value of 5.2 at $s = 0.92$, $\theta = 208.8^o$. The I/Br range remains extensive even when the satellite contributions are included: it extends from 0.99 to 4.59. As in the two potential model, less extensive control is achieved in the presence of a strong natural bias towards a particular product. For example, the I/Br ratio can be controlled over the range of 0.66 to 1.7 at an excitation wavelength of 231 nm and from 33.8 to 1535.5 at $\lambda_1 = 249$ nm.

The dependence of the control plots on θ is also of interest, containing useful information on the nature of the photodissociation dynamics. Inspection of the results in Sect. IVA on the realistic case with two excited states potentials (see Figs. 4-8) reveals that the I/Br branching ratio has its extrema for the case of $\lambda_1 = 248.5$ nm at $\theta \approx 0^o$ or $\theta \approx 180^o$. This is because the "molecular phase" $\alpha_{1,2}^{(q)}$, a quantity of considerable interest [27], is ≈ 0 or $\pm\pi$. That is, in accord with Eq. (28), $\mu_{1,2}^{(q)}$ is essentially a real number at these frequencies. By contrast, as demonstrated in Fig. 11, the model PES discussed in this section results in a

larger molecular phase $\alpha_{1,2}$. As a result, the maxima and minima in the controlled I/Br ratios occur at values other than 0° and 180°. For example, at 239 nm the minimum occurs at $\theta = 43.2°$ and the maximum at $\theta = 208.8°$.

The reason for the $\alpha_{i,j} \approx 0$ in the two-PES-case at various frequencies is due to the similarities in the phases of the $\langle E, f, q^- | \mathrm{d}_{e,g} | E_k \rangle$ transition amplitudes which comprise (see Eq. (28)) the $\mu_{i,j}^{(q)}$ matrix elements. This phenomenon can be traced back to the fact that in the absence of strong inelastic transitions the phases of $\langle E, f, q^- | R, r \rangle$ wave functions appear as mere multiplicative factors. As a result, the $\langle E_k | \mathrm{d}_{e,g} | E, f, q^- \rangle \langle E, f, q^- | \mathrm{d}_{e,g} | E_l \rangle$ product is essentially a real number.

In order to demonstrate this, we have examined a measure of inelasticity of the dissociation process in the q arrangement, defined as, $R_{inelastic} \equiv \sum_{i \neq j} |S_{q;i,j}|^2 / \sum_i |S_{q;i,i}|^2$. Here i, j denote the product vibrational channels and $S_{q:i,j}$ denotes the scattering matrix element for arrangement q starting in state i and going to state j. We find, for example, that for the realistic 2-potentials case, at $\lambda_1 = 260$ nm, for $q = 1$ (i.e. CH_2Br +I) $R_{inelastic} = 2.75 \times 10^{-3}$, while for the model potential, at $\lambda_1 = 230$ nm, $R_{inelastic} = 0.44$ leading $\alpha_{1,2}$ to deviate from the 0 and π. Note that in the realistic two excited PES case, the above criterion could not be used when the A and the B bands overlap because of the interference between the W_a and the W_b mediated dissociation pathways.

C. Control in the Chaotic Regime

It is of interest to study the possibility of phase control when starting from highly-excited bound states that exhibit chaotic dynamics in the classical limit. To do so we first consider the realistic two-PES model of Sect. IVA and create a superposition of two states approximately 40 kcal/mole above the ground vibrational state. These states are above the classical onset of chaos for the ground state of this molecule and exhibit a highly oscillatory uncorrelated [28] behavior. We use two consecutive states with the following energies: $E_1 = -0.128018$ *au* and $E_2 = -0.128008$ *au* measured relative to the threshold for three body dissociation, CH_2+Br+I. In order to obtain converged bound state energies, 70

states of the product and 95 basis functions have been used.

The coherent control results for excitation at $\lambda_1 = 280$ nm are shown in Fig. 12. The range of control is seen to extend from an I/Br ratio of 0.4 at $s = 0.86$, $\theta = 345.6°$ to 2.36 at $s = 0.52$, $\theta = 172.8°$. This corresponds to decrease by 56.7 % of the results obtained for $s = 1$ (where the I/Br ratio is 0.93) and to increase by 38.9 % over the ratio obtained for $s = 0$ (where the I/Br ratio is 1.7). Less extensive control, ranging from product ratios of 0.36 to 1.0 at $\lambda_1 = 248.5$ nm, from 0.29 to 2.13 at $\lambda_1 = 275$ nm, and from 0.3 to 0.82 at $\lambda_1 = 375$ nm, were also obtained.

Results obtained using the same superposition of states for the single-band model gave similar control. In this case the I/Br branching ratio can be varied from 0.55 to 2.26 at $\lambda_1 = 361$ nm, corresponding to a decrease of the product ratio by 34.9% or increase by 45.2% in comparison with the uncontrolled $s = 1$ and $s = 0$ ratios, respectively. Extensive level of control can also be obtained for some other excitation wavelengths, e.g., the I/Br ratio ranges from 1.13 to 5.26 at $\lambda_1 = 380$ nm, and from 2.66 to 6.95 at $\lambda_1 = 400$ nm.

Extensive control is also observed when one prepares superpositions of even higher lying energy levels. For example, the I/Br ratio obtained for the superposition of levels with energies $E_1 = -0.112382$ *au* and $E_2 = -0.112370$ *au*, which are only 5 kcal/mol below the CH_2Br+I dissociation threshold (55 kcal/mol [16]), with $\lambda_1 = 425$ nm, ranges from 0.26 at $s = 0.54$, $\theta = 165.6°$ to 2.16 at $s = 0.06$, $\theta = 345.6°$. A large degree of control was observed at other wavelengths as well, e.g. the I/Br ratio varies from 0.58 to 1.28 at $\lambda_1 = 400$ nm, from 0.28 to 1.66 for $\lambda_1 = 475$ nm, and from 0.21 to 2.96 for $\lambda_1 = 300$ nm.

An equally high level of control over the branching ratio can be achieved for the single band model when utilizing the superposition of the second pair of high-lying states. For instance, at $\lambda_1 = 227$ nm, the I/Br product ratio ranges from 0.62 at $s = 0.44$, $\theta = 172.8°$ to 7.41 at $s = 0.68$, $\theta = 352.8°$.

It is evident from our results that superpositions of highly-excited states provide the same quality of control as obtained using superpositions of low-lying levels, even those above the onset of chaotic motion. Indeed, coherent control over a completely chaotic system has also been recently demonstrated [29].

V. SUMMARY

In this paper we have applied the bichromatic CC scenario to the control of the relative yield of products in the photodissociation of CH_2BrI into CH_2Br + I and CH_2I + Br. To do so we constructed two excited PES to fit the measured absorption spectrum and the I/Br branching ratios at several frequencies. The calculations were performed using a combination of the NIP and the ACM, leading to the identification of a frequency region (near 248.5 nm) where we expect a high level of control. This occurs in the intermediate region between A- and B-bands where both C-I and C-Br fission occur to a significant extent.

The dependence of control on various the parameters, amplitudes ratio and phases, has been examined. The results clearly show that extensive control can be achieved by simply preparing superposition of two levels using a set of phase controlled CW sources. The level of control has been shown to depend strongly on the makeup of the superposition state created in the first step. For example, the most extensive control, ranging in I/Br ratio from 0.06 to 297, was obtained using a superposition of the first and the fifth vibrational levels of the ground state. The effect of taking into account uncontrollable satellite terms has also been examined and we showed that the resulting level of control, though diminished, is still considerable.

Finally, the extent of control afforded for the excitation from the superposition of two states in the chaotic regime has been studied. Our results show that excitation from a superposition of highly excited levels provides the same degree of control as the excitation from low-lying states.

As is evident from our results, an experimental effort at controlling the CH_2BrI and other halomethane bond fission reactions is well warranted. Possible future developments will include the extension of the CH_2BrI model to the non-linear case in order to include the bending of the CH_2 group as well as applications of alternate schemes for coherent control [4].

Acknowledgement

MS wishes to acknowledge support from the EU Commission through Program no. IHP-RTN-99-1. This work was supported by Photonics Research Ontario and by the U.S. Office of Naval Research.

REFERENCES

[1] P. Brumer and M. Shapiro, Chem. Phys. Lett., **126**, 541 (1986).

[2] M. Shapiro and P. Brumer, J. Chem. Phys., **84**, 4103 (1986).

[3] P. Brumer and M. Shapiro, Faraday Discuss. Chem. Soc., **82**, 177 (1986).

[4] P. Brumer and M. Shapiro, Adv. Atom. Mol. and Opt. Phys. **42**, 287 (2000).

[5] S.A. Rice and M. Zhao, Optical Control of Molecular Dynamics, (Wiley, N.Y., 2000)

[6] M. Shapiro and P. Brumer, J. Chem. Phys. **98**, 201 (1993)

[7] For some recent developments in using semiclassical approaches for this purpose see V. Batista and P. Brumer, J. Phys. Chem. **105**, 2591 (2001); V. Batista and P. Brumer, J. Chem. Phys. **114**, 10321 (2001)

[8] D. G. Abrashkevich, M. Shapiro and P. Brumer, J. Chem. Phys. **114**, 54 (2001).

[9] D. Neuhauser and M. Baer, J. Phys. Chem. **90**, 4351 (1989); *ibid.*, **91**, 4651 (1989).

[10] D. Neuhauser, R. S. Judson, R. E. Jaffe, M. Baer, and D. J. Kouri, Chem. Phys. Lett. **176**, 546 (1991).

[11] M. Shapiro, J. Chem. Phys. **56**, 2582 (1972).

[12] M. Shapiro and R. Bersohn, Ann. Rev. Phys. Chem., **33**, 409 (1982).

[13] B.R. Johnson, J. Comp. Phys. **13**, 445 (1973).

[14] S. J. Lee and R. Bersohn, J. Phys. Chem. **86**, 728 (1982).

[15] L.J. Butler, E.J. Hintsa, and Y.T. Lee, J. Chem. Phys. **84**, 4104 (1986).

[16] L.J. Butler, E.J. Hintsa, S.F. Shane, and Y.T. Lee, J. Chem. Phys. **86**, 2051 (1987).

[17] S.-Q. Man, W. M. Kwok, and D. L. Phillips, J. Phys. Chem. **99**, 15705 (1995).

[18] S.-Q. Man, W. M. Kwok, D. L. Phillips, and A. E. Johnson, J. Chem. Phys. **105**, 5842 (1996).

[19] X. Zheng and D. L. Phillips, J. Phys. Chem. **113**, 3194 (2000).

[20] J. C. Mossinger, D. E. Shallcross, and R. A. Cox, J. Chem. Soc. Faraday Trans. **94**, 1391 (1998).

[21] G.G. Balint-Kurti and M. Shapiro, Advan. Chem. Phys., **60**, 403 (1985); P. Brumer and M. Shapiro, Advan. Chem. Phys., **60**, 371 (1985).

[22] M. Shapiro, J. Phys. Chem. **90**, 3644 (1986).

[23] Z.-H. Guo and H. Guo, J. Chem. Phys., **97**, 2110 (1992).

[24] G. Herzberg, Molecular Spectra and Molecular Structure, Vol. 2, (Krieger, Malabar, 1991).

[25] H. Okabe, Photochemistry of Small Molecules (Wiley, New York, 1978).

[26] S. Kanfer and M. Shapiro, J. Phys. Chem. **88**, 3964 (1984).

[27] R.J. Gordon, L.C. Zhu and T. Seidemann, Acct. Chem Res. **32**, 1007 (1999); J.A. Fiss, L.C. Zhu, R.J. Gordon and T. Seidemann, Phys. Rev. Lett. **82**, 65 (1999)

[28] M. Shapiro and G. Goelman, Phys. Rev. Lett. **53**, 1714 (1984).

[29] J. Gong and P. Brumer, Phys. Rev. Lett. **86**, 1741 (2001)

VI. FIGURE CAPTIONS

Figure 1. Contour plot of W_g, the ground PES of CH_2BrI. Energies are given in atomic units, with the zero of energy corresponding to the three body dissociation limit of CH_2BrI, i.e., $E(CH_2 + Br + I) = 0$.

Figure 2. Contour plot of the excited PES: (a) W_a and (b) W_b.

Figure 3. Cut through the three potential surfaces along the CH_2I +Br product channel along with the excitation scheme. The spacing between the two levels $|E_1\rangle$ and $|E_2\rangle$ is exaggerated for clarity.

Figure 4. The calculated absorption spectrum of CH_2BrI. The A-band has a maximum at 274.5 nm and B-band has a maximum at $\lambda_1 = 213.5$ nm.

Figure 5. The I/Br branching ratio ($\times 10$) in the photodissociation of CH_2BrI, at $\lambda_1 = 248.5$ nm, using a superposition of $|E_1\rangle$ and $|E_2\rangle$ states. The lower limit of the measured I/Br branching ratio in the natural photodissociation process is 1.2:1 [16].

Figure 6. Contour plot of the I/Br branching ratio ($\times 100$) in the photodissociation of CH_2BrI at $\lambda_1 = 193.3$ nm, using a superposition of $|E_1\rangle$ and $|E_2\rangle$ states. The measured ratio is 1:3.5 [16].

Figure 7. The same as in Fig. 4, for a superposition of the $|E_1\rangle$ and $|E_5\rangle$ states.

Figure 8. The same as in Fig. 4, including the satellite terms.

Figure 9. Cut through the two model potential surfaces along the CH_2I +Br product channel along with the excitation scheme. The spacing between the two levels $|E_1\rangle$ and $|E_2\rangle$ is exaggerated for clarity.

Figure 10 (a) Contour plot of the model excited PES W_h; (b) The calculated absorption spectrum of the single excited state model of CH_2BrI.

Figure 11. The same as in Fig. 4, for the single excited state model PES, at $\lambda_1 = 239$ nm.

Figure 12. The I/Br branching ratio ($\times 10$) at $\lambda_1 = 280$ nm, using a superposition of two highly excited states (≈ 15 kcal/mol below the CH_2Br+I dissociation threshold).

Fig 1

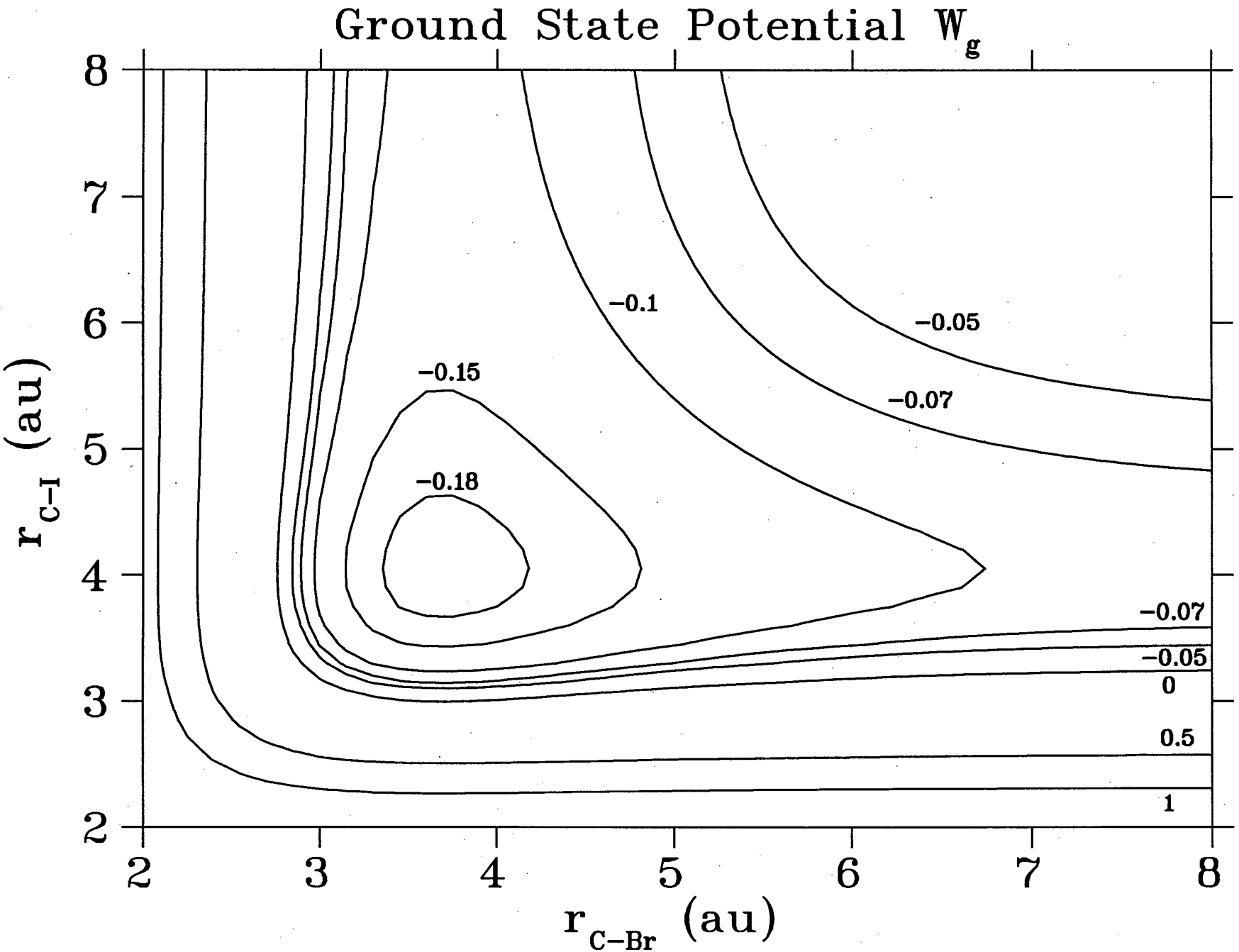
Ground State Potential W_g
r_{C-I} (au)
r_{C-Br} (au)
2
3
4
5
6
7
8
−0.1
−0.05
−0.15
−0.07
−0.18
−0.07
−0.05
0
0.5
1

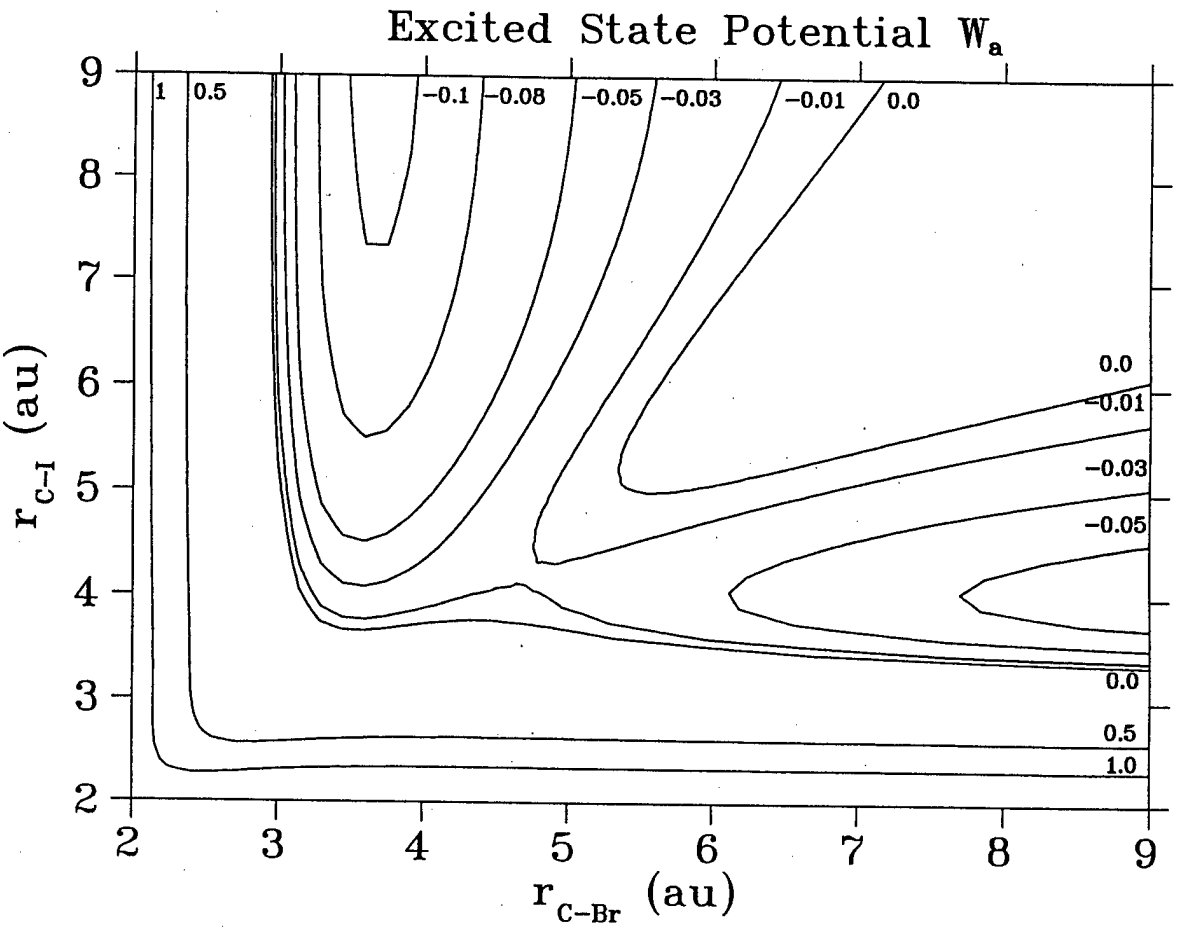
Excited State Potential W_a
1
0.5
−0.1
−0.08
−0.05
−0.03
−0.01
0.0
0.0
−0.01
−0.03
−0.05
0.0
0.5
1.0
r_{C-I} (au)
r_{C-Br} (au)

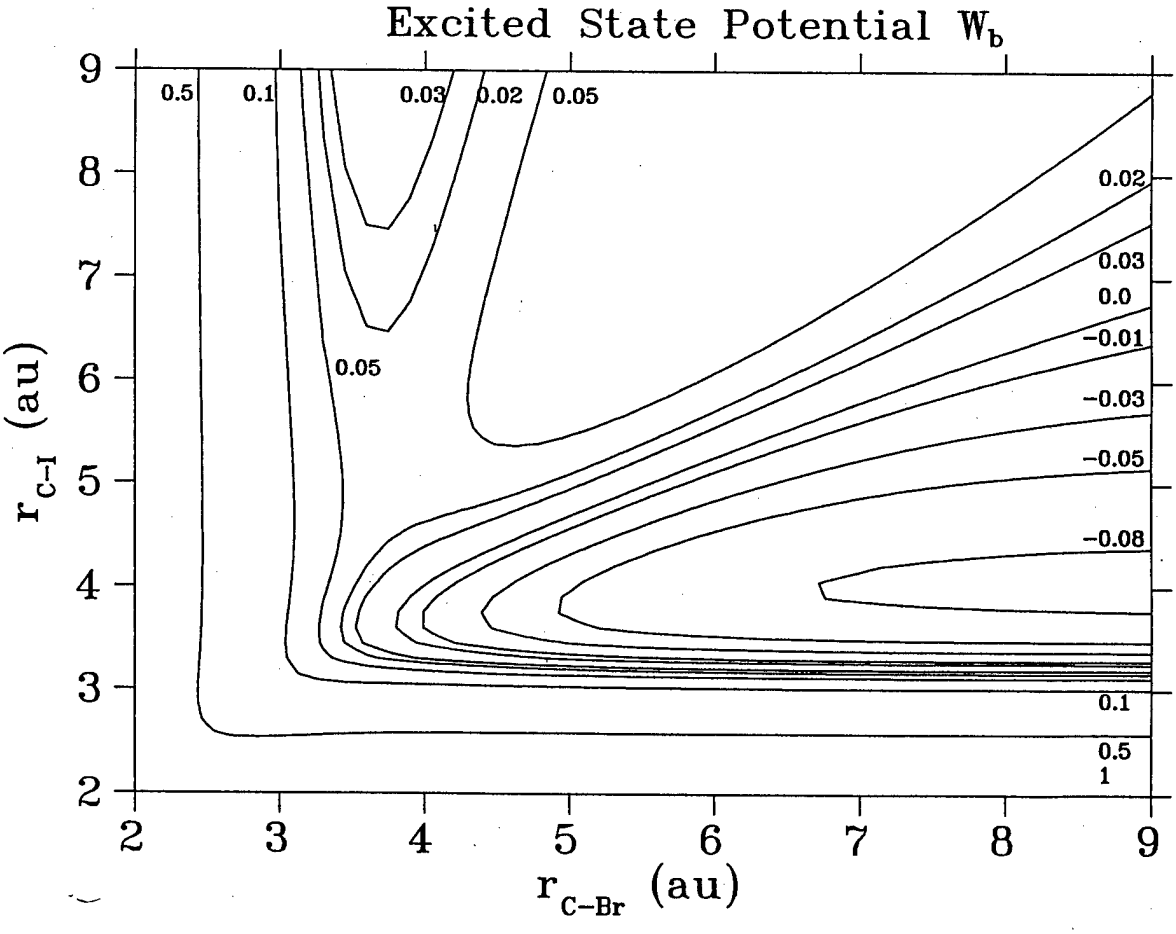
Excited State Potential W_b
0.5
0.1
0.03
0.02
0.05
0.05
0.02
0.03
0.0
−0.01
−0.03
−0.05
−0.08
0.1
0.5
1
r_{C-I} (au)
r_{C-Br} (au)

Fig 3

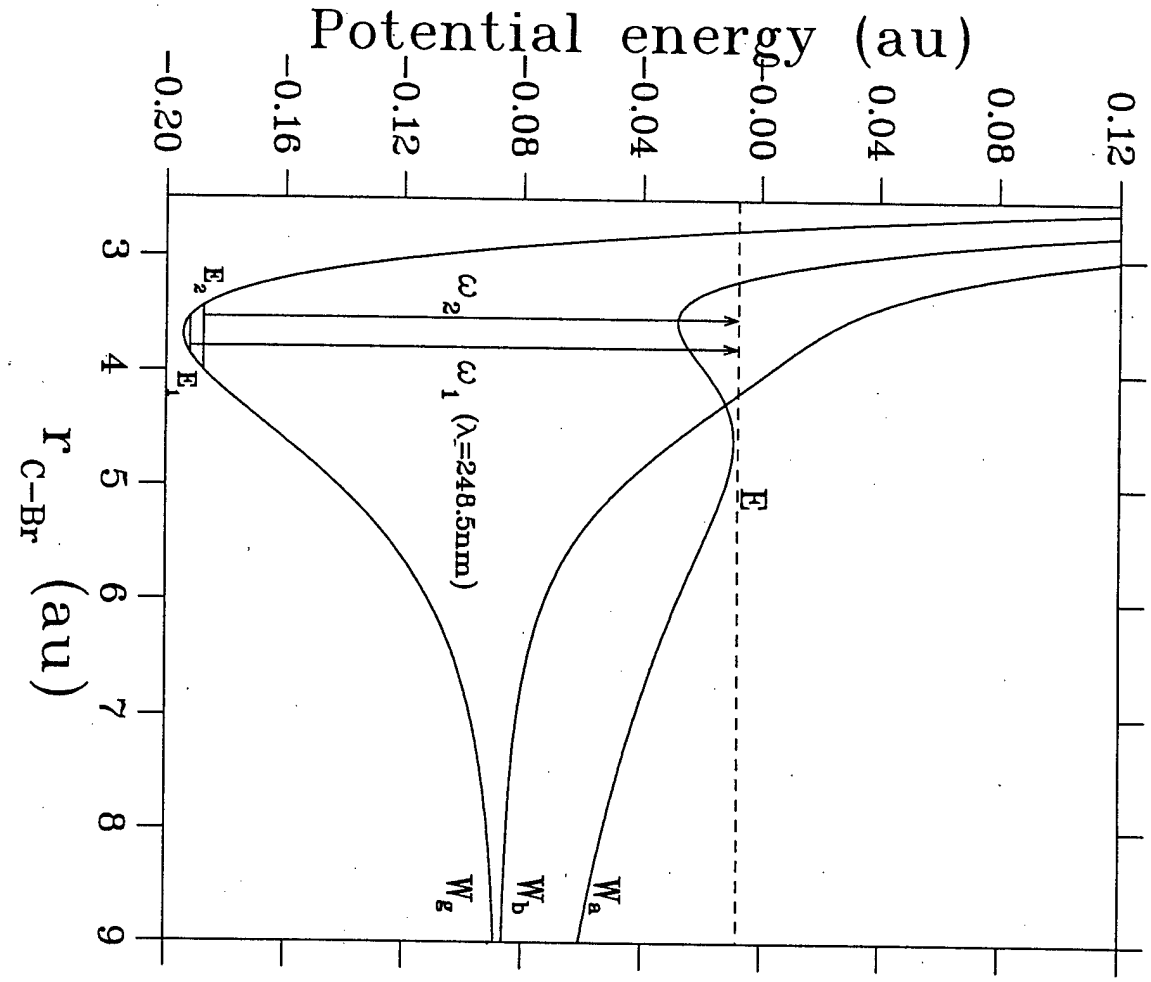
Potential energy (au)
−0.20
−0.16
−0.12
−0.08
−0.04
−0.00
0.04
0.08
0.12
3
4
5
6
7
8
9
r_{C-Br} (au)
E_2
E_1
ω_2
ω_1 (λ=248.5nm)
E
W_g
W_b
W_a

Fig 4

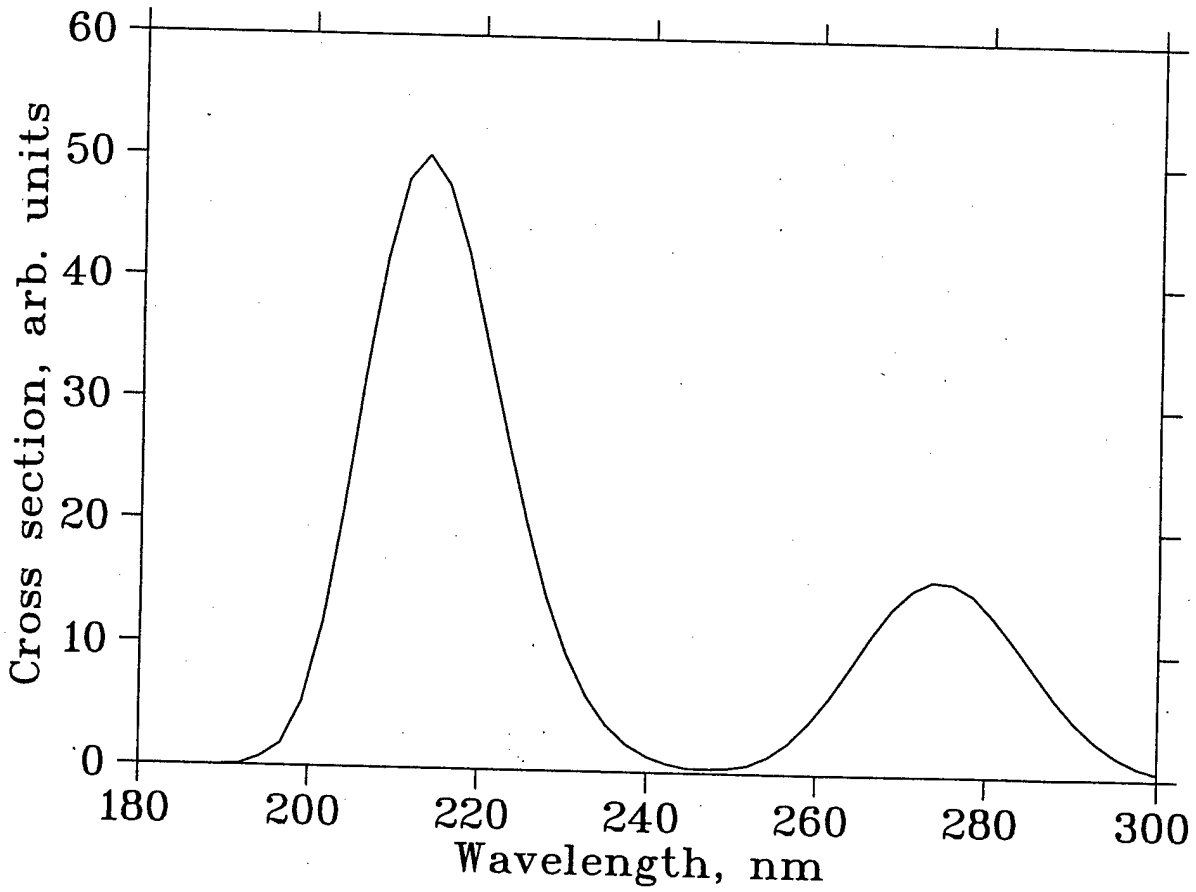
Cross section, arb. units
0
10
20
30
40
50
60
180
200
220
240
260
280
300
Wavelength, nm

Fig 5

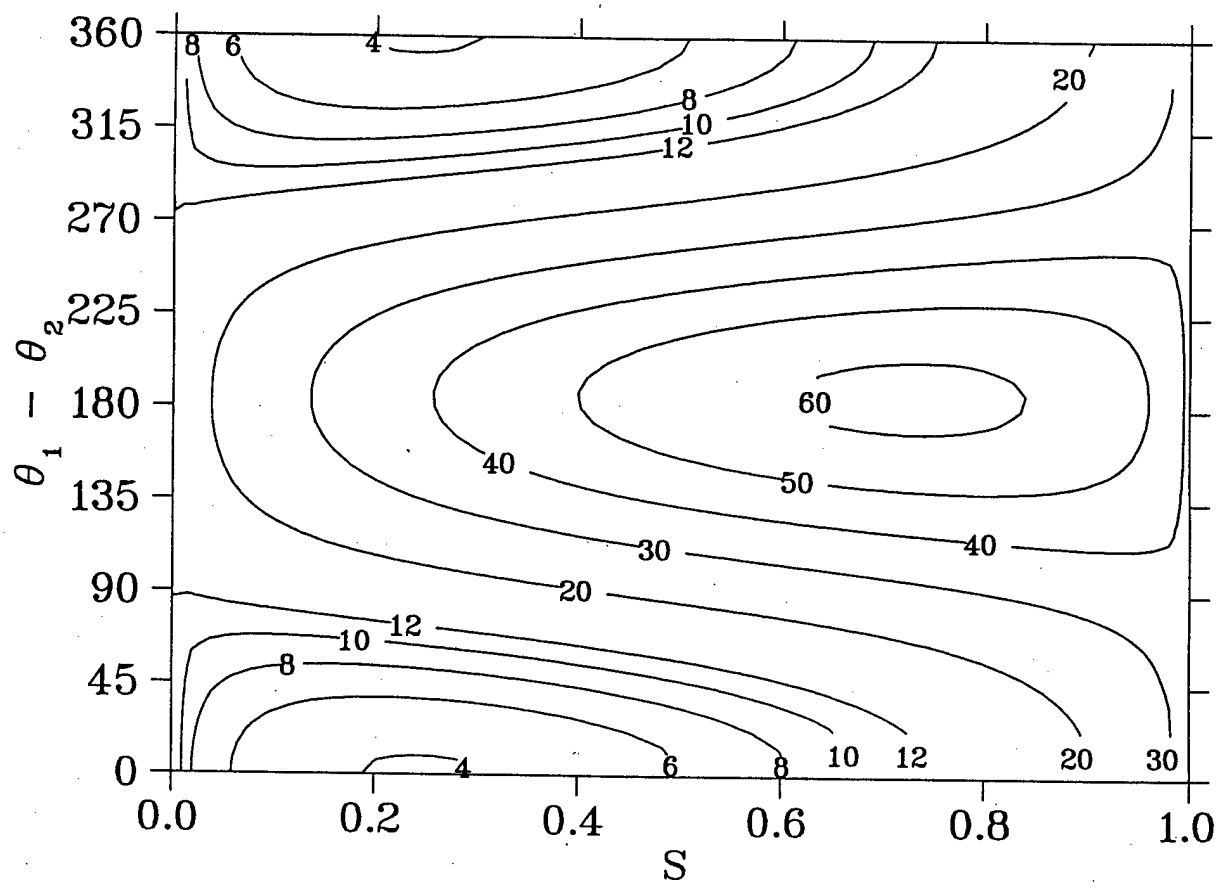
360
315
270
225
180
135
90
45
0
$\theta_1 - \theta_2$
0.0
0.2
0.4
0.6
0.8
1.0
S
8
6
4
8
10
12
20
60
40
50
30
40
20
10
12
8
4
6
8
10
12
20
30

Fig 6

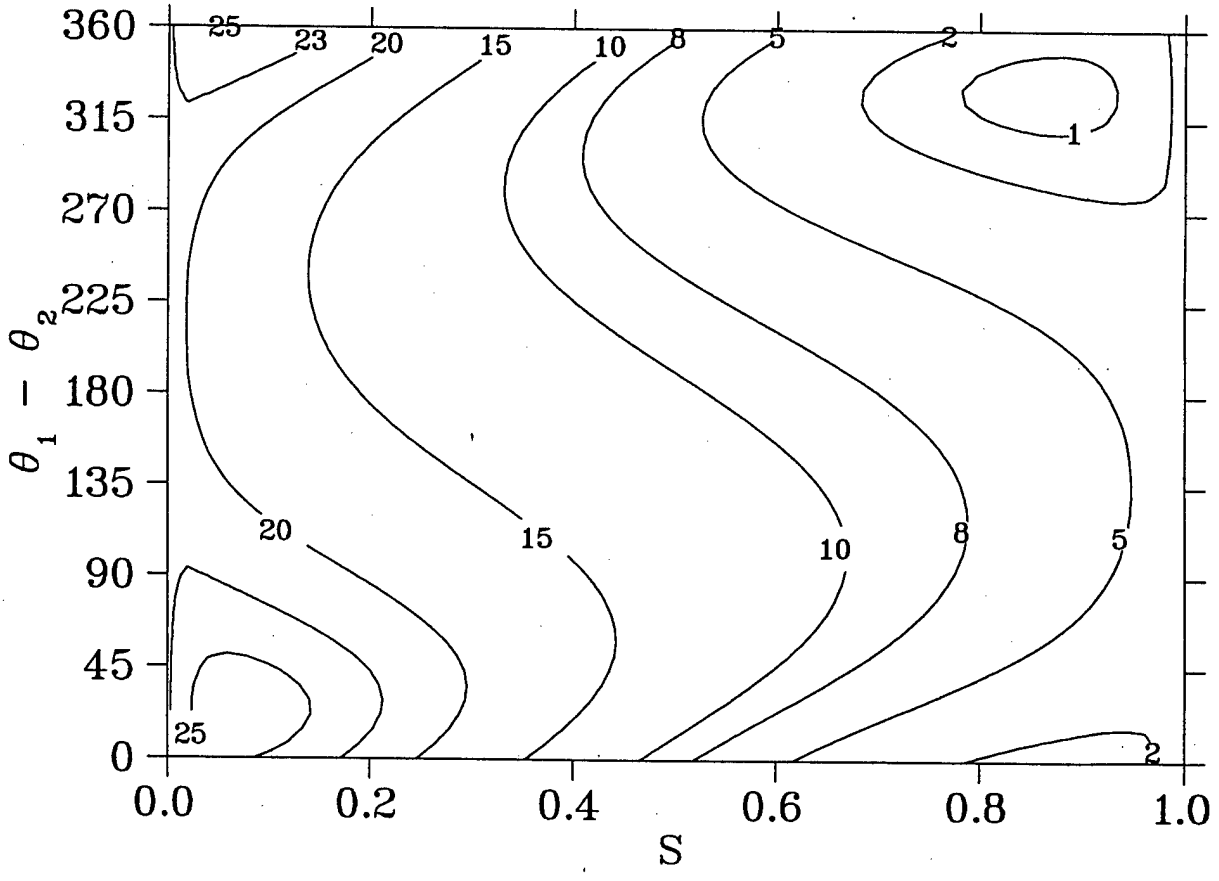
360
315
270
225
180
135
90
45
0
$\theta_1 - \theta_2$
0.0
0.2
0.4
0.6
0.8
1.0
S
25
23
20
15
10
8
5
2
1
20
15
10
8
5
25
2

Fig 7

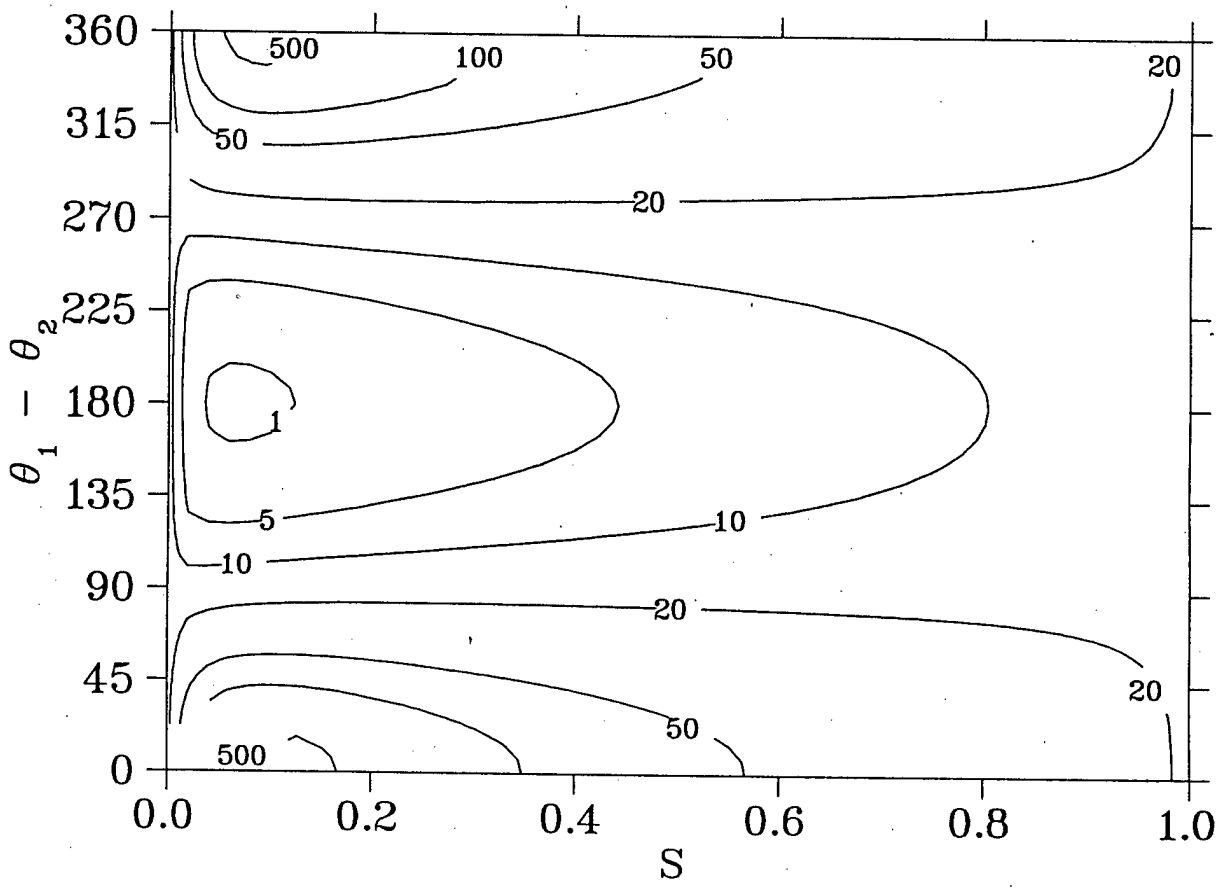
360
315
270
225
180
135
90
45
0
$\theta_1 - \theta_2$
0.0
0.2
0.4
0.6
0.8
1.0
S
500
100
50
20
50
20
1
5
10
10
20
20
50
500

Fig. 8

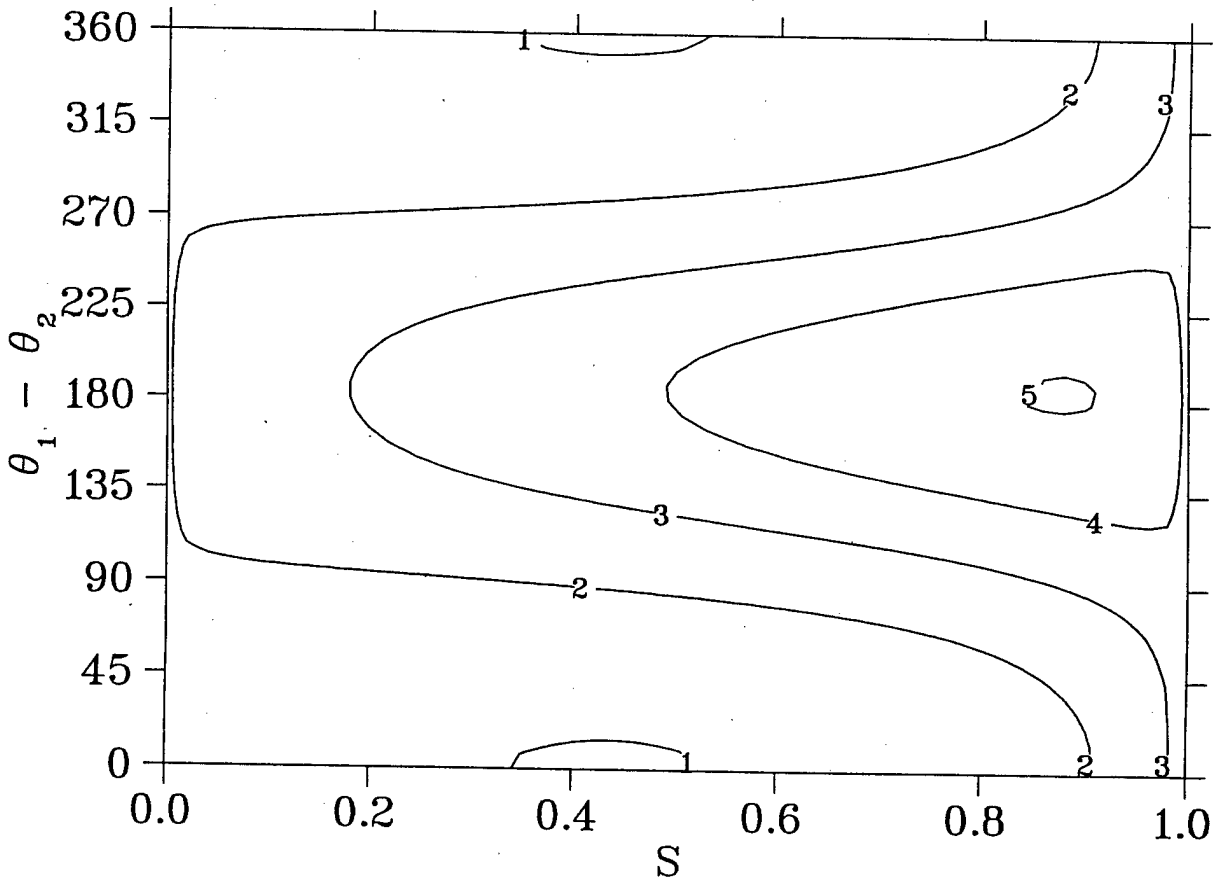
360
315
270
225
180
135
90
45
0
$\theta_1 - \theta_2$
0.0
0.2
0.4
0.6
0.8
1.0
S
1
2
3
5
3
4
2
1
2
3

Fig 9

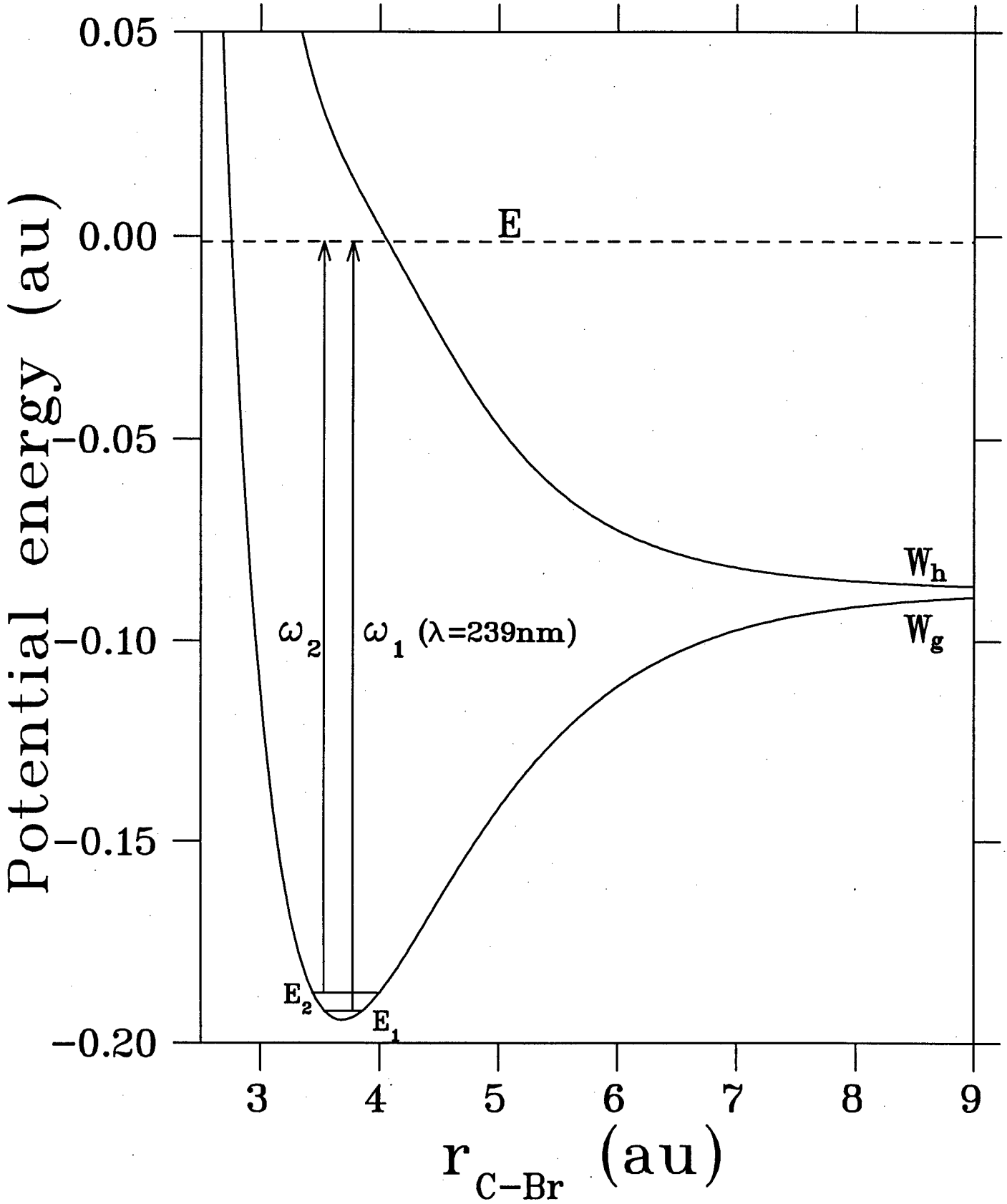
0.05
0.00
−0.05
−0.10
−0.15
−0.20
Potential energy (au)
E
W_h
W_g
ω_2
ω_1 (λ=239nm)
E_2
E_1
3
4
5
6
7
8
9
r_{C-Br} (au)

Fig. 10

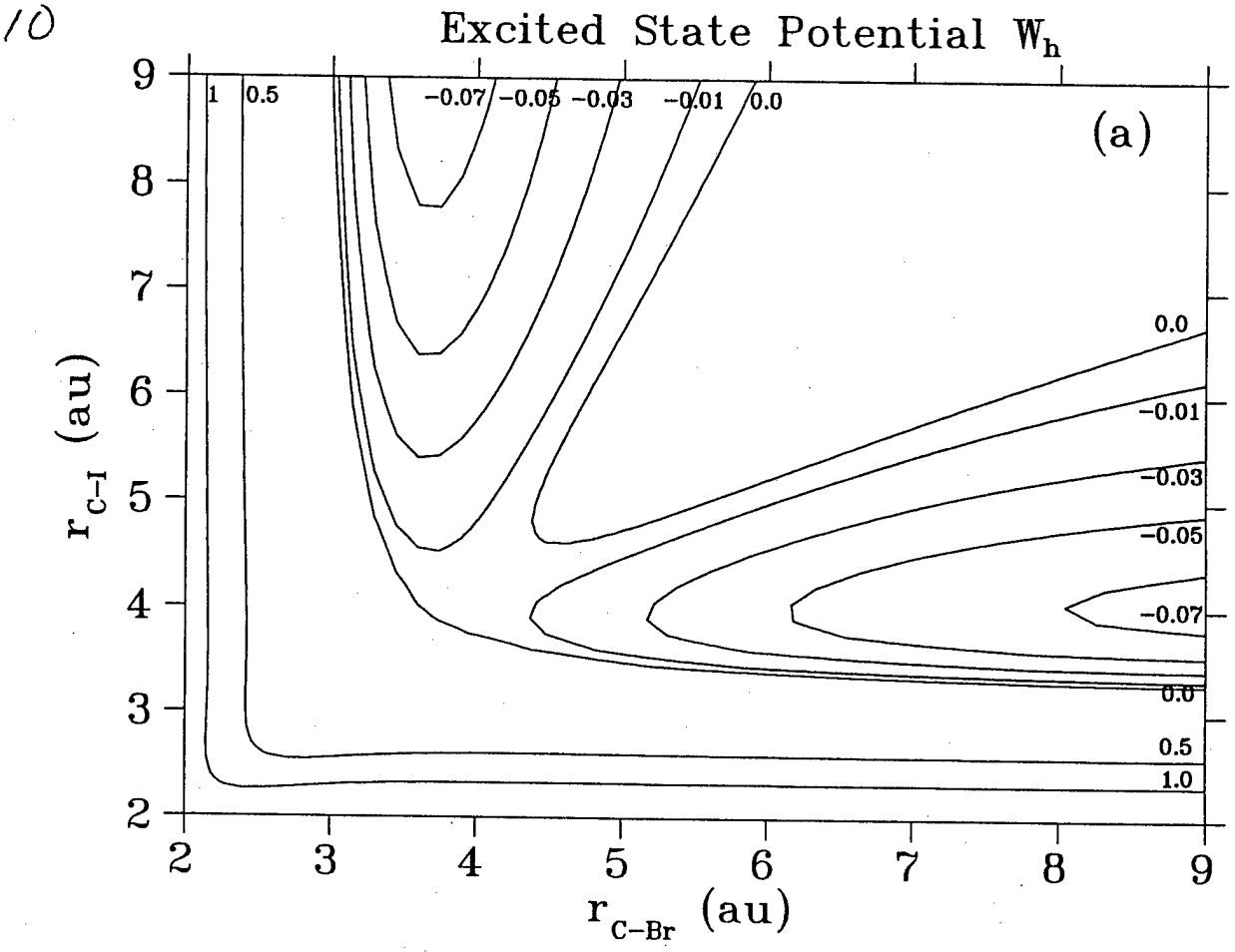
Excited State Potential W_h
(a)
1
0.5
−0.07
−0.05
−0.03
−0.01
0.0
0.0
−0.01
−0.03
−0.05
−0.07
0.0
0.5
1.0
r_{C-I} (au)
r_{C-Br} (au)
2
3
4
5
6
7
8
9

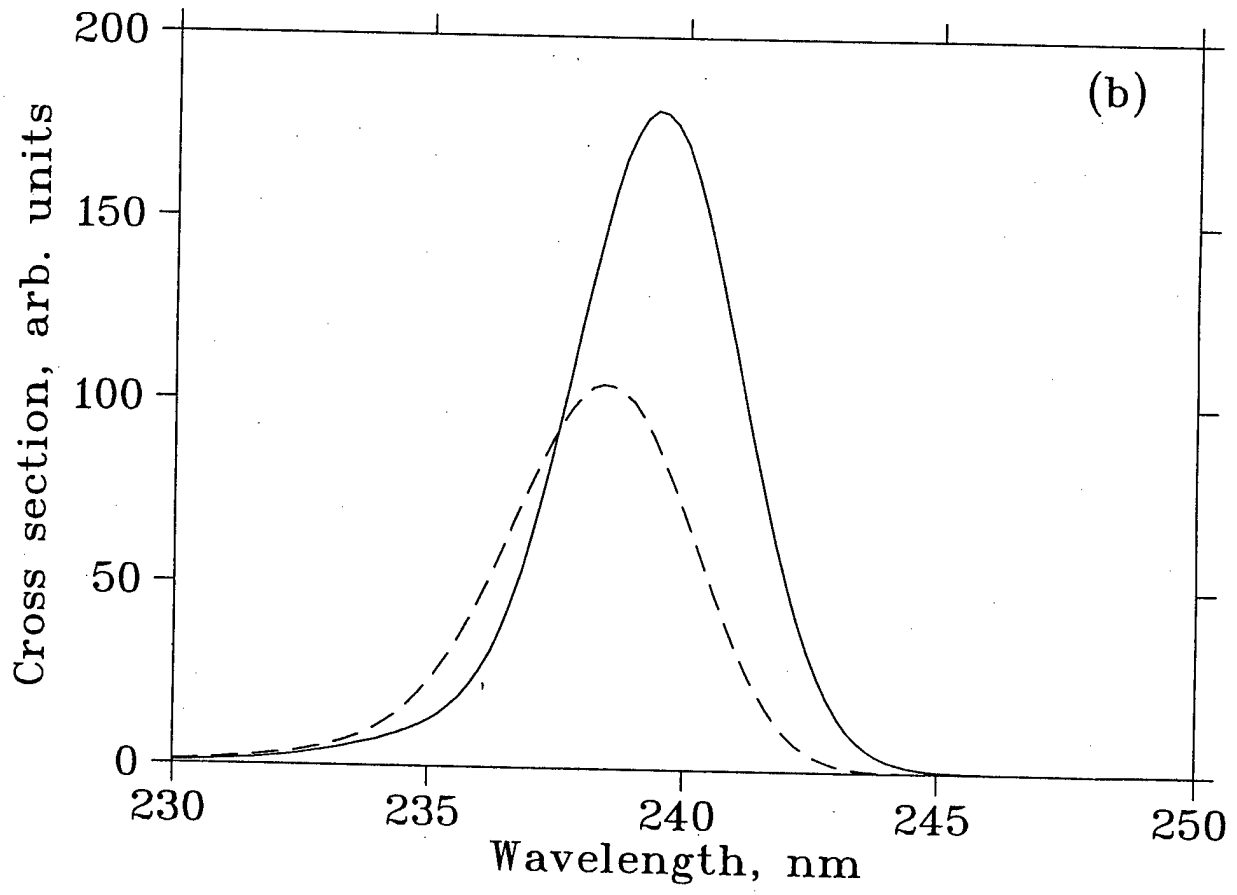
(b)
Cross section, arb. units
Wavelength, nm
0
50
100
150
200
230
235
240
245
250

Fig 11

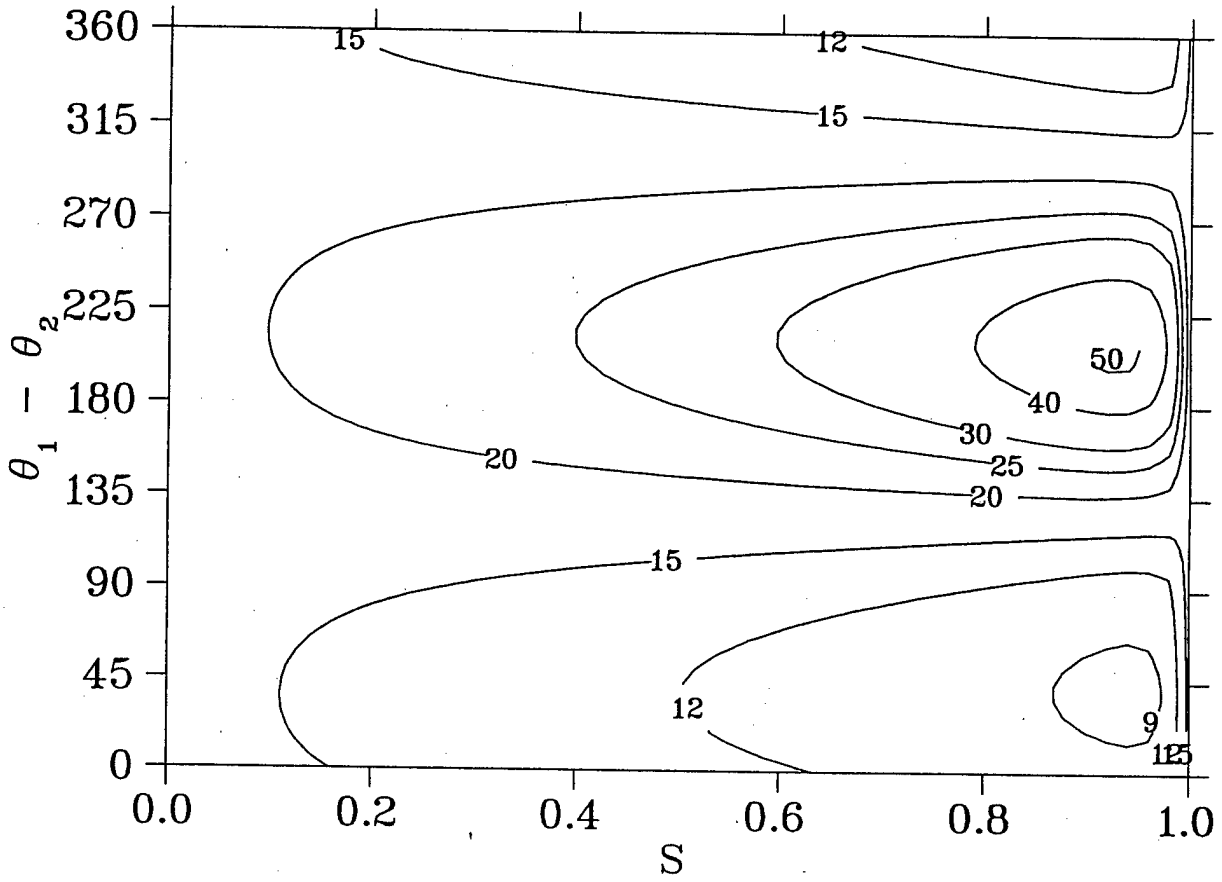
360
315
270
225
180
135
90
45
0
$\theta_1 - \theta_2$
0.0
0.2
0.4
0.6
0.8
1.0
S
15
12
15
50
40
30
25
20
20
15
12
9
12.5

Fig. 12

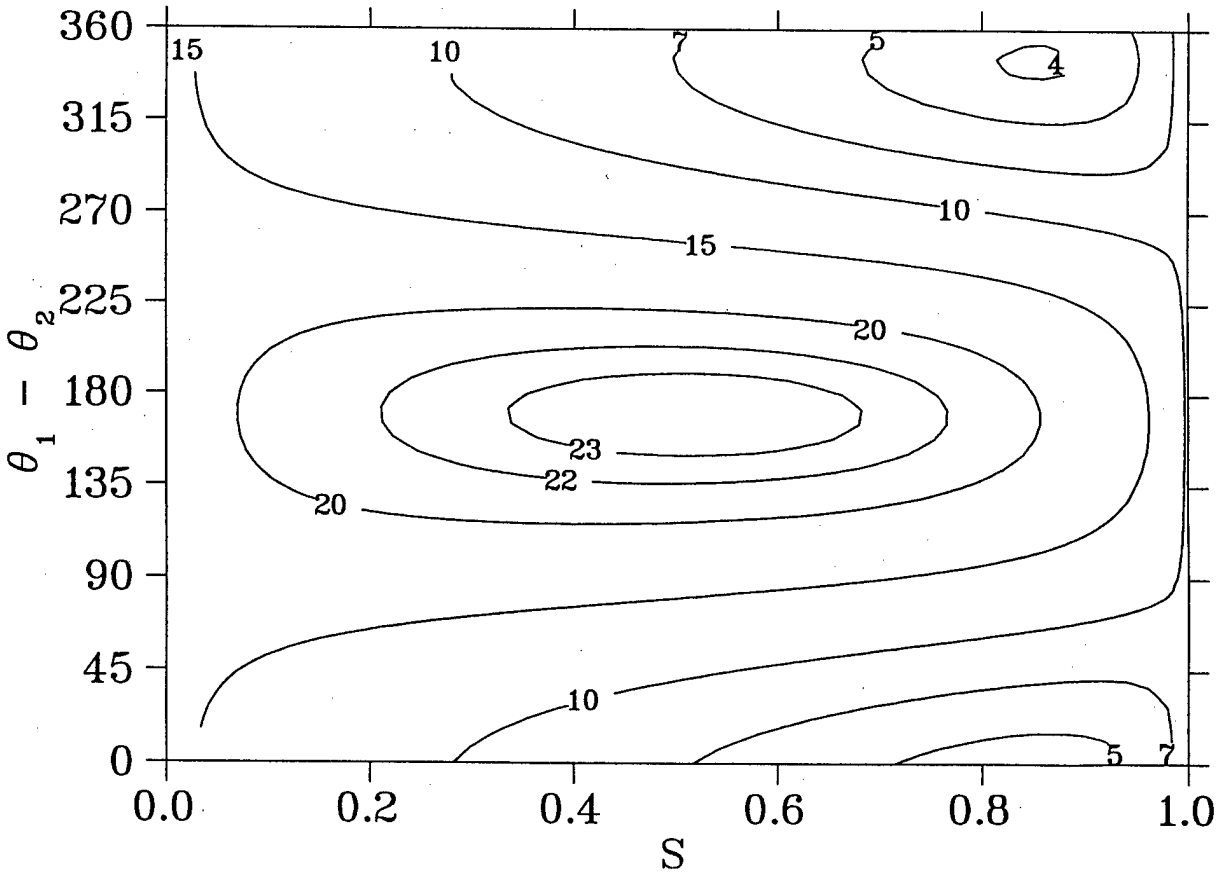
360
315
270
225
180
135
90
45
0
$\theta_1 - \theta_2$
0.0
0.2
0.4
0.6
0.8
1.0
S
15
10
7
5
4
10
15
20
23
22
20
10
5
7

Phys. Rev. Lett. (submitted)

2

Phase Control of Nonadiabaticity-induced Quantum Chaos in An Optical Lattice

Jiangbin Gong and Paul Brumer

Chemical Physics Theory Group,

University of Toronto

Toronto, Canada M5S 3H6

(September 26, 2001)

Abstract

The dynamics of a three-level atom in an optical lattice comprising two standing-wave laser beams is shown to display either regular or chaotic translational motion, depending upon the relative laser phase. Control of this behavior is explained in terms of the nonadiabatic transition between optical potentials and the corresponding regular to chaotic transition in mixed classical-quantum dynamics. The results are of interest to both areas of coherent control and quantum chaos.

PACS numbers: 32.80.Qk, 05.45.Mt, 05.45.Gg

Recent years have witnessed an increasing interest in the coherent control of molecular and atomic processes [1,2]. One central scheme of coherent control is *phase control*, in which different optical phases are introduced into coherent laser-matter interactions in order to manipulate quantum interference effects and thus to achieve target objectives. It has been shown that phase control approaches are widely applicable [1] even to some systems displaying quantum chaotic dynamics [3].

In this Letter we report all-optical phase control of the translational motion of atoms in an optical lattice comprising two standing-wave laser fields. The control mechanism is shown to originate in the nonadiabatic coupling between different optical potentials as well as in the regular to chaotic transition in a mixed classical-quantum description of the model system. The results, which are of broad interest to both coherent control and quantum chaos, substantially enrich our understanding of the role of optical and quantum phases in laser-atom interaction.

Consider a simple model of a Λ-type 3-level atom moving along two co-propagating standing-wave laser beams, with two lower degenerate levels $|1\rangle$ and $|3\rangle$, and one upper level $|2\rangle$. Two laser fields, with different polarizations σ_+ and σ_-, couple $|1\rangle$ with $|2\rangle$ and $|2\rangle$ with $|3\rangle$, respectively. Such a closed 3-level Λ configuration may be realized in, for example, ^{4}He using the $2^3S_1 \rightarrow 2^3P_1$ transition [4]. The laser fields are of the same frequency, with large detuning Δ from $|2\rangle$. We use x, p, M, Ω_1 (Ω_2), k_1 ($= k_2$) to represent the position, momentum, atomic mass, the two Rabi frequencies (assumed real) and the two wavevectors, respectively. The relative phase of the two standing-waves is denoted by ϕ. For generality we employ a set of natural units by scaling all the parameters, i.e., $x^0 = \lambda$ for x, $p^0 = \hbar/\lambda$ for p, $t^0 = M\lambda^2/\hbar$ for the time variable t, $\Omega^0 = 2/t^0$ for Δ, Ω_1 and Ω_2. In terms of these units, the dynamical equations will not explicitly contain the atomic mass, the effective wavevector is given by $k = 2\pi$, and $[x, p] = i$ in the full quantum dynamics. In the rotating wave approximation and in the interaction picture, the Hamiltonian describing the translational motion along the laser beams is $H = p^2/2 + (V_{ij})$, with the potential matrix (V_{ij}) $(i, j = 1, 2, 3)$ given by

$$(V_{ij}) = \begin{pmatrix} 2\Delta & \Omega_1 \sin(kx) & 0 \\ \Omega_1 \sin(kx) & 0 & \Omega_2 \sin(kx+\phi) \\ 0 & \Omega_2 \sin(kx+\phi) & 2\Delta \end{pmatrix}. \quad (1)$$

To demonstrate phase control of the dynamics consider numerical results for the case where (1) $\Omega_1 = 6.0 \times 10^3$, $\Omega_2 = 7.0 \times 10^3$, $\Delta = 1.5 \times 10^4$; (2) the atom is initially in internal state $|1\rangle$; and (3) the average momentum, average position, momentum variance, and position variance of the initial Gaussian wavepacket are given by $\langle p \rangle = 25.0$, $\langle x \rangle = 0.0$, $\delta p = 10/\sqrt{2}$ and $\delta x = 1.0/10\sqrt{2}$, respectively. In ^{4}He, this corresponds to $t^0 \sim 77$ μsec, the detuning $\sim 2\pi \cdot 62$ MHz (about 38 times the linewidth of $|2\rangle$), and the initial kinetic temperature ~ 29 μK. The results shown below represent typical observations for a wide range of system parameters and initial conditions [5].

The solid lines in Fig. 1 show the time dependence of the momentum expectation value $\langle p \rangle$ of time evolving wavepackets for various ϕ. The $\phi = 0$ case [Fig. 1a] displays a perfectly regular recurrence pattern. By contrast, the $\phi = 0.25\pi$ case [Fig. 1b] is characteristic of a relaxation process, in which one sees significantly irregular oscillations of small amplitude. In addition, the associated power spectrum, not shown, is also quite noisy. Further tuning ϕ leads to another totally different situation: in the $\phi = 0.5\pi$ case [Fig. 1c], $\langle p \rangle$ lies very close to its initial value and undergoes regular oscillations, with a characteristic frequency that is much higher than that in the $\phi = 0$ case (The dashed curves in Fig. 1 are discussed later below).

The phase-controlled regular and irregular motion shown in Fig. 1 is associated with entirely different type of sensitivity of the dynamics to slight changes of ϕ. Figure 2 shows the time dependence of the absolute value of the overlap χ of two time evolving wavefunctions emanating from the same initial Gaussian wavepacket, with the relative phase of the two laser fields given by ϕ and $\phi + \pi/400$, respectively. For $\phi = 0$ or $\phi = 0.5\pi$, χ remains nearly one throughout, indicating that the dynamics is highly insensitive to tiny changes of ϕ. By contrast, for $\phi = 0.25\pi$, χ is less than 0.70 at $t = 0.7$. This interesting *hypersensitivity* [6]

quantum chaos. Further, in the $\phi = 0.5\pi$ case [Fig. 3c], the regular classical motion is restored, with a characteristic frequency identical to that in Fig. 1c. Clearly, the essence of the optical phase control shown in Fig. 1 is manifest in our mixed classical-quantum treatment.

Also enlightening is the ensemble statistics in the classical treatment of translational motion. The dashed lines in Fig. 1 display the time dependence of the average momentum $\langle p \rangle$ for a classical ensemble of trajectories initially centered at $x = 0$ and $p = 25.0$, with the same initial variances as in the quantum calculations. Each individual trajectory in the ensemble is obtained by solving Eqs. (2), (3), and (4). The quantum-classical correspondence for the regular dynamics at times $t < 0.15$ in Figs. 1a and 1c is impressive, further confirming our understanding of the full quantum dynamics. On the other hand, as seen in Fig. 1b, $\langle p \rangle$ for the classical ensemble quickly relaxes to zero, whereas $\langle p \rangle$ for the quantum ensemble remains far away from zero. This quantum-classical difference constitutes an excellent example of quantum suppression of classical chaos in an unbounded Hamiltonian system.

Further insights into the origin of phase control can be obtained by considering the dynamics in an adiabatic representation. To do so let us introduce an orthogonal transformation (O_{ij}) $(i, j = 1, 2, 3)$ to diagonalize the potential matrix (V_{ij}). (O_{ij}) is given by

$$(O_{ij}) = \begin{pmatrix} \frac{\Omega_1 \sin kx}{\sqrt{2(\eta^2 - \Delta\eta)}} & \frac{\Omega_2 \sin(kx+\phi)}{\xi} & \frac{\Omega_1 \sin(kx)}{\sqrt{2(\eta^2 + \Delta\eta)}} \\ \frac{\eta - \Delta}{\sqrt{2(\eta^2 - \Delta\eta)}} & 0 & \frac{-\eta - \Delta}{\sqrt{2(\eta^2 + \Delta\eta)}} \\ \frac{\Omega_2 \sin(kx+\phi)}{\sqrt{2(\eta^2 - \Delta\eta)}} & \frac{-\Omega_1 \sin(kx)}{\xi} & \frac{\Omega_2 \sin(kx+\phi)}{\sqrt{2(\eta^2 + \Delta\eta)}} \end{pmatrix}, \tag{5}$$

where $\xi(x, \phi) \equiv \sqrt{\Omega_1^2 \sin^2(kx) + \Omega_2^2 \sin^2(kx + \phi)}$ and $\eta(x, \phi) \equiv \sqrt{\xi^2(x, \phi) + \Delta^2}$. Corresponding to the three eigenvectors (O_{1j}, O_{2j}, O_{3j}) $(j = 1, 2, 3)$, are three eigen-potentials $V_i(x, \phi)$ given by $V_1(x, \phi) = \Delta + \eta(x, \phi)$, the constant potential $V_2 = 2\Delta$, and $V_3(x, \phi) = \Delta - \eta(x, \phi)$. For the special case of $\phi = 0$, V_1 and V_2 are degenerate at $kx = n\pi$, and the eigenvector (O_{12}, O_{22}, O_{32}) is x-independent; for the general cases of $\phi \neq 0$, $V_1(x, \phi) > V_2 > V_3(x, \phi)$, i.e.,

the three potential curves do not cross one another. Of particular interest is the constant potential V_2, associated with the eigenvector (O_{12}, O_{22}, O_{32}). Since

$$\Omega_1 \sin(kx) O_{12} + \Omega_2 \sin(kx + \phi) O_{32} = 0, \tag{6}$$

V_2 results from the complete quantum destructive interference between the two standing-wave laser fields. As such, V_2 is an extension of the "dark optical lattice" in the presence of two counter-propagating plane-wave laser beams [4,9,10].

Now let us transform Eqs. (3) and (4) to the eigen-potential (adiabatic) representation. Specifically, consider the dynamics in terms of $\tilde{C}_i$, $i = 1, 2, 3$, where $\tilde{C}_i = \sum_{k=1}^{3} O_{ki} C_k$. Using $\sum_{k=1}^{3} O_{ki} O_{kj} = \delta_{ij}$ and $\sum_{k=1}^{3} O_{ki} dO_{kj}/dx = -\sum_{k=1}^{3} O_{kj} dO_{ki}/dx$, Eqs. (3) and (4) can be transformed to

$$\frac{dp}{dt} = -|\tilde{C}_1|^2 \frac{dV_1(x,\phi)}{dx} - |\tilde{C}_3|^2 \frac{dV_3(x,\phi)}{dx}, \tag{7}$$

and

$$i \begin{pmatrix} \frac{d\tilde{C}_1}{dt} \\ \frac{d\tilde{C}_2}{dt} \\ \frac{d\tilde{C}_3}{dt} \end{pmatrix} = \begin{pmatrix} V_1(x,\phi) & it_{12} & -it_{13} \\ -it_{12} & V_2 & -it_{23} \\ it_{13} & it_{23} & V_3(x,\phi) \end{pmatrix} \begin{pmatrix} \tilde{C}_1 \\ \tilde{C}_2 \\ \tilde{C}_3 \end{pmatrix}, \tag{8}$$

where the diagonal terms are the three adiabatic potentials given above, and the potential coupling terms are given by $t_{12}(x,\phi) = pk\Omega_1\Omega_2 \sin(\phi)/[2\xi^2(\eta^2 - \Delta\eta)]^{1/2}$, $t_{13}(x,\phi) = pk\Delta[\Omega_1^2 \sin(2kx) + \Omega_2^2 \sin(2kx + 2\phi)]/4\eta^2\xi$, and $t_{23}(x,\phi) = pk\Omega_1\Omega_2 \sin(\phi)/[2\xi^2(\eta^2 + \Delta\eta)]^{1/2}$ [11]. Note that t_{ij} $(i \neq j = 1, 2, 3)$ is proportional to the momentum p. Thus, the coupling between optical potentials is due to the nonadiabatic effects associated with translational motion. Further, for the computational example discussed above (and many other cases in which $\Delta > 0$) one has $\min[V_1(x,\phi) - V_2] << \min[V_2 - V_3(x,\phi)]$ and $t_{12}(x,\phi) >> t_{23}(x,\phi)$, suggesting that $V_3(x,\phi)$ is effectively decoupled from $V_1(x,\phi)$ and V_2. Note also that at the initial location $x = 0$, the initial internal state $|1\rangle$ is a superposition state of the two eigenvectors associated with V_1 and V_2 for $\phi = 0$, and reduces to the eigenvector associated with V_2 for $\phi \neq 0$.

The key role of ϕ becomes clear as one compares the magnitude of the nonadiabatic coupling term $t_{12}(x,\phi)$ with that of $(V_1 - V_2)$. For case (a), $\phi = 0$ and $t_{12}(x, \phi = 0) = 0$, so the dynamics is adiabatic. Thus, in the case of Fig. 1a, the quantum ensemble divides into two sub-ensembles: one is trapped in one well of V_1 around $x = 0$ and undergoes periodic oscillations, and the other experiences the trivial motion on the constant potential V_2. For case (b), $\phi = 0.25\pi$. Here the smallest gap between V_1 and V_2 is given by $g(\phi) = \sqrt{A^2(\phi) + \Delta^2} - \Delta$, where $A^2(\phi) = [\Omega_1^2 + \Omega_2^2 - \sqrt{\Omega_1^4 + \Omega_2^4 + 2\Omega_1^2\Omega_2^2\cos(2\phi)}]/2$. The corresponding ratio of the potential coupling term t_{12} to $g(\phi)$ is given by

$$T(\phi) = \frac{pk\Omega_1\Omega_2\sin(\phi)}{\sqrt{2}[A^2(\phi) + \Delta^2]^{1/4}A(\phi)g^{3/2}(\phi)}. \tag{9}$$

Since $T(\phi = 0.25\pi) \approx 1.0$, the magnitude of the nonadiabatic coupling is comparable to that of $(V_1 - V_2)$, resulting in strong nonadiabatic effects. Thus, the chaotic motion seen in Fig. 3b is induced by the significant nonadiabatic coupling between the two simple one-dimensional potentials V_1 and V_2. Finally, for case (c), $\phi = 0.5\pi$. Here $T(\phi = 0.5\pi) = \min[T(\phi)] \approx 0.16$, i.e., the nonadiabatic coupling is appreciably weaker than in the case of $\phi = 0.25\pi$. As such, the translational motion, initially launched on the adiabatic potential V_2, would essentially remain on V_2, with small perturbations from the insignificant Rabi population oscillation between V_1 and V_2. To further confirm this picture, one finds that the characteristic frequency of the regular dynamics in Fig. 1c and Fig. 3c is ~ 1425, a value consistent with the Rabi frequencies given by $\sqrt{(V_1 - V_2)^2 + 4t_{12}^2}$ [see Eq. (8)].

A number of additional remarks are in order. First, the two-standing-wave configuration is essential in our model. That is, if either or both of the two standing-wave fields are replaced by a traveling-wave, the nonadiabatic coupling or the spacing between V_1 and V_2 is not a sensitive function of ϕ, and there is no significant phase control. On the other hand, a three-level atom in two standing-wave laser fields of different but commensurable frequencies also shows dynamics which is controllable by changing ϕ [12]. Second, in contrast to some recent studies on optical-magneto lattice [13,14], the coupling between different optical potentials discussed above is not due to additional magnetic fields, but directly

due to nonadiabaticity. Further, unlike the work in Ref. [14], here we have observed clear signatures of quantum chaos in the quantum dynamics. Thus, this model is the first all-optics realization of nonadiabaticity-induced quantum chaos, a phenomenon first discovered in molecular systems [15]. Third, in this work we have neglected decoherence effects (e.g., due to the spontaneous emission from the excited state $|2\rangle$). However, based on previous study of decoherence effects in conservative quantum chaotic systems that are far from the classical limit [16], one can expect that including decoherence effects will simply improve the quantum-classical correspondence already seen in this study.

In conclusion, we have demonstrated optical phase control of nonadiabaticity-induced quantum chaos in a Λ-type 3-level system in a two-standing-wave optical lattice. The functional dependence on ϕ has been exposed analytically, guiding experimental studies of the ϕ-dependent regular to chaotic transition. Recent experimental progress in atom optics and quantum chaos [4,10,13,17] suggests that the results should be experimentally achievable with existent technology.

Acknowledgments: This work was supported by the U.S. Office of Naval Research and the Natural Sciences and Engineering Research Council of Canada. J.G. is a Henry Croft Postdoctoral Fellow in Theoretical Chemical Physics.

REFERENCES

[1] M. Shapiro and P. Brumer, Adv. Atom., Mol. and Opt. Phys., **42**, 287 (2000).

[2] S.A. Rice and M. Zhao, *Optical Control of Molecular Dynamics* (John Wiley, New York, 2000).

[3] J. Gong and P. Brumer, Phys. Rev. Lett. **86**, 1741 (2001); J. Chem. Phys. **115**, 3590 (2001).

[4] A. Aspect *et al.*, Phys. Rev. Lett. **61**, 826 (1988).

[5] The system parameters and the initial conditions should be chosen to ensure that the population on level $|2\rangle$ is small ($< 2\%$ in the present case) so that spontaneous emission effects will be insignificant. It is also desirable to ensure negligible tunneling effects between different wells of V_1 so as to achieve good quantum-classical correspondence.

[6] R. Schack and C.M. Caves, Phys. Rev. Lett. **71**, 525 (1993).

[7] J.C. Tully and R.K. Preston, J. Chem. Phys. **55**, 562 (1971).

[8] R. Blümel and B. Esser, Phys. Rev. Lett. **72**, 3658 (1994).

[9] R. Dum and M. Olshanii, Phys. Rev. Lett. **76**, 1788 (1996).

[10] S.K. Dutta, B.K. Teo, and G. Raithel, Phys. Rev. Lett. **83**, 1934 (1999).

[11] The mixed classical-quantum treatment automatically neglects the optical Gauge potential [9,10], which is not of much interest as far as the nonadiabatic coupling is concerned.

[12] J. Gong and P. Brumer, manuscript in preparation.

[13] D.L. Haycock *et al.*, Phys. Rev. Lett. **85**, 3365 (2000).

[14] S. Ghose, P.M. Alsing, and I.H. Deutsch, preprint quan-ph/0102085.

[15] E.J. Heller, J. Chem. Phys. **92**, 1718 (1990); H. Schanz and B. Esser, Phys. Rev. A **55**, 3375 (1997); H. Fujisaki and K. Takatsuka, Phys. Rev. E **63**, 066221 (2001).

[16] J. Gong and P. Brumer, Phys. Rev. E **60**, 1643 (1999).

[17] D.A., Steck, W.H. Oskay, and M.G. Raizen, Science **293**, 274 (2001); W.K. Hensinger *et al*, Nature **412**, 52 (2001).

FIGURE CAPTIONS

Fig. 1:

Time dependence of $\langle p \rangle$ obtained from quantum wavepacket dynamics calculations (solid lines) and the ensemble statistics in a mixed classical-quantum description (dashed lines). The initial internal state is $|1\rangle$, and the $\langle x \rangle$ and $\langle p \rangle$ of the initial Gaussian ensemble are 0.0 and 25.0, respectively. The initial variances in position and momentum are chosen to be $1.0/10\sqrt{2}$ and $10.0/\sqrt{2}$, respectively. The relative phase ϕ equals 0.0, 0.25π, and 0.5π in (a), (b) and (c), respectively.

Fig. 2:

The sensitivity of the quantum dynamics to slight changes of the relative phase parameter ϕ. χ is the absolute value of the overlap between the two time evolving wavefunctions emanating from the same initial state as in Fig. 1, with the relative phase of the two standing-wave laser fields given by ϕ and $\phi + \pi/400$.

Fig. 3:

Time dependence of momentum for classical trajectories obtained by solving Eqs. (2), (3), and (4), with the initial position $x = 0$ and the initial momentum $p = 25.0$. The initial internal state is given by $|1\rangle$. ϕ equals 0.0, 0.25π, and 0.5π in (a), (b) and (c), respectively.

FIGURES

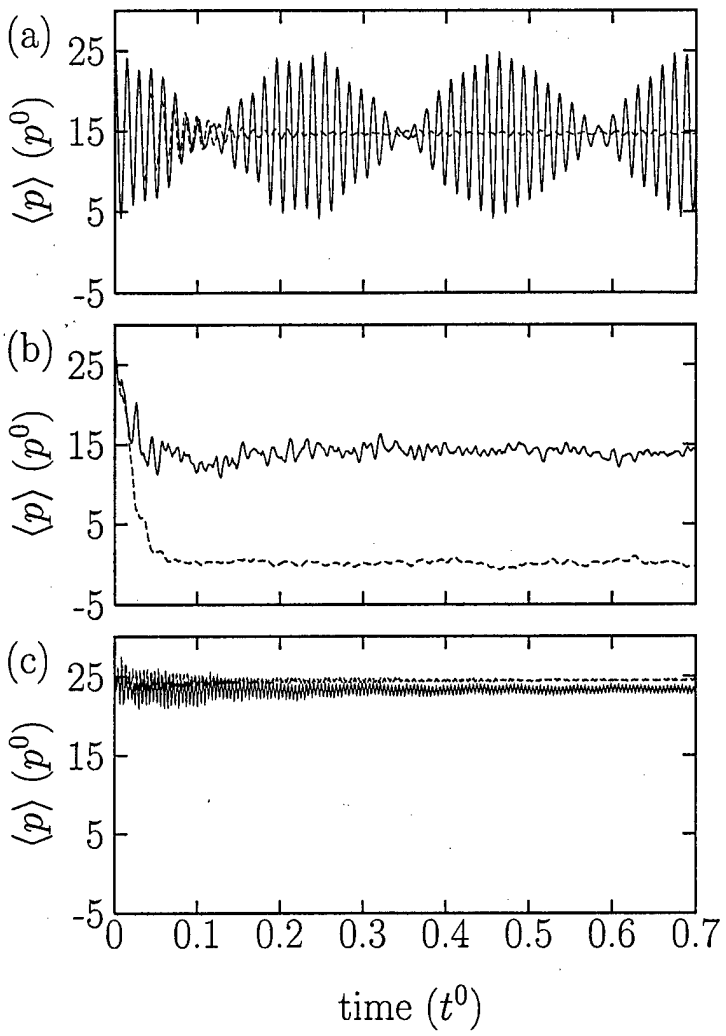

FIG. 1. Gong and Brumer

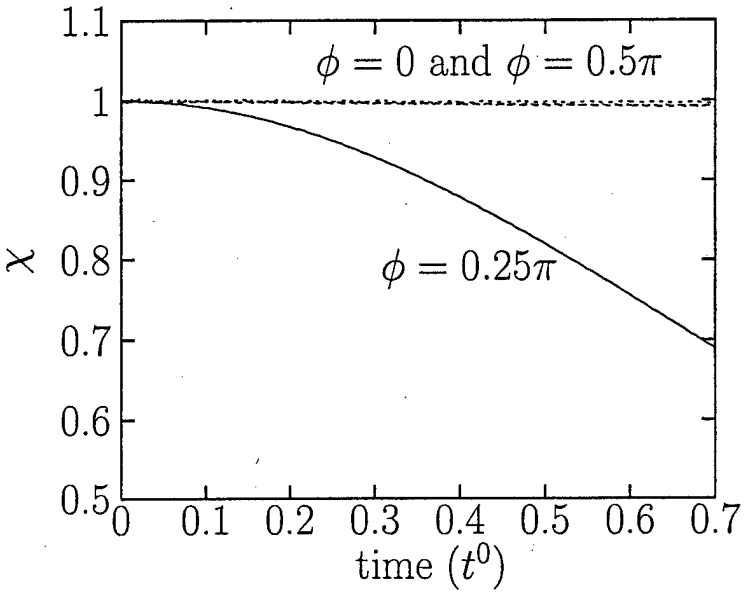

FIG. 2. Gong and Brumer

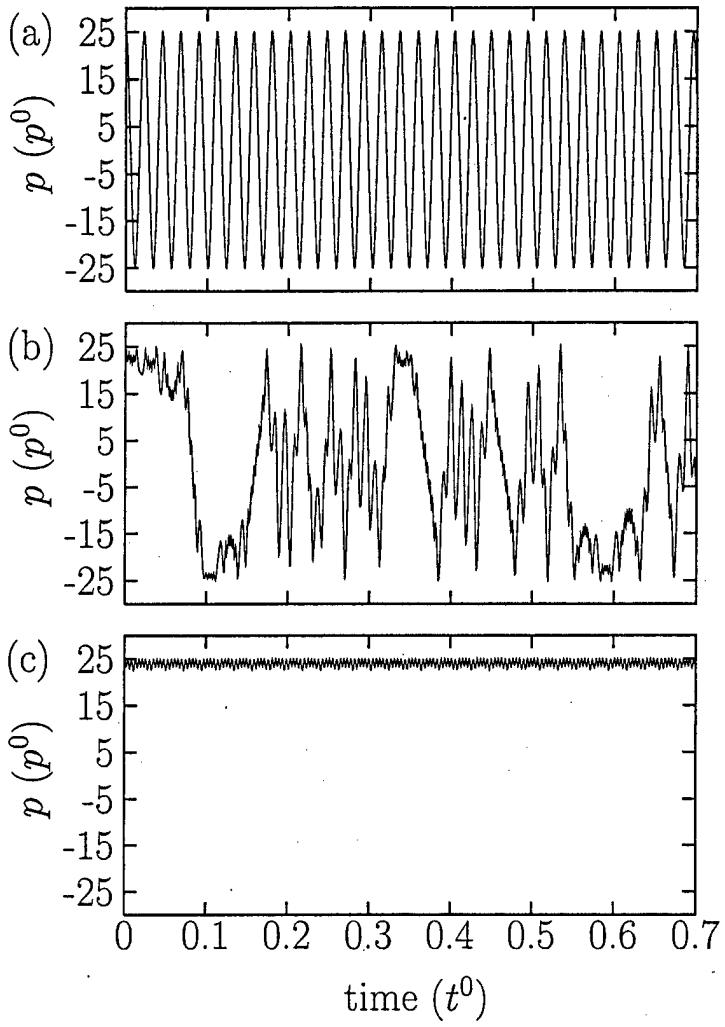

FIG. 3. Gong and Brumer

Phys. Rev. Lett (in press)

Printed on October 4, 2001

Cyclic Population Transfer in Quantum Systems with Broken Symmetry

3

Petr Král and Moshe Shapiro
Department of Chemical Physics, Weizmann Institute of Science, 76100 Rehovot, Israel
(PRL - in press)

We show that quantum systems with broken symmetry which lack an inversion center, e.g. chiral molecules and pairs of asymmetric quantum wells, can be selectively excited due to the coexistence of one- and two-photon transitions between the *same* states. Discrimination between left- and right-handed chiral systems can be accomplished by a "Cyclic Population Transfer" (CPT) process, in which one optically couples states $|1\rangle \leftrightarrow |2\rangle \leftrightarrow |3\rangle \leftrightarrow |1\rangle$, enabling the complete and preferential population of final state $|2\rangle$ and $|3\rangle_M$ (i.e., state $|3\rangle$ of the *mirror imaged* system) or state $|3\rangle$ and $|2\rangle_M$, depending on the laser phases.

33.15.Bh, 33.80.Be, 42.50.Hz, 78.67.-n

Adiabatic Passage phenomena [1] are known to cause complete population transfers between quantum states. In the particular realization of AP, called Stimulated Rapid Adiabatic Passage (STIRAP) [2,3], population in state $|1\rangle$ is transferred to state $|3\rangle$, by a sequence of two one-photon transitions using as an intermediate state $|2\rangle$. The method has been applied to atomic and molecular systems [2,3], as well as to quantum dots [4].

Ordinary STIRAP is only sensitive to the energy levels and the *magnitudes* of transition-dipole coupling matrix elements between them. These quantities are identical for a chiral system and its mirror image (such pairs are called "enantiomers" [5]). Its insensitivity to the *phase* of the transition-dipole matrix elements renders STIRAP, and ordinary weak field absorption [6], incapable of selecting between enantiomers. Recently [7], we have shown, however, that this objective can be realized by other (phase sensitive) optical processes in the weak field regime.

In this Letter, we demonstrate that precisely the *lack of inversion center*, which characterizes chiral and other broken-symmetry systems, allows us to combine the weak-field one- and two-photon method [8–11] with the strong-field STIRAP, to render a phase-sensitive AP method. In the method we term "Cyclic Population Transfer" (CPT), one closes the STIRAP two-photon process $|1\rangle \leftrightarrow |2\rangle \leftrightarrow |3\rangle$ by a one-photon process $|1\rangle \leftrightarrow |3\rangle$. One-photon and two-photon processes cannot coexist in the presence of an inversion center, where all states have a *well defined parity*, because a one-photon absorption (emission) between states $|1\rangle$ and $|3\rangle$, requires that these states have opposite parities, whereas a two-photon process requires that these states have the same parity.

Contrary to systems possessing an inversion center, in which the interference between a one-photon and a two-photon process can only lead to phase-control of *differential* properties, e.g., current directionality [8–11], we show here that the CPT process of broken symmetry systems allows us to control *integral* properties as well, a prime example of which is the control of the excited states population of two enantiomers.

Specific examples for the use of CPT are illustrated in Fig. 1 (upper plot). One example deals with a pair of asymmetric quantum wells, one being the mirror image of the other. Another example, consists of two heteronuclear molecules aligned in an external DC electric field [12], or a mixture of two enantiomeric molecules [7].

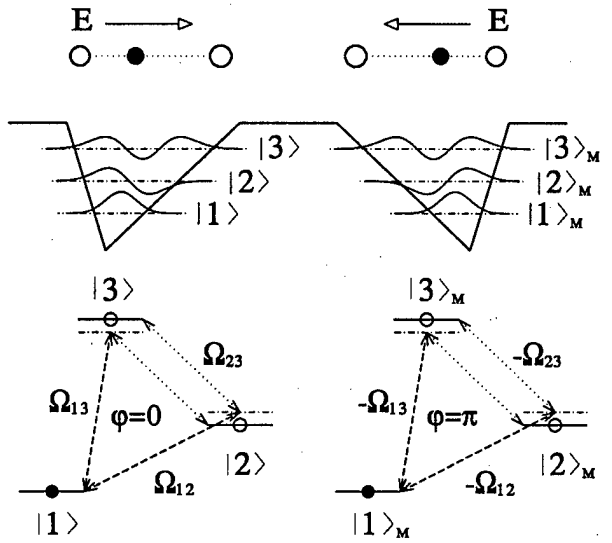

FIG. 1. (Upper plot) An asymmetric quantum well and its mirror image. Also shown are two field-oriented heteronuclear molecules. (Lower plot) Illustration of the three pulses used in these CPT systems. The two systems can be discriminated by their different matter-radiation phases φ.

In the setup of Fig. 1 (lower plot), we consider operating on states $|i\rangle$ and their mirror images $|i\rangle_M$ by three pulses in a "counter-intuitive" order [2,3], i.e., *two* "pump" pulses with Rabi frequencies $\Omega_{12}(t)$ and $\Omega_{13}(t)$, which follow a "dump" pulse $\Omega_{23}(t)$. The Rabi frequencies are defined as, $\Omega_{ij}(t) \equiv \mu_{ij}\,\mathcal{E}_{ij}(t)/\hbar = |\Omega_{ij}(t)|\,e^{i\phi_{ij}} = \Omega^*_{ji}(t)$, where μ_{ij} and $\mathcal{E}_{ij}(t)$ are, respectively, the transition-dipoles and the envelopes of electric fields, of central frequencies ω_{ij}, operating between states $i \neq j$ $(i,j = 1,2,3)$. If we symmetrically detune the pulse center-frequencies, as shown in Fig. 1, we satisfy the $|1\rangle \leftrightarrow |2\rangle \leftrightarrow |3\rangle$ and $|1\rangle \leftrightarrow |3\rangle \leftrightarrow |2\rangle$ two-photon resonance condition, while keeping the one-photon pro-

cesses, $|1\rangle \leftrightarrow |3\rangle$ and $|1\rangle \leftrightarrow |2\rangle$, off-resonance. As a result, the loop formed by the three transitions is not resonantly closed. Therefore, the one and two-photon processes only interfere at isolated points in time, when the pulses are on.

We now solve explicitly the problem by first writing the CPT (radiation + matter) Hamiltonian in the rotating wave approximation as,

$$H = \sum_{j=1}^{3} \omega_j |j\rangle\langle j| + \sum_{i>j=1}^{3} \left(\Omega_{ij}(t) e^{-i\omega_{ij}t} |i\rangle\langle j| + h.c.\right).$$

where ω_j are the energies of the states $|j\rangle$, and atomic units ($\hbar = 1$) are used throughout. The system wave function can be written as

$$|\psi(t)\rangle = \sum_{n=1}^{3} c_n(t)\, e^{-i\omega_n t}\, |n\rangle, \qquad (1)$$

where $\mathbf{c}(t)$, the column vector of the (hopefully slow varying) coefficients $\mathbf{c} = (c_1, c_2, c_3)^{\mathsf{T}}$ (where T denotes the matrix-transpose) can be evaluated from the Schrödinger equation

$$\dot{\mathbf{c}}(t) = -i\,\mathsf{H}(t)\cdot\mathbf{c}(t) \qquad (2)$$

with $\mathsf{H}(t)$, the effective Hamiltonian matrix, given as,

$$\mathsf{H} = \begin{bmatrix} 0 & \Omega_{12}^{*}\, e^{i\Delta_{12}t} & \Omega_{13}^{*}\, e^{i\Delta_{13}t} \\ \Omega_{12}\, e^{-i\Delta_{12}t} & 0 & \Omega_{23}^{*}\, e^{i\Delta_{23}t} \\ \Omega_{13}\, e^{-i\Delta_{13}t} & \Omega_{23}\, e^{-i\Delta_{23}t} & 0 \end{bmatrix}, \qquad (3)$$

where the detunings are defined as, $\Delta_{ij} = \omega_i - \omega_j + \omega_{ij} = -\Delta_{ji}$. For brevity, we have omitted writing explicitly the time-dependence of $\Omega_{ij}(t)$.

In contrast to ordinary STIRAP, unless $\Sigma \equiv \Delta_{12} + \Delta_{23} + \Delta_{31} = 0$, it is not possible to transform away the rapidly oscillating $e^{-i\Delta_{ij}t}$ components from the CPT Hamiltonian (Eq. 3). As a result, the system phase factor varies as $(e^{-i\Sigma t})$ during the time when the three pulses overlap. As a result, in CPT, unless $\Sigma = 0$, null states (i.e. states with zero eigenvalue) cease to be so when the pulses overlap. Moreover, due to non-adiabatic couplings, the population does not follow the adiabatic states during the entire time-evolution, migrating at the near-crossing region from the initially occupied null state.

We can quantify the above statements by examining the eigenvalues of the Hamiltonian of Eq. (3), given as,

$$E_2 = \frac{2^{1/3} a}{3\, c} + \frac{c}{3\cdot 2^{1/3}},$$
$$E_{1,3} = \frac{-(1 \pm i\sqrt{3})\, a}{3\; 2^{2/3}\, c} - \frac{(1 \mp i\sqrt{3})\, c}{6\; 2^{1/3}}, \qquad (4)$$

where $a = 3\left(|\Omega_{12}|^2 + |\Omega_{23}|^2 + |\Omega_{31}|^2\right)$, $b = 3^3\,\mathrm{Det}(\mathsf{H}) = 3^3\, 2\,\mathrm{Re}\,\mathcal{O}$ and $c = \left(b + \sqrt{b^2 + 4\,(-a)^3}\right)^{1/3}$, with $\mathcal{O} = \Omega_{12}\,\Omega_{23}\,\Omega_{31}\, e^{-i\Sigma t}$.

We see that the three eigenvalues depend only on the *overall phase* of $\mathcal{O}$. This phase is composed of a *time-independent* part $\varphi \equiv \phi_{12} + \phi_{23} + \phi_{31}$, of the product of the Rabi frequencies, and a *time-dependent* part Σt. In particular, it follows from Eq. 4, that when $\varphi = \pm\pi/2$ and $\Sigma = 0$, $b = 0$, hence, $c = i2^{1/3}a^{1/2}$ and $E_2 = 0$.

In Fig. 2 we present the time dependence of the eigenvalues $E_i(t)$ $(i = 1,2,3)$ for three Gaussian pulses parameterized as, $|\Omega_{23}(t)| = \Omega_{\max}\exp[-t^2/\tau^2]$, $|\Omega_{12}(t)| = 0.7\,\Omega_{\max}\exp[-(t-t_2)^2/\tau^2]$ and $|\Omega_{13}(t)| = 0.7\,\Omega_{\max}\exp[-(t-t_3)^2/\tau^2]$, with $\Omega_{\max} = 30/\tau$, where τ is the pulse width. The pulse delays are $t_3 = t_2 = 2\tau$ and the detunings, chosen to give maximal selectivity, are $\Delta_{12} = -\Delta_{13} = -\Delta_{23} = 0.08/\tau$. The eigenvalues are presented for the phases $\varphi = 0.235\,\pi$ (see Fig. 4) and $\varphi = (0.235 + 0.5)\,\pi$.

For the problem defined by the parameters of Fig. 2, $(|c_1|, |c_2|, |c_3|)$, the vector of magnitudes of the expansion coefficients of the $|E_i\rangle$ eigenvectors in the "bare" basis, starts in the remote past $(t \to -\infty)$ as $(1,0,0)$ for $|E_2\rangle$, and as $(0,1,1)/\sqrt{2}$ for $|E_1\rangle$ and $|E_3\rangle$. At the end of the process, we have that $(|c_1|, |c_2|, |c_3|) \stackrel{t\to\infty}{\longrightarrow} (0,1,1)/\sqrt{2}$ for $|E_2\rangle$, and $\stackrel{t\to\infty}{\longrightarrow}$ $(\sqrt{2},1,1)/2$ for $|E_1\rangle, |E_3\rangle$. Since the evolution starts with bare state $|1\rangle$, only the $|E_2\rangle$ eigenstate gets initially populated.

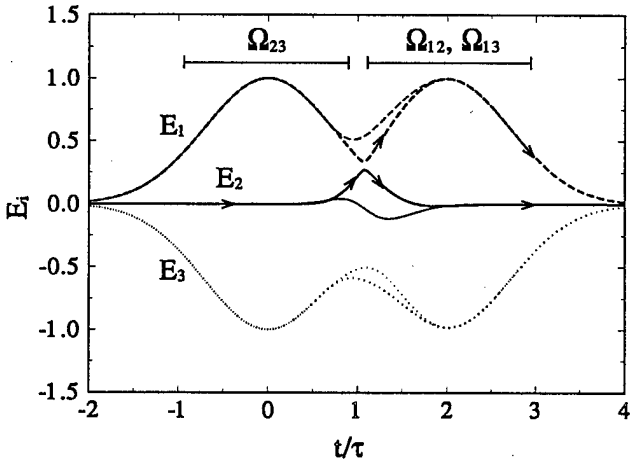

FIG. 2. The three dressed eigenvalues $E_i(t)$ at two different phases. The solution for $\varphi = 0.235\,\pi$ and $\varphi = (0.235 + 0.5)\,\pi$ is plotted by thick and thin lines, respectively. An initial population at state $|1\rangle$ stays on the null state $|E_2(t)\rangle$ with $E_2(t) \approx 0$ up to the avoided crossing region where the population becomes shared with the eigenstate $|E_1(t)\rangle$ or $|E_3(t)\rangle$, depending on the phase φ. The horizontal short lines denote the approximate times of action of the Rabi frequencies Ω_{ij}.

Figure 2 clearly shows that the system evolution is governed by the interference between the "clockwise" $(|1\rangle \to |3\rangle \to |2\rangle)$ and the "counter-clockwise" $(|1\rangle \to |2\rangle \to |3\rangle)$ two-photon processes depicted in Fig. 1. This interference results in the appearance of an avoided-crossing between the $E_2(t)$ eigenvalue and (depending on

the phase φ) either the $E_1(t)$ or the $E_3(t)$ eigenvalue. In the crossing region, the adiabatic description ceases to be valid, and the system populates a *superposition state* $\alpha_2 |E_2\rangle + \alpha_i |E_i\rangle$ ($i = 1$ or $i = 3$).

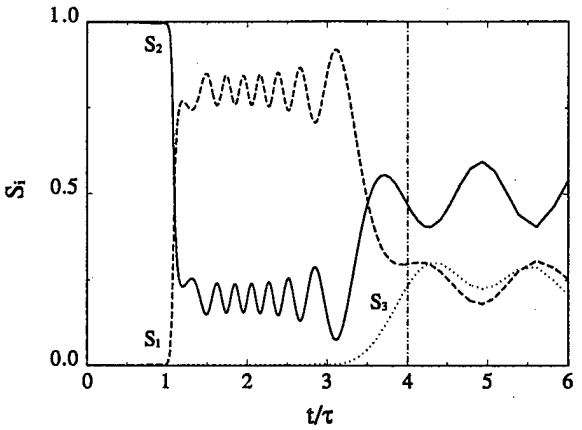

FIG. 3. The populations, given as $S_i(t) \equiv |\langle E_i(t) | \psi(t) \rangle|^2$, of the field-dressed states, given that $|\psi(t=0)\rangle = |1\rangle$ and $\varphi = 0.235\,\pi$. All other parameters are as in Fig. 2. The thin vertical ($- \cdot - \cdot -$) line points at the time after which the populations in the bare states $|i\rangle$ roughly cease to vary.

Figure 3 displays the evolution of the populations $S_i(t) \equiv |\langle E_i(t) | \psi(t) \rangle|^2$ of the field-dressed states, having started with $|\psi(t=0)\rangle = |1\rangle$. The parameters are as in Fig. 2, with φ being confined to the $0.235\,\pi$ value. We see that the eigenstate $|E_2\rangle$ is populated exclusively until the avoided crossing region, where the system goes to the state $\alpha_2 |E_2\rangle + \alpha_1 |E_1\rangle$. As the pulses wane and all $\Omega_{ij}(t) \to 0$, *non-adiabatic* processes populate also the $|E_3\rangle$ state. The populations of the $|E_1\rangle$ and $|E_3\rangle$ states have roughly the same magnitudes $S_1 \approx S_3$ at the end of the process, as expected from the roughly equal final values of the $|c_1|, |c_2|, |c_3|$ coefficients shown above. Hence, by varying φ and Σ we can adjust the α_i coefficients such that $\sum_i \alpha_i |E_i\rangle \overset{t\to\infty}{\longrightarrow} |2\rangle$ or $|3\rangle$.

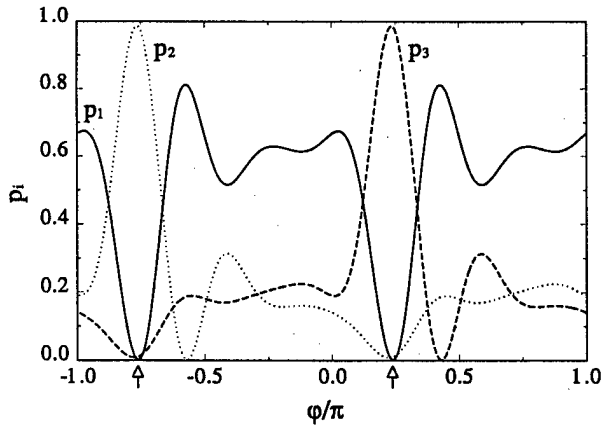

FIG. 4. Dependence of p_i, the final populations of the bare states $|i\rangle$ on the phase φ. The two vertical arrows show the phases for the best separation of the chiral systems, where the population is transferred from state $|1\rangle$ to state $|2\rangle$ or $|3\rangle$.

An example of the degree of control attainable in this manner is given in Fig. 4, where we display the phase dependence of the final populations p_i of the bare states $|i\rangle$, using the parameters of Figs. 2-3. The main feature of Fig. 4 is that the role of state $|2\rangle$ vs. state $|3\rangle$ is *reversed* as we translate the phase φ by π. This features serves, as discussed below, to establish the discrimination between left-handed and right-handed chiral system.

The calculations of Fig. 4 show enhanced sensitivity of the final populations p_i on φ at small detunings Δ_{ij}. The population transfer can be made essentially complete by choosing $\varphi \approx 0.235\,\pi$ (denoted by a small arrow at the bottom of Fig. 4). In that case, 99% of the population is transferred from state $|1\rangle$ to state $|3\rangle$. As the phase φ is shifted by π, the system switches over, with the same efficiency, to the $|1\rangle \to |2\rangle$ population transfer process.

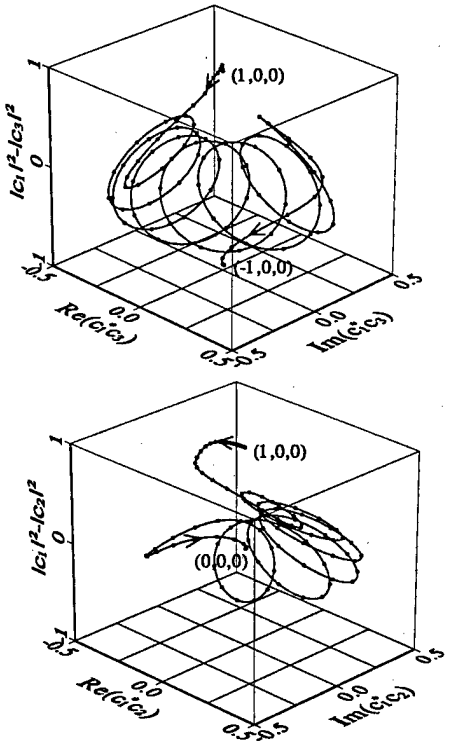

FIG. 5. The Bloch vector $\left(|c_1|^2 - |c_i|^2, \mathrm{Re}(c_1^* c_i), \mathrm{Im}(c_1^* c_i)\right)$ evolution, where $i = 3$ and $i = 2$ holds for the top and bottom plot, respectively. Population starting in the initial state $|1\rangle$ is clearly transferred to the final state $|3\rangle$.

A complementary view of the dynamics is provided by examining the two Bloch vectors with components $\left(|c_1|^2 - |c_i|^2,\ \mathrm{Re}(c_1^* c_i),\ \mathrm{Im}(c_1^* c_i)\right)$ $(i = 2, 3)$, shown in Fig. 5. Starting from the initial position of $(1, 0, 0)$, both vectors leave the avoided-crossing region in a superposition state $\alpha_2 |E_2\rangle + \alpha_1 |E_1\rangle$, where they oscillate with the Rabi frequency $|\Omega_{12}| = |\Omega_{13}|$. The final populations p_i of the bare states $|i\rangle$ are determined by the *second mixing* of the $|E_i\rangle$ states, during the waning of the pulses. This non-adiabatic process reduces the population to the ap-

proximate final state $|3\rangle$, so the two Bloch vectors end in the positions $(-1,0,0)$ and $(0,0,0)$.

The phase-dependence of CPT can be used to discriminate between left and right-handed chiral systems. Denoting by $|i^+\rangle$ (formerly $|i\rangle$) a given symmetry-broken state and by $|i^-\rangle$ (formerly $|i\rangle_M$) its mirror image, we can write these states in terms of symmetric $|S_i\rangle$ and antisymmetric $|A_i\rangle$ states of the two systems as [5,7], $|i^\pm\rangle = s_i|S_i\rangle \pm a_i|A_i\rangle$. Because dipole moments can only connect states of opposite parity, we obtain that the Rabi frequencies for transition between different symmetry-broken states $|i^\pm\rangle$ and $|j^\pm\rangle$ are given as $\Omega_{ij}^\pm = \pm[s_i^* a_j \langle S_i|\mu|A_j\rangle + a_i^* s_j \langle A_i|\mu|S_j\rangle]\mathcal{E}_{ij}$. We see that the Rabi frequencies between any pair of left and right-handed states differ by a sign, i.e., a phase factor of π. Since in the CPT processes the two enantiomers are influenced by the phase $\varphi^\pm$ of the products $\Omega_{12}^\pm\,\Omega_{23}^\pm\,\Omega_{31}^\pm$, we always have that $\varphi^- - \varphi^+ = \pi$. This property is *invariant* to any arbitrary phase change in the individual wave functions of the states $|i^\pm\rangle$.

It therefore follows from Fig. 4, where a change in π of the phase φ is seen to switch the population-transfer process from $|1\rangle \rightarrow |2\rangle$ to $|1\rangle \rightarrow |3\rangle$, and *vice versa*, that we can affect the transfer of population in one chiral system relative to its mirror-image. Because the overall *material phase* $\varphi_s^\pm$ of the product of the dipole matrix elements $\mu_{12}^\pm\,\mu_{23}^\pm\,\mu_{31}^\pm$ is a fixed quantity ($\varphi_s^- - \varphi_s^+ = \pi$), and $\varphi^\pm = \varphi_s^\pm + \varphi_f$, it is the overall phase φ_f of the *three laser fields* $\mathcal{E}_{ij}$ which acts as the laboratory knob allowing us to determines which population-transfer process is experienced by each of the two enantiomers.

The ability of CPT to separate two enantiomers also depends on the individual detuning parameters Δ_{ij} and on the related dynamical phase $2\Sigma\tau$. At resonance $\Delta_{ij} = 0$ and $\varphi = \pm\pi/2$, the exact null eigenstate $|E_2(t)\rangle$ gives a complete population transfer from state $|1\rangle$ to a combination of states $|2\rangle$ and $|3\rangle$. In that case, the p_2/p_3 branching ratio of the final populations is given, as in the double STIRAP case [14,15], by the $|\Omega_{12}/\Omega_{13}|^2$ ratio and no enantiomeric selectivity is then possible.

Once each enantiomer has been excited to a different state ($|2\rangle$ or $|3\rangle$), the pair can be physically separated using a variety of energy-dependent processes, such as ionization, followed by ions extraction by an electric field. If we execute the excitation in the IR range and ionize the chosen excited enantiomer after only a few nsec delay, losses from fluorescence, whose typical lifetimes in that regime are in the msec range, are expected to be minimal.

In summary, we have shown that cyclic population transfer (CPT) in a $|1\rangle$, $|2\rangle$, $|3\rangle$, three level system can operate in molecules and other nano-systems lacking a center of inversion, leading to *phase-sensitive* complete population transfer processes that can discriminate between enantiomers. The scheme is based on the coexistence of a one- and two-photon processes operating between the same initial and final states, leading to interferences between the $|1\rangle \rightarrow |3\rangle \rightarrow |2\rangle$, "clockwise" and the $|1\rangle \rightarrow |2\rangle \rightarrow |3\rangle$, "counter-clockwise" optical processes. This interference, which depends on the (laboratory controlled) overall phase of the three laser fields involved, results in a selective excitation of one asymmetric system relative to its mirror image. Following such a selective excitation, a number of simple, energetically-dependent, physical separation schemes, such as ionization, followed by ions extraction by an electric field, can be employed.

We acknowledge discussions with J. Fiurášek, and support from the Minerva Foundation, GIF, the EU IHP programme HPRN-CT-1999-00129 and the Office of Naval Research, USA.

[1] D. Grischkowsky and M. M. T. Loy, Phys. Rev. A **12**, 1117, (1975); *ibid*, 2514 (1975).

[2] For a review see, K. Bergmann, H. Theuer, and B.W. Shore, Rev. Mod. Phys. **70**, 1003 (1998);

[3] U. Gaubatz, P. Rudecki, S. Schiemann, and K. Bergmann, J. Chem. Phys. **92**, 5363 (1990); H. Theuer, R.G. Unanyan, C. Habscheid, K. Klein, and K. Bergmann, Optics Express **4**, 77 (1999).

[4] U. Hohenester, F. Troiani, E. Molinari, G. Panzarini and C. Macchiavello, Appl. Phys. Lett. **77**, 1864 (2000).

[5] M. Quack, Angew. Chem. Int. Ed. Eng. **28**, 571 (1989).

[6] Chiral molecules exhibit "optical rotatory power" in which the left-handed species rotates the plane of a linearly polarized light in the opposite sense to that of the right-handed species, or "circular dichroism", which is the analogous phenomenon for circularly polarized light. The effect per molecule is usually extremely small, with the *number* of molecules excited being the same for both enantiomers, thereby making the process useless for chiral *separation* purposes.

[7] M. Shapiro, E. Frishman and P. Brumer, Phys. Rev. Lett. **84**, 1669 (2000).

[8] G. Kurizki, M. Shapiro and P. Brumer, Phys. Rev. B **39**, 3435 (1989).

[9] P. B. Corkum, H. C. Liu, M. Buchanan, and Z. R. Wasilewski, Phys. Rev. Lett. **74**, 3596 (1995).

[10] R. Atanasov, A. Haché, L. P. Hughes, H. M. van Driel, and J. E. Sipe, Phys. Rev. Lett. **76**, 1703 (1996).

[11] P. Král and D. Tománek, Phys. Rev. Lett. **82**, 5373 (1999).

[12] J. Ortigoso, G. T. Fraser and B. H. Pate, Phys. Rev. Lett. **82**, 2856 (1999).

[13] B. Sheeny, B. Walker, and L. F. DiMauro, Phys. Rev. Lett. **74**, 4799 (1995).

[14] R. Unayan, M. Fleischhauer, B. W. Shore and K. Bergmann, Opt. Comm. **155**, 144 (1998).

[15] M. N. Kobrak and S. A. Rice, Phys. Rev. A **57**, 2885 (1998).

4

Coherent Control of Quantum Chaotic Diffusion: Diatomic Molecules in a Pulsed Microwave Field

Jiangbin Gong and Paul Brumer

Chemical Physics Theory Group,

Department of Chemistry

University of Toronto

Toronto, Canada M5S 3H6

(October 17, 2001)

Abstract

Extensive phase control of quantum chaotic diffusion is demonstrated for diatomic molecules periodically kicked with microwave pulses. In particular, both complete suppression of chaotic diffusion as well as its enhancement can be achieved by varying the phase of the initial superposition state. The origin of this control in deviations from random matrix theory is also discussed. The results should motivate experiments that are relevant to both coherent control and to quantum chaos.

I. INTRODUCTION

Interference is at the heart of quantum mechanics. The observation that quantum interference and hence molecular dynamics can be altered via experimentally controllable parameters motivated the rapidly developing field of coherent control (CC) of molecular processes [1]. The essence of several scenarios of CC of molecular processes consists of three steps: (1) create a superposition state composed of several basis states, (2) control the relative phases of these basis states, and (3) subject the molecular system to external fields that yield multiple coherent pathways to the same target state. Successful control results when the cross section of particular target states can be extensively and selectively altered by changing the relative phases in the second step. Studies of this kind include, for example, our original bichromatic control scenarios [2], two-pulse control schemes applied to various problems [3], and the CC of molecular scattering [4].

Traditional studies in coherent control typically deal with integrable systems where very few energy levels are involved in the dynamics. By contrast, the majority of real molecular systems are complex: the quantum dynamics may involve many energy levels and the underlying classical dynamics may be strongly chaotic. For this reason, consideration of control for chaotic systems is of general interest and importance.

Classical chaotic systems display intrinsic stochasticity that is generated by the dynamics itself [5]. Thus, even without external noise, a classical chaotic system "loses its memory" of the initial state exponentially fast. Considering the quantum-classical correspondence principle in quantized chaotic systems [6], it is expected that various manifestations of classical chaos should occur in the quantum dynamics when the relevant actions are much larger than Planck's constant [7]. With this perspective, there are those who intuitively believe that quantum phases embedded in initial states should play a minor role in classically chaotic systems, and that controlling quantized chaotic dynamics in the semiclassical regime could be just as difficult as controlling classical Hamiltonian chaos [8]. This is in fact the case. However, coherent control over quantum chaotic dynamics far from the classical limit,

as demonstrated below, should be feasible.

Recently, we computationally demonstrated that extensive phase control of quantum chaotic diffusion is achievable [9] using the delta-kicked planetary rotor (DKPR) model [10] in the quantum regime. In particular, preparing a simple superposition state comprising two basis states allowed for a wide range of control over the ensuing diffusive dynamics. Further, the control was found to persist in the presence of weak decoherence, and diminished, as expected, with increasing decoherence strength. This result opened an interesting direction for coherent control, overlapping with fields such as quantum chaos and chaos control.

In this paper, we consider quantum chaotic diffusion in diatomic molecules in pulsed microwave fields in an effort to extend our studies to realistic systems and in order to motivate experimental coherent control studies of quantum chaotic diffusion. Indeed, experimental studies of microwave-pulse-kicked diatomic molecules appear feasible today and may be easier to realize than, for example, atomic physics approaches discussed in Ref. [9] (e.g., kicked atoms in a single quantum well, or ultracold atoms in a periodic standing wave of near-resonant light).

This paper is organized as follows. In section II, we briefly introduce the DKPR model. In section III, we consider both the classical dynamics and quantum dynamics in detail for diatomic systems kicked by periodic microwave pulses. In section IV, we present representative results, followed by discussions on the mechanism of phase control. Conclusions and a summary comprise section V.

II. THE DELTA-KICKED-PLANETARY ROTOR

Before considering molecular systems, it is beneficial to introduce the DKPR model, a paradigm of both classical and quantum chaos, that will be compared to the kicked diatom. The DKPR Hamiltonian is given by

$$H(\hat{L},\theta) = \frac{\hat{L}^2}{2I} + \lambda\cos(\theta)\sum_n \delta(t/T - n), \tag{1}$$

where $\hat{L} = -i\hbar\frac{\partial}{\partial\theta}$ is the angular momentum operator, θ is the conjugate angle, I is the moment of inertia, λ is the strength of the kicking field, and T is the time interval between kicks. The Hilbert space is spanned by the angular momentum eigenstates $\exp(im\theta)/\sqrt{2\pi}$ $(m = 0, \pm1, \pm2, \cdots)$. The quantum time evolution operator $\hat{M}$ between two kicks is given by [10]

$$\hat{M} = \exp[i\frac{\tau}{4}\frac{\partial^2}{\partial\theta^2}]\exp[-ik\cos(\theta)]\exp[i\frac{\tau}{4}\frac{\partial^2}{\partial\theta^2}], \tag{2}$$

where $\tau \equiv \hbar T/I$ and $k \equiv \lambda T/\hbar$ are dimensionless parameters. The parameter τ plays the role of the effective Planck constant of the system. If we fix the value of the product $k\tau$ and decrease the value of τ, the system approaches the classical limit. This classical limit is given by the standard map [10], which, when expressed in terms of dimensionless variables θ and the scaled classical angular momentum $\tilde{L} = L\tau/\hbar$, takes the following form,

$$\begin{aligned}\theta_N &= \theta_{N-1} + (\tilde{L}_N + \tilde{L}_{N-1})/2, \\ \tilde{L}_N &= \tilde{L}_{N-1} + (k\tau)\sin(\theta_{N-1} + \tilde{L}_{N-1}/2).\end{aligned} \tag{3}$$

As is seen from Eq. (3), the classical dynamics depends only on the product $k\tau$. When $k\tau > 0.9716$, the last KAM invariant curve vanishes and chaotic trajectories can diffuse into the entire unbounded phase space. The scaled mean energy $\langle\tilde{L}^2/2\rangle$ of classical ensembles then displays unrestricted diffusive growth, whose approximate diffusion constant can be evaluated analytically. By contrast, the quantum DKPR displays "quantum localization" [11]. That is, energy absorption is restricted, the external field only excites a finite number of unperturbed energy levels that is related to the classical diffusion constant [12]. Thus, there is a marked difference between the classical and quantum dynamics manifest in qualitatively different energy absorption behavior.

Recently [9], we found that the extent of quantum chaotic diffusion can be actively controlled by manipulating the initial-state coherence. Specifically, we considered the dynamics resulting from an initial superposition state comprising two basis states $\exp(im\theta)/\sqrt{2\pi}$ and $\exp(in\theta)/\sqrt{2\pi}$. By varying the relative phase between the two basis states, we were able to

change the quantum diffusion from almost-completely-suppressed to much-enhanced with the latter behavior much closer to classical diffusion. Thus, quantum chaotic dynamics in the DKPR is both vulnerable to decoherence effects [13] and sensitive to initial-state coherence effects. The DKPR model is experimentally achievable via atom optics [14], but the control experiment in such a system would be difficult. In addition, the system is somewhat contrived. To this end we examine microwave absorption in diatomics, which provides an alternative realistic system for consideration.

III. MICROWAVE KICKED DIATOMIC MOLECULES

The proposal to use microwave kicked diatomic molecules as a molecular analog of the DKPR was advanced more than a decade ago [15]. In particular, with the vibrational degree of freedom frozen, the Hamiltonian for the rotational motion of diatomic molecules subject to periodic microwave pulses resembles that of the DKPR. That is, if the orientation of a diatomic molecule is described by two angles θ and ϕ [16], then the corresponding Hamiltonian is

$$\hat{H} = \frac{\hat{J}^2}{2I} + \mu E_0 \cos(\theta) \sum_n \Delta(\frac{t}{T} - n), \tag{4}$$

where $\hat{J}$ is the angular momentum operator in three dimensions:

$$\hat{J}^2 = -\hbar^2[\frac{1}{\sin(\theta)}\frac{\partial}{\partial\theta}[\sin(\theta)\frac{\partial}{\partial\theta}] + \frac{1}{\sin^2(\theta)}\frac{\partial^2}{\partial\phi^2}], \tag{5}$$

μ is the molecular electric dipole moment, E_0 is the amplitude of the driving field whose polarization direction defines the z direction, I is the moment of inertia of the molecule about an axis perpendicular to the symmetry axis, and $\Delta(t/T - n)$ is the pulse shape function simulating the delta kicking in the DKPR model. Microwave pulses may be realized by an array of phase-locked microwave generators and, following Blümel *et al.* [15], we assume Δ takes the form

$$\Delta(\frac{t}{T} - n) = 1 + 2\sum_{m=1}^{m=7} \cos[2m\pi(\frac{t}{T} - n - 1/2)]. \tag{6}$$

The kicked CsI molecule appears to be an excellent candidate for experimental studies of chaotic rotational excitation by microwave pulses [15] since: (1) it has a large dipole moment, thus dramatically increasing the molecule-field coupling strength, and (2) the excitation energy of the first vibrational energy level in CsI corresponds to that of the $71th$ rotational energy level, so that vibrational excitation and rotation-vibration coupling can generally be neglected. Blümel *et al.* also estimated [15,16] that for CsI, $\tau \equiv \hbar T/I = 1.0$ translates into a driving frequency of $T^{-1} \approx 9\ GHz$, and that $k \equiv \mu E_0 T/\hbar = 5.0$ translates into the relatively moderate field amplitude $E_0 \approx 1\ kV/cm$.

Since the projection of the angular momentum onto the z direction is a constant, we choose it to be zero. As a result, the second term in Eq. (5) gives zero contribution, and the kicked diatomic molecule has only one relevant degree of freedom (θ). Nonetheless, there remain still several important differences between the DKPR model and the kicked diatomic systems. First, the kicking microwave field can only approximate the delta kicks. Second, θ ranges from 0 to 2π in the DKPR model, whereas it ranges from 0 to π for a three-dimensional rotor. Third, the Hilbert space for the kicked molecule case is spanned by the basis states $|j,0\rangle$, where 0 denotes the zero-projection of the angular momentum onto the z axis, and j is the rotational quantum number; while in the DKPR model rotational quantum numbers m can be both positive and negative, representing two possible directions of the angular momentum of the planetary rotor. Fourth, in the DKPR model, the matrix elements of the coupling potential $\cos(\theta)$ are given by

$$\langle m|\cos(\theta)|m'\rangle = \frac{1}{2}(\delta_{m',m-1} + \delta_{m',m+1}), \tag{7}$$

while in the kicked molecule case, we have

$$\langle j,0|\cos(\theta)|j',0\rangle = C_j \delta_{j',j-1} + C_{j+1}\delta_{j',j+1}, \tag{8}$$

where

$$C_j \equiv \frac{j}{\sqrt{(2j-1)(2j+1)}}. \tag{9}$$

Given these differences, it is necessary to independently establish conditions for phase control of quantum diffusion in kicked diatomic systems.

A. Classical Dynamics

With the vibrational degree of freedom frozen and the projection of the angular momentum onto the polarization vector of the driving field being zero, the classical Hamiltonian H_{cl} for diatomic molecules kicked by microwave pulses is given by

$$H_{cl} = \frac{I\dot{\theta}^2}{2} + \mu E_0 \cos(\theta) \sum_n \Delta(\frac{t}{T} - n). \tag{10}$$

The classical equation of motion for θ is then:

$$I\frac{d^2}{dt^2}\theta = \mu E_0 \sin(\theta) \sum_n \Delta(\frac{t}{T} - n). \tag{11}$$

If we define $\xi \equiv t/T$, $\tilde{J} \equiv \dot{\theta}T$, the above equation can be re-expressed as two canonical equations in $\tilde{J}$ and θ:

$$\begin{aligned} \frac{d\theta}{d\xi} &= \tilde{J}, \\ \frac{d\tilde{J}}{d\xi} &= (k\tau)\sin(\theta) \sum_n \Delta(\xi - n). \end{aligned} \tag{12}$$

Clearly, $\tilde{J}$ is the counterpart of $\tilde{L}$ in the DKPR model [see Eq. (3)], and the classical dynamics depends only on the product of k and τ. Note also that the quantum counterpart of $\tilde{J}^2$ is $j(j+1)\tau^2$, where j is the rotational quantum number.

Figure 1 displays the Poincaré surfaces of section for $k\tau = 0.5, 1.0, 2.5$, and 5.0. The results are obtained by numerical integration of 15 different initial trajectories with $\tilde{J}(0) = 0$ and $\theta(0) = l\pi/16$, $l = 1, 2\cdots, 15$, for time equal to 720 kicks. It is clear from Fig. 1 that when $k\tau \geq 5.0$, the classical dynamics is predominately chaotic in the entire $\tilde{J}$ region. We focus below on quantum dynamics in this $k\tau$ regime.

B. Quantum Dynamics

To solve for the time-evolving wavefunction $|\psi(t)\rangle$ for the kicked molecule, we first expand the wavefunction in the Hilbert space basis

$$|\psi(t)\rangle = \sum_j A_j(t)|j,0\rangle. \tag{13}$$

Substituting this expansion into the time-dependent Schrödinger equation and using Eq. (8), we have

$$i\hbar\frac{dA_j(t)}{dt} = \frac{j(j+1)\hbar^2}{2I}A_j(t) + \mu E_0 \sum_n \Delta(\frac{t}{T} - n)(C_j A_{j-1}(t) + C_{j+1}A_{j+1}(t)). \tag{14}$$

The dynamical equations can be further simplified by working with an interaction picture [16]. Specifically, let $B_j(t) = A_j(t)\exp[i\hbar j(j+1)t/(2I)]$, we finally get

$$i\frac{dB_j(\xi)}{d\xi} = k\sum_n \Delta(\xi - n)\{\exp[i\tau j\xi]C_j B_{j-1}(\xi) + \exp[-i\tau(j+1)\xi]C_{j+1}B_{j+1}(\xi)\}. \tag{15}$$

Clearly, in contrast to classical dynamics, the quantum dynamics of the kicked molecule depends on two parameters, τ and k. Thus, by decreasing the magnitude of τ with $k\tau$ fixed, we can arbitrarily decrease the quantum effects due to the quantization of angular momentum while keeping the underlying classical dynamics unaffected.

The coupled equations of motion for the expansion coefficients $B_j(t)$ can be readily solved using the fourth order Runger-Kutta method, with a time step of $10^{-4}T$, and with the number of basis states chosen to be $500/\tau$. With these choices, convergence of the results was excellent.

IV. PHASE CONTROL OF QUANTUM CHAOTIC DIFFUSION IN KICKED MOLECULES

As clearly seen from Eqs. (4) and (6), the Hamiltonian of the system considered here is strictly periodic with time. Hence the time evolution operator $\hat{F}$ associated with one period

T is of particular interest and will prove useful in the analysis of the results. The formal solution for $\hat{F}$ can be written, with the help of the time-ordering operator Γ, as

$$\hat{F} = \Gamma[\exp\{\frac{-i}{\hbar}\int_0^T dt' \hat{H}(t')\}], \tag{16}$$

where

$$\Gamma[\hat{C}(t)\hat{D}(t')] = \hat{C}(t)\hat{D}(t'), if\ t > t'$$
$$\Gamma[\hat{C}(t)\hat{D}(t')] = \hat{D}(t')\hat{C}(t), if\ t < t'. \tag{17}$$

Although it is not possible to give an explicit form of $\hat{F}$ in the kicked molecule case, the existence of this formal solution yields a stroboscopic description of the dynamics,

$$|\psi(nT)\rangle = \hat{F}^{n-1}|\psi((n-1)T)\rangle = \hat{F}^n|\psi(0)\rangle. \tag{18}$$

More importantly, as we will see below, eigenfunctions and eigenphases of the quantum map operator $\hat{F}$ help provide clear insights on how chaotic rotational excitations may be controlled by manipulating quantum phase in the initial state.

A. Formal Dynamics and Initial-state Coherence Effects

Consider now an initial superposition state prepared as

$$|\psi(0)\rangle = \cos(\alpha)|j_1, 0\rangle + \sin(\alpha)\exp(-i\beta)|j_2, 0\rangle. \tag{19}$$

Here we use only two basis states (more basis states can be considered, providing more adjustable parameters for control). After the molecule is kicked N times, the quantum state evolves to $\hat{F}^N|\psi(0)\rangle$. In order to compare quantum results for our case with that for the DKPR model and the classical limit, we define the dimensionless rotational energy $\tilde{E} \equiv \sum_j P_j j(j+1)\tau^2/2$, where $P_j = |B_j|^2$ is the occupation probability of the $|j, 0\rangle$ state. The classical limit of $\tilde{E}$ is given by $\langle \tilde{J}^2/2 \rangle$. $\hat{F}$ can be formally diagonalized by a unitary transformation,

$$< j_a, 0|\hat{F}|j_b, 0\rangle = \sum_{j_c} \exp(-i\phi_{j_c}) U^*_{j_c,j_a} U_{j_c,j_b}, \tag{20}$$

where $U_{j_c,j_a} \equiv \langle j_c, 0|\hat{U}|j_a, 0\rangle$ $(j_a = 0, 1, 2, \cdots)$ is the eigenvector with eigenphase ϕ_{j_c}. Moreover, since the basis states $|j, 0\rangle$ are time-reversal invariant, one can prove that the matrix elements U_{j_c,j_b} can be chosen as real numbers [7], i.e.,

$$U^*_{j_c,j_a} = U_{j_c,j_a}, \quad j_a,\ j_c = 0,\ 1,\ 2,\ \cdots. \tag{21}$$

Further, evaluating $\tilde{E}$ at $t = NT$ with Eqs. (19), (20) and (21) gives

$$\begin{aligned}
\frac{2\tilde{E}}{\tau^2} &= \langle\psi(0)|\hat{F}^{-N}\frac{\hat{J}^2}{\hbar^2}\hat{F}^N|\psi(0)\rangle \\
&= \cos^2(\alpha) \sum_{jj_aj_b} j(j+1) U_{j_aj_1} U_{j_bj} U_{j_aj} U_{j_bj_1} e^{iN(\phi_{j_a} - \phi_{j_b})} \\
&\quad + \sin^2(\alpha) \sum_{jj_aj_b} j(j+1) U_{j_aj_2} U_{j_bj} U_{j_aj} U_{j_bj_2} e^{iN(\phi_{j_a} - \phi_{j_b})} \\
&\quad + \frac{1}{2}\sin(2\alpha)(e^{-i\beta} \sum_{jj_aj_b} j(j+1) U_{j_aj_1} U_{j_bj_2} U_{j_aj} U_{j_bj} e^{iN(\phi_{j_a} - \phi_{j_b})} \\
&\quad + c.c.).
\end{aligned} \tag{22}$$

Evidently, the first two terms are incoherent since they do not depend on the value of β. They represent quantum dynamics associated with each of the states $|j_1, 0\rangle$ and $|j_2, 0\rangle$ independently. The last two terms represent interference effects due to initial-state coherence between $|j_1, 0\rangle$ and $|j_2, 0\rangle$. Below we show that quantum diffusion over the energy space can be extensively controlled by manipulating the initial quantum phase described by β, which corresponds to manipulating the interference term in Eq. (22).

B. Phase Control Results

In Fig. 2 we present two representative examples ($\tau = 1.0, k = 5.0$ in Fig. 2a and $\tau = 1.2$, $k = 4.8$ in Fig. 2b) to illustrate phase control of quantum chaotic diffusion in kicked diatomic molecules. In both examples the underlying classical dynamics of rotational excitation is strongly chaotic, as shown in Fig. 1. We choose $j_1 = 1$ and $j_2 = 2$ to create the initial superposition state $(|1, 0\rangle \pm |2, 0\rangle)/\sqrt{2}$, i.e., $\alpha = \pi/4$ and $\beta = 0, \pi$ in Eq. (19) (Reasons

for choosing β to be 0 or π will be explained in subsection C). As seen in Fig. 2, the phase control is striking. For both examples, $(|1,0\rangle - |2,0\rangle)/\sqrt{2}$ results in almost no diffusion over the energy space whereas $(|1,0\rangle + |2,0\rangle)/\sqrt{2}$ shows extraordinarily fast diffusion (even faster than the semiclassical diffusion shown in Fig. 5 later below) before it essentially stops at $t \approx 10T$. Note (1) that this huge difference is achieved solely by changing the initial relative phase between the two participating states $|1,0\rangle$ and $|2,0\rangle$ in the initial superposition state, and (2) that by contrast, each of $|1,0\rangle$ or $|2,0\rangle$ individually would give very similar diffusion behavior lying between the solid and dashed lines in Fig. 2. In effect, the two participating states $|1,0\rangle$ and $|2,0\rangle$ can either constructively or destructively interfere with each other, even though the underlying classical dynamics is strongly chaotic. Details of the respective wavefunctions at $t = 60T$ are shown in Fig. 3 in terms of the occupation probability P_j versus j. In both Fig. 3a and Fig. 3b, one sees vividly that changing β from 0 to π alters the occupation probability of many states by almost an order of magnitude. This further demonstrates the role of the initial quantum phase embedded in the initial nonclassical states in chaotic molecular processes.

In an effort to gain insight into the nature of this control we examined the evolving wavefunctions $|\psi(nT)\rangle$ in the θ representation. Figure 4 displays $|\langle\theta|\psi(nT)\rangle|^2 \sin(\theta)$ versus θ/π for $n = 0$, 2, 10 and 20, for the case of $\tau = 1.0$ $k = 5.0$ and for $\psi(0)\rangle = (|1,0\rangle + |2,0\rangle)/\sqrt{2}$ or $(|1,0\rangle - |2,0\rangle)/\sqrt{2}$. Note that due to wavefunction normalization $\int_0^\pi |\langle\theta|\psi(nT)\rangle|^2 \sin(\theta) d\theta = 1$. At $t = 0$ [Fig. 4a], the relative phase between the basis states $|1,0\rangle$ and $|2,0\rangle$ is manifest as a difference in molecular orientation. In particular, for the initial state $(|1,0\rangle - |2,0\rangle)/\sqrt{2}$ the highest of the three significant peaks of $|\langle\theta|\psi(0T)\rangle|^2 \sin(\theta)$ is located at $\theta_0 \approx 0.15\pi$, whereas for $|\psi(0)\rangle$=$(|1,0\rangle + |2,0\rangle)/\sqrt{2})$ the peak is at $\pi - \theta_0 \approx 0.85\pi$. However, since the kicking force is proportional to $\sin(\theta)$ and since $\sin(\theta_0) = \sin(\pi - \theta_0)$, such orientation effects can not be the direct origin of our phase control. Indeed, after only two kicks [Fig. 4b], it becomes very hard to see any significant difference between the two evolving wavefunctions in the θ representation, although their energy absorption behavior afterwards (see Fig. 2a) continues to be completely different. Also of interest is the comparison in Fig. 4c and Fig.

4d at times $t = 10T$ and $20T$ (at these times the energy absorption shown in Fig. 2a has stopped). We find that, in the suppressed diffusion cases, the wavefunction displays fairly smooth behavior over the entire range of θ, whereas in the enhanced diffusion cases the magnitude of the wavefunction drastically oscillates with θ. However, the wavefunctions in Fig. 4c and Fig. 4d for both the suppressed and the enhanced cases show similar behavior on the average. Hence, the θ dependence of the wavefunction sheds little light on the origins of the observed control. Indeed, gaining insight into the origins of the control is difficult insofar as it is a nonresonant multi-photon absorption process.

To further demonstrate that our phase control results are quantal in nature, we show [Fig. 5] the dynamics after reducing the effective Planck constant τ by 50 times, while keeping $k\tau$ constant. As further discussed below, when the system is closer to the semiclassical limit, one expects the extent of phase control to decrease. This is confirmed in Fig. 5. For both the case of $\tau = 0.02$ and $k = 250$ in Fig. 5a and the case of $\tau = 0.024$ and $k = 240$ in Fig. 5b, the energy diffusion only shows slight dependence on β. In essence, phase control disappears. We therefore confirm the expectation that quantum chaotic dynamics in the classical limit is insensitive to initial-state coherence.

We have also examined the stability of the results in Fig. 2 for τ far from resonance. We have checked that control in Fig. 2a (Fig. 2b) remains essentially the same when τ is changed from 1.01 to 1.0 to 0.99 or from 1.21 to 1.20 to 1.19. This insensitivity may be important for experimental studies, suggesting that extensive control of quantum diffusion should be robust to small fluctuations of the frequency of the periodic kicking field. It should be noted that for periodically kicked systems, the dynamics can be very sensitive to the exact value of τ. For example, when $\tau = p\pi/q$, where p, q are integers, the free evolution of the kicked system is in resonance with the kicking field, and the corresponding quantum diffusion can be extremely fast [7,10]. Indeed, when the resonance condition is satisfied, the spectrum of the system assumes a completely different form (for example, in the DKPR model, the spectrum is continuous at resonance). Here we have examined cases of τ far from resonance since the uncontrolled dynamics for the case of resonant τ is still poorly

understood. Nevertheless, we note that the possible range of quantum diffusion rates due to phase control, as shown in Fig. 2, is comparable to, or even larger than, that induced by quantum resonances in kicked diatomic systems. For τ near or on resonance, we also observed extensive phase control in many cases (e.g., for $\tau = \pi/2$, $k = 4.5$; or $\tau = 2\pi/5$, $k = 5.0$). However, due to the sensitivity of the dynamics to τ, the phase control for τ near or on resonance is also very sensitive to τ.

Finally, we examine the pulse-shape dependence of our phase control. Our previous calculations have used the microwave pulse given by Eq. (6), which needs seven consecutive harmonically related microwave frequencies. Although this case is indeed very close to delta-kicked dynamics, it is challenging experimentally since one has to phase-lock so many different microwave fields. Fortunately, we found that similar phase control can be observed using only three consecutive harmonically related microwave fields. Figure 6 displays the somewhat less extensive phase control results, where the pulse shape function $\Delta(t/T - n)$ in Eq. (4) is replaced by

$$\Delta'(\frac{t}{T} - n) = 1 + 2\sum_{m=1}^{m=3} \cos[2m\pi(\frac{t}{T} - n - 1/2)]. \tag{23}$$

It is clear that, the main characteristics of the phase control results in Fig. 2 are also observed in Fig. 6. Thus, utilizing Eq. (23) should significantly reduce technical difficulties in experimental studies of phase control of quantum chaotic diffusion.

C. Discussion

The results obtained for CsI are similar to those in the DKPR model [9], despite the fact that there are several differences between the DKPR model and the kicked molecule case. This suggests that the mechanism for phase control of microwave kicked diatomics may be the same as that for the DKPR model. Below we discuss the fact that phase control is based upon, and is a manifestation of, strong statistical deviations from random matrix theory (RMT).

One of the main results of the study of quantum chaos is that statistical properties of eigenfunctions and eigenvalues of the quantum map operator $\hat{F}$ (or the Hamiltonian operator for conservative systems) tend to be well described by RMT if the underlying classical dynamics is chaotic [7]. Indeed, statistical behavior close to RMT predictions are regarded as clear signatures of classical chaos. In particular, RMT claims that eigenvector components of $\hat{F}$ are random and obey universal statistical laws. However, in the case of the DKPR model and the kicked diatoms, deviations from RMT are observed in the suppressed quantum diffusion [10]. Here we demonstrate that quantum control is another strong manifestation of the deviation from RMT.

We first note that Eq. (22) can be further simplified, for relatively large N, by making a fairly good approximation. That is, the factor $e^{iN(\phi_{j_a}-\phi_{j_b})}$ tends to oscillate so rapidly that essentially only those terms with $j_a = j_b$ contribute in the sum over j_a and j_b. We then obtain

$$\begin{aligned}\frac{2\tilde{E}}{\tau^2} &= \cos^2(\alpha)\sum_j j(j+1)\sum_{j_a}|U_{j_aj}|^2|U_{j_aj_1}|^2 \\ &+ \sin^2(\alpha)\sum_j j(j+1)\sum_{j_a}|U_{j_aj}|^2|U_{j_aj_2}|^2 \\ &+ \sin(2\alpha)\cos(\beta)\sum_j j(j+1)\sum_{j_a}|U_{j_aj}|^2 U_{j_aj_1}U_{j_aj_2}. \end{aligned} \tag{24}$$

Evidently, the last term in Eq. (24) arising from quantum interference is proportional to $\cos(\beta)$, and would be most effective when $\beta = 0$ or $\beta = \pi$. This explains our previous choice of $\beta = 0,\ \pi$ for the demonstration of extensive phase control.

Consider then RMT applied to the statistics of the eigenvectors U_{j_c,j_b} in Eq. (24). Suppose the effective dimension of the Hilbert space is $D \propto 1/\tau$, τ being the effective Planck constant. We then assume that U_{j_aj}, $U_{j_aj_1}$, and $U_{j_aj_2}$ are independent random numbers with mean value 0 and variance $1/D$, in accord with RMT. With this statistical description, we are now ready to compare the magnitudes of the interference term and the incoherent terms in Eq. (24). Consider first the interference term. As an approximation, $\sum_{j_a}|U_{j_aj}|^2 U_{j_aj_1}U_{j_aj_2} \approx 1/D\sum_{j_a}(U_{j_aj_1}U_{j_aj_2})$, where high order correlations between $|U_{j_aj}|^2$ and $U_{j_aj_1}U_{j_aj_2}$ are neglected. Note that the ensemble average of $U_{j_aj_1}U_{j_aj_2}$ $(j_1 \neq j_2)$ is zero.

Hence the the standard deviation of $1/D\sum_{j_a}(U_{j_a j_1}U_{j_a j_2})$ is given by $1/\sqrt{D}$ times the standard deviation of $U_{j_a j_1}U_{j_a j_2}$ (which is of the order of $1/D$). It follows that the standard deviation of $\sum_{j_a}(U_{j_a j_1}U_{j_a j_2})$ from zero is of the order of $1/\sqrt{D}$. On the other hand, for the incoherent terms, say, the first term, $\sum_{j_a}|U_{jj_a}|^2|U_{j_a j_1}|^2 \approx 1/D\sum_{j_a}|U_{j_a j_1}|^2 = 1/D$. Thus, according to RMT, the interference term is zero statistically, and the magnitude of the fluctuation of the interference term is $1/\sqrt{D}$ times smaller than that of the incoherent term. That is, RMT predicts that phase control of quantum diffusion is bound to fail. Further, since D scales with $1/\tau$, we have that the magnitude of the fluctuations of the quantum interference term in Eq. (24) scales with $\tau^{1/2}$. As we approach the classical limit by decreasing the effective Planck constant τ, initial state coherent effects, and thus phase control necessarily vanish.

Thus, our control results imply that RMT is not a good statistical description when the periodically kicked molecular system is not close to the semiclassical limit. Just as in the DKPR model, when quantum effects are large, the $\hat{F}$ matrix and thus the $\hat{U}$ matrix are banded matrices [17] in the representation of angular momentum eigenstates. This band structure causes strong statistical deviations from RMT expectations. In particular, in the sum $\sum_{ja}|U_{jj_a}|^2U_{j_a j_1}U_{j_a j_2}$, only those terms with $|j - j_a|$ less than the band width of the $\hat{U}$ matrix (or the localization length of the eigenvector U_{j,j_a}) will contribute, i.e., the number of contributing terms in the sum will be much less than D, the effective dimension of the Hilbert space. This directly leads to enhanced fluctuations of $\sum_{ja}|U_{jj_a}|^2U_{j_a j_1}U_{j_a j_2}$, i.e., the interference term in Eq. (24) can be comparable to the first two incoherent terms. As a result, extensive phase control of quantum chaotic diffusion becomes possible.

Based on the observation that statistical deviations from RMT are responsible for control, in Ref. [9] we quantitatively obtained a necessary condition for extensive phase control. Specifically, in the DKPR model, we require $k < 50/\kappa$ or $\tau > \kappa^2/50$ for control. The essence of this condition is evident. That is, larger quantum effects induce more phase control. It is thus very natural to conjecture that this condition could also apply to the model of periodically kicked molecules. Indeed: (1) under this condition, for numerous cases

of varying α, β, k and τ, we have obtained extensive phase control results similar to those in Fig. 2, and (2) outside that domain, phase control is not extensive in general.

V. CONCLUSION AND SUMMARY

The results of this paper should impact strongly on two research areas, that of quantum chaos and that of coherent control. The focus of traditional studies in quantum chaos is quantum-classical correspondence, i.e., the conditions under which quantum and classical dynamics agree, and how this agreement breaks down with time as a result of quantum interference effects. In order to understand interference effects, most studies have used classical initial states and have avoided using nonclassical initial states. As such, the literature of quantum chaos rarely considers initial-state coherence effects. Rather, people often take the semiclassical view that the classical chaotic dynamics leads to a randomization of the phase in quantum evolution, and that the quantum dynamics is insensitive to the form of the initial condition [18]. By contrast, studies in coherent control [1] emphasize the significance of quantum phases, both in the initial state and the ensuing dynamics.

Our study clearly demonstrates the importance of initial-state coherence in quantized chaotic dynamics. Specifically, we have demonstrated that initial-state coherence can dramatically alter the dynamics of quantum diffusion when the system is far from the semiclassical limit. This sensitivity is lost as the system approaches the classical limit. This phase control is based on, and is a manifestation of, strong statistical deviations from RMT. Further, it is distinct from other studies of control in diatomic excitation [19,20], which can essentially be described classically [21].

Having theoretically shown that initial-state coherence can be used to control chaotic rotational excitation of diatomic molecules, the only remaining issue is the experimental preparation of initial superposition states such as $(|1,0\rangle \pm |2,0\rangle)/\sqrt{2}$, or, more generally, the generation of rotational coherence before the periodic kicking field is turned on. We note that STIRAP [22] provides a natural choice for such superposition state preparation. In

REFERENCES

[1] M. Shapiro and P. Brumer, Adv. Atom., Mol. and Opt. Phys. **42**, 287 (2000).

[2] P. Brumer and M. Shapiro, Chem. Phys. Lett. **126**, 541 (1986).

[3] T. Seideman, M. Shapiro, and P. Brumer, J. Chem. Phys. **90**, 7132 (1989); D.G. Abrashkevich, M. Shapiro, and P. Brumer, J. Chem. Phys. **108**, 3585 (1998).

[4] J.L. Krause, M. Shapiro, and P. Brumer, J. Chem. Phys. **92**, 1126 (1990); A. Abrashkevich, M. Shapiro, and P. Brumer, Phys. Rev. Lett. **81**, 3789 (1998); E. Frishman, M. Shapiro, and P. Brumer, J. Chem. Phys. **110**, 1 (1999); E. Frishman, M. Shapiro, and P. Brumer, J. Phys. Chem. A **49**, 10333 (1999).

[5] A.J. Lichtenberg and M.A. Lieberman, *Regular and Chaotic Dynamics* (Springer-Verlag, New York, 1992).

[6] For a general approach that deals with classical quantum correspondence for both classical and nonclassical states, in both integrable and chaotic systems, see J. Wilkie and P. Brumer, Phys. Rev. A **55**, 27 (1997); **55**, 43 (1997).

[7] F. Haake, *Quantum Signatures of Chaos* (Springer-Verlag, Berlin, 1992); L.E. Reichl, *The Transition to Chaos in Conservative Classical Systems : Quantum Manifestations* (Springer-Verlag, New York, 1992).

[8] Most studies on classical chaos control focus on dissipative systems. Controlling Hamiltonian chaos presents a challenge. See, e.g., Y.C. Lai, M. Ding, and C. Grebogi, Phys. Rev. E **47**, 86 (1993); J. Botina, H. Rabitz, and N. Rahman, Phys. Rev. A **51**, 923 (1995).

[9] J. Gong and P. Brumer, Phys. Rev. Lett. **86**, 1741 (2001).

[10] G. Casati and B. Chirikov, *Quantum chaos: between order and disorder* (Cambridge University Press, New York, 1995).

[11] G. Casati, B.V. Chirikov, F.M. Izrailev, and J. Ford, in *Stochastic Behaviors in Classical and Quantum Hamiltonian Systems*, edited by G. Casati and J. Ford, Lecture Notes in Physics Vol. 93 (Springer Verlag, Berlin, 1979), p. 334.

[12] D.L. Shepelyansky, Physica D **28**, 103 (1987).

[13] J. Gong and P. Brumer, Phys. Rev. E **60**, 1643 (1999) and references therein.

[14] F.L. Moore *et al.*, Phys. Rev. Lett. **75**, 4598 (1995); H. Ammann *et al.*, Phys. Rev. Lett. **80**, 4111 (1998).

[15] R. Blümel, S. Fishman, and U. Smilansky, J. Chem. Phys. **84**, 2604 (1986).

[16] R. Blümel and W.P. Reinhardt, *Chaos in Atomic Physics* (Cambridge University Press, New York, 1997).

[17] G. Casati, I. Guarneri, F.M. Izrailev, and R. Scharf, Phys. Rev. Lett. **64**, 5 (1990).

[18] See, e.g., C.F. Bharucha, J.C. Robinson, F.L. Moore, B. Sundaram, Q. Niu, and M.G. Raizen, Phys. Rev. E **60**, 3881 (1999).

[19] S. Chelkowski, A.D. Bandrauk, and P.B. Corkum, Phys. Rev. Lett. **65**, 2355 (1990).

[20] J. Karczmarek, J. Wright, P. Corkum, and M. Ivanov, Phys. Rev. Lett. **82**, 3420 (1999); D.M. Villeneuve, S. A. Aseyev, P. Dietrich, M. Spanner, M.Y. Ivanov, and P.B. Corkum, Phys. Rev. Lett. **85**, 542 (2000).

[21] W.K. Liu, B. Wu, and J.M. Yuan, Phys. Rev. Lett. **75**, 1992 (1995); J.H. Kim, W.K. Liu, and J.M. Yuan, J. Chem. Phys. **111**, 216 (1999).

[22] K. Bergmann, H. Theur, and B.W. Shore, Rev. Mod. Phys. **70**, 1003 (1998).

[23] R.G. Unayan, M. Fleischhauer, K. Bergmann, and B.W. Shore, Opt. Commun. **155**, 144 (1998); H. Theuer, R.G. Unanyan, C. Habscheid, K. Kelin, and K. Bergmann, Optics Express **4**, 77 (1999).

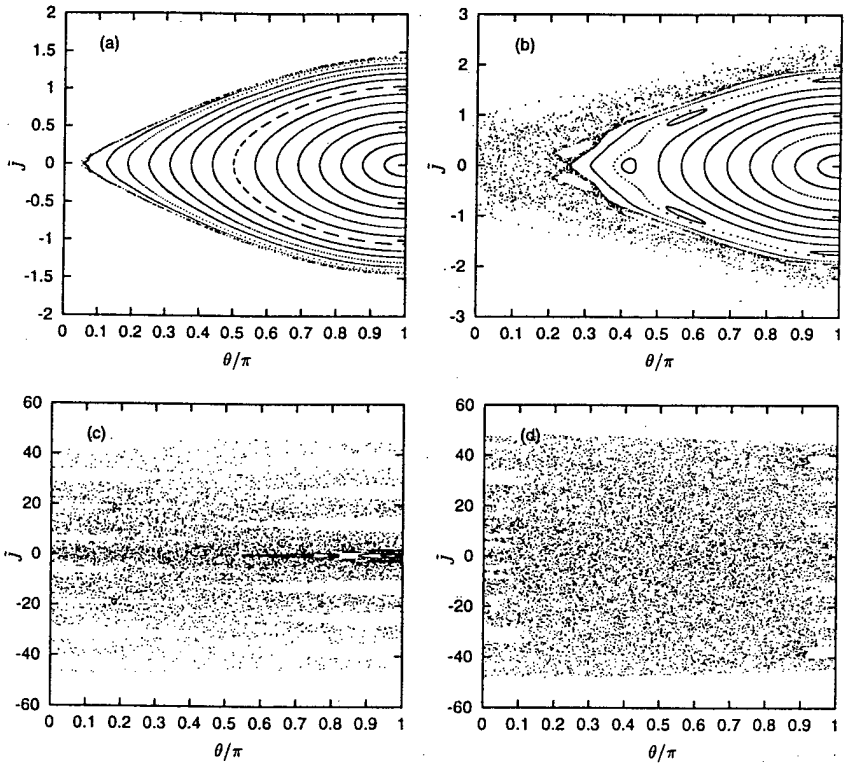

FIG. 1.

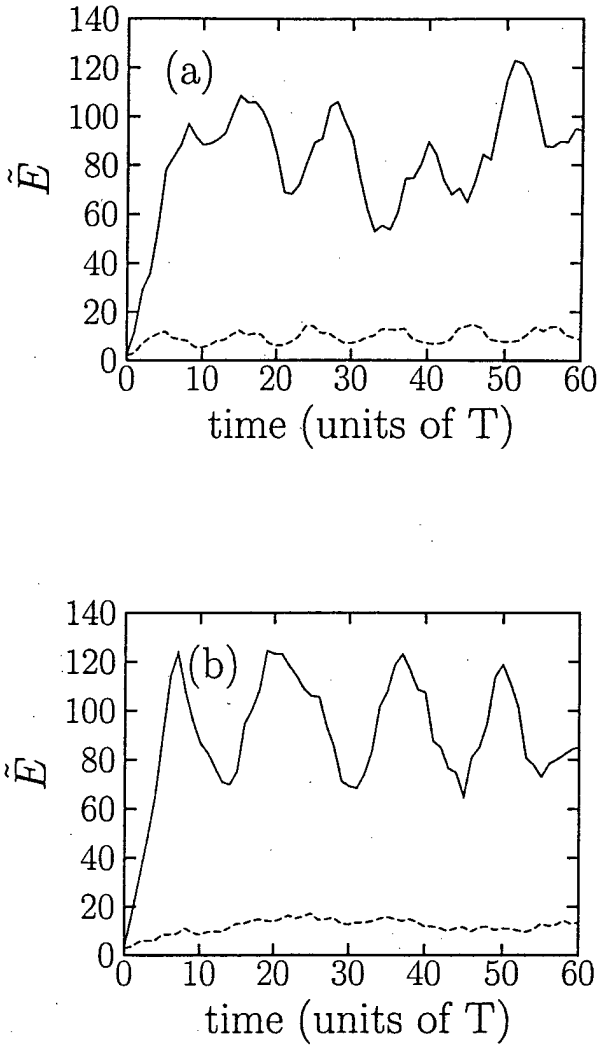

FIG. 2.

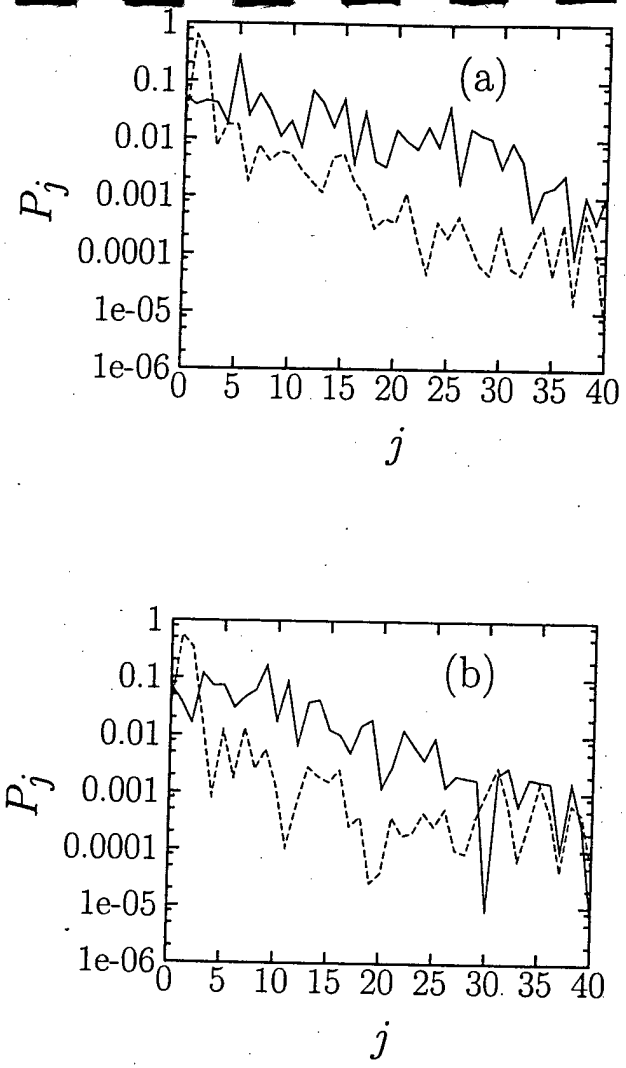

FIG. 3.

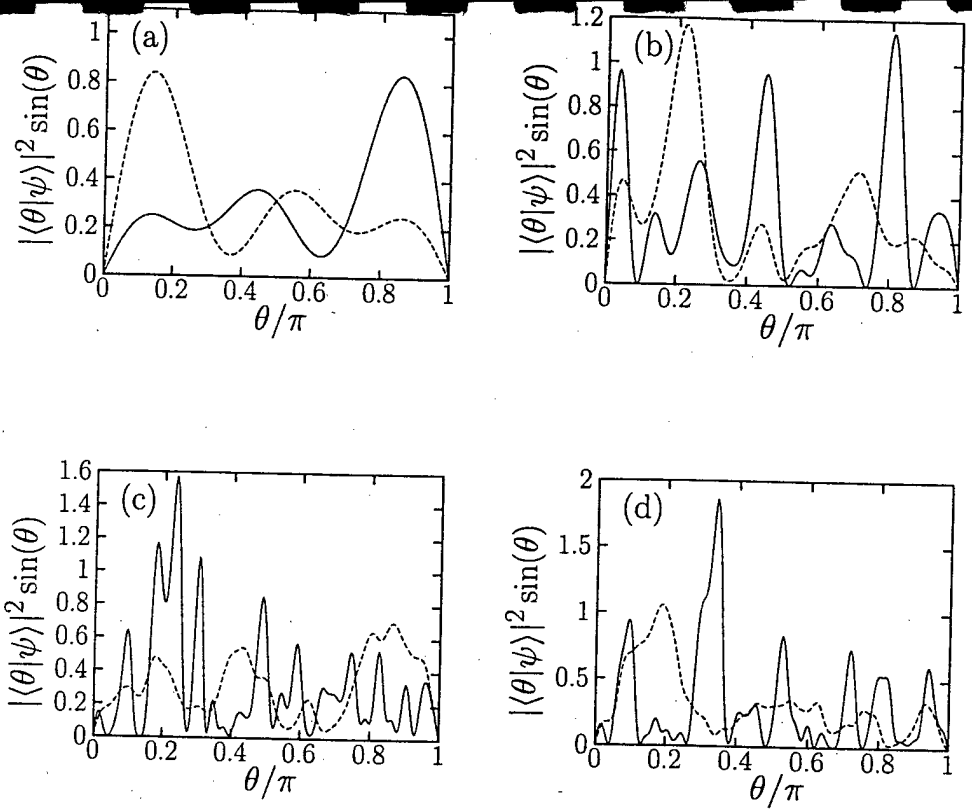

FIG. 4.

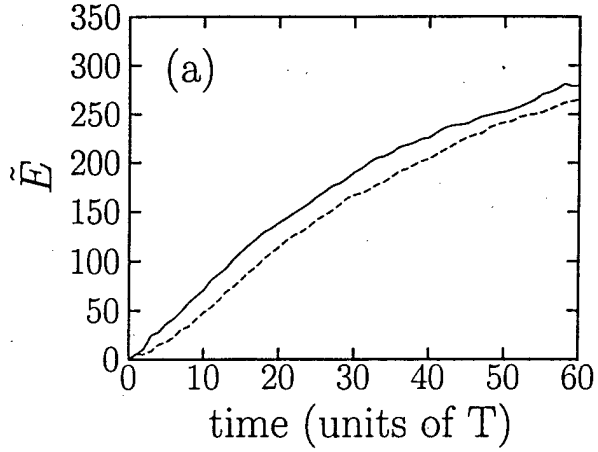

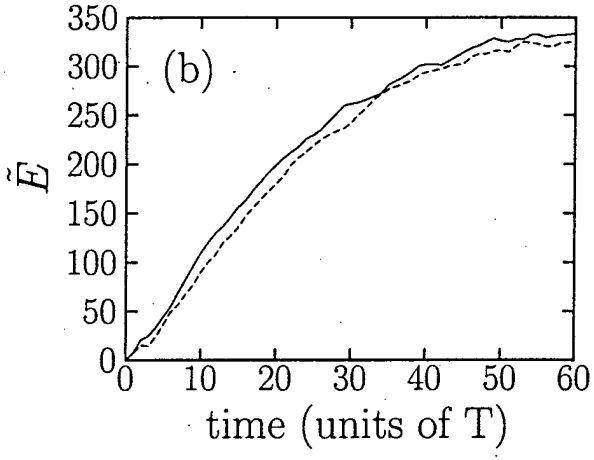

FIG. 5.

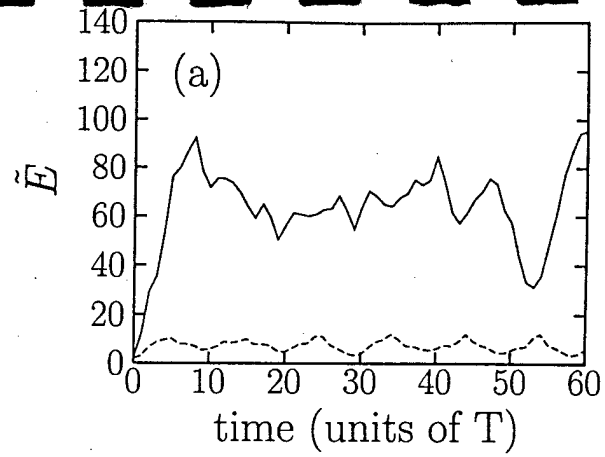

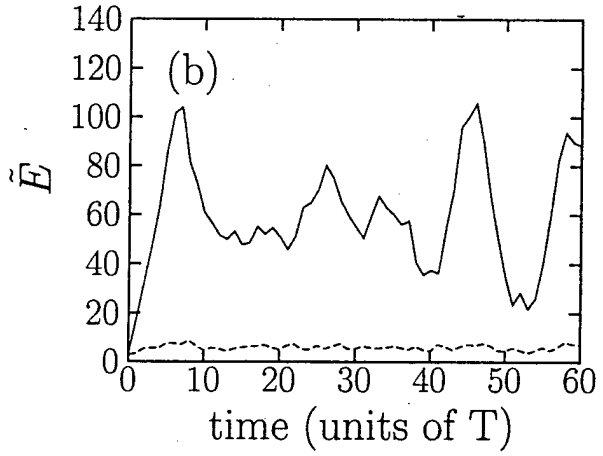

FIG. 6.

Gong and Brumer

5

Principles of Electric-Dipole Allowed Optical Control of Molecular Chirality

Paul Brumer

Chemical Physics Theory Group,

Department of Chemistry

University of Toronto

Toronto, Canada M5S 3H6,

and

Einat Frishman and Moshe Shapiro

Chemical Physics Department,

The Weizmann Institute of Science,

Rehovot, Israel 76100

(October 24, 2001)

Abstract

Conditions for achieving "optical asymmetric synthesis", an example of controlled chiral symmetry breaking, using the electric-dipole light field interaction are derived. These include scenarios in which neither the medium nor the light is chiral by itself. Specifically, parity requirements are used to show that any optical scenario in which the dynamics of the molecule depends on the overall sign of the electric field allows for control over the production of one chiral species in preference to its mirror image. A sample laser-molecule scenario is used to demonstrate these conditions.

Typeset using REVTEX

The ability to produce a specific broken-symmetry system and in particular a chiral system of specific handedness, in preference to its equal energy broken-symmetry forms, is of great interest, both practically as well as theoretically. Examples of broken-symmetry systems of interest include a pair of asymmetric quantum wells, one being the mirror image of the other; two heteronuclear molecules aligned in a DC electric field; and a 1:1 mixture (called a "racemic" mixture) of chiral molecules and their mirror images (such pairs are called "enantiomers"). Although the results described below may be applied to a rather general class of broken-symmetry systems, we focus here on the conversion of a racemic mixture to a single enantiomeric form, a process we term "optical asymmetric synthesis". Our interest is in identifying general conditions under which linearly polarized light can be used to achieve this goal.

The use of circularly polarized light [1–3] to selectively enhance a desired enantiomer, results in a very small effect for most molecules. The reason for this can be traced to the reliance on the presence of the weak molecular magnetic-dipole. Alternatively we can explain the minuteness of the effect by noting that although circularly polarized light is chiral, this chirality, which is due to the combined sense of the rotation of the electric (or magnetic) field and the direction of propagation, is hardly felt by the molecule due to the differences of at least three orders of magnitudes between the wavelength of light in the visible range and the molecular size.

In contrast, coherent control methods which utilize the far stronger electric-dipole interaction, in conjunction with either polarization (M_J selection) of photofragments [4] or of the initial racemic mixture [5,6], or orientation [7,8] of the initial sample, have been shown theoretically to yield a very high degree of enantio-selectivity. In the former cases [4,5], linearly polarized light was used, so that neither the system, nor the light, was chiral by itself. As discussed below, chiral molecules of specific handedness may be generated, in a process we term "optical asymmetric synthesis", by combining a phase-specific electromagnetic field with a polarized racemic mixture.

In this note we derive the general conditions under which an optical asymmetric synthesis

based purely on the electric-dipole light-field interaction is possible. The conditions are completely general, taking into account the properties of both the medium and the incident light.

Consider a molecule, described by the total Hamiltonian (including electrons and nuclei) H_M. Within the Born-Oppenheimer approximation adopted below, the nuclear wavefunction associated with the ground electronic state has two enantiomers denoted L and D, related to one another through inversion $\mathcal{I}$. Specifically, H_M eigenstates describing L and D and are denoted $|\, L_i \,\rangle$ and $|\, D_i \,\rangle$ $(i = 1, 2, 3....)$ and satisfy

$$\mathcal{I}|\, L_i \,\rangle = -|\, D_i \,\rangle; \quad \mathcal{I}|\, D_i \,\rangle = -|\, L_i \,\rangle, \tag{1}$$

The dipole interaction of this molecule with an incident time dependent electric field $\mathbf{E}(t)$ is described by the Hamiltonian:

$$H(\mathbf{E}) = H_M - \mu \cdot \mathbf{E}, \tag{2}$$

Here μ is the total dipole operator, including both electron and nuclear contributions, and we have explicitly indicated the dependence of the Hamiltonian on the electric field. Consider now the effect of inversion on H. Since $\mathcal{I}$ operates on the coordinates of the molecule, we first note that it reverses the sign of the dipole operator, i.e, $\mathcal{I}^\dagger \mu \mathcal{I} = -\mu$. Secondly we note that the molecular Hamiltonian is invariant to the action of $\mathcal{I}$. Thus, since $\mathcal{I}^\dagger = \mathcal{I}$, that $[H_M, \mathcal{I}] = 0$. Combining the above results, we have [9] that, $\mathcal{I}H(\mathbf{E})\mathcal{I} = H(-\mathbf{E})$, where $H(-\mathbf{E}) = H_M + \mu \cdot \mathbf{E}$. This implies, defining $U(\mathbf{E})$ and $U(-\mathbf{E})$ as the propagators corresponding to dynamics under $H(\mathbf{E})$ and $H(-\mathbf{E})$, respectively, that,

$$U(\mathbf{E})\mathcal{I} = \mathcal{I}U(-\mathbf{E}). \tag{3}$$

To expose the underlying principles allowing optical asymmetric synthesis, consider irradiating a racemic mixture of D and L in its ground electronic state with an electric field $\mathbf{E}$ and examine the difference δ between the amount of D and L formed. We consider first the coherent process using transform limited light in the absence of collisions. Then, the difference δ is given by

$$\delta = \sum_i P_i \sum_j [|\langle D_j|\, U(\mathbf{E})\,|D_i\rangle|^2 + |\langle D_j|\, U(\mathbf{E})\,|L_i\rangle|^2] - [|\langle L_j|\, U(\mathbf{E})\,|D_i\rangle|^2 + |\langle L_j|\, U(\mathbf{E})\,|L_i\rangle|^2] \tag{4}$$

where P_i is the probability of state $|L_i\rangle$ and $|D_i\rangle$ in the initial mixed state. (Since the initial state is a racemic mixture, the states $|L_i\rangle$ and $|D_i\rangle$ appear with equal probability.) If $\delta = 0$ then there is no control over the chirality in the scenario defined by $U(\mathbf{E})$.

To determine the conditions under which δ is nonzero, we rewrite Eq. (4) as

$$\delta = \sum_i P_i \sum_j [|\langle D_j|\, U(\mathbf{E})\,|D_i\rangle|^2 - |\langle L_j|\, U(\mathbf{E})\,|L_i\rangle|^2] + [|\langle D_j|\, U(\mathbf{E})\,|L_i\rangle|^2 - |\langle L_j|\, U(\mathbf{E})\,|D_i\rangle|^2] \tag{5}$$

and recast the second and third terms using:

$$\begin{aligned} |\langle L_j|\, U(\mathbf{E})\,|L_i\rangle|^2 &= |\langle D_j|\, \mathcal{I}^\dagger U(\mathbf{E})\mathcal{I}\,|D_i\rangle|^2 = |\langle D_j|\, U(-\mathbf{E})\,|D_i\rangle|^2 \\ |\langle D_j|\, U(\mathbf{E})\,|L_i\rangle|^2 &= |\langle D_j|\, U(\mathbf{E})\mathcal{I}\,|D_i\rangle|^2 = |\langle D_j|\, \mathcal{I}U(-\mathbf{E})\,|D_i\rangle|^2 = |\langle L_j|\, U(-\mathbf{E})\,|D_i\rangle|^2 \end{aligned} \tag{6}$$

giving

$$\delta = \sum_i P_i \sum_j [|\langle D_j|\, U(\mathbf{E})\,|D_i\rangle|^2 - |\langle D_j|\, U(-\mathbf{E})\,|D_i\rangle|^2] + [|\langle L_j|\, U(-\mathbf{E})\,|D_i\rangle|^2 - |\langle L_j|\, U(\mathbf{E})\,|D_i\rangle|^2] \tag{7}$$

Equation (7), the essential result of this work, provides the general condition under which electric fields, assuming a dipole interaction, can break the right/left symmetry of the initial state, and result in enhanced production of a desired enantiomer. Specifically, the difference between the amount of D and L formed is seen to depend entirely on the difference between the molecular dynamics when irradiated by $\mathbf{E}$ and by $-\mathbf{E}$. Hence, barring cancellation of matrix elements of different j, *any scenario where the dynamics of the molecules depends on the overall sign of the electric field can give a nonzero enantiomeric excess and a breaking of the left-right symmetry, even for cases with initial achiral precursors.* Note that the fact that molecular dynamics can depend on the phase of the incident electric field is well substantiated [10,11], but its utility for asymmetric synthesis is only evident from this result. Finally, note that the result is completely consistent with symmetry based arguments that

can usefully provide conditions under which δ must equal zero. For example, a racemic mixture of thermally equilibrated molecules is rotationally invariant. Hence any rotation that converts $\mathbf{E}$ to $-\mathbf{E}$ could not, in this case, result in enantiomeric control. In particular, in this case the sum over M_J (where M_J is the component of the total angular momentum along the direction of laser polarization) implicit in the sum over P_i in Eq. (7) would result in $\delta = 0$. By contrast, for example, a racemic mixture of M_J polarized molecules irradiated with linearly polarized light [5] gives nonzero δ. New $\delta \neq 0$ examples emanating from Eq. (7) are also expected to display similar non-traditional characteristics.

Both qualitative and quantitative applications of Eq. (7) are possible. Qualitatively, for example, a traditional scheme where the ground electronic state of L and D are incoherently excited to bound levels of an excited state, gives $\delta = 0$. This is because all processes connecting the initial and final $|\, L_i \,\rangle$ and $|\, D_i \,\rangle$ states, i.e. contributions to the matrix elements in Eq. (7), are even in the power of the electric field. Hence, propagation under $\mathbf{E}$ and $-\mathbf{E}$ are identical. By contrast, consider the four level model scheme in Fig. 1, where the states $|\, D_1 \,\rangle$ and $|\, L_1 \,\rangle$ are denoted $|\, D \,\rangle$ and $|\, L \,\rangle$. (E.g. these may be four levels of fixed M_J). In this enhanced version of the scenario introduced in Ref. [5], two states $|\, 1 \,\rangle$ and $|\, 2 \,\rangle$ of energy E_1 and E_2, which are associated with an excited electronic state, are coupled to the ground state at energies $E_D = E_L$ by two narrow pulses $\varepsilon_1(t)$, $\varepsilon_2(t)$ of linearly polarized coherent light. Here the ro-vibrational component of $|\, 1 \,\rangle$ is symmetric with respect to $\mathcal{I}$ whereas $|\, 2 \,\rangle$ is antisymmetric [12]. The latter two levels are coupled to one another by an additional pulse of coherent linearly polarized light of amplitude $\varepsilon_0(t)$. When $\varepsilon_0(t) \neq 0$ there exist processes connecting the initial and final $|\, L \,\rangle$ and $|\, D \,\rangle$ states which are of the form $|\, L \,\rangle \rightarrow |\, 1 \,\rangle \rightarrow |\, 2 \,\rangle \rightarrow |\, D \,\rangle$ and hence there are terms in Eq. (7) that are odd in the power of the electric field. One therefore anticipates the possibility of altering the enantiomeric excess using this combination of pulses, providing the basis for the control results reported in Ref [5]. Further, if $\varepsilon_0 = 0$ then the situation reverts to the case discussed above, where only processes even in the electric field contribute to transitions between the initial $|\, D \,\rangle, |\, L \,\rangle$ and final $|\, D \,\rangle, |\, L \,\rangle$ transitions, and hence control over the enantiomeric excess is lost. For this

reason, the $\varepsilon_0(t)$ coupling laser is crucial to enantiomeric control. This qualitative picture is substantiated quantitatively, below.

Quantitatively, the time evolution of the system shown in Fig. 1 is given by the wavefunction

$$|\Psi(t)\rangle = b_D(t)\exp(-iE_Dt/\hbar)|D\rangle + b_L(t)\exp(-iE_Lt/\hbar)|L\rangle + b_1(t)\exp(-iE_1t/\hbar)|1\rangle + b_2(t)\exp(-iE_2t/\hbar)|2\rangle. \tag{8}$$

Inserting Eq. (8) into the time dependent Schrödinger Equation, invoking the rotating wave approximation, and noting the symmetry properties of the nuclear component of $|1\rangle$ and $|2\rangle$ gives a set of equations [5] which can be solved numerically for the time dependence of the coefficients $b_i(t)$. Specifically,

$$\begin{aligned}
\dot{b}_1 &= i\exp(i\Delta_1 t)\Omega^*_{D,1}[b_D + b_L] + i\exp(i\Delta_0 t)\Omega^*_0 b_2 \\
\dot{b}_2 &= i\exp(i\Delta_2 t)\Omega^*_{D,2}[b_D - b_L] + i\exp(-i\Delta_0 t)\Omega_0 b_1 \\
\dot{b}_D &= i\exp(-i\Delta_1 t)\Omega_{D,1} b_1 + i\exp(-i\Delta_2 t)\Omega_{D,2} b_2 \\
\dot{b}_L &= i\exp(-i\Delta_1 t)\Omega_{D,1} b_1 - i\exp(-i\Delta_2 t)\Omega_{D,2} b_2
\end{aligned} \tag{9}$$

where the Rabi frequencies $\Omega_{ij}(t) \equiv \mu_{ij}\varepsilon_j(t)/\hbar$, $i = D, L$, $j = 1, 2, \Omega_0 \equiv \mu_{21}\varepsilon_0(t)/\hbar$, and detunings $\Delta_j \equiv \omega_{jD} - \omega_j, \Delta_0 \equiv \omega_{21} - \omega_0$, where $\mu_{ij} \equiv \langle i|\mu\cdot\hat{\epsilon}_k|j\rangle$, with $i = D, L; k = 0, 1, 2$ and $j = 1, 2$. Here $\omega_{ij} = (E_i - E_j)/\hbar$ and $\hat{\epsilon}_k$ defines the direction of the linearly polarized pulse $\varepsilon_k(t)$. We take the pulses ε_1 and ε_2 much narrower in bandwidth than ω_{21}, and neglect the effect of pulse 1 on level 2 and of pulse 2 on level 1.

Analytically, the solution to Eq. (9) depends on the sign of $\mathbf{E}$ when $\varepsilon_0 \neq 0$, Specifically, changing $\mathbf{E}$ to $-\mathbf{E}$ means changing all $\varepsilon_j(t)$ to $-\varepsilon_j(t)$. Doing so, and defining $b'_1 = -b_1$ and $b'_2 = -b_2$ converts Eq. (9) into

$$\begin{aligned}
\dot{b}'_1 &= i\exp(i\Delta_1 t)\Omega^*_{D,1}[b_D + b_L] - i\exp(i\Delta_0 t)\Omega^*_0 b'_2 \\
\dot{b}'_2 &= i\exp(i\Delta_2 t)\Omega^*_{D,2}[b_D - b_L] - i\exp(-i\Delta_0 t)\Omega_0 b'_1 \\
\dot{b}_D &= i\exp(-i\Delta_1 t)\Omega_{D,1} b'_1 + i\exp(-i\Delta_2 t)\Omega_{D,2} b'_2 \\
\dot{b}_L &= i\exp(-i\Delta_1 t)\Omega_{D,1} b'_1 - i\exp(-i\Delta_2 t)\Omega_{D,2} b'_2
\end{aligned} \tag{10}$$

Thus, Eq. (10) is the same as Eq. (9) barring the change of sign in the Ω_0 terms. Hence by the above argument, this scenario therefore allows for chirality control when $\varepsilon_0(t) \neq 0$.

Numerical studies indeed confirm that control over the $|D\rangle$ and $|L\rangle$ populations is, indeed, extensive when laser properties (pulse widths, central frequencies, time delay, etc.) are varied in this scenario. Consider, for example, excitation from a racemic mixture. Fig. 2a shows the dependence of the populations of $|D\rangle$ and $|L\rangle$ on the phase $\theta \equiv \theta_2$ of $\varepsilon_2(t)$, where the pulses are assumed Gaussians [5] of the form $\varepsilon_k(t) = \beta_k \exp[-((t-t_k)/\alpha_k)^2]$ $(k = 0, 1, 2)$, with $\beta_k = |\beta_k| \exp(i\theta_k)$. Clearly, one can preferentially deplete ground state L or ground state D just by changing θ by π. Similarly, Fig. 2b shows the extensive dependence of the L and D populations on the intensity ratio β_0/β_1.

Finally, we note that control depends upon the ability to coherently prepare excited state levels by one or more simultaneous excitation routes, embodied in the simultaneous radiative coupling of levels $|1\rangle$ and $|2\rangle$ to one another and to $|D_i\rangle$ and $|L_i\rangle$. Thus, this constitutes a demonstration of the use of coherent control [13] to alter the overall chirality of a system without the use of chiral input. What is required experimentally is control over the phase of the electric field. One possible approach is to use ultra short pulses [14,15] which allow defining the overall electric field phase.

In summary, we have derived the basic principle that allows, using the dominant electric-dipole light interaction, for phase selective transfer of a racemic mixture into the pure D or L enantiomeric form. In doing so we have ignored collisional effects, as well as radiative emission to the ground state, discussed in Ref. [5], because they do not modify the principles described above.

Acknowledgments: This research was supported by the U.S. Office of Naval Research; by the Minerva Foundation and by the German Israeli Foundation.

REFERENCES

[1] L. D. Barron, "*Molecular Light Scattering and Optical Activity*", (Cambridge Univ. Press, Cambridge, 1982).

[2] e.g., A. Salam and W. J. Meath, Chem. Phys. **228**, 115 (1998).

[3] J. Shao and P. Hänggi, J. Chem. Phys. 10799351997

[4] M. Shapiro and P. Brumer J. Chem. Phys. **95**, 8658 (1991)

[5] M. Shapiro, E. Frishman and P. Brumer, Phys. Rev. Letters **84**, 1669 (2000).

[6] The system analyzed in Ref. [5] consists of four levels coupled by linearly polarized light, an example being a medium composed of a single value of M_J. Note that such a system is not chiral. For a detailed discussion of the role of angular momentum in coherently controlled asymmetric synthesis, see M. Shapiro, E. Frishman and P. Brumer (manuscript in preparation).

[7] Y. Fujimura, L. Gonalez, K. Hoki,, J. Manz and Y. Ohtsuki, Chem. Phys. Lett. **306**, 1 (1999); errata: ibid. **310**, 578 (1999). Note, that these authors study control over an initial superposition state, rather than a racemic mixture.

[8] Y. Fujimura, (presented at Pacifichem 2000, Hawaii)

[9] C.S. Maierle and R.A. Harris, J. Chem. Phys. **109**, 3713 (1998)

[10] J.H. Shirley, Phys. Rev. **138**B, 979 (1965)

[11] A. Brown and W.J. Meath, J. Chem. Phys. **109**, 9351 (1998)

[12] References to molecules which are proposed to have level structure with these characteristics have been given in Ref. 4. More recently we have shown (E. Deretey, M. Shapiro and P. Brumer, submitted) that 1,3 dimethylallene does display this level structure and is extensively controllable (D. Gerbasi, M. Shapiro and P. Brumer, submitted) using the proposed laser scenario. Other molecules are under study.

[13] For recent reviews see M. Shapiro, P. Brumer, Adv. Atomic, Molecular and Optical Phys. **42**, 287 (2000); S. Rice and M. Zhao, Optical Control of Molecular Dynamics, (Wiley, N.Y., 2000)

[14] A. Apolonski, A. Poppe, G. Tempea, C. Spielmann, T. Udem, R. Holzwarth, T.W. Hänsch and F. Krausz, Phys. Rev. Lett. **85**, 740 (2000)

[15] C. Raman, T.C. Weinacht and P.H. Bucksbaum, Phys. Rev. A, **55**, R3995 (1997)

Figure Captions

Figure 1: Model system and laser scenario, as described in text.

Figure 2: Probability of observing D (solid lines) and of observing L (dot-dashed lines) after laser excitation of a racemic mixture as function of (a) the phase θ of $\varepsilon_2(t)$ and (b) the ratio of amplitudes β_0/β_1. System parameters are: $\mu_{1L} = \mu_{1D} = 1$ a.u., $\mu_{2L} = -\mu_{2D} = 1$ a.u., $\beta_i = 1 * 10^{-5}$ a.u., $i = 1, 2$, $\alpha_i = 2$ psec ,$i = 0, 1, 2$, $\Delta_1 = \Delta_2 = -5$ cm^{-1}, $t_1 = t_2$ and (a) $\beta_0 = 4 \times 10^{-5}$ a.u., $\Delta_0 = 0$ and $t_0 = t_1$. (b) $\beta_0 = 1 \times 10^{-5}$ a.u., $\Delta_0 = -5$ cm^{-1} and $t_0 - t_1 = -2$ psec.

FIGURES

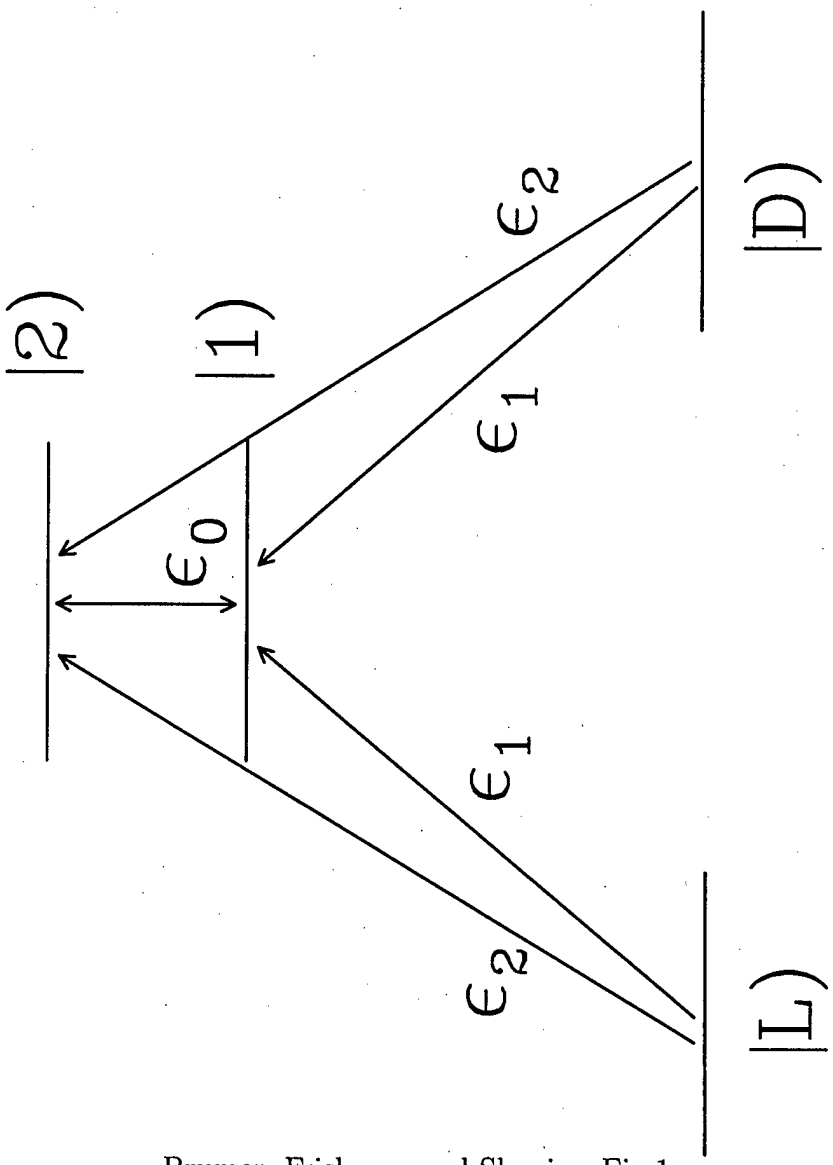

Brumer, Frishman and Shapiro, Fig.1

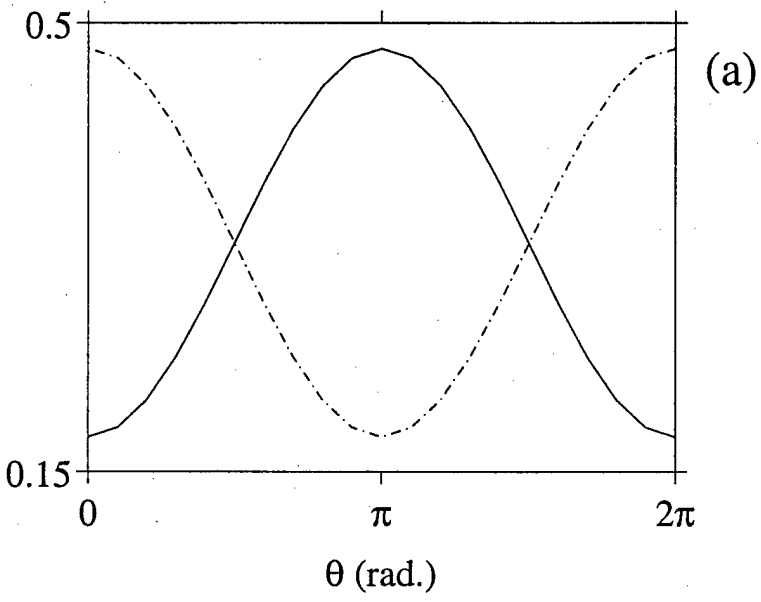

Brumer,

Frishman and Shapiro, Fig.2a

6

Chiral Molecules With Achiral Excited States: A Computational Study of 1,3-Dimethylallene

Eugen Deretey, Moshe Shapiro* and Paul Brumer

Chemical Physics Theory Group, Department of Chemistry

University of Toronto, Toronto M5S 3H6, Canada

Abstract

Molecular orbital computations using the configuration interaction singles (CIS) method and complete active space self-consistent field (CASSCF) method were used to map out the electronic ground and excited states of 1,3-dimethylallene. Both open shell and closed shell singlet configurations were taken into account. Potential Energy Surfaces (PES) for the ground and the first two excited states were obtained over a two-mode grid composed of the C–C–C bending angle and the dihedral angle between the planes defined by the carbon atoms of the H_3C–C=C and C=C–CH_3 groups. Several critical points located on the ground and first excited PES were fully optimized by allowing all degrees of freedom to relax. The ground state racemization reaction from the left-handed enantiomer to the right-handed was found to proceed via a barrier of 41 kcal/mol, in excellent agreement with the experimental value of 45.1kcal/mol for the enthalpy of racemization. The ground state transition state geometry is shown to be planar-bent. The results indicate that 1,3-dimethylallene shows chiral structures in the ground state and achiral structures in the first excited state. Coupled with the reported dipole moment function, 1,3-dimethylallene is shown to be a useful molecule for coherently-controlled racemic purification using our "laser distillation" scheme[*Phys. Rev. Lett.*, **2000**, *84*, 1669].

---

*Permanent Address: Chemical Physics Department, The Weizmann Institute of Science, Rehovot, 76100, Israel

I. INTRODUCTION

There has been a great deal of interest recently [1–5] in the interaction of chiral molecules or racemic mixtures with coherent light. This includes, for example, efforts to understand the nature of coherent superpositions of chiral molecules [1] as well work such as ours on coherently controlled asymmetric synthesis using linearly polarized light [3], a process that we term "laser distillation". Many of these studies share the common feature that the molecules are assumed to have a ground state potential which supports chiral structures and an electronically excited state which is achiral. Despite the interest in such molecules, however, there has been no systematic effort to identify molecules displaying these characteristics.

In this paper we show that 1,3-dimethylallene is a molecule of this type. 1,3-dimethylallene, a chiral molecule by virtue of the perpendicular positioning of the two methyl groups, was initially chosen for consideration due to its unique geometry, which allows the interconversion between the D and L enantiomers by simply breaking either of the double bonds, followed by a 180° rotation about that bond (see Figure 1). This suggests, as confirmed below, that although the breaking of a double bond is expected to be prohibited energetically on the ground state, it may well be facile on some of the excited states. Subsequent work, reported elsewhere [6] showed that the structure of the potential surfaces, coupled with the dipole moment function reported in this paper, allows for extensive chiral selectivity using our laser distillation scenario [3].

To assess the utility of a molecule for laser distillation, or for the other studies cited above, requires that we characterize all critical points. In the case of 1,3-dimethylallene there are a few studies of the spectra and internal rotation [7,8]. However, the many experimental [9–14] and computational [15–18] studies on the ground and excited states of allene, amongst them the computational study of the ring opening of substituted cyclopropylidenes to cyclic allenes [16], suggest that computations must be done with care. Specifically, computational

studies on the excited states of non-substituted allene are inconclusive regarding the character of local minima and other critical points on the first excited state surface. While Density Functional Theory (DFT) results in the first excited PES having a single minimum [16], CASSCF based computations [17] suggest that the critical point at that geometry is a saddle point. For this reason we have initiated a careful and systematic exploration of the ground and excited state surface of 1,3-dimethylallene of all relevant critical points, characterizing their geometries and electronic configurations.

Section II below describes the methods of computation, followed by results for ground and excited state critical points and the dipole moment function, in Section III.

II. METHOD OF CALCULATION

The ground and excited state surfaces were computed over a rigid grid using single-excitation configuration interaction (CIS) [19,20] spanned by a double-zeta 6-31+G(d,p) basis set. In addition, full geometry optimizations of the critical points on the first excited PES of the planar 1,3-dimethylallene geometries were carried out using the "Complete Active Space Multiconfiguration Self Consistent Field" [21,22] (CASSCF) with a triple zeta 6-311+G(d,p) basis set. As the active CASSCF space, termed CASSCF(4,6), we have chosen four electrons and six orbitals. In the C_s planar configurations we have chosen four $\mathbf{A'}$ and two $\mathbf{A''}$ molecular orbitals, whereas for C_{2v} geometries the active space includes a single $\mathbf{b_1}$, $\mathbf{b_2}$, and $\mathbf{a_2}$ orbital and three $\mathbf{a_1}$ orbitals. The active space for the C_{2h} geometries is composed of an $\mathbf{a_g}$, $\mathbf{b_g}$, $\mathbf{a_u}$ and three $\mathbf{b_u}$ orbitals.

All the calculations were carried out using the GAUSSIAN 94 [23] program. The molecular orbital diagrams were generated by MOLDEN [24].

III. RESULTS

A. Two variable PES for the ground and first excited states

The potential surfaces were computed on a grid as a function of two variables, α, the C–C–C bending angle, and θ, defined as the dihedral angle between the H_3C–C=C and C=C–CH_3 planes (see Fig. 2), for "in-plane" α and $\alpha = 0, 180°$, and as $\phi - 90°$ where ϕ is the dihedral angle between the H_3C–C=C plane and the C=C=C plane for the out-of-plane bending angle $\alpha' \neq 0, 180°$.

For linear 1,3-dimethylallene θ is identical to the torsional angle H_3C–C...C–CH_3. The range of θ explored was [0°, 180°] , where (see Figure 1) 0° and 180° correspond to the two planar geometries and 90° - to one of the orthogonal 1,3-dimethylallene geometries. Because of symmetry we did not need to explore the 180° to 360° range.

Due to the methyl substituents there are three principal inequivalent bending directions of the linear C=C=C group (see Figure 3): (a) "In-plane" bending by angle α - confined to the frozen H_3C–C=C plane. (b) "Out-of-plane" bending by angle α' - i.e. bending in a direction orthogonal to the frozen H_3C–C=C plane. This bending will generate non-planar geometries, which are precursors for ring closure to yield the cyclopropylidene [16]. (c) Bending at 45° between the above directions. Bending in this direction preserves the C_2 symmetry of 1,3-dimethylallene.

We have computed the potential energy surfaces for the bending motion in the (a) and (b) directions, where the bending angle was allowed to vary between 100° and 260°. Figure 4 shows the ground and the first two excited PES generated by the CIS method for the in-plane bending. Figure 5 shows the same data for the out-of-plane bending. Note that in both cases the ground state shows two wells with a barrier between them along $\theta = 180°$, corresponding to the two ground state chiral species, whereas the first excited state shows a well with a minimum at $\theta = \alpha = 180°$. This is precisely the PES structure one seeks for

the chiral studies cited above–i.e. the ground state is chiral whereas the (first) excited state is not.

The geometries of the rigid scan critical points are shown in Fig. 6 and Fig. 7. In Fig. 6 we display six critical geometries of the planar 1,3-dimethylallene molecule. Since the planar geometries at (θ, α)=(180°,120°), and (180°,240°) geometries are identical, there are five independent critical geometries. We note that the structure located at (360°,240°), for which the two methyl groups are very close to one another, is very unfavorable energetically.

In Fig. 7 we display six critical geometries in the out-of-plane bending configurations of the first excited state. Only two of them, $(\theta, \alpha') = (180°,180°)$ and (360°,180°) are of sufficient low energy to be of interest in this study. They are similar to the in-plane critical points. The other four geometries are precursors to the cyclopropylidene ring closure.

B. CASSCF optimization at the planar critical points

The limited scan over two angles reported above only yields approximate locations for the critical points. In order to refine our understanding we have performed, using CASSCF, full-dimensional optimization at the planar critical geometries uncovered by our two-dimensional search. These calculations were performed for both closed- and open-shell singlets and for one open-shell triplet state.

Figure 8 shows the six orbitals and the four electrons considered in the active space. The electronic configurations are identified by four numbers composed of the orbital number (1,2,...,6), with the first two numbers carrying an α spin and the last two number a β spin. For example, the notation (1,2)(1,2) implies that the first electron is assigned to orbital 1, the second electron to orbital 2, both with α spins; the third electron to orbital 1 and the fourth electron to orbital 2, both with β spins.

Save for some specific configurations, all the geometric parameters were relaxed in the optimization, with no symmetry constraints imposed. The resultant energies [25] and

coefficients for the most important electronic states are given in Table I and Table II. The calculated geometries, the atom serial numbers, the bond length and bond angles are given in Figs. 2,9,10, Table III and Table IV. The highest occupied and lowest unoccupied molecular orbitals are shown in Fig. 11.

It is instructive to follow the way in which the bending of the C–C–C angle affects the closed shell planar energies. To do so we performed single point CASSCF calculations at the linear-*anti* and the slightly bent C–C–C geometries. The results are shown in Fig. 12. Bending from 180^o to $\approx 165^o$ shows smooth energy variations on the excited electronic state with closed shell singlet configuration. Additional bending below $\approx 165^o$ leads to the sudden "collapse" of the CASSCF calculation to the lower energy open-shell ground state configuration. At bending angles of 130^o and below, the stable excited state CASSCF configuration again returns to a closed-shell excited state.

Figure 12 shows the presence of a near crossing between the open-shell (1,2)(1,2) singlet and the closed-shell (1,2)(1,3) singlet at $\approx 165^o$. The existence of an "avoided crossing" is further confirmed by the interchange of the HOMO-LUMO orbitals in linear and bent geometries as seen in Fig. 11 . It is conceivable that the "collapse" of the CASSCF calculation noted above is due to the failure of the Born-Oppenheimer approximation in this near crossing region. In the present study we did not try to locate the crossing point more accurately because our main purpose was to study the planar structures, further details about which are given in section IV.

C. The electric dipole-moment for the ground and the first excited states

Studies of light induced processes in chiral molecules, the motivation for this study, require the electric dipole moment as input into the computation of Franck-Condon factors. Computational results on the electric dipole are provided in this section.

We have computed the electric dipole moment for the ground state and first electronic

excited state of 1,3-dimethylallene using the same procedure as for the potential energy surfaces. The X, Y and Z components (see note [26]) of the dipole in ground and excited electronic states are shown in Figs. 13 and 14 for fixed α, and as a function of θ. We find that for the linear orthogonal-conformation $(\theta, \alpha) = (90, 180)$ the dipole moment of the first excited state is four times larger than that of the ground state. In contrast, the dipole moment for the planar anti-conformation $(\theta, \alpha) = (180, 180)$ is essentially zero in both ground and first excited states and remaining linear planar conformations show a generally small dipole in both the ground and excited states. The dipole functions for the bent conformations are somewhat more complicated. The total electric dipole moment surfaces for the ground state and first electronic excited state are shown in Fig. 15.

IV. OPTIMIZED CONFIGURATIONS AND RACEMIZATION

In this section we discuss the results of fully optimized studies, carried out at select geometries using the CASSCF method, as well as the energetics of the 1,3-dimethylallene racemization reaction.

¿From the viewpoint of electronic structure, our most important finding is that the ground PES is dominated by a closed-shell (1,2)(1,2) configuration in the orthogonal geometry and by an open-shell (1,2)(1,3) configuration in the planar geometries. The *reverse* occurs in the first excited state: this state is dominated by the open-shell (1,2)(1,3) configurations in the orthogonal geometries and by a closed-shell configuration (1,2)(1,2) in the planar geometries. This alternation between open and closed shell configurations is similar to that found for allene [16].

We find that at the same geometry, the ground PES has a saddle point and the first excited PES has a minimum. We identify the ground PES saddle point with the transition state for the interconversion of L 1,3-dimethylallene to D 1,3-dimethylallene. In addition, we find that, a) the first excited surface minimum is characterized by a closed-shell

configuration; b) at the geometry of the first excited state minimum the first excited state is higher in energy than the ground state; c) the ground PES saddle point, occurring at the same geometry, is dominated by an open shell configuration.

A. Planar Geometries

1. Planar-Linear Geometries

At the planar-linear geometries the CASSCF coefficients show that the ground PES is almost entirely made up of the (1,2)(1,3) open-shell configuration, while the first excited PES is dominated by the (1,2)(1,2) closed-shell configuration. We find that the energy difference between the open and closed shell planar-linear geometries is ≈26 kcal/mol. These findings are qualitatively similar to the situation in non-substituted allene, though for 1,3-dimethylallene the energy gap is higher.

In both electronic states there is no difference in energy between the *anti* and *syn* planar-linear geometries. Presumably the distance between the methyl groups is so large that there is essentially no interaction between these two groups at these geometries (see Table III and Ref. [27]).

2. Planar-Bent Geometries

At the planar-bent geometries the ground and first excited states have a similar electronic character to that of the planar-linear geometries, except for some mixing with the (2,3)(2,3) doubly-excited closed shell configuration [28] (see Table I).

Contrary to the situation in the planar-linear case, in the planar-bent case the energy difference between the ground and first excited state *does* depend on whether the system is in the *anti* or *syn* geometry: The energy difference is ≈8.6 kcal/mol for the planar-bent

anti geometries, and ≈1.0 kcal/mol for the planar-bent *syn* geometries (see Table II, Fig. 9 and Fig. 10), the *syn* being always lower in energy in the first excited state. The energy difference between these two planar-bent geometries is ≈ 7 kcal/mol. By contrast, there is essentially no difference in energy between these geometries in the ground state.

The *syn-anti* energy difference is a direct result of the C–C–C bending angle where the PES has a local minimum. In the first excited state *anti* configuration this angle is 113°, whereas in the *syn* configuration it is 108°, both values being much smaller than the C–C–C bending angle minimizing the ground PES, which is 139° in the *anti* configuration and 137.5° in the *syn* configuration (see Table IV). As a result, the methyl groups are much closer in the first excited state [27] and interact more, thereby explaining the difference in energy between the *syn* and *anti* geometries in the first excited state.

One of the most prominent features, seen from Table III, to come out of our calculation is the shortening of the C–C bond-lengths in the first excited state planar-linear geometry. The optimized geometries are displayed in Fig. 9(**1a**) for the first excited state C_{2h} symmetry and in Fig. 9(**2a**) for the first excited state C_s symmetry. The ground state geometry having a C_{2h} symmetry is shown in Fig. 9(**1b**), and that belonging to the C_{2v} symmetry is shown in Fig. 9(**2b**). The shortening of the C–C bond length occurs for both the *anti* and the *syn* geometries.

The open shell triplet planar structures are about 2 kcal/mol lower in energy than the open shell singlet structures. There is almost no difference between the open shell singlet and the open shell triplet geometries, as shown in Table III.

B. The Racemization Reaction

In order to complete the calculation of the minimum energy path for the racemization reaction, which is the transition from one orthogonal-linear geometry to its enantiomeric form, we have performed CASSCF optimization at the *orthogonal* geometry. At this geome-

try the ground state was found to be composed essentially of a single closed-shell (1,2)(1,2) configuration. In contrast, the first excited state was found to be composed of a number of open-shell configurations, with the (1,2)(1,3) configuration being most prominent.

Having performed the optimization for both the orthogonal-linear and planar geometries the current calculation suggests that the racemization reaction proceeds via the planar-bent geometry. The transition-state energy-barrier at this geometry without any temperature correction was computed here to be 41 kcal/mol. This barrier height and the transition-state geometries are in good agreement with experimental findings [8]. In particular, the experimental value for the enthalpy of racemization was found to be 45.1 kcal/mol [8], is in excellent agreement with our computed energy barrier. In contrast, the path which proceeds via the planar-linear geometry is more costly in energy: it involves a barrier of 50 kcal/mol.

V. CONCLUSIONS

We have computed the ground and first excited state PES of 1,3-dimethylallene as a function of the C–C–C bending angle and the dihedral angle between H_3C–C=C and C=C–CH_3 planes at the CIS level. We have also performed a full CASSCF optimization at a number of critical configurations in both the ground and first excited PES.

We have shown that the ground state racemization reaction from one enantiomeric form of 1,3-dimethylallene to the other proceeds via a barrier of 41 kcal/mol, in excellent agreement with the experimental value of 45.1kcal/mol for the enthalpy of racemization. The ground state transition state geometry was shown to be planar-bent.

We have also found that the first excited PES possesses a stable low energy critical point at the planar-bent geometry corresponding to the ground state transition state. Thus, this study suggests that 1,3-dimethylallene has a ground state potential energy surface that supports chiral structures, and an excited electronic state that is achiral. Further, the

minimum in the upper potential lies above the ground state transition state from the Dextro to the Levo form. As a consequence 1,3-dimethylallene is a useful molecule for many of the proposed studies of coherent light interacting with a chiral species [1–4]. In particular, in a subsequent publication [6] we demonstrate the ability to "laser distill" [3] 1,3-dimethylallene so as to selectively produce a large enantiomeric excess using linearly polarized light and a polarized dimethylallene medium.

Acknowledgments

We thank Professor Malcolm Bersohn, University of Toronto, for his suggestion that we consider 1,3-dimethylallene as a candidate for laser distillation, and for subsequent discussions. This work was partially supported by a grant from the EU IHP IHP-RTN-99-1 Program and by the U.S. Office of Naval Research.

TABLES

TABLE I. The CAS coefficients of the most important configuration[a].

State	*anti*-linear	*syn*-linear	*anti*-bent	*syn*-bent
Closed shell singlet (1,2)(1,2)	0.99926	0.99940	0.96199	0.96601
Open shell singlet (1,2)(1,3)	0.99998	0.99998	0.99999	0.99999
Open shell triplet (1,2,3)(1)	0.99998	0.99997	0.99999	0.99998

[a] Planar-linear geometries with a (1,2)(1,2) CAS coefficient bigger then 0.999 are considered to be "pure". In the planar-bent geometries, in addition to the dominant (1,2)(1,2) configuration, there is a small contribution from the doubly excited (2,3)(2,3) configuration.

TABLE II. CAS(4,6)/6-311+G(d,p) energies for the ground state and excited state planar 1,3-dimethyl allene[a].

	CAS energy [hartree]			
Electronic state	*anti*-linear	*syn*-linear	*anti*-bent	*syn*-bent
Closed shell singlet (1,2)(1,2)	-193.866194	-193.867627[c]	-193.909096	-193.920042
Open shell singlet (1,2)(1,3)	-193.908078	-193.907871	-193.922921	-193.921624
Open shell triplet (1,2,3)(1)	-193.911049	-193.910845	-193.926780	-193.925483
	CAS energy relative to the open shell singlet species [kcal/mol][b]			
Closed shell singlet (1,2)(1,2)	26.283 (76.439)	25.253 (75.540)	8.675 (49.518)	0.993 (42.649)
Open shell singlet (1,2)(1,3)	0.000 (50.156)	0.000 (50.287)	0.000 (40.843)	0.000 (41.656)
Open shell triplet (1,2,3)(1)	-1.864 (48.293)	-1.866 (48.421)	-2.422 (38.421)	-2.422 (39.235)

[a]For ground state, orthogonal 1,3-dimethylallene E_{CAS} = -193.988008,CAS_{coeff} = 0.99999, C=C=C angle = 179.9°; [b]Numbers are given to three significant figures, as obtained in the calculation. No claim of such accuracy is of course claimed here. If judging by the agreement with the experimental [8] $\Delta H_{racemization}$= 45.1 kcal/mol value, than these numbers are only accurate to $\pm 2-3$ kcal/mol. [c]See [25]; [d]Bracketed numbers are calculated with respect to the orthogonal 1,3-dimethylallene.

TABLE III. Bond lengths and bending angles for linear and planar-bent geometries[a]

	Linear *anti*			Linear *syn*		
	Bond length [Å]			Bond length [Å]		
Atom label	**1a**	**1b**	**1c**	**2a**	**2b**	**2c**
2,1	1.318	1.344	1.343	1.318	1.344	1.343
3,1	1.318	1.344	1.343	1.318	1.344	1.343
4,2	1.517	1.507	1.507	1.518	1.508	1.508
5,2	1.079	1.083	1.083	1.078	1.083	1.083
6,3	1.079	1.083	1.083	1.078	1.083	1.083
7,3	1.517	1.507	1.507	1.518	1.508	1.508
8,4	1.086	1.088	1.088	1.086	1.088	1.088
9,4	1.085	1.083	1.083	1.085	1.084	1.084
10,4	1.086	1.088	1.088	1.086	1.088	1.088
11,7	1.086	1.088	1.088	1.086	1.088	1.088
12,7	1.086	1.088	1.088	1.086	1.088	1.088
13,7	1.085	1.083	1.083	1.085	1.084	1.084
	Bending angle [degrees]			Bending angle [degrees]		
3,1,2	180.000	180.000	180.000	179.634	180.000[b]	180.000[b]
4,2,1	123.822	124.881	124.952	123.410	125.031	125.107
5,2,1	114.285	119.123	119.114	114.852	118.978	118.965
6,3,1	114.285	119.123	119.114	114.852	118.978	118.965
7,3,1	123.822	124.881	124.952	123.410	125.031	125.107
8,4,2	111.281	110.608	110.611	111.257	110.808	110.809
9,4,2	111.065	111.480	111.476	111.241	111.136	111.138
10,4,2	111.281	110.608	110.611	111.257	110.808	110.809
11,7,3	111.281	110.608	110.611	111.257	110.808	110.809
12,7,3	111.281	110.608	110.611	111.257	110.808	110.809

13,7,3	111.065	111.480	111.476	111.241	111.136	111.138

[a]The triplet open shell geometries, **1c** and **2c**, were included for comparative purposes

[b] The C–C–C bending angle together with four dihedral angles were frozen during the optimization.

TABLE IV. Bond lengths and bending angles for planar-bent geometries[a]

	Bent *anti*			Bent *syn*		
	Bond lengths [Å]			Bond angles [Å]		
Atom label	**3a**	**3b**	**3c**	**4a**	**4b**	**4c**
2,1	1.399	1.413	1.413	1.392	1.357	1.357
3,1	1.392	1.321	1.321	1.392	1.357	1.357
4,2	1.506	1.503	1.503	1.492	1.500	1.500
5,2	1.083	1.075	1.075	1.091	1.082	1.082
6,3	1.087	1.083	1.083	1.091	1.082	1.082
7,3	1.493	1.504	1.504	1.492	1.500	1.500
8,4	1.088	1.088	1.088	1.089	1.088	1.088
9,4	1.080	1.083	1.083	1.081	1.084	1.084
10,4	1.088	1.088	1.088	1.089	1.088	1.088
11,7	1.089	1.088	1.088	1.089	1.088	1.088
12,7	1.089	1.088	1.088	1.089	1.088	1.088
13,7	1.081	1.084	1.084	1.081	1.084	1.084
	Bond angles [degree]			Bond angles [degree]		
3,1,2	113.442	139.161	138.763	108.746	137.530	137.202
4,2,1	133.243	123.932	124.103	124.461	124.704	124.737
5,2,1	115.738	118.000	117.927	121.364	117.772	117.806
6,3,1	123.571	118.606	118.638	121.364	117.772	117.806
7,3,1	123.134	124.917	124.850	124.461	124.704	124.737
8,4,2	108.722	110.764	110.764	109.826	110.929	110.905
9,4,2	115.292	111.948	111.968	111.048	111.211	111.219
10,4,2	108.722	110.764	110.764	109.826	110.929	110.905
11,7,3	109.845	110.779	110.780	109.826	110.929	110.905
12,7,3	109.845	110.779	110.780	109.826	110.929	110.905

13,7,3	110.967	111.178	111.188	111.048	111.211	111.219

[a]The triplet open shell geometries, **3c** and **4c**, were included for comparison.

REFERENCES

[1] Maierle, C.S. ; Harris, R.A., *J. Chem. Phys.* **1998** *109*, 3713; Cina, J.A. ; Harris, R.A., *J. Chem. Phys.* **1994** *100*, 2531.

[2] Quack, M., Angew. Chem. Ed. Engl. **1989** *28*, 571

[3] Shapiro, M.; Frishman, E.; Brumer, P. *Phys. Rev. Lett.*, **2000**, *84*, 1669.

[4] Fujimura Y.; Gonzalez, L.; Hoki, K.; Manz, J.; Ohtsuki, Y.; *Chem. Phys. Lett.* **1999** *306*, 1.

[5] Salam A.; Meath, W.J., *J. Chem. Phys.* **1997** *106*, 7865; Salam A.; Meath, W.J., *ibid.* **1998** *228*, 115

[6] D. Gerbasi, M. Shapiro and P. Brumer, (manuscript in preparation)

[7] Rauk, A.; Drake, A. F.; Mason, S. F. *J. Am. Chem. Soc.* **1979**, *101*, 2284.

[8] Roth, W. R.; Bastigkeit, T. *Liebigs Ann.* **1996**, 2171.

[9] Iverson, A. A.; Russel, B. R. *Spectrochim. Acta* **1972**, *28A*, 447.

[10] Fuke, K.; Schnepp, O. *Chem. Phys.* **1979**, *38*, 211.

[11] Baltzer, P.; Wannberg, B.; Lundqvist, M.; Karlsson, L.; Holland, D. M. P.; MacDonald, M. A.; von Niessen, W. *Chem. Phys.* **1995**, *196*, 551.

[12] Bawagan, A. D. O.; Ghanty, T. K.; Davidson, E. R.; Tan, K. H. *Chem. Phys. Lett.* **1998**, *287*, 61.

[13] Holland, D. M. P.; Shaw, D. A. *Chem. Phys.* **1999**, *243*, 333.

[14] Mahapatra, S.; Cederbaum, L. S.; Koppel, H. *J. Chem. Phys.* **1999**, *111*, 10452.

[15] Seeger, R.; Krishnan, R.; Pople, J. A.; Schleyer, P. v. R. *J. Am. Chem. Soc.* **1977**, *99*, 7103.

[16] Bettinger, H. F.; Schreiner, P. R.; Schleyer, P. v. R.; Schaefer, III, H. F. *J. Phys. Chem.* **1996**, *100*, 16147. *ibid J. Org. Chem.* **1997** *62* 9267.

[17] Jackson, W. M.; Mebel, A. M.; Lin, S. H.; Lee, Y. T. *J. Phys. Chem. A* **1997**, *101*, 6638 and references wherein.

[18] Otto, P.; Ruiz, M. B. *J. Mol. Struct. (Theochem)* **1998**, *433*, 131.

[19] Foresman, J. B.; Head-Gordon, M.; Pople, J. A.; Frisch, M. J. *J. Phys. Chem.* **1992**, *96*, 135.

[20] Stanton, J. F.; Gauss, J.; Ishikawa, N.; Head-Gordon, M. *J. Chem. Phys.*, **1995**, *103*, 4160.

[21] Schlegel, H. B.; Robb, M. A. *Chem. Phys. Lett.* **1982**, *93*, 43.

[22] Bernardi, F.; Bottoni, A.; McDougall, J. J. W.; Robb, M. A.; Schlegel, H. B. *Faraday Symp. Chem. Soc.* **1984**, *19*, 137.

[23] Gaussian 94, Revision D.4, M. J. Frisch, G. W. Trucks, H. B. Schlegel, P. M. W. Gill, B. G. Johnson, M. A. Robb, J. R. Cheeseman, T. Keith, G. A. Petersson, J. A. Montgomery, K. Raghavachari, M. A. Al-Laham, V. G. Zakrzewski, J. V. Ortiz, J. B. Foresman, J. Cioslowski, B. B. Stefanov, A. Nanayakkara, M. Challacombe, C. Y. Peng, P. Y. Ayala, W. Chen, M. W. Wong, J. L. Andres, E. S. Replogle, R. Gomperts, R. L. Martin, D. J. Fox, J. S. Binkley, D. J. Defrees, J. Baker, J. P. Stewart, M. Head-Gordon, C. Gonzalez, and J. A. Pople, Gaussian, Inc., Pittsburgh PA, 1995.

[24] Schaftenaar, G.; Noordik, J. H. *J. Comput. -Aided Mol. Design*, **2000**, *14*, 123.

[25] The optimization of the **2a** geometry yielded two CASSCF(4,6) structures, both of them having mostly (1,2)(1,2) configuration. The higher-energy structure, with $E_{cas} = -193.867624$, has a CAS coefficient of 0.999, indicating that it is completely dominated by the (1,2)(1,2) configuration. This structure has three imaginary

frequencies. The C–C bond-length and the C–C–C bending angle are 1.318Å and 179.634°, respectively. The lower energy structure, with $E_{cas} = -193.888821$ hartree, has a CAS coefficient of 0.982. In this case the main (1,2)(1,2) configuration is mixed with the doubly excited (1,3)(1,3) configuration. The lower energy structure has four imaginary frequencies. The C–C bond-length and the C–C–C bending angle are 1.329Å and 179.690°, respectively. In this structure the symmetries of the active space orbitals changed from (A″A″A′A′A′A′) to (A″A″A″A′ A′A′). The closeness of the two structures suggests the existence of an avoided curve-crossing or of a conical intersection near the **2a** conformation.

[26] The central C=C=C carbon atom defines the origin of XYZ axis. The C=C=C group is located along the Z axis, the X axis is contained in the frozen plane defined by CH_3–C-H group and the Y axis is orthogonal to this plane.

[27] In the ground state the distance between the two Carbons belonging to the two Methyl groups in the syn configuration is 4.32Å. The smallest distance between two Hydrogens belonging to the two Methyls is 3.06Å. These distances are well outside the sum of the van der Waals radii of two Carbon atoms, which is 3.40 Å and that of two Hydrogen atoms which is 2.40 Å.

[28] On the basis of previous DFT calculations for the non-substituted allene, where a first-excited-state minimum in the planar-linear configuration was found, we have used the DFT method to optimize the planar geometries of 1,3-dimethylallene. Since the DFT methods is strictly applicable to ground closed-shell configurations, the use of DFT for excited state calculations might appear questionable. However, in our case, the excited state geometries have closed shell electronic states, for which DFT is applicable. Using DFT in conjunction with the B3LYP method with a smaller basis set [6-31+G(d,p)] yielded a *non-planar* minimum energy geometry of the C_i symmetry, with the two C-H hydrogen atoms oriented out-of-plane. This finding was confirmed

by a preliminary CASSCF optimization, yielding a critical point at a non-planar conformation.

FIGURE CAPTION

Figure 1: Racemization of 1,3-dimethylallene through internal rotation. The orthogonal left-handed enantiomer is converted to the right-handed enantiomer via the planar geometry.

Figure 2: The geometry of the 1,3-dimethylallene used in the two dimensional scan. The two variables in the rigid scan are (1) θ - the dihedral angle between the H_3C–C=C and C=C–CH_3 planes; (2) α - the C–C–C bending angle, here shown by an arrow which brings the H_3C–C-H out of the plane of the paper.

Figure 3: Three main modes of distortion for the 1,3-dimethylallene C=C=C group. The Newmann projection is shown along the C=C=C moiety. Arrows show the movement of the CH_3–C–H mobile group (the second C atom from the left is symbolized by a black dot).

Figure 4: In-plane bending surfaces. α is the C–C–C bending angle and θ is the dihedral angle. The orthogonal linear 1,3-dimethylallene is the global ground state minimum.

Figure 5: The same as in Fig. 4 but for the out-of-plane bending surfaces. In this case the C-C-C bending angle is denoted α'.

Figure 6: The geometries of some low energy critical points found by an "in-plane" rigid scan over the ground and first excited PES. Numbers below the figures denote values of (θ, α). Note that the figure in the center is on the ground electronic state and those on the outside are on the first excited electronic state.

Figure 7: The same as in Fig. 4 but for the "out-of-plane" scan. In this case the numbers below the figures denote values of (θ, α').

Figure 8: Examples of closed and open shell electronic configurations included in the active space in CAS(4,6) and their symbolic notation.

Figure 9: Calculated planar-linear geometries. The **1a**, **2a** geometries have closed shell configurations. The **1b**, **2b** geometries have open shell configurations.

Figure 10: Calculated planar-bent geometries. The **3a**, **4a** geometries have closed shell configurations. The **3b**, **4b** geometries have open shell configurations.

Figure 11: Molecular orbitals of the planar-linear C_{2h} and planar-bent C_{2v} symmetries.

Figure 12: The energy of planar-*anti* 1,3-dimethylallene as a function of the C–C–C bending.

Figure 13: The ground state electric-dipole moment as a function of θ for two values of α [$\alpha = 180$ for the linear configuration in the upper panel, and $\alpha = 160$ in a bent configuration in the lower panel]. Shown are the X (denoted by plus signs), Y (denoted by x's), and Z (stars) components of the electric dipole, as well as the total electric dipole moment (denoted by boxes).

Figure 14: As in Fig. 13, but for the first excited state electric-dipole moment.

Figure 15: The electric dipole moment as a function of θ and α - the dihedral and bending angles.

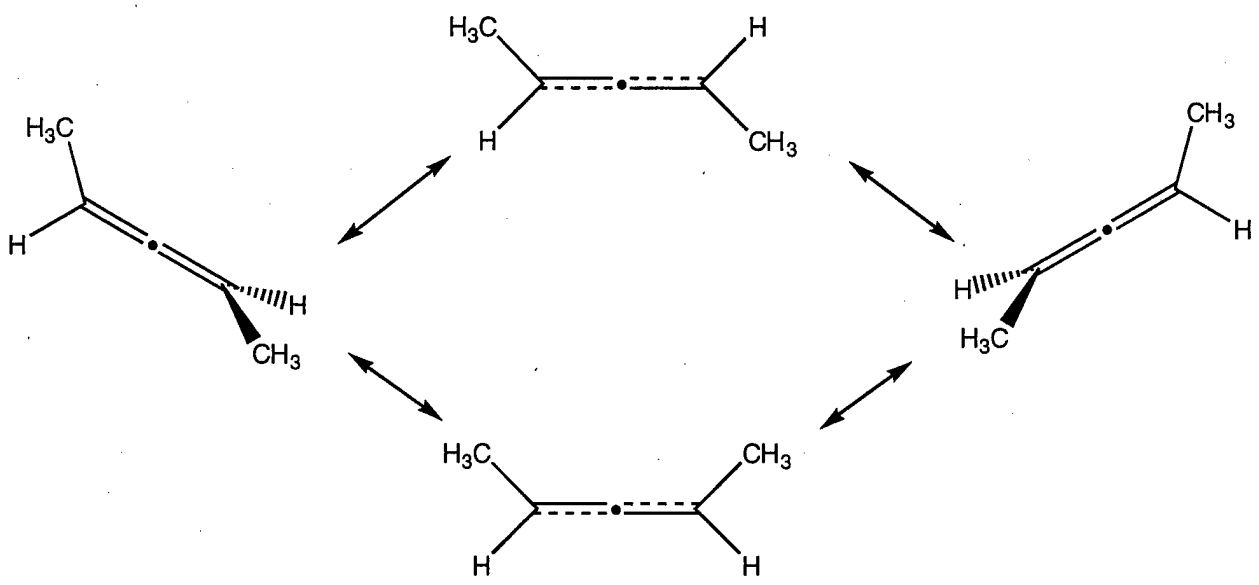
H3C
H
H
CH3
H3C
H
H
CH3
CH3
H
H
H3C
H3C
CH3
H
H

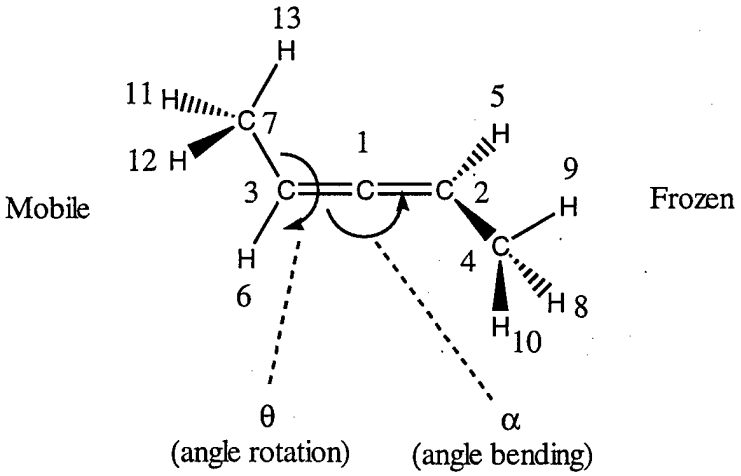
13
H
11 H
C 7
12 H
1
5
H
9
H
Mobile
3 C
C
C
2
Frozen
H
6
4
C
H 8
H 10
θ
(angle rotation)
α
(angle bending)

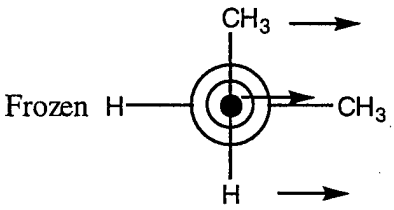

(a) In-plane bending

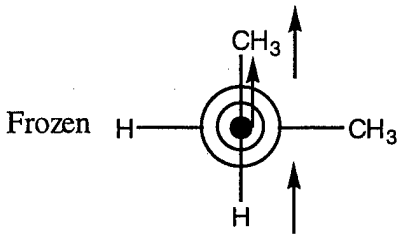

(b) Out-of-plane bending

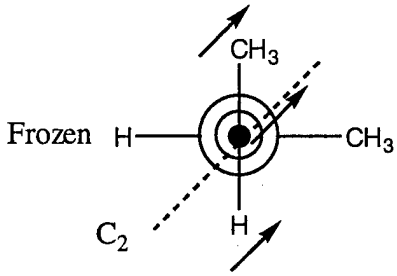

(c) Bending at 45 ^{o}

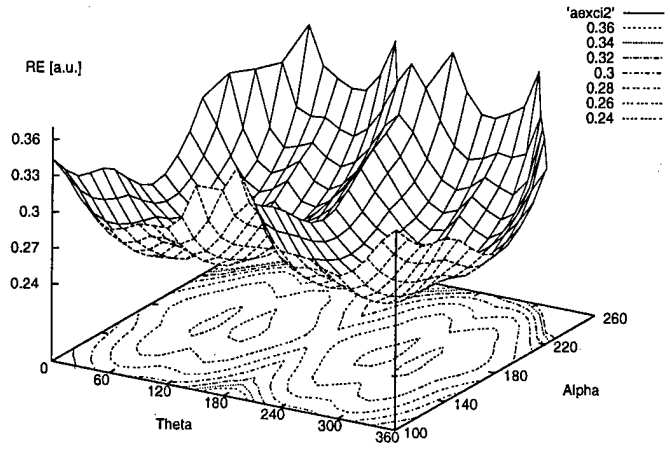

Second excited state surface.

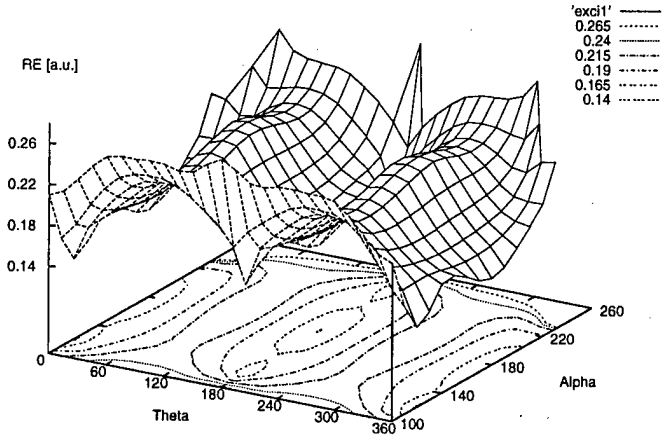

First excited state surface.

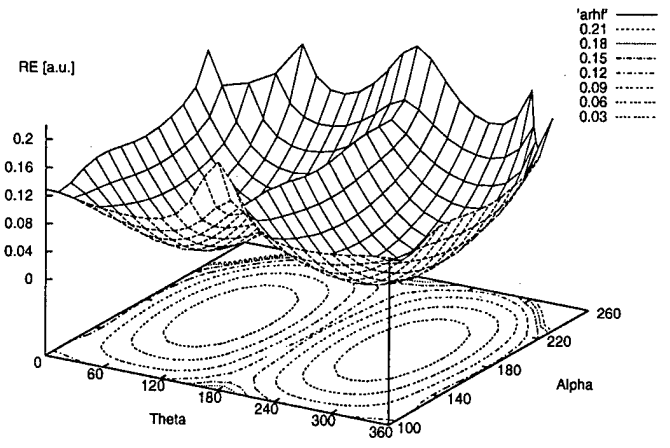

Ground state surface.

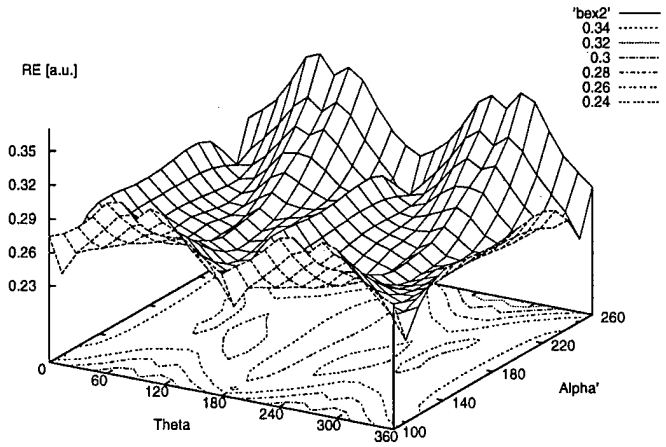

Second excited state surface.

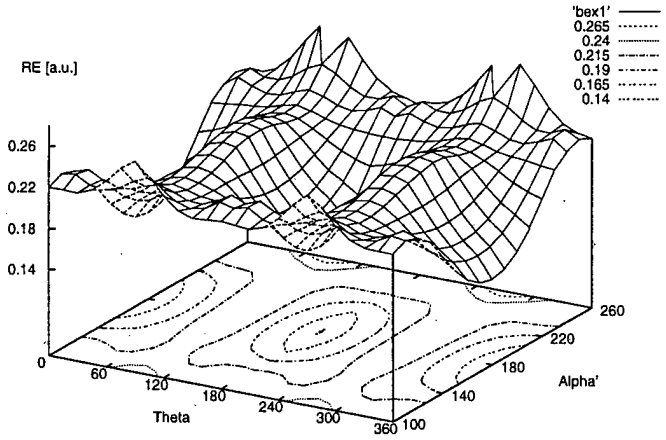

First excited state surface.

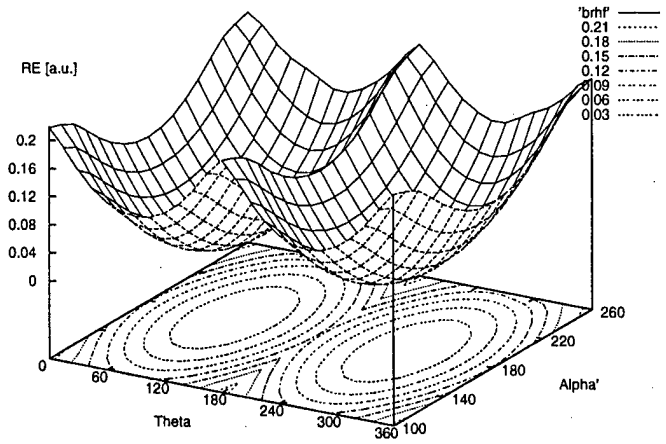

Ground state surface.

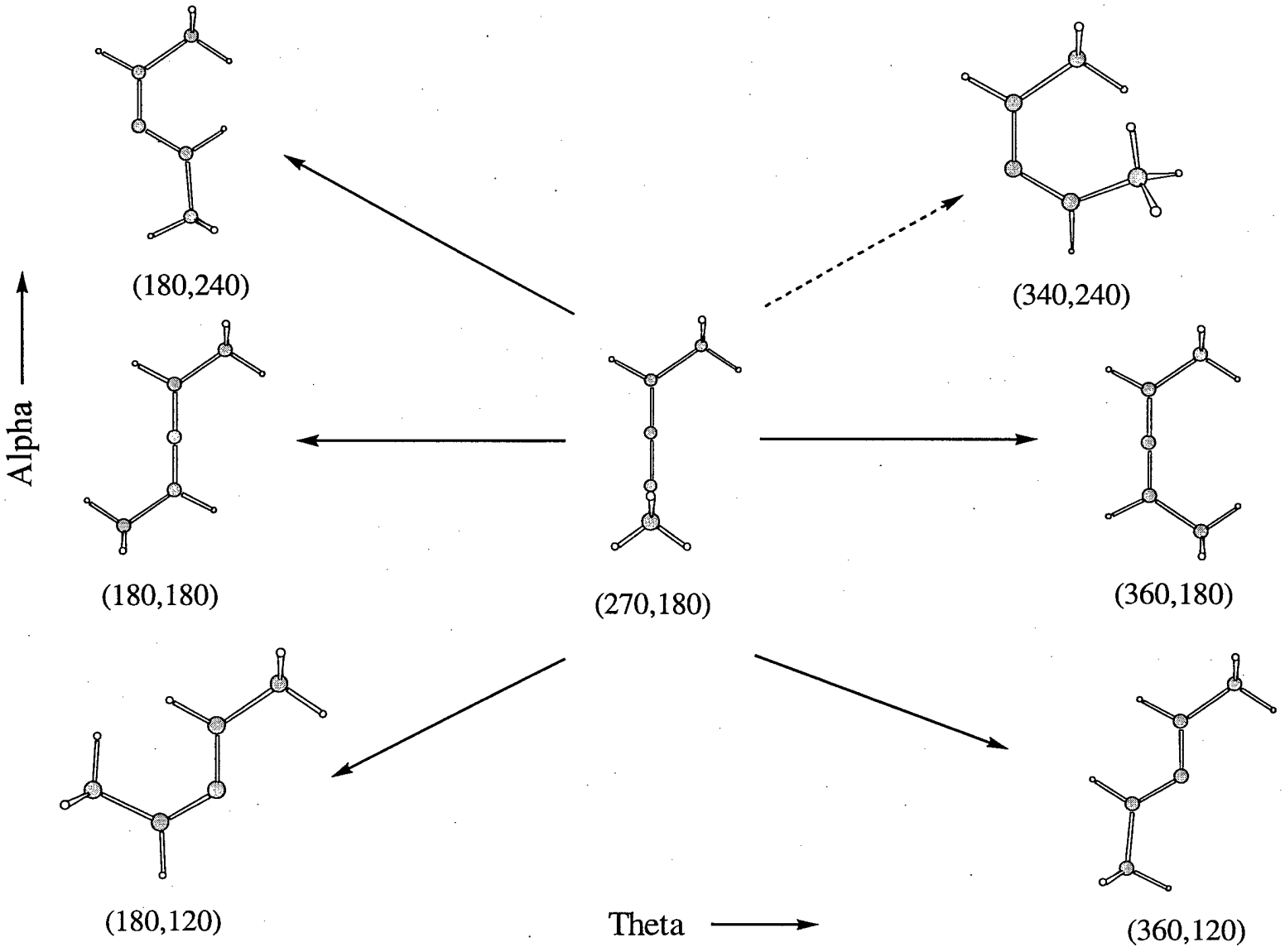
(180,240)
(340,240)
Alpha
(180,180)
(270,180)
(360,180)
(180,120)
Theta
(360,120)

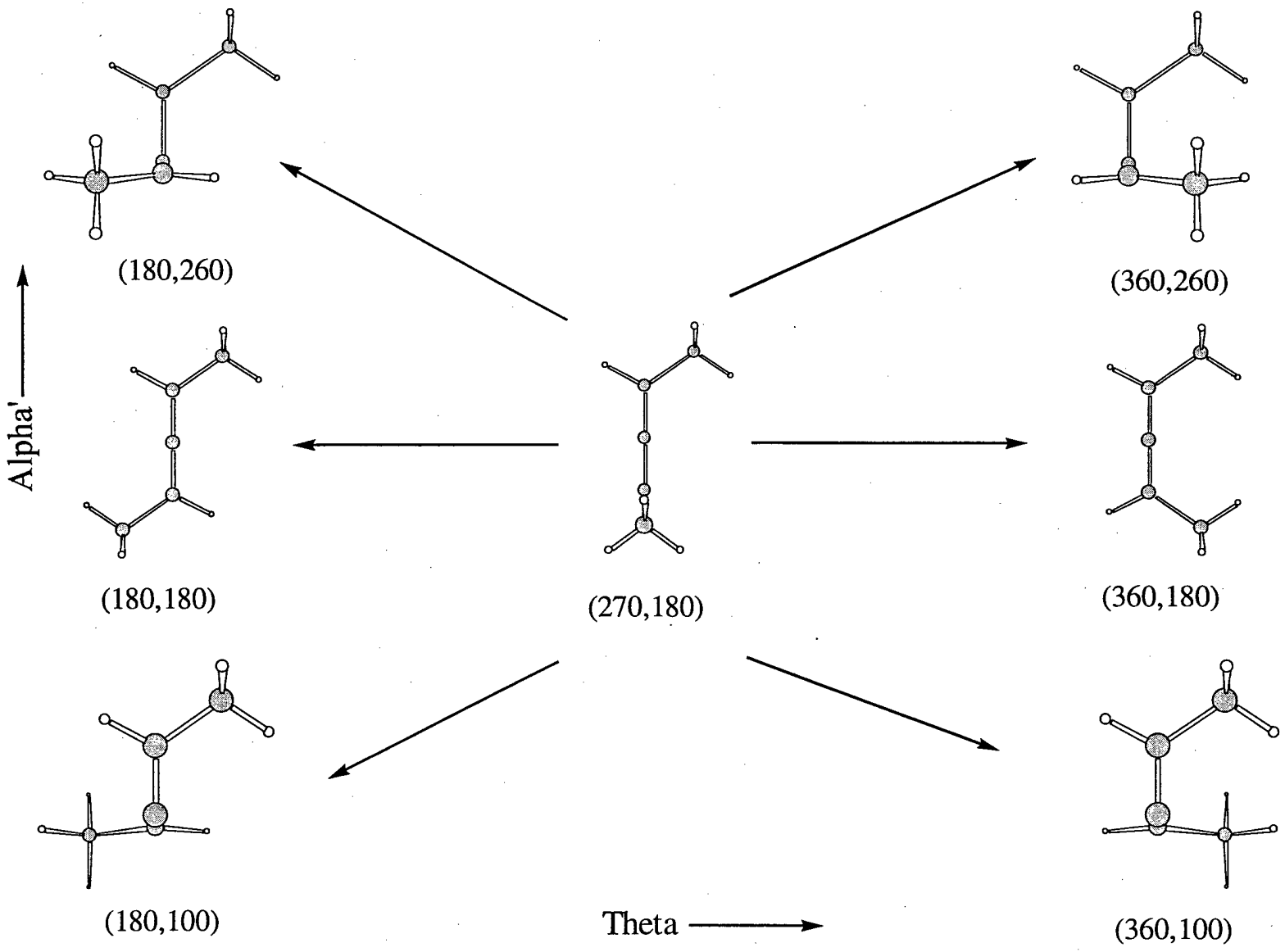
(180,260)
(360,260)
Alpha'
(180,180)
(270,180)
(360,180)
(180,100)
Theta
(360,100)

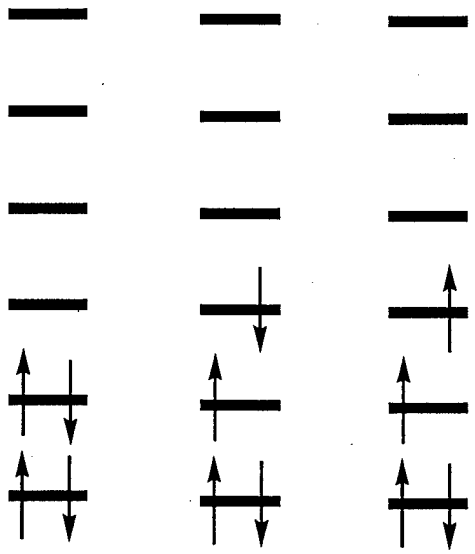

Closed shell
singlet
(1,2),(1,2)
a ß

Open shell
singlet
(1,2),(1,3)
a ß

Open shell
triplet
(1,2,3),(1)
a ß

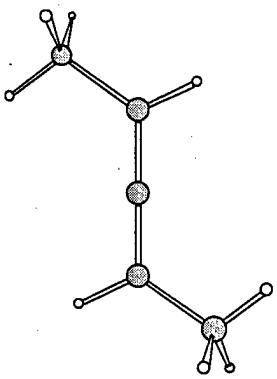

1a

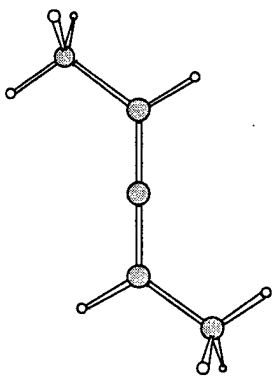

1b

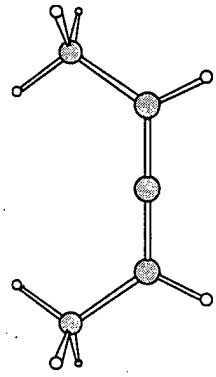

2a

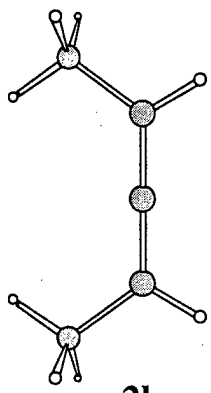

2b

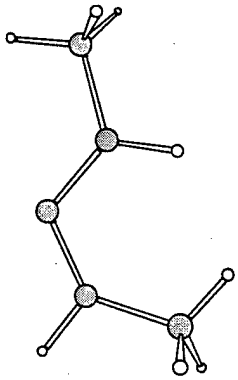

3a

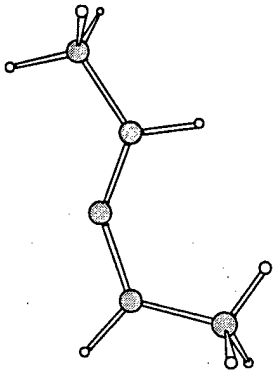

3b

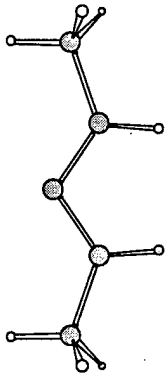

4a

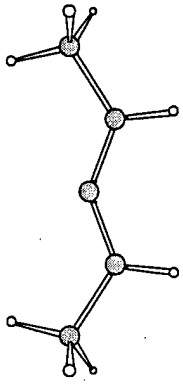

4b

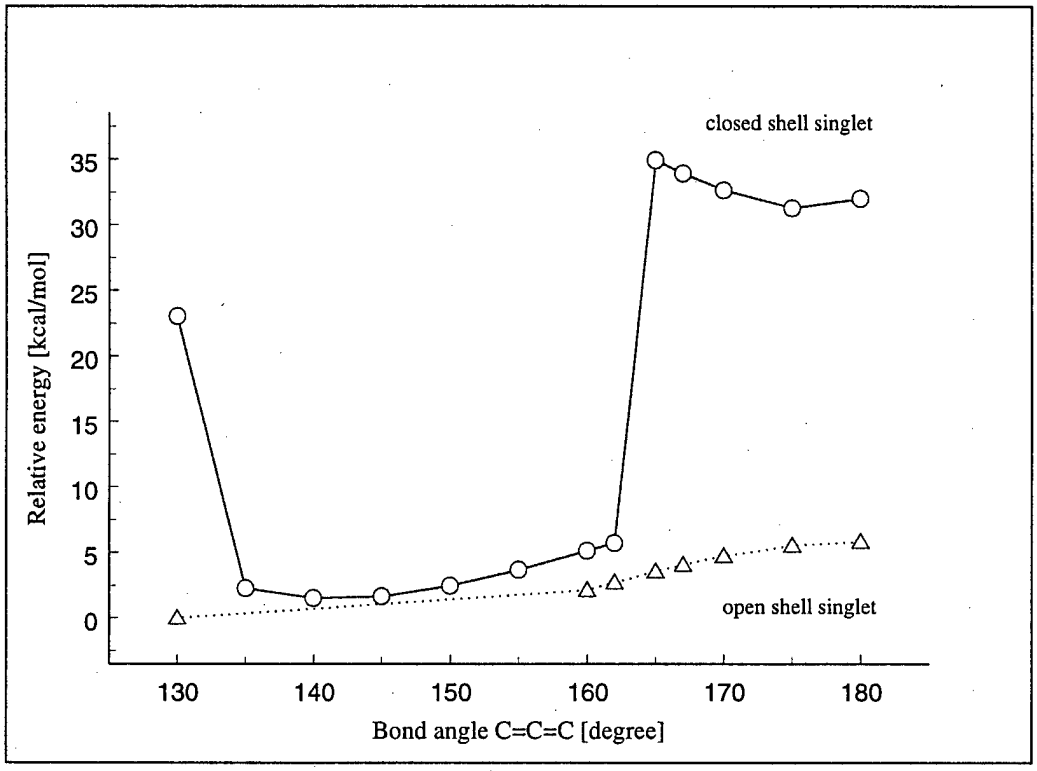
closed shell singlet
open shell singlet
Relative energy [kcal/mol]
0
5
10
15
20
25
30
35
130
140
150
160
170
180
Bond angle C=C=C [degree]

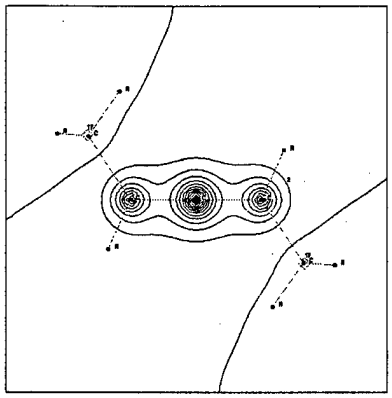

HOMO-1

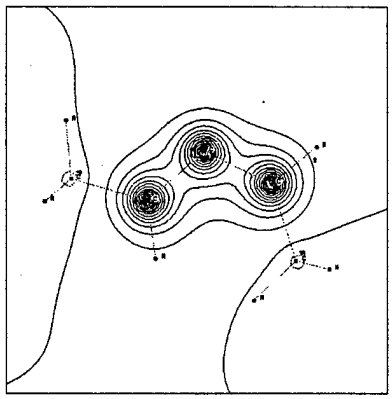

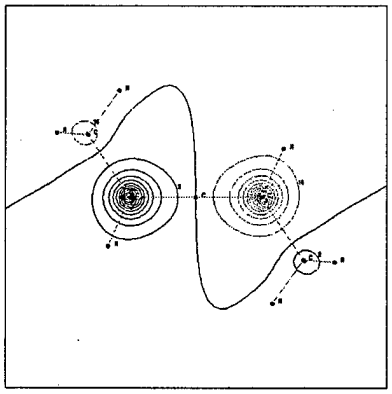

HOMO

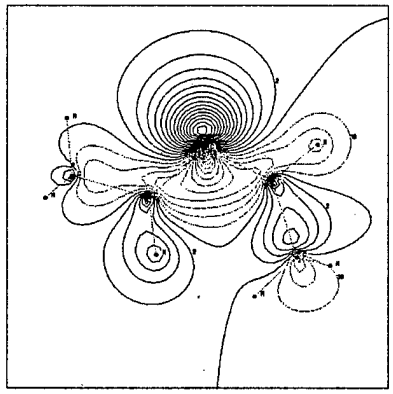

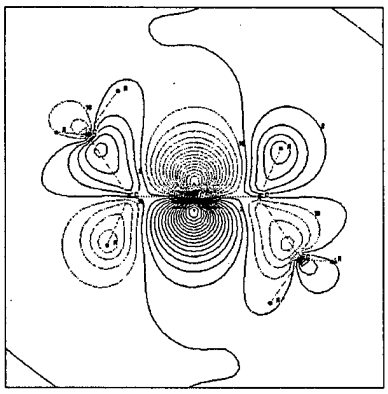

LUMO

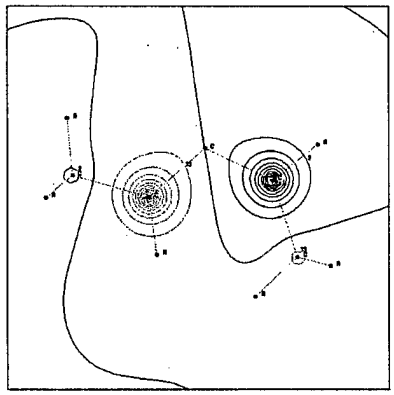

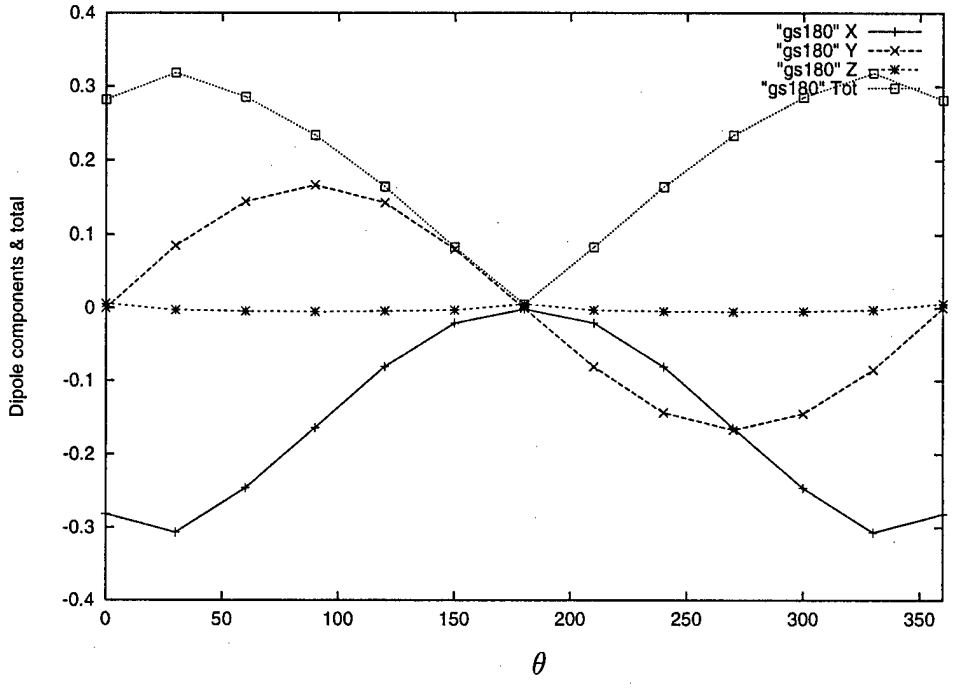
"gs180" X
"gs180" Y
"gs180" Z
"gs180" Tot
Dipole components & total
0.4
0.3
0.2
0.1
0
-0.1
-0.2
-0.3
-0.4
0
50
100
150
200
250
300
350
θ

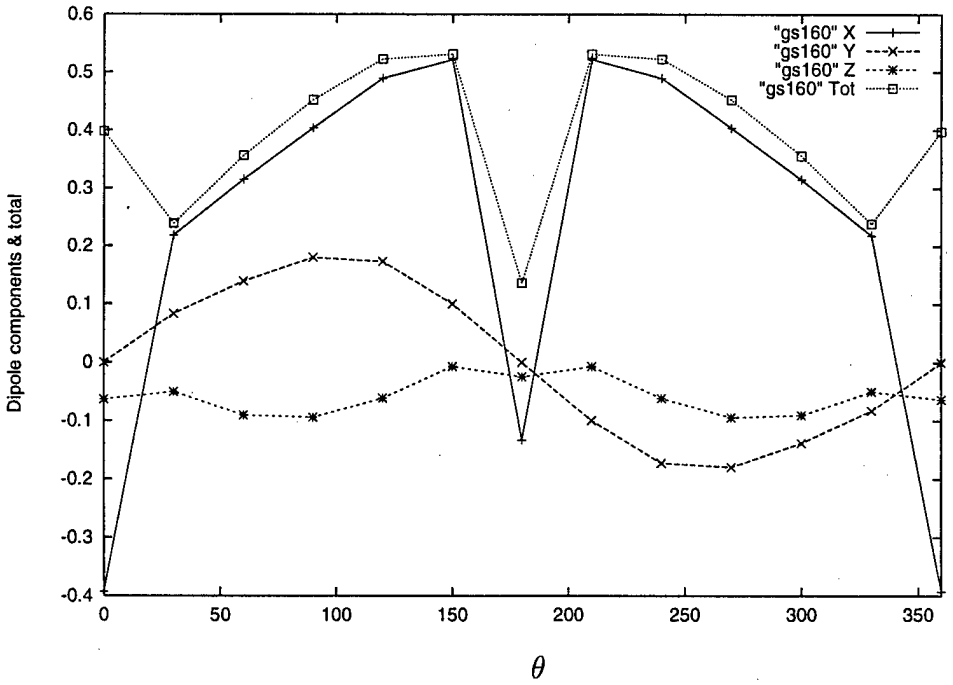
"gs160" X
"gs160" Y
"gs160" Z
"gs160" Tot
Dipole components & total
0.6
0.5
0.4
0.3
0.2
0.1
0
-0.1
-0.2
-0.3
-0.4
0
50
100
150
200
250
300
350
θ

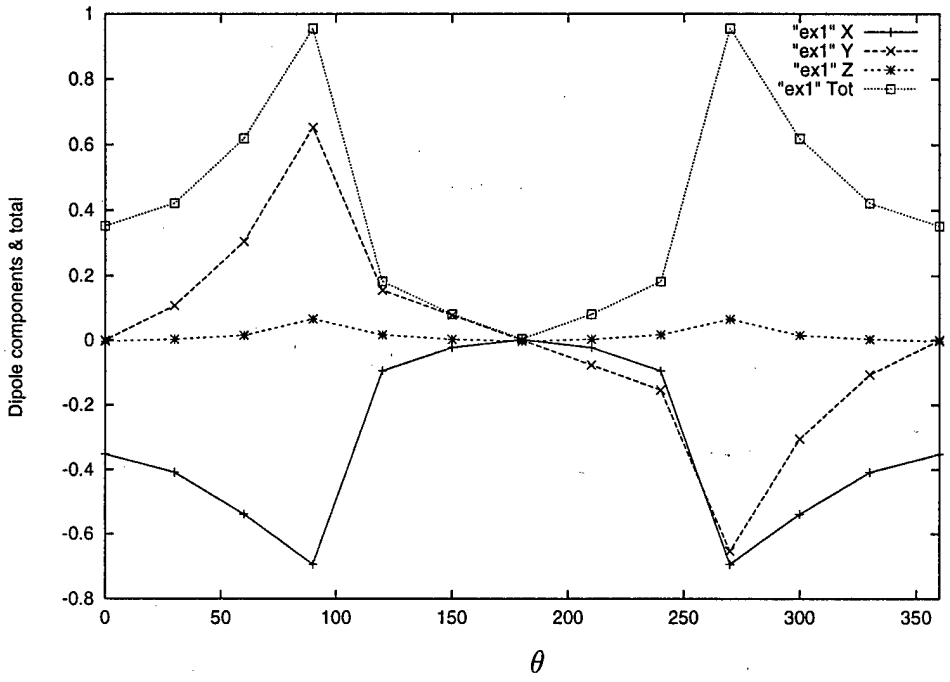
"ex1" X
"ex1" Y
"ex1" Z
"ex1" Tot
Dipole components & total
θ

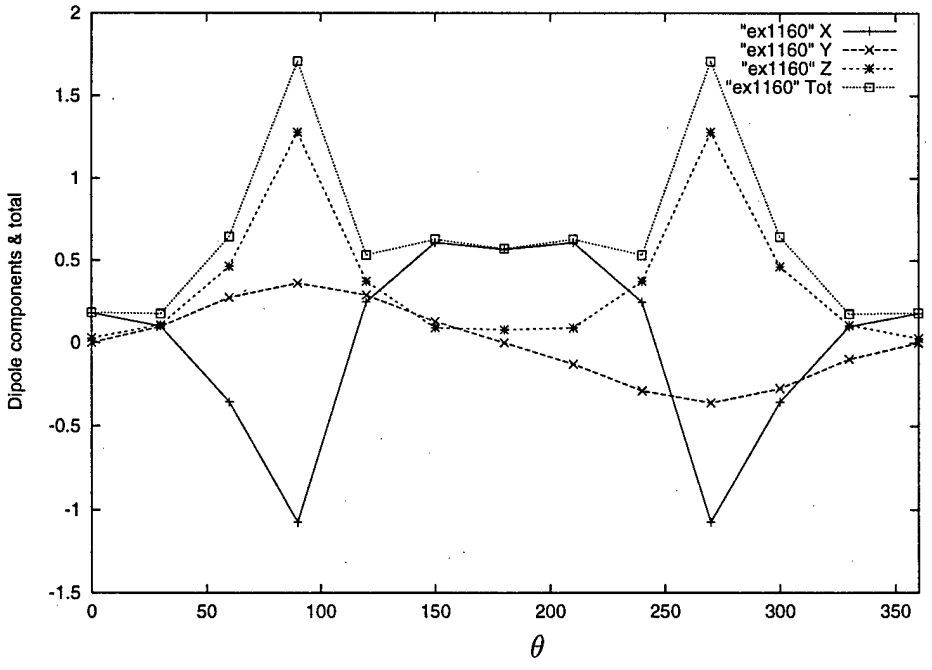
"ex1160" X
"ex1160" Y
"ex1160" Z
"ex1160" Tot
Dipole components & total
θ

First excited state total dipole moment

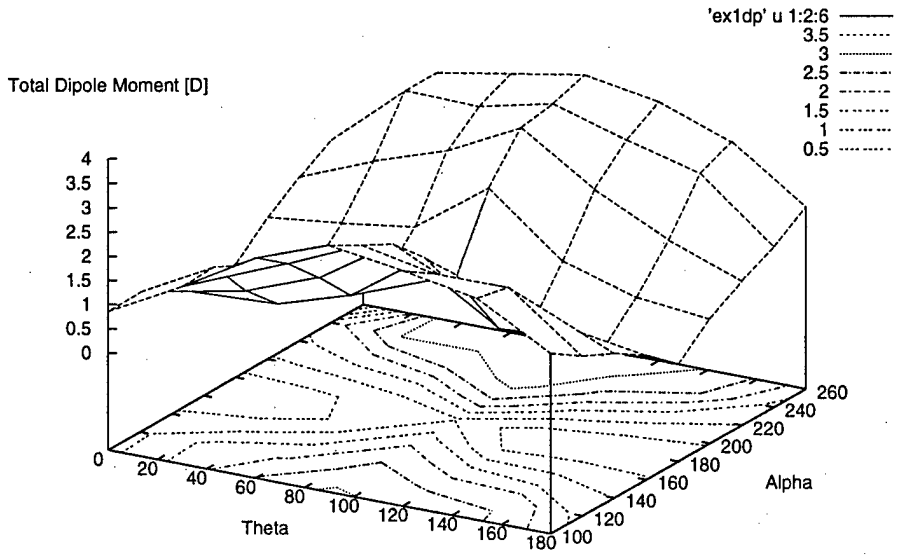

Ground state total dipole moment

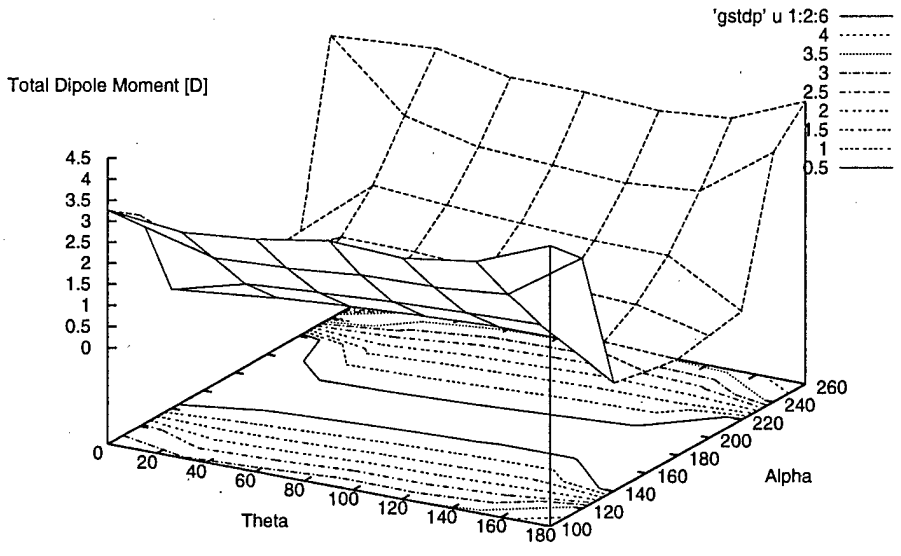

Theory of enantiomeric control in dimethylallene using achiral light

David Gerbasi, Moshe Shapiro,[a] and Paul Brumer
Chemical Physics Theory Group, The Department of Chemistry, University of Toronto, Toronto M5S 3H6, Canada

(Received 20 March 2001; accepted 1 August 2001)

Extensive control over enantiomer populations using achiral light is computationally demonstrated for J, M_J-selected 1,3 dimethylallene. In particular, by altering the detuning of one of three lasers incident on an J, M_J-polarized racemic mixture, one can alter the enantiomeric excess from ≈93% of the L enantiomer to ≈93% of the D enantiomer. © *2001 American Institute of Physics.* [DOI: 10.1063/1.1405116]

Considerable attention has recently been directed towards using lasers to alter the enantiomeric excess of an initially racemic mixture.[1–5] Traditionally, light-induced asymmetric synthesis scenarios have relied on the ability of left or right circularly polarized light[1] to differentiate between enantiomers via the (weak) magnetic dipole interaction. Recently[2,5] we demonstrated that it is possible to use linearly polarized light, and hence the strong dipole–electric field interaction, to control the interconversion of enantiomers if the molecules that are laser excited are M_j-selected, where M_j is the projection of the total angular momentum J along the direction of laser polarization.[6] Related arguments have been made by others about enantiomer control for oriented molecules,[3,4] with Ref. 4 relying upon the excitation of oriented molecules with shaped laser pulses. In both cases, specifying conditions on the molecules plus including laser phase introduces chirality into the total electric field-molecule system.

In our M_j-selected scenario a particular laser arrangement, discussed below, serves to excite more or less of the population of one enantiomer than the other. The excited molecules then collisionally relax and radiate back to the D and L ground state.[7] Laser pumping followed by relaxation in the ground and excited states is repeated again and again until convergence, leading to an excess of population of the desired enantiomer. This scenario, which we call laser distillation, is one example of a more general theorem[8] on possible scenarios for asymmetric synthesis based on the dipole–electric field interaction. It is of interest since neither the incident light nor the initial molecular system are chiral, but chiral discrimination and the enhancement of the population of one enantiomer over the other in a racemic mixture is nonetheless possible.

In this communication we demonstrate computationally that 1,3 dimethylallene provides an excellent candidate for this scenario, and that virtually total control over the enantiomeric excess resulting from irradiating a racemic mixture of 1,3 dimethylallene is possible. Specifically, we use our recently computed[9] potential energy surfaces and electric dipole moments for 1,3 dimethylallene in conjunction with a three-laser version of the laser distillation scenario, to demonstrate a vast range of control over the enantiomeric excess in an irradiated M_j polarized racemic mixture of D and L 1,3 dimethylallene.

Consider first the initial laser excitation scheme. Specifically, we examine a three-laser extension[10] of the scenario discussed in Ref. 2. Here, an electric field $\mathbf{E}(t)$ comprising three pulses is incident on a racemic mixture of chiral molecules in a fixed M_j state. The field $\mathbf{E}(t)$ is given by

$$\mathbf{E}(t)=\sum_{k=0,1,2}\mathbf{E}_k(t)\equiv\sum_{k=0,1,2}2\hat{\epsilon}_k\,\mathrm{Re}[\epsilon_k(t)\exp(i\omega_k(t))], \tag{1}$$

where $\epsilon_k(t)$ is the pulse envelope, ω_k is the central laser frequency, and $\hat{\epsilon}_k$ is the polarization direction. The central frequency of $\epsilon_1(t)$ is chosen to couple the ground vibrational states $|D\rangle$ and $|L\rangle$ of the right and left handed enantiomers with energies $E_D=E_L$ to eigenstate $|1\rangle$ of energy E_1, $\epsilon_2(t)$ to couple eigenstates $|D\rangle$ and $|L\rangle$ to state $|2\rangle$ of energy E_2, and $\epsilon_0(t)$ couples states $|1\rangle$ and $|2\rangle$ to one another. Here $|1\rangle$ and $|2\rangle$ are eigenstates of nuclear motion in the excited electronic state, and we choose $\hat{\epsilon}_0=\hat{\epsilon}_1=\hat{\epsilon}_2$ to define the z axis.

The molecule under consideration is assumed characterized by an achiral excited potential energy surface[11] so that $|1\rangle$ can be chosen to be symmetric with respect to inversion and $|2\rangle$ is antisymmetric with respect to inversion. By choosing ω_i near-resonant with $\omega_{iD}\equiv(E_i-E_D)/\hbar$, $(i=1,2)$ and $\omega_0\approx\omega_{21}\equiv(E_2-E_1)/\hbar$, and by making the pulse widths narrow, the system is well described as a laser coupled four level system. This being the case, we expand the total wave function $|\Psi\rangle$ as

$$\begin{aligned}|\Psi\rangle=&b_D(t)\exp(-iE_Dt/\hbar)|D\rangle+b_L(t)\\&\times\exp(-iE_Lt/\hbar)|L\rangle+b_1(t)\exp(-iE_1t/\hbar)|1\rangle\\&+b_2(t)\exp(-iE_2t/\hbar)|2\rangle.\end{aligned} \tag{2}$$

Substituting Eq. (2) into the time dependent Schrodinger equation gives the following set of coupled differential equations within the rotating wave approximation:

[a]Permanent address: Chemical Physics Department, The Weizmann Institute of Science, Rehovot, Israel 76100.

 © 2001 American Institute of Physics

Downloaded 24 Oct 2001 to 142.150.224.5. Redistribution subject to AIP license or copyright, see http://ojps.aip.org/jcpo/jcpcr.jsp

$$\begin{aligned}
\dot{b}_1 &= i\exp(i\Delta_1 t)\Omega^*_{D,1}[b_D + b_L] + i\exp(i\Delta_0 t)\Omega^*_0 b_2 \\
\dot{b}_2 &= i\exp(i\Delta_2 t)\Omega^*_{D,2}[b_D - b_L] + i\exp(-i\Delta_0 t)\Omega_0 b_1 \\
\dot{b}_D &= i\exp(-i\Delta_1 t)\Omega_{D,1} b_1 + i\exp(-i\Delta_2 t)\Omega_{D,2} b_2 \\
\dot{b}_L &= i\exp(-i\Delta_1 t)\Omega_{D,1} b_1 - i\exp(-i\Delta_2 t)\Omega_{D,2} b_2 .
\end{aligned} \tag{3}$$

Here $\Omega_{ij}(t) \equiv \mu_{ij}\epsilon_j(t)/\hbar$, $\Delta_j \equiv \omega_{j_D} - \omega_j$, $\mu_{ij} \equiv \langle i|\vec{\mu}_k \cdot \hat{\epsilon}_k|j\rangle$, with $i = D,L$, $k = 0,1,2$, $j = 1,2$, $\Delta_0 \equiv \omega_{21} - \omega_0$, and $\Omega_0(t) \equiv \mu_{12}\epsilon_0(t)/\hbar$. The quantity $\vec{\mu}_i$ is the electric dipole operator relevant to the particular transition. In obtaining Eq. (3) we have used the relations $\Omega_{D,1} = \Omega_{L,1}$, and $\Omega_{D,2} = -\Omega_{L,2}$, which are consequences[2] of the symmetric and antisymmetric nature of $|1\rangle$ and $|2\rangle$. The extent to which control can be achieved over enantiomer populations depends upon numerous system parameters, including the nature of the states $|1\rangle$, $|2\rangle$, the laser parameters, etc. Equation (3) can be solved numerically for various system parameters to display this dependence, as shown below. Specifically, we present results for the probabilities $|b_D|^2$ and $|b_L|^2$ at long times. Note that control arises, as in all coherent control scenarios, through quantum interference effects. Specifically, the presence of the three excitation frequencies in Eq. (1) allows for at least two interfering routes for excitation from states $|D\rangle$ and $|L\rangle$ to state $|1\rangle$ or $|2\rangle$.

To apply this approach to dimethylallene we require the Franck–Condon factors for excitation from the D and L eigenstates of the ground electronic state to the excited state levels. Essential input into this study are the results of our previous molecular structure computations.[9] Specifically, we constructed a cut through the full dimethylallene potential surface by computing ground and excited state energies as a function of the dihedral angle α between the $H_3C—C{=}C$ and $C{=}C—CH_3$ planes and the C—C—C bending angle θ. Consideration of these cuts showed that dimethylallene, a chiral molecule by virtue of its overall molecular geometry, possesses two stable conformations in the ground state, corresponding to the right- and left-handed enantiomeric states, and does have an achiral first electronic state,[9] as required above. Further, we computed the electronic dipole moment[9] and the eigenstates of the potentials as a function of θ and α, the latter using the discrete variable representation with periodic boundary conditions[12] in α. Only high lying states were found to give significant Franck–Condon overlap with the ground state wave functions, hence the DVR computations required very large numbers of basis function (e.g., on the order of 25 000) for convergence. In addition, we approximate the rotational eigenfunctions of dimethylallene by those of a symmetric top with quantum numbers J, M_J, λ, where λ is the projection of J on a body fixed axis.

The reliability of our calculated eigenstates was verified by comparing computed absorption spectra to experimental data. Starting with Fermi's golden rule, the absorption cross section is given by $\sigma = D^2\omega L(\omega)/(6\epsilon_0\hbar c)$, where $D^2 = e^2|\mu|^2$ is the square of the transition dipole moment, ω is the transition frequency, and $L(\omega)$ is the lineshape function which includes both spontaneous emission and Doppler Broadening. The results are remarkably accurate when compared to experimental values.[13] That is, the computed extinction coefficient at the absorption maximum of 196.3 nm is 6601 ($cm^{-1}\,mol^{-1}\,L$) as compared to the experimental value of 6300, with the absorption maxima shifted by only 6 nm.

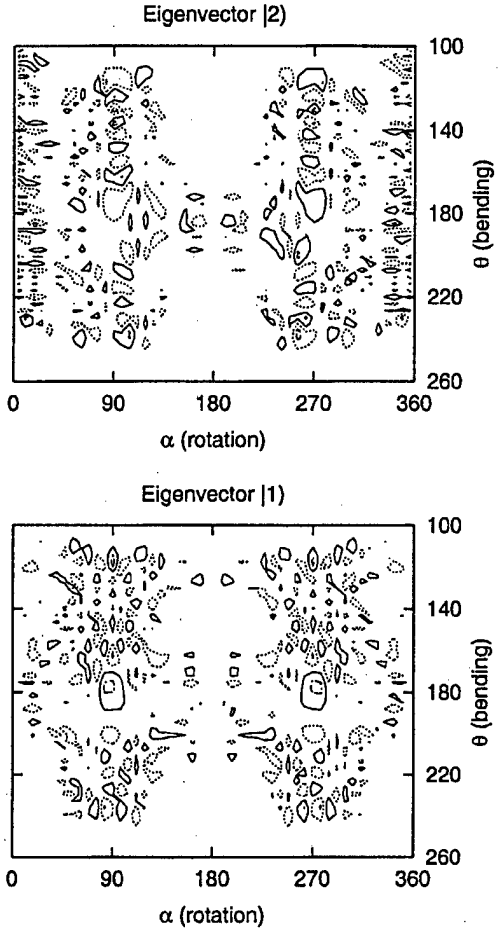

FIG. 1. Contour plots of $|1\rangle$ and $|2\rangle$ where dash–dash lines = 0.012 a.u., dot–dot lines = 0.004 a.u., solid lines = −0.004 a.u., and dot–dash lines = −0.012 a.u. Note that $|1\rangle$ is symmetric with respect to inversion and $|2\rangle$ is antisymmetric. Inversion here corresponds to changing $(\alpha - 180°)$ to $(\alpha + 180°)$.

Below we choose two eigenstates which have large Franck–Condon transition probabilities to demonstrate the extent of possible control. The α, θ dependence of the wave functions for these two states, shown in Fig. 1, make clear the symmetric and antisymmetric character of the states, as well as the very high level of excitation to which they correspond. Since we approximate dimethylallene by a symmetric top, we consider specific J, M_J, λ to J',M_J,λ' transitions. Our computations gave, for these wave functions and, for example, for rotational quantum numbers J, M_J,λ of 3, 2, 2 and 4, 2, 2 for the ground and excited electronic states: $\langle 1|\mu|D\rangle = \langle 1|\mu|L\rangle = 5.44\times10^{-3}$ a.u., $\langle 2|\mu|D\rangle = -\langle 2|\mu|L\rangle = 4.01\times10^{-3}$ a.u., $\langle 1|\mu|2\rangle = -8.17\times10^{-4}$ a.u., and $\omega_{21} = 261.78\,cm^{-1}$. Many other pairs of states defined by different vibrational or rotational quantum numbers show qualitatively similar control to the results for this case, discussed below.

We consider the extent of control achievable using Gaussian pulses of the form

Downloaded 24 Oct 2001 to 142.150.224.5. Redistribution subject to AIP license or copyright, see http://ojps.aip.org/jcpo/jcpcr.jsp

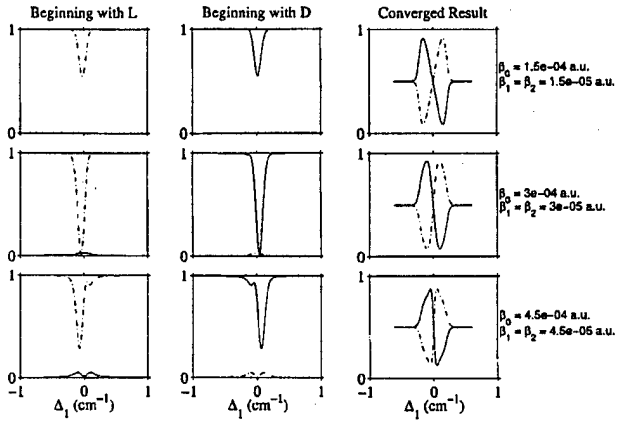

FIG. 2. Control over dimethylallene enantiomer populations as a function of the detuning Δ_1 for various laser powers. The first column corresponds to probabilities of L (dot–dash curves) and D (solid curves) after a single laser pulse, assuming that the initial state is all L, the second column are similar, but for an initial state which is all D. The right most column corresponds to the probabilities of L and D when one starts with a racemic mixture and carries out repeated excitations followed by spontaneous emission and collisional relaxation.

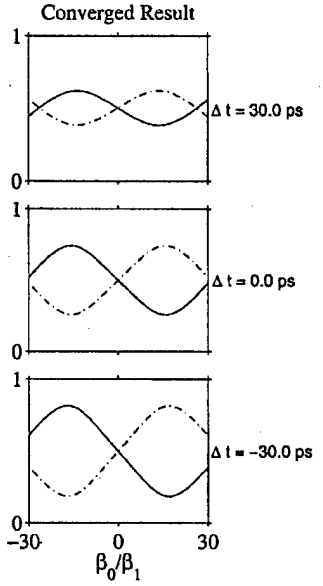

FIG. 3. Control over dimethylallene enantiomer probability as a function of the field ratio β_0/β_1 for $\beta_1=\beta_2=3.0\times10^{-5}$ a.u., $\Delta_1=0.09\ \mathrm{cm}^{-1}$ and various values of the time delay $\Delta t=t_1-t_0$ with $t_1=t_2$.

$$\epsilon_\ell(t)=\beta_\ell\exp\{-[(t-t_\ell)/\alpha_\ell]^2\}\quad(l=0,1,2). \tag{4}$$

Results are presented for pulses with $\beta_0=10\beta_1$, $\beta_1=\beta_2$ and with all pulses of 100 ps duration full width at half maximum. These pulses are sufficiently narrow in frequency so that they excite only single levels in the excited state region, where the density of states for our 2-dimensional model is 0.34 states per wave number. Control results are shown in Fig. 2 as a function of the detuning Δ_1 of ω_1 from $(E_1-E_D)/\hbar$ and with $\Delta_2=\Delta_1$ for various laser powers. The other pulse, $\omega_0=261.78\ \mathrm{cm}^{-1}$, is resonant with the transition noted above. Three different sets of results are shown—those corresponding to a single pulse sequence starting with an initial state which is solely L (column 1), those corresponding to a single pulse sequence where the initial state is solely D (column 2), and the "converged result" which are composed of repeated steps of radiative excitation followed by relaxation until equilibrium has been established (column 3). In the latter case the initial state is taken as a racemic mixture. The results clearly show outstanding enantiomeric control over the dimethylallene enantiomers for a wide variety of powers. For example, the most impressive result is achieved for $\Delta_1=-0.0986\ \mathrm{cm}^{-1}$ and $\beta_0=3.0\times10^{-4}$ a.u., $\beta_1=\beta_2=3.0\times10^{-5}$ a.u., corresponding to laser powers of $3.16\times10^9\ \mathrm{W/cm^2}$ and $3.16\times10^7\ \mathrm{W/cm^2}$, respectively. Here a racemic mixture of dimethylallene can be converted, after a series of pulses, to a mixture of dimethylallene, containing 92.7% of the D-dimethylallene in this state. Similarly, detuning to $\Delta_1=0.0986\ \mathrm{cm}^{-1}$ results in a similar enhancement of L-dimethylallene. Slightly lower extremes of control are seen to be achievable for the two other laser powers shown. Further, control was achievable to field strengths down to $10^4\ \mathrm{W/cm^2}$. Control can also be affected by varying other laser parameters such as the time ordering of the pulses, the relative laser powers, the remaining detunings, etc. For example, Fig. 3 shows control as a function of the field strength ratio β_0/β_1 for $\beta_1=\beta_2=3.0\times10^{-5}$ a.u. for various different time orderings $\Delta t=t_0-t_1$, with $t_1=t_2$. Control is clearly affected by a wide range of control parameters.

More detailed consideration of the results shown in Fig. 2 is enlightening. To do so, note that the probability $\mathcal{P}_D$ for forming the D enantiomer, after repeated iterations of laser excitation followed by collisional and radiative relaxation is given by[2]

$$\mathcal{P}_D=\frac{1+P_D'-P_L'}{2-P_D+P_L+P_D'-P_L'}, \tag{5}$$

where P_D and P_L denote the probabilities of $|D\rangle$ and $|L\rangle$ resulting from a single laser pulse sequence assuming that the system is initially solely in $|D\rangle$ (i.e. the results in column 2 of Fig. 2), and P_D' and P_L' denote results of a single laser pulse sequence exciting a system composed solely of $|L\rangle$ (i.e. the results shown in column 1 of Fig. 2). The probability of forming L in the specific J, M_J-state after the full iterative process is $\mathcal{P}_L=1-\mathcal{P}_D$. (Note that it is $\mathcal{P}_L$ and $\mathcal{P}_D$ that are shown as the "converged results" in Figs. 2 and 3.)

Given Eq. (5) we may extract trends that are responsible for increasingly good enantiomeric discrimination in the converged results. For example, results in Fig. 2 show that the enantiomeric discrimination is best for $|P_D-P_L|\approx1$ and $|P_D'-P_L'|\approx1$, but with $P_D\neq P_L'$ and $P_D'\neq P_L$. For example, at the maximal control point $\Delta_1=-0.153\ \mathrm{cm}^{-1}$ in the top row in Fig. 2 $P_D=0.998\,40$, $P_L'=0.975\,92$, and $P_D'\approx P_L\approx7.0\times10^{-3}$. In this instance the iterative laser distillation process gives an excellent result of $\mathcal{P}_D=0.915$. (Note that the small difference between P_D and P_L' and between P_D' and P_L is necessary for control; if these quantities are equal then enantiomeric control is lost.) Such large values of P_D and P_L' are, of course, not necessary for high quality control. For example, the maximum control in the middle row of Fig.

Downloaded 24 Oct 2001 to 142.150.224.5. Redistribution subject to AIP license or copyright, see http://ojps.aip.org/jcpo/jcpcr.jsp

2 (at $\Delta_1 = -0.0986\,\mathrm{cm}^{-1}$, giving the results noted above, i.e., $\mathcal{P}_D = 0.927$) is obtained with $P'_L = 0.452\,99$, $P_D = 0.973\,50$, $P_L = P'_D = 0.017\,75$.

Finally, note that each Δ_1 point in the converged result column in Fig. 2 required a different number of iterations for convergence, although none required an excessive number of pulses. For example, the point of maximal control the top row of Fig. 2 required 852 pulses, the middle row required 42 pulses, and the bottom row required 29 pulses. In general, the number of pulses required is related to the difference between P_D and P'_L; the greater the difference, the less amount of pulses will be needed to reach equilibrium. These numbers constitute lower bounds to the real experiment which include other levels to which the system radiatively and collisionally relaxes.

To implement the above procedure experimentally one could impose an external magnetic field to split the M_J levels and excite the system on the required J, M_J to J',M_J transitions by appropriate laser tuning. Collisions and radiative relaxation re-equilibrate the J, M_J levels within each enantiomer. The laser pulses followed by re-equilibration is repeated many times. In this way we are able to affect the populations of all J, M_J levels of the system, converting them from L to D, even though we pump only on a particular J, M_J to J',M_J transition.

In summary, we have shown that dimethylallene is a strong candidate for laser control over the enantiomeric excess, which can be extensively enhanced using linearly polarized light from an initial racemic mixture. The method emphasizes the role of quantum interference in the symmetry-breaking control. Enantiomeric excesses of up to 92.7% can be achieved using very realistic pulse parameters. A full computation utilizing the asymmetric top levels of dimethylallene and including alternate pulse durations, collisional effects and competition due to internal conversion are underway.

The authors are grateful to Professor Malcolm Bersohn, University of Toronto, for suggesting that they consider dimethylallene as a candidate for the laser distillation scenario. Einat Frishman is acknowledged for helpful discussion and for computer programs. One of the authors (D.G.) holds a PGSA Fellowship from NSERC, Canada. M.S. acknowledges partial support for this work from the EU IHP Program (COCOMO Network) and the Minerva Foundation, Germany. This work was supported by the U.S. Office of Naval Research.

[1] A. Salam and W. J. Meath, Chem. Phys. **228**, 115 (1998); J. Chem. Phys. **106**, 7865 (1997).
[2] M. Shapiro, E. Frishman, and P. Brumer, Phys. Rev. Lett. **84**, 1669 (2000).
[3] Y. Fujimura, L. Gonalez, K. Hoki, J. Manz, and Y. Ohtsuki, Chem. Phys. Lett. **306**, 1 (1999); **310**, 578 (1999). Note, that this paper studies control starting with an initial superposition state, rather than with a racemic mixture.
[4] K. Hoki, Y. Ohtsuki, and Y. Fujimura, J. Chem. Phys. **114**, 1575 (2001). See also, Y. Fujimura, L. Gonzalez, K. Hoki, D. Kroner, J. Manz, and Y. Ohtsuki, Angew. Chem. Int. Ed. Engl. **39**, 4586 (2000); K. Hoki, D. Kroner, and J. Manz, Chem. Phys. **267**, 59 (2001).
[5] See also a related approach, M. Shapiro and P. Brumer, J. Chem. Phys. **95**, 8658 (1991).
[6] The restriction to a single M_J state is implicit, rather than explicit, in Ref. 2. If, in addition, the molecule is a symmetric top then one must consider inducing excitations between specific pairs of J,M_J, λ levels, where λ is the projection of J along a body fixed axis. A detailed discussion of angular momentum and associated selection rules is provided in M. Shapiro, E. Frishman, and P. Brumer (in preparation).
[7] In actuality, radiative emission occurs to all levels in the ground state. However, we assume rapid thermal equilibration of state populations so that the overall final control will be the same as if populations did radiate to the single ground state.
[8] P. Brumer and M. Shapiro, J. Chem. Phys. (submitted).
[9] E. Deretey, P. Brumer, and M. Shapiro, J. Phys. Chem. (submitted).
[10] In the previously considered scenario (Ref. 2) $\epsilon_1(t)$ and $\epsilon_2(t)$ were considered components of a single electric field.
[11] Systems with chiral electronic ground states and achiral excited electronic states are well established models in studies of chiral systems. See, for example, M. Quack, Angew. Chem. Int. Ed. Engl. **28**, 571 (1989); J. A. Cina and R. A. Harris, J. Chem. Phys. **100**, 2531 (1994); C. S. Maierle and R. A. Harris, *ibid.* **109**, 3713 (1998).
[12] D. T. Colbert and W. H. Miller, J. Chem. Phys. **96**, 1982 (1992).
[13] A. Rauk, A. F. Drake, and S. F. Mason, J. Am. Chem. Soc. **101**, 2284 (1979).

Downloaded 24 Oct 2001 to 142.150.224.5. Redistribution subject to AIP license or copyright, see http://ojps.aip.org/jcpo/jcpcr.jsp

8

A direct approach to one photon interference contributions in the coherent control of photodissociation

Victor S. Batista[a] and Paul Brumer
Chemical Physics Theory Group, Department of Chemistry, and Photonics Research Ontario, University of Toronto, Toronto, Ontario M5S 3H6, Canada

(Received 13 March 2001; accepted 29 March 2001)

Formally exact quantum mechanical expressions for cumulative transition matrix elements $\mu_{jk}(\xi,E)=\Sigma_n\langle j|\mu_\varepsilon|E,\xi,n^-\rangle\langle E,\xi,n^-|\mu_\varepsilon|k\rangle$, central to one photon coherent control scenarios of photodissociation, are derived. The resultant approach bypasses the need for solving the complete state-to-state quantum mechanical reactive scattering problem to obtain control results. These exact expressions are implemented both quantum mechanically and via a semiclassical initial value representation method to investigate coherent control in the generic photodissociation of a triatomic into more than one product. The semiclassical approach is shown to provide an accurate description of bimolecular control in this system. © *2001 American Institute of Physics.*
[DOI: 10.1063/1.1372713]

I. INTRODUCTION

Developing new laser techniques for controlling the quantum dynamics of polyatomic systems is one of the important challenges in modern photochemistry. The most successful of these approaches is coherent control,[1,2] where quantum interference effects are manipulated to alter the dynamics. With coherent control having been demonstrated both computationally and experimentally for simple photodissociation reactions, the challenges ahead range from investigating yield control in complex molecular environments to demonstrating routes to new products in realistic polyatomic reactions.

Progress in coherent control relies heavily on theoretical and computational approaches which allow an understanding of the dominant interference phenomena and provide a means of designing new control scenarios. However, such approaches are currently restricted to small systems, a limitation of modern computational quantum mechanics. The purpose of this paper is to develop an efficient and rigorous semiclassical approach to simulate coherent control scenarios to allow applications to larger molecular systems. We focus on coherent control scenarios involving interference via one photon routes. This includes controlled photodissociation via bichromatic coherent control[3] or weak field pump–dump schemes.[4]

We consider photodissociation from an initial bound state $|i\rangle$ to the final continuum state $|E,\xi,n^-\rangle$. Here, E,ξ,n denote the total energy, arrangement channel and internal quantum numbers of the product state with which the continuum state $|E,\xi,n^-\rangle$ correlates. In coherent control of photodissociation involving one photon routes, the probability of forming a desired product is a sum of terms, some corresponding to the direct photodissociation of a bound state $|k\rangle$ of the form $\mu_{kk}=\Sigma_n\langle k|\mu_\varepsilon|E,\xi,n^-\rangle\langle E,\xi,n^-|\mu_\varepsilon|k\rangle$, and some to terms of the form $\mu_{jk}=\Sigma_n\langle j|\mu_\varepsilon|E,\xi,n^-\rangle\times\langle E,\xi,n^-|\mu_\varepsilon|k\rangle$. The latter correspond to interference between one photon absorption routes to the continuum from level $|j\rangle$ and from level $|k\rangle$. Both of these terms involve a sum over all final states. It therefore appears that obtaining μ_{jk} requires solving the scattering problem at the complete state-to-state level, a task which becomes increasingly difficult as the size of the system increases. In this paper we show that this is not the case, i.e., that a direct method for obtaining these terms, based on a correlation function approach, considerably simplifies this computation.

In particular, in this paper we make two contributions towards the goal of developing useful methods for coherent control computations. First, we develop formally exact quantum expressions for cumulative transition matrix elements that circumvent the need to solve the reactive scattering problem at the complete state-to-state level. Second, we implement this approach semiclassically via the initial value representation (SC-IVR) to examine a specific control scenario, bichromatic control, on a (collinear) polyatomic problem dissociating to two chemically distinct products, and show that the results are in very good agreement with exact quantum computations.

In recent years, there has been a rebirth of interest in the SC-IVR approach, a method originally due to Miller,[5] as a means of including quantum effects in molecular dynamics.[6–21] However, to date, the only SC-IVR application to coherent control is our recent study of bichromatic coherent control of nonadiabatic ICN photodissociation.[22] In that work, the SC-IVR was shown capable of reproducing both amplitudes and *phases* of the μ_{ij} in an approach that required solving the full scattering problem at the asymptotic state-to-state level. The resultant semiclassical photofragmentation ratios were found to be in good agreement with quantum simulations. Here we extend this approach, dealing with a reactive photodissociation problem via the "direct"

[a]Current address: Department of Chemistry, Yale University, New Haven, Connecticut 06520-8107.

 © 2001 American Institute of Physics

Downloaded 03 Oct 2001 to 142.150.224.5. Redistribution subject to AIP license or copyright, see http://ojps.aip.org/jcpo/jcpcr.jsp

implementation procedure of the SC-IVR for computations of cumulative transition matrix elements.

The paper is organized as follows: In Sec. II, and the Appendix, we review the bichromatic coherent control scenario and derive formally exact expressions for the cumulative transition matrix elements. Sections III and IV describe procedures to implement these expressions in terms of the SC-IVR, and also in terms of exact quantum mechanical methods based on the split-operator propagation scheme.[23] Section V evaluates these expressions for a simple example of unimolecular decomposition, and compares the semiclassical results with full quantum mechanical simulations. The Appendix contains a derivation of an important expression for the projection operator onto fixed total energy and specific product channel. Section VI contains a summary and conclusions.

II. COHERENT CONTROL IN A CONTINUUM STATE

We consider bichromatic coherent control[3] in the unimolecular decomposition reaction of a generic polyatomic molecular system ABC that photodissociates according to

$$ABC+\hbar\omega \begin{array}{l} \overset{(\xi=1)}{\rightarrow} C+AB(n) \\ \overset{(\xi=2)}{\rightarrow} A+BC(n). \end{array} \tag{2.1}$$

Here $\xi=1,2$ denotes the final arrangement and n denotes the internal states of the product.

The molecule ABC is prepared in an initial superposition state,

$$|\Psi_0(j,k)\rangle=|\Phi_g\rangle[c_j|j\rangle+c_k|k\rangle], \tag{2.2}$$

where $|\Phi_g\rangle$ is the ground electronic state wave function, and $|j\rangle$ is the nuclear eigenstate of energy E_j associated with excitation in the jth vibrational state. The system is subsequently photo-excited with two CW lasers with a total electric field $\bar{\varepsilon}(t)$,

$$\bar{\varepsilon}(t)=\bar{\varepsilon}_j e^{-i(\omega_j t+\theta_j)}+\bar{\varepsilon}_k e^{-i(\omega_k t+\theta_k)}+\text{c.c.}, \tag{2.3}$$

where the field amplitudes $\bar{\varepsilon}_j$ and $\bar{\varepsilon}_k$ are time independent vectors of length $|\bar{\varepsilon}_j|$, and $|\bar{\varepsilon}_k|$. The quantities θ_j and θ_k, in Eq. (2.3), are the phases of the two CW fields. If the frequencies ω_j and ω_k are chosen such that $\hbar\omega_k+E_k=\hbar\omega_j+E_j=E$, then both $|j\rangle$ and $|k\rangle$ are raised by the laser field to continuum states $|E,\xi,n^-\rangle$ of an electronic excited state with energy E. These two photoexcitation routes interfere with one another, and assuming that the field is sufficiently weak to allow the use of first order perturbation theory, the relative probability ratio $R(\xi,\xi',E)$, of producing product in arrangement channel ξ to that in arrangement ξ', at energy E, is given by[3]

$$R(\xi,\xi';E)=\frac{|\mu_{jj}(\xi,E)|+x^2|\mu_{kk}(\xi,E)|+2x\cos(\theta_j-\theta_k+\Phi_{jk}(\xi,E))|\mu_{jk}(\xi,E)|}{|\mu_{jj}(\xi',E)|+x^2|\mu_{kk}(\xi',E)|+2x\cos(\theta_j-\theta_k+\Phi_{jk}(\xi',E))|\mu_{jk}(\xi',E)|}. \tag{2.4}$$

Here, x is the ratio of controllable parameters $x=|(c_k|\bar{\varepsilon}_k|)/(c_j|\bar{\varepsilon}_j|)|$, and $\Phi_{jk}(\xi,E)$ is the phase of the cumulative transition matrix element $\mu_{jk}(\xi,E)$,

$$\mu_{j,k}(\xi,E)=|\mu_{jk}(\xi,E)|e^{i\Phi_{jk}(\xi,E)} =\langle\Psi_0(j)|\left[\sum_{n=0}^{\infty}|E,\xi,n^-\rangle\langle E,\xi,n^-|\right]|\Psi_0(k)\rangle, \tag{2.5}$$

where $|\Psi_0(j)\rangle\equiv\mu_\varepsilon|j\rangle$, and μ_ε is the dipole operator along the direction of the field. Note that the off-diagonal μ_{jk} manifest the interference between components of the continuum wave function which are excited by independent coherent excitation pathways.

Equations (2.4) and (2.5) show that the relative product yields can be experimentally controlled by changing either the composition of the initial superposition state, or the relative phase or amplitude associated with the photoexcitation laser pulses. Essentially all simulations to date have computed the cumulative transition matrix elements $\mu_{j,k}(\xi,E)$, according to Eq. (2.5), after solving first the time-independent scattering problem at the complete state-to-state level. The only exception to this has been our recent study of ICN coherent control,[22] where the photodissociation process was described in the time dependent picture, and the transition matrix elements were computed according to

$$\mu_{j,k}(\xi,E)=\lim_{t\rightarrow\infty}\sum_{n=0}^{\infty}\langle\Psi_t(j)|E,\xi,n^o\rangle\langle E,\xi,n^o|\Psi_t(k)\rangle. \tag{2.6}$$

Here $|E,\xi,n^o\rangle$ are the asymptotic states associated with photofragments that are in product channel ξ, at energy E, and internal state n. The quantities $|\Psi_t(j)\rangle$ and $|\Psi_t(k)\rangle$ result from time evolving $|\Psi_0(j)\rangle$ and $|\Psi_0(k)\rangle$ according to the excited state Hamiltonian $\hat{H}$. Hence, all methods implemented to date have required resolution into individual product states.

We wish to derive an expression that allows the determination of μ_{jk} without the need to compute dynamics into each product channel. To do so we first rewrite Eq. (2.5). The Appendix shows that the sum in brackets, in Eq. (2.5), can be written as

$$\sum_{n=0}^{\infty}|E,\xi,n^-\rangle\langle E,\xi,n^-|=\hat{P}_\xi\delta(E-\hat{H}), \tag{2.7}$$

to obtain

$$\mu_{j,k}(\xi,E)=\langle\Psi_0(j)|\hat{P}_\xi\delta(E-\hat{H})|\Psi_0(k)\rangle. \tag{2.8}$$

Downloaded 03 Oct 2001 to 142.150.224.5. Redistribution subject to AIP license or copyright, see http://ojps.aip.org/jcpo/jcpcr.jsp

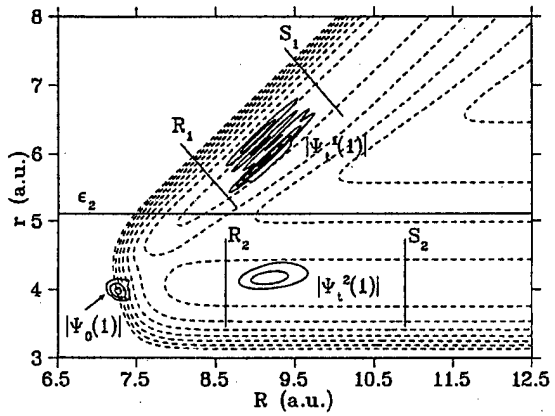

FIG. 1. Excited state potential-energy surface for unimolecular dissociation [Eq. (2.1)]. Here, $r=r_{BC}$ and $R=r_{AB}+r_{BC}m_C/(m_C+m_B)$, are the Jacobi coordinates associated with the vibrational and translational coordinates, respectively, in photofragmentation channel $\xi=2$. Shown are the dividing surfaces $R=R_1$ and $R=R_2$, the asymptotic cuts S_1 and S_2 in the free interaction regions, and the position of the absorbing potential ϵ_2 that would absorb the wave packet components $\Psi_t^1(1)$ and $\Psi_t^1(2)$ that correlate with asymptotic product channel $\xi=1$. Also shown are contour plots for the modulus of the initial wave packet, $\Psi_0(1)$, that results from photoexcitation of the ground vibrational state, and the time evolved wave packet components $\Psi_t^1(1)$ and $\Psi_t^2(1)$ at $t=40$ fs after photoexcitation of the system.

Here, $\hat{P}_\xi$ is the projection operator onto asymptotic product channel ξ, defined as

$$\hat{P}_\xi = \lim_{t\to\infty} e^{i\hat{H}t/\hbar} h_\xi(R) e^{-i\hat{H}t/\hbar}, \tag{2.9}$$

and, $h_\xi(R)$ is a function of the dissociating bond length R, associated with asymptotic channel ξ. Specifically, $h_\xi(R)$ is one on the right of the dividing surface $R=R_\xi$ and zero on the left (see Fig. 1).

Substituting Eq. (2.9) into Eq. (2.8), gives that $\mu_{j,k}(\xi,E)$ can be computed according to

$$\mu_{j,k}(\xi,E) = (2\pi\hbar)^{-1} \int_{-\infty}^{\infty} dt e^{i\omega t/\hbar} \zeta_{j,k}(\xi,t), \tag{2.10}$$

with $E=\hbar\omega$, i.e., as the Fourier transform of the survival amplitude $\zeta_{j,k}(\xi,t)$,

$$\zeta_{j,k}(\xi,t) = \langle \Psi_0^\xi(j) | \Psi_t(k) \rangle. \tag{2.11}$$

Here, $|\Psi_0^\xi(j)\rangle$ is defined according to

$$|\Psi_0^\xi(j)\rangle \equiv \hat{P}_\xi |\Psi_0(j)\rangle = \lim_{t\to\infty} e^{i\hat{H}t/\hbar} h_\xi e^{-i\hat{H}t/\hbar} |\Psi_0(j)\rangle, \tag{2.12}$$

and is the wave packet component of the initial state $|\Psi_0(j)\rangle$ that correlates with the asymptotic product channel ξ.

Semiclassical and quantum mechanical calculations, reported in Sec. V, are essentially straightforward implementations of Eq. (2.10), where the survival amplitudes $\zeta_{j,k}(\xi,t)$ are obtained according to Eqs. (2.11) and (2.12). These equations provide an efficient procedure to obtain cumulative transition matrix elements, solely in terms of survival amplitudes. These survival amplitudes are expected to decay quite rapidly during the early time relaxation process in the continuum state, since the initially interacting constituents of the system separate from one another according to alternative reaction pathways, and cease to interact thereafter.

Finally, two comments are in order. First, we note that Eq. (2.10) provides the useful computational check that

$$\sum_\xi \mathrm{Im}[\mu_{j,k}(\xi,E)] = 0, \tag{2.13}$$

when both $\Psi_0(j)$ and $\Psi_0(k)$ are real functions. Here Im[] denotes the imaginary part function of its argument. Equation (2.13) follows from noting that, according to Eq. (2.10), the sum

$$\sum_\xi \mu_{j,k}(\xi,E) = \langle \Psi_0(j) | \delta(E-\hat{H}) | \Psi_0(k) \rangle, \tag{2.14}$$

is real, since

$$\langle \Psi_0(j) | \delta(E-\hat{H}) | \Psi_0(k) \rangle = (2\pi\hbar)^{-1} 2\,\mathrm{Re}\left[\int_0^\infty dt e^{i\omega t/\hbar} \zeta_{j,k}(t) \right], \tag{2.15}$$

when $\Psi_0(j)$ and $\Psi_0(k)$ are real wave functions with $j\neq k$, and always when $j=k$. Here the survival amplitudes $\zeta_{j,k}(t)$ [Eq. (2.15)], are defined as

$$\zeta_{j,k}(t) \equiv \langle \Psi_0(j) | e^{-i\hat{H}t/\hbar} | \Psi_0(k) \rangle = \langle \Psi_0(j) | \Psi_t(k) \rangle. \tag{2.16}$$

Second, we note that the survival amplitudes $\zeta_{j,k}(\xi,t)$ could also be computed in terms of the flux through the dividing surface, $R=R_\xi$, according to the time average over motion

$$\zeta_{j,k}(\xi,t) = \langle \Psi_0(j) | h_\xi | \Psi_t(k) \rangle + \int_0^\infty dt' \langle \Psi_{t'}(j) | \hat{F}_\xi | \Psi_{t+t'}(k) \rangle, \tag{2.17}$$

where $\hat{F}_\xi$, in Eq. (2.17), is the flux operator defined as

$$\hat{F}_\xi \equiv \left(\frac{i}{\hbar}\right) [\hat{H}, h_\xi]. \tag{2.18}$$

Equation (2.17) follows from Eqs. (2.11) and (2.12), by noting that

$$\lim_{t\to\infty} e^{i\hat{H}t/\hbar} h_\xi e^{-i\hat{H}t/\hbar} = h_\xi + \frac{i}{\hbar} \int_0^\infty dt' e^{i\hat{H}t'/\hbar} (\hat{H}h_\xi - h_\xi \hat{H}) e^{-i\hat{H}t'/\hbar}. \tag{2.19}$$

A semiclassical procedure for implementing Eq. (2.17) is presented in Sec. IV B.

III. QUANTUM MECHANICAL APPROACH

The quantum mechanical procedure to compute $\mu_{jk}(E,\xi)$ in terms of Eqs. (2.10), (2.11), and (2.12), requires the propagation of each wave packet component $|\Psi_0(k)\rangle$ and $|\Psi_0(j)\rangle$ which comprise the initial superposition state. We do so in accord with the standard split-operator propagation scheme.[23]

Computations of survival amplitudes $\zeta_{j,k}(\xi,t)$ involve projections of the time evolved wave packet $|\Psi_t(k)\rangle$ onto

Downloaded 03 Oct 2001 to 142.150.224.5. Redistribution subject to AIP license or copyright, see http://ojps.aip.org/jcpo/jcpcr.jsp

the initial state component $|\Psi_0^{\xi}(j)\rangle$ that correlates with asymptotic product channel ξ. To compute $|\Psi_0^{\xi}(j)\rangle$ we replace the infinite time limit, in Eq. (2.11), by a finite propagation time, τ,

$$|\Psi_0^{\xi}(j)\rangle = e^{i\hat{H}\tau/\hbar} h_{\xi} e^{-i\hat{H}\tau/\hbar} |\Psi_0(j)\rangle. \tag{3.1}$$

The quantity $|\Psi_0^{\xi}(j)\rangle$ is obtained, according to Eq. (3.1), by propagating $|\Psi_0(j)\rangle$ forward for time τ, applying h_{ξ} and then propagating the resultant wave packet backwards in time for time τ. Doing so only requires evolving the initial state $|\Psi_0(j)\rangle$ for the minimum time τ after which there is no significant overlap between the wave packet component exiting in channel ξ and the wave packet components associated with the other photofragmentation channels. Note that τ can be much shorter than the relaxation time necessary to reach the asymptotic noninteracting region.

The result of this procedure to prepare $|\Psi_0^{\xi}(j)\rangle$, is to absorb completely those wave packet components that do not correlate with the asymptotic product state ξ. This preparation of $|\Psi_0^{\xi}(j)\rangle$ can also be performed according to

$$|\Psi_0^{\xi}(j)\rangle = e^{i\hat{H}\tau/\hbar} e^{-i(\hat{H}-i\hat{\epsilon}_{\xi})\tau/\hbar} |\Psi_0(j)\rangle, \tag{3.2}$$

by performing the forward propagation in the presence of an appropriate absorbing potential, $\hat{\epsilon}_{\xi}$.[24–27] Note, that here we take advantage of the underlying simplicity of photodissociation dynamics in the continuum state, where the system cannot recross back to the interaction region after reaching a specific product region. The absorbing potential is chosen to be zero in the interaction region where the relevant dynamics for determining the survival amplitude occurs, and is "switched on" to absorb the product in the region of products that do not correlate with channel ξ (see Fig. 1). The finite propagation time τ, in Eq. (3.2), can then be chosen as the minimum propagation time (in the presence of the absorbing potential), necessary to absorb all wave packet components that do not correlate with the asymptotic product state ξ.

IV. SEMICLASSICAL APPROACH

Section IV A describes a semiclassical procedure to compute the cumulative transition matrix elements $\mu_{jk}(E,\xi)$ in terms of Eq. (2.10), where the survival amplitudes $\zeta_{j,k}(\xi,t)$ are obtained according to Eqs. (2.11) and (2.12). Section IV B describes a semiclassical procedure to compute the survival amplitudes $\zeta_{j,k}(\xi,t)$, according to Eq. (2.17), in terms of the flux through a dividing surface along the dissociative coordinate.

A. Absorbing boundary: Semiclassical implementation of Eqs. (2.10) and (2.11)

The semiclassical implementation of Eq. (2.10), is quite straightforward. The survival amplitudes $\zeta_{j,k}(\xi,t)$ are computed, by writing Eq. (2.12) in the form of Eq. (3.2), according to

$$\zeta_{j,k}(\xi,t) = \langle \Psi_0(j)| e^{-i\hat{H}t/\hbar} e^{i\hat{H}\tau/\hbar} e^{-i(\hat{H}-i\hat{\epsilon}_{\xi})\tau/\hbar} |\Psi_0(k)\rangle, \tag{4.1}$$

and the three time evolution operators, in Eq. (4.1), are combined into one overall SC-IVR time propagation, according to

$$\zeta_{j,k}(\xi,t) = (2\pi\hbar)^{-N} \int d\mathbf{p}_0 \int d\mathbf{q}_0 e^{i[S_t(\mathbf{p}_0,\mathbf{q}_0)+i\epsilon_{\tau}]/\hbar} \times C_t(\mathbf{p}_0,\mathbf{q}_0) \langle \Psi_0(j)|\mathbf{p}_t,\mathbf{q}_t\rangle \langle \mathbf{p}_0,\mathbf{q}_0|\Psi_0(k)\rangle, \tag{4.2}$$

where the exponential damping factor $e^{-\epsilon_{\tau}}$, arising from the absorbing potential,[28] is

$$\epsilon_{\tau} \equiv \int_0^{\tau} dt' \, \epsilon(\mathbf{q}(\mathbf{q}_0,\mathbf{p}_0;t')), \tag{4.3}$$

and can be approximated according to

$$e^{-\epsilon_{\tau}} = h_{\xi}(R_{\tau}), \tag{4.4}$$

since its only effect, in the long time limit ($\tau \to \infty$), is to eliminate the contributions of trajectories that do not dissociate into channel ξ.

Equation (4.2) is obtained by using the Herman–Kluk,[29] or coherent state IVR for the time evolution operator. The quantities $\mathbf{q}_t \equiv \mathbf{q}_t(\mathbf{p}_0,\mathbf{q}_0)$, and $\mathbf{p}_t \equiv \mathbf{p}_t(\mathbf{p}_0,\mathbf{q}_0)$, in Eq. (4.2), are the coordinates and momenta evolved for time t from the initial phase space point $(\mathbf{p}_0,\mathbf{q}_0)$, using the Hamiltonian H of the excited state. The classical action along this trajectory, $S_t(\mathbf{p}_0,\mathbf{q}_0)$, is obtained by integrating the following equation:

$$\frac{dS_t}{dt} = \mathbf{p}_t \cdot \dot{\mathbf{q}}_t - H(\mathbf{p}_t,\mathbf{q}_t), \tag{4.5}$$

along with the usual classical equations of motion,

$$\frac{dq(j)}{dt} = \frac{\partial H(\mathbf{q},\mathbf{p})}{\partial p(j)} \quad \text{and} \quad \frac{dp(j)}{dt} = -\frac{\partial H(\mathbf{q},\mathbf{p})}{\partial q(j)}. \tag{4.6}$$

The Hamiltonian $H(\mathbf{p}_t,\mathbf{q}_t)$, in Eqs. (4.5) and (4.6) above, is

$$H(\mathbf{q},\mathbf{p}) = \tfrac{1}{2}\mathbf{p}\cdot\mathbf{m}^{-1}\cdot\mathbf{p} + V(\mathbf{q}), \tag{4.7}$$

written in terms of normal mode coordinates and momenta, $\mathbf{q}$ and $\mathbf{p}$, respectively. $V(\mathbf{q})$, in Eq. (4.7), is the dissociative excited state potential energy that describes the photodissociation reaction for the generic molecule ABC.

The pre-exponential factor in the integrand of Eq. (4.2) is given by

$$C_t(\mathbf{p}_0,\mathbf{q}_0) = \sqrt{\det[\mathbf{M}]}, \tag{4.8}$$

where $\mathbf{M}$ is a linear combination of components of the monodromy matrix,

$$M(j,k) = \frac{1}{2}\left(\frac{\partial q_t(k)}{\partial q_0(j)} + \frac{\gamma(j)}{\gamma(k)} \frac{\partial p_t(k)}{\partial p_0(j)} - \frac{1}{2i\hbar\gamma(k)} \frac{\partial p_t(k)}{\partial q_0(j)} - 2i\hbar\gamma(j) \frac{\partial q_t(k)}{\partial p_0(j)} \right), \tag{4.9}$$

where $\gamma(j)$ are the constant parameters in the coherent states,

Downloaded 03 Oct 2001 to 142.150.224.5. Redistribution subject to AIP license or copyright, see http://ojps.aip.org/jcpo/jcpcr.jsp

$$\langle \mathbf{q}|\mathbf{q}_t,\mathbf{p}_t\rangle=\prod_{j=1}^{N}\left(\frac{2\gamma(j)}{\pi}\right)^{1/4}\exp\Big(-\gamma(j)[q(j)-q_t(j)]^2 + \frac{i}{\hbar}p_t(j)[q(j)-q_t(j)]\Big), \tag{4.10}$$

and similarly for $\langle \mathbf{q}|\mathbf{q}_0,\mathbf{p}_0\rangle$.

The various time dependent partial derivatives are obtained by numerically integrating the following equations for the stability matrix

$$\frac{d}{dt}\left(\frac{\partial p_t(i)}{\partial z(j)}\right)=-\sum_{k=1}^{N}\left(\frac{\partial^2 H(\mathbf{p}_t,\mathbf{q}_t)}{\partial p_t(k)\partial q_t(i)}\frac{\partial p_t(k)}{\partial z(j)} + \frac{\partial^2 H(\mathbf{p}_t,\mathbf{q}_t)}{\partial q_t(k)\partial q_t(i)}\frac{\partial q_t(k)}{\partial z(j)}\right)$$

$$\frac{d}{dt}\left(\frac{\partial q_t(i)}{\partial z(j)}\right)=+\sum_{k=1}^{N}\left(\frac{\partial^2 H(\mathbf{p}_t,\mathbf{q}_t)}{\partial p_t(k)\partial p_t(i)}\frac{\partial p_t(k)}{\partial z(j)} + \frac{\partial^2 H(\mathbf{p}_t,\mathbf{q}_t)}{\partial q_t(k)\partial p_t(i)}\frac{\partial q_t(k)}{\partial z(j)}\right),$$

where $z=p_0$ or q_0.[30]

B. Flux evaluation: Semiclassical implementation of Eq. (2.17)

The first term on the r.h.s. of Eq. (2.17) can be computed according to the standard implementation of the SC-IVR for computations of survival amplitudes. Also, in general, this term can be neglected since the dividing surface of h_ξ can be chosen sufficiently far from the Franck–Condon region. The discussion that follows concerns practical aspects of the semiclassical implementation of Eq. (2.17) and disregards the first term on the r.h.s of Eq. (2.17).

The second term in Eq. (2.17) can also be written in the form

$$\zeta_{jk}(\xi,t')=(2\pi\hbar)^{-1}\int_0^\infty dt\langle\Psi_0(j)| \times e^{i\hat{H}t'/\hbar}\hat{F}_\xi e^{-i\hat{H}(t+t')/\hbar}|\Psi_0(k)\rangle. \tag{4.11}$$

Using the Herman–Kluk,[29] or coherent state IVR for the time evolution operator, $\zeta_{jk}(\xi,t')$ becomes a double phase space average over initial conditions for the time average over motion,

$$\zeta_{jk}(\xi,t')=(2\pi\hbar)^{-2N-1}\int d\mathbf{p}_0\int d\mathbf{q}_0\int d\mathbf{p}_0'\int d\mathbf{q}_0'\int_0^\infty dt \times e^{i(S_{t+t'}(\mathbf{p}_0,\mathbf{q}_0)-S_t(\mathbf{p}_0',\mathbf{q}_0'))/\hbar} \times C_t^*(\mathbf{p}_0',\mathbf{q}_0')C_{t+t'}(\mathbf{p}_0,\mathbf{q}_0)\times\langle\Psi_0(j)|\mathbf{p}_0',\mathbf{q}_0'\rangle \times\langle\mathbf{p}_t',\mathbf{q}_t'|\hat{F}_\xi|\mathbf{p}_{t+t'},\mathbf{q}_{t+t'}\rangle\langle\mathbf{p}_0,\mathbf{q}_0|\Psi_0(k)\rangle. \tag{4.12}$$

The integration variables $(\mathbf{p}_0,\mathbf{q}_0)$ and $(\mathbf{p}_0',\mathbf{q}_0')$, in Eq. (4.12), are the initial conditions for pairs of classical trajectories. Propagating first a trajectory that evolves according to $\mathbf{q}_{t'+t}\equiv\mathbf{q}_{t'+t}(\mathbf{p}_0,\mathbf{q}_0)$ and $\mathbf{p}_{t'+t}\equiv\mathbf{p}_{t'+t}(\mathbf{p}_0,\mathbf{q}_0)$, the time average over motion could be evaluated while one is computing the second trajectory of each pair, $\mathbf{q}_t'\equiv\mathbf{q}_t(\mathbf{p}_0',\mathbf{q}_0')$, and $\mathbf{p}'_t \equiv\mathbf{p}_t(\mathbf{p}'_0,\mathbf{q}'_0)$. Doing the t integral, in Eq. (4.12), thus would not entail any extra effort in the calculation, other than storing the time dependent quantities associated with the first trajectory. Also, the structure of Eq. (4.12) allows doing the calculation for many different values of t', i.e., all from the same set of trajectories. We have found, however, that the implementation of this method is not as efficient as the implementation procedure described in Sec. IV A, where survival amplitudes are obtained from the very early time relaxation dynamics. Hence, we utilize below the method of Sec. IV A. The direct semiclassical procedure described in this section, however, has the advantage that could be easily generalized to simulate coherent control in the presence of nonadiabatic photodissociation dynamics, as formulated in terms of the Meyer–Miller Hamiltoninan.[31,22]

V. RESULTS

Results are presented in two sections after describing the specific model Hamiltonian and the initial state in Sec. V A; Sec. V B compares the semiclassical results for survival amplitudes and transition matrix elements to the corresponding cumulative, and state-to-state resolved quantum mechanical results. Section V C then presents our semiclassical results of bichromatic coherent control, after photoexcitation of an initial superposition state to various final energy states in the continuum, and compares them to the corresponding full quantum mechanical calculations.

Semiclassical results are converged with 5×10^5 trajectories, integrated using the standard fourth-order Runge–Kutta algorithm,[32] according to the parallel programming model described in Ref. 6. Trajectories are initialized through Monte Carlo sampling of coordinates and momenta according to localized phase space distributions, determined by the coherent state transform of the initial wave packet components. This excited state population is created under the artifice that the photolysis event promotes molecules instantaneously from the ground electronic state to the optically allowed excited state that is resonant with the excitation wavelength.

A. Model Hamiltonian and initial state

The nuclear wave function that represents the initial population in the excited electronic state is assumed to be

$$\langle\mathbf{q}|\Psi_0(j)\rangle=\left(\frac{\alpha(1)\alpha(2)}{\pi^2}\right)^{1/4}H_j(\sqrt{\alpha(1)/\hbar}q(1)) \times e^{(-1/2)[\alpha(1)q(1)^2-\alpha(2)q(2)^2]}, \tag{5.1}$$

where H_j is a Hermite polynomial of degree j. The coordinates $q(1)$ and $q(2)$, in Eq. (5.1), are the symmetric and antisymmetric stretching normal modes of the ABC molecule. The initial state for the control studies, introduced in Eq. (2.2), involves a linear superposition of vibrational states with $j=0$ and $j=1$. The transition dipole that couples the ground and excited electronic states is assumed to be independent of nuclear coordinates (Condon approximation).

Downloaded 03 Oct 2001 to 142.150.224.5. Redistribution subject to AIP license or copyright, see http://ojps.aip.org/jcpo/jcpcr.jsp

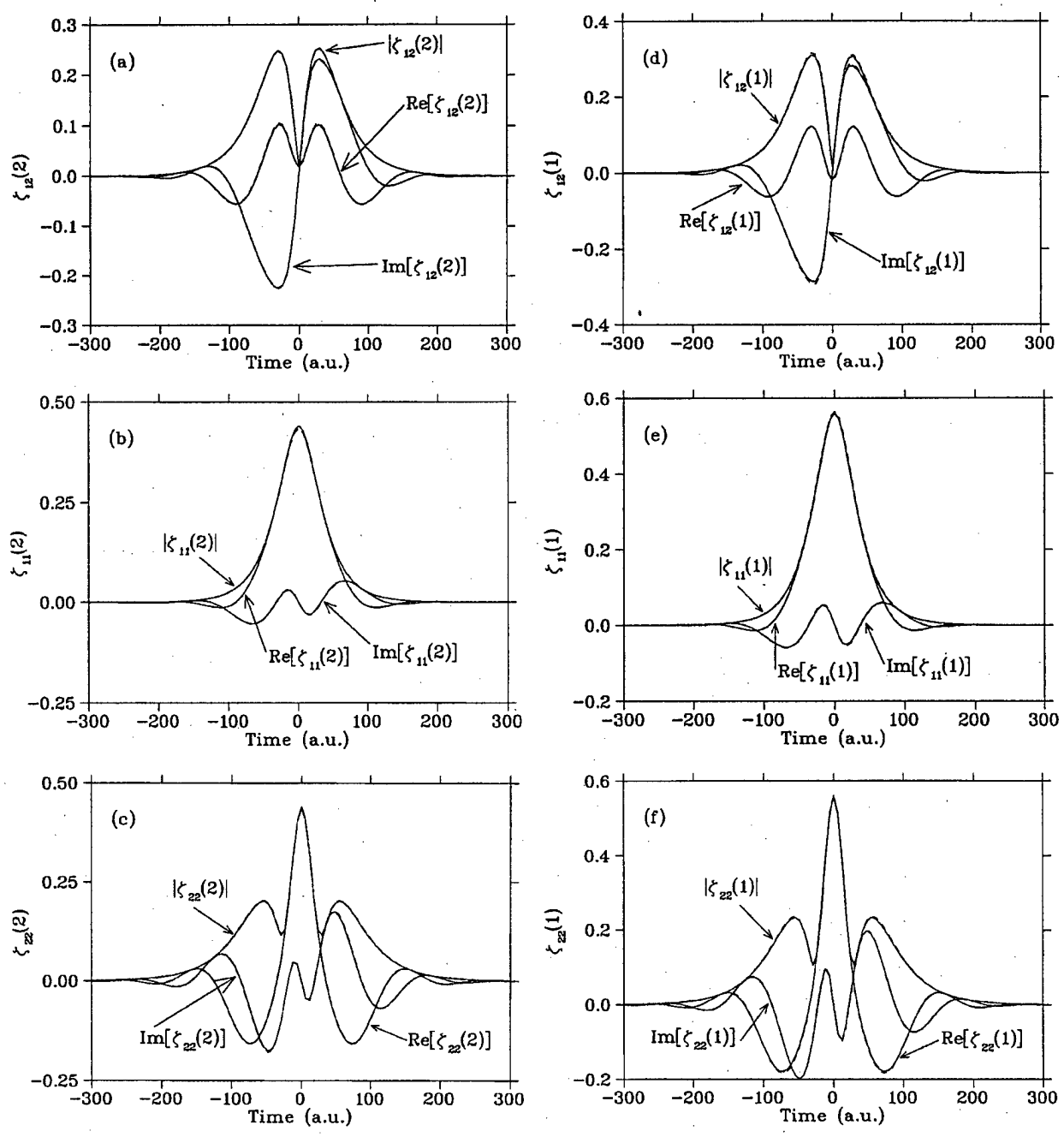

FIG. 2. Comparison of semiclassical (solid lines), and quantum mechanical results (dashes) for the modulus, real, and imaginary parts of the survival amplitudes $\zeta_{12}(\xi)$, $\zeta_{11}(\xi)$, and $\zeta_{22}(\xi)$, with $\xi=(1,2)$ as a function of time. Panels (a), (b), and (c) correspond to photodissociation channel $\xi=2$, while panels (d), (e), and (f) correspond to channel $\xi=1$.

We examine a simple collinear model for photodissociation where the ground electronic state potential energy surface is defined as a sum of two Morse potentials,

$$V_{nm}(r_{nm})=D_{nm}[e^{-\alpha_{nm}(r_{nm}-r_{nm}^{e})}-1]^2-D_{nm}, \qquad (5.2)$$

where $nm=AB$, or $nm=BC$ labels the corresponding molecular fragment. The Morse potentials are parametrized as follows: $D_{AB}=0.0874$ a.u., $\alpha_{AB}=0.87094$ a.u., $r_{AB}^{e}=4.043$ a.u., $D_{BC}=0.1069$ a.u., $\alpha_{BC}=0.9155$ a.u., $r_{BC}^{e}=3.685$ a.u. The masses for the molecular fragments A, B, and C are chosen to be those of I, CH_2, and Br, respectively. Specifically, $m_A=126.904\ m_H$, $m_B=14.011\ m_H$, and $m_C=79.904\ m_H$, respectively, where m_H is the mass of a hydrogen atom.

The excited state potential energy surface, $V(r_{AB},r_{BC})$, is defined in terms of the internal coordinates r_{AB} and r_{BC} according to the following expression:

$$\begin{aligned}V(r_{AB},r_{BC})=&(A_{AB}e^{-\beta_{AB}r_{AB}}+V_{BC}(r_{BC}))f(x)\\&+(A_{BC}e^{-\beta_{BC}r_{BC}}+V_{AB}(r_{AB}))(1.0-f(x))\\&+D_2e^{-\alpha_2(r_{AB}-r_{AB}^{e})-\alpha_3(r_{BC}-r_{BC}^{e})}, \qquad (5.3)\end{aligned}$$

Downloaded 03 Oct 2001 to 142.150.224.5. Redistribution subject to AIP license or copyright, see http://ojps.aip.org/jcpo/jcpcr.jsp

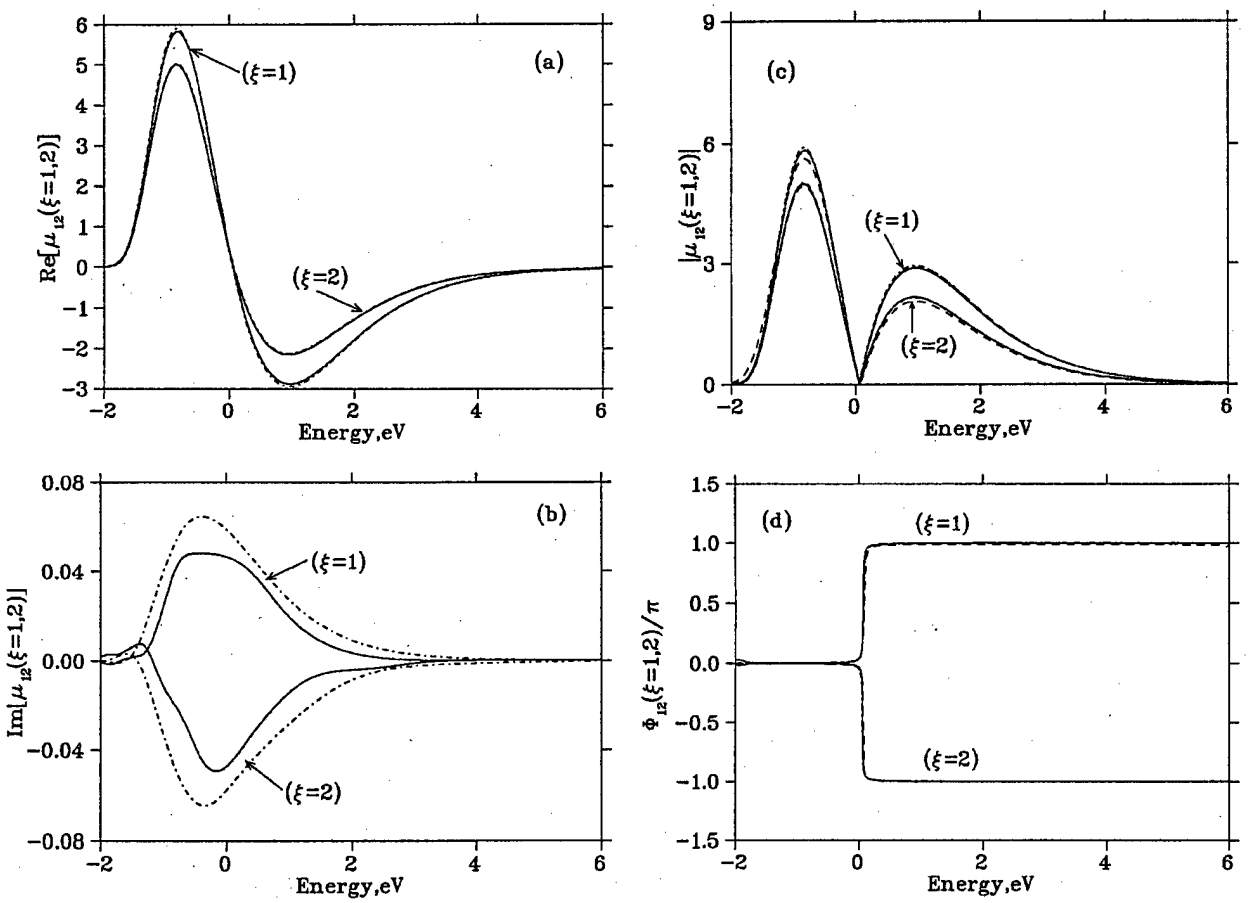

FIG. 3. Comparison of the semiclassical results (solid lines) for the cumulative transition matrix elements $\mu_{12}(\xi=1,2)$, as a function of the total energy E in the continuum state, to state-resolved (dashes) and cumulative (broken dashes) quantum mechanical calculations. Panels (a) and (b) show the real and imaginary parts of $\mu_{12}(\xi=1,2)$, respectively. Note the difference in scale of the ordinate of panel (b). Panel (c) shows the modulus $|\mu_{12}(\xi=1,2)|$, and panel (d) the phases Φ_{12}, as a function of final energy E in the continuum.

where $V_{BC}(r_{BC})$ and $V_{AB}(r_{AB})$ are the Morse potentials, introduced by Eq. (5.2), that parametrize the ground electronic state; $A_{AB}=0.37$, $\beta_{AB}=1.5$, $\alpha_2=4.8$, $\alpha_3=4.8$, $D_2=0.08824$. The function $f(x)$, in Eq. (5.3), is defined according to

$$f(x)=1/(1+e^{\alpha_h(x-x_h)}), \quad \text{with} \quad x=r_{BC}/(r_{AB}+r_{BC}), \tag{5.4}$$

where, $\alpha_h=90$, and $x_h=0.44643$.[33]

All forces and second derivatives necessary for integrating the equations of motion are calculated using finite difference expressions. Full quantum mechanical results are obtained using the fast Fourier transform (FFT) method with an extended grid of 1024 points in both the r and R Jacobi coordinates, defined in the range of coordinates $|R-9.5$ a.u.$|<3$ a.u. and $|r-6$ a.u.$|<3$ a.u.

B. Survival amplitudes and transition matrix elements

Figure 2 compares the semiclassical results (solid lines), with the corresponding full quantum mechanical results (dashes) for the modulus, real, and imaginary parts of survival amplitudes $\zeta_{12}(\xi)$, $\zeta_{11}(\xi)$, and $\zeta_{22}(\xi)$, with $\xi=(1,2)$, as a function of time. Panels (a), (b), and (c) correspond to photodissociation channel $\xi=2$, while panels (d), (e), and (f) show the corresponding quantities for channel $\xi=1$. The comparison shows that the semiclassical survival amplitudes are in excellent agreement with quantum mechanical results; so good, in fact, that the dashed and solid lines often overlap. Figure 2 shows that both the diagonal and off-diagonal survival amplitudes decay for this particular model system within 7 fs (~290 a.u.). This relaxation time is significantly shorter than the time necessary to reach the asymptotic noninteracting region at ~40 fs after photoexcitation of the system. Figure 2 also shows a significant difference between the diagonal and the off-diagonal survival amplitudes; while $\zeta_{11}(\xi=1,2)$ and $\zeta_{11}(\xi=1,2)$ are symmetric relative to $t=0$, and satisfy the condition that $\zeta_{jj}(\xi,t)=\zeta^*_{jj}(\xi,-t)$, the off-diagonal survival amplitudes $\zeta_{jk}(\xi=1,2)$ are slightly asymmetric relative to $t=0$. For example, note that the maximum of $|\zeta_{jk}(\xi=1,2)|$ at positive times is slightly higher than the maximum at negative times. This asymmetry results from an asymmetric potential energy surface, and makes its Fourier transform μ_{12} a complex quantity with nonzero real and imaginary parts.

Figure 3 shows the comparison of semiclassical (solid lines), and quantum mechanical (dashes) results for the real [panel (a)] and imaginary [panel (b)] parts of $\mu_{12}(\xi=1,2)$.

Downloaded 03 Oct 2001 to 142.150.224.5. Redistribution subject to AIP license or copyright, see http://ojps.aip.org/jcpo/jcpcr.jsp

Figure 3, also compares of the modulus $|\mu_{12}(\xi=1,2)|$ [see panel (c)], and phase $\Phi_{12}(\xi=1,2)$ [panel (d)] of the cumulative transition matrix elements $\mu_{12}(\xi=1,2)$, as a function of the total energy E in the continuum state, obtained according to the semiclassical method (solid lines), the quantum state-resolved (dashes) approach, and quantum cumulative (broken dashes) methodology. Although one can see small differences, both the modulus and the phase of the cumulative transition matrix elements obtained semiclassically are in very good agreement with full quantum mechanical simulations over the whole energy range. The semiclassical results are able to reproduce the correct shape of $|\mu_{12}(\xi=1,2)|$, and the position of the amplitude nodes as a function of E, as well as the energy dependence of the phase $\Phi_{12}(\xi=1,2)|$, that is found to be in almost quantitative agreement with full quantum mechanical calculations in both photofragmentation channels. Figure 3 shows that the most important features of $\mu_{12}(\xi=1,2)$ include the energy position of the node, the quality of the node (the amplitude does not totally vanish at the node), and the change in sign of $\mu_{12}(\xi=1,2)$ when going through the energy node ($\Delta\Phi_{12}=+/-\pi$). These features can be understood in terms of the symmetry properties of the product of the two wave packet components that contribute to $\mu_{12}(\xi=1,2)$ at each n, as defined by Eq. (2.6). The comparison of real and imaginary parts shows more clearly the level of agreement between the quantum and semiclassical results for a model system where the imaginary parts of $\mu_{12}(\xi=1,2)$ are much smaller than the real parts throughout the whole energy range.

Figure 4 compares the semiclassical results (solid lines) for the diagonal cumulative matrix elements $\mu_{11}(\xi=1,2)$ [see panel (a)], and $\mu_{22}(\xi=1,2)$ [see panel (b)], with the corresponding state-resolved [dashes], and cumulative (broken dashes) quantum mechanical results. One sees that with the exception of small deviations there is almost quantitative agreement between semiclassical and full quantum mechanical calculations of the cumulative transition amplitudes associated with ground and excited vibrational states, for both photodissociation channels.

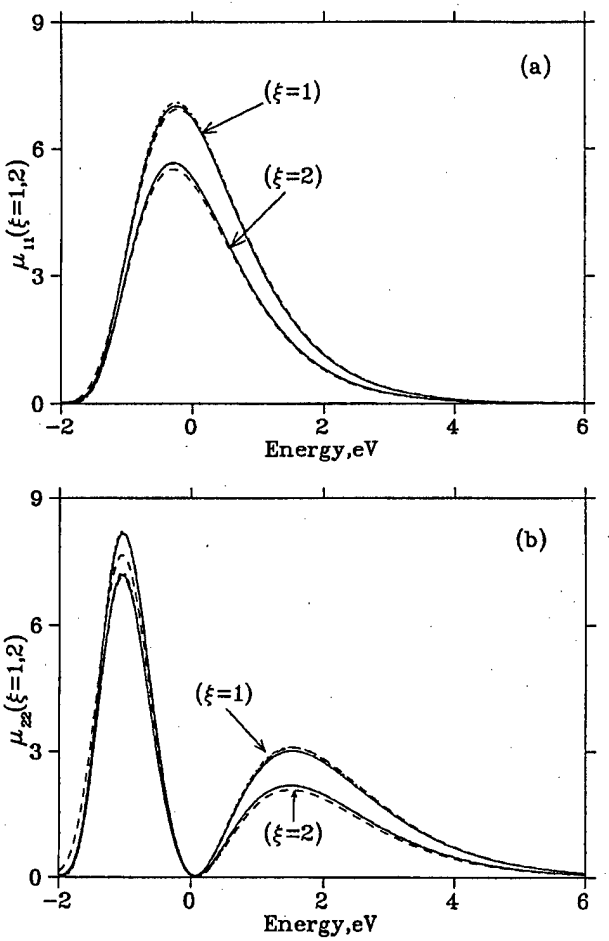

FIG. 4. Comparison between the semiclassical results (solid lines) for the cumulative matrix elements $\mu_{11}(\xi)$ and $\mu_{22}(\xi)$, with $\xi=(1,2)$, and the corresponding state-resolved (dashes) and cumulative (broken lines) quantum mechanical results. Panel (a) shows the comparison of $\mu_{11}(\xi=1,2)$, and panel (b) displays the corresponding results for $\mu_{22}(\xi=1,2)$.

C. Coherent control of photofragmentation product yields

Figure 5 shows the percentage product yields $100\times A/(A+C)$, obtained from Eq. (2.4), after photodissociation in the continuum. Bichromatic coherent control is simulated for an initial superposition of vibrational states with quantum numbers $v=1$ and $v=2$, respectively. Figure 5 compares the SC (solid lines) and full quantum mechanical (dashed lines) results obtained at various photoexcitation energies. Percentage product yields are presented in the form of contour plots for the photoexcitation energies indicated in panels (a)–(f), as a function of both the relative pulse phase parameter, $\Theta_1-\Theta_2$, and the relative amplitude $S=(c_1^2\bar{\varepsilon}_1^2/(c_2^2\bar{\varepsilon}_2^2+c_1^2\bar{\varepsilon}_1^2)$.

Figure 5 shows that the model system considered herein is particularly challenging, since the relative product yields change only moderately as a function of the relative phase parameter. However, the overall comparison between SC and full quantum dynamics simulations of coherent control, indicates that the structure of the diagrams, the trend in these structures with photoexcitation energy, and the range of quantum mechanical product yields, are reproduced by the semiclassical calculations within an error of approximately 1%–5%.

At the lowest photoexcitation energy [see panel (a)], there is maximum control at $S\leqslant 0.5$, where the production of A can be reduced from 50% to 40%, by changing the relative phase parameter from 0° to 180°. At higher values of S (when $S\rightarrow 1$), the semiclassical and full quantum mechanical product yields still agree with one another within an error of 1%–5%, and show a qualitatively different behavior from that observed at smaller values of S. The major difference to note is that the degree of yield control becomes only weakly dependent on the relative phase parameter, $\Theta_1-\Theta_2$ at larger S, and is therefore no longer possible to control the final outcome of the chemical reaction via interference effects.

At higher photoexcitation energies [panel (b)] the SC and full quantum mechanical product yields again agree within about 1%–5% error and show a diagram structure as

Downloaded 03 Oct 2001 to 142.150.224.5. Redistribution subject to AIP license or copyright, see http://ojps.aip.org/jcpo/jcpcr.jsp

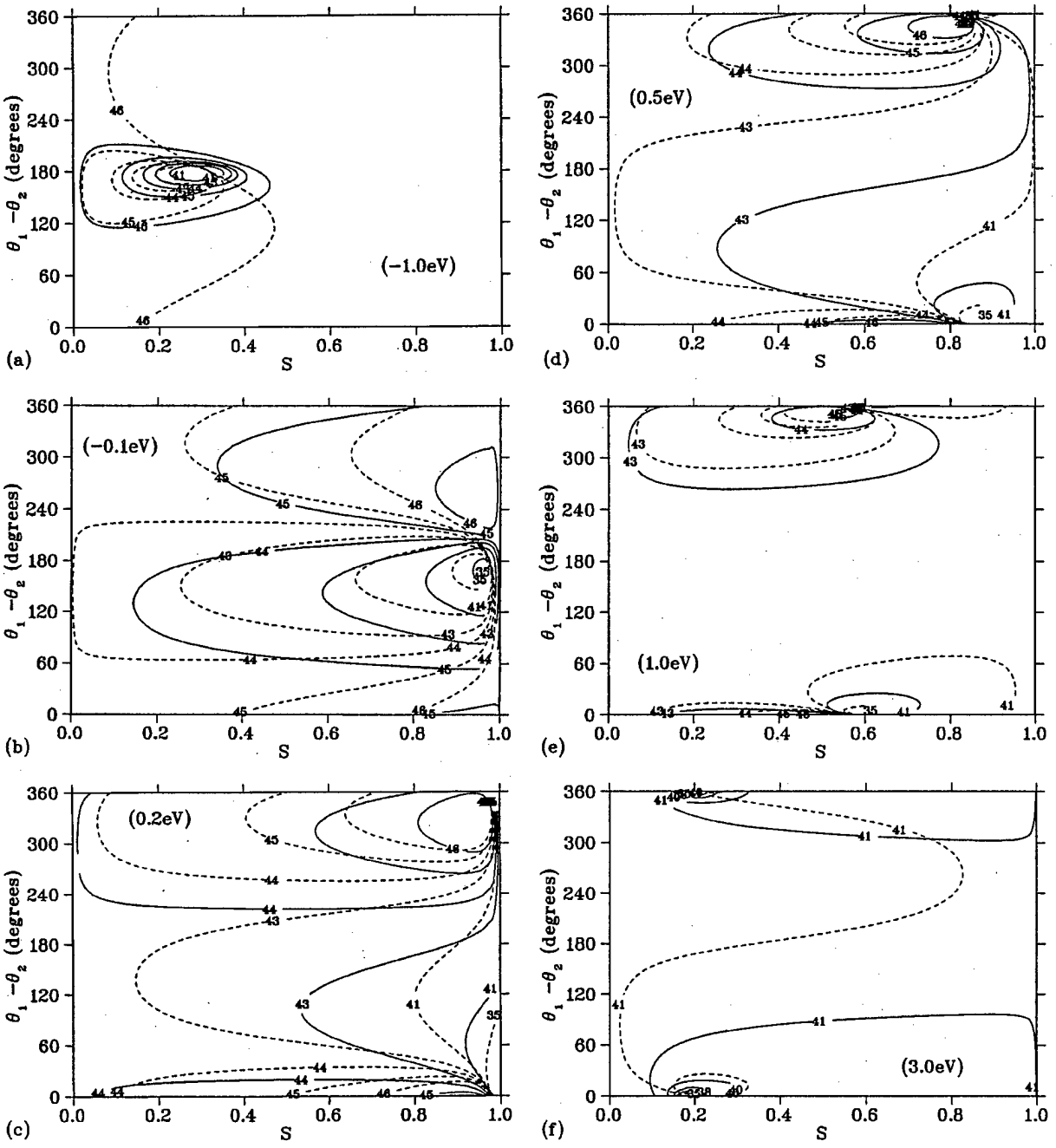

FIG. 5. Contour plots of the relative product yields $100 \times A/(A+C)$, for bichromatic coherent control of an initial ABC superposition state with symmetric stretch vibrational quantum numbers $v=1$ and $v=2$, respectively. The photoexcitation energy is indicated in each panel, relative to the energy of the isolated fragments.

a function of controllable parameters that is completely different from the diagram obtained at lower photoexcitation energies. The degree of yield control is found to be maximum in the $0.9 \leqslant S \leqslant 1.0$ range, where the production of A can be reduced from more than 45% to less than 35% by changing the relative phases from about 0° to 180°.

At even higher photoexcitation energies [panel (c)] the contour diagram is once again totally different from the diagrams obtained at lower photoexcitation energies, however, the SC and full quantum mechanical calculations agree in predicting that a maximum degree of yield control can be achieved in the $0.9 \leqslant S \leqslant 1.0$ range. Within this range of relative amplitude parameter the production of A is less than 38%, at approximately 30°, and can be increased to more than 45%, by changing the relative phases to the 280°–300° range.

Coherent control vanishes when the final energy is > 3.0 eV [panel (f)]. Panel (f) shows than SC and full quantum calculations agree in predicting that there is practically no coherent control at this particular final energy, in terms of contour lines of percentage yields that agree within 1%–5% error.

Downloaded 03 Oct 2001 to 142.150.224.5. Redistribution subject to AIP license or copyright, see http://ojps.aip.org/jcpo/jcpcr.jsp

Finally, at intermediate photoexcitation energies [panels (d) and (e)], SC and full quantum mechanical calculations agree once again with one another within the same error range and predict that moderate coherence control is recovered.

VI. CONCLUSIONS

In this article we have derived formally exact quantum mechanical expressions for cumulative transition matrix elements, and we have shown that these expressions provide a useful means for simulating one photon control scenarios, such as bichromatic control of an initial superposition state, without having to solve the complete state-to-state quantum mechanical reactive scattering problem.

We have shown how to implement these exact quantum mechanical expressions both quantum mechanically, and semiclassically by using an initial value representation method, in order to investigate quantum control in a generic reaction that describes unimolecular decomposition into more than one possible product.

We have demonstrated the capabilities of the semiclassical approach by comparing the semiclassical results to full quantum mechanical calculations of photofragmentation product yields, as controlled by the relative pulse phase, and the relative amplitude parameters. We have shown that semiclassical results, obtained through quantization of the classical Hamiltonian, according to the Herman–Kluk SC-IVR methodology, together with stationary phase MC methods, were able to reproduce the correct structure of the relative product yield diagrams for various different photoexcitation energies. These results demonstrate that the cumulative SC-IVR methodology, developed in this paper, is an efficient and reliable approach to describe laser induced quantum interferences between alternative photodissociation pathways.

According to the present implementation, semiclassical simulations of coherent control require only the evaluation of survival amplitudes. The SC-IVR has already been successfully implemented for computing survival amplitudes, associated with diagonal transition matrix elements, for systems of up to 35 coupled degrees of freedom.[10] Therefore, one expects that the computational method developed in this paper should be a tractable and reliable approach for simulating coherent control in systems of high dimensionality. Such work is in progress.[34]

ACKNOWLEDGMENTS

We gratefully acknowledge financial support for this work from Photonics Research Ontario and from the U.S. Office of Naval Research. We also acknowledge a generous allocation of supercomputing time from the National Energy Research Scientific Computing Center (NERSC).

APPENDIX: DERIVATION OF EQ. (3.6)

In this Appendix we show that

$$\hat{P}_{E,\xi}\equiv\sum_{n=0}^{\infty}|E,\xi,n^-\rangle\langle E,\xi,n^-|=\hat{P}_{\xi}\delta(E-\hat{H}), \tag{A1}$$

where the spatial projection operator $\hat{P}_{\xi}$ is defined as

$$\hat{P}_{\xi}=\lim_{t\to\infty}e^{i\hat{H}t/\hbar}h_{\xi}(R)e^{-i\hat{H}t/\hbar}. \tag{A2}$$

Here, $h_{\xi}(R)$ is a function of the dissociating bond length R associated with asymptotic channel ξ. The function $h_{\xi}(R)$ is defined as 1(0) on the right(left) of a dividing surface $R=R_{\xi}$. The scattering states $|E,\xi,n^-\rangle$, in Eq. (A1), satisfy the Schrödinger equation,

$$(\hat{H}-E)|E,\xi,n^-\rangle=0, \tag{A3}$$

and are normalized according to

$$\langle E',\xi',n'^-|E,\xi,n^-\rangle=\delta(E-E')\,\delta_{\xi,\xi'}\,\delta_{n,n'}. \tag{A4}$$

First, we insert the delta function $\delta(\hat{H}-E)$, into Eq. (A1), according to

$$\hat{P}_{E,\xi}=\sum_{n=0}^{\infty}\int_{-\infty}^{\infty}dE'\,\delta(\hat{H}-E)|E',\xi,n^-\rangle\langle E',\xi,n^-|, \tag{A5}$$

and then we evoke time-dependent scattering theory[35] to express the scattering states $|E,\xi,n^-\rangle$ in terms of the asymptotic free states $|E,\xi,n^o\rangle$,

$$|E,\xi,n^-\rangle=\lim_{t\to\infty}e^{i(\hat{H}-E)t/\hbar}|E,\xi,n^o\rangle. \tag{A6}$$

Substituting Eq. (A6) into Eq. (A5) we obtain

$$\hat{P}_{E,\xi}=\lim_{t\to\infty}e^{i\hat{H}t/\hbar}\delta(\hat{H}-E)\times\left[\sum_{n=0}^{\infty}\int_{-\infty}^{\infty}dE'|E',\xi,n^o\rangle\langle E',\xi,n^o|\right]e^{-i\hat{H}t/\hbar}. \tag{A7}$$

Here, $|E',\xi,n^o\rangle$ are free states of photofragments that evolve according to the free Hamiltonian in the ξ channel,

$$\hat{H}^o\equiv\lim_{R\to\infty}\hat{H}=\frac{K^2}{2\mu}+\epsilon_n, \tag{A8}$$

in the recoil direction of *positive* momenta K (conjugate to the jacobi coordinate R), energy E', and internal quantum states n of energy ϵ_n.

Hence, we can change integration variables, in Eq. (A7), to obtain

$$\hat{P}_{E,\xi}=\lim_{t\to\infty}e^{i\hat{H}t/\hbar}\delta(\hat{H}-E)\times\left[\sum_{n=0}^{\infty}\int_{0}^{\infty}dK|K,n^o\rangle\langle K,n^o|\right]e^{-i\hat{H}t/\hbar}, \tag{A9}$$

where the free states $|K,n^o\rangle$, introduced by Eq. (A9), are normalized according to

$$\langle K',n'^o|K,n^o\rangle=\delta(K-K')\,\delta_{n,n'}. \tag{A10}$$

Equation (A9) involves the sum over a complete set in the space of the vibrational coordinate. However, the translational scattering wavefunctions are not complete, since they cover only the range of positive momenta. In order to com-

Downloaded 03 Oct 2001 to 142.150.224.5. Redistribution subject to AIP license or copyright, see http://ojps.aip.org/jcpo/jcpcr.jsp

plete the integration range in Eq. (A9), we introduce the step function $h_\xi(K)$, defined as 1(0) for positive(negative) values of its argument, and obtain

$$\hat{P}_{E,\xi}=\lim_{t\to\infty} e^{i\hat{H}t/\hbar}\delta(\hat{H}-E) \times\left[\sum_{n=0}^{\infty}\int_{-\infty}^{\infty} dK h_\xi(K)|K,n^o\rangle\langle K,n^o|\right]e^{-i\hat{H}t/\hbar}. \tag{A11}$$

After substituting the closure,

$$\hat{1}=\sum_{n=0}^{\infty}\int_{-\infty}^{\infty} dK|K,n^o\rangle\langle K,n^o|, \tag{A12}$$

we can rewrite Eq. (A11) in terms of the translation momentum operator $\hat{K}$,

$$\hat{P}_{E,\xi}=\lim_{t\to\infty}\delta(\hat{H}-E)e^{i\hat{H}t/\hbar}h_\xi(\hat{K})e^{-i\hat{H}t/\hbar}. \tag{A13}$$

Equation (A1) can be directly obtained from Eq. (A13), by replacing the momentum projection operator,

$$\hat{P}_\xi=\lim_{t\to\infty} e^{i\hat{H}t/\hbar}h_\xi(\hat{K})e^{-i\hat{H}t/\hbar}, \tag{A14}$$

by the spatial projection operator introduced in Eq. (A2). These two projection operators are equivalent, as explicitly shown in Appendix A of Ref. 36.

Finally, we note that Eq. (A13) can also be written in the symmetric form,

$$\hat{P}_{E,\xi}=\hat{P}_\xi\delta(\hat{H}-E)\hat{P}_\xi=\lim_{t\to\infty} e^{i\hat{H}t/\hbar}h_\xi\delta(\hat{H}-E)h_\xi e^{-i\hat{H}t/\hbar}, \tag{A15}$$

noting that $\hat{P}_\xi^2=\hat{P}_\xi$, and that $\hat{P}_\xi$ and $\delta(\hat{H}-E)$ commute.

Comment: The procedure described in Sec. IV A, is more efficient than a more standard "forward-backward" approach, such as

$$\zeta_{j,k}(\xi,t)=(2\pi\hbar)^{-N}\int_{-\infty}^{\infty}dp_s(2\pi i p_s)^{-1}\int d\mathbf{p}_0\int d\mathbf{q}_0 \times e^{iS_t(\mathbf{p}_0,\mathbf{q}_0)/\hbar}C_t(\mathbf{p}_0,\mathbf{q}_0)\times\langle\Psi_0(j)|\mathbf{p}_t,\mathbf{q}_t\rangle \times\langle\mathbf{p}_0,\mathbf{q}_0|\Psi_0(k)\rangle, \tag{A16}$$

where the partial contribution of a single trajectory would require forward propagation from the initial phase point $(\mathbf{p}_0,\mathbf{q}_0)$ to the resulting phase point $(\mathbf{p}_\tau,\mathbf{q}_\tau)$ at time τ, then a "momentum jump" at time τ,

$$\mathbf{p}'_\tau=\mathbf{p}_\tau+p_s\left[\frac{\partial s(\mathbf{q})}{\partial\mathbf{q}}\right]_{\mathbf{q}=\mathbf{q}_\tau}, \tag{A17}$$

then backward propagation from the phase point $(\mathbf{p}'_\tau,\mathbf{q}_\tau)$ to phase point $(\mathbf{p}'_0,\mathbf{q}'_0)$, and finally propagation for time t, from phase point $(\mathbf{p}'_0,\mathbf{q}'_0)$ to phase point $(\mathbf{p}_t,\mathbf{q}_t)$ (see Ref. 31). Note that in contrast to Eq. (4.2), the integrand in Eq. (A16) does not include any damping factor. Therefore, according to Eq. (A16), all contributions of trajectories that do not photodissociate into channel ξ would have to be cancelled out through destructive interference.

[1] M. Shapiro and P. Brumer, in *Adv. in Atom., Mol. and Opt. Phys.*, edited by B. Bederson and H. Walther (Academic, San Diego, 2000), pp. 287–343.
[2] S. A. Rice and M. Zhao, in *Optical Control of Molecular Dynamics* (Wiley, New York, 2000).
[3] P. Brumer and M. Shapiro, Chem. Phys. Lett. **126**, 541 (1986).
[4] T. Seodeman, M. Shapiro, and P. Brumer, J. Chem. Phys. **90**, 7132 (1989).
[5] W. H. Miller, J. Chem. Phys. **53**, 3578 (1970).
[6] V. S. Batista and W. H. Miller, J. Chem. Phys. **108**, 498 (1998).
[7] V. S. Batista, M. T. Zanni, B. T. Greenblatt, D. M. Neumark, and W. H. Miller, J. Chem. Phys. **110**, 3736 (1999).
[8] V. Guallar, V. S. Batista, and W. H. Miller, J. Chem. Phys. **110**, 9922 (1999).
[9] E. A. Coronado, V. S. Batista, and W. H. Miller, J. Chem. Phys. **112**, 5566 (2000).
[10] V. Guallar, V. S. Batista, and W. H. Miller, J. Chem. Phys. **113**, 9510 (2000).
[11] G. Campolieti and P. Brumer, Phys. Rev. A **50**, 997 (1994).
[12] K. G. Kay, J. Chem. Phys. **100**, 4432 (1994).
[13] K. G. Kay, J. Chem. Phys. **101**, 2250 (1994).
[14] M. L. Brewer, J. S. Hulme, and D. E. Manolopoulos, J. Chem. Phys. **106**, 4832 (1997).
[15] B. E. Guerin and M. F. Herman, Chem. Phys. Lett. **286**, 361 (1998).
[16] E. J. Heller, J. Chem. Phys. **95**, 9431 (1991).
[17] F. Grossmann and E. J. Heller, Chem. Phys. Lett. **241**, 45 (1995).
[18] S. Garashchuk, F. Grossmann, and D. J. Tannor, J. Chem. Soc., Faraday Trans. **93**, 781 (1997).
[19] D. V. Shalashilin and B. Jackson, Chem. Phys. Lett. **291**, 143 (1998).
[20] D. Provost and P. Brumer, Phys. Rev. Lett. **74**, 250 (1995).
[21] X. Sun and W. H. Miller, J. Chem. Phys. **110**, 6635 (1999).
[22] V. S. Batista and P. Brumer, J. Phys. Chem. A **105**, 2591 (2001).
[23] J. A. Fleck, Jr., J. R. Morris, and M. D. Feit, Appl. Phys. **10**, 129 (1976).
[24] A. Goldberg and B. W. Shore, J. Phys. B **11**, 3339 (1978).
[25] C. Leforestier and R. Wyatt, J. Chem. Phys. **78**, 2334 (1983).
[26] R. Kosloff and D. Kosloff, J. Comput. Phys. **63**, 363 (1986).
[27] D. Neuhauser and M. Baer, J. Chem. Phys. **90**, 4351 (1989).
[28] B. Spath and W. H. Miller, J. Chem. Phys. **104**, 95 (1996).
[29] M. F. Herman and E. Kluk, Chem. Phys. **91**, 27 (1984).
[30] See Eqs. (A16) and (A17) in the Appendix.
[31] X. Sun and W. H. Miller, J. Chem. Phys. **106**, 6346 (1997).
[32] W. H. Press, B. P. Flannery, S. A. Teukolsky, and W. T. Vetterling, in *Numerical Recipes* (Cambridge University Press, Cambridge, 1986).
[33] This potential, however, is not designed to model true CH_2IBr photodissociation. For the latter, see D. Abrashkevich and P. Brumer (to be published).
[34] V. S. Batista and P. Brumer, J. Phys. Chem. (to be submitted).
[35] R. G. Newton, in *Scattering Theory of Waves and Particles* (McGraw–Hill, New York, 1966).
[36] W. H. Miller, S. D. Schwartz, and J. W. Tromp, J. Chem. Phys. **79**, 4889 (1983).

Downloaded 03 Oct 2001 to 142.150.224.5. Redistribution subject to AIP license or copyright, see http://ojps.aip.org/jcpo/jcpcr.jsp

On the Origin of Pulse Shaping Control of Molecular Dynamics†

Moshe Shapiro

Department of Chemical Physics, The Weizmann Institute of Science, Rehovot, 76100 Israel and ITAMP, Center for Astrophysics, Harvard University, 60 Garden Street, Cambridge, Massachusetts 02138

Paul Brumer*

Chemical Physics Theory Group, Department of Chemistry, University of Toronto, Toronto, Ontario, M5S3H6, Canada

Received: October 20, 2000; In Final Form: January 30, 2001

Pulsed laser control of photodissociation in the strong and the weak coupling regimes is analyzed. Simple pulse shaping conditions are derived and are given explicitly in the weak coupling regime. Implicit equations in the strong coupling regime are also derived. Short, shaped pulses, yielding optimal control, are shown to work due to quantum interference among routes to the same final energy. This is contrary to the prevailing view that the role of a short pulse is to be fast enough so as to "beat the process of intramolecular vibrational redistribution (IVR)".

I. Introduction

Coherent control constitutes a method in which quantum interference effects are used to control molecular processes.[1] There are, at present, two distinct paradigms for the coherent control of chemical reactions. One, due to Brumer and Shapiro,[2] approaches control in energy space. This is done by expanding the molecular states in terms of the eigenstates of the molecular Hamiltonian. Control is shown to be attainable by populating each continuum state using multiple interfering pathways. Ideally, this interference is made to be destructive for all states but one, the ("target" or "objective") state of interest.

The alternative paradigm, originally due to Tannor and Rice[3] and central to the optimal control approach,[4] attempts to achieve the same goal by considering the explicit time dependence of states that evolve to a desired target. Although not as manifestly evident, this approach also relies upon the existence of multiple interfering pathways to bring about control.

Both of these paradigms bring their own correct insights to coherent control. In addition, they each motivate appropriate experiments in different technological domains. Thus, the energy-resolved viewpoint has been used mainly to motivate ns pulsed laser experiments, whereas the time-dependent perspective was used mainly to devise and interpret ultrafast experiments.[5]

Consider now control of the dynamics of isolated systems (e.g., photodissociation processes). Adopting the time-dependent approach to this case has a conceptual drawback that has led to some misunderstanding. Specifically, despite efforts to counter this incorrect viewpoint,[6] there is still talk about the need for faster laser pulses, or more complex laser pulse shapes, to "beat out the effects of intramolecular vibrational redistribution (IVR)". That is, there remains the incorrect perception that control over chemical reactions in isolated molecules is achieved by creating molecular states whose controlled time scale of evolution is faster than IVR rates.[7]

It is the purpose of this paper to show that the energy resolved perspective both corrects this perception and adds considerably to our understanding of pulse-shaped control. Specifically, we show that even for strong laser fields, the shape of the exciting laser pulse, and hence certainly the time scale of the subsequent molecular evolution, is irrelevant to the control over unimolecular processes in the case where a *single* bound state is photodissociated. Second, we explicitly consider pulsed laser excitation when *many* bound states are coupled to a continuum, and show that in this case control is possible. We also derive the pulse shaping conditions that allow for control in this case and show the origin of control in quantum interference.

II. Multichannel Dissociation/Ionization of a Single Precursor State

Consider first the case of a single bound state excited to dissociation using a pulsed laser. Naive thinking would suggest that shaping the pulse, either to enhance particular frequencies or to shorten the pulse in time, might prove useful in order to increase the yield of a desired product state. Here we show that this is not the case. In particular, we show that, contrary to common wisdom, as long as only a single bound state is effectively involved, the situation is uncontrollable, irrespective of the pulse shape used.

Consider the action of a pulse of light, described by a classical time-evolving electric field of polarization $\hat{\epsilon}$,

$$\vec{\epsilon} = 2\hat{\epsilon}\,\mathcal{R}_e\{\epsilon(t)e^{i\omega_L t}\} \tag{1}$$

on an initially bound molecular system. Given the total radiation−matter Hamiltonian in the "electric-dipole" approximation,

$$H_{tot} = H - \vec{\mu}\cdot\vec{\epsilon}(t) \tag{2}$$

where H is the molecular Hamiltonian and $\vec{\mu}$ is the dipole operator, the outcome of the action of the pulse is obtained by

† Part of the special issue "William H. Miller Festschrift".

10.1021/jp0038781 CCC: $20.00 © 2001 American Chemical Society
Published on Web 03/06/2001

solving the time-dependent Schrödinger equation,

$$i\hbar\frac{\partial}{\partial t}|\Psi\rangle = H_{\rm tot}|\Psi\rangle \tag{3}$$

The bound and continuum eigenstates of the molecular Hamiltonian H satisfy the time-independent Schrödinger equation,

$$[E_i - H]|E_i\rangle = [E - H]|E, \mathbf{n}^-\rangle = 0 \tag{4}$$

where $|E_i\rangle$ denote the bound eigenstates and $|E, \mathbf{n}^-\rangle$ the continuum eigenstates, labeled by the indices $\mathbf{n}$ and E, with $\mathbf{n}$ comprising a set of quantum numbers that specify the final ($t \rightarrow \infty$) internal (vibrational, rotational, etc.) states of the dissociated polyatomic fragments as well as the product arrangement. These indices label the eigenstates $|E, \mathbf{n}; 0\rangle$ of the separated fragments Hamiltonian, $H_0 = H - V$. That is,

$$[E - H_0]|E, \mathbf{n}; 0\rangle = 0 \tag{5}$$

Here V is the interaction between the fragments, which naturally decays as R, the distance between the fragments, becomes sufficiently large,

$$\lim_{R\rightarrow\infty} V(R) = 0 \tag{6}$$

We denote the "incoming" eigenstates of H by $|E, \mathbf{n}^-\rangle$. These states satisfy the incoming Lippmann Schwinger equation,

$$|E, \mathbf{n}^-\rangle = |E, \mathbf{n}; 0\rangle + \lim_{\zeta\rightarrow 0}[E - i\zeta - H_0]^{-1}V|E, \mathbf{n}^-\rangle \tag{7}$$

which guarantees[8] that the incoming states correlate in the $t \rightarrow \infty$ limit with a single $|E, \mathbf{n}; 0\rangle$ eigenstate of H_0. That is, we say that

$$\lim_{t\rightarrow\infty}|E, \mathbf{n}^-\rangle e^{-iEt/\hbar} = |E, \mathbf{n}; 0\rangle e^{-iEt/\hbar} \tag{8}$$

meaning more precisely that an arbitrarily narrow wave packet of scattering states $|E, \mathbf{n}^-\rangle$ correlates with an equally narrow wave packet of product states $|E, \mathbf{n}; 0\rangle$ in the long time limit:

$$\lim_{\Delta\rightarrow 0}\lim_{t\rightarrow\infty}\int_\Delta c_E|E, \mathbf{n}^-\rangle e^{-iEt/\hbar}\,dE = \int_\Delta c_E|E, \mathbf{n}; 0\rangle e^{-iEt/\hbar}\,dE \tag{9}$$

The above radiation-free basis set enables us to explicitly include the $t \rightarrow \infty$ limit in the full time dependent wave function. Considering now the case where only a *single* bound state $|E_1\rangle$ is coupled to the continuum, we can expand $|\Psi(t)\rangle$ as[9-11]

$$|\Psi(t)\rangle = b_1(t)|E_1\rangle e^{-iE_1t/\hbar} + \sum_{\mathbf{n}}\int dE b^{(1)}_{E,\mathbf{n}}(t)|E, \mathbf{n}^-\rangle e^{-iEt/\hbar} \tag{10}$$

Substituting this expansion into the time-dependent Schrödinger equation and using the orthogonality of the basis functions yields a set of first-order differential equations for the expansion coefficients,

$$\frac{d}{dt}b_1 = i\int dE\sum_{\mathbf{n}}\Omega_{1,E,\mathbf{n}}(t)b^{(1)}_{E,\mathbf{n}}(t)\,e^{-i\Delta_{E,1}t} \tag{11a}$$

$$\frac{d}{dt}b^{(1)}_{E,\mathbf{n}} = \Omega^*_{1,E,\mathbf{n}}(t)e^{i\Delta_{E,1}t}b_1(t), \text{ for each } E \text{ and } \mathbf{n} \tag{11b}$$

where we have retained only the rotating waves terms. $\Delta_{E,i}$, the detuning, is defined as

$$\Delta_{E,i} \equiv \omega_{E,i} - \omega_L \text{ with } \omega_{E,i} \equiv (E - E_i)/\hbar,\ i = 1, ..., \tag{12}$$

and $\Omega_{1,E,\mathbf{n}}(t)$, the (time-varying) Rabi-frequency, is defined as

$$\Omega_{1,E,\mathbf{n}}(t) \equiv \langle E_1|\mu|E, \mathbf{n}^-\rangle\epsilon(t)/\hbar \tag{13}$$

where μ is the projection of the dipole operator along the polarization vector of the field.

We proceed[12] by integrating the $b^{(1)}_{E,\mathbf{n}}$ continuum coefficients of eq 11 over time, while imposing the boundary condition that only the $|E_1\rangle$ state is initially populated, i.e., that $b^{(1)}_{E,\mathbf{n}}(t \rightarrow -\infty) = 0$. With this boundary condition, we have that

$$b^{(1)}_{E,\mathbf{n}}(t) = i\int_{-\infty}^{t} dt'\Omega^*_{1,E,\mathbf{n}}(t')b_1(t')e^{i\Delta_{E,1}t} \tag{14}$$

Of interest is the state-specific probability, $P_{\mathbf{n}}(E)$, which is the long-time probability, at fixed energy E, of observing a particular internal state $|\mathbf{n}\rangle$ of the dissociated fragments. It is given using eq 14 as

$$P_{\mathbf{n}}(E) = P_{\mathbf{n}}(E, t\rightarrow\infty) = |b^{(1)}_{E,\mathbf{n}}(t\rightarrow\infty)|^2 = \left|\frac{1}{\hbar}\langle E_1|\mu|E, \mathbf{n}^-\rangle\int_{-\infty}^{\infty} dt'\epsilon^*(t')b_1(t')e^{i\Delta_{E,1}t'}\right|^2 \tag{15}$$

It follows from eqs 14 and 15 that the long-time ratio of probabilities (which is the key quantity to control in chemical reactions) to observe two internal fragment states is given by

$$\frac{P_{\mathbf{n}}(E)}{P_{\mathbf{m}}(E)} = \frac{P_{\mathbf{n}}(E, t)}{P_{\mathbf{m}}(E, t)} = \left|\frac{b^{(1)}_{E,\mathbf{n}}(t)}{b^{(1)}_{E,\mathbf{m}}(t)}\right|^2 = \left|\frac{\langle E_1|\mu|E, \mathbf{n}^-\rangle}{\langle E_1|\mu|E, \mathbf{m}^-\rangle}\right|^2 \tag{16}$$

We see that the relative probabilities of populating different asymptotic states at a fixed energy E are independent of the laser pulse attributes (save for the polarization direction). Moreover, the branching ratio does not change during the pulse. This result, which coincides with that of perturbation theory, holds true irrespective of the laser power, provided that only one bound state $|E_1\rangle$ is coupled to the continuum.

The above result holds true even when the rotating waves approximation, adopted above, breaks down, because even in this case the probability can be written as

$$P_{\mathbf{n}}(E) = |b^{(1)}_{E,\mathbf{n}}(t\rightarrow\infty)|^2 = \left|\frac{1}{\hbar}\langle E_1|\mu|E, \mathbf{n}^-\rangle\int_{-\infty}^{\infty} dt'\{\epsilon^*(t')e^{i\Delta_{E,1}t'} + \epsilon(t')e^{i(\omega_{E,1}+\omega_L)t'}\}b_1(t')\right|^2 \tag{17}$$

and the pulse attributes still cancel out when the $P_{\mathbf{n}}(E)/P_{\mathbf{m}}(E)$ branching ratio is evaluated.

We conclude that pulse shaping does not provide a means of controlling the ratio of products formed in the excitation of a single bound state. Hence, the common phrase that it is advantageous to shorten the laser pulse "in order to beat IVR" is totally misleading: the fate of the system merely follows the nature of the radiation-free $|E, \mathbf{n}^-\rangle$ molecular eigenstates.

III. Quantum Interference Control

The lack of pulse-shaping control demonstrated above can be overcome by photodissociating not just one $|E_1\rangle$ bound state, but a superposition of several bound states $|E_i\rangle$. Such a superposition state can be created separately by a preparation

pulse. This is in essence the pump−dump control scenario.[3,13] Alternatively, the superposition state can be created by the photolysis pulse itself (by, e.g., a stimulated Raman process), provided that the bandwidth of the pulse is comparable to the energy spacings between the $|E_i\rangle$ levels.

Mathematically speaking, the object of control is the preparation of a single $|E, \mathbf{n}^-\rangle$ state. If this is achieved, we are guaranteed, by eq 8, complete control insofar as only one fragment target state $|E, \mathbf{n}; 0\rangle$ is populated as $t \rightarrow \infty$. With this in mind, we rewrite eq 10 in matrix notation as

$$|\Psi^{(1)}(t)\rangle = \int dE e^{-iEt/\hbar} (b^{(1)}_{E,\mathbf{n}_1}(t), b^{(1)}_{E,\mathbf{n}_2}(t), b^{(1)}_{E,\mathbf{n}_3}(t), ...) \begin{pmatrix} |E, \mathbf{n}_1^-\rangle \\ |E, \mathbf{n}_2^-\rangle \\ |E, \mathbf{n}_3^-\rangle \\ . \\ . \\ . \end{pmatrix} \quad (18)$$

where $|\Psi^{(1)}(t)\rangle$ is the excited portion of the wave packet that originated from state $|E_1\rangle$, namely,

$$|\Psi^{(1)}(t)\rangle \equiv |\Psi(t)\rangle - b_1|E_1\rangle e^{-iE_1t/\hbar} \quad (19)$$

To achieve the control target we consider preparing a whole array of wave packets, by, for example, starting with other initial states composed of the system bound states $|E_i\rangle$. That is,

$$\underline{\Psi}(t) = \int dE e^{-iEt/\hbar} \underline{\underline{b}}(E) \cdot \underline{\psi}(E) \quad (20)$$

where

$$\underline{\psi}(t) \equiv \begin{pmatrix} |\Psi^{(1)}(t)\rangle \\ |\Psi^{(2)}(t)\rangle \\ |\Psi^{(3)}(t)\rangle \\ . \\ . \\ . \end{pmatrix} \quad (21)$$

$$\underline{\underline{b}}(E) \equiv \begin{pmatrix} b^{(1)}_{E,\mathbf{n}_1}, b^{(1)}_{E,\mathbf{n}_2}, b^{(1)}_{E,\mathbf{n}_3}, ... \\ b^{(2)}_{E,\mathbf{n}_1}, b^{(2)}_{E,\mathbf{n}_2}, b^{(3)}_{E,\mathbf{n}_3}, ... \\ b^{(3)}_{E,\mathbf{n}_1}, b^{(3)}_{E,\mathbf{n}_2}, b^{(3)}_{E,\mathbf{n}_3}, ... \\ . \\ . \\ . \end{pmatrix} \quad (22)$$

and

$$\underline{\psi}(E) \equiv \begin{pmatrix} |E, \mathbf{n}_1^-\rangle \\ |E, \mathbf{n}_2^-\rangle \\ |E, \mathbf{n}_3^-\rangle \\ . \\ . \\ . \end{pmatrix} \quad (23)$$

It is easy to see that the $\underline{\underline{b}}(E)$ matrix factorizes as

$$\underline{\underline{b}}(E) = \underline{\underline{\hat{E}}}(E) \cdot \underline{\underline{M}}(E) \quad (24)$$

where

$$\underline{\underline{M}}(E) = \begin{pmatrix} \langle E_1|\mu|E, \mathbf{n}_1^-\rangle, \langle E_1|\mu|E, \mathbf{n}_2^-\rangle, ... \\ \langle E_2|\mu|E, \mathbf{n}_1^-\rangle, \langle E_2|\mu|E, \mathbf{n}_2^-\rangle, ... \\ . \\ . \\ . \end{pmatrix} \quad (25)$$

and where $\underline{\underline{\hat{E}}}(E)$ is a diagonal matrix of the Fourier transform of the pulse amplitude times the bound states coefficients, at the transition frequencies $\omega_{E,i}$,

$$\underline{\underline{\hat{E}}}(E) = \begin{pmatrix} E_1(E), 0, 0, 0, ... \\ 0, E_2(E), 0, 0, ... \\ 0, 0, E_3(E), 0, ... \\ . \\ . \\ . \end{pmatrix} \quad (26)$$

with

$$E_i(E) = \int_{-\infty}^{\infty} dt \epsilon^*(t) e^{i\Delta_{E,i}t} b_i(t) \quad (27)$$

Writing the array of possible wave function produced as,

$$\underline{\Psi}(t) = \int dE e^{-iEt/\hbar} \underline{\underline{\hat{E}}}(E) \cdot \underline{\underline{M}}(E) \cdot \underline{\psi}(E) \quad (28)$$

allows us to examine the possibility of taking different linear combinations of the components of the $\underline{\Psi}(t)$ vector so as to satisfy the control objectives of producing a single $|E, \mathbf{n}_i^-\rangle$ state. In this way different pathways starting with different precursor states leading to the same $|E, \mathbf{n}_i^-\rangle$ state will be seen to interfere to achieve the desired goal.

As an example, we consider a superposition state composed of the sum over the components of $\underline{\psi}(t)$,

$$\Psi'(t) = \sum_k \int dE e^{-iEt/\hbar} E_k(E) \sum_j \underline{\underline{M}}(E)_{k,j} |E, \mathbf{n}_j^-\rangle \quad (29)$$

In the weak field limit, the population and the phase of the initial levels can be assumed constant with time,

$$b_k(t) \approx b_k \equiv b_k(-\infty) \quad (30)$$

in which case all the $E_k(E)$ matrix elements factor as

$$E_k(E) \approx b_k \int_{-\infty}^{\infty} dt \epsilon^*(t) e^{i\Delta_{E,k}t} = 2\pi b_k \bar{\epsilon}(\Delta_{E,k}) \quad (31)$$

where

$$\bar{\epsilon}(\omega) \equiv (1/2\pi) \int_{-\infty}^{\infty} dt \epsilon^*(t) e^{i\omega t} \quad (32)$$

Our objective to populate exclusively the ith fragment state $|E, \boldsymbol{n}_i^-\rangle$ can be realized in the weak field domain by choosing the pulse shape which defines $\Psi'(t)$ [eq 29] to satisfy the condition,

$$b_k \bar{\epsilon}_i(\Delta_{E,k}) = (\underline{\underline{M}}(E)^{-1})_{i,k} \quad (33)$$

This choice eliminates all but a single $|E, \boldsymbol{n}_i^-\rangle$ state in $\Psi'(t)$ given by eq 29.

Thus, the control objective, the ith product state, is seen to be realized by starting out with an initial superposition of bound

states,

$$|\Phi(t)\rangle = \sum_k b_k |E_k\rangle e^{-iE_k t/\hbar} \tag{34}$$

and subjecting the system to the action of a pulse shaped according to eq 33. This allows for multiple-path interference between the various ways of generating the $|E, \boldsymbol{n}_i^-\rangle$ state. The weight of each pathway is chosen so as to cause destructive interference in the production of all the $|E, \boldsymbol{n}^-\rangle$ states but one, the $|E, \boldsymbol{n}_i^-\rangle$ state.

Thus, pulse shaping leads to control only insofar as it allows for interference between different coherently related bound states comprising Φ, or more generally, between different pathways leading to the same product. Hence, the effect of a short pulse is not to "beat IVR", but rather, due to its increased bandwidth, to allow processes originating in more bound states to interfere with each other in forming the same $|E, \boldsymbol{n}_i^-\rangle$ state.

In general, control is incomplete because the pulse shaping conditions of eq 33 cannot be satisfied simultaneously for all energies. This can be seen by noting that the $(\underline{\underline{M}}(E)^{-1})$ matrix element, which (for a single i) is a function of two variables, k and E, has to be equated to a product of a function of k, b_k, and a function of E, $\bar{\epsilon}_i(\Delta_{E,k})$. In general, this equality cannot be satisfied. There are nevertheless important cases in which eq 33 can be satisfied. These are: either when $\underline{\underline{M}}(E)$ does not vary too rapidly with E, or, conversely, when the $\langle E_1|\mu|E, \boldsymbol{n}^-\rangle$ matrix elements, which determine $\underline{\underline{M}}(E)$ (and the absorption spectrum), span a very narrow range of energies (e.g., a narrow resonance).

The weak field control discussed here must be achieved in two steps. First it is necessary to create the $\Phi(t)$ superposition state of eq 34. This state is then irradiated with the pulse satisfying eq 33. This is the essence of the weak field pump–dump scenario. However, in the strong field domain these two processes cannot be separated because the factorization of eq 31 does not hold. In that case the control conditions become

$$E_{i,k}(E) = (\underline{\underline{M}}(E)^{-1})_{i,k} \tag{35}$$

In this strong field regime the $b_k(t)$ coefficients are embedded in $E_k(E)$ (see eq 27) and are themselves functions of $\epsilon(t)$. Hence the problem is inherently nonlinear, necessitating an iterative solution. Nevertheless, the same interference mechanism outlined in the weak field domain applies. The only difference is that the pulse-shaping conditions are given implicitly via eq 35, rather than explicitly via eq 33, as in the weak field domain.

IV. Bichromatic Control

As an example of the general procedure described above we now examine the simple case—bichromatic control[2]—achieved by considering a two-dimensional $\underline{\Psi}(t)$ vector. Constructing a linear superposition of just two initial states

$$|\Phi(t)\rangle = b_1|E_1\rangle e^{-iE_1 t/\hbar} + b_2|E_2\rangle e^{-iE_2 t/\hbar} \tag{36}$$

we have that

$$b_{E,\mathbf{n}}(t \to \infty) = \frac{i}{\hbar}\{\langle E, \mathbf{n}^-|\mu|E_1\rangle \int_{-\infty}^{\infty} dt' \epsilon^*(t') e^{i\Delta_{E,1}t'} b_1(t') + \langle E, \mathbf{n}^-|\mu|E_2\rangle \int_{-\infty}^{\infty} dt' \epsilon(t') e^{i\Delta_{E,2}t'} b_2(t')\} \tag{37}$$

In first-order perturbation theory, $b_1(t)$ and $b_2(t)$ are constant. Hence in the weak field regime,

$$b_{E,\mathbf{n}}(t \to \infty) \approx \frac{2\pi i}{\hbar}\{\langle E, \mathbf{n}^-|\mu|E_1\rangle \bar{\epsilon}(\Delta_{E,1}) b_1 + \langle E, \mathbf{n}^-|\mu|E_2\rangle \bar{\epsilon}(\Delta_{E,2}) b_2\} \tag{38}$$

where $\bar{\epsilon}(\omega)$ is defined in eq 32. Recognizing that $\bar{\epsilon}(\omega)$ has a phase, we can write

$$\bar{\epsilon}(\Delta_{E,1}) = |\bar{\epsilon}(\Delta_{E,1})| e^{-i\theta(\Delta_{E,1})}, \bar{\epsilon}(\Delta_{E,2}) = |\bar{\epsilon}(\Delta_{E,2})| e^{-i\theta(\Delta_{E,2})} \tag{39}$$

and transform eq 38 into

$$b_{E,\mathbf{n}}(\infty) = \frac{2\pi i}{\hbar}\{\langle E, \mathbf{n}^-|\mu|E_1\rangle |\bar{\epsilon}(\Delta_{E,1})| e^{-i\theta(\Delta_{E,1})} b_1 + \langle E, \mathbf{n}^-|\mu|E_2\rangle |\bar{\epsilon}(\Delta_{E,2})| e^{-i\theta(\Delta_{E,2})} b_2\} \tag{40}$$

The probability of observing the product state $\mathbf{n}$ at infinite time is therefore now given as

$$P_{\mathbf{n}}(E) = \frac{4\pi^2}{\hbar^2}|\langle E, \mathbf{n}^-|\mu|E_1\rangle|\bar{\epsilon}(\Delta_{E,1})| e^{-i\theta(\Delta_{E,1})} b_1 + \langle E, \mathbf{n}^-|\mu|E_2\rangle|\bar{\epsilon}(\Delta_{E,2})| e^{-i\theta(\Delta_{E,2})} b_2|^2 \tag{41}$$

It is clear that in this configuration the pulse attributes have been "entangled" with the material matrix elements. As a result, by shaping the pulse (e.g., by tuning the relative phase $\theta(\Delta_{E,2}) - \theta(\Delta_{E,1})$ or the relative amplitude $|\bar{\epsilon}(\Delta_{E,2})/\bar{\epsilon}(\Delta_{E,1})|$), we can change the branching ratios to different channels. The above mechanism serves as the basis for the so-called bichromatic coherent control scenario.[2]

It is possible to deviate from the weak field regime and incorporate some of the effects of strong fields in a simple manner by assuming that state $|E_1\rangle$ is decoupled from state $|E_2\rangle$. In that case it is possible to solve explicitly for the $b_1(t)$ coefficient by substituting eq 14 in eq 11a to obtain a first-order integro-differential equation for b_1,

$$\frac{db_1}{dt} = \frac{-1}{\hbar^2}\int dE \sum_{\mathbf{n}} |\langle E, \mathbf{n}^-|\mu|E_1\rangle|^2 \epsilon(t) \int_{-\infty}^{t} dt' \epsilon^*(t') e^{-i\Delta_{E,1}(t-t')} b_1(t') \tag{42}$$

Equation 42 can be solved numerically in a straightforward fashion. Nevertheless, it is instructive to analyze it in terms of $F_1(t-t')$, the "spectral autocorrelation function",[12,14,11,15] defined as the Fourier transform of the absorption spectrum,

$$F_1(t-t') = \int_0^{\infty} dE A_1(E) e^{-i\omega_{E,1}(t-t')} \tag{43}$$

where $E = 0$ is taken to be the lowest (threshold) energy in the continuum, and $A_i(E)$, the absorption spectrum from the ith state, is given as

$$A_i(E) \equiv \sum_{\mathbf{n}} |\langle E, \mathbf{n}^-|\mu|\psi_i\rangle|^2 \tag{44}$$

With the above definition of $F_1(t-t')$, we can rewrite eq 42 as

$$\frac{db_1}{dt} = \frac{-\epsilon(t)}{\hbar^2}\int_{-\infty}^{t} dt' \epsilon^*(t') F_1(t-t') b_1(t') \tag{45}$$

We see that the value of the ground-state coefficient at time t

is determined by its past history at $t' < t$ through the "memory kernel" $\epsilon(t)\epsilon(t')F_1(t - t')$.

The simplest (though approximate) solution of eq 45 is obtained if one can assume that all the continua are "flat", i.e., that the bound continuum matrix elements vary slowly with energy and can be replaced by their value at some average energy, say $E_L = E_1 + \hbar\omega_L$

$$\sum_{\mathbf{n}}|\langle E, \mathbf{n}^-|\mu|E_1\rangle|^2 \approx \sum_{\mathbf{n}}|\langle E_L, \mathbf{n}^-|\mu|E_1\rangle|^2 \qquad (46)$$

If in addition one assumes that $\langle E = 0, \mathbf{n}^-|\mu|E_1\rangle \approx 0$ (i.e., the photoabsorption spectrum starts at post-threshold energies), the above approximation, called the "slowly varying continuum approximation" (SVCA),[12,16,17] localizes the autocorrelation function in time. To see this, we note that under the SVCA assumptions it follows from eq 43 that

$$F_1(t - t') \approx \int_{-\infty}^{\infty} dE A_1(E)e^{-i\omega_{E,1}(t-t')} \approx A_1(E_L)\int_{-\infty}^{\infty} dE e^{-i\omega_{E,1}(t-t')} = 2\pi\hbar A_1(E_L)\delta(t - t') \quad (47)$$

Substituting eq 47 in eq 45 and performing the integration over E and t', we obtain that

$$\frac{db_1}{dt} = -\Omega(t)b_1(t) \qquad (48)$$

hence,

$$b_1(t) = b_1(-\infty)e^{-\int_{-\infty}^{t}\Omega(t')dt'} \qquad (49)$$

where $\Omega(t)$—the "imaginary Rabi frequency"—is defined as

$$\Omega(t) \equiv \pi A_1(E_L)|\epsilon(t)|^2/\hbar = \pi\sum_{\mathbf{n}}|\langle E_L, \mathbf{n}^-|\mu|E_1\rangle\epsilon(t)|^2/\hbar \qquad (50)$$

The factor of 1/2 relative to eq 47 arises because the integration over $t' - t$ in eq 45 is performed over the $[-\infty, 0]$ range rather than the usual $[-\infty, +\infty]$ range.

It follows from eq 49 that a "slowly varying" continuum acts as an irreversible "perfect absorber", since in this approximation $b_1(t)$ decreases monotonically (though not necessarily purely exponentially) with time. In many cases the continuum may have structures that are narrower than the effective bandwidth of the pulse (which depends on its frequency profile and its intensity). Such structures may be due to either the natural spectrum of the nonradiative Hamiltonian[18,19] or to the interaction with the strong external field.[20,21] Under such circumstances we expect the SVCA approximation to break down, yielding nonmonotonic decay dynamics.

Using the SVCA we can now write an analytic formula for bichromatic control that goes beyond perturbation theory. Allowing the initial coefficients to decay according to eq 49, we obtain from eq 37 that

$$b_{E,\mathbf{n}}(t \to \infty) = \frac{i}{\hbar}\{\langle E, \mathbf{n}^-|\mu|E_1\rangle b_1\int_{-\infty}^{\infty} dt'\epsilon_1^*(t')e^{i\Delta_{E,1}t' - \pi/\hbar A_1(E_L)\int_{-\infty}^{t'}|\epsilon_1(t'')|^2dt''} + \langle E, \mathbf{n}^-|\mu|E_2\rangle b_2\int_{-\infty}^{\infty} dt'\epsilon_2^*(t')e^{i\Delta_{E,2}t' - \pi/\hbar A_2(E_L)\int_{-\infty}^{t'}|\epsilon_2(t'')|^2dt''}\} \quad (51)$$

where $b_i \equiv b_i(-\infty)$, $i = 1, 2$. Therefore, the probability of observing a particular channel $\mathbf{n}$ is given as

$$P_{\mathbf{n}}(E) = \frac{4\pi^2}{\hbar^2}|\langle E, \mathbf{n}^-|\mu|E_1\rangle|\bar{\eta}(\Delta_{E,1})|e^{-i\theta(\Delta_{E,1})}b_1 + \langle E, \mathbf{n}^-|\mu|E_2\rangle|\bar{\eta}(\Delta_{E,2})|e^{-i\theta(\Delta_{E,2})}b_2 \quad (52)$$

where

$$\bar{\eta}(\omega) \equiv (1/2\pi)\int_{-\infty}^{\infty} dt\epsilon^*(t)e^{-\pi/\hbar A_1(E_L)\int_{-\infty}^{t}|\epsilon(t')|^2dt'}e^{i\omega t} \quad (53)$$

This formulation therefore gives a result that is correct (within the range of validity of the SVCA) to all field strengths and that resembles the weak field bichromatic control result (eq 41). The only difference is that instead of the Fourier transform of the pulse electric field, eq 52 depends on the Fourier transform of the product of the pulse electric field and the $e^{-\pi/\hbar A_1(E_L)\int_{-\infty}^{t}|\epsilon(t')|^2dt'}$ decaying factor, describing the depletion of the initial state(s) due to the action of the pulse.

Given this result, the optimal control pulse shaping conditions (eq 33) now become

$$b_k\bar{\eta}_i(\Delta_{E,k}) = (\underline{\underline{M}}(E)^{-1})_{i,k} \qquad (54)$$

This result resembles the weak field condition of eq 33, but due to the replacement of $\bar{\epsilon}_i(\Delta_{E,k})$ by $\bar{\eta}_i(\Delta_{E,k})$, it applies (within the range of validity of the SVCA) to strong fields as well.

V. Summary

We have elucidated the nature of pulsed-shaping control of photodissociation from the viewpoint of energy resolved coherent control theory. The result is a clear-cut demonstration that control is not dependent on time dependent aspects of the pulse in cases where excitation is from a single initial bound state. When excitation is from a superposition of states, the pulse shaping is seen to enhance or reduce the role of multiple interfering pathways that are responsible for control. This discussion should, therefore, lay to rest any attempt to attribute control to effective competition with internal relaxation processes in the molecule which, by their very nature, are coherent and phase preserving.

Acknowledgment. We are pleased to submit this paper in honor of the 60th birthday of W. H. Miller, a leader in the field of chemical physics for over three decades. We thank the U.S. Office of Naval Research and the Minerva Foundation, Germany, for support of this research. M.S. thanks the Institute for Theoretical Atomic and Molecular Physics, Harvard University, for its hospitality during the time this paper was written.

References and Notes

(1) For reviews, see Shapiro, M.; Brumer, P. *Adv. Atom. Mol. and Opt. Physics* **2000**, *42*, 287. Rice, S. A.; Zhao, M. *Optical Control Of Molecular Dynamics*; Wiley: New York, 2000.

(2) Brumer, P.; Shapiro, M. *Chem. Phys. Lett.* **1986**, *126*, 541. Shapiro, M.; Brumer, P. *J. Chem. Soc., Faraday Trans. 2* **1997**, *93*, 1263.

(3) Tannor, D.; Rice, S. A. *J. Chem. Phys.* **1985**, *83*, 5013. Tannor, D.; Kosloff, R.; Rice, S. A. *J. Chem. Phys.* **1986**, *85*, 5805.

(4) For a recent review, see Rabitz, H.; de Vivie-Riedle, R.; Motzkus, M.; Kompa, K. R. *Science* **2000**, *288*, 824.

(5) See, e.g., Assion, T., et al. *Science* **1998**, *282*, 919. Kleiman, V. D.; Zhu, L.; Li, X.; Gordon, R. J. *J. Chem. Phys.* **1995**, *102*, 5863. Shnitman, A.; Sofer, I.; Golub, I.; Yogev, A.; Shapiro, M.; Chen, Z.; Brumer, P. *Phys. Rev. Lett.* **1996**, *76*, 2886.

(6) Brumer, P.; Shapiro, M. *Chem. Phys.* **1989**, *139*, 221.

(7) Of course, there may be a need for fast pulses to compete with decoherence processes which emanate from coupling to systems outside the molecule (e.g., decoherence due to either spontaneous emission or to collision with molecules in the environment). These, however, are processes that are distinct from intramolecular vibrational redistribution which cannot decohere the system.

(8) Levine, R. D.; *Quantum Mechanics of Molecular Rate Processes*; Clarendon Press: Oxford, 1969.

(9) Shapiro, M. *Isr. J. Chem.* **1973**, *11*, 691.

(10) Cohen-Tannoudji, C.; *Quantum Mechanics*; John Wiley & Sons: New York, 1977; Vol. 2, ch XIII.

(11) Shapiro, M. *J. Phys. Chem.* **1993**, *97*, 7396. Shapiro, M. *J. Chem. Phys.* **1993**, *99*, 2453.

(12) Shapiro, M. *J. Chem. Phys.* **1994**, *101*, 3844.

(13) Seideman, T.; Shapiro, M.; Brumer, P. *J. Chem. Phys.* **1989**, *90*, 7132.

(14) Heller, E. J. In *Potential Energy Surfaces; Dynamics Calculations*; Truhlar, D. G., Ed.; Plenum: New York, 1981. Heller, E. J. *Acc. Chem. Res.* **1981**, *14*, 368.

(15) Abrashkevich, A. G.; Shapiro, M. *J. Phys. B* **1996**, *29*, 627.

(16) Frishman, E.; Shapiro, M. *Phys. Rev. A* **1996**, *54*, 3310.

(17) Vardi, A.; Shapiro, M. *J. Chem. Phys.* **1996**, *104*, 5490.

(18) Shapiro, M. *J. Phys. Chem.* **1998**, *102*, 9570.

(19) Shapiro, M.; Vrakking, M. J. J.; Stolow, A. *J. Chem. Phys.* **1999**, *110*, 2465.

(20) See, for example, Knight, P. L.; Lauder, M. A.; Dalton, B. J. *Phys. Rep.* **1990**, *190*, 1 and references therein. Faucher, O.; Charalambidis, D.; Fotakis, C.; Zhang, J.; Lambropoulos, P. *Phys. Rev. Lett.* **1993**, *70*, 3004.

(21) Chen, Z.; Shapiro, M.; Brumer, P. *J. Chem. Phys.* **1995**, *102*, 5683. Shnitman, A.; Sofer, I.; Golub, I. I.; Yogev, A.; Shapiro, M.; Chen, Z.; Brumer, P. *Phys. Rev. Lett.* **1996**, *76*, 2886.

10

Coherent Control of Quantum Chaotic Diffusion

Jiangbin Gong and Paul Brumer
Chemical Physics Theory Group, University of Toronto, Toronto, Canada M5S 3H6
(Received 30 May 2000)

Extensive coherent control over quantum chaotic diffusion using the kicked rotor model is demonstrated and its origin in deviations from random matrix theory is identified. Further, the extent of control in the presence of external decoherence is established. The results are relevant to both areas of quantum chaos and coherent control.

DOI: 10.1103/PhysRevLett.86.1741 PACS numbers: 05.45.Gg, 05.45.Mt, 05.60.Gg, 32.80.Qk

The kicked rotor and its classical limit, the standard map, have long served as paradigms for classical and quantum chaos [1]. The classical dynamics shows characteristic diffusive energy growth whereas the quantum dynamics shows similar chaotic short time behavior, followed by the suppression of diffusion at longer times. In this Letter, we demonstrate that the quantum features of the chaotic kicked rotor allow for extensive coherent control [2] over quantum chaotic diffusion, even in the presence of modest decoherence. In particular, we show that quantum relaxation dynamics in the kicked rotor model is sensitive to the coherence characteristics of the initial state, and that altering these characteristics allows for control over the energy diffusion. The extent of the controlled behavior is vast, from strong suppression to strong enhancement of diffusion.

Consider the kicked rotor whose Hamiltonian is given by

$$H(\hat{L},\theta,t) = \frac{\hat{L}^2}{2I} + \lambda\cos(\theta)\sum_n \delta(t/T - n), \quad (1)$$

where $\hat{L}$ is the angular momentum operator, θ is the conjugate angle, I is the moment of inertia, λ is the strength of the "kicking field," and T is the time interval between kicks. The quantum time evolution operator $\hat{F}$ for times $(N - 1/2)T$ to $(N + 1/2)T$ is [1]

$$\hat{F} = \exp\left[i\frac{\tau}{4}\frac{\partial^2}{\partial\theta^2}\right]\exp[-ik\cos(\theta)]\exp\left[i\frac{\tau}{4}\frac{\partial^2}{\partial\theta^2}\right], \quad (2)$$

with dimensionless parameters $\tau = \hbar T/I$ and $k = \lambda T/\hbar$. The classical limit [1] of this quantum map is given by the standard map, which, when expressed in terms of dimensionless variables θ and the scaled c-number angular momentum $\tilde{L} = L\tau/\hbar$, takes the following form:

$$\begin{aligned}\theta_N &= \theta_{N-1} + (\tilde{L}_N + \tilde{L}_{N-1})/2,\\ \tilde{L}_N &= \tilde{L}_{N-1} + \kappa\sin(\theta_{N-1} + \tilde{L}_{N-1}/2),\end{aligned} \quad (3)$$

where $\kappa = k\tau$, and $(\tilde{L}_N, \theta_N)$ represents the phase space location of a classical trajectory after N kicks. The system is chaotic for $\kappa > \kappa_{cr} = 0.9716\ldots$. The resultant diffusion constant can be defined as the absorption rate of the average scaled rotational energy $\tilde{E} \equiv \langle\tilde{L}^2\rangle/2$. Comparing classical and quantum dynamics for typical initial classical states shows that quantum dynamics displays significant suppression of the classical chaotic diffusion, i.e., the external field can only excite a finite number of unperturbed energy levels [3].

The fact that the rotor is a Hamiltonian system and the kick is coherent implies that the system maintains its quantum phase throughout the evolution. If this is the case then the system should be controllable via coherent control [2], i.e., by using quantum interference phenomena to affect the dynamics. To demonstrate this, and to examine the extent of possible control, we consider the dynamics of states which are initially composed of superpositions of two arbitrary angular momentum eigenstates, $|m\rangle = \exp(im\theta)/\sqrt{2\pi}$ and $|n\rangle = \exp(in\theta)/\sqrt{2\pi}$. Each of these eigenstates is classically allowed, with a corresponding classical distribution function given by $\rho^c_m(\theta,\tilde{L}) = \delta_{\tilde{L}/\tau,m}/2\pi$ and $\rho^c_n(\theta,\tilde{L}) = \delta_{\tilde{L}/\tau,n}/2\pi$, respectively [4].

To show that changing the coherent characteristics of the initial state significantly alters the subsequent dynamics, we consider the dynamics of states given initially by the superposition $|\psi\rangle = \cos(\alpha)|m\rangle + \sin(\alpha)\exp(i\beta)|n\rangle$. Typical results, culled from numerous cases of varying α, β, k, and τ are shown below and correspond to a weaker and stronger chaotic case, and to two values of β, i.e., $\beta = 0$, and $\beta = \pi$. Specifically, we display below results for case (a) $|\psi^{\pm}_a\rangle = (|+2\rangle \pm |-1\rangle)/\sqrt{2}$, with $\tau = 0.5$, $k = 5.0$, and for case (b) $|\psi^{\pm}_b\rangle = (|+1\rangle \pm |+2\rangle)/\sqrt{2}$, with $\tau = 1.0$, $k = 5.0$. Note that neither the basis states nor the superposition states are eigenstates of the parity operator.

Figure 1 shows $\tilde{E}$ for each of these two systems and for each of the values of β. Figure 1a, for example, displays $\tilde{E}$ for $|\psi^-_a\rangle$ (dashed curve) and for $|\psi^+_a\rangle$ (solid curve). Clearly, the initial state $|\psi^-_a\rangle$ gives clear diffusive behavior during the first 40 kicks whereas energy absorption in the case of $|\psi^+_a\rangle$ is completely suppressed. As a result, $\tilde{E}(t = 40T) = 9.6$ for the $|\psi^-_a\rangle$ case, while $\tilde{E}(t = 40T) = 1.6$ for propagation from the initial state $|\psi^+_a\rangle$. Note (i) that this huge difference is achieved solely by changing the initial relative phase β between the two participating states $|+2\rangle$ and $|-1\rangle$ in the initial

 © 2001 The American Physical Society

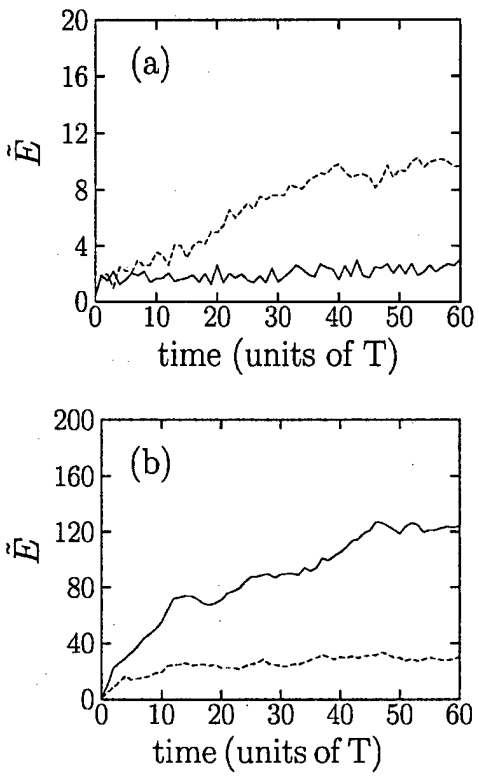

FIG. 1. The expectation value of the dimensionless scaled rotational energy $\tilde{E} = \langle \hat{L}^2 \rangle \tau^2 / 2\hbar^2$ versus time (in units of T). (a) Solid and dashed lines are for the initial states $|\psi_a^+\rangle$ and $|\psi_a^-\rangle$, respectively, $\tau = 0.5$, $k = 5.0$. (b) Solid and dashed lines are for the initial states $|\psi_b^+\rangle$ and $|\psi_b^-\rangle$, respectively, $\tau = 1.0$, $k = 5.0$.

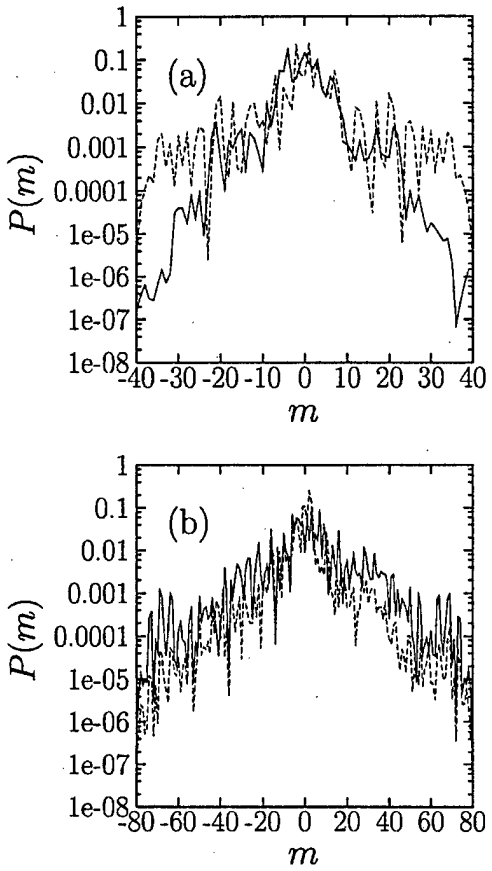

FIG. 2. Probability $P(m)$ of finding the system in the state $|m\rangle$ at $t = 60T$. Results are for the cases shown in Fig. 1.

superposition, and (ii) that by contrast, each of $|+2\rangle$ or $|-1\rangle$ individually would behave similarly to one another with respect to energy absorption, giving $\tilde{E}(t = 40T) = 5.4$ and 6.0, respectively. Hence, the observed control is due entirely to changing the coherent properties of the initial superposition state.

Similar control persists for the more chaotic case shown in Fig. 1b. Here $|\psi_b^+\rangle$ (solid line) shows extensive chaotic diffusion (i.e., compare ordinates scale for Figs. 1a and 1b) for up to 45 kicks, giving $\tilde{E}(t = 45T)$ far higher than the value of 70.4 and 77.1 reached by propagating either of the basis functions $|+1\rangle$ and $|+2\rangle$ independently. Further, and by contrast, there is essentially no quantum diffusion after $t = 4T$ for $|\psi_b^-\rangle$ (dashed line). Control (not shown) is possible for the resonant case as well, e.g., where $\tau = \pi/3$, but it is somewhat less extensive.

These differences are also reflected in the details of the evolving wave functions. For example, Fig. 2 shows the probability $P(m)$ of finding the system in the state $|m\rangle$ at $t = 60T$. For case (a), $P(m)$ for $|m| \geq 10$ is 15.8% and 3.4% for $\beta = \pi$ and for $\beta = 0$, respectively. Similarly, for case (b) $P(m)$ differs by a factor of 5.4 for the two β values (3.2% vs 17.2%) in the probability of exciting the rotor to high-energy rotational states $|m\rangle$, $|m| \geq 20$. In both Figs. 2a and 2b it is evident that the difference in final populations resulting from the evolution of the two superpositions is an erratic function of m with few evident trends.

The behavior shown in Fig. 1 is in sharp contrast to that which would be observed for the same initial distributions propagated classically. These computations are shown in Fig. 3 and result from classical propagation of the initially non-positive-definite Wigner function $\rho^W(\theta, \tilde{L})$ associated with the wave function $\cos(\alpha)|m\rangle + \sin(\alpha)\exp(i\beta)|n\rangle$. That is, we classically propagate

$$\rho^W(\theta, \tilde{L}) = \cos^2(\alpha)\rho_m^c(\theta, \tilde{L}) + \sin^2(\alpha)\rho_n^c(\theta, \tilde{L}) + \frac{1}{2\pi}\sin(2\alpha)\cos[\beta - (m - n)\theta]\delta_{\tilde{L}/\tau,(m+n)/2}, \quad (4)$$

for each of $|\psi_a^\pm\rangle$ and $|\psi_b^\pm\rangle$. In all cases, the classical results show (Fig. 3) strong diffusion, characteristic of the chaotic dynamics of the standard map. There are only small differences in the $\tilde{E}$ diffusion between $|\psi_a^+\rangle$ and $|\psi_a^-\rangle$ and between $|\psi_b^+\rangle$ and $|\psi_b^-\rangle$.

Consider then the origins of coherent control of chaotic systems in the quantum dynamics and the behavior in the classical limit. To this end we diagonalize the quantum map operator $\hat{F}$ by a unitary operator $\hat{U}$, i.e., $\langle i|\hat{F}|j\rangle = \sum_k e^{-i\phi_k} U^*_{ki} U_{kj}$, where $U_{ij} \equiv \langle i|\hat{U}|j\rangle$, $j = 1, 2, \ldots$ is the eigenvector with eigenphase ϕ_i. After the initial superposition state $|\psi\rangle = \cos(\alpha)|m\rangle + \sin(\alpha)\exp(i\beta)|n\rangle$ is kicked N times, we have

$$\frac{2\tilde{E}}{\tau^2} = \cos^2(\alpha) \sum_{ljj'} l^2 U^*_{jm} U^*_{j'l} U_{jl} U_{j'm} e^{iN(\phi_j - \phi_{j'})} + \sin^2(\alpha) \sum_{ljj'} l^2 U^*_{jn} U^*_{j'l} U_{jl} U_{j'n} e^{iN(\phi_j - \phi_{j'})} + \left[\frac{1}{2} \sin(2\alpha) e^{-i\beta} \sum_{ljj'} l^2 U^*_{jm} U_{j'n} U_{jl} U^*_{j'l} e^{iN(\phi_j - \phi_{j'})} + \text{c.c.} \right], \quad (5)$$

where c.c. denotes the complex conjugate of the immediately preceding term within the brackets. The total term in brackets corresponds to interference effects due to initial-state coherence. For large N only the $j = j'$ terms will survive in the summations due to rapid oscillations of $e^{iN(\phi_j - \phi_{j'})}$. Hence the last two terms reduce to $1/2 \sin(2\alpha) e^{-i\beta} \sum_l l^2 \sum_j |U_{jl}|^2 U^*_{jm} U_{jn}$ + c.c.

If there is no structure in $|U_{jl}|^2$ and the eigenvector components U^*_{jm} and U_{jn} are perfectly independent, as expected from random matrix theory [5], then $\sum_j |U_{jl}|^2 U^*_{jm} U_{jn}$ is small and the magnitude of the interference term is $1/\sqrt{D}$ times smaller than that of the incoherent terms (where D is the effective dimension of the Hilbert space) [6], interference vanishes, and control is lost. Hence, the coherent control of quantum chaotic diffusion relies upon the residual statistical correlations between eigenvector components $\{U_{ij}\}$. Indeed, in this system the matrix $\langle i|\hat{F}|j\rangle$ is known to display a band structure

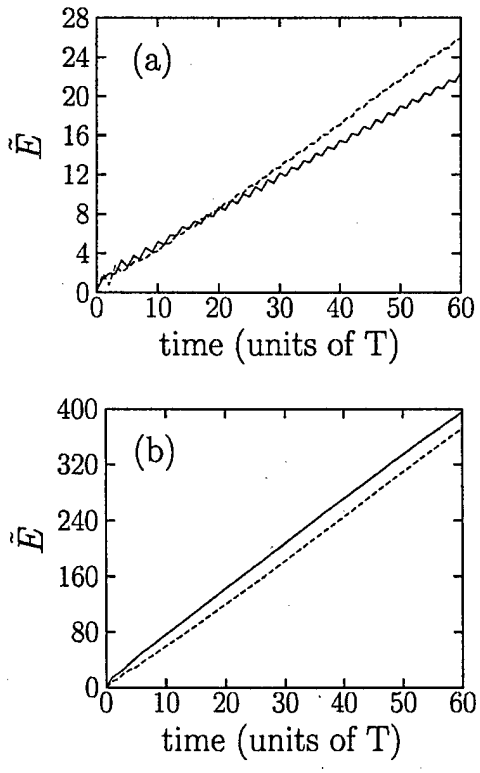

FIG. 3. As in Fig. 1 except that $\tilde{E}$ is calculated by classically propagating the initial non-positive-definite Wigner function in Eq. (4).

with the bandwidth $2k$ where the quantity k^2/N, where N is the size of the banded random matrices, provides a measure of the statistical deviations from random matrix theory [7]. Numerical results show that $k^2/N < 0.2$ is sufficiently small for control to persist. This being the case, we obtain a necessary condition to ensure the significance of the interference term, namely, $k < 0.2N_\kappa/\kappa$ or $\tau > \kappa^2/(0.2N_\kappa)$, where N_κ is the minimum grid size for accurate fast-Fourier transform calculations with $\tau = 1$. Numerical studies indicate that, for $\kappa < 10.0$, $N_\kappa \approx 256$, implying that we require $k < 50/\kappa$ or $\tau > \kappa^2/50$ for control. This makes it clear that as one approaches the classical limit (by increasing k or decreasing τ with fixed κ), coherent control is lost.

Further evidence that deviations from random matrix theory are responsible for control was obtained by examining control using a model composed of a banded matrix with random matrix elements. Control was obtained in this case as well, but was not as extensive as the kicked rotor system since the latter displays less random matrix character.

The dynamics of the kicked rotor in the presence of decoherence effects has also been examined both experimentally [8] and theoretically [9]. The survival of control in the presence of decoherence is of interest both in general and for this particular case. To examine this issue we introduce a simple decoherence model. Here, the quantum map operator between $(N - 1/2)T$ and $(N + 1/2)T$ is taken as $\hat{R}\hat{F}$, where $\hat{R}$ introduces random phases into the system. Specifically, $\hat{R}|m\rangle = e^{i2\pi r \xi(m,N)}|m\rangle$, where $m = 0, \pm 1, \pm 2, \ldots$, and $\xi(m, N)$ takes on random values that are distributed uniformly between 0 and 1 for each different m or N. Note that this model is such that its $r \to 1$ limit corresponds to measurement-induced quantum diffusion [10].

The density matrix $\hat{\rho}$ for the dynamics governed by $\hat{R}\hat{F}$ can then be obtained as an average over many realizations of $\xi(m, N)$. We take the linear entropy $S \equiv Tr\hat{\rho}^2$ as a useful additional measure of the purity of quantum states and hence of the effect of decoherence.

Numerical studies show that for $r < 0.05$, coherent control of quantum diffusion is hardly affected by the decoherence. For stronger decoherence, e.g., $r = 0.15$, phase control is essentially lost. Examination of the corresponding values of $S(t = 60T)$ shows that this is consistent with maintenance of control when the decoherence is sufficiently small so that $S(t = 60T) > 0.4$. Sample results

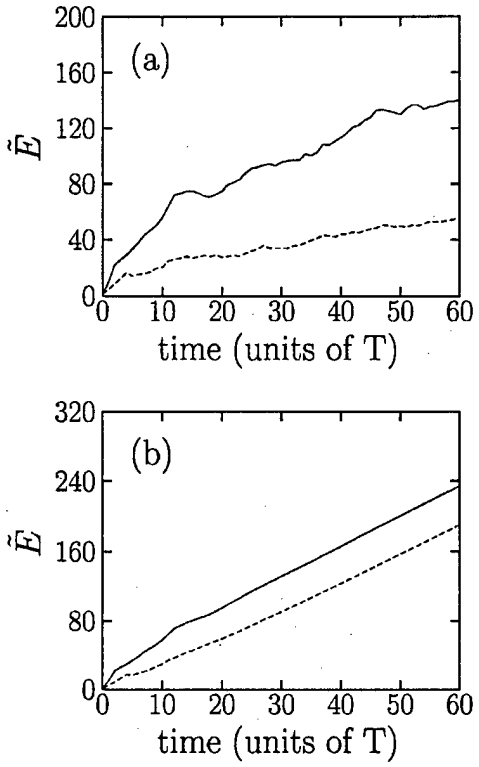

FIG. 4. As in Fig. 1b but in the presence of (a) modest decoherence and (b) stronger decoherence.

are shown in Fig. 4 where we plot the time dependence $\tilde{E}$ versus the time in the presence of small decoherence (Fig. 4a, $r = 0.05$) and of appreciable decoherence (Fig. 4b, $r = 0.15$). Both panels refer to the case of stronger chaos. Comparison of Fig. 4a with the decoherence-free dynamics in Fig. 1b shows that control is still significant, but decoherence is beginning to have an effect insofar as $\tilde{E}$ at $t = 60T$ is larger in Fig. 4a than in Fig. 1b. That is, the results show a slight tendency towards the classical behavior. In the case of stronger decoherence (Fig. 4b) phase control is greatly reduced and long time linear diffusive growth of $\tilde{E}$ is observed. A careful examination of Fig. 4b suggests that phase control persists until $t \approx 20T$ when the slopes of the dashed and solid curves become virtually identical. However, the slopes of these curves are still significantly less than those in Fig. 3b, suggesting that quantum coherence is still maintained at these longer times. In essence, it appears that phase control over the diffusion rate vanishes before quantum coherence is completely destroyed.

Note, finally, that the possibility of control does not rely heavily on the specific choice of basis states [11]. For example, we have also obtained extensive phase control by adding together either negative parity real basis states $\sin(m\theta)/\sqrt{\pi}$ or by adding together positive parity states $\cos(m\theta)/\sqrt{\pi}$. Since the states $\sin(m\theta)/\sqrt{\pi}$ satisfy the boundary condition of an infinitely deep square well potential $V(\theta)$ with $V(0) = V(2\pi) = +\infty$ and since the dynamics of a kicked particle in a well is similar to the kicked rotor for similar initial states [12], this indicates that one can also demonstrate coherent control of chaotic diffusion using superpositions of Hamiltonian eigenstates of a kicked particle in a potential well.

A number of possible experimental demonstrations of the proposed control scenario are evident. For example, the kicked diatomic molecule *CsI* [6,13] is a promising molecular system for demonstrating controlled quantum chaotic diffusion. In this case, preliminary controlled laser excitation could be used to prepare the desired initial superposition state (which are here superpositions of $|J, M\rangle$ and $|J', M\rangle$, where J and J' are the angular momentum and M is their projection on the z axis) and to vary β. Alternatively, one can utilize the square well analogy described above to experimentally study kicked dynamics of a particle in a well. By contrast, implementation of the atom-optics approach [14] to studies of control appears more difficult, insofar as it is necessary to prepare initial quantum superposition states, a considerable extension of previous work [15].

This work was supported by the U.S. Office of Naval Research and the Natural Sciences and Engineering Research Council of Canada. We thank Professor Aephraim Steinberg for discussions on the atom-optics approach to δ kicked dynamics.

[1] G. Casati and B. Chirikov, *Quantum Chaos: Between Order and Disorder* (Cambridge University Press, New York, 1995).
[2] M. Shapiro and P. Brumer, Adv. At. Mol. Opt. Phys. **42**, 287 (2000); P. Brumer and M. Shapiro, Sci. Am. **272**, No. 3, 34 (1995).
[3] D.L. Shepelyansky, Physica (Amsterdam) **28D**, 103 (1987).
[4] For example, C. Jaffe and P. Brumer, J. Chem. Phys. **82**, 2330 (1985).
[5] F. Haake, *Quantum Signatures of Chaos* (Springer-Verlag, Berlin, 1992).
[6] J. Gong and P. Brumer (to be published).
[7] G. Casati, I. Guarneri, F.M. Izrailev, and R. Scharf, Phys. Rev. Lett. **64**, 5 (1990).
[8] B.G. Klappauf *et al.*, Phys. Rev. Lett. **81**, 1203 (1998); H. Ammann *et al.*, Phys. Rev. Lett. **80**, 4111 (1998).
[9] E. Ott, T.M. Antonsen, Jr., and J.D. Hanson, Phys. Rev. Lett. **53**, 2187 (1984).
[10] P. Facchi, S. Pascazio, and A. Scardicchio, Phys. Rev. Lett. **83**, 61 (1999).
[11] We have also obtained similar control results with $\cos\theta$ in Eq. (1) replaced by $\cos(\theta + \pi/10)$, which gives a Hamiltonian that does not conserve parity.
[12] R. Sankaranarayanan, A. Lakshminarayan, and V.B. Sheorey, preprint nlin 0005035.
[13] R. Blümel, S. Fishman, and U. Smilansky, J. Chem. Phys. **84**, 2604 (1986).
[14] R. Graham, M. Schlautmann, and P. Zoller, Phys. Rev. A **45**, R19 (1992).
[15] F.L. Moore *et al.*, Phys. Rev. Lett. **75**, 4598 (1995).

Semiclassical Dynamics in the Coherent Control of Nonadiabatic ICN Photodissociation†

Victor S. Batista* and Paul Brumer

Chemical Physics Theory Group, Department of Chemistry, and Photonics Research Ontario, University of Toronto, Toronto, Ontario M5S 3H6, Canada

Received: October 2, 2000

The utility of a semiclassical initial value representation (SC-IVR) to simulate coherent control is explored. Specifically, bichromatic control of the state specific ICN photodissociation in the Ã continuum is investigated both quantum mechanically and semiclassically, and the ability of the SC-IVR method to reproduce *phases* of transition matrix element products is examined. Control over the $I(^2P_{1/2})/I(^2P_{3/2})$ product ratio is considerable and the resultant semiclassical photofragmentation ratios are in good agreement with full quantum dynamics calculations.

I. Introduction

Understanding, manipulating, and utilizing laser-induced quantum interference effects in chemical reaction dynamics is a central problem in the development of the new optical technology to control atomic and molecular processes. These quantum mechanical effects require detailed investigation using new computational techniques for modeling excited state chemical dynamics. Indeed, quantum mechanics simulations have already proven useful in understanding and developing coherent control techniques.[1] However, these rigorous computational methods are currently limited to systems with only a few degrees of freedom, since they usually require computational effort and storage space that scales exponentially with the number of coupled degrees of freedom. Future computations of larger systems must, in the forseeable future, rely on developments in semiclassical dynamics techniques.

In this paper we examine the utility of semiclassical initial value representation SC-IVR techniques for coherent optical control simulations, and we investigate coherent control of nonadiabatic ICN photodissociation in the Ã continuum. Specifically, we consider control of the I/I* ratio in ICN photodissociation using the bichromatic coherent control scenario.[2,3] In this scenario, two lasers are used to photodissociate ICN, prepared in a superposition of coherent states. Control can be achieved by varying the relative phases and intensities of the two photodissociation lasers, or by varying the expansion coefficients in the superposition state. This particular coherent control scenario has yet to be demonstrated experimentally but has been investigated theoretically, using quantum mechanical simulations as applied to ICH_3 photodissociation dynamics, demonstrating a broad range of control over the possible photofragmentation channels.[2,3]

Of particular interest in this paper is the SC-IVR approach, which is a generalization of classical molecular dynamics simulation methods. This approach combines the quantum superposition of probability amplitudes with real-valued classical trajectories in the computation of the quantum mechanical propagator.[4−17] These methods aim to provide a tractable alternative to exact quantum mechanical computations[18] as well as an intuitive understanding of complex quantum dynamics associated with chemical reactions. In this paper we implement a SC-IVR approach that is able to describe electronically nonadiabatic processes through the quantization of the classical electron−nuclear model Hamiltonian of Meyer and Miller.[19] This SC method has been successfully applied to the three 1-dimensional model problems suggested by Tully for testing nonadiabatic dynamics,[20] and to the spin-boson model for dissipative systems.[21,22] However, the only applications to date for a real molecular system have been the studies of ultrafast photodissociation dynamics of ozone,[5] and the nonadiabatic photodissociation dynamics of ICN in the Ã continuum.[23] The latter computations demonstrated the capabilities of the SC-IVR for simulating both the absorption band, and the rotational distributions of CN photofragments. There remains, however, the nontrivial question as to whether this method can also be successfully implemented to simulate coherent control, which requires quantum phases as well as amplitudes.

In this paper we show that such semiclassical approach can indeed be effectively implemented to describe the complex quantum interference terms required in coherent control of ICN photodissociation dynamics. Specifically, we evaluate the cumulative ICN state specific photofragmentation amplitudes using the Herman−Kluk SC-IVR methodology, together with stationary phase MC methods (see refs 5 and 23). For the sake of presenting a rigorous comparison between semiclassical and full quantum mechanical results, we solve first the scattering problem at the complete state-to-state level, and then compute the cumulative transition amplitudes by summing over final states. As a byproduct we also produce the cross sections for ICN photodissociation into various product channels with excitation from a variety of initial ICN states.

The ICN Ã continuum is a broad absorption band in the 200−300 nm range.[24] Photolysis at approximately 266 nm induces predominately $^3\Pi_{0+} \leftarrow X$ parallel transitions, and produces two peaks in the translational photofragment spectra. These peaks are assigned to two photodissociation pathways, indicated below

$$\begin{aligned} ICN + \hbar\omega &\rightarrow I^*(^2P_{1/2}) + CN(X^2\Sigma^+) \\ &\rightarrow I(^2P_{3/2}) + CN(X^2\Sigma^+) \end{aligned} \qquad (1.1)$$

that produce either iodine atoms in the $I^*(^2P_{1/2})$ spin−orbit state, through adiabatic photodissociation, or iodine atoms in the

† Part of the special issue "William H. Miller Festschrift".

10.1021/jp0035939 CCC: $20.00 © 2001 American Chemical Society
Published on Web 02/13/2001

$I(^2P_{3/2})$ spin−orbit state, through nonadiabatic dynamics at the conical intersection between electronic excited states $^3\Pi_{0+}$ and $^1\Pi_1$, respectively. Here $\hbar\omega$ is the photoexcitation energy, and the CN radicals are produced in the ground electronic state CN-$(X^2\Sigma^+)$. Little vibrational excitation is found in the CN fragment (>98% in $v = 0$), but the rotational distribution of CN involves highly excited states and exhibits a bimodal structure.[25] Experiments have shown that the CN fragment is formed with rotational distributions that peak at low quantum numbers when dissociation of the molecule produces excited state iodine atoms $I^*(^2P_{1/2})$. The channel forming ground state iodine $I(^2P_{3/2})$, however, produces CN fragments that are rotationally hot. Experiments have also shown that the I/I* branching ratio in the CN rotational distribution is not very sensitive to the initial temperature of the parent molecule but can be strongly controlled in terms of the photoexcitation wavelength, with I* production accounting for approximately 62% of the total product at 266 nm, but much less at both lower and higher photoexcitation energies.[26]

In this paper we show that the I/I* branching ratio can also be controlled over a broad range of values, simply by changing the relative phases of two laser pulses that photoexcite an initial superposition state to the same final energy state in the $\tilde{A}$ continuum. Considering the longstanding interest in ICN photodissociation, we anticipate considerable experimental interest in examining this control scenario.

The paper is organized as follows. In section II we first outline the CC technique based on bichromatic excitation of a superposition state, and the SC-IVR methods implemented in our simulations to calculate the degree of yield control in terms of state-to-state specific transition matrix elements. Section III then summarizes our semiclassical results, and compares them with full quantum dynamics simulations. Section IV summarizes and concludes.

II. Methods

A. Bichromatic Coherent Control. We consider bichromatic coherent control in a model of ICN photodissociation.[2,3] In accord with this scenario, the system is prepared in an initial superposition state

$$|\Psi_0(j,k)\rangle = |\Phi_g\rangle(c_j|\chi_0(j)\rangle + c_k|\chi_0(k)\rangle) \qquad (2.1)$$

where $|\Phi_g\rangle$ is the ICN ground electronic state wave function. Here $|\chi_0(j)\rangle$ is the nuclear eigenstate of energy E_j associated with excitation in the j-th vibrational state of the Jacobi coordinate R, which represents the distance between the iodine atom and the CN center of mass. The system is subsequently photoexcited with two CW lasers with frequencies ω_j and ω_k, where $\omega_j = E - E_j$, and E represents the final energy of the system after photoexcitation to the $\tilde{A}$ continuum. That is, we excite the system with the electric field $\epsilon(t)$

$$\bar{\epsilon}(t) = \bar{\epsilon}_j e^{-i(\omega_j t+\theta_j)} + \bar{\epsilon}_k e^{-i(\omega_k t+\theta_k)} + \text{c.c.} \qquad (2.2)$$

where $\bar{\epsilon}_j$ and $\bar{\epsilon}_k$ are time independent vectors of length $|\bar{\epsilon}_j|$ and $|\bar{\epsilon}_k|$. θ_j and θ_k are the phases of the two pulses. As a consequence, both $|\chi_0(j)\rangle$ and $|\chi_0(k)\rangle$ are raised by the laser field with frequencies ω_j and ω_k, to states with energy E in the continuum, denoted $|E,\xi,J^-\rangle$. Here J is the CN angular momentum and $\xi = (I_{1/2}$ or $I_{3/2})$, denotes the state of the iodine product. The CN vibration is ignored since experiments show little CN vibrational excitation after photodissociation. These two photoexcitation routes interfere with one another.

Assuming that the field is sufficiently weak to allow the use of first-order perturbation theory, the relative product ratio $R(\xi,\xi',E)$, of producing product in arrangement channel ξ to that in arrangement ξ', at energy E, is given by

$$R(\xi,\xi',E) = \{|\mu_{jj}(\xi,E)| + x^2|\mu_{kk}(\xi,E)| + 2x\cos(\theta_j - \theta_k + \Phi_{jk}(\xi,E))|\mu_{jk}(\xi,E)|\}/\{|\mu_{jj}(\xi',E)| + x^2|\mu_{kk}(\xi',E)| + 2x\cos(\theta_j - \theta_k + \Phi_{jk}(\xi',E))|\mu_{jk}(\xi',E)|\} \qquad (2.3)$$

Here x is the ratio of controllable parameters $x = |(c_k|\bar{\epsilon}_k|)/(c_j|\bar{\epsilon}_j|)|$, and $\Phi_{jk}(\xi,E)$ is the phase of the cumulative transition matrix element $\mu_{jk}(\xi,E)$, where

$$\mu_{j,k}(\xi,E) = |\mu_{jk}(\xi,E)|e^{i\Phi_{jk}(\xi,E)} = \sum_{J=0}^{\infty}\langle\chi_0(k)|\mu_\epsilon|E,\xi,J^-\rangle\langle E,\xi,J^-|\mu_\epsilon|\chi_0(j)\rangle \qquad (2.4)$$

with μ_ϵ being the dipole operator along the direction of the field. Note that the off-diagonal μ_{jk} manifest the interference between components of the continuum wave function which are excited by independent coherent excitation pathways. The matrix element $\langle E,\xi,J^-|\mu_\epsilon|\chi_0(j)\rangle$ in eq 2.4, is the state-to-state specific transition matrix element associated with the initial vibrational state $|\chi_0(j)\rangle$, and the final photodissociation channel corresponding to electronic state ξ, CN rotational state J, energy E, and incoming boundary conditions.

Equations 2.3 and 2.4 show that the relative product yield $R(I_{1/2}:I_{3/2},E)$ of product in $I_{1/2}$ to product in $I_{3/2}$ can be computed in terms of the state-to-state specific transition matrix elements $\langle E,\xi,J^-|\mu_\epsilon|\chi_0(j)\rangle$, and can be experimentally controlled by changing either the initial superposition state, or the relative phase and amplitude of the CW photoexcitation lasers.

The state-to-state specific transition matrix elements are obtained in the time dependent picture by evolving each wave packet component $|\chi_0(j)\rangle$ in the initial superposition times the dipole function, to obtain $|\chi_t(j)\rangle$ as determined by the nonadiabatic excited state dynamics at time t. We then compute the desired matrix element as

$$\langle E,\xi,J^-|\mu_\epsilon|\chi_0(j)\rangle \equiv \lim_{t\to\infty}\langle K(E),J,\xi|\chi_t(j)\rangle e^{iEt/\hbar} \qquad (2.5)$$

where $\langle K,J,\xi|\chi_t(j)\rangle$ is the asymptotic nuclear wave packet, in the $K - J$ representation, associated with the final electronic state ξ. Note that the integral associated with the rhs of eq 2.5 should include the appropriate Jacobian factors. Here K is the nuclear momentum conjugate to the Jacobi coordinate R, and $K(E)$ is its asymptotic value at final energy E and CN rotational state J, given by the formula

$$K(E) = \left[2M\left(\frac{E - E_0(\xi)}{\hbar^2} - \frac{J(J+1)}{2mr^2}\right)\right]^{1/2} \qquad (2.6)$$

where $E_0(\xi)$ is the asymptotic energy of the electronic state potential energy surface associated with photodissociation channel ξ, M is the reduced mass associated with coordinate R, and m is the C−N reduced mass.

To obtain $\langle K,\xi,J|\chi_t(j)\rangle$, we compute the asymptotic wave function $\langle \mathbf{x},R,\theta|\Psi_t(j)\rangle$ that results from nonadiabatic dynamics propagation, after instantaneous photoexcitation of the $|\Phi_g\rangle|\chi_0(j)\rangle$ state component in the initial superposition to the optically active electronic excited state resonant with the excitation energy. Here $\mathbf{x}$ are the electronic degrees of freedom,

and Θ is the angle between the I to CN distance and the CN axis. Projecting out the corresponding electronic state $|\phi^{\xi}\rangle$ gives

$$\Psi^{\xi}_{i}(R,\theta;j) = \int dx \langle \phi^{\xi}|\mathbf{x}\rangle\langle \mathbf{x},R,\theta|\Psi_{i}(j)\rangle \qquad (2.7)$$

and transforming $\Psi^{\xi}_{i}(R,\theta;j)$ to the $K-J$ representation according to

$$\langle K,J,\xi|\chi_{i}(j)\rangle = A\int_{0}^{\infty} dR \int_{0}^{\pi} d\Theta\, Y^{*}_{J0}(\Theta) \sin\Theta\, e^{-iKR}\Psi^{\xi}_{i}(R,\Theta;j) \qquad (2.8)$$

gives the desired $\langle K,J,\xi|\chi_{i}(j)\rangle$. Here A is a normalization constant, and the spherical harmonic $Y_{J0}(\Theta)$ represents the J-th rotational state of the CN fragment. The computational task for predicting the degree of yield control is therefore reduced to calculating the cumulative transition matrix elements $\mu_{i,j}(\xi,E)$, in terms of the asymptotic state components $|\Psi_{i}(j)\rangle$ obtained according to the SC-IVR methodology described in section IIB.

B. State-Resolved Semiclassical Approach. The semiclassical approach considered in this paper computes $\mu_{i,j}(\xi,E)$ from $|\chi_{i}(j)\rangle$, in accord with eqs 2.4 and 2.5. The $|\chi_{i}(j)\rangle$ are computed by propagating each state $|\Psi_{0}(j)\rangle$ in the initial superposition according to the semiclassical methodology outlined in ref 23. Specifically, the Herman–Kluk propagator is used in conjunction with a stationary phase Monte Carlo method to simulate nonadiabatic dynamics using the Miller–Meyer Hamiltonian for the ICN system. This Hamiltonian includes both electronic and nuclear degrees of freedom.

Semiclassical results were found to be converged with 2×10^{7} trajectories, using the parallel programming model described in ref 5. However, we have observed that a good qualitative description of coherence control can already be obtained with an ensemble of 2×10^{6} trajectories. For comparison purposes, we computed quantum mechanical results using the fast Fourier transform (FFT) method with an extended grid of 512 points in both the R and Θ coordinates, defined in the range of coordinates $|R - 9|$ au < 5 au, and $|\Theta| < 2\pi$ radians.

The initial wave packet components $\Psi_{0}(x,R,\theta;j)$, after instantaneous photoexcitation of the system, are defined according to the Meyer–Miller formalism as a product of electronic and nuclear wave functions

$$\Psi_{0}(x,R,\theta;j) = \phi^{n}(\mathbf{x})\chi_{0}(j;R,\theta) \qquad (2.9)$$

assuming that the transition dipole that couples the ground electronic state g with the optically active electronic excited state n is independent of nuclear coordinates (Condon approximation). We take as $\chi_{0}(j;R,\theta)$, in eq 2.9, the harmonic nuclear wave function

$$\chi_{0}(j;R,\theta) = \left(\frac{\alpha_{R}}{\pi}\right)^{1/4} H_{j}(\sqrt{\alpha_{R}/\hbar}(R - R_{0}))e^{-(\alpha_{R}/2)(R-R_{0})^{2}}\left(\frac{\alpha_{\theta}}{\pi}\right)^{1/4} \times \exp\left[-\frac{\alpha_{\theta}}{2}(\theta - \theta_{0})^{2}\right] \qquad (2.10)$$

where H_{j} is a Hermite polynomial of degree j, α_{R} and α_{Θ} are obtained from the ICN stretching and bending force constants,[27] and the equilibrium values of the Jacobi coordinates (R,Θ) are $R_{0} = 4.99$ bohrs, and $\theta_{0} = 0.0$ rad, respectively. The electronic wave function $\phi^{n}(\mathbf{x})$ in eq 2.9 is defined as the product of two one-dimensional harmonic oscillator wave functions, each representing the eigenfunctions of the electronic part of the quantum Hamiltonian. For example, the electronic wave function for state n is a ground state harmonic oscillator wave function for all electronic modes except the nth one, which has one quantum of excitation:

$$\phi^{n}(x) = x_{n}e^{-(1/2)(x_{1}^{2}+x_{2}^{2})} \qquad (2.11)$$

In our calculations we use the empirical ICN potential energy surfaces derived by Goldfield et al.,[28] and assume that the dominant contributions to the excited state dynamics result from parallel transitions from the ground state $^{1}\Sigma_{0+}$ potential energy surface to the excited electronic state with $^{3}\Pi_{0+}$ symmetry. These empirical potentials consist of two coupled excited state potential energy surfaces, associated with the $^{3}\Pi_{0+}$ and $^{1}\Pi_{1}$ electronic excited states that correlate to the $I_{1/2}$ and $I_{3/2}$ channel, respectively. Rigorous comparisons with experimental data, however, might require calculations on the complete set of ab initio potential energy surfaces, e.g., those reported by Morokuma and co-workers.[29]

III. Results

Results are presented in two sections. First, section IIIA presents the cumulative transition matrix elements obtained according to the semiclassical methodology, described in section II, and compares the results to those obtained using quantum mechanics. We considered the case where $\chi_{0}(j) = \chi_{0}(1)$ is the ground vibrational state, and $\chi_{0}(k) = \chi_{0}(3)$ is the second excited vibrational state along the R coordinate. Section IIIA also compares the semiclassical results for individual wave packet components in the $E-J$ representation, for both the $^{3}\Pi_{0+}$ and the $^{1}\Pi_{1}$ electronic excited states, with the corresponding quantum mechanical results. This comparison of individual wave packet components provides a comprehensive picture of the energy dependence of individual transition matrix elements and demonstrates the ability of the semiclassical methodology to describe both real and imaginary parts of the state-to-state specific transition matrix elements associated with alternative photoexcitation pathways. Finally, section IIIB presents molecular dynamics simulation results of coherent control, after photoexcitation of an initial superposition state to various final energy levels in the $\tilde{A}$ continuum. In particular, we provide a detailed comparison between the relative product yields obtained using semiclassical mechanics to the corresponding quantum mechanical results.

A. Transition Matrix Elements. Consider first results that correlate with the $I_{1/2}$ product channel. Besides the calculation of the photodissociation cross sections, coherent control studies require $\mu_{ij}(\xi,E)$, i.e., the off-diagonal channel-dependent complex quantities. Figure 1 compares the semiclassical (solid) and quantum (dashed) results for the modulus $|\mu_{13}(I_{1/2},E)|$ (see panel a), and phase $\Phi_{13}(I_{1/2},E)$ (panel b) of the cumulative transition matrix element $\mu_{13}(I_{1/2},E)$ [see eq 2.4]. Although one sees differences of up to 15–20% between the semiclassical and quantum mechanical results, the overall qualitative features are in excellent agreement with one another; that is, both the overall shape of $|\mu_{13}(I_{1/2},E)|$ and the position of the amplitude nodes as a function of E, as well as the energy dependence of the phase $|\Phi_{13}(I_{1/2},E)|$ are in good agreement. Note that the phase of μ_{ij} is the most elementary phase-dependent quantity to which we can apply a test of the utility of semiclassical mechanics. That is, the phase of a matrix element involving the continuum, as opposed to the product considered herein, does not allow for quantum-semiclassical comparisons since the phase of the continuum wave function is arbitrary and therefore computer-code dependent.

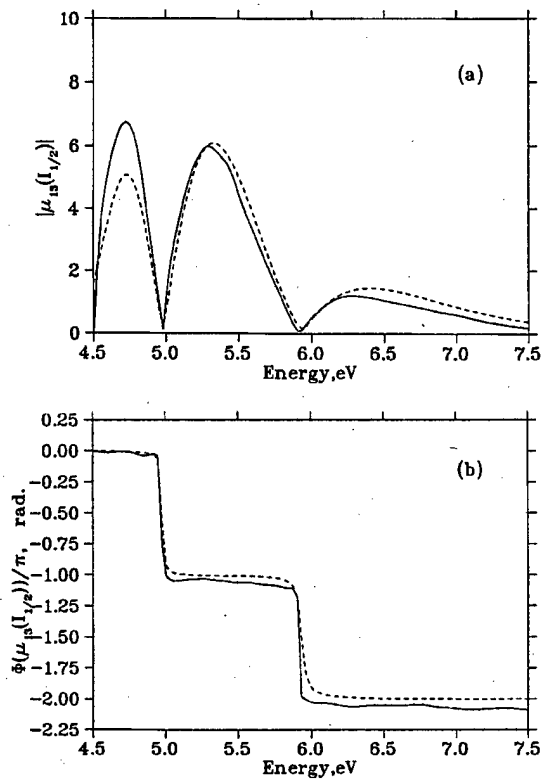

Figure 1. Semiclassical (solid lines), and quantum mechanical (dashes) cumulative matrix elements $\mu_{13}(I_{1/2},E) = |\mu_{13}(I_{1/2},E)| \exp(i\Phi_{13}(I_{1/2},E))$, associated with final photodissociation channel $I_{1/2}$, as a function of final energy E in the Ã continuum.

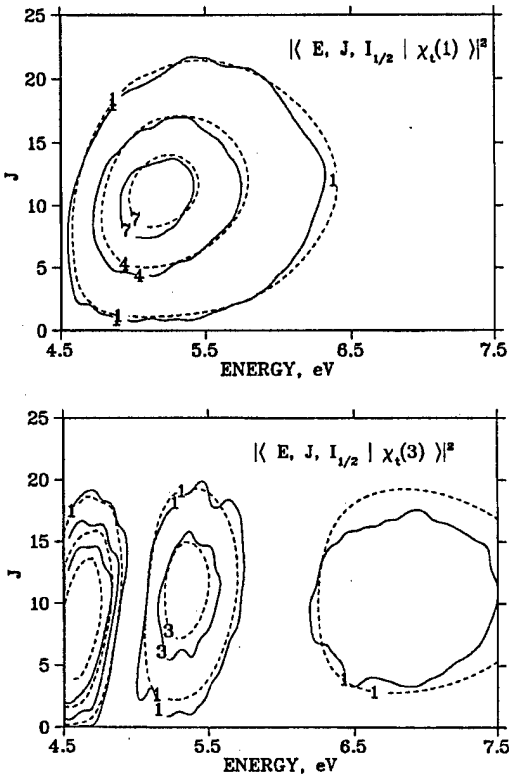

Figure 2. Contour plots for the norm of the $^3\Pi_{0+}$ asymptotic wave packet components in the $E-J$ representation at 50 fs after $^3\Pi_{0+} \leftarrow X$ photoexcitation of the molecule that is initially in the ground (panel a), or second excited vibrational states (panel b). Semiclassical results (solid lines), and the corresponding quantum mechanical results (dashed lines) are shown.

Figure 1 shows important qualitative features of $\mu_{13}(I_{1/2},E)$, such as the energy position of the nodes, and the change in sign of $\mu_{13}(I_{1/2},E)$ when going through an energy node. Both of these features are determined by the symmetry properties of the product of the two wave packet components that contribute to $\mu_{13}(I_{1/2},E)$ at each J, as defined by eq 2.4. The origin of the deviations between semiclassical and full quantum mechanical results, displayed in Figure 1, can be attributed to differences in the asymptotic wave packet components that correlate with the $I_{1/2}$ photodissociation channel, as discussed later in this section. The wave packet components also provide a comprehensive understanding of the energy dependence of $|\mu_{13}(I_{1/2},E)|$ since, as mentioned above, $|\mu_{13}(I_{1/2},E)|$ is obtained according to eq 2.4, by summing the product of the two wave packet components that correlate to the $I_{1/2}$ photodissociation channel over all rotational states.

Figure 2 compares contour plots for the asymptotic wave packet components that correlate to the $I_{1/2}$ photodissociation product. Results are shown for wave packet components obtained in the photoexcitation of ICN that are initially in the ground vibrational state $|\chi_0(1)\rangle$ (panel a), or in the second excited vibrational state $|\chi_0(3)\rangle$ (panel b). Here, semiclassical wave packet results (solid lines) are compared to the corresponding quantum results (dashed lines), obtained at 50 fs after photoexcitation of the molecule to the $^3\Pi_{0+}$ electronic excited state. At this time, the wave packet components in the $E-J$ representation are asymptotic since the wave packet is unchanged at times greater than 45 fs after photoexcitation. Figure 2 shows that for this empirical potential energy model, the CN rotational distributions associated with both photoexcitation pathways are centered at approximately $J = 10$ for all final energy states in the Ã continuum, However, they differ with respect to one another in the number of nodes along the energy coordinate, reflecting features of the corresponding initial vibrational state. The agreement between semiclassical and full quantum mechanical calculations is quite satisfactory at the center of the band, while deviations become more significant at the tails.

Similar considerations apply to product associated with the $I_{3/2}$ channel. Figure 3 shows the modulus $|\mu_{13}(I_{3/2},E)|$ (see panel a), and phase $\Phi_{13}(I_{3/2},E)$ (panel b) of $\mu_{13}(I_{3/2},E)$, and compares the semiclassical (solid lines) and quantum mechanical (dashed) results. Figure 3 shows that both the modulus and the phase of the semiclassical $\mu_{13}(I_{3/2},E)$ are in very good agreement with quantum results. Significantly, for all cases the convergence of the modulus, and the phase, occur at essentially the same rate.

Figure 4 compares the contour plots for the asymptotic wave packet components that correlate to the $I_{3/2}$ spin–orbit state in the $^1\Pi_1$ photodissociation channel. These wave packets result entirely from nonadiabatic dynamics at the conical intersection, after $^3\Pi_{0+} \leftarrow X$ photoexcitation of ICN molecules that are initially in the ground vibrational state (panel a), or in the second excited vibrational state (panel b). As above, semiclassical wave packets (solid lines) are compared to the corresponding quantum results (dashed lines), at 50 fs. Figure 4 shows that for this photodissociation channel the CN rotational distributions associated with both photoexcitation pathways have maximum amplitudes at $40 \leq J \leq 60$ for all final energy states in the Ã continuum, and are significantly more structured than the wave packet components that correlate to the $I_{1/2}$ spin–orbit state. The agreement between semiclassical and quantum calculations, for these rather hot and complicated rotational distributions, is once again very satisfactory. Evident from Figure 4 is the origin of the two more prominent band intensities displayed by Figure 3, in the 4–6 eV energy range, as well as the quality of the

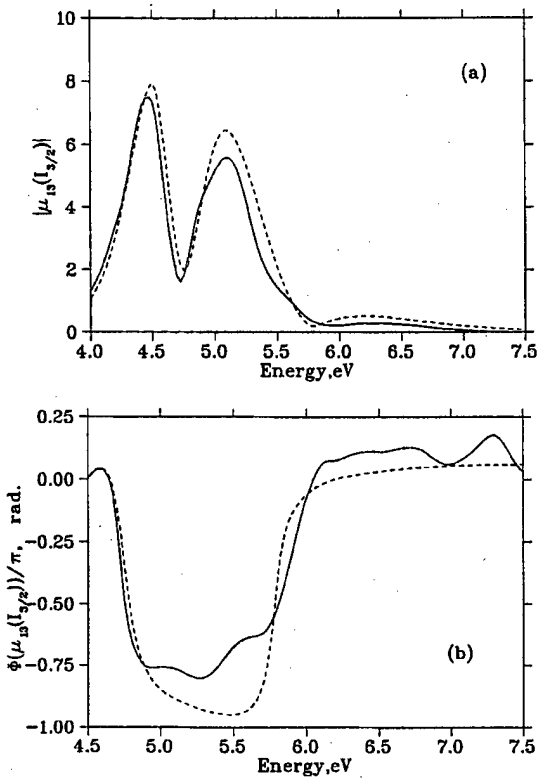

Figure 3. Semiclassical (solid lines), and quantum mechanical (dashes) cumulative matrix elements $\mu_{13}(I_{3/2},E) = |\mu_{13}(I_{3/2},E)|\exp(i\Phi_{13}(I_{3/2},E))$, associated with final photodissociation channel $I_{3/2}$, as a function of final energy E in the Ã continuum.

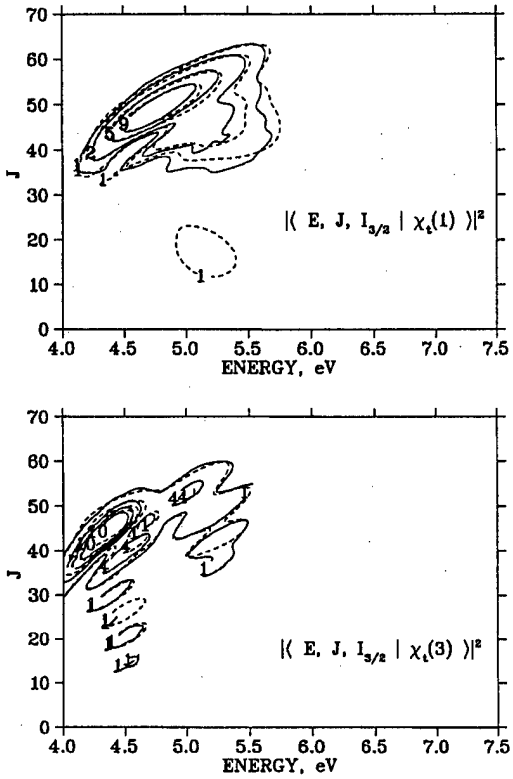

Figure 4. Comparison of contour plots for the norm of the $^1\Pi_1$ asymptotic wave packet components in the $E-J$ representation at 50 fs after $^3\Pi_{0+} \leftarrow X$ photoexcitation of the molecule that is initially in the ground (panel a), or second excited vibrational states (panel b). Semiclassical results (solid lines), and the corresponding quantum mechanical results (dashed lines) are shown.

"node" at ~4.75 eV as determined by the structure of the rotational distribution as a function of J. Figure 3 also shows that the same level of agreement displayed in Figure 3 for the cumulative transition matrix element as a function of energy can also be observed in the rotational state specific transition amplitudes. Thus, one would anticipate that the SC-IVR techniques could also be implemented for simulating rotational state specific CC techniques.

In these computations, we have included only contributions from parallel transitions $^3\Pi_{0+} \leftarrow X$, in order to facilitate the comparison between semiclassical and quantum calculations. Therefore, the cumulative transition matrix element $\mu_{13}(I_{3/2},E)$ results exclusively from population that crosses from the initially populated $^3\Pi_{0+}$ state to the $^1\Pi_1$ electronic excited state at the conical intersection. The agreement displayed in Figure 3 demonstrates that the Meyer–Miller Hamiltonian, quantized according to the Herman–Kluk SC-IVR methodology together with stationary phase MC methods, is able to describe not only the modulus but also the phase of the off-diagonal cumulative transition matrix elements in semiquantitative agreement with full quantum mechanical calculations. This is an important result because it demonstrates that even when the system undergoes purely nonadiabatic dynamics the semiclassical methodology correctly describes both coherences, i.e., the relative phases of asymptotic wave functions in the Ã continuum, and probability distributions.

Finally, Figures 5 and 6 compare the semiclassical cumulative matrix elements $\mu_{ii}(I_{1/2},E)$ (see panel a), and $\mu_{ii}(I_{3/2},E)$ (see panel b), with the corresponding quantum results (dashes). With the exception of small deviations in the high energy tail of $\mu_{11}(\xi,E)$ ($\xi = {}^3/_2, {}^1/_2$) there is almost quantitative agreement between semiclassical and full quantum mechanical results. By contrast, Figure 6 shows somewhat poorer agreement for $\mu_{33}(I_{1/2},E)$ (see panel a), and $\mu_{33}(I_{3/2},E)$ (see panel b). In this case, when the system is photoexcited from higher vibrational states, the semiclassical calculations show more significant deviations from the exact quantum mechanical results. These deviations are similar to those observed in previous studies,[5,23,30] and are the subject of further investigation. However, the overall qualitative features of these higher vibrational state cumulative matrix elements obtained according to semiclassical mechanics are still in good agreement with full quantum mechanical calculations throughout the whole energy range.

The comparison of Figures 5, 6, 1, and 3 shows that the "nodes" of the cumulative transition matrix element are smeared out by the coupling between the two electronic states, leaving only a very narrow 5.7–6.0 eV energy range where coherent control is expected to be inefficient, since both $|\mu_{13}(I_{3/2},E)|$ and $|\mu_{13}(I_{1/2},E)|$ are small compared to the diagonal transition matrix elements $|\mu_{jj}(I_{3/2},E)|$.

B. Coherent Control of Photofragmentation Product Yields. Figure 7 shows the relative product yields $R(I_{1/2}:I_{3/2},E)$, (eq 2.3), after ICN photodissociation in the Ã continuum, obtained through bichromatic coherent control of an initial superposition of vibrational states with quantum numbers $v = 1$ and $v = 3$. Figure 7 compares the semiclassical (solid lines) and quantum (dashed lines) results obtained at various photoexcitation energies. Relative product yields are presented in the form of contour plots for the photoexcitation energies indicated in panels a–f, as a function of both the relative pulse phase parameter, $\Theta_1 - \Theta_2$, and the relative amplitude $S = c_1^2\epsilon_1'^2/(c_3^2\epsilon_3'^2 + c_1^2\epsilon_1'^2)$.

Note first, that Figure 7 shows that the product ratio varies significantly as a function of the relative pulse phase parameter,

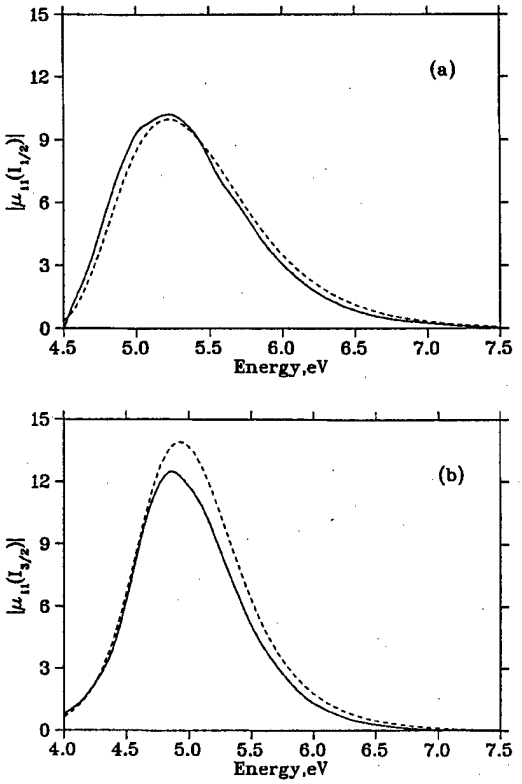

Figure 5. Semiclassical cumulative matrix elements $\mu_{11}(\xi)$, with $\xi = (I_{1/2},I_{3/2})$ (solid lines), and the corresponding quantum mechanical results (dashes). Panel a shows the comparison of $\mu_{11}(I_{1/2})$, and panel b displays the corresponding results for $\mu_{11}(I_{3/2})$.

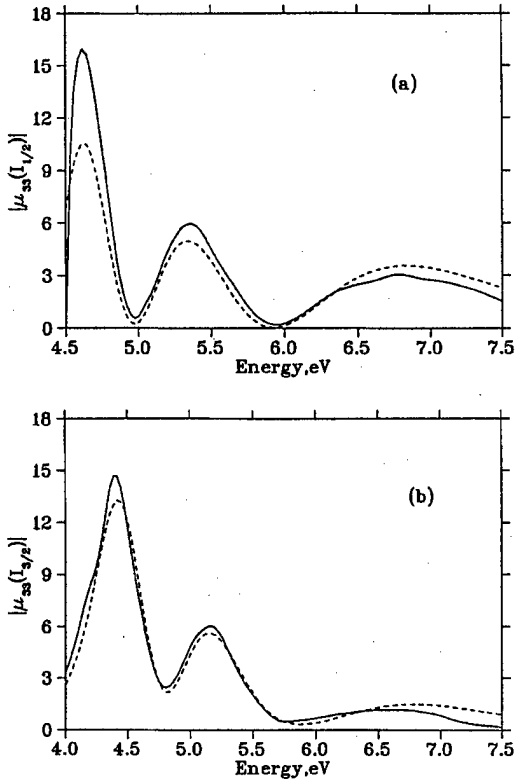

Figure 6. Semiclassical cumulative matrix elements $\mu_{33}(\xi)$, with $\xi = (I_{1/2},I_{3/2})$ (solid lines), and the corresponding quantum mechanical results (dashes). Panel a shows the comparison of $\mu_{33}(I_{1/2})$, and panel b displays the corresponding results for $\mu_{33}(I_{3/2})$.

demonstrating a broad range of yield control over an extended range of S (i.e., strong dependence on $(\Theta_1 - \Theta_2)$) for all photoexcitation energies, with the exception of $E = 6$ eV [see panel (d)]. Here coherent control is expected to vanish since *both* off-diagonal matrix elements $|\mu_{13}(I_{1/2},E)|$ and $|\mu_{13}(I_{3/2},E)|$ are much smaller than the diagonal terms $|\mu_{jj}(\xi,E)|$, with $\xi = (I_{1/2},I_{3/2})$ and $j = (1,3)$ (see Figures (5, 6, 1 and 3)).

Second, note that the overall comparison between semiclassical and full quantum dynamics simulations of coherent control, displayed by the contour diagrams in Figure 7, indicates that the structure of the diagrams, the trend in these structures with photoexcitation energy, and the range of quantum mechanical product yields are reproduced by the semiclassical calculations within an error of approximately 5−10%.

At the lowest photoexcitation energy (see panel a), maximum control is attained at $S \leq 0.5$, where the production of $I_{1/2}$ can be reduced from 40% to less than 1%, simply by varying the relative phase parameter from 0° to 180° at $S \sim 0.25$. At higher values of S (as $S \rightarrow 1$), the semiclassical and full quantum mechanical product yields still agree with one another within an error of 5−10% and show a qualitatively different behavior from that observed at smaller values of S. In particular, the ratio R, as $S \rightarrow 1$, becomes only weakly dependent on the relative pulse phase parameter, $\Theta_1 - \Theta_2$, and it is therefore no longer possible to control the final outcome of the photodissociation reaction.

At higher photoexcitation energies (see panel b) the semiclassical and full quantum mechanical product yields again agree within about 5−10% error and show dependence on $\Theta_1 - \Theta_2$ and S that is completely different from that obtained at lower photoexcitation energies. Here, the degree of yield control is found to be maximum in the $0.5 \leq S \leq 0.8$ range, where the production of $I_{1/2}$ can be reduced from more than 70% to less than 30% by changing the relative phase from about 330° to 150°.

Various different trends are observed at the other energies shown in Figure 7, it being clear that (a) ICN is an excellent candidate for studies of coherent control and (b) semiclassical IVR computations do an adequate job of predicting control.

IV. Conclusions

In this article we have shown that coherent control over ICN photodissociation is extensive and that SC-IVR techniques are able to simulate bichromatic coherent control of an initial ICN superposition state in semiquantitative agreement with exact quantum mechanical results.

We have demonstrated the capabilities of a semiclassical technique that involves quantization of the Meyer−Miller classical Hamiltonian for nuclear and electronic dynamics, by comparing the semiclassical and full quantum mechanical results of relative photofragmentation product yields, as controlled by the relative pulse phase, or the relative amplitude parameters. Some quantitative disagreement was observed for dynamics initiated in the higher vibrational states. Its origin is the subject of further study.

The SC results obtained through quantization of the Meyer−Miller Hamiltonian, according to the Herman−Kluk SC-IVR methodology, together with stationary phase MC methods, were able to reproduce the correct structure of the relative product yield for various different photoexcitation energies, demonstrating that the SC-IVR methodology correctly describes excited

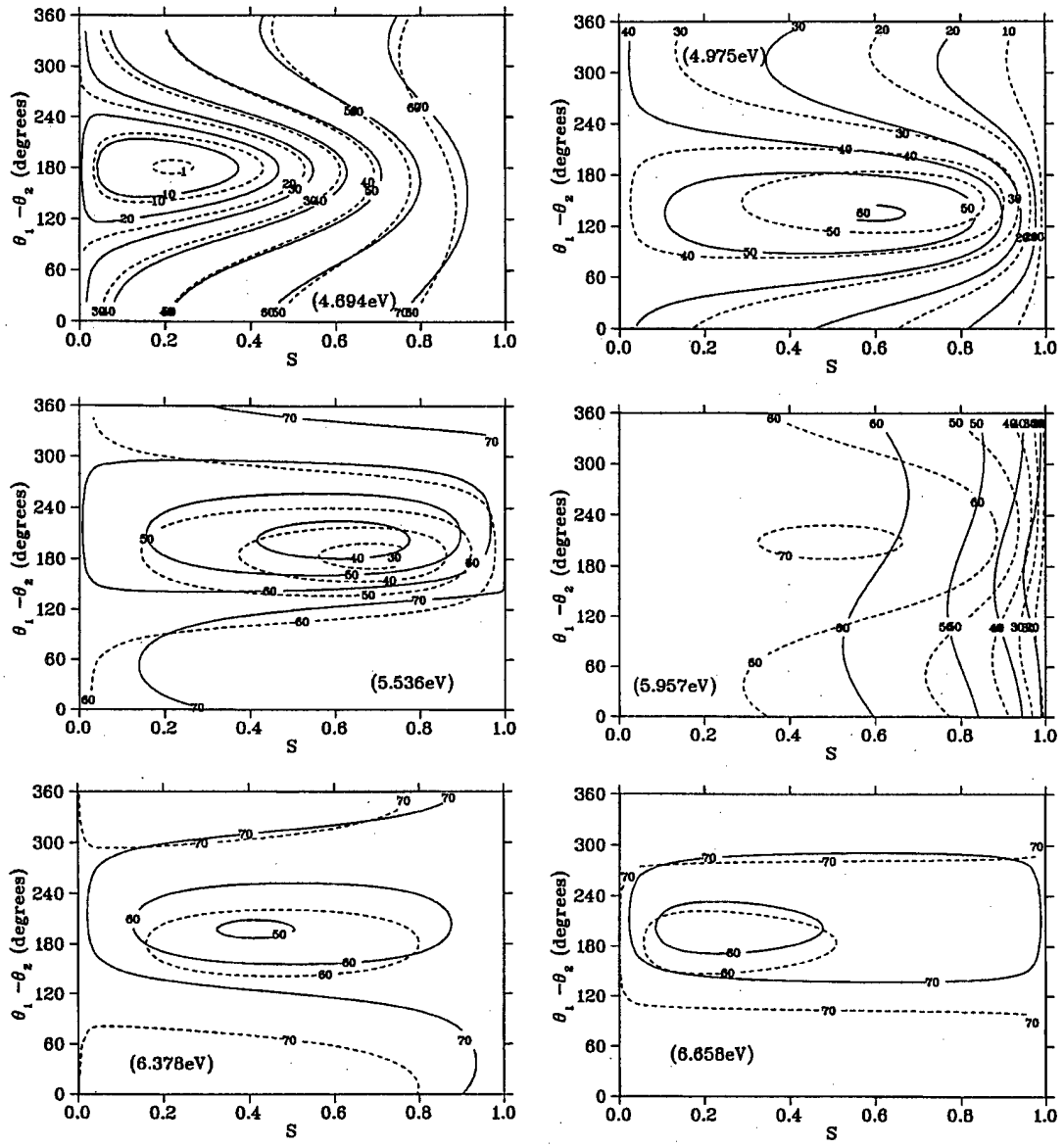

Figure 7. Contour plots of the relative product yields $R(I_{1/2}:I_{3/2},E) = I_{1/2}/(I_{1/2} + I_{3/2})$, for bichromatic coherent control of an initial ICN superposition state with vibrational quantum numbers $v = 1$ and $v = 3$, respectively. The photoexcitation energy is indicated in each panel.

state nonadiabatic dynamics as influenced by laser induced quantum interference effects.

According to the present implementation, semiclassical simulations of ICN coherent control require the evaluation of quite a large number of trajectories ($\sim 2 \times 10^7$), and of course they would be even more demanding for systems with many more degrees of freedom. This is clearly the aspect of the calculation that needs further development. It is expected that the combination of the HK SC-IVR, together with stationary phase MC, and direct implementation methodologies under development, should provide a more tractable approach for simulating coherent control on higher dimensionality problems.

Acknowledgment. The authors are grateful to Bill Miller for teaching them many things in many different ways. We gratefully acknowledge financial support for this work from the U.S. Office of Naval Research and from Photonics Research Ontario. We also acknowledge a generous allocation of supercomputing time from the National Energy Research Scientific Computing Center (NERSC). V.S.B. thanks Dr. Eduardo A. Coronado for very encouraging comments on an early version of this manuscript.

References and Notes

(1) Shapiro, M.; Brumer, P. In *Advances in Atomic, Molecular and Optical Physics*; Bederson, B., Walther, H., Eds.; Academic Press: San Diego, CA, 2000; pp 287−343.
(2) Brumer, P.; Shapiro, M. *Chem. Phys. Lett.* **1996**, *126*, 541.
(3) Shapiro, M.; Brumer, P. *Faraday Discuss. Chem. Soc.* **1987**, *82*, 177.
(4) Miller, W. H. *J. Chem. Phys.* **1970**, *53*, 3578.
(5) Batista, V. S.; Miller, W. H. *J. Chem. Phys.* **1998**, *108*, 498.
(6) Batista, V., et al., *J. Chem. Phys.* **1999**, *110*, 3736.
(7) Guallar, V.; Batista, V.; Miller, W. *J. Chem. Phys.* **1999**, 110, 9922.
(8) Campolieti, G.; Brumer, P. *Phys. Rev. A* **1994**, *50*, 997.
(9) Kay, K. G. *J. Chem. Phys.* **1994**, *100*, 4432.
(10) Kay, K. G. *J. Chem. Phys.* **1994**, *101*, 2250.
(11) Brewer, M. L.; Hulme, J. S.; Manolopoulos, D. E. *J. Chem. Phys.* **1997**, *106*, 4832.

(12) Guerin, B. E.; Herman, M. F. *Chem. Phys. Lett.* **1998**, *286*, 361.
(13) Heller, E. *J. Chem. Phys.* **1991**, *95*, 9431.
(14) Grossmann, F.; Heller, E. J. *Chem. Phys. Lett.* **1995**, *241*, 45.
(15) Garashchuk, S.; Grossmann, F.; Tannor, D. J. *J. Chem. Soc., Faraday Trans.* **1997**, *93*, 781.
(16) Shalashilin, D. V.; Jackson, B. *Chem. Phys. Lett.* **1998**, *291*, 143.
(17) Provost, D.; Brumer, P. *Phys. Rev. Lett.* **1995**, *74*, 250.
(18) Guo, H.; Schatz, G. C. *J. Chem. Phys.* **1990**, *92*, 1634.
(19) Meyer, H.; Miller, W. H. *J. Chem. Phys.* **1979**, *70*, 3214.
(20) Tully, J. *J. Chem. Phys.* **1990**, *93*, 1061.
(21) Stock, G.; Thoss, M. *Phys. Rev. Lett.* **1997**, *78*, 578.
(22) Wang, H.; Song, X.; Chandler, D.; Miller, W. *J. Chem. Phys.* **1999**, *110*, 4828.
(23) Coronado, E. A.; Batista, V. S.; Miller, W. H. *J. Chem. Phys.* **2000**, *112*, 5566.
(24) H. W. P.; L. S. R., *J. Chem. Phys.* **1987**, *86*, 3773.
(25) Nadler, I.; Mahgerefteh, D.; Reisler, H.; Wittig, C. *J. Chem. Phys.* **1985**, *82*, 3885.
(26) Pitts, W.; Baronavski, A. *Chem. Phys. Lett.* **1980**, *71*, 395.
(27) Herzberg, G. *Molecular Spectra and Molecular Structure, Volume II* ; Krieger Publishing Co: Malabar, FL, 1991; p 174.
(28) Goldfield, E. M.; Houston, P. L.; Ezra, G. S. *J. Chem. Phys.* **1986**, *84*, 3120.
(29) Qian, J.; Tannor, D.; Amatatsu, Y.; Morokuma, K. *J. Chem. Phys.* **1994**, *101*, 9597.
(30) Sun, X.; Miller, W. H. *J. Chem. Phys.* **1999**, *110*, 6635.

ELSEVIER

Chemical Physics 267 (2001) 81–92

Chemical Physics

www.elsevier.nl/locate/chemphys

Coherent control of atom–diatom reactive scattering: isotopic variants of $H + H_2$ in three dimensions

Alexander Abrashkevich, Moshe Shapiro [1], Paul Brumer *

Chemical Physics Theory Group, University of Toronto, Photonics Research Ontario, Toronto, Canada M5S 3H6

Received 3 January 2001

Abstract

Control over reactive and non-reactive cross-sections in 3D atom–diatom scattering is shown to be possible using a superposition of non-degenerate ro-vibrational states of the target-diatomic molecule. Depending on the phase and magnitude of the coefficients which describe the initial superposition state, one can, through quantum interference, enhance or suppress the reactive or non-reactive scattering to predetermined product states. Fully converged 3D quantum computations reveal extensive control over the reactive/non-reactive branching ratios in the $D + H_2 \rightarrow DH + H$ and the $H + H'D \rightarrow HH' + D$; $HD + H'$ reactions, where H and H′ denote hydrogen atoms which are considered distinguishable. © 2001 Published by Elsevier Science B.V.

PACS: 82.40.Dm; 34.50.Rk; 34.50.Lf

1. Introduction

The coherent control (CC) approach for controlling dynamical processes [1–24] makes use of quantum interference effects to manipulate the wave-like nature of matter. Specifically, CC utilizes coherent light sources to induce constructive or destructive interferences in the matter molecules. In this way one can enhance (or suppress) desired (or undesired) products. Numerous experimental demonstrations of the CC principle are now available [1–3].

Thus far, CC has been realized experimentally in the control of *unimolecular* processes, such as molecular photodissociation and photoionization [1–15]. Controlling the yield of *bimolecular reactions* [16–24] presents a much greater experimental challenge, since, as explained below, in this case one starts with an initially unbound state.

In recent years we have developed a number of scenarios by which bimolecular control could be achieved. Initially we investigated bimolecular laser control at energies below or near the reaction threshold [16–19]. Later, we presented a general theory for the control of bimolecular collisions, capable of dealing with energies above the reaction threshold [20]. This general theory has been applied to the control of isotopic variants of the $H + H_2 \rightarrow H_2 + H$ reaction [21] in the collinear domain. We have also studied the control of differential cross-sections of these reactions. Because

* Corresponding author. Fax: +1-416-978-5325.
E-mail address: pbrumer@tikva.chem.utoronto.ca (P. Brumer).
[1] Permanent address: Department of Chemical Physics, The Weizmann Institute of Science, 76100 Rehovot, Israel.

0301-0104/01/$ - see front matter © 2001 Published by Elsevier Science B.V.
PII: S0301-0104(01)00256-7

of kinematic constraints [22], to be discussed below, we utilized, in both cases, superpositions of nearly degenerate diatomic states [23,24].

In the present paper we consider a more ambitious control scenario, involving fully realistic computations on superpositions of non-degenerate target-diatomic states. The experimental difficulty inherent in utilizing such target states as a basis for a superposition of scattering states, requiring correlating the translational energy of the atom with the internal energy of the target-diatomic molecule, is offset by the extensive degree of control afforded in this scheme. Below we demonstrate, with exact 3D quantum-mechanical calculations for isotopic variants of the $H + H_2 \rightarrow H_2 + H$ reaction using realistic potential energy surface, that total reactive vs non-reactive cross-sections can be extensively controlled by varying the phases and amplitudes of the initially prepared superposition state.

This paper is organized as follows: The preparation of the superposition of scattering state is discussed in Section 2.1. In Section 2.2 we summarize the implementation of CC for 3D atom–diatom quantum reactive scattering. The results of our calculations for $D + H_2$ and $H + H'D$ reactions (where H and H′ denote hydrogen atoms which are assumed to be distinguishable) are discussed in Section 3, where the wide range of control over reactive vs non-reactive cross-sections is demonstrated. Section 4 contains a brief summary.

2. Coherent control of atom–diatom reactive scattering

2.1. Initial preparation of a superposition of scattering state

Consider an atom A colliding with a diatomic molecule BC. The three possible outcomes (arrangements) of this collision are A + BC, B + AC, C + AB and we label each arrangement by the symbol $\alpha = a(A + BC)$, $b(B + AC)$, or $c(C + AB)$. Denoting the masses of the three atoms as M_A, M_B, M_C, and their positions as $\mathbf{r}_A$, $\mathbf{r}_B$, $\mathbf{r}_C$, we define $\mathbf{r}_{BC}$, the position of one target atom relative to the other, $\mathbf{K}$, the total center-of-mass wave vector, and $\mathbf{R}$, the total center-of-mass position, as,

$$\begin{aligned} &M_{BC} = M_B + M_C, \quad M = M_A + M_{BC}, \\ &\mu_{BC} = M_B M_C/(M_B + M_C), \\ &\mathbf{R}_{BC} = (M_B\mathbf{r}_B + M_C\mathbf{r}_C)/M_{BC}, \\ &\mathbf{R} = (M_A\mathbf{r}_A + M_B\mathbf{r}_B + M_C\mathbf{r}_C)/M, \\ &\mathbf{r}_{BC} = \mathbf{r}_B - \mathbf{r}_C, \quad \mathbf{k}_{BC} = \mathbf{k}_B + \mathbf{k}_C, \\ &\mathbf{K} = \mathbf{k}_A + \mathbf{k}_{BC}. \end{aligned} \tag{1}$$

We also define the arrangement-specific relative atom–diatom wave vector $\mathbf{k}$, and the relative atom–diatom position $\mathbf{r}$ for arrangement a as

$$\mathbf{k} = (M_{BC}\mathbf{k}_A - M_A\mathbf{k}_{BC})/M, \quad \mathbf{r} = \mathbf{r}_A - \mathbf{R}_{BC}. \tag{2}$$

Similar definitions hold for the two other (b and c) arrangements.

The total Hamiltonian of the system can be divided into four parts,

$$H = T(\mathbf{R}) + T(\mathbf{r}) + h_a(\mathbf{r}_{BC}) + V_a(\mathbf{r}, \mathbf{r}_{BC}), \tag{3}$$

where T denotes a kinetic-energy operator, h_a is the Hamiltonian for the BC diatomic and V_a is the atom–diatom interaction potential in the a arrangement, satisfying the asymptotic condition,

$$V_a \overset{r\to\infty}{\rightarrow} 0. \tag{4}$$

The breakup of the Hamiltonian can be carried out in (three) different ways, depending on the arrangement index, α.

As shown previously [20], in order to assume control we need to create a superposition of continuum states, denoted as $|E, a, \mathbf{c}; 0\rangle$, comprised of $|E, a, \mathbf{n}; 0\rangle$, the eigenstates of the asymptotic arrangement Hamiltonian H_a,

$$H_a \equiv T(\mathbf{r}) + h_a(\mathbf{r}_{BC}), \tag{5}$$

satisfying the eigenvalue relation,

$$[E - H_a]|E, a, \mathbf{n}; 0\rangle = 0, \tag{6}$$

with $\mathbf{n}$ denoting the quantum numbers (such as vibration or rotation) describing the internal energetic states of the a arrangement separated products.

Assuming that we can create a superposition of two such states, we choose the atomic and diatomic incident wave functions ψ_A and ψ_{BC} as,

$$|\psi_A\rangle = |\phi_A(g)\rangle\{c_1 \exp[i\mathbf{k}_A(1)\cdot\mathbf{r}_A] + c_2 \exp[i\mathbf{k}_A(2)\cdot\mathbf{r}_A]\}, \quad (7)$$

$$|\psi_{BC}\rangle = c_3|\phi_{BC}(3)\rangle \exp[i\mathbf{k}_{BC}(3)\cdot\mathbf{R}_{BC}] + c_4|\phi_{BC}(4)\rangle \exp[i\mathbf{k}_{BC}(4)\cdot\mathbf{R}_{BC}], \quad (8)$$

where $|\phi_A(g)\rangle$ is the ground electronic state of atom A and $|\varphi_{BC}(j)\rangle$ are internal diatomic states with energy $e_{BC}(j)$. The total incident wave function is then given as,

$$|E,a,\mathbf{c};0\rangle = |\psi_A\rangle|\psi_{BC}\rangle = \sum_{i=1}^{2}\sum_{j=3}^{4} |A\rangle_{ij} \exp(i\mathbf{k}_{ij}\cdot\mathbf{r}) \exp(i\mathbf{K}_{ij}\cdot\mathbf{R}), \quad (9)$$

where $|A\rangle_{ij} = c_i c_j |\phi_A(g)\rangle|\phi_{BC}(j)\rangle$, $\mathbf{k}_{ij} = (M_{BC}\mathbf{k}_A(i) - M_A\mathbf{k}_{BC}(j))/M$, and $\mathbf{K}_{ij} = \mathbf{k}_A(i) + \mathbf{k}_{BC}(j)$ with $(i = 1,2; j = 3,4)$.

If each term in the wave function has a different center-of-mass wave vector $\mathbf{K}_{ij}$, then Eq. (9) is composed of four independent incident waves. Since the V_a potential depends solely on the relative coordinates, $\mathbf{r}$ and $\mathbf{r}_{BC}$, and not on $\mathbf{R}$, the center-of-mass momentum is conserved (which is why we are able to separate out the center-of-mass coordinate from the relative coordinates). As a result, as shown in Ref. [22], only those $|\mathbf{K}\rangle$ components of the incident superposition state having the same center-of-mass momentum can interfere with each other to affect the final cross-sections. The interference between components with different $\mathbf{K}_I$ values is quickly washed away during the collision. However, conditions can be set in such a way that interference, and hence control, may be achieved. In order to do that, we require the equality of the center-of-mass motion of at least two energetically degenerate components,

$$\mathbf{K}_{13} = \mathbf{K}_{24}, \qquad \hbar^2 k_{13}^2/2\mu + e_{BC}(3) = \hbar^2 k_{24}^2/2\mu + e_{BC}(4), \quad (10)$$

with $\mu = M_A M_{BC}/M$. Eq. (9) then becomes

$$|E,a,\mathbf{c};0\rangle = \{|A\rangle_{13}\exp(i\mathbf{k}_{13}\cdot\mathbf{r}) + |A\rangle_{24}\exp(i\mathbf{k}_{24}\cdot\mathbf{r})\}\exp(i\mathbf{K}_{13}\cdot\mathbf{R}) + |A\rangle_{23}\exp(i\mathbf{k}_{23}\cdot\mathbf{r})\exp(i\mathbf{K}_{23}\cdot\mathbf{R}) + |A\rangle_{14}\exp(i\mathbf{k}_{14}\cdot\mathbf{r})\exp(\mathbf{K}_{14}\cdot\mathbf{R}), \quad (11)$$

where the term in the first bracket, due to Eq. (10), is a linear superposition of two degenerate states.

The cross-section resulting from the initial state in Eq. (11) is comprised of the first two terms of Eq. (11), which can interfere with each other because they have the same center-of-mass momentum, and by the last two ("satellite") terms, which are non-interfering because they have different center-of-mass momenta.

As a particular realization of Eq. (10) we choose $\mathbf{K}_{13} = \mathbf{K}_{24} = 0$ and $\mathbf{K}_{23} = -\mathbf{K}_{14}$, which means that $\mathbf{k}_A(1) = -\mathbf{k}_{BC}(3)$ and $\mathbf{k}_A(2) = -\mathbf{k}_{BC}(4)$. Since in that case $\mathbf{k}_{13} = \mathbf{k}_A(1)$, $\mathbf{k}_{24} = \mathbf{k}_A(2)$, we have from Eq. (10) that,

$$\hbar^2[k_A^2(1) - k_A^2(2)] = (2M_A M_{BC})[e_{BC}(4) - e_{BC}(3)]/(M_{BC} + M_A). \quad (12)$$

We also have in that case that, $\mathbf{k}_{23} + \mathbf{k}_{14} = \mathbf{k}_{13} + \mathbf{k}_{24} = \mathbf{k}_A(1) + \mathbf{k}_A(2)$, and assuming that $\mathbf{k}_A(1)$ is parallel to $\mathbf{k}_A(2)$, the energies of the satellite terms become,

$$E_{23}^{sat} = \frac{\hbar^2}{2\mu}k_{23}^2 + e_{BC}(3), \qquad E_{14}^{sat} = \frac{\hbar^2}{2\mu}k_{14}^2 + e_{BC}(4), \quad (13)$$

where

$$k_{23}^2 = [M_{BC}^2 k_A^2(2) + M_A^2 k_A^2(1) + 2M_A M_{BC} k_A(1)k_A(2)]/M^2,$$

$$k_{14}^2 = [M_{BC}^2 k_A^2(1) + M_A^2 k_A^2(2) + 2M_A M_{BC} k_A(1)k_A(2)]/M^2.$$

Note that in the specific case where we superpose degenerate states of the BC, Eq. (12) becomes $k_A^2(1) = k_A^2(2)$. Indeed, in this case we can choose $\mathbf{k}_A(1) = \mathbf{k}_A(2) = -\mathbf{k}_{BC}(3) = -\mathbf{k}_{BC}(4)$ so that all of the $\mathbf{K}_{ij}$ are equal and at the same time all of the four terms in Eq. (9) are energetically degenerate. Therefore, in the case corresponding to the scattering of an atom off a diatom in a superposition

of degenerate diatomic states, there are no extraneous uncontrollable satellite contributions. Results for this class of coherent control obtained for $D + H_2$, $H + D_2$ and $H + H'D$ reactions have been discussed in Refs. [22–24]. In this paper we consider another class of control, that utilizing superpositions of non-degenerate internal diatomic states.

2.2. Atom–diatom scattering using non-degenerate initial superposition states

Consider a superposition state involving non-degenerate diatomic states, given as,

$$|E,a,\mathbf{c};0\rangle = \sum_{i=1,2} c_i |\varphi_A(g)\rangle |\varphi_{BC}(v_i j_i m_i)\rangle |E_a^{kin}(i)\rangle, \tag{14}$$

where, as above, c_i are complex coefficients. $|E_a^{kin}(i)\rangle$ are plane waves describing the free motion of the A atom relative to the BC diatomic, whose energies are correlated to the energy levels of BC according to,

$$E_a^{kin}(i) = E - e_{BC}(v_i, j_i). \tag{15}$$

In this way all the components which make up the superposition state have the same total energy E.

With m_i quantum numbers taken to be helicities [25–27], i.e., the projections of $\mathbf{j}_i$ on $\mathbf{r}$, the relative atom–diatom (center-of-mass) position vector, the differential cross-section for forming the α-arrangement at scattering angles θ and φ, having started from the $|E,a,\mathbf{c};0\rangle$ superposition state, is given by

$$\sigma_{\alpha v j m \leftarrow a,\mathbf{c}}(E|\theta,\varphi) = \left| \sum_{i=1,2} c_i f_{\alpha v j m \leftarrow a v_i j_i m_i}(\pi-\theta,\varphi) \right|^2, \tag{16}$$

where

$$f_{\alpha v j m \leftarrow a v_i j_i m_i}(\theta,\varphi) = \frac{\mathrm{i}^{j_i - j + 1}\, \mathrm{e}^{\mathrm{i} m_i \varphi}}{2k_{a,v_i j_i}} \sum_J (2J+1) \times d^J_{m m_i}(\theta) T^J_{\alpha v j m \leftarrow a v_i j_i m_i} \tag{17}$$

is the scattering amplitude [27], $T^J_{\alpha v j m \leftarrow a v_i j_i m_i} = S^J_{\alpha v j m \leftarrow a v_i j_i m_i} - \delta_{\alpha a}\delta_{v v_i}\delta_{j j_i}\delta_{m m_i}$, $S^J_{\alpha v j m \leftarrow a v_i j_i m_i}$ are the elements of scattering S matrix in the helicity representation. Here J is the total angular momentum, m is the helicity of the product diatom, $d^J_{m m_i}(\theta)$ are the reduced rotation matrices [26,28], and $k_{a,v_i j_i} = (2\mu_a(E - e_{BC}(v_i, j_i)))^{1/2}/\hbar$, with μ_a being the atom–diatom reduced mass in the a arrangement. The use of $\pi - \theta$, rather than θ, on the right-hand side of Eq. (16) is discussed in Ref. [29].

Explicitly squaring the sum in Eq. (16) (and dropping the initial state labels for convenience) and constructing the differential cross-section

$$\sigma^R_{v j m}(\theta) = \int_0^{2\pi} \sigma^R_{v j m}(\theta,\varphi)\, \mathrm{d}\varphi, \tag{18}$$

gives

$$\sigma^R_{v j m}(\theta) = |c_1|^2 \sigma^R_{v j m}(11|\theta) + |c_2|^2 \sigma^R_{v j m}(22|\theta) + 2\,\mathrm{Re}\left\{ c_1 c_2^* \sigma^R_{v j m}(12|\theta) \right\}, \tag{19}$$

$$\sigma^R_{v j m}(ii|\theta) = \frac{\pi}{2k^2_{a,v_i j_i}} \sum_{J,J'} (2J+1)(2J'+1) d^J_{m m_i}(\pi-\theta) \times d^{J'}_{m m_i}(\pi-\theta) \times S^J_{\alpha v j m \leftarrow a v_i j_i m_i} \left[S^{J'}_{\alpha v j m \leftarrow a v_i j_i m_i} \right]^*, \quad a \neq \alpha, \ i = 1,2, \tag{20}$$

and

$$\sigma^R_{v j m}(12|\theta) = \frac{\pi \mathrm{i}^{j_1 - j_2}}{2k_{a,v_1 j_1} k_{a,v_2 j_2}} \sum_{J,J'} (2J+1)(2J'+1) \times d^J_{m m_1}(\pi-\theta) d^{J'}_{m m_2}(\pi-\theta) S^J_{\alpha v j m \leftarrow a v_1 j_1 m_1} \times \left[S^{J'}_{\alpha v j m \leftarrow a v_2 j_2 m_2} \right]^* \delta_{m_1,m_2}, \quad a \neq \alpha. \tag{21}$$

Here we have taken into account that

$$\int_0^{2\pi} \mathrm{d}\varphi\, \mathrm{e}^{\mathrm{i}(m_1 - m_2)\varphi} = 2\pi \delta_{m_1,m_2}, \tag{22}$$

so that the interference term $\sigma^R_{v j m}(12|\theta)$ is non-zero only when $m_1 = m_2$ and control therefore disappears for $m_1 \neq m_2$. Below, all superposition states used adhere to the $m_1 = m_2$ requirement. Note that above, the superscript R denotes reactive scattering into a specific final arrangement channel $\alpha \neq a$.

The total differential cross-section, $\sigma^R(\theta)$, for reaction out of a state $|E,a,\mathbf{c};0\rangle$ is given as a sum over final states of the state-specific cross-sections,

$$\sigma^{R}(\theta) = \sum_{v,j,m} \sigma^{R}_{vjm}(\theta). \quad (23)$$

Integration of Eq. (19) over angle $\theta \in [0, \pi]$ gives the state-resolved integral reactive cross-section σ^{R}_{vjm}. This can also be written as three terms, as in Eq. (19), but with $\sigma^{R}_{vjm}(ij|\theta)$ replaced by $\sigma^{R}_{vjm}(ij)$, where

$$\sigma^{R}_{vjm}(ii) = \frac{\pi}{k^2_{a,v_i j_i}} \sum_{J} (2J+1) \left| S^{J}_{\alpha vjm \leftarrow a v_i j_i m_i} \right|^2, \quad i = 1,2, \quad (24)$$

$$\sigma^{R}_{vjm}(12) = \frac{\pi i^{j_1 - j_2}}{k_{a,v_1 j_1} k_{a,v_2 j_2}} \sum_{J} (2J+1) S^{J}_{\alpha vjm \leftarrow a v_1 j_1 m_1} \times \left[S^{J}_{\alpha vjm \leftarrow a v_2 j_2 m_2} \right]^{*} \delta_{m_1, m_2}, \quad \alpha \neq a. \quad (25)$$

Averaged integral cross-sections are obtained by averaging over initial states and summing over the final states (we assume that $\Delta j = j_2 - j_1 > 0$)

$$\sigma^{R}_{vj} = \frac{1}{2j_1 + 1} \sum_{m} \sum_{m_1} \left[|c_1|^2 \sigma^{R}_{vjm}(11) + |c_2|^2 \sigma^{R}_{vjm}(22) + 2\,\mathrm{Re}\left\{ c_1^{*} c_2 \sigma^{R}_{vjm}(12) \right\} \right]. \quad (26)$$

Summing over the final states at energy E, we obtain the total integral cross-section as

$$\sigma^{R} = \sum_{v,j} \sigma^{R}_{vj}. \quad (27)$$

Note that state-to-state cross-sections $\sigma^{R}_{vjm}(ii|\theta)$ and $\sigma^{R}_{vjm}(ii)$ in Eqs. (20) and (24), as well as the corresponding total cross-sections $\sigma^{R}(ii|\theta)$ and $\sigma^{R}(ii)$, are the differential and integral cross-sections that appear in standard scattering theory (see, e.g., Ref. [25]), while $\sigma^{R}_{vjm}(12|\theta)$ and $\sigma^{R}_{vjm}(12)$ in Eqs. (22) and (25) and corresponding total cross-sections $\sigma^{R}(12|\theta)$ and $\sigma^{R}(12)$, are new types of interference terms which allow for control by varying the c_i coefficients. It is important to mention that significant control requires substantial $\sigma^{R}(12)$ which follows from the Schwartz inequality $[|\sigma^{R}(12)| \leqslant (\sigma^{R}(11)\sigma^{R}(22))^{1/2}]$, i.e., large $\sigma^{R}(12)$ requires also large $\sigma^{R}(11)$ and large $\sigma^{R}(22)$. Therefore, extensive control is not limited to regions near the reactive threshold [16–19].

We can rewrite the total reactive cross-section in the more convenient form

$$\sigma^{R} = [\sigma^{R}(11) + x^2 \sigma^{R}(22) + 2x|\sigma^{R}(12)| \cos(\delta^{R}(12) + \phi_{12})]/(1 + x^2), \quad (28)$$

where $x = |c_2/c_1|$, $\phi_{12} = \arg(c_2/c_1)$, and $\delta^{R}(12) = \arg(\sigma^{R}(12))$. Eq. (28) has the familiar form (see, e.g., Ref. [1]) which depicts the essence of CC. Specifically, there are two terms, $\sigma^{R}(11)$ and $\sigma^{R}(22)$, which result from independent routes to the product, plus an interference term, which is proportional to the complex term $\sigma^{R}(12)$. The last term results from the simultaneous contributions of the two pathways.

In many cases, controlling the branching ratio between the reactive and non-reactive total cross-sections is of greatest interest. This ratio is given as,

$$\frac{\sigma^{R}}{\sigma^{NR}} = \frac{\sigma^{R}(11) + x^2 \sigma^{R}(22) + 2x|\sigma^{R}(12)| \cos\left(\delta^{R}(12) + \phi_{12}\right)}{\sigma^{NR}(11) + x^2 \sigma^{NR}(22) + 2x|\sigma^{NR}(12)| \cos\left(\delta^{NR}(12) + \phi_{12}\right)}. \quad (29)$$

In Eq. (29) the NR symbol denotes the non-reactive terms. These terms are analogous to the reactive terms except that α is replaced by a and T matrix elements replace the S matrix elements. A formula similar to Eq. (29) holds for the ratio of reactive to non-reactive differential cross-sections with $\sigma^{R}(mn)$ replaced by $\sigma^{R}(mn|\theta)$, etc.

It follows from Eqs. (28) and (29) that by varying the relative magnitude, x, and the relative phase, ϕ_{12} of the c_i coefficients, we can directly alter the interference term $\sigma(12)^{R}$ (and/or $\sigma^{NR}(12)$) and hence control the scattering cross-sections. The above approach can be readily extended to the case of a superposition of $N > 2$ interfering states.

3. Results and discussion

3.1. Computational details

We have applied this formulation to control the isotopic variants of the $H + H_2$ reaction: $D + H_2 \rightarrow DH + H$ and $H + H'D \rightarrow HH' + D$; $HD + H'$, where H and H′ are considered distinguishable. In our three-dimensional quantum-mechanical calculations, the $A + B_2$ symmetry [29] has been exploited for the first reaction for which there are only two final outcomes. We have restricted attention to initial superpositions made up of even H_2 rotational states (and assorted vibrational levels), i.e., only the even parity manifold for each partial wave was considered. In the second reaction, no such symmetry was assumed and three final arrangements were considered. The LSTH [30–32] potential energy surface was used in all calculations and the S matrices were obtained using a contracted-basis [33] log–derivative version of the Kohn variational principle [34].

The calculations in the $D + H_2$ reaction were carried out at two energies, $E = 0.93$ and 1.25 eV, for total angular momentum $J = 0, 1, \ldots, 31$ with $E_{max} = 2.5$ eV and $j = 0, 2, 4, \ldots, 12$ and $j = 0, 2, 4, \ldots, 14$, respectively. The $H + H'D$ calculations were performed at total energy $E = 0.8$ eV for total angular momentum up to $J = 32$ with $j_{max} = 14$ and $E_{max} = 2.6$ eV. Here, E_{max} and j_{max} are respectively the maximum (cutoff) energy and maximum diatomic rotational quantum number of all diatomic basis states. The above sets of parameters ensure fully converged cross-sections for the chosen energies. The calculations reported here are CPU intensive, requiring in excess of 30 h of CRAY T90 time for each scattering computation.

3.2. Control of integral cross-sections

Of greatest practical interest is the ability to control integral cross-sections. We have explored the control of integral cross-sections of the $D + H_2 \rightarrow H + HD$ reaction at total energy $E = 1.25$ eV, which is well above the reaction threshold, thereby allowing us to demonstrate substantial control in the presence of a significant natural reactive cross-section.

Our numerical tests, carried out for various combinations of initial (v, j) states of H_2, show that control is substantial when superpositions of states with the same v quantum numbers are used. Initial superposition states with different v's do not lead to appreciable control. Hence, only equal-v results are reported here.

We first present results for scattering from an initial superposition state comprised of the $v_1 = 1$, $j_1 = 2$ and $v_2 = 1$, $j_2 = 4$ diatomic states (see Eq. (11)). Panel (a) of Fig. 1 presents a contour plot of σ^R/σ^{NR} ratio with contributions from the satellite terms ignored. The branching ratios are plotted as a function of the ϕ_{12} and $s = x^2/(1 + x^2)$ control parameters. (Note added in proof: a programming error requires that one change the ϕ_{12} to $-\phi_{12}$ in all figures in which it appears, in this paper as well as in Refs. [22,23].) Varying s from 0 to 1 corresponds to changing the initial superposition from being composed (at $s = 0$) of state 1 only, to being composed (at $s = 1$) of state 2 only .

The results clearly show substantial control over σ^R/σ^{NR}. This ratio can be increased by a factor of 2.5, from 0.14 for $s = 0.72$, $\phi_{12} = 131°$, to 0.35 for $s = 0.23$, $\phi_{12} = 308°$. These numbers should be compared with the "natural" branching ratios of 0.25 at $s = 0$ and 0.18 at $s = 1$.

Panel (b) of Fig. 1 shows the the σ^R/σ^{NR} ratio when the satellite terms are included. This has the effect of reducing slightly the range of control, which now only extends from 0.20 up to 0.33.

The range of control achievable gradually decreases with Δj of the rotational states which make up the superposition state. The origin of this behavior is evident from analysis of the results presented in Table 1 where the magnitude of both the reactive and non-reactive $\sigma(12)$ terms are seen to decrease sharply with increasing Δj. This leads, according to Eq. (29), to a decrease in the degree of control. The above behavior holds for both the $v_i = 0$ and $v_i = 1$ diatomic states.

In our computations the computational effort needed to evaluate the satellite terms of Eq. (11) at the two additional energies associated with the satellite terms was reduced by evaluating them at the same $E = 1.25$ eV energy of the main (interfering) term. The approximate σ^R/σ^{NR} ratios ob-

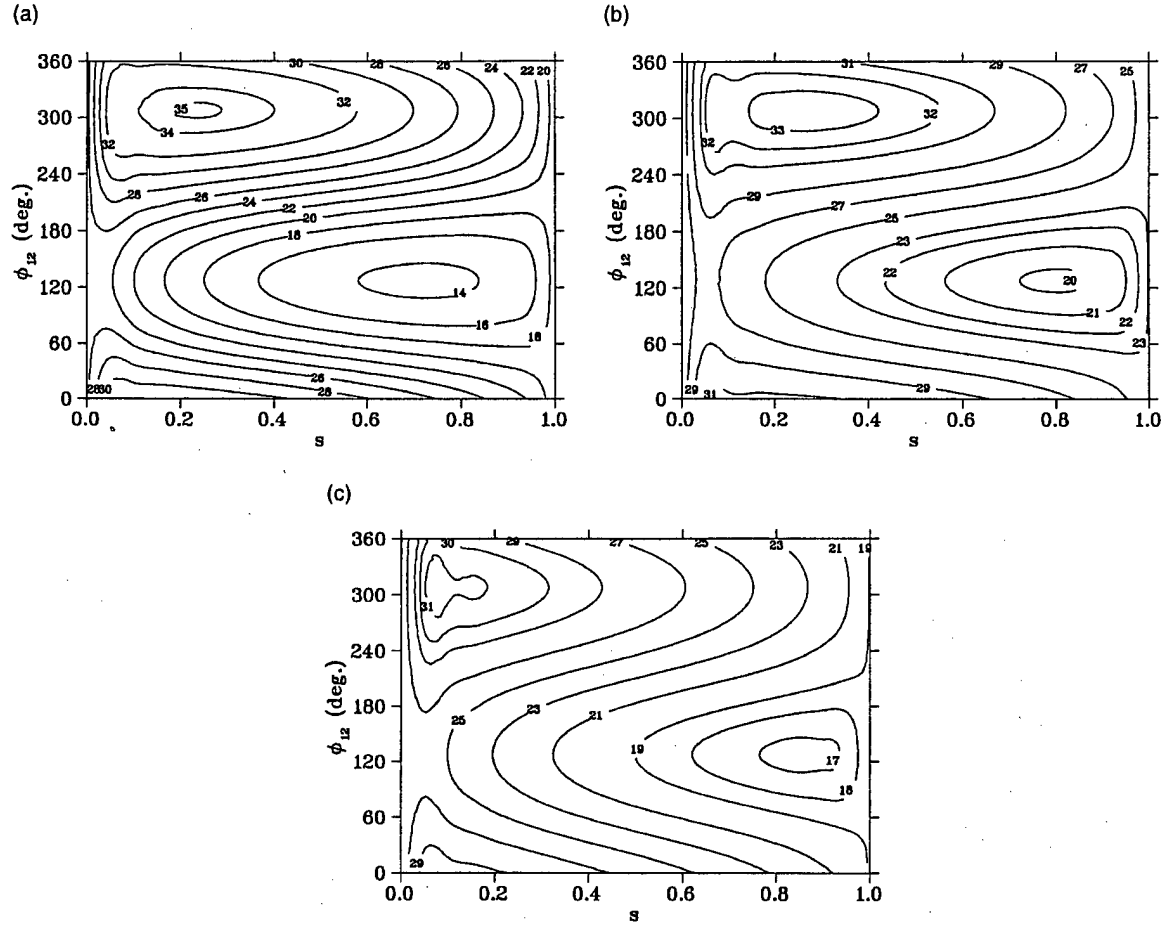

Fig. 1. Contour plot of the integral cross-sections ratio $\sigma^{R}/\sigma^{NR}(\times 10^2)$ for the $D + H_2$ reaction at total scattering energy $E = 1.25$ eV as a function of ϕ_{12} and s for a transition from an initial superposition state with $v_1 = 1, j_1 = 2, v_2 = 1, j_2 = 4$ calculated (a) without satellite terms, (b) with satellite terms obtained at energies given by Eq. (13) and (c) with satellite terms evaluated at energy $E = 1.25$ eV.

tained in this way, are in good agreement (compare panels (b) and (c) of Fig. 1) with the exact results. For example, the overall range of control is 72%, as compared to 65% in the more exact scheme. This favorable comparison has led us to use this approximation (which reduces the computational effort by a factor of 3) in all the calculations reported below.

Similar control results to those reported above are obtained for superposition states composed of $v = 0$ diatomic states. The best control has been obtained for scattering from the initial $(v_1 = 0, j_1 = 4, v_2 = 0, j_2 = 6)$ superposition state (see Table 1).

We now examine the range of control at $E = 0.93$ eV, an energy closer to the reaction threshold. Of the many cases studied, the most extensive control at that energy is obtained by choosing $(v_1 = 0, j_1 = 2, v_2 = 0, j_2 = 4)$ to build the initial superposition state. Fig. 2 shows the σ^{R}/σ^{NR} ratios for this case. By changing the phase angle ϕ_{12} from 93° at $s = 0.75$ to 269° at $s = 0.19$ we can vary σ^{R}/σ^{NR} from 0.16 to 0.29, as compared with the uncontrolled ratios of 0.24 at $s = 0$ and 0.18 at $s = 1$.

Control is also evident for scattering from the $(v_1 = 1, j_1 = 0; v_2 = 1, j_2 = 2)$ initial state, but in that case the ICS ratio is smaller by two orders of

Table 1
Integral cross-sections $\sigma^{NR,R}(mn)$ (in a_0^2), $m \leqslant n = 1, 2$, for $D + H_2$ collisions at $E = 1.25$ eV

v_1	j_1	v_2	j_2	$\sigma^{NR}(11)$	$\sigma^{NR}(22)$	$\sigma^{NR}(12)$	$\sigma^{R}(11)$	$\sigma^{R}(22)$	$\sigma^{R}(12)$
0	0	0	2	4.736(+1)	4.610(+1)	2.070(+0)	5.713(+0)	6.728(+0)	2.177(+0)
0	0	0	4	4.736(+1)	5.037(+1)	5.558(−1)	5.713(+0)	6.521(+0)	4.653(−1)
0	0	0	6	4.736(+1)	6.908(+1)	8.610(−3)	5.713(+0)	5.738(+0)	2.219(−1)
0	0	0	8	4.736(+1)	9.758(+1)	2.299(−1)	5.713(+0)	3.614(+0)	1.310(−1)
0	2	0	4	4.744(+1)	5.043(+1)	1.705(+0)	5.656(+0)	6.256(+0)	1.581(+0)
0	2	0	6	4.744(+1)	6.892(+1)	3.295(−1)	5.656(+0)	5.583(+0)	4.197(−1)
0	2	0	8	4.744(+1)	9.765(+1)	1.792(−1)	5.656(+0)	3.513(+0)	1.511(−1)
0	4	0	6	5.098(+1)	6.838(+1)	1.492(+0)	5.258(+0)	5.182(+0)	1.521(+0)
0	4	0	8	5.098(+1)	9.782(+1)	3.394(−1)	5.258(+0)	3.229(+0)	3.391(−1)
0	6	0	8	6.696(+1)	9.813(+1)	1.409(+0)	4.284(+0)	2.759(+0)	1.370(+0)
1	0	1	2	1.109(+2)	1.217(+2)	3.697(+0)	7.594(+0)	7.098(+0)	3.445(+0)
1	0	1	4	1.109(+2)	1.419(+2)	1.081(+0)	7.594(+0)	4.447(+0)	1.010(+0)
1	0	1	6	1.109(+2)	1.647(+2)	2.047(+0)	7.594(+0)	4.472(−1)	2.257(−1)
1	2	1	4	1.231(+2)	1.423(+2)	2.321(+0)	6.166(+0)	4.250(+0)	2.371(+0)
1	2	1	6	1.231(+2)	1.644(+2)	1.362(−1)	6.166(+0)	3.989(−1)	1.253(−1)
1	4	1	6	1.440(+2)	1.638(+2)	6.420(−1)	2.993(+0)	3.105(−1)	5.752(−1)

Quantum numbers v_i and j_i are explained in the text. The numbers in parentheses denote powers of 10.

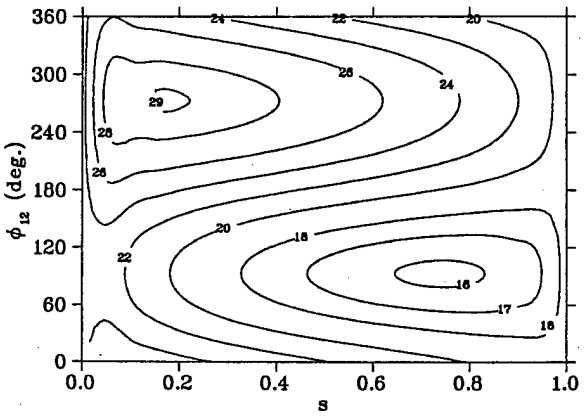

Fig. 2. The same as in Fig. 1 for scattering from an initial superposition state with $v_1 = 0$, $j_1 = 2$, $v_2 = 0$, $j_2 = 4$ at scattering energy $E = 0.93$ eV, including contributions from the uncontrolled satellite terms.

magnitude compared to the $v_i = 0$ case, due to the fact that at this energy the reactive cross-sections for $v_i = 1$ are much smaller than the non-reactive ones. The range of control quickly diminishes when higher values of j_i are involved or when $\Delta j > 2$. This can be understood by looking at Table 2 where the interference terms $\sigma(12)$ for $v_1 = v_2 = 1$ are tabulated and are seen to be much smaller than the diagonal $\sigma(nn)$ terms.

Consider next the $H + H'D$ reactions, calculated at total scattering energy of $E = 0.8$ eV, where H and H′ denote hydrogen atoms which are assumed distinguishable. In this case, we have two final reactive arrangement channels, $H' + HD(\alpha = b)$ and $D + HH'(\alpha = c)$. Our calculations show that control here is also attained mainly by choosing $\Delta v = 0$ and $\Delta j = 1, 2$. By contrast, control is practically non-existent for $\Delta v > 0$, or $\Delta j > 5$ or for $j_i > 8$. This behavior is consistent with Table 3 where we present the contributions of the diagonal and off-diagonal $\sigma(mn)$. We see that the $\sigma^R(12)$ terms are similar in magnitude to the corresponding diagonal terms for $\Delta j = 1$ or 2. This results in very extensive control (see Fig. 3). With increasing Δj, σ_{12}^R decreases, resulting, according to Eq. (29), in a smaller degree of control.

Looking specifically at scattering into the $H' + HD(\alpha = b)$ arrangement channel, our computations show that control is largest for superposition states composed of $v_1 = 0$, $j_1 = 2$, and $v_2 = 0$, $j_2 = 3$. The same holds true for the $v_1 = 0$, $j_1 = 2$, and $v_2 = 0$, $j_2 = 4$ superposition. σ^R/σ^{NR} for these cases, excluding the satellite contributions, are shown in Fig. 3(a) and (b), respectively. These figures display a very large range of control: The reactive to non-reactive ratio is seen to vary

Table 2
Integral cross-sections $\sigma^{NR,R}(mn)$ (in a_0^2), $m \leqslant n = 1, 2$, for $D + H_2$ collisions at $E = 0.93$ eV

v_1	j_1	v_2	j_2	$\sigma^{NR}(11)$	$\sigma^{NR}(22)$	$\sigma^{NR}(12)$	$\sigma^{R}(11)$	$\sigma^{R}(22)$	$\sigma^{R}(12)$
0	0	0	2	6.231(+1)	7.178(+1)	2.855(+0)	3.855(+0)	4.648(+0)	2.807(+0)
0	0	0	4	6.231(+1)	9.487(+1)	5.105(−1)	3.855(+0)	3.323(+0)	5.092(−1)
0	0	0	6	6.231(+1)	1.269(+2)	2.106(−1)	3.855(+0)	7.584(−1)	1.904(−1)
0	0	0	8	6.231(+1)	1.603(+2)	1.810(−2)	3.855(+0)	7.412(−3)	1.689(−2)
0	2	0	4	7.225(+1)	9.529(+1)	1.714(+0)	3.315(+0)	2.934(+0)	1.716(+0)
0	2	0	6	7.225(+1)	1.275(+2)	1.447(−1)	3.315(+0)	6.807(−1)	1.627(−1)
0	2	0	8	7.225(+1)	1.602(+2)	1.413(−2)	3.315(+0)	6.756(−3)	1.442(−2)
0	4	0	6	9.659(+1)	1.289(+2)	6.379(−1)	1.971(+0)	5.180(−1)	6.860(−1)
0	4	0	8	9.659(+1)	1.599(+2)	3.021(−2)	1.971(+0)	5.474(−3)	3.210(−2)
0	6	0	8	1.312(+2)	1.595(+2)	1.969(−2)	3.700(−1)	4.176(−3)	2.948(−2)
1	0	1	2	1.612(+2)	1.689(+2)	1.795(+0)	1.846(−1)	8.315(−2)	1.220(−1)
1	0	1	4	1.612(+2)	1.966(+2)	1.488(−2)	1.846(−1)	2.421(−5)	1.623(−3)
1	2	1	4	1.668(+2)	1.948(+2)	1.055(−1)	2.420(−2)	2.008(−5)	4.341(−4)

Table 3
Integral cross-sections $\sigma^{NR,R}(mn)$ (in c_1^2), $m \leqslant n = 1, 2$, for $H + H'D$ collisions at $E = 0.8$ eV[a]

j_1	j_2	$\alpha = 1$			$\alpha = 2$			$\alpha = 3$		
		$\sigma^{NR}(11)$	$\sigma^{NR}(22)$	$\sigma^{NR}(12)$	$\sigma^{R}(11)$	$\sigma^{R}(22)$	$\sigma^{R}(12)$	$\sigma^{R}(11)$	$\sigma^{R}(22)$	$\sigma^{R}(12)$
0	1	1.29(+2)	1.29(+2)	4.75(−1)	9.08(−1)	1.72(+0)	1.23(+0)	7.74(−1)	1.57(+0)	1.09(+0)
0	2	1.29(+2)	1.30(+2)	1.29(+0)	9.08(−1)	1.39(+0)	4.48(−1)	7.74(−1)	1.36(+0)	9.06(−1)
0	3	1.29(+2)	1.32(+2)	7.00(−2)	9.08(−1)	1.01(+0)	4.75(−1)	7.74(−1)	1.08(+0)	5.07(−1)
0	4	1.29(+2)	1.35(+2)	3.10(−1)	9.08(−1)	6.80(−1)	1.31(−1)	7.74(−1)	9.43(−1)	1.77(−1)
0	5	1.29(+2)	1.39(+2)	4.56(−2)	9.08(−1)	3.14(−1)	4.19(−2)	7.74(−1)	6.93(−1)	1.14(−1)
0	6	1.29(+2)	1.41(+2)	2.23(−1)	9.08(−1)	8.77(−2)	4.25(−2)	7.74(−1)	3.89(−1)	1.09(−1)
0	7	1.29(+2)	1.48(+2)	5.32(−2)	9.08(−1)	1.30(−2)	1.81(−2)	7.74(−1)	1.58(−1)	6.27(−2)
1	2	1.30(+2)	1.30(+2)	6.24(−1)	8.76(−1)	1.18(+0)	9.35(−1)	7.60(−1)	1.09(+0)	8.44(−1)
1	3	1.30(+2)	1.32(+2)	1.11(+0)	8.76(−1)	1.04(+0)	7.00(−1)	7.60(−1)	1.11(+0)	6.75(−1)
1	4	1.30(+2)	1.35(+2)	4.47(−2)	8.76(−1)	6.61(−1)	3.81(−1)	7.60(−1)	9.10(−1)	3.95(−1)
1	5	1.30(+2)	1.39(+2)	3.44(−1)	8.76(−1)	2.95(−1)	1.50(−1)	7.60(−1)	6.45(−1)	1.69(−1)
1	6	1.30(+2)	1.43(+2)	4.50(−2)	8.76(−1)	8.27(−2)	4.42(−2)	7.60(−1)	3.69(−1)	7.83(−2)
1	7	1.30(+2)	1.48(+2)	7.82(−2)	8.76(−1)	1.24(−2)	1.14(−2)	7.60(−1)	1.52(−1)	4.71(−2)
2	3	1.31(+2)	1.33(+2)	5.95(−1)	7.80(−1)	8.04(−1)	7.33(−1)	7.15(−1)	8.48(−1)	7.16(−1)
2	4	1.31(+2)	1.35(+2)	9.55(−1)	7.80(−1)	5.67(−1)	5.07(−1)	7.15(−1)	7.88(−1)	5.41(−1)
2	5	1.31(+2)	1.39(+2)	5.18(−2)	7.80(−1)	2.62(−1)	2.59(−1)	7.15(−1)	5.82(−1)	3.07(−1)
2	6	1.31(+2)	1.43(+2)	2.22(−1)	7.80(−1)	7.44(−2)	9.53(−2)	7.15(−1)	3.37(−1)	1.34(−1)
2	7	1.31(+2)	1.48(+2)	3.71(−2)	7.80(−1)	1.14(−2)	2.34(−2)	7.15(−1)	1.41(−1)	5.47(−2)
3	4	1.33(+2)	1.36(+2)	3.70(−1)	5.90(−1)	4.39(−1)	4.78(−1)	6.22(−1)	6.16(−1)	5.70(−1)
3	5	1.33(+2)	1.39(+2)	7.99(−1)	5.90(−1)	2.15(−1)	2.85(−1)	6.22(−1)	4.87(−1)	3.98(−1)
3	6	1.33(+2)	1.43(+2)	8.53(−2)	5.90(−1)	6.33(−2)	1.22(−1)	6.22(−1)	2.95(−1)	2.09(−1)
3	7	1.33(+2)	1.48(+2)	1.17(−1)	5.90(−1)	9.94(−3)	3.47(−2)	6.22(−1)	1.26(−1)	8.53(−2)
4	5	1.36(+2)	1.39(+2)	1.21(−1)	3.44(−1)	1.72(−1)	2.31(−1)	4.84(−1)	3.94(−1)	4.03(−1)
4	6	1.36(+2)	1.43(+2)	6.45(−1)	3.44(−1)	5.22(−2)	1.11(−1)	4.84(−1)	2.48(−1)	2.52(−1)
4	7	1.36(+2)	1.48(+2)	9.07(−2)	3.44(−1)	8.46(−3)	3.54(−2)	4.84(−1)	1.10(−1)	1.17(−1)
5	6	1.40(+2)	1.43(+2)	5.71(−1)	1.41(−1)	4.32(−2)	7.46(−2)	3.24(−1)	2.07(−1)	2.39(−1)
5	7	1.40(+2)	1.48(+2)	4.22(−1)	1.41(−1)	7.14(−3)	2.64(−2)	3.24(−1)	9.40(−2)	1.28(−1)
6	7	1.43(+2)	1.48(+2)	1.01(+0)	3.66(−2)	6.08(−3)	1.42(−2)	1.75(−1)	8.05(−2)	1.10(−1)

[a] Cross-sections for $\alpha = 2$ and $\alpha = 3$ correspond to the $H' + HD$ and $D + H_2$ final arrangements, respectively. Results for scattering from initial states with $v_i = 0$ only are shown.

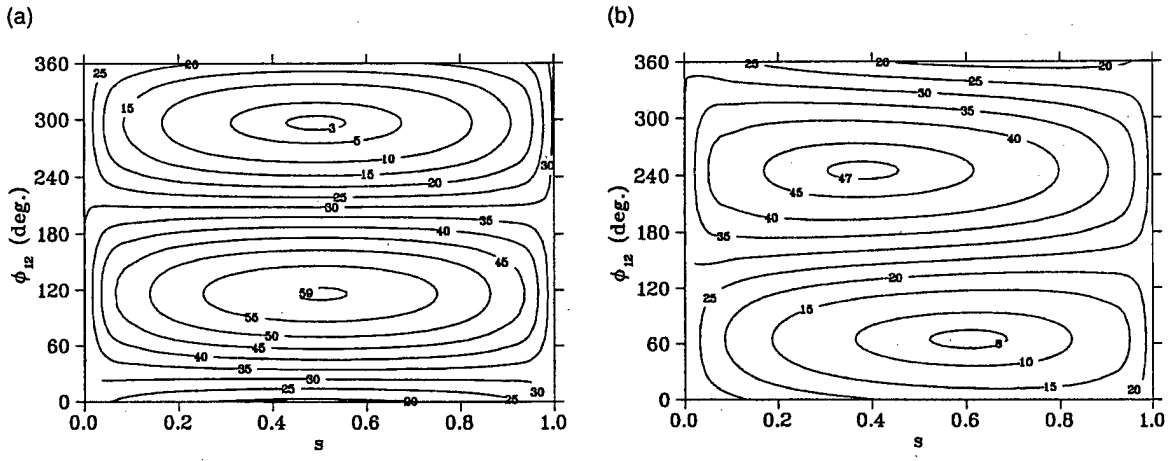

Fig. 3. Contour plot of the integral cross-sections ratio $\sigma^{R}/\sigma^{NR}(\times 10^3)$, obtained without accounting for satellite terms, for the H + H'D reaction at total scattering energy $E = 0.8$ eV as a function of ϕ_{12} and s, for a transition to the H' + HD final arrangement from an initial superposition state with (a) $v_1 = 0$, $j_1 = 2$, $v_2 = 0$, $j_2 = 3$, and (b) $v_1 = 0$, $j_1 = 2$, $v_2 = 0$, $j_2 = 4$.

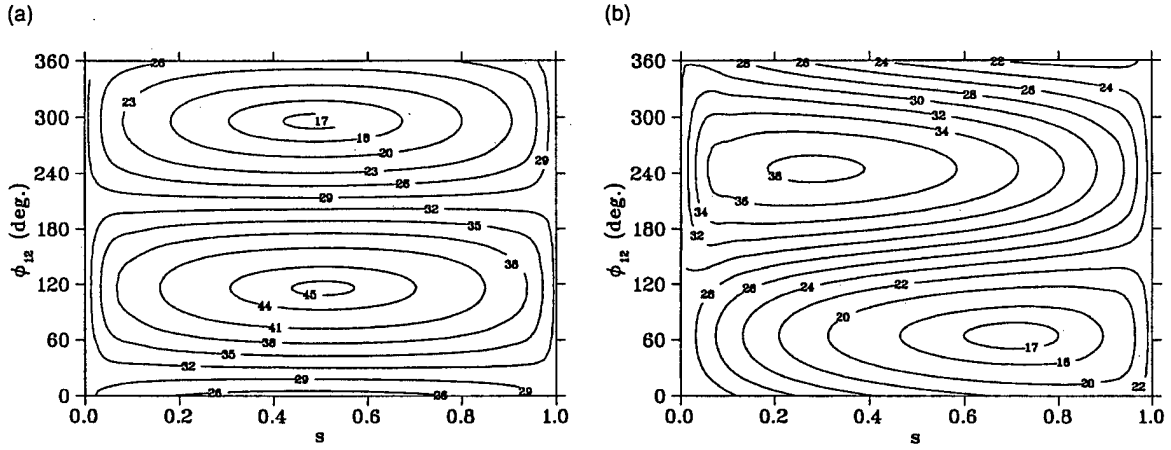

Fig. 4. The same as in Fig. 3 including the contribution from the uncontrolled satellite terms.

from 0.003 to 0.059 (a factor of 19.7) for the first case, and from 0.008 to 0.047 (a factor of 5.9) for the second case.

The results for the same superposition states obtained by taking into account the contributions from two uncontrolled satellite terms are presented in Fig. 4(a) and (b). Substantial control over σ^{R}/σ^{NR} ratio is clearly seen even in the presence of the satellite terms. One can also see that control is larger for the transition with $\Delta j = 1$ (see Fig. 4(a)). For example, by changing ϕ_{12} from 120° to 300° at $s = 0.51$, we can change σ^{R}/σ^{NR} for an initial superposition of the $v_1 = 0$, $j_1 = 2$, and $v_2 = 0$, $j_2 = 3$ states from 0.017 to 0.045, as compared with the "natural" ratio of 0.031.

Essentially the same level of control may be achieved by using a superposition of the $v_1 = 0$, $j_1 = 2$ and $v_2 = 0$, $j_2 = 4$ states (see Fig. 4(b)). In this case, the ICS ratio varies from 0.017 to 0.038. Here too we find that the range of control decreases with increasing Δj (see, e.g., Table 3), and that control is essentially non-existent for $\Delta v > 0$.

Finally, consider the D + HH' ($\alpha = c$) arrangement. In this case, the largest control is

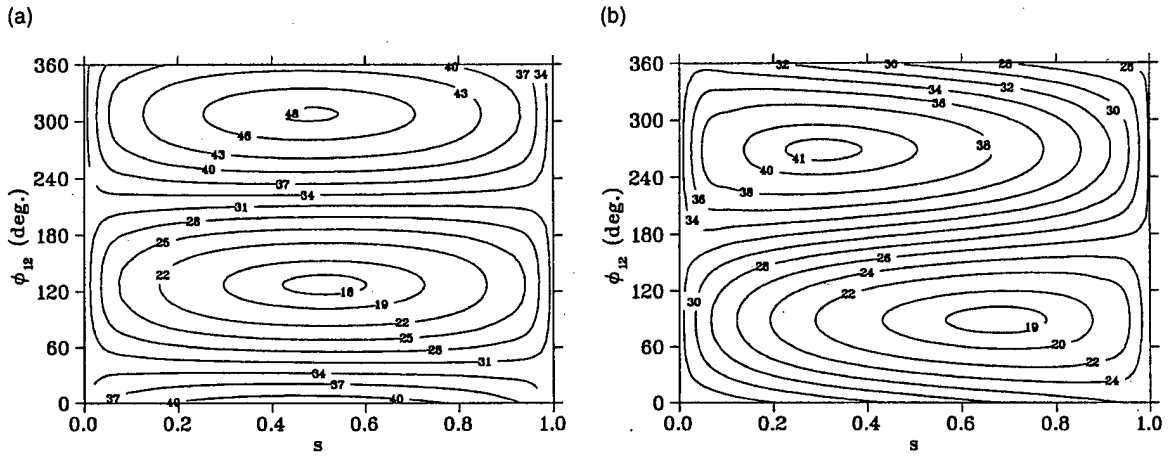

Fig. 5. Contour plot of the integral cross-sections ratio $\sigma^{R}/\sigma^{NR}(\times 10^3)$ (with uncontrolled satellite terms) for the H + H′D reaction at total scattering energy $E = 0.8$ eV as a function of ϕ_{12} and s, for a transition to the D + HH′ final arrangement from an initial superposition state with (a) $v_1 = 0$, $j_1 = 3$, $v_2 = 0$, $j_2 = 4$, and (b) $v_1 = 0$, $j_1 = 3$, $v_2 = 0$, $j_2 = 5$.

achieved by scattering from a superposition of the $v_1 = 0$, $j_1 = 3$ and $v_2 = 0$, $j_2 = 4$ states or the $v_1 = 0$, $j_1 = 3$ and $v_2 = 0$, $j_2 = 5$ states. A substantial range of control over reactive to non-reactive branching ratios in these two cases is displayed in Fig. 5(a) and (b), respectively. As shown in Fig. 5(a), the ICS ratio can be made to change from 0.018 to 0.048, compared with the "natural" ratio of 0.033. The results for the second case are similar.

4. Summary

In this work, we have demonstrated that it is possible to substantially control the reactive to non-reactive integral branching ratios by using a superposition of non-degenerate continuum states. The demonstration was carried out for realistic 3D reactive scattering models of the $D + H_2 \rightarrow DH + H$ and the $H + H'D \rightarrow HH' + D$; $HD + H'$ reactions. Control is due to both a constructive enhancement of reactive cross-sections and a destructive depletion of the non-reactive ones, or vice versa.

Kinematic laboratory constraints pertaining to bimolecular control lead to uncontrolled satellite terms. Nevertheless, even in the presence of these uncontrolled terms, extensive control over total cross-sections has been demonstrated, making the laboratory confirmation of our present predictions a realistic possibility.

Acknowledgements

This work was supported in part by the US Office of Naval Research, Photonics Research Ontario and by a grant of HPC time on the CRAY T90 and SV1 from the DoD NAVOCEANO MSRC Center.

References

[1] M. Shapiro, P. Brumer, Trans. Far. Soc. 93 (1997) 1263.
[2] P. Brumer, M. Shapiro, Annu. Rev. Phys. Chem. 43 (1992) 257.
[3] A. Shnitman, I. Sofer, I. Golub, A. Yogev, M. Shapiro, Z. Chen, P. Brumer, Phys. Rev. Lett. 76 (1996) 2886.
[4] C. Asaro, M. Shapiro, P. Brumer, Phys. Rev. Lett. 60 (1988) 1634.
[5] M. Shapiro, J.W. Hepburn, P. Brumer, Chem. Phys. Lett. 149 (1988) 451.
[6] C. Chen, Y.-Y. Yin, D.S. Elliott, Phys. Rev. Lett. 64 (1990) 507.
[7] C. Chen, Y.-Y. Yin, D.S. Elliott, Phys. Rev. Lett. 65 (1990) 1737.
[8] S.M. Park, S.-P. Lu, R.J. Gordon, J. Chem. Phys. 94 (1991) 8622.
[9] B.A. Baranova, A.N. Chudinov, B.Ya. Zel'dovitch, Opt. Commun. 79 (1990) 116.

[10] V.D. Kleiman, L. Zhu, X. Li, R.G. Gordon, J. Chem. Phys. 102 (1995) 5863.
[11] B. Kohler, J.L. Krause, F. Raski, K.R. Wilson, V.V. Yakovlev, R.M. Whitnell, Y. Yan, Acct. Chem. Res. 28 (1995) 133.
[12] W.S. Warren, H. Rabitz, M. Dahleh, Science 259 (1993) 1581.
[13] S.A. Rice, Science 258 (1992) 412.
[14] B. Sheehy, B. Walker, L.F. DiMauro, Phys. Rev. Lett. 74 (1995) 4799.
[15] E. Dupont, P.B. Corkum, H.C. Liu, M. Buchanan, Z.R. Wasilewski, Phys. Rev. Lett. 74 (1995) 3596.
[16] M. Shapiro, Y. Zeiri, J. Chem. Phys. 85 (1986) 6449.
[17] T. Seideman, M. Shapiro, J. Chem. Phys. 88 (1988) 5525.
[18] T. Seideman, J.L. Krause, M. Shapiro, Faraday Disc. Chem. Soc. 91 (1991) 271.
[19] J.L. Krause, M. Shapiro, P. Brumer, J. Chem. Phys. 92 (1990) 1126.
[20] M. Shapiro, P. Brumer, Phys. Rev. Lett. 77 (1996) 2574.
[21] D. Holmes, M. Shapiro, P. Brumer, J. Chem. Phys. 105 (1996) 9162.
[22] A. Abrashkevich, M. Shapiro, P. Brumer, Faraday Discuss. 113 (1999) 291.
[23] A. Abrashkevich, M. Shapiro, P. Brumer, Phys. Rev. Lett. 81 (1998) 3789.
[24] A. Abrashkevich, M. Shapiro, P. Brumer, Phys. Rev. Lett. 82 (1999) 3002.
[25] J.R. Taylor, Scattering Theory, Wiley, New York, 1972.
[26] W.H. Miller, J. Chem. Phys. 50 (1969) 407.
[27] G.C. Schatz, A. Kuppermann, J. Chem. Phys. 65 (1976) 4642.
[28] R.T. Pack, G.A. Parker, J. Chem. Phys. 87 (1987) 3888.
[29] J.Z.H. Zhang, W.H. Miller, J. Chem. Phys. 91 (1989) 1528.
[30] P. Siegbahn, B. Liu, J. Chem. Phys. 68 (1978) 2457.
[31] D.G. Truhlar, C.J. Horowitz, J. Chem. Phys. 68 (1978) 2466.
[32] D.G. Truhlar, C.J. Horowitz, J. Chem. Phys. 71 (1979) 1514.
[33] D.E. Manolopoulos, M. D'Mello, R.E. Wyatt, J. Chem. Phys. 93 (1990) 403.
[34] D.E. Manolopoulos, R.E. Wyatt, Chem. Phys. Lett. 152 (1988) 23.

13

Multiarrangement photodissociation calculations utilizing negative imaginary potentials

Dmitri G. Abrashkevich and Paul Brumer
Chemical Physics Theory Group, Department of Chemistry and Photonics Research Ontario, University of Toronto, Toronto M5S 3H6, Canada

Moshe Shapiro
Chemical Physics Department, The Weizmann Institute of Science, Rehovot 76100, Israel

(Received 6 July 2000; accepted 10 October 2000)

A new method for calculating total and partial cross sections for photodissociation processes which produce more than one chemical product is presented. By using negative imaginary absorbing potentials, the method reduces the multiarrangement problem to a set of single-arrangement problems. In this way, the state-to-state photodissociation transition amplitudes are calculated directly using the artificial channel method coupled to an efficient log–derivative propagator. In addition, the discrete position operator representation is used to significantly simplify the calculations of the potential matrix elements. The method is shown to provide accurate cross sections for the resonant photodissociation of a model CO_2 system. © *2001 American Institute of Physics.* [DOI: 10.1063/1.1329642]

I. INTRODUCTION

Branching, or multiarrangement, photodissociation, leading to a number of chemically distinct products, is the subject of many theoretical and experimental studies. Recently, interest has turned to controlling the ratio of products of such a photodissociation process. This goal can be achieved using quantum interference phenomena, via the methods of coherent and optimal control.[1–8]

Continued progress towards this goal demands the development of effective theoretical tools for treating multiarrangement photodissociation reactions. Multiarrangement photodissociation is in essence a reactive scattering process which occurs on an excited potential surface, accessed from a bound state of the ground electronic state. As such, it is subject to many of the computational difficulties associated with multiarrangement problems, the main one being the need to simultaneously solve the Schrödinger equation in all the product arrangements. This heavy computational burden grows roughly as the third power of the number of arrangements. In spite of these difficulties, significant progress has been made in the past few decades via the development of efficient theoretical methods for treating the multiarrangement reactive scattering problem. In particular, various collinear[9] and three-dimensional[10] reactive scattering systems have been treated using both the time-dependent and time-independent versions of the negative imaginary absorbing potential (NIAP) method. In this article we make use of this approach to develop a method of computing photodissociation amplitudes for multiarrangement photodissociation problems.

The negative imaginary potential approach is of special interest since it enables one to convert a multiarrangement problem in real arithmetic into a set of (complex arithmetic) single-arrangement problems. In this way the numerical effort grows, in principle, linearly with the number of product arrangements, a significant reduction by comparison with the third power law noted above. However, this reduction in computational effort is usually accompanied by a loss of information. In particular, in the NIAP approach to reactive scattering one introduces absorbing potentials in order to capture all the flux entering the products' region. The negative imaginary potential is introduced at the entrance to the products' configuration subspace, while not affecting the wave function in the reactants subspace.[9] When this is achieved, the resulting nonunitarity in the S-matrix of the reactants subspace reflects exactly the flux arriving at the products' channels. In this way the (reactants)-state-to-all-(products)-states reactive *flux* can be estimated.

In this study we show how in the context of the artificial channel method (ACM)[11] it is possible to use the NIAP method to calculate *state-to-state* photodissociation amplitudes. NIAP method allows the direct calculation of the detailed state-to-state *amplitudes*[12] because in photodissociation the initial state is a bound state of the combined system which belongs to neither products. With the NIAP method, it is therefore possible to separately calculate transitions from the initial state to any of the final states of any chemical product.

Photodissociation calculations necessitate the calculation of dipole matrix elements from an initial bound state to a final scattering state describing the reactive scattering process. This task can be done very efficiently using the ACM,[11] which allows for the direct evaluation of the state-to-state transition amplitudes, without the explicit generation of the bound or the continuum wave functions. The ACM has been used extensively in the past and shown to be highly accurate for single arrangement photodissociation calculations.[13] It is therefore eminently suitable, as shown below, for applications of the NIAP method.

Additional features of the methodology introduced here

 © 2001 American Institute of Physics

Downloaded 03 Oct 2001 to 142.150.224.5. Redistribution subject to AIP license or copyright, see http://ojps.aip.org/jcpo/jcpcr.jsp

$$\left[\left(-\frac{\hbar^2}{2\mu}\frac{d^2}{dR^2}-E\right)\mathsf{I}+\boldsymbol{\epsilon}^s+\mathsf{V}^s\right]\mathsf{F}^{(s)}(R)=0, \tag{9}$$

where $\mathsf{F}^{(s)}$ is the matrix of solutions and I is the unity matrix, both of dimension $N_s\times N_s$. The matrices $\boldsymbol{\epsilon}^s$ and V^s are defined as

$$\epsilon^s_{n,m}=\epsilon^s_n\delta_{n,m} \tag{10}$$

and

$$V^s_{n,m}(R)=\int dr\,\phi^{*s}_n(r)V^s(R,r)\phi^s_m(r). \tag{11}$$

Here $V^s(R,r)$ is the interaction potential defined as

$$V^s(R,r)=W_s(R,r)-v_s(r). \tag{12}$$

We now reduce these equations to a set of single arrangement equations. To do so, we modify $V^s(R,r)$ by placing short-range NIAPs, $U_I(R,r)$, well into the entrance region of all the products, save for the product of interest. A perfectly absorbing potential, if placed sufficiently far into the products region, will not significantly affect the wave function in the region of the product of interest. When the "perfect absorbance" condition is met, the photodissociation amplitude to the product of interest will include the loss of flux due to transitions to all other products. By repeating the calculations for different products of interest we can thus extract all the state-to-state photodissociation amplitudes.

Various forms of absorbing potential can be used. The convenient form adopted here is the linear ramp:[10]

$$U_I(R,r)=\begin{cases}-iU_{I0}\dfrac{r-r_{1I}}{r_{2I}-r_{1I}}, & r_{1I}\leqslant r\leqslant r_{2I},\\ 0, \quad \text{otherwise},\end{cases} \tag{13}$$

where $0\leqslant R\leqslant\infty$. The constant U_{I0} must fulfill the following two conditions:[10]

$$\hbar E_t^{1/2}/(\Delta r_I\sqrt{8\mu})\ll U_{I0}\ll\Delta r_I\sqrt{8\mu}E_t^{3/2}/\hbar, \tag{14}$$

where, E_t is the translational energy in the product of interest arrangement, μ is the reduced mass in that arrangement, and $\Delta r_I=r_{2I}-r_{1I}$. The left-hand inequality [Eq. (14)] guarantees that all the flux entering into this potential region is absorbed, and the right-hand one guarantees that there is no reflection off the imaginary potential.

The V^e matrix [Eq. (11)] is now replaced by a matrix, denoted $\tilde{\mathsf{V}}^e$, derived from the

$$\tilde{V}^e(R,r)=W_e(R,r)+U_I(R,r)-v_e(r) \tag{15}$$

potential.

With $\tilde{\mathsf{V}}^e$ matrix replacing V^e, we now utilize Eq. (9) to obtain the photodissociation amplitudes. To do so we utilize the ACM, wherein one solves a combined set of coupled-channels equations for the bound and continuum manifolds.[11] To account for the different boundary conditions of the bound and continuum parts, one introduced an additional "artificial" channel (identified by subscripts a), serving as a source term for the bound manifold. The resultant set of equations can be written as

$$\left(-\frac{\hbar^2}{2\mu}\frac{d^2}{dR^2}+\epsilon^e_n-E\right)F^{(f)}_n(R)+\sum_{n'}\tilde{V}^e_{n,n'}(R)F^{(f)}_{n'}(R)$$
$$=-\sum_{m'}d_{n,m'}(R)F^{(i)}_{m'}(R), \tag{16}$$

$$\left(-\frac{\hbar^2}{2\mu}\frac{d^2}{dR^2}+\epsilon^g_m-E\right)F^{(i)}_m(R)+\sum_{m'}V^g_{m,m'}(R)F^{(i)}_{m'}(R)$$
$$=-V^a_m(R)F_a(R), \tag{17}$$

$$\left(-\frac{\hbar^2}{2\mu}\frac{d^2}{dR^2}-E+\epsilon_a+V_a(R)\right)F_a(R)=0, \tag{18}$$

where the dipole matrix, $d_{m,n}(R)$, is given by

$$d_{m,n}=\int dr\,\phi^{*e}_m(r)d_{e,g}\phi^g_n(r). \tag{19}$$

Equation (16) describes a continuum manifold, coupled to a bound manifold of Eq. (17) which, in turn, is coupled to the artificial channel introduced in Eq. (18). The artificial channel, serving as a source term, is governed by the ϵ_a asymptotic energy, the V_a potential, and the choice of V^a_n coupling potentials. The $\tilde{V}^e_{n,m}(R)$ and $V^g_{n,m}(R)$ matrices are given by matrix elements of Eqs. (12) and (15). In the Franck–Condon approximation used here, these matrix elements are given as

$$d_{m,n}=\bar{d}_{e,g}\int dr\,\phi^{*e}_m(r)\phi^g_n(r). \tag{20}$$

Although the combined set of equations is now somewhat larger than the separate set of scattering equations of Eq. (9), the difference is not too large because the number of additional equations due to the bound part is usually small. This is more than compensated for by obviating the need to calculate wave functions.

Equations (16)–(18) can be written in a more compact form using matrix notation

$$\left\{\left(-\frac{\hbar^2}{2\mu}\frac{d^2}{dR^2}+\boldsymbol{\epsilon}-E\right)\mathsf{I}+\mathsf{V}(R)\right\}\mathsf{F}(R)=0, \tag{21}$$

where the potential matrix is of the form

$$\mathsf{V}(R)=\begin{pmatrix}V_a(R) & \mathbf{O}^\dagger & \mathbf{O}^\dagger\\ \mathbf{O} & \tilde{\mathsf{V}}^e(R) & d_{e,g}(R)\\ \mathbf{V}^a(R) & \mathsf{O} & \mathbf{V}^g(R)\end{pmatrix}, \tag{22}$$

with $\boldsymbol{\epsilon}$ given by

$$\boldsymbol{\epsilon}=\begin{pmatrix}\epsilon_a & \mathbf{O}^\dagger & \mathbf{O}^\dagger\\ \mathbf{O} & \boldsymbol{\epsilon}^e & \mathsf{O}\\ \mathbf{O} & \mathsf{O} & \boldsymbol{\epsilon}^g\end{pmatrix}. \tag{23}$$

Here, A represents a rectangular matrix, $\mathbf{A}$ represents a column vector, and the † symbol denotes the Hermitian adjoint (the complex-conjugate transpose).

The S-matrix derived from Eq. (21) can be obtained using a variety of multichannel propagation schemes.[25] Of greatest interest to us are the elements of the S-matrix which

Downloaded 03 Oct 2001 to 142.150.224.5. Redistribution subject to AIP license or copyright, see http://ojps.aip.org/jcpo/jcpcr.jsp

connect the artificial channel to the continuum subspace. These matrix elements can be written, using standard expressions, as

$$S_{f,a}(E)=2\pi i\langle \mathbf{F}^{-(f)}|\cdot \mathbf{d}_{e,g}\cdot|\mathbf{F}^{+(a)}(E)\rangle. \tag{24}$$

Here, an $|\mathbf{A}\rangle$ symbol represents a column of ket vectors and an $\langle\mathbf{A}|$ symbol represents a row of bra vectors. The $\pm(j)$ superscript represents a scattering solution with an incoming/outgoing flux in the jth channel.

It can be shown[11,14] that with the special nonsymmetric form of Eq. (21) the above matrix elements become

$$S_{f,a}(E)=2\pi i \times\sum_i \frac{\langle \mathbf{F}^{-(f)}|\cdot \mathbf{d}_{e,g}\cdot|\mathbf{F}^{(i)}\rangle\langle\mathbf{F}^{(i)}|\cdot\mathbf{V}^a|F_a^{+(a)}(E)\rangle}{E-E_i}. \tag{25}$$

It follows from Eq. (25) that all the elements belonging to the $S_{f,a}$ column have poles at E_i, the bound state energies of the system, and that the residues of these poles are directly related to the desired photodissociation amplitudes of Eq. (6),

$$A_{f,i}(E)=\langle \mathbf{F}^{-(f)}|\cdot \mathbf{d}_{e,g}\cdot|\mathbf{F}^{(i)}\rangle=\frac{1}{2\pi i}\mathrm{Res}_i\left\{\frac{S_{f,a}(E)}{a_i(E)}\right\}, \tag{26}$$

where Res_i is the ith residue, and

$$a_i(E)=\langle\mathbf{F}^{(i)}|\cdot\mathbf{V}^a|F_a^{+(a)}(E)\rangle. \tag{27}$$

The pole energies E_i and the a_i coefficients are calculated separately by replacing all the channels belonging to the excited electronic state by a single additional artificial channel a'. Channel a' is identical in form to channel a, namely we choose $\epsilon_{a'}=\epsilon_a$, $\mathbf{V}^{a'}=\mathbf{V}^{a\dagger}$, and $V_{a'}=V_a$. The $S_{a',a}$ matrix element resulting from this truncated set of equations, which is identical in structure to Eq. (21), is of the form

$$S_{a',a}(E)=2\pi i\sum_i \frac{\langle F_{a'}^{-(a')}(E)|\mathbf{V}^{a'}\cdot|\mathbf{F}^{(i)}\rangle\langle\mathbf{F}^{(i)}|\cdot\mathbf{V}^a|F_a^{+(a)}(E)\rangle}{E-E_i}=2\pi i\exp(2i\delta_a)\sum_i |a_i(E)|^2/(E-E_i). \tag{28}$$

Hence $|a_i(E_i)|^2$ are obtained as

$$|a_i(E_i)|^2=\left|\frac{1}{2\pi}\mathrm{Res}_i S_{a',a}(E)\right|, \tag{29}$$

and E_i are obtained as the corresponding poles positions. These poles can be located very efficiently[26] using only a few iterations (see Appendix A of Ref. 26).

Once $a_i(E_i)$ and E_i are known, the desired bound-free matrix elements are computed directly from Eq. (25). A simple shift of $E-E_i$ in the definition of the ϵ_a asymptotic energy guarantees that it suffices to solve Eq. (29) only once, i.e., that the value of $a_i(E_i)$ may be used for all energies.[11]

The above procedure guarantees[11] that the results for the final bound-free matrix elements are insensitive to the exact form of $V_a(R)$ and $V_n^a(R)$. The only limitation on the choice of $V_a(R)$ and $V_n^a(R)$ is imposed by the requirement that the artificial wave function F^a overlaps well with the bound wave functions. In the present application we have chosen V_a to be of the form, $V_a(R)=V_0\exp(-aR)$, with the value of a fixed so as to guarantee a good overlap with the bound manifold.

The calculations are then repeated in a similar fashion for each of the products of interest by placing the negative imaginary potential at the entrance to other products.

The numerical method used by us to solve Eq. (21) and to obtain the $S_{f,a}(E)$ matrix elements is the log–derivative propagation method.[25] The method converges rapidly and eliminates instability problems which can arise when the integration is started deep inside the classically forbidden region.[25,27]

In addition, in order to speed up the computations we have used the DPOR[15] to calculate the potential matrix elements. According to this method, the matrix elements $V_{n,m}(R)$ are calculated using a quadrature of the form

$$V^g_{m,m'}(R)=\sum_{j=1}^{N_g} C^g_{m,j}V^g(R,r^g_j)C^g_{m',j}, \quad m,m'=1,\ldots,N_g,$$
$$\tilde{V}^e_{n,n'}(R)=\sum_{j=1}^{N_e} C^e_{n,j}\tilde{V}^e(R,r^e_j)C^e_{n',j}, \quad n,n'=1,\ldots,N_e, \tag{30}$$

where $C^s_{n,i}$, $s=g,e$, are the eigenvectors, r^s_j being the eigenvalues, of the position operator matrix, r,

$$\mathsf{r}^{(s)}_{n,m}=\int_{-\infty}^{\infty} dr\,\phi^{*s}_n(r)r\phi^s_m(r), \quad s=g,e. \tag{31}$$

If the basis is complete, $C^s_{n,i}$ also diagonalizes the potential matrix $\mathsf{V}(R,r)$, since the potential matrix can be written[15] as a function of the r matrix, $V(R,\mathsf{r})$. This is the justification for Eqs. (30). With the points and weights chosen in this way, even a small number of quadrature points can give highly accurate evaluation of the potential matrix.[15]

III. THE $CO_2\rightarrow CO+O$ PHOTODISSOCIATION

To test the utility and efficiency of this method we have examined the photodissociation of the well-studied[19,20,22–24] case of collinear CO_2 photodissociation, where the photodissociation branches to two identical products,

$$OC+O\leftarrow OCO\rightarrow CO+O.$$

Downloaded 03 Oct 2001 to 142.150.224.5. Redistribution subject to AIP license or copyright, see http://ojps.aip.org/jcpo/jcpcr.jsp

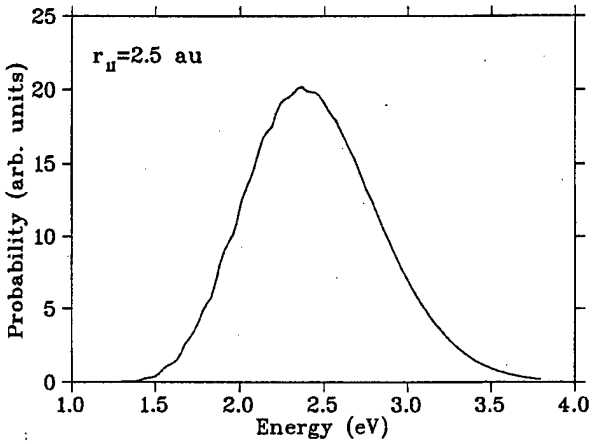

FIG. 1. The CO_2 absorption spectrum with $r_{1I}=2.5$ a.u.

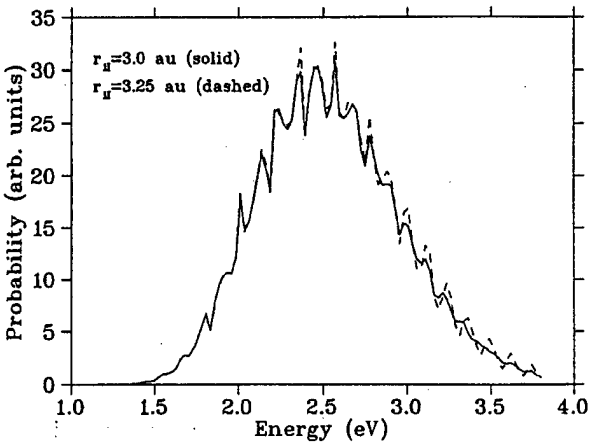

FIG. 2. The CO_2 absorption spectra obtained with $r_{1I}=3.0$ a.u. (solid line) and $r_{1I}=3.25$ a.u. (dashed line).

At the vacuum ultraviolet (VUV) photon energies of interest, the absorption spectrum consists of a sequence of resonances superimposed on a smooth continuum. From a semiclassical perspective, these structures reflect to underlying unstable periodic orbits on the excited electronic surface.[28] The large background is due to the dominant direct dissociation. We compute photodissociation into one product channel, the total photodissociation probability being twice that obtained for one channel.

In this case the $W_e(R,r)$ [Eq. (4)] is given by the Kulander–Light LEPS potential surface,[19] a surface which has a saddle point at $r_{CO}=2.41$ a.u., which is somewhat displaced from the ground state equilibrium position of 2.2 a.u. The ground state surface was composed of Morse functions in both bond-stretching coordinates r_{CO} and r_{OC}:[29,30]

$$W_g(R,r)\equiv W_g(r_{CO},r_{OC}) = v^{\text{Morse}}(r_{CO})+v^{\text{Morse}}(r_{OC}). \tag{32}$$

Here,

$$v^{\text{Morse}}(r)=D_e\{\exp[-2\alpha(r-r_{CO}^e)] - 2\exp[-\alpha(r-r_{CO}^e)]\}, \tag{33}$$

where $\alpha=1.641a_0^{-1}$, $D_e=5.453$ eV, and $r_{CO}^e=2.2a_0$. In this case, parameters of the Morse function were fitted to the equilibrium distances and force constants for the ground PES taken from the harmonic potential of Kulander *et al.*[22] The relevant reduced masses chosen are defined as, $\mu=m_Om_{CO}/(m_C+2m_O)$ and $m=m_Cm_O/(m_C+m_O)$.

We consider the transition from the ground vibrational state of CO_2 to energies ranging from 1.4 to 3.7 eV above the CO+O dissociation threshold. The eigenfunctions $\{\phi_n^s(r)\}$ of the Eq. (7) with $v(r)=\lim_{R\to\infty}W_e^{\text{LEPS}}(R,r)$ were used as a basis for both the initial and final CO_2 states. The vibrational eigenenergies and the corresponding eigenfunctions of the product diatomic potentials were obtained via the renormalized Numerov method[31] and a Simpson-type quadrature was used to obtain the Franck–Condon transition matrix [Eq. (20)]. The potential parameters U_{I0} and $\Delta r=(r_{2I}-r_{1I})$ were chosen to satisfy the inequalities, Eq. (14), that guarantee no reflected flux from the $r>r_{1I}$ region. Note that the conditions in Eq. (14) must be satisfied for all translational energies at given dissociation energy E. Note also that with increasing dissociation energy E the number of open channels increases as well and more basis wave functions have to be included in the expansion of Eq. (5) in order to achieve convergence.

The specific choice of r_{1I} was found to be quite important to the quality of the results. It was obtained by starting close to the reaction region, and *gradually* increasing r_{1I} until further *small* incremental increases did not influence the results. Sample results are shown in Figs. 1–3 for $\Delta r_I=2$ a.u., $U_{I0}=0.05$ a.u., and the fixed number of channels [Eq. (5)] $N_e=80$. When r_{1I} is too small ($r_{1I}=2.5$ a.u., shown in Fig. 1) the structure atop the broad background is almost absent. In this case the absorbing boundary interferes with the oscillatory wave packet motion that produces the diffuse structure, so that the peaks are suppressed. As r_{1I} is increased the spectra begin to display the proper diffuse vibrational structure. For example, the results for $r_{1I}=3.0$ a.u. (solid line) and $r_{1I}=3.25$ a.u. (dashed line) are presented in Fig. 2 and show the convergence of the spectra. (Note, however, that complete convergence for the chosen number of channels is still not achieved for the dissociation

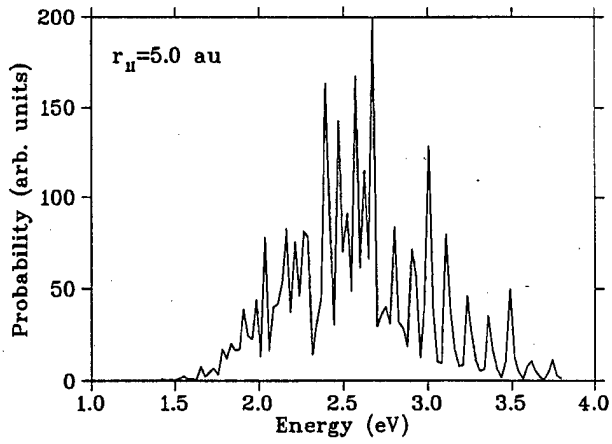

FIG. 3. The CO_2 absorption spectrum as obtained with $r_{1I}=5.0$ a.u.

Downloaded 03 Oct 2001 to 142.150.224.5. Redistribution subject to AIP license or copyright, see http://ojps.aip.org/jcpo/jcpcr.jsp

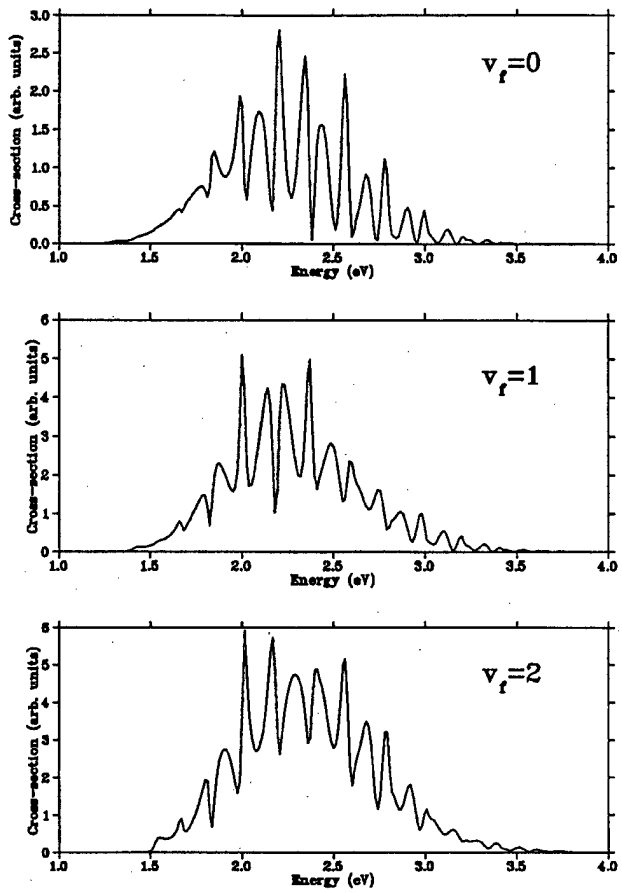

FIG. 4. Partial photodissociation probabilities excitation to the first three final vibrational quantum numbers of the CO fragment. Excitation is from the ground state of CO_2.

energies above 3 eV. In this case one would need larger values of N_e for convergence, since more channels become open as the dissociation energy increases.)

Finally, when the absorbing potential is too far from the reaction region (as Fig. 3 for $r_{1/}=5$ a.u.), we obtain nonconverged results for the number of channels used. In this case, substantially more channels would be required for convergence. Thus, choosing $r_{1/}$ too large ($r_{1/}>4.9$ a.u.) results in a poor representation of the diffuse background, whereas choosing $r_{1/}$ too small ($r_{1/}<3.0$ a.u.) led to poor results for the vibrational structure.

Considerations of this kind led to the best parameter choice of $r_{1/}=3.0$ a.u., $\Delta r_I=2$ a.u., and $U_{I0}=0.05$ a.u. For each $r_{1/}$, full convergence with respect to the number of vibrational states N_e in the basis for the excited state was reached for $E<3$ eV. The final results of our calculations of the resonant CO_2 spectrum are given by the solid line in Fig. 2. The spectrum obtained displays the series of irregular peaks, peaking at 2.36 eV, in good agreement with the results of Kulander and Light,[19] with small differences being a result of the extreme sensitivity of the results to the ground state potential.[21,23] The vibrationally resolved partial probabilities into the first three final vibrational quantum numbers ($v_f=0,1,2$) are presented in Fig. 4. Our results show that partial cross sections display the similar diffuse resonant structure as the total probabilities, and are in good agreement with previous results.[19,23]

IV. CONCLUSIONS

In this article we have introduced a new fully quantum-mechanical method of calculating photodissociation cross sections for triatomic molecules with more than one product arrangement. A short range imaginary absorbing potential has been added to the Hamiltonian operator, reducing a multiarrangement photodissociation problem to a set of single arrangement photodissociation problems. The resulting single-arrangement photodissociation is solved with the artificial channel method, utilizing an efficient log–derivative propagator. The method has been successfully applied to the photodissociation of collinear CO_2 and the diffuse vibrational structure of the CO_2 photoabsorption spectrum has been successfully reproduced in good agreement with the previous results.

This study can be readily generalized to the full three-dimensional problem. Work to that end is in progress. Applications of this method to the coherent control of collinear CH_2IBr photodissociation are the subject of a forthcoming article.[32]

ACKNOWLEDGMENT

We thank the U.S. Office of Naval Research and Photonics Research Ontario for the funding of this research.

[1] M. Shapiro and P. Brumer, Adv. At., Mol., Opt. Phys. **42**, 287 (2000); J. Chem. Soc., Faraday Trans. **93**, 1263 (1997); P. Brumer and M. Shapiro, Acc. Chem. Res. **22**, 407 (1989).
[2] S. A. Rice and M. Zhao, *Optical Control of Molecular Dynamics* (Wiley, New York, in press).
[3] W. S. Warren, H. Rabitz, and M. Dahleh, Science **259**, 1581 (1993).
[4] B. Kohler, J. L. Krause, F. Raski, K. R. Wilson, V. V. Yakovler, R. M. Whitnell, and Y. Yan, Acc. Chem. Res. **28**, 133 (1995).
[5] I. Zhu, V. Kleiman, X. Li, S.-P. Liu, K. Trentelman, and R. J. Gordon, Science **270**, 77 (1995).
[6] E. Dupont, P. B. Corkum, H. C. Liu, M. Buchanan, and Z. R. Wasilewski, Phys. Rev. Lett. **74**, 3596 (1995).
[7] A. Shnitman, I. Sofer, I. Golub, A. Yogev, M. Shapiro, Z. Chen, and P. Brumer, Phys. Rev. Lett. **76**, 2886 (1996).
[8] T. Assion, T. Baumert, M. Bergt, T. Brixner, B. Kiefer, U. Seyfried, M. Strehle, and G. Gerber, Science **282**, 919 (1998).
[9] D. Neuhauser and M. Baer, J. Phys. Chem. **90**, 4351 (1989); **91**, 4651 (1989).
[10] D. Neuhauser, R. S. Judson, R. E. Jaffe, M. Baer, and D. J. Kouri, Chem. Phys. Lett. **176**, 546 (1991).
[11] M. Shapiro, J. Chem. Phys. **56**, 2582 (1972).
[12] For NIAP calculations of state to state reactive transition probabilities see D. Neuhauser, J. Chem. Phys. **93**, 7836 (1990); D. Neuhauser, R. S. Judson, D. J. Kouri, and D. E. Adelman, Science **257**, 519 (1992); H. Szichman, M. Baer, and H. Nakamura, J. Chem. Phys. **107**, 3521 (1997).
[13] M. Shapiro, Chem. Phys. Lett. **46**, 442 (1977); E. Segev and M. Shapiro, J. Chem. Phys. **73**, 2001 (1980); **77**, 5604 (1982); S. Kanfer and M. Shapiro, J. Phys. B **16**, L655 (1983); I. Levy and M. Shapiro, J. Chem. Phys. **89**, 2900 (1988); M. Shapiro, M. J. J. Vrakking, and A. Stolow, *ibid.* **110**, 2465 (1999).
[14] M. Shapiro and R. Bersohn, Annu. Rev. Phys. Chem. **33**, 409 (1982); G. G. Balint-Kurti and M. Shapiro, Adv. Chem. Phys. **60**, 403 (1985).
[15] S. Kanfer and M. Shapiro, J. Phys. Chem. **88**, 3964 (1984).
[16] R. W. Heather and J. C. Light, J. Chem. Phys. **79**, 147 (1983).
[17] See, for example, K. C. Kulander, Phys. Rev. A **35**, 445 (1987); G. Ashkenazi, U. Banin, A. Bartana, R. Kosloff, and S. Ruhman, Adv. Chem. Phys. **100**, 229 (1997), and references therein; G. G. Balint-Kurti, R. N. Dixon, and C. C. Marston, Int. Rev. Phys. Chem. **11**, 317 (1992); H.

Downloaded 03 Oct 2001 to 142.150.224.5. Redistribution subject to AIP license or copyright, see http://ojps.aip.org/jcpo/jcpcr.jsp

Flöthmann, C. Beck, R. Schinke, C. Woywod, and W. Domcke, J. Chem. Phys. **107**, 7296 (1997).
[18] M. Shapiro, J. Phys. Chem. **97**, 7396 (1993); M. Shapiro, Z. Chen, and P. Brumer, Chem. Phys. **217**, 325 (1997).
[19] K. C. Kulander and J. C. Light, J. Chem. Phys. **73**, 4337 (1980).
[20] J. P. Henshaw and D. C. Clary, J. Phys. Chem. **91**, 1580 (1987).
[21] R. Schinke and V. Engel, Chem. Phys. Lett. **124**, 504 (1986).
[22] K. C. Kulander, C. Cerjan, and A. E. Orel, J. Chem. Phys. **94**, 2571 (1991).
[23] R. Schinke and V. Engel, J. Chem. Phys. **93**, 3252 (1990).
[24] R. Sadeghi and R. T. Skodje, J. Chem. Phys. **105**, 7504 (1996).
[25] B. R. Johnson, J. Comput. Phys. **13**, 445 (1973).
[26] M. Shapiro and G. G. Balint-Kurti, J. Chem. Phys. **71**, 1461 (1978).
[27] E. B. Stechel, R. B. Walker, and J. C. Light, J. Chem. Phys. **69**, 3518 (1978).
[28] For a discussion see R. Schinke, *Photodissociation Dynamics* (Cambridge University Press, Cambridge, 1993), Chap. 8.
[29] S. Sato, J. Chem. Phys. **23**, 592 (1955); R. Weston, *ibid.* **31**, 892 (1959).
[30] M. Shapiro and R. Bersohn, J. Chem. Phys. **73**, 3810 (1980); M. Shapiro, J. Phys. Chem. **90**, 3644 (1986).
[31] B. R. Johnson, J. Chem. Phys. **67**, 4086 (1977).
[32] D. G. Abrashkevich, M. Shapiro, and P. Brumer (unpublished).

Downloaded 03 Oct 2001 to 142.150.224.5. Redistribution subject to AIP license or copyright, see http://ojps.aip.org/jcpo/jcpcr.jsp

14

Coherently Controlled Nanoscale Molecular Deposition

Bijoy K. Dey, Moshe Shapiro,* and Paul Brumer

Chemical Physics Theory Group, Department of Chemistry, University of Toronto, Toronto, Ontario M5S 3H6, Canada

(Received 9 June 2000)

Quantum interference effects are shown to provide a means of controlling and enhancing the focusing of a collimated neutral molecular beam onto a surface. The nature of the aperiodic pattern formed can be altered by varying laser field characteristics and the system geometry.

PACS numbers: 32.80.Qk, 34.50.Dy, 79.20.Rf

Light induced forces have been used to deflect, slow, accelerate, cool, and confine [1] neutral atoms. Similarly, and of particular interest here, atoms have been focused and deposited on surfaces on the nanometer scale [2,3]. In these cases, preliminary laser cooling followed by passage through an optical standing wave resulted in the formation of a periodic submicron atomic pattern on a surface. There are far fewer results for molecules, the most noteworthy being experiments [4] and theory [5] on focusing of molecules using intense laser fields. In this Letter we show that coherent control techniques [6] can be used to enhance and control the deposition of molecules on a surface, in *aperiodic,* nanometric scale patterns. The essence of the technique lies in the prepreparation of an initial controlled superposition of molecular eigenstates, followed by passage through an optical standing wave composed of two fields of related frequency. By varying the characteristics of the prepared superposition, or the characteristics of the optical standing wave, one can vary the induced dipole-electric field interaction, and hence alter the deposited pattern. The result demonstrates the utility of coherent control to manipulate the translational motion of molecules. Below we describe the general theory and provide computational results for the computationally convenient [7] molecule, N_2.

The general configuration of the proposed control scenario is illustrated in Fig. 1. A beam of neutral molecules propagating along the z direction is prepared in a superposition of vibrotational states with a highly cooled transverse velocity distribution. Preparation is achieved either by passing a precooled or precollimated beam through a preparatory electric field to create a superposition of vibrotational states in the ground electronic state, or by simultaneously preparing the superposition and cooling the transverse velocity by an extension of a recently proposed radiative association approach [8]. For simplicity we focus on a two-level superposition, i.e.,

$$|\Psi(t)\rangle = c_1 |\phi_1\rangle e^{-iE_1 t/\hbar} + c_2 |\phi_2\rangle e^{-iE_2 t/\hbar}, \quad (1)$$

where $|\phi_i\rangle$ are the eigenstates of the molecular Hamiltonian, of energy E_i.

The molecules then pass through a standing wave $\mathbf{E}(x,t)$ composed of two electromagnetic fields which lie parallel to the surface and are polarized in the z direction. That is,

$$\begin{aligned}\mathbf{E}(x,t) &= [2E_1^{(0)} \cos(k_1 x) e^{i\omega_1 t} + \text{c.c.}]\hat{\mathbf{k}} \\ &\quad + [2E_2^{(0)} \cos(k_2 x + \theta_F) e^{i\omega_2 t} + \text{c.c.}]\hat{\mathbf{k}} \\ &\equiv [E(\omega_1) + \text{c.c.}]\hat{\mathbf{k}} + [E(\omega_2) + \text{c.c.}]\hat{\mathbf{k}} \quad (2)\end{aligned}$$

Here $\hat{\mathbf{k}}$ denotes a unit vector in the z direction, c.c. denotes the complex conjugate of the terms preceding it, θ_F is the relative phase of the two standing waves (SW), $E_j^{(0)}$, k_j, and ω_j are the maximum amplitude, wave vector, and frequency of the jth standing wave, of wavelength λ_j.

The potential energy of interaction $V(x)$ of the molecule with the field $\mathbf{E}(x,t)$ is $V(x) = -\mu^{\text{ind}} \cdot \mathbf{E}(x,t)$, where μ^{ind} is the induced dipole moment. Within first order perturbation theory, the induced dipole of the superposition state in the presence of the two fields, chosen so that $E_1 + \hbar\omega_1 = E_2 + \hbar\omega_2$, is given by [7]

$$\begin{aligned}\mu^{\text{ind}} &= \chi^{\text{in}}(\omega_1)E(\omega_1) + \chi^{\text{ni}}(\omega_1)E(\omega_1) + \chi^{\text{in}}(\omega_2)E(\omega_2) + \chi^{\text{ni}}(\omega_2)E(\omega_2) + \chi^{\text{in}}(\omega_{21} + \omega_1)E(\omega_{21} + \omega_1) \\ &\quad + \chi^{\text{in}}(\omega_{21} - \omega_2)E(\omega_{21} - \omega_2) + \text{c.c.}, \quad (3)\end{aligned}$$

where $E(\omega_{21} + \omega_1) = 2E_1^{(0)} \cos(k_1 x) e^{i(\omega_{21}+\omega_1)t}$ and $E(\omega_{21} - \omega_2) = 2E_2^{(0)} \cos(k_2 x + \theta_F) e^{i(\omega_{21}-\omega_2)t}$. The χ are the following contributions to the zz component of the polarizability:

$$\chi^{\text{in}}(\omega_1) = \frac{1}{\hbar} \sum_j c_1 c_2^* \left[\frac{\mu_{j1}^z \mu_{2j}^z}{\omega_{j1} + \omega_2} + \frac{\mu_{j2}^z \mu_{1j}^z}{\omega_{j2} - \omega_2} \right] \frac{E_2^{(0)}}{E_1^{(0)}},$$

$$\chi^{\text{in}}(\omega_2) = \frac{1}{\hbar} \sum_j c_2 c_1^* \left[\frac{\mu_{j2}^z \mu_{1j}^z}{\omega_{j2} + \omega_1} + \frac{\mu_{j1}^z \mu_{2j}^z}{\omega_{j1} - \omega_1} \right] \frac{E_1^{(0)}}{E_2^{(0)}},$$

$$\chi^{\text{ni}}(\omega_1) = \frac{1}{\hbar} \sum_j \sum_{i=1,2} |c_i|^2 \mu_{ji}^z \mu_{ij}^z \left[\frac{1}{\omega_{ji} + \omega_1} + \frac{1}{\omega_{ji} - \omega_1} \right],$$

0031-9007/00/85(15)/3125(4)$15.00 © 2000 The American Physical Society

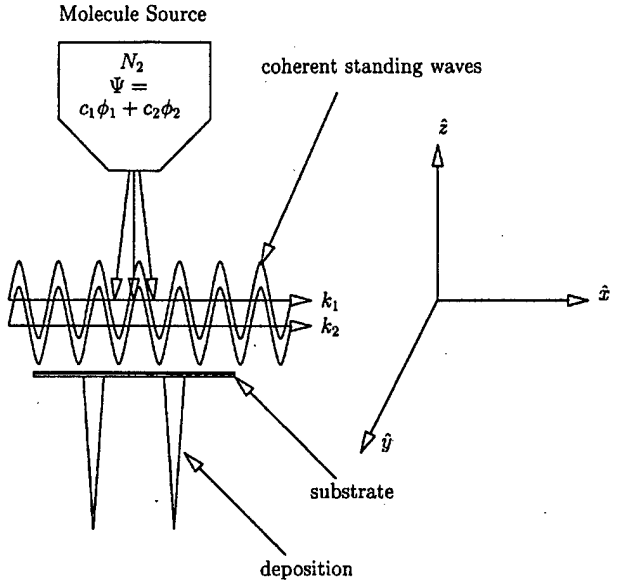

FIG. 1. Schematic of the proposed control scenario.

$$\chi^{\rm ni}(\omega_2) = \frac{1}{\hbar}\sum_j \sum_{i=1,2} |c_i|^2 \mu^z_{ji}\mu^z_{ij}\left[\frac{1}{\omega_{ji} + \omega_2} + \frac{1}{\omega_{ji} - \omega_2}\right],$$

$$\chi^{\rm in}(\omega_{21} + \omega_1) = \frac{1}{\hbar}\sum_j \left[c_1 c_2^* \frac{\mu^z_{j1}\mu^z_{2j}}{\omega_{j1} + \omega_1} + c_1^* c_2 \frac{\mu^z_{j2}\mu^z_{1j}}{\omega_{j2} - \omega_1}\right],$$

$$\chi^{\rm in}(\omega_{21} - \omega_2) = \frac{1}{\hbar}\sum_j \left[c_1 c_2^* \frac{\mu^z_{j1}\mu^z_{2j}}{\omega_{j1} - \omega_2} + c_1^* c_2 \frac{\mu^z_{j2}\mu^z_{1j}}{\omega_{j2} + \omega_2}\right],$$

where $\omega_{ij} = (E_j - E_i)/\hbar$ and $\mu^z_{ij} = \langle\phi_i|\mu\cdot\hat{\mathbf{k}}|\phi_j\rangle$. Here the superscripts "in" and "ni" refer to the interference and noninterference contributions to χ, the interference terms being the direct consequence of the established coherence between $|\phi_1\rangle$ and $|\phi_2\rangle$ [Eq. (1)]. The summation in the above equations runs over all the vibrational and rotational states. For example, in the particular case of N_2, examined below, vibrotational states of six excited electronic states ($b'^1\Sigma_u^+$, $c'^1\Sigma_u^+$, $e'^1\Sigma_u^+$, $b^1\Pi_u$, $c^1\Pi_u$, and $o^1\Pi_u$) are included.

The final expression for the potential within the rotating wave approximation is then given by

$$V(x) = -\mu^{\rm ind}\cdot\mathbf{E}(x,t) = V^{\rm ni}(x) + V^{\rm in}(x), \tag{4}$$

where

$$\begin{aligned} -V^{\rm ni}(x) = {} & 2[4E_1^{(0)^2}\cos^2(k_1x)\chi^{\rm ni}(\omega_1) + 4E_2^{(0)^2}\cos^2(k_2x + \theta_F)\chi^{\rm ni}(\omega_2) \\ & + 4E_1^{(0)}E_2^{(0)}\cos(k_1x)\cos(k_2x + \theta_F)[\chi^{\rm ni}(\omega_1) + \chi^{\rm ni}(\omega_2)]\cos(\omega_1 - \omega_2)t \end{aligned} \tag{5}$$

and

$$\begin{aligned} -V^{\rm in}(x) = {} & 2\{4E_1^{(0)^2}\cos(k_1x)\cos(k_2x + \theta_F)\chi_r^{\rm in}(\omega_1) + 4E_2^{(0)^2}\cos(k_1x)\cos(k_2x + \theta_F)\chi_r^{\rm in}(\omega_2) \\ & + 4E_1^{(0)}E_2^{(0)}\cos^2(k_2x + \theta_F)[\chi_r^{\rm in}(\omega_1)\cos(\omega_1 - \omega_2)t - \chi_I^{\rm in}(\omega_1)\sin(\omega_1 - \omega_2)t] \\ & + 4E_1^{(0)}E_2^{(0)}\cos^2(k_1x)[\chi_r^{\rm in}(\omega_2)\cos(\omega_2 - \omega_1)t - \chi_I^{\rm in}(\omega_2)\sin(\omega_2 - \omega_1)t]\}. \end{aligned} \tag{6}$$

Here $\chi_r^{\rm in}$ and $\chi_I^{\rm in}$ denote the real and imaginary parts of the zz component of $\chi^{\rm in}$. Computations show that the time dependent contributions to Eqs. (5) and (6) average out and may be neglected. The resultant time independent "optical potential" displays a series of maxima and minima along x, with each minima serving to focus the molecules, and each maxima serving to defocus them. The structure of $V(x)$ and hence its effect on the molecule's dynamics depends upon the *control parameters* $E_1^{(0)}$, $E_2^{(0)}$, c_1, c_2, θ_F and the quantum numbers ν_i, J, M.

The extent to which control is possible is evident from the computational results shown below on N_2 (a molecule chosen solely for computational convenience). Here $|\phi_i\rangle \equiv |\nu_i, J_i, M_i\rangle$, where ν_i and J_i are the vibrational and rotational quantum numbers, respectively, and M_i is the projection of J_i along the z direction. Selection rules imply [7] that $\chi^{\rm in}$ is zero unless $|\phi_1\rangle$ and $|\phi_2\rangle$ are of the same parity. To this end we employ a two photon preparatory step so that $J_2 = J_1 + 2$, $M_1 = M_2$.

As an example, we compute classical trajectories for the deposition of N_2 on a surface, reported as the number of trajectories $N(x)$ incident on the surface in a Δx interval of 1.403 nm. Our initial studies examined deposition using a nozzle width of 20 μm and a similar sample size. Results for the chosen parameters ($\lambda_1 = 0.628$ μm, $\lambda_2 = 0.736$ μm) showed an almost periodic repeating of patterns of 3–4 μm width. Hence we here focus down to this subregion, with computations simplified by reducing the nozzle diameter and sample size to $4\lambda_2 = 3$ μm. The initial velocity along z is taken as 600 m/sec, and the transverse velocity is assumed to be zero. Additional computations show that corrections to include a transverse velocity distribution can be incorporated in accord with Ref. [3]. That is, for a Gaussian transverse velocity distribution peaked about zero and of width σ, we find that the deposited peaks are broadened by $\approx\sqrt{2}\,t_{\rm int}\sigma$ while the ratios of peak height to background level are decreased by

$\approx 1/\sqrt{\pi} t_{int} \sigma$, where $t_{\rm int}$ is the interaction time between the molecule and the field.

Classical trajectories are computed for the motion of the N_2 center of mass in the presence of $V(x)$, which is encountered for the time period $t = 0$ to $t = t_{\rm int}$ [9]. We adopt an aspect of the ballistic aggregation model [10] and assume that all molecules that strike the surface stick without diffusing. Note also that although trajectories are computed for N_2 as a point particle, the $V(x)$ encountered by N_2 depends on the molecule's J, M through its effect on χ [11].

Consider first simple cases involving only a single superposition of states. Figure 2 shows the results in the presence and absence of interference contributions for a superposition composed of $|0,0,0\rangle$ and $|0,2,0\rangle$. Specifically, 2(a) and 2(b) show the pattern of deposition, and the associated optical potential, for dynamics in the presence of $V(x) = V^{\rm in}(x) + V^{\rm ni}(x)$. For comparison we show, in 2(c) and 2(d), the corresponding results assuming that there is no coherence between $|\phi_1\rangle$ and $|\phi_2\rangle$, i.e., neglecting $V^{\rm in}(x)$. In the absence of molecular coherence the optical potential is seen to be [Fig. 2(d)] periodic, resulting in a series of short periodic deposition peaks [Fig. 2(c)]. By contrast, the inclusion of interference contributions [Figs. 2(a) and 2(b)] result in significant enhancement and narrowing of peaks [5 times narrower (FWHM of less than 4 nm) and 4 times more intense], as well as the appearance of an aperiodic potential and associated aperiodic deposition pattern. Quantitative consideration of the peaks shows that they are in general in accord with the theory outlined in Ref. [3]. That is, a sharp peak forms in the region of the potential minima when $t_{\rm int} \sim (2n + 1)T/4$, where T is the optical period for a particular potential well. In the presence of $V^{\rm in}(x)$ not all potential wells have the same period. Hence, deposition is not periodic and is dependent on the interrelationship between $t_{\rm int}$ and the period T of each different well.

The optical potential $V(x)$ and hence the nature of the deposition pattern is seen to depend analytically [see Eqs. (4)–(6)] on the contributing $|\phi_i\rangle$, the coefficients c_i, the phase θ_F, the fields $E_i^{(0)}$, and the time of interaction $t_{\rm int}$ between the field and the molecule. Of these, numerical studies on the relative phase θ of the c_i, an important parameter in coherent control studies of photodissociation and bimolecular scattering [6], show that it does not significantly affect the deposition pattern. Consideration of Eq. (4) shows that this is because changes in θ do not affect the positions of the extrema of $V(x)$, and result only in small changes in the depth of the minima. By contrast, changes in the other parameters can strongly affect the structure of the deposited pattern. For example, Figs. 3(a) and 3(b) show significant differences in both the position and the intensity of the peaks as a function of θ_F. By contrast, consideration of the analogous plot where only $V^{\rm ni}$ is considered (not shown) shows no variation in peak intensity as a function of θ_F. Similarly, Figs. 3(c) and 3(d) show the strong dependence of the deposition upon the magnitude of the coefficients of the created superposition. Clearly, varying these parameters affords a wide range of control over the deposited pattern.

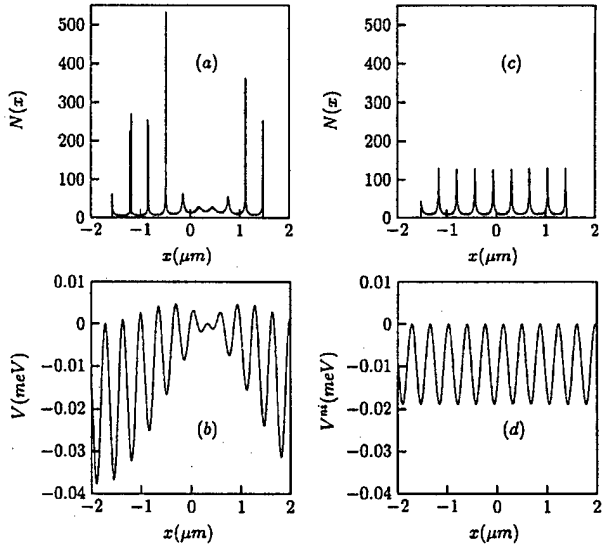

FIG. 2. Molecular deposition and associated optical potential for the initial superposition $\sqrt{0.8}\,|0,0,0\rangle + \sqrt{0.2}\,|0,2,0\rangle$ due to $V(x) = V^{\rm in}(x) + V^{\rm ni}(x)$ [(a) and (b)], and due to $V(x)^{\rm ni}$ only [(c) and (d)]. Here $\frac{E_2^0}{E_1^0} = 1.0 \times 10^4$, $E_1^0 = 1.0 \times 10^2$ V/cm, $\lambda_1 = 0.628$ μm, $\lambda_2 = 0.736$ μm, $\theta_F = -2.65$ radian, and $t_{\rm int} = 0.625$ μsec. Results are from a sample of 20 000 trajectories.

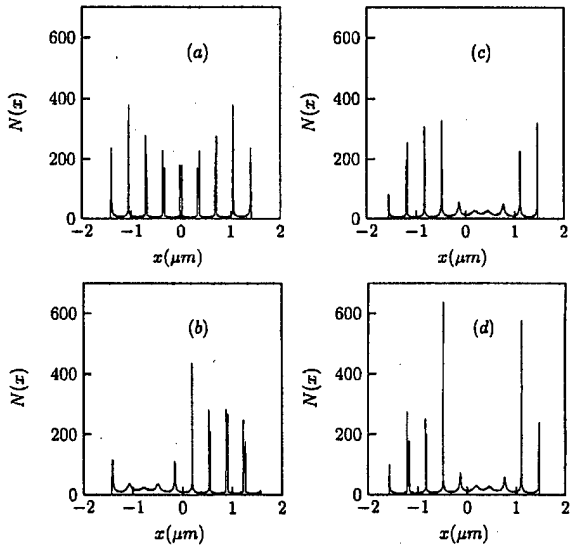

FIG. 3. (a),(b) Molecular deposition associated with $\sqrt{(0.8)}\,|000\rangle + \sqrt{(0.2)}\,|1,2,0\rangle$ for varying θ_F, i.e., (a) $\theta_F = 0$ and (b) $\theta_F = 2.0$. (c),(d) Sample variation of deposition with changes in $|c_1|, |c_2|$: (c) $\sqrt{0.99}\,|0,0,0\rangle + \sqrt{(0.01)}\,|0,2,0\rangle$; (d) $\sqrt{(0.4)}\,|0,0,0\rangle + \sqrt{0.6}\,|0,2,0\rangle$. Other parameters are as in Fig. 2.

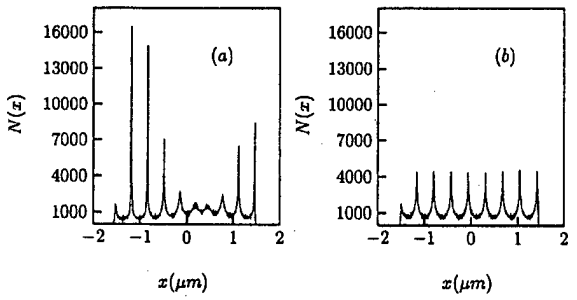

FIG. 4. Molecular deposition with (a) and without (b) molecular coherence for the mixed state at temperature $T = 298$ K, as described in text. Remaining parameters are as in Fig. 2 except that results are obtained from 1.23×10^6 trajectories and $r_{\text{int}} = 0.467$ μm.

Finally, consider control over a beam of molecules with a thermal distribution of molecular level populations. That is, consider the case where the initial collimated molecular beam is in a mixture of states $\sum_{i,j} w_{i,j} |0, J_i, M_j\rangle\langle 0, J_i, M_j|$, with the weights w_{ij} given by a Boltzmann distribution at $T = 298$ K. In this instance 20 J states are populated. By passing this mixture through a square pulse of field strength 3.25×10^9 V/m and frequency width 75.4 cm^{-1}, we excite all 19 states to pairwise superpositions of J states. That is, we produce the mixture $\sum_{i,j} w_{i,j}[c_{i,j} |0, J_i, M_j\rangle\langle 0, J_i, M_j| + d_{i,j} |0, J_i + 2, M_j\rangle\langle 0, J_i + 2, M_j|]$ where $|d_{i,j}|^2 = 1 - |c_{i,j}|^2$. At the chosen field strength, d_{ij} can be computed in perturbation theory [7], the final result being that the mixture of superpositions has the coefficient $c_{0,0}$ associated with the state $|0, 0, 0\rangle$ on the order of $\sqrt{0.8}$. This mixed state is then passed through the two stationary fields and the deposition pattern computed. Results for one such case are shown in Fig. 4 where results including the coherence contributions V^{in} are shown in 4(a) and contrasted with the results where only the noninterference terms are included [Fig. 4(b)]. The results are quite similar to those of the single superposition shown in Figs. 2 and 3 above. That is, including the interference, in addition to eliminating the periodicity, results in more intense, sharper lines. Examination of $V(x)$ as a function of J, M shows that the lack of broadening of the peaks with the mixing of J, M levels is a result of the fact that changing J, M alters only the depth of the $V(x)$ minima, and not their location.

In summary, we have shown that introducing a coherence between molecular energy levels, in conjunction with two frequency related electromagnetic fields, introduces a set of parameters that allow for control over the nanoscale molecular deposition pattern. Further work is needed to consider the possibility of depositing any arbitrary pattern, to examine the focusing of larger molecules (which have inherently larger polarizabilities and should be more easily focused), and to consider the effects of more intense cw fields. Work to this effect is in progress.

Support from the U.S. of Naval Research is gratefully acknowledged.

*Permanent address: Chemical Physics Department, The Weizmann Institute of Science, Rehovot, Israel.

[1] J. P. Gordon and A. Ashkin, Phys. Rev. A **21**, 1606 (1980); P. E. Moskowitz, P. L. Gould, and D. E. Pritchard, J. Opt. Soc. Am. B **2**, 1784 (1985); J. Prodan, A. Migdall, W. D. Phillips, I. So, H. Metcalf, and J. Dalibard, Phys. Rev. Lett. **54**, 992 (1985); A. P. Kazantsev, Sov. Phys. JETP **39**, 784 (1974); C. N. Cohen-Tannoudji and W. D. Phillips, Phys. Today **43**, 33 (1990); M. Kasevich and S. Chu, Phys. Rev. Lett. **69**, 1741 (1992); C. Salomon, J. Dalibard, A. Aspect, H. Metcalf, and C. N. Cohen-Tannoudji, Phys. Rev. Lett. **59**, 1659 (1987).

[2] G. Timp, R. E. Behringer, D. M. Tennant, J. E. Cunningham, M. Prentiss, and K. K. Berggren, Phys. Rev. Lett. **69**, 1636 (1992).

[3] K. Berggren, M. Prentiss, G. L. Timp, and R. E. Behringer, J. Opt. Soc. Am. B **11**, 1166 (1994).

[4] H. Stapelfeldt, H. Sakai, E. Constant, and P. B. Corkum, Phys. Rev. Lett. **79**, 2787 (1997); H. Sakai, A. Tarasevitch, J. Danilov, H. Stapelfeldt, R. W. Yip, C. Ellert, E. Constant, and P. B. Corkum, Phys. Rev A **57**, 2794 (1998).

[5] T. Seideman, J. Chem. Phys. **106**, 2881 (1997); Phys. Rev. A **56**, R17 (1997).

[6] M. Shapiro and P. Brumer, Adv. At. Mol. Opt. Phys. **42**, 287 (2000).

[7] E. McCullough, M. Shapiro, and P. Brumer, Phys. Rev. A **61**, 041801 (2000).

[8] A. Vardi, D. G. Abrashkevich, E. Frishman, and M. Shapiro, J. Chem. Phys. **107**, 6166 (1997); A. Vardi, M. Shapiro, and K. Bergmann, Opt. Express **4**, 91 (1999).

[9] For simplicity in the computation, we do not include a free flight time from the nozzle to the onset of the field in the computation. Including this time would increase both the number of molecules lost from the target area due to the transverse velocity spread as well as the width of the individual peaks.

[10] D. N. Sutherland, J. Colloid Interface Sci. **25**, 373 (1967); Nature (London) **226**, 1241 (1974).

[11] Thus, for example, molecules may well arrive at the surface with some degree of alignment, since molecules with different M are subject to different forces.

JOURNAL OF CHEMICAL PHYSICS VOLUME 113, NUMBER 6 8 AUGUST 2000

COMMUNICATIONS

Identical collision partners in the coherent control of bimolecular reactions

Paul Brumer
Chemical Physics Theory Group, Department of Chemistry, University of Toronto, Toronto M5S 3H6, Canada

Klaas Bergmann
Fachbereich Physik, Universitat Kaiserslautern, Kaiserslautern, Germany 36226

Moshe Shapiro
Chemical Physics Department, The Weizmann Institute of Science, Rehovot, Israel 76100

(Received 7 March 2000; accepted 7 June 2000)

The coherent control of bimolecular processes typically requires that the system be initiated in a superposition of correlated translational and internal reactant states. We show that by colliding identical molecules one bypasses many of these complexities, allowing for direct studies of coherently controlled collision phenomena. © *2000 American Institute of Physics.* [S0021-9606(00)01930-9]

Coherent control provides a route to controlling reaction dynamics via laser-induced quantum interference effects.[1,2] The vast majority of work has been done on controlling unimolecular processes. However, we recently[3,4] showed that it is possible to apply the principle of coherent control to control bimolecular reactions. These considerations indicate that bimolecular control requires conditions additional to those operative in unimolecular processes, making bimolecular control more challenging. Here we show, however, that reactions of the form $A+A\rightarrow B+C$ afford a unique opportunity for studying controlled bimolecular reactions.

The essential principle of coherent control requires that one create a controllable superposition of degenerate Hamiltonian eigenstates in the center of mass coordinate system.[1] By altering the composition of this superposition, one can alter the ratio of reaction products. Consider then the bimolecular case

$$A+D\rightarrow F+G, \tag{1}$$

where A, D, F, G are, in general, molecules of mass M_A, M_D, M_F, and M_G. Here F and G can be identical to A and D (nonreactive scattering) or different from A and D (reactive scattering). We label $A+D$ as arrangement q and $F+G$ as arrangement q'.

In accord with standard scattering theory[5] the cross section $\sigma_E(\mathbf{n},q';\mathbf{m},q)$ for scattering between the incident Hamiltonian eigenstates $|E,q,\mathbf{m};0\rangle$ of $A+D$ (labeled q) and the product Hamiltonian eigenstates $\langle E,q',\mathbf{n};0|$ of $F+G$ (labeled q') is given by

$$\sigma_E(\mathbf{n},q';\mathbf{m},q)=|\langle E,q',\mathbf{n}^-|V_q|E,q,\mathbf{m};0\rangle|^2. \tag{2}$$

Here $\mathbf{n}$, $\mathbf{m}$ denote quantum numbers associated with the reactants and products, respectively, $|E,q',\mathbf{n}^-\rangle$ are the incoming scattering solutions associated with product in state $|E,q',\mathbf{n};0\rangle$, and V_q is the component of the total potential that vanishes as the A to D distance becomes arbitrarily large. The cross section for scattering into arrangement q', independent of the product internal state $\mathbf{n}$, is then

$$\sigma_E(q';\mathbf{m},q)=\sum_{\mathbf{n}}|\langle E,q',\mathbf{n}^-|V_q|E,q,\mathbf{m};0\rangle|^2. \tag{3}$$

Control of bimolecular collisions is achieved by constructing an initial state $|E,q,\{a_\mathbf{m}\}\rangle$ comprised of a superposition of N energetically degenerate asymptotic states $|E,q,\mathbf{m};0\rangle$:

$$|E,q,\{a_\mathbf{m}\}\rangle=\sum_{\mathbf{m}}a_\mathbf{m}|E,q,\mathbf{m};0\rangle. \tag{4}$$

The cross section associated with using Eq. (4) as the initial state, obtained by replacing $|E,q,\mathbf{m};0\rangle$ by Eq. (4) in Eq. (2), is

$$\begin{aligned}\sigma_E(\mathbf{n},q';\{a_\mathbf{m}\},q)&=|\langle E,q',\mathbf{n}^-|V_q\sum_{\mathbf{m}}a_\mathbf{m}|E,q,\mathbf{m};0\rangle|^2\\&=\sum_{\mathbf{m}}|a_\mathbf{m}|^2|\langle E,q',\mathbf{n}^-|V_q|E,q,\mathbf{m};0\rangle|^2+\sum_{\mathbf{m}'}\sum_{\mathbf{m}\neq\mathbf{m}'}a_\mathbf{m}a^*_{\mathbf{m}'}\langle E,q',\mathbf{n}^-|V_q|E,q,\mathbf{m};0\rangle\langle E,q,\mathbf{m}';0|V_q|E,q',\mathbf{n}^-\rangle\\&\equiv\sum_{\mathbf{m}}|a_\mathbf{m}|^2\sigma(\mathbf{n},q';\mathbf{m};q)+\sum_{\mathbf{m}'}\sum_{\mathbf{m}\neq\mathbf{m}'}a_\mathbf{m}a^*_{\mathbf{m}'}\sigma(\mathbf{n},q';\mathbf{m}',\mathbf{m},q),\end{aligned} \tag{5}$$

 © 2000 American Institute of Physics

Downloaded 03 Oct 2001 to 142.150.224.5. Redistribution subject to AIP license or copyright, see http://ojps.aip.org/jcpo/jcpcr.jsp

where $\sigma(\mathbf{n},q';\mathbf{m}',\mathbf{m},q)$ is defined via Eq. (5). The total cross section into arrangement q' is then given by

$$\sigma_E(q';\{a_\mathbf{m}\},q)=\sum_\mathbf{n}\sigma_E(\mathbf{n},q';\{a_\mathbf{m}\},q). \tag{6}$$

Note that Eq. (5), and hence Eq. (6), are now of a standard coherent control form, i.e., direct contributions from each member of the superposition, proportional to $|a_\mathbf{m}|^2$, plus interference terms which are proportional to $a_\mathbf{m}a^*_{\mathbf{m}'}$. It is clear that if we control the $a_\mathbf{m}$, through assorted preparation methods, then we can control the interference term, and hence the scattering cross section. In the case of bimolecular collisions, coherent control arises only from states that are of equal energy and that have the same center of mass momentum.

Consider now the laboratory preparation of the generalized superposition states [Eq. (4)] where for simplicity we limit consideration to a superposition of two states. To emphasize the role of the center of mass motion and the particular utility of choosing $A=D$ we first treat this problem in general (i.e., any D). To do so we examine the scattering of A and D, each in a previously prepared superposition of Hamiltonian eigenstates $|\phi_A(i)\rangle$ and $|\phi_D(i)\rangle$ of molecules A and D. These states are of energy $e_A(i)$ and $e_D(i)$, respectively. We denote $\mathbf{r}_A$ and $\mathbf{r}_D$ as the laboratory position of A and D with $\hbar\mathbf{k}^A$, $\hbar\mathbf{k}^D$ denoting their laboratory momenta. The relative momentum $\mathbf{k}$, relative coordinate $\mathbf{R}$, center of mass momentum $\mathbf{K}$, and position $\mathbf{R}_{\text{c.m.}}$ are defined as

$$\begin{aligned}&\mathbf{K}=\mathbf{k}^A+\mathbf{k}^D,\quad \mathbf{R}_{\text{c.m.}}=(M_A\mathbf{r}_A+M_D\mathbf{r}_D)/(M_A+M_D),\\ &\mathbf{k}=(M_D\mathbf{k}^A-M_A\mathbf{k}^D)/(M_A+M_D),\quad \mathbf{R}=\mathbf{r}_A-\mathbf{r}_D.\end{aligned} \tag{7}$$

The wave functions of A and D in the laboratory frame, ψ_A and ψ_D, are of the general form:

$$\psi_A=a_1|\phi_A(1)\rangle\exp(i\mathbf{k}_1^A\cdot\mathbf{r}_A)+a_2|\phi_A(2)\rangle\exp(i\mathbf{k}_2^A\cdot\mathbf{r}_A), \tag{8}$$

$$\psi_D=b_1|\phi_D(1)\rangle\exp(i\mathbf{k}_1^D\cdot\mathbf{r}_D)+b_2|\phi_D(2)\rangle\exp(i\mathbf{k}_2^D\cdot\mathbf{r}_D). \tag{9}$$

The incident wave function is then the product

$$\begin{aligned}\psi_{\text{in}}&=\psi_A\psi_D\\ &=[a_1|\phi_A(1)\rangle\exp(i\mathbf{k}_1^A\cdot\mathbf{r}_A)+a_2|\phi_A(2)\rangle\exp(i\mathbf{k}_2^A\cdot\mathbf{r}_A)]\\ &\quad\times[b_1|\phi_D(1)\rangle\exp(i\mathbf{k}_1^D\cdot\mathbf{r}_D)+b_2|\phi_D(2)\rangle\exp(i\mathbf{k}_2^D\cdot\mathbf{r}_D)]\\ &=\sum_{i,j=1}^{2}A_{ij}\exp(i\mathbf{k}_{ij}\cdot\mathbf{R})\exp(i\mathbf{K}_{ij}\cdot\mathbf{R}_{\text{c.m.}}),\end{aligned} \tag{10}$$

where $A_{ij}=a_ib_j|\phi_A(i)\rangle|\phi_D(j)\rangle$, $\mathbf{k}_{ij}=(M_D\mathbf{k}_i^A-M_A\mathbf{k}_j^D)/(M_A+M_D)$, and $\mathbf{K}_{ij}=\mathbf{k}_i^A+\mathbf{k}_j^D$.

As constructed, Eq. (10) is composed of four independent noninterfering incident states since each has a different center of mass wave vector $\mathbf{K}_{ij}$. However, we can set conditions so that interference, and hence control, is allowed. That is, we require the equality of the center of mass motion of two components, plus energy degeneracy:

$$\begin{aligned}&\mathbf{K}_{12}=\mathbf{K}_{21},\\ &\hbar^2k_{12}^2/2\mu+e_A(1)+e_D(2)=\hbar^2k_{21}^2/2\mu+e_A(2)+e_D(1),\end{aligned} \tag{11}$$

with $\mu=M_AM_D/(M_A+M_D)$. Equation (10) then becomes

$$\begin{aligned}\psi_{\text{in}}&=[A_{12}\exp(i\mathbf{k}_{12}\cdot\mathbf{R})+A_{21}\exp(i\mathbf{k}_{21}\cdot\mathbf{R})]\exp(i\mathbf{K}_{12}\cdot\mathbf{R}_{\text{c.m.}})\\ &\quad+A_{11}\exp(i\mathbf{k}_{11}\cdot\mathbf{R})\exp(i\mathbf{K}_{11}\cdot\mathbf{R}_{\text{c.m.}})\\ &\quad+A_{22}\exp(i\mathbf{k}_{22}\cdot\mathbf{R})\exp(\mathbf{K}_{22}\cdot\mathbf{R}_{\text{c.m.}}),\end{aligned} \tag{12}$$

where the term in the square brackets, due to Eq. (11), is a linear superposition of two *degenerate* states. We therefore expect that the scattering cross section will be comprised of noninterfering contributions from three components with differing $\mathbf{K}_{ij}$, but where the first term allows for control via the interference between the A_{12} and A_{21} terms. The two remaining terms, proportional to A_{11} and A_{22}, are uncontrolled satellite contributions.

For example, if we design the experiment so that $\mathbf{k}_1^A=-\mathbf{k}_2^D$ and $\mathbf{k}_2^A=-\mathbf{k}_1^D$ then $\mathbf{K}_{12}=\mathbf{K}_{21}=0$, and $\mathbf{k}_{12}=\mathbf{k}_1^A$, $\mathbf{k}_{21}=-\mathbf{k}_1^D$, so that the degeneracy requirement [Eq. (11)] becomes

$$\begin{aligned}&\hbar^2(k_1^A)^2/2\mu+e_A(1)+e_D(2)\\ &\quad=\hbar^2(k_1^D)^2/2\mu+e_A(2)+e_D(1).\end{aligned} \tag{13}$$

In general, this condition necessitates a method of preparing ψ_A and ψ_D which correlates the internal states $|\phi_A(i)\rangle$ and $|\phi_D(i)\rangle$ with their associated momenta $\mathbf{k}_i^A$, $\mathbf{k}_i^D$ so as to obtain Eq. (13). This requires a considerable extension of currently available experimental techniques. However, the situation simplifies enormously for the case of $D=A$, the subject of this note. Specifically, consider

$$A+A'\rightarrow B+C. \tag{14}$$

Here we have used A' to denote the molecule A, but in a superposition state which is not necessarily the same as A. If we prepare each of the two initial A and A' superposition states from the same molecular bound states, e.g., $|\phi_A(1)\rangle=|\phi_{A'}(1)\rangle$ and $|\phi_A(2)\rangle=|\phi_{A'}(2)\rangle$ then the requirement for conservation of energy in the center of mass [Eq. (11)] becomes

$$\hbar^2(k_{12})^2/2\mu=\hbar^2(k_{21})^2/2\mu. \tag{15}$$

This condition is satisfied for a standard scattering arrangement where $\mathbf{k}_1^A=\mathbf{k}_2^A$ and $\mathbf{k}_1^{A'}=\mathbf{k}_2^{A'}$, since then $k_{12}=|0.5(\mathbf{k}_1^A-\mathbf{k}_2^{A'})|=|0.5(\mathbf{k}_2^A-\mathbf{k}_1^{A'})|=k_{21}$.

This scenario opens up a wide range of possible experimental studies of control in bimolecular collisions. Specifically, we need only prepare A and A' in a controlled superposition of two states (e.g., by resonant excitation of $|\phi_A(1)\rangle$) to produce a superposition with $|\phi_A(2)\rangle$, scatter them, and vary the coefficients in the superposition to affect the reaction probabilities. Control originates in quantum interference between two degenerate states associated with the contributions of $|\phi_A(1)\rangle|\phi_{A'}(2)\rangle$ and $|\phi_A(2)\rangle|\phi_{A'}(1)\rangle$. This is accompanied by two uncontrolled scattering contributions corresponding to the contributions of

Downloaded 03 Oct 2001 to 142.150.224.5. Redistribution subject to AIP license or copyright, see http://ojps.aip.org/jcpo/jcpcr.jsp

$|\phi_A(1)\rangle|\phi_{A'}(1)\rangle$ and $|\phi_A(2)\rangle|\phi_{A'}(2)\rangle$. Control is achieved by varying the four coefficients a_i, b_i, $i=1,2$.

STIRAP[6] provides a natural choice for such state preparation. A particularly promising version is the tripod-STIRAP variant which was recently suggested[7] and experimentally demonstrated.[8] In the tripod-STIRAP scheme, an additional laser couples the intermediate level (through which the initial and final state are radiatively connected via the pump and Stokes laser) with another unpopulated state. Depending on the overlap in time of the interaction of the additional laser with that of the pump and Stokes laser, any coherent superposition of the initial and final state can be created. The system remains in the superposition state after the interaction with the lasers has ceased and the superposition so created is robust, i.e., it is not sensitive to small variations of the laser intensities or the overlap.

The above-described control approach can be generalized to a superposition of N levels in each of the two A and A' reactants. Specifically, choosing all $\mathbf{k}_i^A=\mathbf{k}^A$ and all $\mathbf{k}_i^{A'}=\mathbf{k}^{A'}$ we have

$$\psi_A=\exp(i\mathbf{k}^A\cdot\mathbf{r}_A)\left[\sum_{i=1}^{N} a_i|\phi_A(i)\rangle\right],$$
$$\psi_{A'}=\exp(i\mathbf{k}^{A'}\cdot\mathbf{r}_{A'})\left[\sum_{j=1}^{N} b_j|\phi_A(j)\rangle\right]. \tag{16}$$

The scattering wave function is then

$$\psi_{\text{in}}=\psi_A\psi_{A'}=\exp(i\mathbf{K}\cdot\mathbf{R}_{\text{c.m.}})\exp(i\mathbf{k}\cdot\mathbf{R})\left[\sum_{i=1}^{N} a_i|\phi_A(i)\rangle\right]\times\left[\sum_{j=1}^{N} b_j|\phi_A(j)\rangle\right]. \tag{17}$$

Since $M_A=M_{A'}$, $\mathbf{k}=(\mathbf{k}^A-\mathbf{k}^{A'})/2$ and $\mathbf{K}=\mathbf{k}^A+\mathbf{k}^{A'}$. The kinetic energy $k^2/2\mu$ is the same for each term in Eq. (17) so that degenerate states in the center of mass frame correspond to states $|\phi_A(i)\rangle|\phi_{A'}(j)\rangle$ in Eq. (17) which are of equal internal energy $e_A(i)+e_{A'}(j)$. Expanding the product in Eq. (17) gives N^2 terms, N terms of which are of differing energy $2e_A(i)$, $i=1,\ldots,N$ and (N^2-N) states of energy $e_A(i)+e_{A'}(j)$, $i\neq j$. Of the latter terms, each is accompanied by another term of equal energy [i.e., $e_A(i)+e_{A'}(j)=e_A(j)+e_{A'}(i)$]. Hence the N^2 terms are comprised of N direct terms plus $(N^2-N)/2$ degenerate pairs which are a source of interference, and hence control. Here control is achieved by altering the $2N$ coefficients a_i,b_i in the initially prepared state [Eq. (17)], e.g., by shaped pulsed laser excitation of $|\phi_A(1)\rangle$ and $|\phi_{A'}(1)\rangle$. The extent to which increasing N affects control must be the subject of further study.

Finally, we note that $OH+OH\rightarrow H_2O+H$ is an excellent candidate for study. Experimentally, this system is desirable because cooled OH has only a few populated rotational levels, the first electronic state (needed in STIRAP) is accessible with conveniently available near-UV radiation, and the H atom product can be detected by resonance enhanced multiphoton ionization, possibly in combination with ion imaging to obtain information of the internal energy of the H_2O product.

Theoretical and experimental efforts to examine this control scenario, with initial applications to isotopes of molecular hydrogen and to $OH+OH\rightarrow H_2O+H$, are under way.

This work was supported by the U.S. Office of Naval Research, the Israel Science Foundation, and the Israel–German D.I.P. Strategic Collaborative Project.

[1] M. Shapiro and P. Brumer, Adv. At., Mol., Opt. Phys. **42**, 287 (2000).
[2] R. J. Gordon and S. A. Rice, Annu. Rev. Phys. Chem. **48**, 595 (1997).
[3] P. Brumer, A. Abrashkevich, and M. Shapiro, Discuss. Faraday Soc. **113**, 291 (1999); the present paper corrects a typographical error in this reference, in which the outgoing scattering state, rather than the incoming scattering state, was indicated.
[4] A. Abrashkevich, M. Shapiro, and P. Brumer, Phys. Rev. Lett. **81**, 3789 (1998); Erratum: **82**, 3002 (1999); M. Shapiro and P. Brumer, *ibid.* **77**, 2574 (1996); E. Frishman, M. Shapiro, and P. Brumer, J. Phys. Chem. A **103**, 10333 (1999).
[5] J. R. Taylor, *Scattering Theory* (Wiley, New York, 1972).
[6] K. Bergmann, H. Theuer, and B. W. Shore, Rev. Mod. Phys. **70**, 1003 (1998); U. Gaubatz, P. Rudecki, S. Schiemann, and K. Bergmann, J. Chem. Phys. **92**, 5363 (1990).
[7] R. G. Unanyan, M. Fleischhauer, K. Bergmann, and B. W. Shore, Opt. Commun. **155**, 144 (1998).
[8] H. Theuer, R. G. Unanyan, C. Habscheid, K. Klein, and K. Bergmann, Opt. Express **4**, 77 (1999).

Downloaded 03 Oct 2001 to 142.150.224.5. Redistribution subject to AIP license or copyright, see http://ojps.aip.org/jcpo/jcpcr.jsp

10 March 2000

ELSEVIER

Chemical Physics Letters 319 (2000) 27–44

CHEMICAL PHYSICS LETTERS

www.elsevier.nl/locate/cplett

Semiclassical initial value representation techniques for chaotic systems

B.R. McQuarrie [1], Paul Brumer *

Chemical Physics Theory Group, Department of Chemistry, University of Toronto, Toronto, ONT M5S 3H6, Canada

Received 8 November 1999; in final form 28 December 1999

Abstract

Semiclassical wavefunction propagation for chaotic systems suffer from numerical difficulties due to the chaotic nature of classical trajectories, resulting in reduced accuracy for standard initial value representation (IVR) methods. We compare four recent IVR methods developed to overcome these difficulties (Herman–Kluk with trajectory truncation; stationary-phase Herman–Kluk (SPHK); cellularized frozen Gaussian approximation; stationary-phase Monte Carlo) by computing the Franck–Condon spectrum of the 2-dimensional Henon–Heiles and quartic oscillator systems. The SPHK is found to be the most successful of the four methods. The SPHK is then used to determine the spectrum for collinear CO_2 photodissociation.
© 2000 Elsevier Science B.V. All rights reserved.

1. Introduction

There has been a great deal of recent interest in semiclassical methods to treat the dynamics of atoms and molecules based upon an initial value representation (IVR) [1–7]. An IVR expresses the system dynamics as an integral over initial phase-space (coordinate and momenta) variables. Dynamical system quantities are evaluated along the classical trajectories which emanate from these initial phase-space points. The primary advantage of IVR methods is that they do not require a search for trajectories which satisfy both initial and final time constraints, which is the case for any boundary value representation such as the Van Vleck propagator [8]. The central deficiency of IVR methods is in the need to integrate over highly oscillatory integrands. Here we examine IVR propagators for the numerically difficult case of chaotic dynamics.

Extensive studies have been carried out to compare IVR propagators for non-chaotic systems. In this case, the Herman–Kluk (HK) frozen Gaussian approximation [2], an improved version of the original frozen Gaussian approximation of Heller [1], has proven particularly useful. In addition to providing reliable results, the method does not require the computation of the Maslov index [5], a simplifying feature. For example, Kay compared several IVR methods for non-chaotic systems [4], and concluded that the HK propagator can produce highly accurate results which converge quickly. Similarly, Garashchuk and Tannor [9] found the HK formalism to be far better at treating reactive scattering than other semiclassical methods, and van de Sand and

* Corresponding author. Fax: (416) 978-5325; e-mail: pbrumer@tikva.chem.utoronto.ca

[1] E-mail: bmcquar@tikva.chem.utoronto.ca

0009-2614/00/$ - see front matter © 2000 Elsevier Science B.V. All rights reserved.
PII: S0009-2614(00)00053-1

Rost [10] successfully treated 3-dimensional Coulomb scattering using the HK propagator. This propagator has also been used by Walton and Manolopoulos to treat collinear CO_2 photodissociation [11] (cf. Section 3). The method converged but required 10^8 trajectories. The large number of trajectories is undoubtably due to the dissociative nature of the problem, but the authors also identified unstable periodic orbits as a contributing factor.

Far fewer studies have been directed at chaotic dynamics. Here chaotic trajectories and associated exponential growth cause serious convergence problems for the oscillatory integrals that dominate IVR methods. Kay treated bound chaotic systems [12] and noted that the HK method was not very successful due to chaotic trajectories which caused the integrand to grow exponentially. To resolve this problem Kay proposed discarding excessively unstable trajectories, an ad hoc procedure (which we term HKK) that produced good results. Subsequently, Campolieti and Brumer [13] introduced a stationary-phase approach that automatically weighted chaotic trajectories, obviating the need for arbitrary truncation of any trajectories. The resultant technique, a stationary-phase Monte Carlo (SPMC) not related to the HK approach, provided good results for bound chaotic dynamics.

Attempts have also been made to modify the HK integral to treat chaotic dynamics. We examine two such methods: the stationary-phase Herman–Kluk (SPHK) of Herman [7] and the cellularized frozen Gaussian approximation (CFGA) of Walton and Manolopoulos [6]. In this Letter, we will consider these three modified HK methods (HKK, SPHK, and CFGA) and compare their utility on a number of chaotic systems. We also include a comparison with our previously proposed stationary-phase Monte Carlo (SPMC) method [13]. Comparisons are made by computing the Franck–Condon spectrum for three 2-dimensional systems of varying degrees of chaotic behavior (Henon-Heiles (HH) and quartic oscillator potential). Our goal is to assess both accuracy and to determine the method which requires the fewest trajectories for convergence. The results are compared, and the SPHK approach is found to be the most successful. This method is then used to treat collinear CO_2 photodissociation. We show that the SPHK method can obtain reasonable estimates of the spectrum using orders of magnitude fewer trajectories than the unmodified HK approach.

Note that the systems we consider have been examined previously by some type of semiclassical IVR method (Henon–Heiles in Ref. [6]; quartic oscillator in Refs. [12,13]; collinear CO_2 in Ref. [11]). However, this Letter provides a systematic comparison of the methods, crucial to further development of this area. A comparison of the IVR methods applied to chaotic systems, as presented in this Letter, leads to the unambiguous conclusion that the SPHK is the best of the four approaches for the properties studied.

2. Semiclassical propagation of wavefunctions

In Section 2, we outline the Franck–Condon spectral theory, and describe the four IVR procedures.

The absorption spectrum $I(E)$, the quantity we wish to compute, can be expressed as the Fourier transform of an autocorrelation function [14]

$$I(E) = \mathrm{Re}\frac{1}{2\pi\hbar}\int_{-\infty}^{\infty} \mathrm{d}t \exp(iEt/\hbar)C(t)\,, \qquad (1)$$

where $C(t) = \langle\Psi_0|\exp(-i\hat{H}t/\hbar)|\Psi_0\rangle$ is the autocorrelation function for an initial Ψ_0 propagating under Hamiltonian $\hat{H}$. The initial state is chosen to be a Gaussian in the coordinate representation

$$\Psi_0(q') = \langle q'|\bar{p}\bar{q}\alpha 0\rangle \equiv (2\alpha/\pi)^{d/4} \times \exp\left(-\alpha|q'-\bar{q}|^2 + i\bar{p}\cdot(q'-\bar{q})/\hbar\right), \qquad (2)$$

where $\bar{q}$ and $\bar{p}$ are the coordinate and momentum shift, respectively, and α is a width parameter. The (q,p) phase space is of dimension $2d$.

A wavefunction at time t is given in terms of the wavefunction at time zero by

$$\Psi_t(x) = \int \mathrm{d}x'\, K_t(x,x')\Psi_0(x')\,, \qquad (3)$$

where $K_t(x,x')$ is the Feynman propagator

$$K_t(x,x') = \langle x|\exp(-i\hat{H}t/\hbar)|x'\rangle\,. \qquad (4)$$

The autocorrelation function is therefore given by

$$C(t) = \int \mathrm{d}x \Psi_0^*(x) \int \mathrm{d}x' \, K_t(x,x') \Psi_0(x') . \quad (5)$$

A semiclassical approximation to the quantum wavefunction at t is obtained by replacing K_t by a semiclassical propagator K_t^{sc}, giving the semiclassical approximation $C^{\mathrm{sc}}(t)$ to the autocorrelation function.

2.1. Herman–Kluk propagator

To appreciate the differences between the semiclassical propagators, we consider the structure of each method studied. The HK propagator is given by [3]

$$K_t^{\mathrm{sc}}(x,x') = \frac{1}{(2\pi\hbar)^d} \int \mathrm{d}p \int \mathrm{d}q \, R_{pqt} \, \mathrm{e}^{iS_{pqt}/\hbar} \times \langle x | p(t) q(t) \alpha' 0 \rangle \langle p q \alpha' 0 | x' \rangle , \quad (6)$$

where

$$S_{pqt} = \int_0^t \mathrm{d}t' \, p(t') \cdot \dot{q}(t') - H(p(t'), q(t')) , \quad (7)$$

$$R_{pqt} = \pm \left\{ \det \left[\frac{1}{2} \left(M_{pp} + M_{qq} - 2i\alpha'\hbar M_{qp} + \frac{i}{2\alpha'\hbar} M_{pq} \right) \right] \right\}^{\frac{1}{2}} . \quad (8)$$

Here q,p denote phase-space points at $t = 0$, which evolve classically to $q(t),p(t)$ at time t. The stability matrix M consists of the sub-matrices given by $M_{qq} = \partial q(t)/\partial q$, $M_{qp} = \partial q(t)/\partial p$, $M_{pq} = \partial p(t)/\partial q$, $M_{pp} = \partial p(t)/\partial p$. The sign of the prefactor R_{pqt} is chosen to keep R_{pqt} differentiable at all times. Note that the Maslov index does not appear in Eq. (6); instead R_{pqt} must be kept differentiable over the entire trajectory.

The quantity α' (Eq. (6)) is an adjustable parameter [3], which defines the width of the frozen Gaussians which are propagated [15]. The effect of varying α' has been examined by Kay [4] for the HK, who recommends determining α' by examining energy conservation of a wavepacket, and by Herman [7]. Below, we take $\alpha' = \alpha$ for the initial wavefunction, a reasonable choice used in many cases [6,9,11,12,16].

Substituting Eqs. (2) and (6) into Eq. (5) and performing the x and x' integrations gives the HK representation of the autocorrelation function

$$C_{\mathrm{HK}}^{\mathrm{sc}}(t) = \left(\frac{1}{2\pi\hbar} \right)^d \int\int \mathrm{d}p \, \mathrm{d}q \, R_{pqt} \, \mathrm{e}^{iS_{pqt}/\hbar} \times \exp\left[-\frac{\alpha}{2}(q(t) - \bar{q})^2 - \frac{i}{2\hbar}(p(t) + \bar{p}) \cdot (q(t) - \bar{q}) - \frac{(p(t) - \bar{p})^2}{8\alpha\hbar^2} \right] \exp\left[-\frac{\alpha}{2}(q - \bar{q})^2 + \frac{i}{2\hbar}(p + \bar{p}) \cdot (q - \bar{q}) - \frac{(p - \bar{p})^2}{8\alpha\hbar^2} \right] . \quad (9)$$

Eq. (9) is the unmodified version of the HK method which has been used successfully to treat non-chaotic systems [4,9–11]. The integrand in Eq. (9) is highly oscillatory due to rapid variations of the phase, and R_{pqt} can grow exponentially fast for chaotic trajectories. For these reasons Eq. (9) is unable to provide accurate spectral estimates for chaotic systems.

A simple, surprisingly successful method [12] to treat chaotic systems using the HK propagator is to truncate trajectories when the prefactor R_{pqt} grows large (HKK). In particular, contributions to the integral are kept until $|R_{pqt}|^2 > D_t$, where D_t is some arbitrarily defined function of time.

More systematic methods involve pre-averaging the integrand to reduce the oscillatory behavior [6,7,16–20], e.g. by application of a Filinov transform [21]. In a particular Filinov transformation [7], the oscillatory $2d$-dimensional integral

$$I = \int \mathrm{d}z A(z) \exp[if(z)] , \quad (10)$$

is replaced by the approximation

$$I \sim I_\epsilon = \int \mathrm{d}z A(z) \exp[if(z)] \exp\left[-\epsilon |\nabla f(z)|^2 \right] . \quad (11)$$

This form emphasizes regions of stationary phase in the integral, and contains the adjustable parameter ϵ.

In general, $\lim_{\epsilon\to 0} I_\epsilon = I$, and I_ϵ approaches, as $\epsilon\to\infty$, the result of summing over stationary-phase points [17,18]. For computational purposes, ϵ should be chosen relatively small so that the series expansions used in developing I_ϵ are valid [18]. However, it is desirable to use large ϵ, since fewer trajectories are needed to converge I_ϵ. Unfortunately, as $\epsilon\to\infty$, determining the stationary-phase points becomes increasingly difficult, and any brute force numerical implementation is bound to fail. These considerations are used to determine a suitable ϵ; the converged Monte Carlo integral should be stable for a range of non-zero ϵ. This range is typically 3–4 orders of magnitude.

2.2. Stationary-phase Herman–Kluk approach

Applying Eq. (11) to Eq. (9), gives the first-order SPHK approximation [7,16,20]

$$C^{sc}_{SPHK}(t) = \left(\frac{1}{2\pi\hbar}\right)^d \int\int dp\, dq R_{pqt} e^{iS_{pqt}/\hbar} D_{\epsilon pqt} \times \exp\left[-\frac{\alpha}{2}(q(t)-\bar{q})^2 - \frac{i}{2\hbar}(p(t)+\bar{p})\cdot(q(t)-\bar{q}) - \frac{(p(t)-\bar{p})^2}{8\alpha\hbar^2}\right] \exp\left[-\frac{\alpha}{2}(q-\bar{q})^2 + \frac{i}{2\hbar}(p+\bar{p})\cdot(q-\bar{q}) - \frac{(p-\bar{p})^2}{8\alpha\hbar^2}\right], \quad (12)$$

where

$$D_{\epsilon pqt} = \exp\left\{-\frac{\epsilon}{4\hbar^2} + \left[\left(M_{qq}\cdot(p(t)-\bar{p}) - M_{pq}\cdot(q(t)-\bar{q}) - p + \bar{p}\right)^2 \left(M_{qp}\cdot(p(t)-\bar{p}) - M_{pp}\cdot(q(t)-\bar{q}) + q - \bar{q}\right)^2\right]\right\}. \quad (13)$$

2.3. Cellularized frozen Gaussian approach

Another method based on the Filinov transformation, is the cellularized frozen Gaussian approximation (CFGA) of Walton and Manolopoulos [6]. Since the expansions used in deriving the CFGA are to a higher order than those used for the SPHK, it is possible that the CFGA will be able to obtain the correct result for larger ϵ, and hence require fewer trajectories.

The CFGA result is [6]

$$C^{sc}_{CFGA}(t) = \left(\frac{1}{2\pi\hbar}\right)^d \int\int dp\, dq R_{pqt} e^{iS_{pqt}/\hbar} \times \left(\frac{(4\epsilon)^{-2d}}{\det[A_{pqt}]}\right)^{1/2} \times \exp\left(\tfrac{1}{4} b^T_{pqt} A^{-1}_{pqt} b_{pqt} - c_{pqt}\right), \quad (14)$$

where

$$A_{pqt} = \begin{pmatrix} A_{qq} & A_{qp} \\ A_{pq} & A_{pp} \end{pmatrix} \quad (15)$$

$$A_{qq} = \frac{\alpha}{2} M^T_{qq} M_{qq} + \frac{1}{8\alpha\hbar^2} M^T_{pq} M_{pq} + \left(\frac{\alpha}{2} + \frac{1}{4\epsilon}\right) I, \quad (16)$$

$$A_{qp} = \frac{\alpha}{2} M^T_{qq} M_{qp} + \frac{1}{8\alpha\hbar^2} M^T_{pq} M_{pp}, \quad (17)$$

$$A_{pq} = \frac{\alpha}{2} M^T_{qp} M_{qq} + \frac{1}{8\alpha\hbar^2} M^T_{pp} M_{pq}, \quad (18)$$

$$A_{pp} = \frac{\alpha}{2} M^T_{qp} M_{qp} + \frac{1}{8\alpha\hbar^2} M^T_{pp} M_{pp} + \left(\frac{1}{8\alpha\hbar^2} + \frac{1}{4\epsilon}\right) I, \quad (19)$$

$$b_{pqt} = \begin{pmatrix} b_q \\ b_p \end{pmatrix}, \quad (20)$$

$$b_q = \alpha\left[M_{qq}^T(q(t)-\bar{q})+(q-\bar{q})\right] + \frac{1}{4\alpha\hbar^2}\left[M_{pq}^T(p(t)-\bar{p})\right] + \frac{i}{2\hbar}\left[M_{pq}^T(q(t)-\bar{q}) - M_{qq}(p(t)-\bar{p}) + (p-\bar{p})\right], \quad (21)$$

$$b_p = \alpha\left[M_{qp}^T(q(t)-\bar{q})\right] + \frac{1}{4\alpha\hbar^2} \times\left[M_{pp}^T(p(t)-\bar{p})+(p-\bar{p})\right] + \frac{i}{2\hbar}\left[M_{pp}^T(q(t)-\bar{q}) - M_{qp}(p(t)-\bar{p}) - (q-\bar{q})\right], \quad (22)$$

$$c_{pqt} = \frac{\alpha}{2}\left[(q(t)-\bar{q})^2+(q-\bar{q})^2\right] + \frac{1}{8\alpha\hbar^2}\left[(p(t)-\bar{p})^2+(p-\bar{p})^2\right] + \frac{i}{2\hbar}\left[(p(t)+\bar{p})^T(q(t)-\bar{q}) - (p+\bar{p})^T(q-\bar{q})\right]. \quad (23)$$

Although the CFGA introduces significant numerical complexity, it has been used successfully to treat 2- and 3-dimensional bound-state systems [6], and to obtain the photodissociation spectrum of Ar_nI^- [22].

2.4. Stationary-phase Monte Carlo

A non-HK-based propagator can also be used. We consider the method of Campolieti and Brumer [13] which uses the first-order stationary-phase method applied to the coordinate-based expression for $C(t)$. Methods of this type have been successfully used to treat both non-chaotic and chaotic systems [4,13,19,23]. This coordinate propagator yields the following result for the autocorrelation function [5]

$$C^{sc}(t) = \left(\frac{1}{2\pi i\hbar}\right)^{d/2} \times\int\int dp\, dq\, |\det M_{qp}|^{1/2} e^{iS_{pqt}/\hbar} e^{i\pi\nu/2} \times\Psi_0^*(q)\Psi_0(q(t)), \quad (24)$$

Table 1
Numerical details associated with the spectra in Figs. 1–3 for the three systems studied

	Parameters	Number of trajectories	Average (t_f)	Trajectories truncated
HH Case 1				
SPHK	$\epsilon = 10^{-3}$	2000	428	0
SPMC	$\epsilon = 10^{-2}$	10000	428	0
CFGA	$\epsilon = 10^{-3}$	2000	421	8
HKK	$D_t = 5000$	2000	374	24
HH Case 2				
SPHK	$\epsilon = 10^{-4}$	40000	304	0
SPMC	$\epsilon = 10^{-3}$	80000	304	0
CFGA	$\epsilon = 10^{-4}$	40000	241	32
HKK	$D_t = 1000$	40000	133	71
Quartic oscillator				
SPHK	$\epsilon = 10^{-6}$	100000	50	0
SPMC	$\epsilon = 10^{-5}$	200000	50	0
CFGA	$\epsilon = 10^{-5}$	100000	6	100
HKK	$D_t = 100e^{0.2t}$	100000	6	99

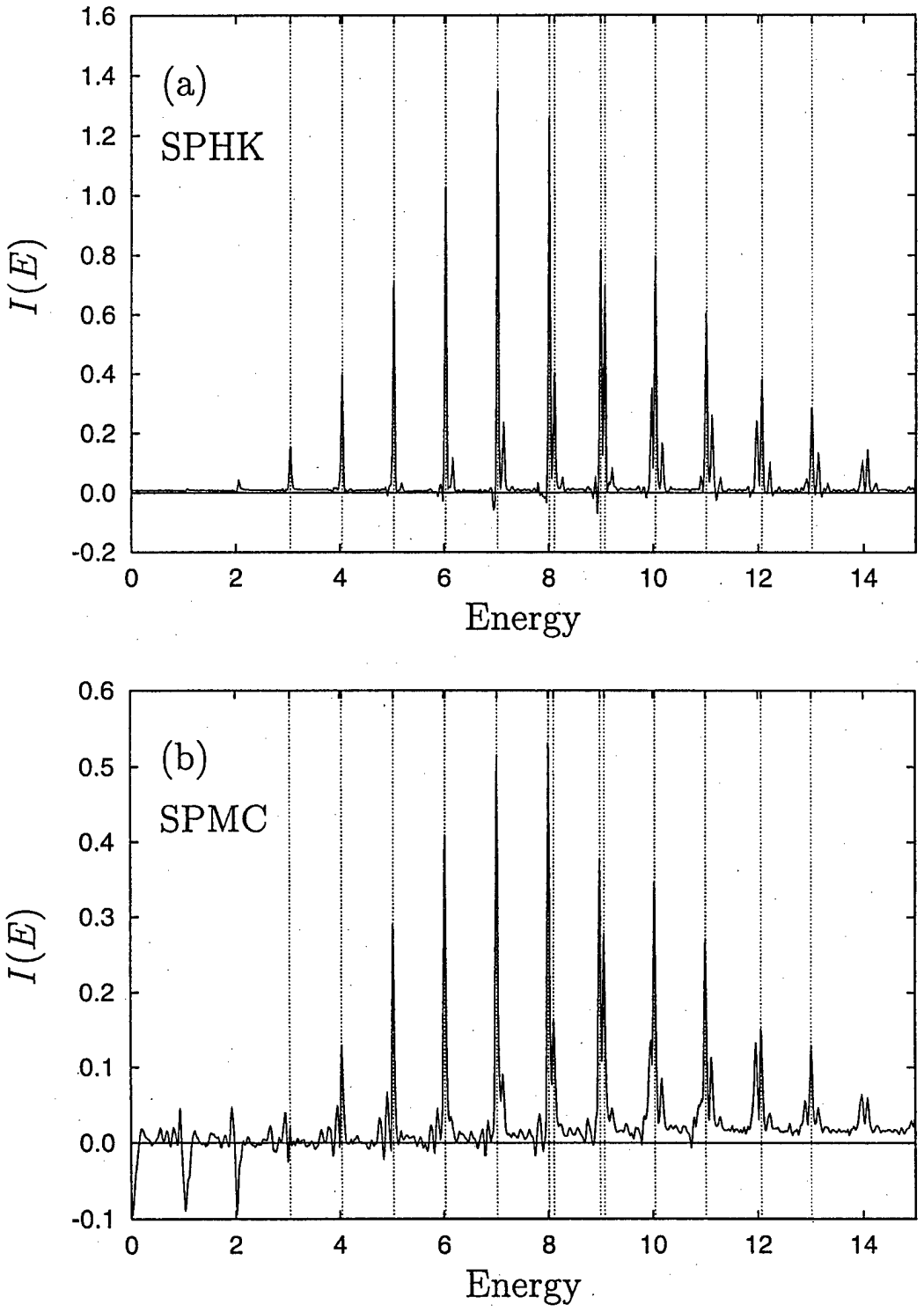

Fig. 1. HH Case 1. The vertical lines are some of the dominant quantum eigenvalues [6], although the additional peaks (above the noise) also reproduce the quantum result.

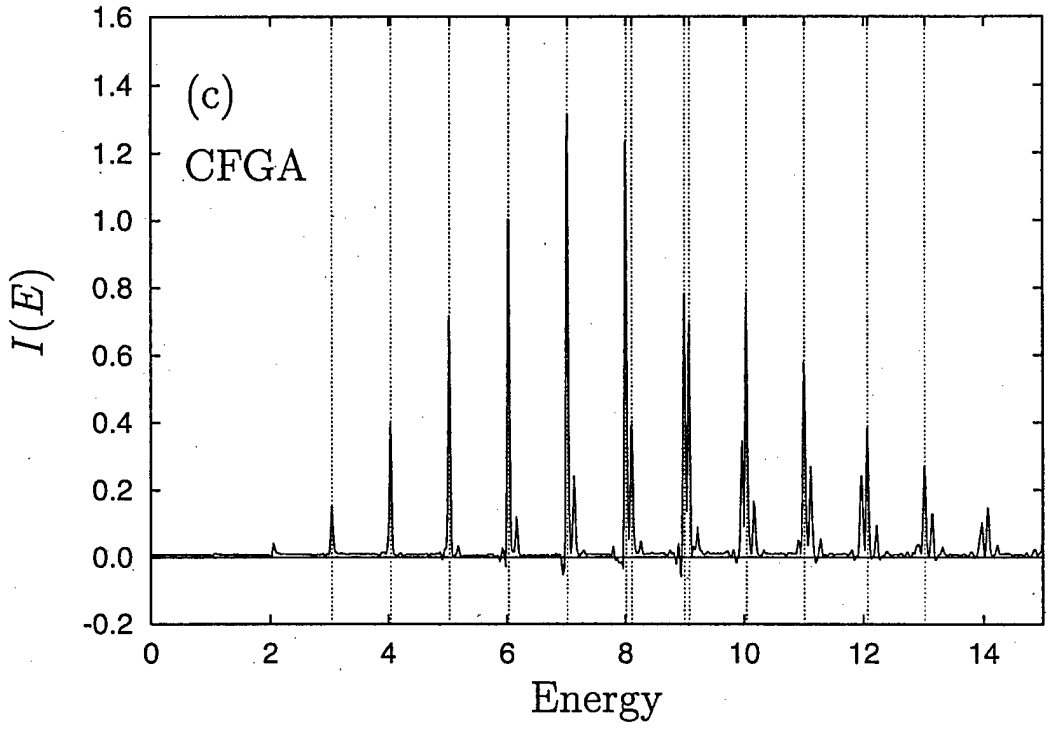

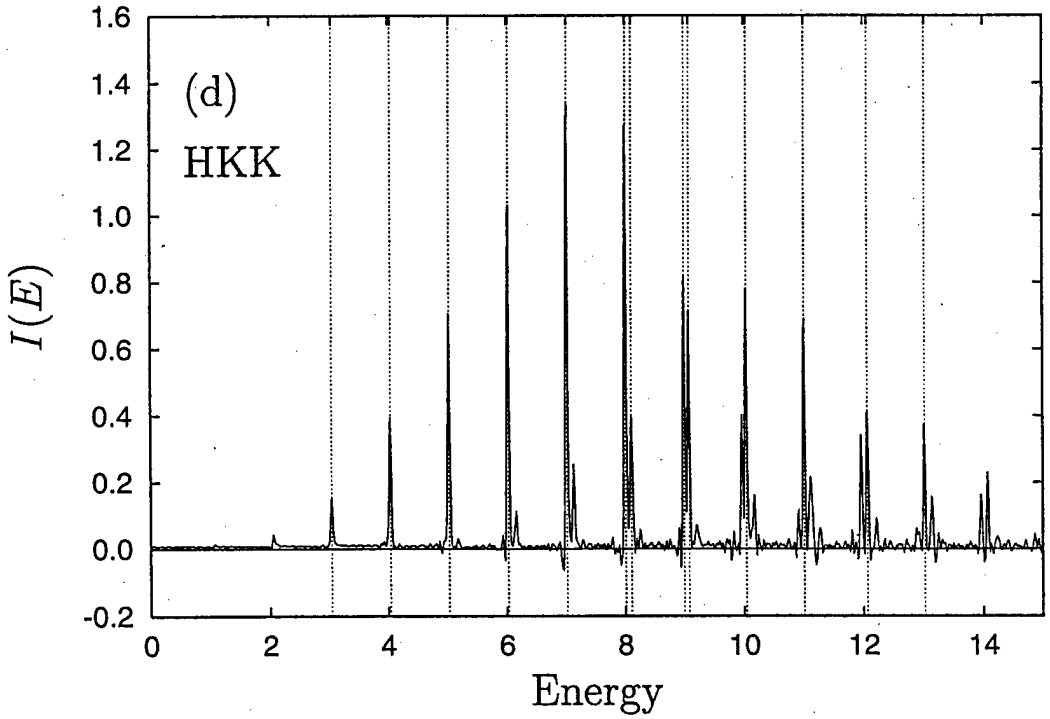

Fig. 1 (continued).

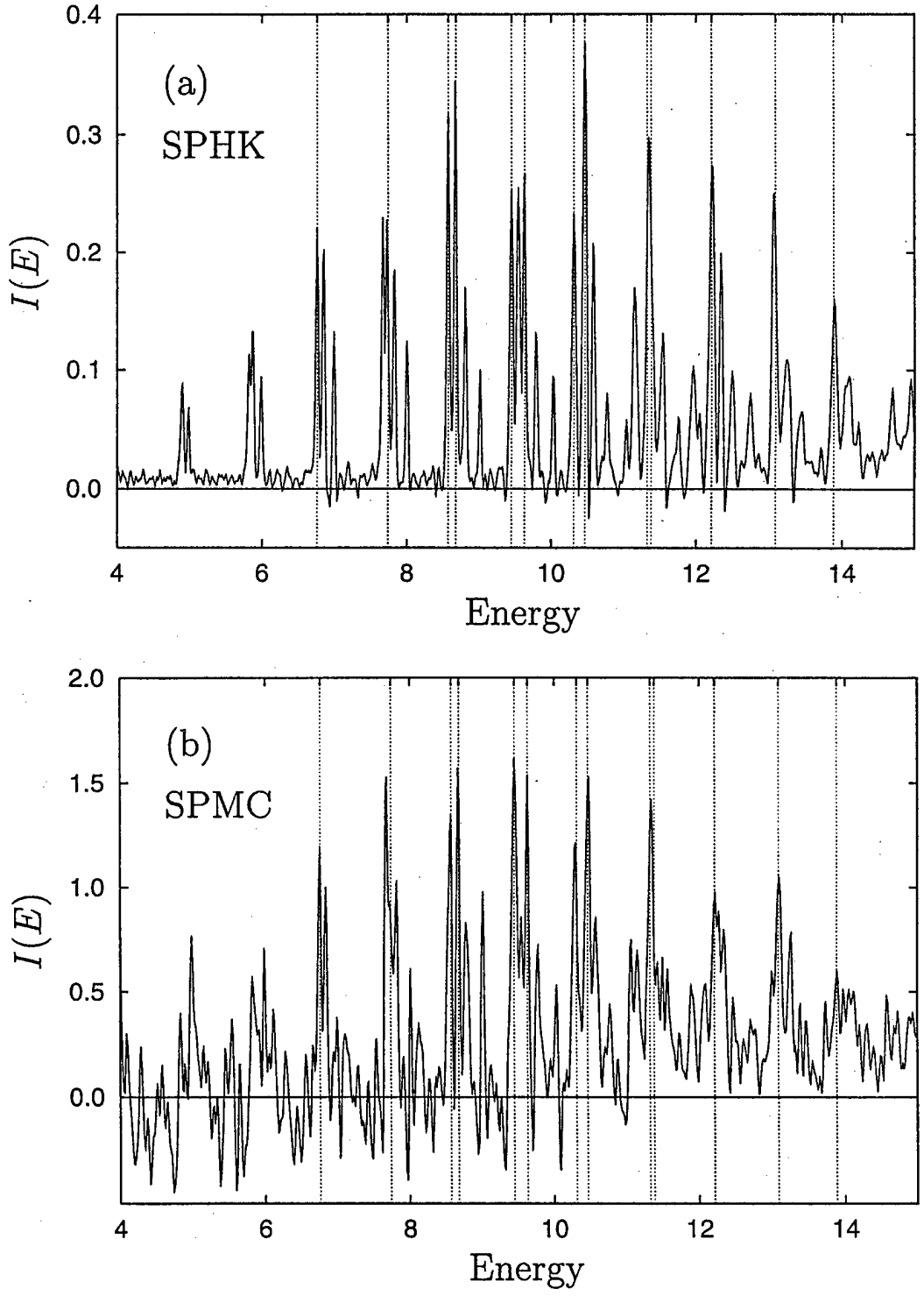

Fig. 2. HH Case 2. The vertical lines are some of the dominant quantum eigenvalues [6], although the additional peaks (above the noise) also reproduce the quantum result.

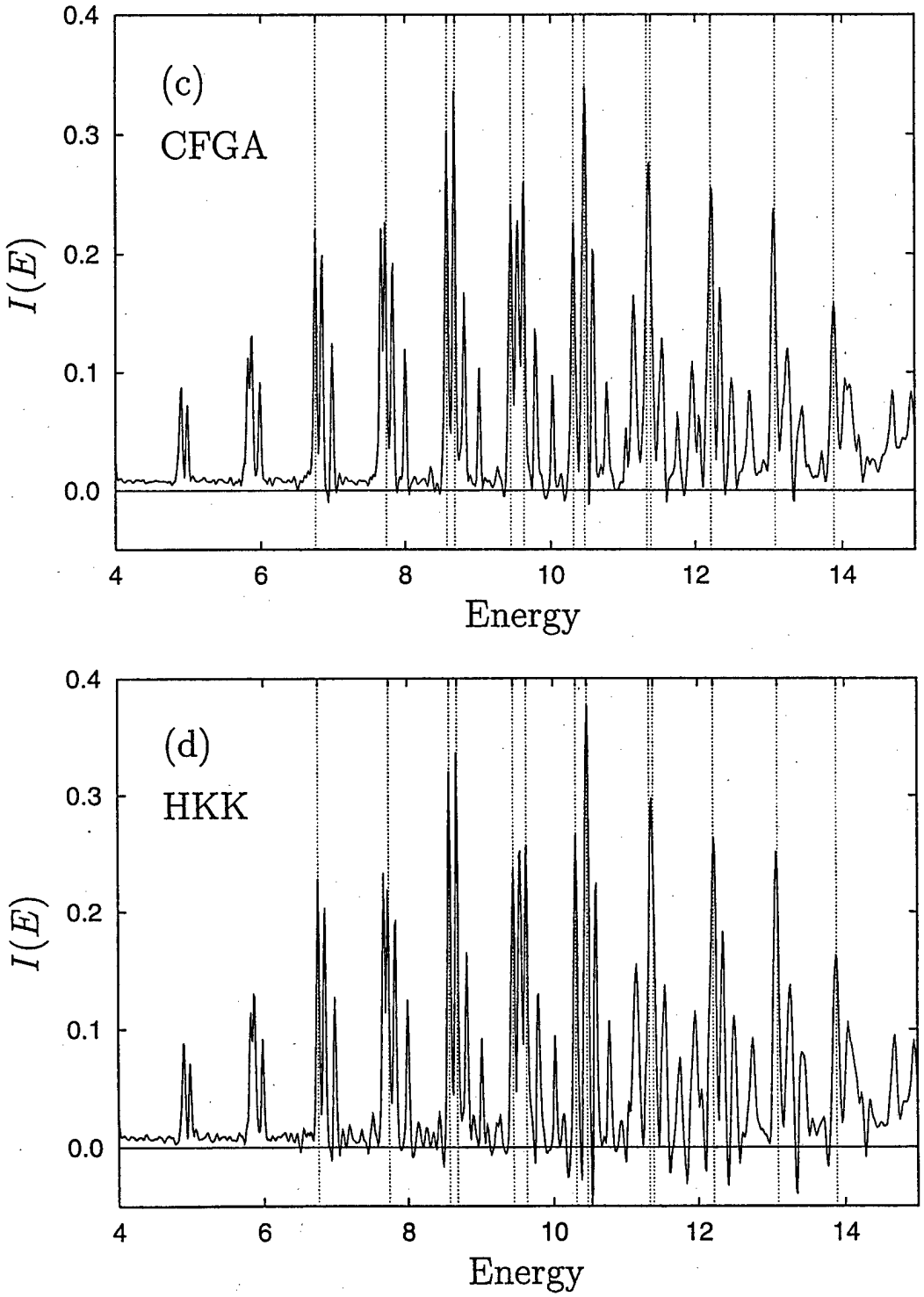

Fig. 2 (continued).

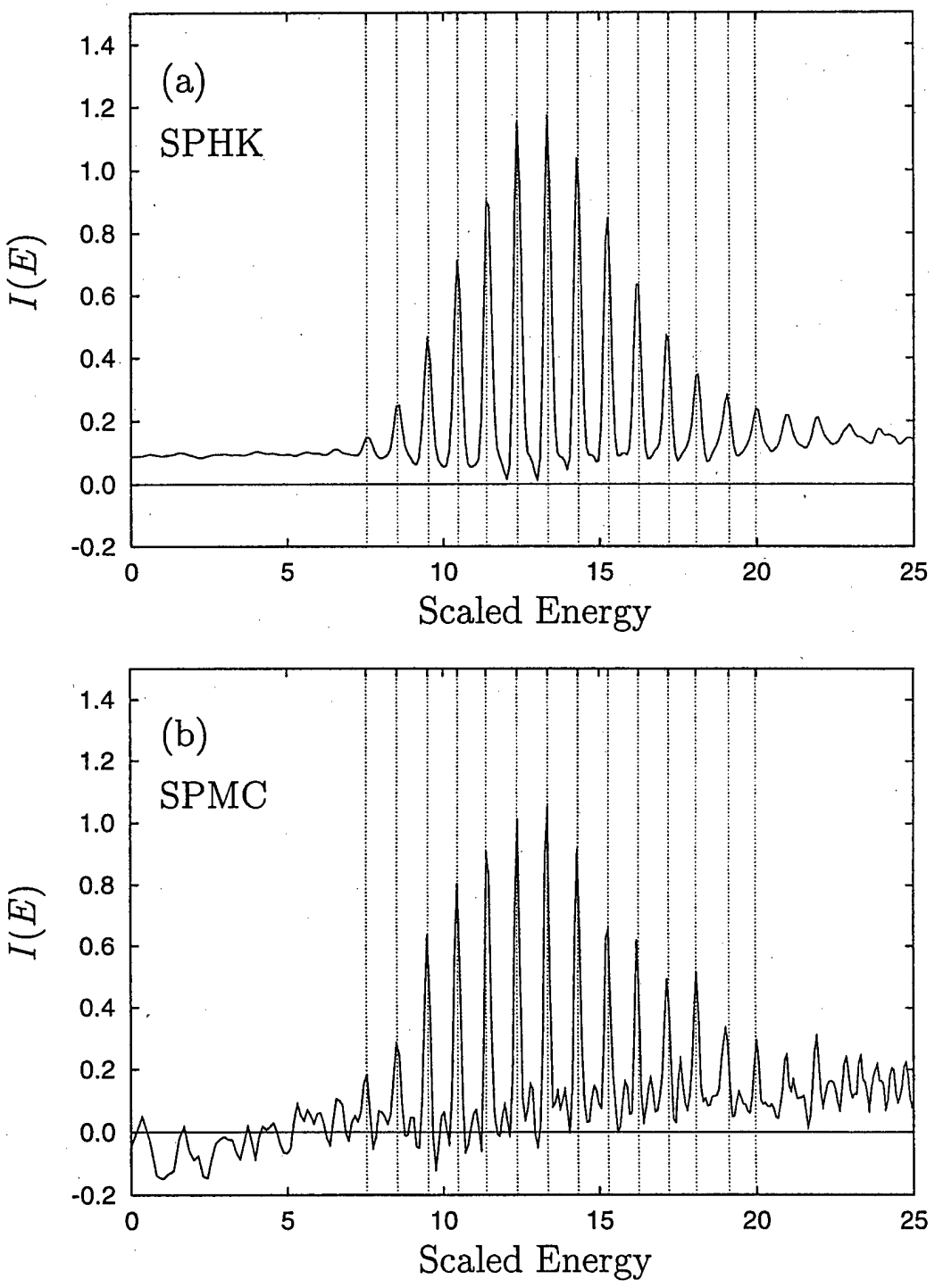

Fig. 3. Quartic oscillator. The vertical lines are some of the dominant quantum eigenvalues [28], although the additional peaks (above the noise) also reproduce the quantum result.

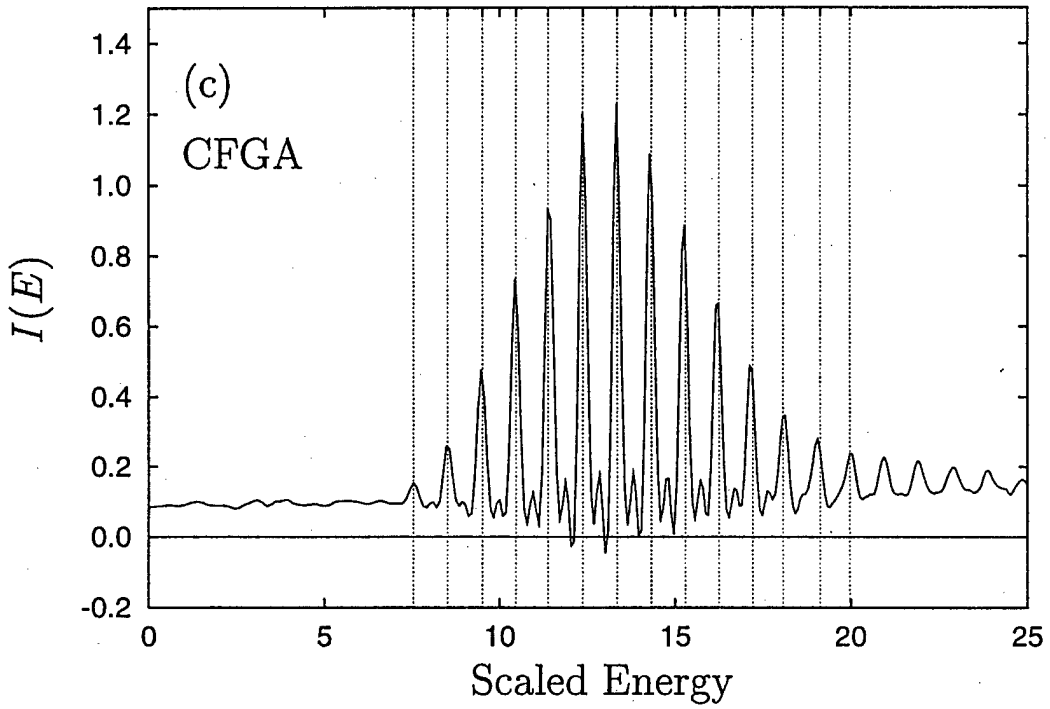

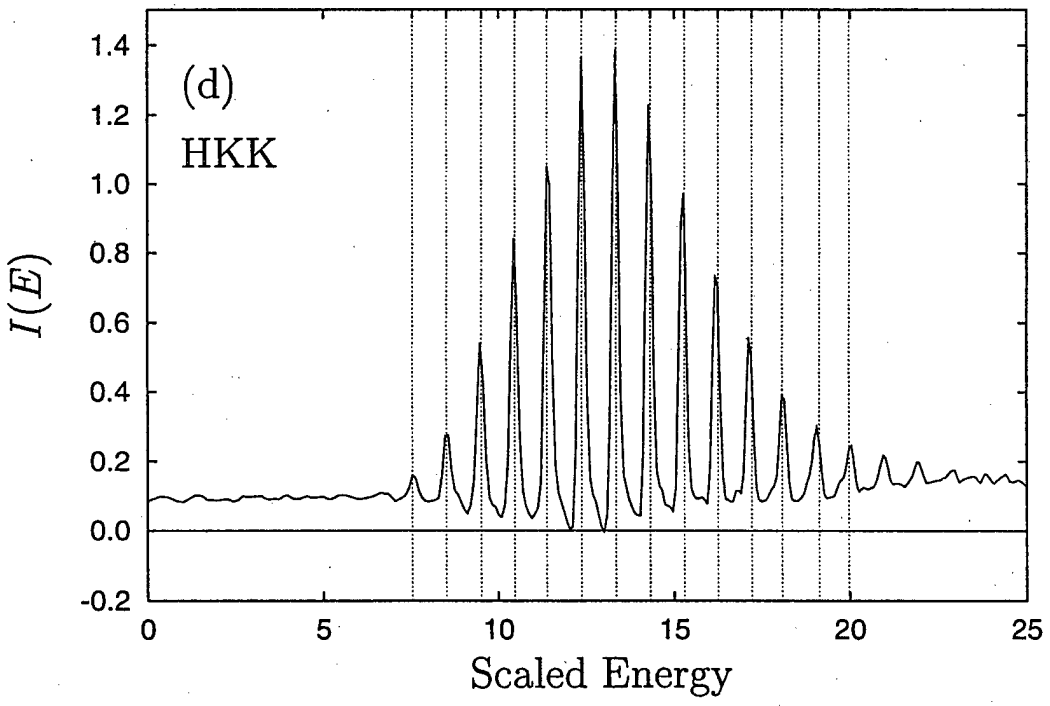

Fig. 3 (continued).

where ν is the Maslov index and the initial wavefunction is given by Eq. (2). Applying a stationary-phase procedure to Eq. (24) similar to that which generated Eq. (12) from Eq. (9), gives the sta-

tionary-phase Monte Carlo (SPMC) result (it is assumed that the Maslov index is constant within phase-space regions)

$$C^{sc}_{SPMC}(t) = \left(\frac{\alpha}{\pi^2 i\hbar}\right)^{d/2} \times \int\int dp\, dq\, |\det M_{qp}|^{1/2} e^{iS_{pqt}/\hbar} e^{i\pi\nu/2} \times D_{\epsilon p q t} \exp\left[-\alpha|q-\bar{q}|^2 - \alpha|q(t)-\bar{q}|^2 + i(q(t)-q)\cdot\bar{p}/\hbar\right], \quad (25)$$

where

$$D_{\epsilon p q t} = \exp\left\{-\frac{\epsilon}{\hbar^2}\left[\left(M_{qq}\cdot(p(t)+\bar{p})-(p+\bar{p})\right)^2 + \left(M_{qp}\cdot(p(t)+\bar{p})\right)^2\right]\right\}. \quad (26)$$

This result is quite different from the methods based on Herman–Kluk. In particular, the p and q are treated differently in this equation. Specifically the p integration does not benefit from a Gaussian decay factor. In addition, the $t \to 0$ limit of Eq. (24) is not obvious (it does, in fact, reproduce the result $C^{sc}(0) = 1$ [5]). These two considerations are drawbacks of the SPMC method.

The differences between the stationary-phase conditions for SPHK and SPMC should also be noted. For SPHK, the phase contains a momentum dependence which is not in the SPMC. This results in a stationary-phase term (Eq. (13)) which is more symmetric in coordinate and momentum than that for SPMC (Eq. (26)). The SPHK is therefore expected to be better at damping down regions of phase space which contribute a negligible amount to the integral.

3. Results and discussion

3.1. Essentially bound systems

In Section 3.1, we compare results for these four semiclassical IVR methods as applied to increasingly chaotic 2-dimensional bound-state systems. In each case, the IVR integrals are evaluated by Monte Carlo integration. A box Muller transformation [24] is used to perform the p and q integrals for the HK-based methods (HKK, CFGA, SPHK), and the q integral in the SPMC method. The p integral in the SPMC method is carried out using a simple Monte Carlo method over a rectangular region. The spectra are found from the autocorrelation function by an FFT [24], and are artificially broadened to be consistent with previous treatments using a windowing function $W(t) = \exp[-t^2/(2W_T^2)]$.

We consider two cases, a modified HH Hamiltonian and a quartic oscillator, where the Hamiltonian $H = (1/2)p^2 + V(q)$ and where $\hbar = 1$. The modified 2-dimensional HH system [25] has the potential

$$V(q_x, q_y) = \tfrac{1}{2}w_x^2 q_x^2 + \tfrac{1}{2}w_y^2 q_y^2 + \lambda q_x^2 q_y - \mu q_y^3. \quad (27)$$

We consider two parameter sets [1,6]: Case 1 has $w_x = 1.1$, $w_y = 1$, $\lambda = -0.11$, $\mu = 0.0$, $\alpha = 0.5$, $\bar{q}_x = 0$, $\bar{q}_y = 4$, $\bar{p} = 0$, $W_T = 57.0$; Case 2 has $w_x = w_y = 1$, $\lambda = 0.111803$, $\mu = 0.037268$, $\alpha = 0.5$, $\bar{q}_x = 0$, $\bar{q}_y = -1.914$, $\bar{p}_x = 3.976$, $\bar{p}_y = 0.961$, $W_T = 57.0$. The average Lyapunov exponents for the two cases are 0.2 and 0.16, respectively. That is, these systems are only mildly chaotic. The systems have dissociative classical trajectories above $E_d \sim 15.125$ and 13.333, respectively. Such trajectories are included in the phase-space average only up until the time of dissociation. The final time is taken as $T = 450$.

The quartic oscillator, which is much more chaotic than the HH potential [26,27], has [28]

$$V(q_x, q_y) = \tfrac{1}{2}q_x^2 q_y^2 + \frac{\beta}{4}\left(q_x^4 + q_y^4\right), \quad (28)$$

with [12] $\beta = 0.01$, $\alpha = 0.5$, $\bar{q}_x = 0$, $\bar{q}_y = 8.32$, $\bar{p} = 0, W_T = 17.7$. For the quartic oscillator, the results are presented in terms of the scaled energy, $(2E)^{3/4}$ [28]. In this case, the average Lyapunov exponent is 0.8, which is an order of magnitude larger than for the least chaotic HH case considered. Since the

Table 2
Average Lyapunov exponent and number of trajectories to converge the spectrum using the SPHK method

	λ	No. of trajectories
HH Case 1	0.02	2000
HH Case 2	0.16	40000
Quartic Case 2[a]	0.83	100000
Quartic Case 1	0.93	100000

[a] $\beta = 0.01, \alpha = 2.0, \bar{q}_x = 0, \bar{q}_y = 5.0, \bar{p}_x = 5.0, \bar{p}_y = 0, \epsilon = 10^{-6}$.

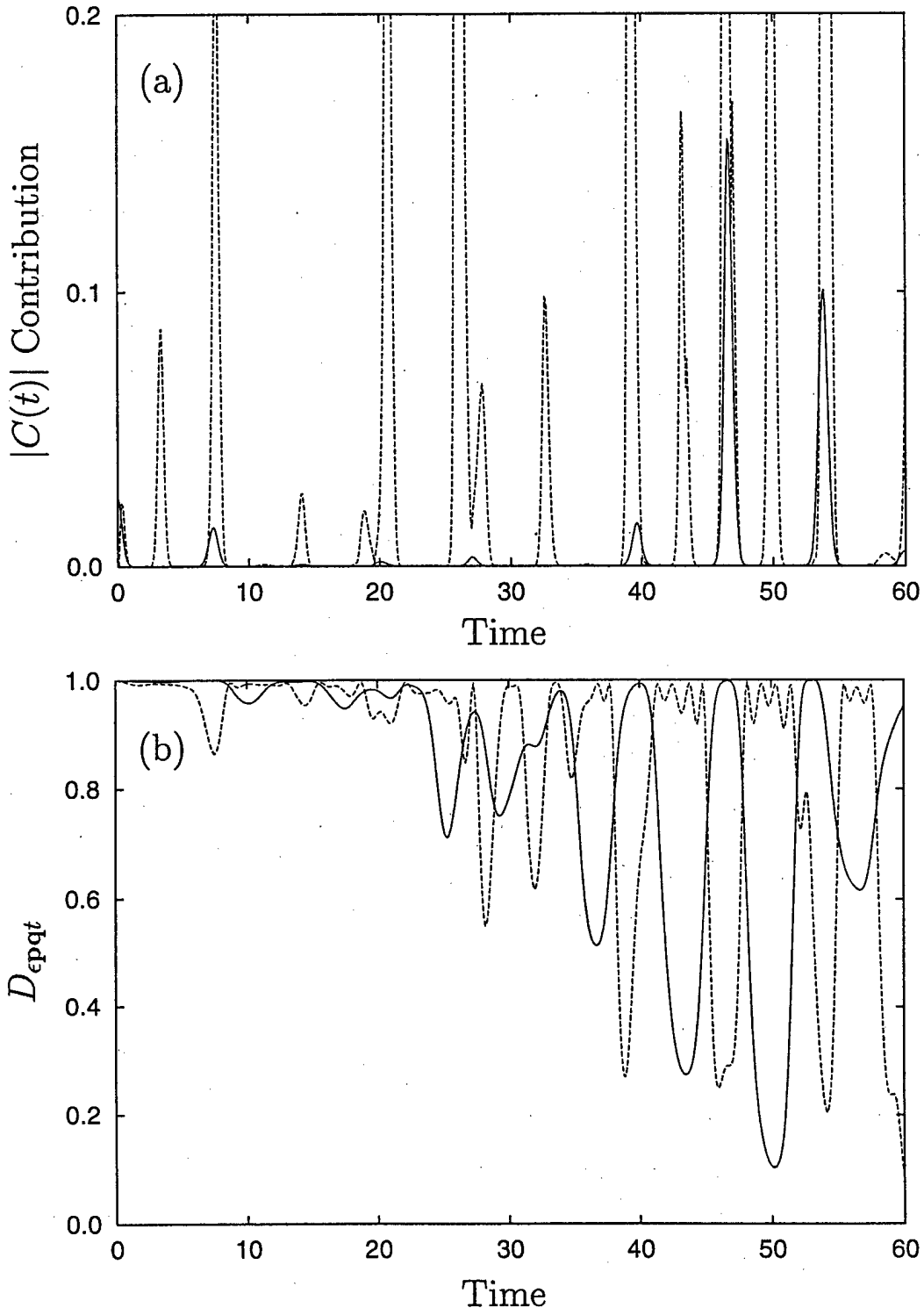

Fig. 4. (a) Single trajectory contributions to $|C(t)|$ and (b) the stationary-phase damping term ($D_{\epsilon p\, q t}$) with $\epsilon = 10^{-7}$ for HH Case 2 (Eqs. (13) and (26)); solid lines are SPHK, dashed lines are SPMC. The initial conditions for the trajectory are $q = \bar{q}, p = \bar{p}$. For ease of comparison, the $D_{\epsilon p\, q t}$ term is not included in the $|C(t)|$ contribution.

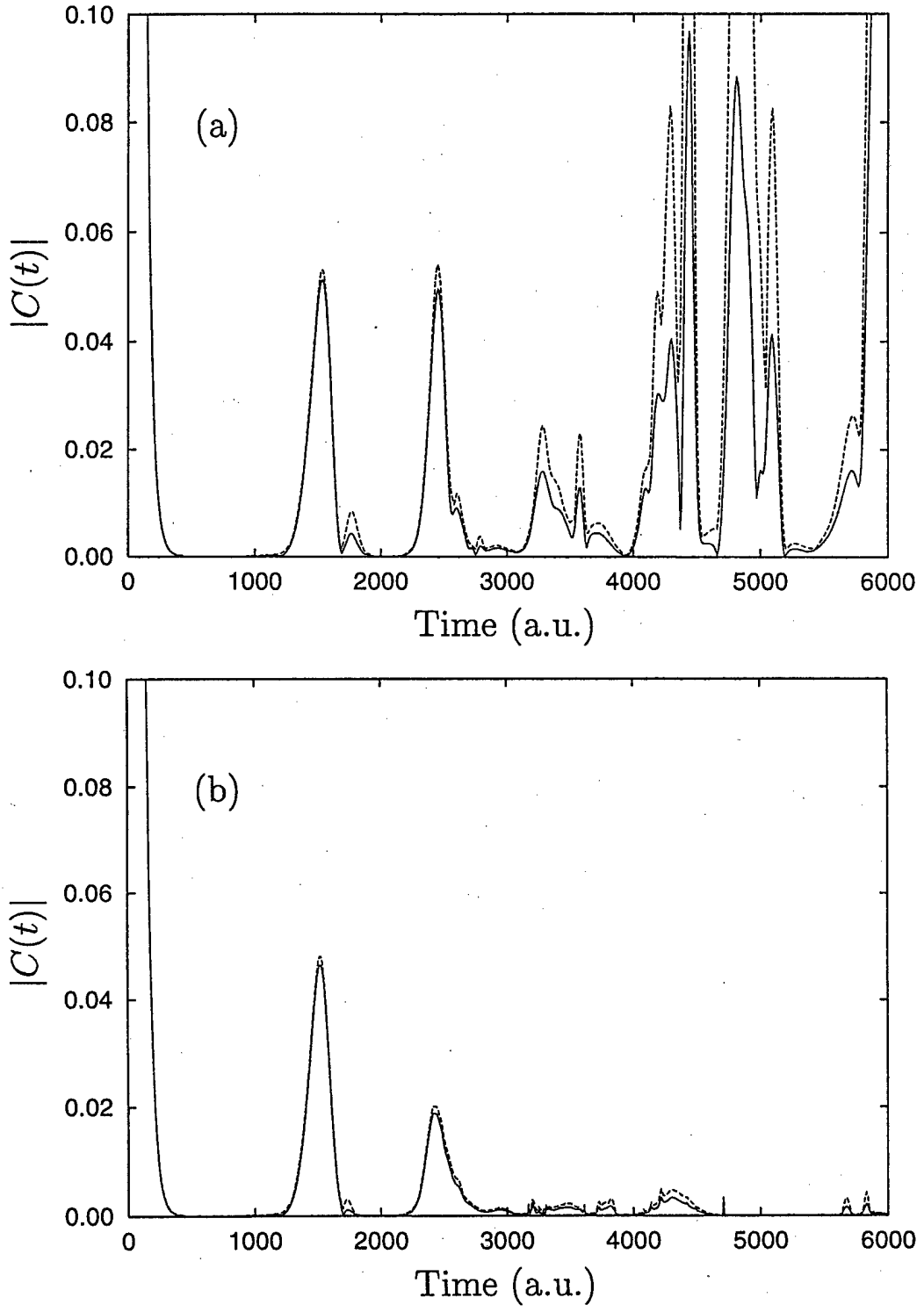

Fig. 5. Results for CO_2 photodissociation with 10^6 trajectories: (a) HK autocorrelation, dashed line is one standard deviation error in the Monte Carlo sum; (b) SPHK autocorrelation with $\epsilon = 10^{-7}$; (c) HK spectrum (dash) and SPHK spectrum (solid).

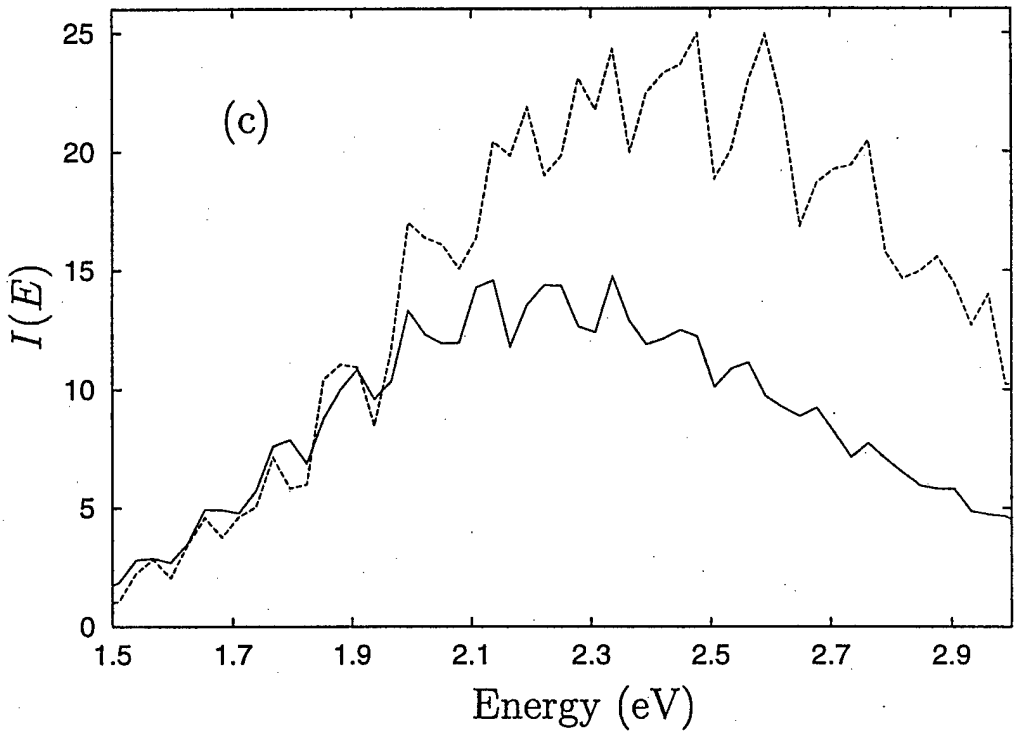

Fig. 5 (continued).

quartic oscillator is a confining potential, no trajectories dissociate. The final time is taken as $T = 50$.

The quartic oscillator posseses C_{4v} symmetry [29], and we only consider states with A_1 symmetry, i.e. wavefunctions which are symmetric under reflections across the axes and symmetric under reflections across the diagonals. An arbitrary function G can be modified in the following manner to satisfy A_1 symmetry

$$\begin{aligned}
&\hat{p}_{A_1} G(\bar{q}_x,\bar{p}_x,\bar{q}_y,\bar{p}_y) \\
&\quad = G(\bar{q}_x,\bar{p}_x,\bar{q}_y,\bar{p}_y) + G(-\bar{q}_y,-\bar{p}_y,\bar{q}_x,\bar{p}_x) \\
&\qquad + G(\bar{q}_y,\bar{p}_y,-\bar{q}_x,-\bar{p}_x) \\
&\qquad + G(-\bar{q}_x,-\bar{p}_x,-\bar{q}_y,-\bar{p}_y) \\
&\qquad + G(-\bar{q}_x,-\bar{p}_x,\bar{q}_y,\bar{p}_y) \\
&\qquad + G(\bar{q}_x,\bar{p}_x,-\bar{q}_y,-\bar{p}_y) \\
&\qquad + G(\bar{q}_y,\bar{p}_y,\bar{q}_x,\bar{p}_x) \\
&\qquad + G(-\bar{q}_y,-\bar{p}_y,-\bar{q}_x,-\bar{p}_x). \qquad (29)
\end{aligned}$$

Thus, our initial Gaussian wavefunction is replaced by the sum of eight Gaussians.

Table 1 contains the values of the adjustable parameters, the number of trajectories, the average final time (t_f) of the trajectories, and the percent of trajectories truncated for each of the cases studied. Note that although the CFGA method does not explicitly call for discarding trajectories, we found that the complex matrix manipulations required the truncation of trajectories in order to obtain results (these matrix manipulations have previously been noted as a possible weakness, confirmed herein, by Garashchuk and Tannor [9]). Specifically, we found that for some chaotic trajectories the matrix A_{pqt} would grow to such a size as to make inversion inaccurate. If these trajectories were not truncated then the integrand grew to infinity and the results became meaningless. Note also that the data in Table 1 makes clear that the SPMC method requires 2–5 times the number of trajectories than does the HK-based methods to achieve convergence.

The resultant $I(E)$ for all cases is shown in Figs. 1 and 3. The results are all in good agreement with

the quantum $I(E)$ [6,12] except for the extra noise seen in the SPMC results. Further, a comparison of the $I(E)$ in Figs. 1 and 3 makes clear that all the HK-based methods are in basic agreement with one another. By contrast, the SPMC results are somewhat noisier even though the method utilizes more trajectories.

Table 2 shows a comparison of the Lyapunov exponent and the number of trajectories required for convergence. Clearly, increasing λ necessitates a larger trajectory sample. As is evident from Fig. 3, however, the system with the largest λ need not display the most chaotic spectrum (compare Fig. 2 and Fig. 3). Rather, in the case of the quartic oscillator, a large number of trajectories had to be run in order to expose the underlying, simple autocorrelation function. Indeed, for the quartic oscillator the HKK methods obtains results with only very short time trajectories. This is because the correct quartic oscillator autocorrelation function is quasiperiodic, so that a nearly correct spectrum would result from a computation over a single period. This is not, however, a general result. For example, the HH system requires the proper computation of a large number of resonances since the autocorrelation function is not quasiperiodic.

Also of interest is the extent to which spectral results can be obtained with a small number of trajectories. In general, the spectrum which results from using fewer trajectories is noisier. However, in many cases it is possible to determine the eigenvalues to sufficient accuracy with far fewer trajectories than reported in Table 1. For example, all HK-based methods gave good results for the HH Case 1 with as few as 500 trajectories. Similarly, the SPHK quartic oscillator spectrum ($\epsilon = 10^{-6}$) can be estimated quite accurately using only 10^4 trajectories. However, convergence is only attained with 10^5 trajectories.

Finally, we comment on the inefficiency of the SPMC method. This is due to the lack of localization of the $\boldsymbol{p}$ integration. That is, since the integrand does not contain localizing terms of the form $\exp[-\xi(\boldsymbol{p}-\bar{\boldsymbol{p}})^2]$ or $\exp[-\xi(\boldsymbol{p}(t)-\bar{\boldsymbol{p}})^2]$, the SPMC relies to a greater degree on numerical cancellation than do the HK methods. For example, Fig. 4 shows the difference in single trajectory contributions to the SPMC and the SPHK methods. Specifically, the single trajectory contribution to the autocorrelation (Fig. 4a) is seen to be both much larger and have more peaks for the SPMC. Some of these peaks will have to be cancelled by contributions from other trajectories in order to obtain a near zero result, which the SPHK obtains automatically. The stationary-phase damping term $D_{\epsilon pqt}$ (Fig. 4b) is also seen to be smoother and spends less time near unity for the SPHK, due to the extra terms in Eq. (13) which are not present in Eq. (26). The stationary-phase procedure therefore achieves better damping of chaotic trajectories for the SPHK than it does for the SPMC.

3.2. Photodissociation

Our particular interest is in the use of IVR techniques for coherent control [30] and hence for processes like photodissociation. Previous studies of 3D photodissociation using the SPMC method [31] showed good results but required many trajectories. In an effort to see the utility of other IVR methods we consider collinear CO_2, a system which has been previously examined in great detail [11,32–34]. In particular, we compare the HK and SPHK approaches to explore the effect of the stationary-phase method. CO_2 provides an interesting case because its spectrum depends heavily on a relatively small number of periodic orbits [33,34]. For example, Walton and Manolopoulos studied collinear CO_2 using the HK formalism [11], and required 10^8 trajectories for convergence, due to both periodic orbits (specifically, the symmetric stretch motion), as well as the dissociative nature of the system. Here we extend the SPHK to photodissociation and demonstrate substantially improved efficiency over the HK approach.

The model CO_2 Hamiltonian is given by [33]

$$H = \frac{1}{2\mu}p^2 - \frac{1}{m_C}p_1 p_2 + V(R_1, R_2) \tag{30}$$

where R_1 and R_2 are CO and OC interatomic distances, and $\mu = m_O m_C/(m_O + m_C)$. The potential used is the LEPS potential [35], parameters are taken from Ref. [32], and energy is measured relative to CO_2 dissociation. The initial state of the system is given by Eq. (2), with equilibrium separation $R_e = \bar{q}_1 = \bar{q}_2 = 2.20\ a_0$, $\bar{p} = 0$ a.u., $\alpha = 69.2\ a_0^{-2}$. The CO_2 spectrum was computed with $\epsilon = 10^{-7}$ from

the autocorrelation function with no windowing function.

Fig. 5 shows the autocorrelation and spectrum obtained using 10^6 trajectories for both the HK and the SPHK methods. As can be seen from Fig. 5a, the HK autocorrelation has not converged for large times, resulting in an inaccurate representation of the spectrum (Fig. 5c). By contrast, the SPHK autocorrelation is well converged (Fig. 5b), and the associated spectrum is in good agreement with quantum results [32], allowing for accurate estimates of the energy eigenvalues (Fig. 5c). Thus, the autocorrelation and associated eigenvalues can be estimated using the SPHK with two orders of magnitude fewer trajectories than that required by the HK method.

The extent to which this spectrum agrees with the true quantum spectrum was found to depend greatly on the choice of ϵ. If ϵ is chosen too large, important long time information can be lost (cf. Section 2). Note, however, that even though the autocorrelation in Fig. 5b does not contain the actual structure of the correct CO_2 autocorrelation for times greater than 3000 a.u. (due to an insufficient number of trajectories), it does contain enough of the actual autocorrelation structure to provide good results for the photodissociation spectrum (computed from all time points). This is largely due to the simplicity of the CO_2 autocorrelation.

Finally, since periodic orbits are important in the CO_2 system, we note the effect of the stationary-phase procedure on periodic orbits. For the important symmetric stretch periodic orbits in the CO_2 system, $D_{\epsilon p\, q t} \sim 1$ for $\epsilon = 10^{-7}$, so the SPHK procedure includes the symmetric stretch effects which are essentially unmodified from the HK results. This is quite different from a HKK treatment which would have discarded the trajectory once the prefactor $R_{p\, q t}$ became large. Trajectories which return to the Frank–Condon region but which are far from periodic have $D_{\epsilon p\, q t} \sim 0$.

4. Conclusions

We have applied four semiclassical IVR methods to a number of chaotic systems, in order to determine the method with best overall performance. All methods gave reasonable spectra but differed in utility.

The SPMC method required more trajectories than any of the HK-based results, due to the lack of a Gaussian damping function on the p integral in Eq. (24). Further, the noise in the resultant $I(E)$ was considerable, and an expression which is not numerically tractable at $t = 0$ made this the least effective method of those studied.

The CFGA method also suffers from numerical difficulties involving matrix inversion when the trajectories are chaotic. It required the truncation of trajectories, a procedure which we prefer to avoid.

The HKK is still seen to be a good method for chaotic systems, although the trajectory truncation procedure remains unsatisfying. Nonetheless, this relatively simple method was able to provide results which matched the quality of the more numerically ambitious methods.

The most successful of the four methods for calculating the bound-state Frank–Condon spectrum is the SPHK. It produced accurate results and did not require the truncation of any trajectories. It also produced good estimates of the spectrum for collinear CO_2 photodissociation and required a relatively small number of trajectories. The SPHK is able to determine the autocorrelation for chaotic systems very accurately, and requires only a small amount of numerical calculation beyond that of the HK method. Further, the SPHK method is such that if greater accuracy is required one can decrease the smoothing parameter ϵ giving a result approaching that of the converged HK method. The ability of SPHK to give reasonable results for a small number of trajectories is useful for initial treatments of systems, and also allows some systems to be solved accurately using only modest computing power.

The HK-based methods were found to be especially well suited to the problem studied, where the overlap of the initial and time-evolved wavefunction is calculated. However, if one wishes to calculate the propagated wavefunction, then we note that HK-based methods require an integration over the full-phase space (q,p), whereas the SPMC requires only an integration over q-space. This extra integration may prove advantageous: Kay has shown [4], by calculating the overlap of the semiclassical wavefunction with the quantum wavefunction, that the HK for non-chaotic systems (and the HKK for chaotic systems [12]) produce very accurate propagated

wavefunctions. These results suggest that HK-based methods like the SPHK should be useful in obtaining more detailed properties of the system (such as photofragmentation matrix elements) which do not rely on an overlap with the initial state. Work in this direction is in progress.

Acknowledgements

The authors would like to thank Prof. Ken Kay (Bar-Ilan University) for a helpful communication regarding symmetry adaption for the quartic oscillator potential. This work was supported by the US Office of Naval Research and by the Natural Sciences and Engineering Research Council of Canada.

References

[1] E.J. Heller, J. Chem. Phys. 75 (1981) 2923.
[2] M.F. Herman, E. Kluk, Chem. Phys. 91 (1984) 27.
[3] K.G. Kay, J. Chem. Phys. 100 (1994) 4377.
[4] K.G. Kay, J. Chem. Phys. 100 (1994) 4432.
[5] G. Campolieti, P. Brumer, Phys. Rev. A 50 (1994) 997.
[6] A.R. Walton, D.E. Manolopoulos, Mol. Phys. 87 (1996) 961.
[7] M.F. Herman, Chem. Phys. Lett. 275 (1997) 445.
[8] J.H. Van Vleck, Proc. Natl. Acad. Sci. USA 14 (1928) 178.
[9] S. Garashchuk, D. Tannor, Chem. Phys. Lett. 262 (1996) 477.
[10] G. van de Sand, J.M. Rost, Phys. Rev. A. Rapid Comm. 59 (1999) R1723.
[11] A.R. Walton, D.E. Manolopoulos, Chem. Phys. Lett. 244 (1995) 448.
[12] K.G. Kay, J. Chem. Phys. 101 (1994) 2250.
[13] G. Campolieti, P. Brumer, J. Chem. Phys. 109 (1998) 2999.
[14] E.J. Heller, J. Chem. Phys. 68 (1978) 2066.
[15] E.J. Heller, J. Chem. Phys. 94 (1991) 2723.
[16] B.E. Guerin, M.F. Herman, Chem. Phys. Lett. 286 (1998) 361.
[17] N. Makri, W.H. Miller, Chem. Phys. Lett. 139 (1987) 10.
[18] N. Makri, W.H. Miller, J. Chem. Phys. 89 (1988) 2170.
[19] B.W. Spath, W.H. Miller, J. Chem. Phys. 104 (1996) 95.
[20] V.S. Batista, W.H. Miller, J. Chem. Phys. 108 (1998) 498.
[21] V.S. Filinov, Nucl. Phys. B 271 (1986) 717.
[22] M.L. Brewer, J.S. Hulme, D.E. Manolopoulos, J. Chem. Phys. 106 (1997) 4832.
[23] J. Cao, G.A. Voth, J. Chem. Phys. 104 (1996) 273.
[24] W.H. Press, S.A. Teukolsky, W.T. Vetterling, B.P. Flannery, Numerical Recipes: the Art of Scientific Computing, 2nd edn., Cambridge University Press, Cambridge, 1996.
[25] M. Hénon, C. Heiles, Astron. J 69 (1964) 73.
[26] H.D. Meyer, J. Chem. Phys. 84 (1986) 3147.
[27] A. Carnegie, I.C. Percival, J. Phys. A 17 (1983) 801.
[28] B. Eckhardt, G. Hose, E. Pollak, Phys. Rev. A 39 (1989) 3776.
[29] F.A. Cotton, Chemical Applications of Group Theory, Wiley–Interscience, New York, 1971.
[30] M. Shapiro, P. Brumer, Adv. Atomic Mol. Opt. Phys. 42 (2000) 287.
[31] G. Campolieti, P. Brumer, J. Chem. Phys. 107 (1997) 791.
[32] K.C. Kulander, J.C. Light, J. Chem. Phys. 73 (1980) 4337.
[33] R. Schinke, V. Engel, J. Chem. Phys. 93 (1990) 3252.
[34] K.C. Kulander, C. Cerjan, A.E. Orel, J. Chem. Phys. 94 (1991) 2571.
[35] S. Sato, J. Chem. Phys. 23 (1955) 592.

17

Coherently Controlled Asymmetric Synthesis with Achiral Light

Moshe Shapiro and Einat Frishman
Chemical Physics Department, The Weizmann Institute of Science, Rehovot, Israel 76100

Paul Brumer
Chemical Physics Theory Group, Department of Chemistry, University of Toronto, Toronto, Canada M5S 3H6

(Received 10 June 1999)

A laser-based method of increasing the enantiomeric excess of a chiral enantiomer in a racemic mixture is described. Neither the initial reagents nor the incident light need be chiral. Both formal and computational results show that enhancement of the enantiomer of choice, controlled by laser parameters, can be extensive.

PACS numbers: 31.10.+z, 33.80.–b

The existence of enantiomers, i.e., pairs of chiral molecules related to one another through inversion I, is one of the fundamental broken symmetries in nature [1]. It is also one of great practical importance because biological processes are often stereospecific, motivating a long-standing interest in asymmetric synthesis, i.e., molecular processes which preferentially produce one of the enantiomeric pairs.

It is a long-standing belief that asymmetric synthesis must necessary involve either reactants or reaction conditions which are chiral [2], i.e., display a decided handedness. Thus, for example, previous efforts to use light-matter interactions to alter the enantiomeric excess in a racemic mixture used either circular or elliptically polarized light [3]. Here we show that preferential production of a chiral molecule in a molecular process can occur even though neither the system Hamiltonian nor the initial conditions are chiral. In particular, we show that one can design *achiral* laser scenarios which encode quantum coherences in the molecule to selectively enhance the production of either the right- (denoted D) or left- (denoted L) handed enantiomer, even when starting with a racemic mixture.

To do so we consider a molecule with two enantiomers L and D, with a common excited electronic state whose potential surface, denoted G, is achiral [4]. This excited electronic state has stationary rovibrational states which are either symmetric or antisymmetric with respect to I. The scenario that we advocate, which is a significant extension of the coherent control approach [6,7], is described below. In particular, a racemic mixture of L and D is irradiated with a well-defined sequence of achiral coherent laser pulses to form a specified coherent superposition of rovibrational states of G. This excited system then returns to the ground electronic state by radiative emission. By successively irradiating the system and allowing radiative emission and collisional relaxation, we show that one can enhance the concentration of either enantiomer L or D by varying the laser pulse characteristics. We call this scenario the "laser distillation of chiral enantiomers."

Consider then the time dependent Schrödinger equation for a molecule with Hamiltonian H_M in the presence of a series of laser pulses. In general we may deal with lasers which are not fully coherent but for simplicity we focus here on transform limited pulses of linearly polarized light. The electric field, here comprised of two pulses, is given by $\mathbf{E}(t) = \sum_{k=0,1} \mathbf{E}_k(t) \equiv \sum_{k=0,1} 2\hat{\epsilon}_k \mathrm{Re}[\varepsilon_k(t) \exp(i\omega_k t)]$, where $\varepsilon_k(t)$ is the pulse envelope, ω_k is the central laser frequency, and $\hat{\epsilon}_k$ is the polarization direction. The time dependent Schrödinger equation is $i\hbar\partial|\Psi\rangle/\partial t = H_{\mathrm{tot}}(t)|\Psi\rangle$ with

$$H_{\mathrm{tot}}(t) = H_M - \sum_k \vec{\mu}_k \cdot \mathbf{E}_k(t), \tag{1}$$

and $\vec{\mu}_k$ is the transition-dipole moment for the electronic transition induced by $\mathbf{E}_k(t)$. Expanding $|\Psi\rangle$ in eigenstates $|j\rangle$ of the molecular Hamiltonian [i.e., $H_M|j\rangle = E_j|j\rangle$] as $|\Psi\rangle = \sum_j b_j \exp(-iE_j t/\hbar)|j\rangle$ and substituting into the Schrödinger equation gives the standard set of coupled equations:

$$\dot{b}_i = \frac{i}{\hbar} \sum_{jk} b_j \exp(-i\omega_{ji}t) \langle i|\vec{\mu}_k \cdot \mathbf{E}_k(t)|j\rangle, \tag{2}$$

where $\omega_{ji} = (E_j - E_i)/\hbar$.

As an example of an effective control scenario, consider the D or L enantiomer in its ground electronic states with $|D\rangle$ and $|L\rangle$ denoting vibrotational eigenstates of energy $E_D = E_L$. We choose $\varepsilon_1(t)$ so as to excite the system to two eigenstates $|1\rangle$ and $|2\rangle$, of energies E_1 and E_2, of the electronically excited G. The states $|1\rangle$ and $|2\rangle$ are coupled by an additional laser field (see Fig. 1) $\varepsilon_0(t)$. Specifically, we choose $\mathbf{E}(t)$ to be composed of two linearly polarized light pulses, with ω_0 in near resonance with $\omega_{21} \equiv (E_2 - E_1)/\hbar$, and ω_1 chosen to lie

 © 2000 The American Physical Society

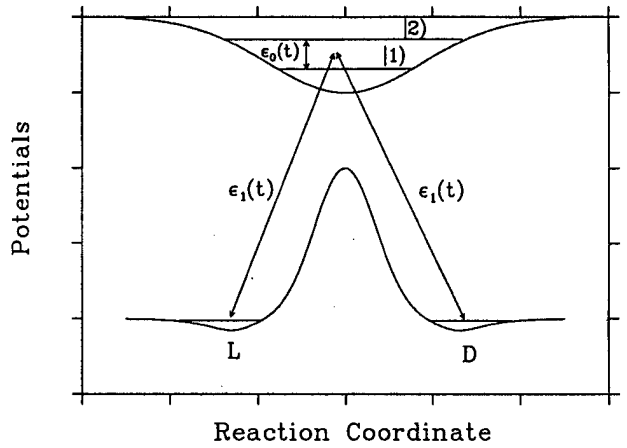

FIG. 1. Sample control scenario.

between $\omega_{1D} \equiv (E_1 - E_D)/\hbar$, and $\omega_{2D} \equiv (E_2 - E_D)/\hbar$ (see Fig. 1). In this case only four molecular states are relevant and $|\Psi\rangle$ is expanded as

$$|\Psi\rangle = b_D(t)\exp(-iE_Dt/\hbar)|D\rangle + b_L(t)\exp(-iE_Lt/\hbar)|L\rangle + b_1(t)\exp(-iE_1t/\hbar)|1\rangle + b_2(t)\exp(-iE_2t/\hbar)|2\rangle. \tag{3}$$

Equation (2), in the rotating wave approximation, is then given by

$$\begin{aligned}
\dot{b}_1 &= i\exp(i\Delta_1 t)[\Omega^*_{D,1}b_D + \Omega^*_{L,1}b_L] + i\exp(i\Delta^{(2)}t)\Omega^*_0 b_2,\\
\dot{b}_2 &= i\exp(i\Delta_2 t)[\Omega^*_{D,2}b_D + \Omega^*_{L,2}b_L] + i\exp(-i\Delta^{(2)}t)\Omega_0 b_1,\\
\dot{b}_D &= i\exp(-i\Delta_1 t)\Omega_{D,1}b_1 + i\exp(-i\Delta_2 t)\Omega_{D,2}b_2,\\
\dot{b}_L &= i\exp(-i\Delta_1 t)\Omega_{L,1}b_1 + i\exp(-i\Delta_2 t)\Omega_{L,2}b_2,
\end{aligned} \tag{4}$$

where $\Omega_{ij}(t) \equiv \mu^{(1)}_{ij}\varepsilon_1(t)/\hbar$, $\Omega_0 \equiv \mu^{(0)}_{21}\varepsilon_0(t)/\hbar$, $\Delta_j \equiv \omega_{jD} - \omega_1$, $\Delta^{(2)} \equiv \omega_{21} - \omega_0$, where $\mu^{(k)}_{ij} \equiv \langle i|\vec{\mu}_k \cdot \hat{\epsilon}_k|j\rangle$, with $i = D, L$; $k = 0, 1$ and $j = 1, 2$. Note, to avoid confusion, that all computations carried out below assume that the initial state is either $|D\rangle$ [i.e., $b_L(0) = 0$] or $|L\rangle$ [i.e., $b_D(0) = 0$]. No initial superposition of $|D\rangle$ and $|L\rangle$ is assumed.

The essence of the laser distillation process lies in choosing the laser of central frequency ω_1 so that it excites the system to a state $|1\rangle$ which is *symmetric* with respect to the inversion operation I, and to a state $|2\rangle$ which is *antisymmetric* with respect to I. By contrast, $|D\rangle$ and $|L\rangle$ do not share these symmetries but are related to one another through inversion (i.e., $I|D\rangle = -|L\rangle$, $I|L\rangle = -|D\rangle$ whereas $I|1\rangle = |1\rangle$, $I|2\rangle = -|2\rangle$). Hence, $\varepsilon_1(t)$ is chosen unimodal if $|1\rangle$ and $|2\rangle$ are adjacent levels, or bimodal if the pulse needs to be shaped to predominantly excite states of the desired symmetries. Note that $|D\rangle$ and $|L\rangle$ are not eigenstates of the parity operator or of H_M. Hence there are no parity constraints [5,8] preventing either the dipole excitation of both $|1\rangle$ and $|2\rangle$ from $|D\rangle$ and $|L\rangle$, or dipole transitions between $|1\rangle$ and $|2\rangle$.

To consider the nature of the Rabi frequencies Ω in Eq. (4) we rewrite $|D\rangle$ and $|L\rangle$ in terms of a symmetric state $|S\rangle = [|D\rangle - |L\rangle]/2$ and an antisymmetric state $|A\rangle = [|D\rangle + |L\rangle]/2$. The relevant matrix elements are then of the form:

$$\begin{aligned}
\langle 1|\mu^{(1)}|D\rangle &= \langle 1|\mu^{(1)}|A + S\rangle = \langle 1|\mu^{(1)}|A\rangle,\\
\langle 1|\mu^{(1)}|L\rangle &= \langle 1|\mu^{(1)}|A - S\rangle = \langle 1|\mu^{(1)}|A\rangle,\\
\langle 2|\mu^{(1)}|D\rangle &= \langle 2|\mu^{(1)}|A + S\rangle = \langle 2|\mu^{(1)}|S\rangle,\\
\langle 2|\mu^{(1)}|L\rangle &= \langle 2|\mu^{(1)}|A - S\rangle = -\langle 2|\mu^{(1)}|S\rangle.
\end{aligned} \tag{5}$$

That is, $\Omega_{D,1} = \Omega_{L,1}$, $\Omega_{D,2} = -\Omega_{L,2}$, and Eq. (4) therefore becomes

$$\begin{aligned}
\dot{b}_1 &= i\exp(i\Delta_1 t)\Omega^*_{D,1}[b_D + b_L] + i\exp(i\Delta^{(2)}t)\Omega^*_0 b_2,\\
\dot{b}_2 &= i\exp(i\Delta_2 t)\Omega^*_{D,2}[b_D - b_L] + i\exp(-i\Delta^{(2)}t)\Omega_0 b_1,\\
\dot{b}_D &= i\exp(-i\Delta_1 t)\Omega_{D,1}b_1 + i\exp(-i\Delta_2 t)\Omega_{D,2}b_2,\\
\dot{b}_L &= i\exp(-i\Delta_1 t)\Omega_{D,1}b_1 - i\exp(-i\Delta_2 t)\Omega_{D,2}b_2.
\end{aligned} \tag{6}$$

The essence of optically controlled enantioselectivity lies in the relationship $\Omega_{D,2} = -\Omega_{L,2}$ and its effect on the dynamical equations for the level populations [Eq. (6)]. Note specifically that the equation for $\dot{b}_D(t)$ is different than the equation for $\dot{b}_L(t)$, due to the sign difference in the last term to Eq. (6). Although not sufficient to ensure enantiomeric selectivity, the ultimate consequence of this difference is that populations of $|D\rangle$ and $|L\rangle$ after laser excitation are different in the presence of radiative coupling between levels $|1\rangle$ and $|2\rangle$.

To obtain quantitative estimates for the extent of obtainable control we have numerically solved Eq. (4) for model cases assuming Gaussian pulses: $\varepsilon_\ell(t) = \beta_\ell \exp\{-[(t - t_\ell)/\alpha_\ell]^2\}$ $(\ell = 0, 1)$ and system parameters $\langle 1|\mu^{(1)}|D\rangle = \langle 1|\mu^{(1)}|L\rangle = \langle 2|\mu^{(1)}|L\rangle = -\langle 2|\mu^{(1)}|D\rangle = 1$ a.u., $\langle 1|\mu^{(0)}|2\rangle = 1$ a.u., $\omega_{2,1} = 100\ \text{cm}^{-1}$, and $\Delta^{(2)} = 0$. Figure 2 displays the final probabilities $P_D = |b_D(\infty)|^2$, $P_L = |b_L(\infty)|^2$ in $|D\rangle$ and $|L\rangle$, after a single pulse sequence, for a variety of pulse parameters. Results are shown for various values of Δ_1 at various different pulse powers assuming that one starts solely with D, solely with L, or with a racemic mixture of both enantiomers. Clearly, the responses of D and L to the pulses are quite different and, for particular parameters, one can significantly enhance the population of one chiral enantiomer over the other. For example, for $\Delta_1 = -125\ \text{cm}^{-1}$, $\beta_0 = \beta_1 = 1.5 \times 10^{-3}$, a racemic mixture of D and L can be converted, after a single pulse, to an enantiomerically enriched mixture with predominantly D. Tuning to $\Delta_1 = 25\ \text{cm}^{-1}$ at the same power results in a significant enhancement of L.

Figure 2, however, only provides input into a computation of the overall result. In the overall process we begin

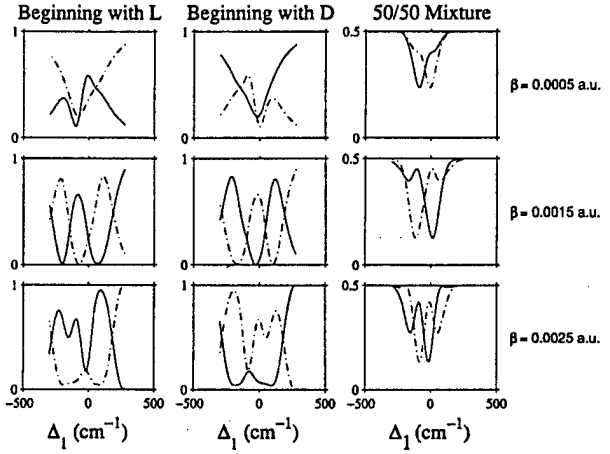

FIG. 2. Probabilities of populating the $|D\rangle$ (solid lines) and $|L\rangle$ (dot-dashed lines) after laser excitation, but prior to relaxation, as a function of Δ_1. Three different cases are shown, corresponding to three different initial conditions: (1) only state $|L\rangle$ occupied, (2) only state $|D\rangle$ occupied, and (3) both $|D\rangle$ and $|L\rangle$ equally occupied. Results are shown for three different laser powers ($\beta \equiv \beta_0 = \beta_1$), where Gaussian pulses are assumed with $\alpha_0 = \alpha_1 = 0.15$ psec, and $t_0 = t_1$.

with an incoherent mixture of N_D molecules of type D and N_L molecules of type L. In the first step the system is excited, as above, with a laser pulse sequence. In the second step, the system collisionally and radiatively relaxes so that all the population returns to the ground state to produce an incoherent mixture of $|L\rangle$ and $|D\rangle$. This pair of steps is then repeated until the populations of $|L\rangle$ and $|D\rangle$ reach convergence.

To obtain the result computationally note that the population after laser excitation, but before radiative relaxation, consists of the weighted sum of the results of two computations: N_D times the results of laser excitation starting solely with molecules in $|D\rangle$, plus N_L times the results of laser excitation starting solely with molecules in $|L\rangle$. If P_D and P_L denote the probabilities of $|D\rangle$ and $|L\rangle$ resulting from laser excitation assuming the first of these initial conditions, and P'_D and P'_L for the results of excitation following from the second of these initial conditions, then the populations of $|D\rangle$ and $|L\rangle$ after laser excitation of the mixture are $N_D P_D + N_L P'_D$ and $N_D P_L + N_L P'_L$, respectively. The remainder of the population, $N_D[1 - P_D - P_L] + N_L[1 - P'_D - P'_L]$, is in the upper two levels $|1\rangle$ and $|2\rangle$. Radiative emission from levels $|1\rangle$ and $|2\rangle$ then follows, with the excited population dividing itself equally between $|D\rangle$ and $|L\rangle$. The resultant populations $\mathcal{N}_D$ and $\mathcal{N}_L$ is ground state $|D\rangle$ and $|L\rangle$ are then $\mathcal{N}_D = 0.5N_D[1 + P_D - P_L] + 0.5N_L[1 + P'_D - P'_L]$ and $\mathcal{N}_L = N_D + N_L - \mathcal{N}_D$.

The sequence of laser excitation followed by collisional relaxation and radiative emission is then iterated to convergence, i.e., $\mathcal{N}_D = N_D$, and $\mathcal{N}_L = N_L$. These conditions reduce to $N_D(1 - P_D + P_L) = N_L(1 + P'_D - P'_L)$. If the total population is chosen to be normalized ($N_D + N_L = 1$), then the final probabilities $\mathcal{P}_D, \mathcal{P}_L$ of populating states $|D\rangle$ and $|L\rangle$ are

$$\mathcal{P}_D = \frac{1 + P'_D - P'_L}{2 - P_D + P_L + P'_D - P'_L} \tag{7}$$

with $\mathcal{P}_L = 1 - \mathcal{P}_D$.

Results for the converged probabilities for the cases depicted in Fig. 2 are shown in Fig. 3. The results clearly show substantially enhanced enantiomeric ratios at various choices of control parameters. For example, at $\beta \equiv \beta_0 = \beta_1 = 1.5 \times 10^{-3}$, tuning Δ_1 to 50 cm^{-1} gives a preponderance of L whereas tuning to the $\Delta_1 = -125$ cm^{-1} gives more D.

Numerous parameters in this system, such as the pulse shape, time delay between pulses, pulse frequencies, and pulse powers, etc., can be varied to affect the final L to D ratio. For example, Fig. 4 shows the dependence on the ratio of field strengths β_0/β_1 for various values of $\Delta t = t_0 - t_1$. Changing these parameters is clearly seen to alter the L to D ratio.

Conditions on the structure of the molecule under which this method is applicable have been described above and such molecules are expected to exist [4]. However, in many cases an excited state G with the required characteristics does not exist below the dissociation energy. In such cases one may be able to apply the laser distillation procedure by adding a molecule B to the initial L, D

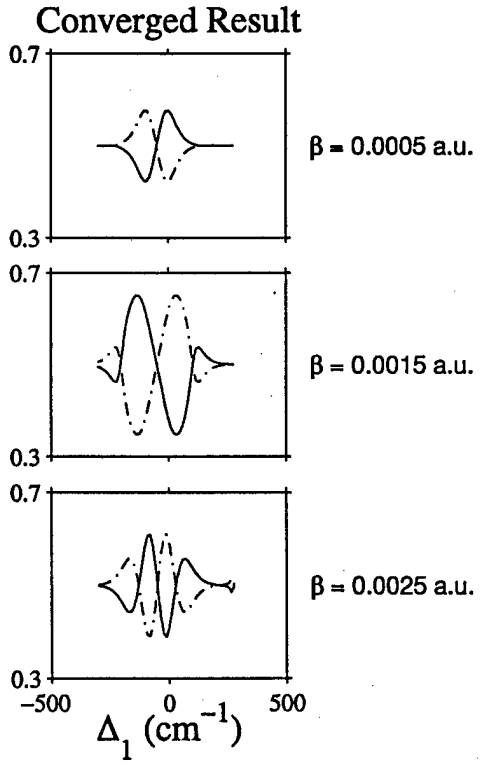

FIG. 3. Results for the cases in Fig. 2, but after a convergent series of steps comprised of radiative excitation, followed by collisional and radiative relaxation.

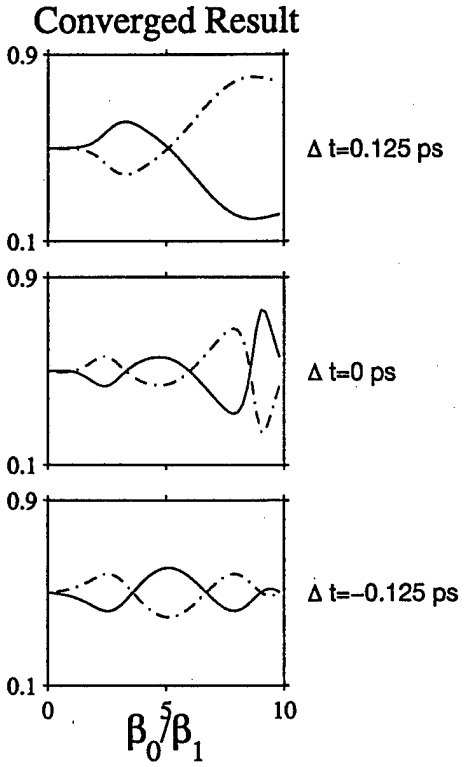

FIG. 4. Converged results as a function of field strength ratios with $\Delta_1 = 0$, $\alpha_0 = \alpha_1 = 0.25$ psec, and $\beta_1 = 1.0 \times 10^{-4}$ a.u. for three values of Δt.

mixture to form weakly bound $L - B$ and $B - D$, which are themselves right- and left-handed enantiomeric pairs. The molecule B is chosen so that electronic excitation of $B - D$ and $L - B$ forms an excited species G which has stationary rovibrational states which are either symmetric or antisymmetric with respect to inversion through I. The species $L - B$ and $B - D$ now serve as the L and D enantiomers in the general scenario above and the laser distillation procedure described above then applies. Further, the molecule B serves a catalyst that may be removed from the final product by traditional chemical means.

For example, L and D might be the left- and right-handed enantiomers of a chiral alcohol, and B is the ketone derived from this alcohol (see Fig. 5). In this case, preliminary studies [9] of the electronic structure of the alcohol-ketone system show that there are weakly bound chiral alcohol-ketone minima in the ground electronic state, as desired; further work is in progress to determine the excited state structures [9].

In summary, we have shown that a chiral outcome, the enhancement of a particular enantiomer, can arise by coherently encoding quantum interference information in the excitation of a racemic mixture. The fact that the initial state displays a broken symmetry and that the excited state has states which are either symmetric or antisymmetric with respect to I allows for the creation of a superposition

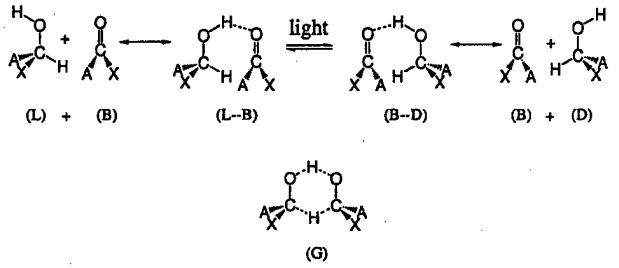

FIG. 5. Sample scenario for enhanced enantiomeric selectivity in a racemic mixture of two chiral alcohols related by inversion. An alcohol and a ketone exchange two hydrogen atoms so as to produce the ketone, but with an alcohol of reverse handedness. Here A and X are distinct organic groups; dashes denote, in the upper panel, hydrogen bonds. The electronically excited species G is postulated to be given by the structure at the bottom of the figure.

state which does not have these transformation properties. Radiatively coupling the states in the superposition then allows for the transition probabilities from L and D to differ, allowing for depletion of the desired enantiomer. Work is in progress to obtain qualitative insights into the essence of this symmetry breaking scheme and to design other scenarios based on a common symmetry breaking principle.

This research was supported by internal funds of the Weizmann Institute of Science and by the Natural Sciences and Engineering Research Council of Canada.

[1] R. G. Wooley, Adv. Phys. **25**, 27 (1975); *Origins of Optical Activity in Nature,* edited by D. C. Walker (Elsevier, Amsterdam, 1979).
[2] For a discussion, see L. D. Barron, in *New Developments in Molecular Chirality,* edited by P. G. Mezey (Kluwer, Dordrecht, 1991); L. D. Barron, *Molecular Light Scattering and Optical Activity* (Cambridge University Press, Cambridge, 1982).
[3] See, for example, A. Salam and W. J. Meath, J. Chem. Phys. **106**, 7865 (1997); **228**, 115 (1998).
[4] Potential surfaces of this type have been discussed before [see, e.g., M. Quack, Angew. Chem. Int. Ed. Engl. **28**, 571 (1989); J. A. Cina and R. A. Harris, J. Chem. Phys. **100**, 2531 (1994), as well as Ref. [5]. However, none of these proposed schemes are able to lead to the enhancement of one enantiomer over another, when starting with a racemic mixture.]
[5] C. S. Maierle and R. A. Harris, J. Chem. Phys. **109**, 3713 (1998).
[6] For a recent review, see M. Shapiro and P. Brumer, Adv. At. Mol. Opt. Phys. **42**, 287 (2000); R. G. Gordon and S. A. Rice, Annu. Rev. Phys. Chem. **48**, 595 (1997).
[7] M. Shapiro and P. Brumer, J. Chem. Phys. **95**, 8658 (1991).
[8] M. Quack, Chem. Phys. Lett. **132**, 147 (1986).
[9] E. Brumer, K. Baldridge, E. Deretey, M. Shapiro, and P. Brumer (to be published).

PHYSICAL REVIEW A, VOLUME 61, 041801(R)

18

Coherent control of refractive indices

E. McCullough, M. Shapiro,* and P. Brumer
Chemical Physics Theory Group, Department of Chemistry, University of Toronto, Toronto, Canada M5S 3H6
(Received 1 June 1999; published 6 March 2000)

The application of coherent control to modify the real and imaginary parts of the refractive index n of a material is described. Parameters to control the refractive index, and to minimize absorption, are identified. An application to gaseous N_2 shows that extensive control over n is possible.

PACS number(s): 42.50.Gy

There is considerable ongoing interest in manipulating quantum interference effects in order to alter the nonlinear optical properties of materials [1]. Here we show that one of the earliest coherent control scenarios [2,3] affords a versatile means of significantly increasing or decreasing the refractive index of molecules both off resonance and near resonance. Previous work on modifying the refractive index through coherence effects includes Refs. [4–6]. Harris and co-workers [4] focuses on broadband generation with concomitant reduction of the index of refraction in the case where electromagnetically induced transparency (EIT) is used to establish maximal two-level coherence (i.e., $|c_1|^2 = |c_2|^2 = 0.5$ below). Hau, Harris, and co-workers [5] invoke EIT in a Bose-Einstein condensate to modify the refractive index of sodium atoms by many orders of magnitude, slowing down the speed of light in this medium to ≈ 17 m/sec. Scully [6] focuses on increasing the refractive index, with low absorption, near resonances. By contrast, this work introduces new control parameters in the weak-field regime that allow for direct and extensive control over the real and imaginary parts of the refractive index both off resonance and near resonance.

We consider a system that has been prepared (e.g., by two-photon excitation) in a superposition state

$$|\psi(t)\rangle = c_1|\phi_1\rangle \exp(-iE_1 t/\hbar) + c_2|\phi_2\rangle \exp(-iE_2 t/\hbar) \tag{1}$$

of Hamiltonian eigenstates $|\phi_i\rangle$ of energy E_i and that is then subjected to two cw fields of the form ($k=1,2$)

$$\vec{\varepsilon}_k = [F_k \exp(i\omega_k t) + F_k^* \exp(-i\omega_k t)]\hat{\varepsilon}_k . \tag{2}$$

where $\hat{\varepsilon}_k$ is the unit vector along $\vec{\varepsilon}_k$. We choose $(\omega_2 - \omega_1) = (E_2 - E_1)/\hbar \equiv \Omega_{21}$, so that excitation of $|\phi_1\rangle$ by ω_1 and of $|\phi_2\rangle$ by ω_2 lead to the same energy $E = E_1 + \hbar\omega_1 = E_2 + \hbar\omega_2$ [2]. Our interest is in modifying the refractive index of the material at frequencies ω_1 or ω_2. We examine the case of isolated molecules, or molecules in a very dilute gas, where collisional relaxation and dephasing effects can be ignored. Further, the system and states are chosen so that the radiative decay of $|\phi_1\rangle$ and $|\phi_2\rangle$ is negligibly small on the time scale associated with observing the effect described below.

An application of first-order perturbation theory gives the average value of the resultant system dipole moment as

$$\langle \vec{\mu} \rangle = \sum_m c_m^{(1)}(t)(c_1^* \vec{\mu}_{1m} e^{-i\Omega_{m1}t} + c_2^* \vec{\mu}_{2m} e^{-i\Omega_{m2}t}) + \text{c.c.}, \tag{3}$$

where $\vec{\mu}_{1m} = \langle \phi_1 | \vec{\mu} | \phi_m \rangle$ is the transition-dipole matrix element, and c.c. denotes the complex conjugate of the sum that precedes it and where the sum is over all $|\phi_m\rangle$. Here

$$\begin{aligned} c_m^{(1)}(t) &= \frac{1}{\hbar} c_1 \sum_{k=1}^{2} \mu_{m1}^{\varepsilon_k} \left(F_k^* \frac{e^{i(\Omega_{m1} - \omega_k)t}}{\Omega_{m1} - \omega_k - i\gamma} + F_k \frac{e^{i(\Omega_{m1} + \omega_k)t}}{\Omega_{m1} + \omega_k - i\gamma} \right) \\ &\quad + \frac{1}{\hbar} c_2 \sum_{k=1}^{2} \mu_{m2}^{\varepsilon_k} \left(F_k^* \frac{e^{i(\Omega_{m2} - \omega_k)t}}{\Omega_{m2} - \omega_k - i\gamma} \right. \\ &\quad \left. + F_k \frac{e^{i(\Omega_{m2} + \omega_k)t}}{\Omega_{m2} + \omega_k - i\gamma} \right), \end{aligned} \tag{4}$$

where γ is the average linewidth of bound levels that has been introduced phenomenologically, $\Omega_{mn} = (E_m - E_n)/\hbar$, $\vec{\mu}_{jm} = \langle \phi_j | \vec{\mu} | \phi_m \rangle$ and $\mu_{jm}^{\varepsilon_k} = \langle \phi_j | \vec{\mu} \cdot \hat{\varepsilon}_k | \phi_m \rangle$. Here we assume that (a) the cw fields are turned on at $t \to -\infty$, at which time the system is in its initial superposition state [Eq. (1)]; (b) the medium has no permanent dipole moment; and (c) $\langle \phi_1 | \vec{\mu} | \phi_2 \rangle = 0$ due to parity requirements discussed later below. Inserting Eq. (4) in Eq. (3) gives 32 term contributions to $\langle \mu \rangle$: half are proportional to $|c_1|^2$ or $|c_2|^2$ and hence involve the independent effects of ω_1 and ω_2 and half, proportional to $c_i c_j^* (i \neq j)$, are interference terms originating from the fact that we are dealing with an initial coherent superposition of $|\phi_i\rangle$. Of these 16 interference terms, eight do not oscillate with frequency ω_1 or ω_2 and hence do not contribute to the susceptibility $\chi(\omega)$ at these frequencies. Noting that $\vec{\mu}(\omega) = (\epsilon_0/\rho)\chi(\omega)\vec{F}(\omega)\exp(i\omega t)$, where ϵ_0 is the permittivity of the vacuum, $\vec{F}(\omega)$ is the electric field at frequency ω, and ρ is the density of material, and using the expression for $\vec{\mu}(\omega)$ obtained as described above, we have

*Permanent address: Chemical Physics Department, The Wiezmann Institute of Science, Rehovot, Israel.

 ©2000 The American Physical Society

$$\epsilon_0\hbar\chi(\omega_1)/\rho = \sum_m |c_1|^2\vec{\mu}_{1m}\vec{\mu}_{m1}\left(\frac{1}{\Omega_{m1}-\omega_1-i\gamma}+\frac{1}{\Omega_{m1}+\omega_1-i\gamma}\right) + |c_2|^2\vec{\mu}_{2m}\vec{\mu}_{m2}\left(\frac{1}{\Omega_{m2}-\omega_1-i\gamma}+\frac{1}{\Omega_{m2}+\omega_1-i\gamma}\right) + (c_1^*c_2F_2^*/F_1^*)\left[\frac{\vec{\mu}_{1m}\vec{\mu}_{m2}}{\Omega_{m1}-\omega_1-i\gamma}+\frac{\vec{\mu}_{m2}\vec{\mu}_{1m}}{\Omega_{m2}+\omega_1-i\gamma}\right], \quad (5)$$

$$\epsilon_0\hbar\chi(\omega_2)/\rho = \sum_m |c_1|^2\vec{\mu}_{1m}\vec{\mu}_{m1}\left(\frac{1}{\Omega_{m1}-\omega_2-i\gamma}+\frac{1}{\Omega_{m1}+\omega_2-i\gamma}\right) + |c_2|^2\vec{\mu}_{2m}\vec{\mu}_{m2}\left(\frac{1}{\Omega_{m2}-\omega_2-i\gamma}+\frac{1}{\Omega_{m2}+\omega_2-i\gamma}\right) + (c_1c_2^*F_1^*/F_2^*)\left[\frac{\vec{\mu}_{2m}\vec{\mu}_{m1}}{\Omega_{m2}-\omega_2-i\gamma}+\frac{\vec{\mu}_{m1}\vec{\mu}_{2m}}{\Omega_{m1}+\omega_2-i\gamma}\right]. \quad (6)$$

Below we assume that all of the incident light is linearly polarized along the z axis and denote the laboratory zz component of χ as χ_{zz}. The desired index of refraction is given by $n(\omega_i)=\sqrt{1+\chi_{zz}(\omega_i)}$. Control over both the real and imaginary parts of $n(\omega)$ is of interest.

Examination of Eqs. (5) and (6) shows that $\chi(\omega)$ is comprised of two terms that are proportional to $|c_i|^2$ and that are associated with the traditional contribution, plus two field-dependent terms, proportional to $d_{ij}=c_i^*c_jF_j^*/F_i^*$, which results from the coherent excitation of $|\phi_1\rangle$ and $|\phi_2\rangle$ to the same total energy $E=E_1+\hbar\omega_1=E_2+\hbar\omega_2$. As a consequence, changing d_{ij} alters the interference between excitation routes and allows for coherent control over the susceptibility, and hence control over the refractive index. Experimentally, this control is achieved by altering the parameters in the state preparation in order to affect c_1,c_2 and/or by varying the relative phase [7] and relative magnitude of F_1,F_2.

Three comments are in order. First, with $|\phi_1\rangle$ and $|\phi_2\rangle$ assumed to belong to the same electronic state, nonzero dipole products such as $\vec{\mu}_{1m}\vec{\mu}_{m2}$ require that $|\phi_1\rangle$ and $|\phi_2\rangle$ be of the same party. Thus, a superposition state that allows for control must be prepared via a parity-preserving process, e.g., by two-photon absorption. In this case, using a laser of frequency ω_p and of field amplitude $F_p\hat{\varepsilon}_p$, gives

$$d_{12}=\sum_n \frac{\mu_{2n}^{\varepsilon_p}\mu_{n1}^{\varepsilon_p}F_p^{2*}F_2^*}{(\Omega_{n1}-\omega_p)(-i\gamma)F_1^*}. \quad (7)$$

Here the ε_p superscript denotes the component of the vector matrix element along $\hat{\varepsilon}_p$. Second, Eqs. (5) and (6) make clear that control over $\chi(\omega_i)$ is expected to be substantial if F_i/F_j is large. However, under these circumstances control over $\chi(\omega_j)$ is minimal since the corresponding interference term is proportional to F_j/F_i. Hence, effective control over the refractive index is possible only at one of ω_1 or ω_2. Third, the assumption of perturbation theory implies that $|c_2|^2$ cannot exceed ≈ 0.2, the value used below.

As an example of this general theory we consider modifying the refractive index of gaseous N_2. Sample control results for $n(\omega)$, both off resonance and near resonance, are shown below. The off-resonance computations, carried out to convergence, included over 120 transition dipole matrix elements from rovibrational states of the ground $X\Sigma_g^+$ electronic state to the vibrotational states of $b'^1\Sigma_u^+$, $c''\Sigma_u^+$, $e''\Sigma_u^+$, $b'\Pi_u$, $c'\Pi_u$, and $0'\Pi_u$ electronic states. The near-resonance computations approximate N_2 as a three-level system. We assume the Condon approximation, use the electronic dipole transition matrix elements of Stahel *et al.* [8] with radial wave-function overlap calculated via uniform WKB, and include all vibrotational states needed for convergence. Control is shown as a function of the relative laser phase $\theta=2\theta_p+\theta_2-\theta_1$ where θ_p is the phase of F_p^* and $\theta_i(i=1,2)$ is the phase of F_i^*.

Figure 1 shows the dependence of the real [panel (a)] and imaginary [panel (b)] parts of $n(\omega_1)=n'(\omega_1)+in''(\omega_1)$, which are linked by causality, on $|F_2/F_1|$ for various different values of θ. Results are shown for the nonresonant excitation of a superposition state comprised of $|\phi_1\rangle=|v_1=0,J_1=0,M_1=0\rangle$ plus $|\phi_2\rangle=|v_2=0,J_2=2,M_2=0\rangle$, where $|c_2|^2=0.2$, $\omega_1=3\times10^{15}$ Hz, and $\omega_2=2.99775\times10^{15}$ Hz. The quantities (v_i,J_i,M_i) denote quantum numbers for vibration, rotation, and for the projection of the angular momentum along the z axis.

Consider first the case of $\theta=-\pi/2$. Here $n''(\omega_1)=0$ (i.e., no absorption of the field) and $n'(\omega_1)$ is seen to grow linearly on the log-log plot for $|F_2/F_1|\rangle 10$; i.e., once the interference term in Eq. (6) dominates. Extensive control over n' is evident; e.g., n' has changed by well over 10% by $|F_2/F_1|\sim10^4$. This is in sharp contrast with the tiny refractive-index changes associated, for example, with the optical Kerr effect or self-focusing (e.g., changing the index of refraction of N_2 by as little as 10^{-6} via either of these effects requires laser intensities of $>10^{12}$ W/cm^2).

Figures 1(a) and 1(b) display a broad range of behavior of n' and n''. For example, for the case of $\theta=0$ and π the n' increases for $|F_2/F_1|>1100$. For $\theta=0$ this increase is accompanied by positive n'', and hence by the absorption of the field. By contrast, the case of $\theta=\pi$ shows negative n'', i.e., the field is amplified. Also of interest is the case of $\theta=\pi/2$, which shows rapidly decreasing n' with increasing F_2/F_1, accompanied by zero n''.

Additional computations indicated a strong dependence of control on $|c_i|$ and on the particular choice of $|\phi_i\rangle$. For example, results for initial superpositions comprised of $|\phi_1\rangle=|v_1=0,J_1=0,M_1=0\rangle$ and $|\phi_2\rangle=|v_2,J_2,M_2=0\rangle$ depended weakly on the choice of $J_2=0$ or $J_2=2$, but were heavily dependent on v_2. In particular, the larger the v_2, the smaller the n' at fixed $|F_2/F_1|$. This behavior is a direct consequence of the reduced size, for larger v_2, of the radial

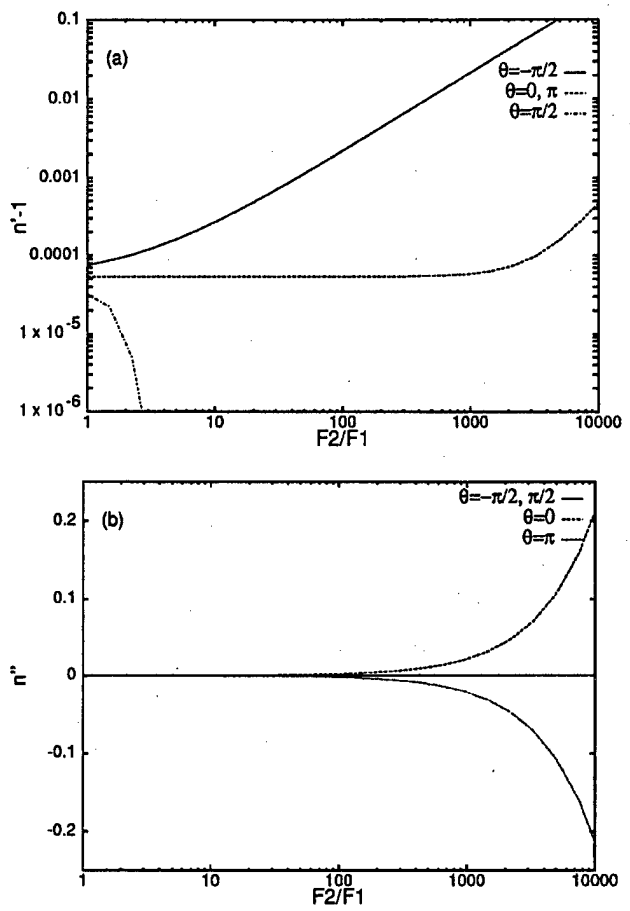

FIG. 1. Dependence of $n(\omega)$ on F_2/F_1 in N_2 (in the superposition state described in the text) for different values of the relative laser phase θ. (a) Real part $n'(\omega)$ for $\theta=-\pi/2$ (solid), $\theta=0$ and π (dashed), and $\theta=\pi/2$ (dot-dashed); (b) imaginary part $n''(\omega)$ for $\theta=-\pi/2$ and $\pi/2$ (solid), $\theta=0$ (dashed) and $\theta=\pi$ (dotted).

overlap matrix elements which, in turn, lower the value of dipole products such as $\vec{\mu}_{1m}\vec{\mu}_{m2}$, and hence reduce the interference contribution.

Altering $|c_1|$, either in a controlled fashion or, e.g., due to thermalization of population among various states, leads to a change in n. For example, Fig. 2 shows n' for the case of $\theta=-\pi/2$, but where coefficients $|c_1|^2$ are extracted from state populations at $T=298°$ K. Two examples are shown, the first is associated with having prepared a superposition of $|v_1=0,J_1=0,M_1=0\rangle$ with $|v_2=1,J_2=0,M_2=0\rangle$ and the second for a density matrix comprised of $(2J_1+1)$ of superpositions of $|v_1=0,J_1=6,M_i\rangle$ with $|v_2=1,J_2=6,M_i\rangle$, $M_i=-J_1$ to J_1, where $(v_1=0,J_1=6)$ is the most populated state at the given T. These superpositions (only a part of the full density matrix) would result from preparation via excitation [Eq. (7)] that is two-photon resonant with the energy spacing between the indicated levels. The results in Fig. 2 show a significant reduction in control over that shown in Fig. 1. Nonetheless, extensive control is predicted.

Consider now near-resonant excitation of the superposition state used in Fig. 1. Excitation with $\omega_1=1.900\,884\,279\times10^{16}$ Hz, and $\omega_2=1.900\,659\,420\times10^{16}$ Hz excites the sys-

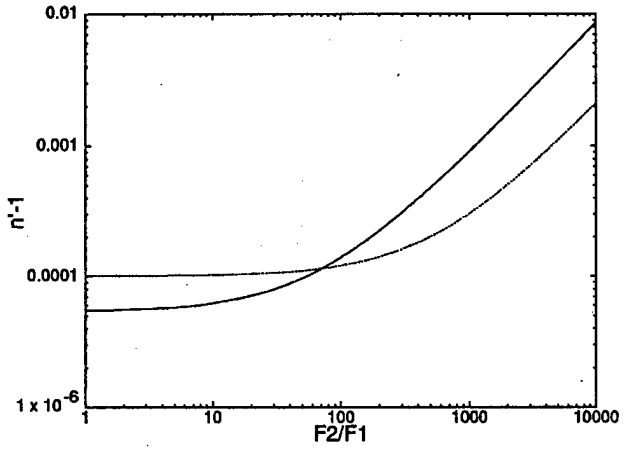

FIG. 2. Dependence of $n'(\omega)$ on F_2/F_1 for a superposition of $|v_1=0,J_1=0,M_1=0\rangle$ with $|v_2=1,J_2=0,M_2=0\rangle$ where (solid line) molecules are in the ground state with $|c_1|^2$ determined by thermal populations at $T=298°$ K and (dashed line) for a density matrix comprised of superpositions of $|v_1=0,J_1=6,M_1=(-6\text{ to }6)\rangle$ with $|v_2=1,J_2=6,M_2=(-6\text{ to }6)\rangle$.

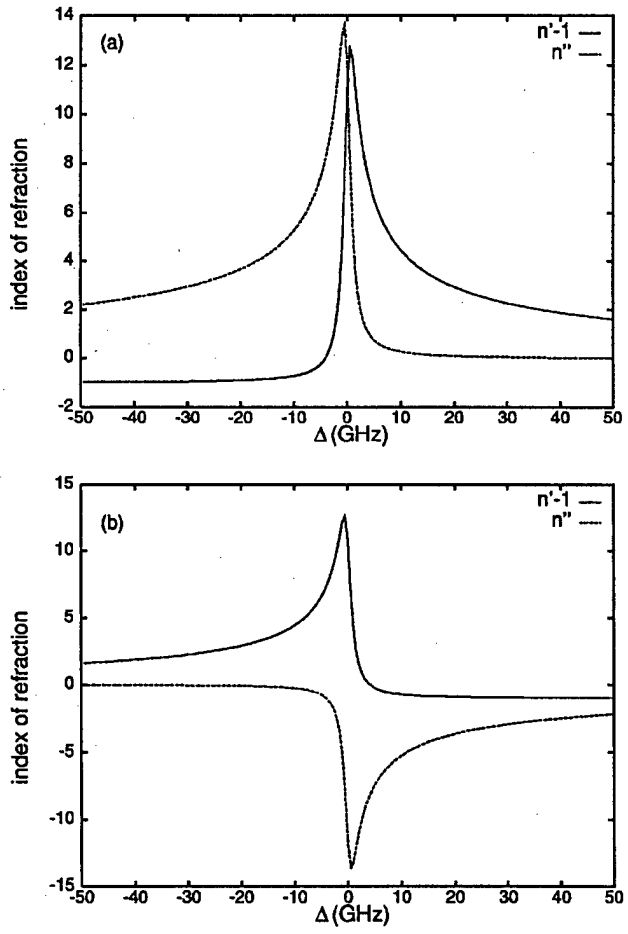

FIG. 3. Real and imaginary parts of the index of refraction of N_2 as a function of the detuning Δ for the initial superposition state described in the text with $F_2/F_1=1000$. (a) $\theta=-\pi/2$, (b) $\theta=\pi/2+10^{-6}$.

tem, on resonance, to the $|v=0,J=1,M=0\rangle$ bound state of energy E_b of the $b^1\Pi_u$ electronic state of N_2. Consider then the refractive index as a function of detuning Δ (i.e., $E=E_1+\hbar\omega_1=E_2+\hbar\omega_2=E_b-\hbar\Delta$). Figure 3(a) shows n' and n'' as a function of the detuning Δ for the choice $\theta=-\pi/2$, $F_2/F_1=1000$. Here large values of the index of refraction are seen to be associated with negligible absorption at $\Delta>20$ GHz, and the group velocity of light $v_g=c/[n'+\omega_1 dn'/d\omega_1]$ in this regime [5] can be estimated to be 150 m/sec. The sensitivity to the control parameters is evident by changing θ to $\pi/2+10^{-6}$, shown in Fig. 3(b). Here n'' is negative, corresponding to amplification of the beam. One should note then that a rich range of behavior is possible in near-resonance cases as the control variables d_{ij} are altered. Numerous examples are provided in Ref. [9].

In summary, this simple control scenario affords the possibility of a broad range of control over the refractive index. Applications to N_2 show that the control range is extensive. The scenario discussed in this Rapid Communication, where a superposition of two levels is excited by two cw lasers, is just one of many possible coherent control scenarios that take advantage of quantum interference effects [3]. Other coherent control scenarios, as well as the possibility of lasing in the region of negative n'', are currently under investigation.

Support from the U.S. Office of Naval Research is gratefully acknowledged.

[1] See, e.g., M.O. Scully and M.S. Zubairy, *Quantum Optics* (Cambridge University Press, Cambridge, 1997).

[2] P. Brumer and M. Shapiro, Chem. Phys. Lett. **126**, 541 (1986).

[3] For a recent review, see M. Shapiro and P. Brumer, J. Chem. Soc., Faraday Trans. **93**, 1263 (1997).

[4] M. Jain, H. Xia, G.Y. Yin, A.J. Merriam, and S.E. Harris, Phys. Rev. Lett. **77**, 4326 (1996); S.E. Harris and A.V. Sokolov, Phys. Rev. A **55**, R4019 (1997).

[5] L.V. Hau, S.E. Harris, Z. Dutton, and C.H. Behroozi, Nature (London) **397**, 594 (1999).

[6] M.O. Scully, Phys. Rev. Lett. **67**, 1855 (1991); A.S. Zibrov, M.D. Lukin, L. Hollberg, D.E. Nikonov, M.O. Scully, H.G. Robinson, and V.L. Velichansky, *ibid.* **76**, 3935 (1996); M. Fleischhauer, C.H. Keitel, M.O. Scully, C. Su, B.T. Ulrich, and S-Y Zhu, Phys. Rev. A **46**, 1468 (1992).

[7] C. Chen, Y-Y. Yin, and D.S. Elliott, Phys. Rev. Lett. **64**, 507 (1990); S.M. Park, S-P. Lu, and R.J. Gordon, J. Chem. Phys. **94**, 8622 (1991).

[8] D. Stahel, M. Leoni, and K. Dressler, J. Chem. Phys. **79**, 2541 (1983).

[9] E. McCullough, M.Sc. dissertation, University of Toronto, 1997 (unpublished).

ADVANCES IN ATOMIC, MOLECULAR, AND OPTICAL PHYSICS -- Volume 42

Edited by B. Bederson and H. Walther

Academic Press, San Diego, 2000

COHERENT CONTROL OF ATOMIC, MOLECULAR, AND ELECTRONIC PROCESSES

MOSHE SHAPIRO

Department of Chemical Physics, The Weizmann Institute, Rehovot, Israel

PAUL BRUMER

Chemical Physics Theory Group, Department of Chemistry, University of Toronto, Toronto, Canada

I. Introduction 287
II. Preparation and Dynamics of a Continuum State 289
III. Bichromatic Control of a Superposition State 296
IV. The Coherent Control Principle 304
V. Weak-Field Coherent Control: Unimolecular Processes 304
A. Interference Between N-Photon and M-Photon Routes 304
1. One-Photon versus Three-Photon Interference 305
2. One-Photon versus Two-Photon Interference 309
3. Two-Photon versus Two-Photon Interference 311
4. Polarization Control of Differential Cross Sections 313
B. Pump-Dump Control: Two-Level Excitation 315
C. Symmetry Breaking and the Generation of Chirality 321
VI. Strong-Field Incoherent Interference Control 325
A. Theory of Incoherent Interference Control 326
B. Computational and Experimental Demonstration 330
VII. Coherent Control of Bimolecular Processes 332
A. Degenerate e_m Superpositions 334
B. Sculpted Imploding Waves 337
C. Optimized Bimolecular Scattering: Enhancement and Total Suppression 339
VIII. Summary 342
IX. Acknowledgments 343
X. References 343

I. Introduction

One of the central questions in the physical sciences is the extent to which the present determines the future. Quantum mechanics, although a probabilistic theory, gives a deterministic answer to this question: given the wavefunction of an isolated system in the present, the system wavefunction in the future is

Copyright © 2000 by Academic Press
All rights of reproduction in any form reserved.
ISBN 0-12-003842-0/ISSN 1049-250X/00 $30.00

61

completely determined. This is a consequence of the fact that the Schrödinger equation is a first-order differential equation in the time variable.

Thus, if we wish to *predict* future probabilities, all we need to do is numerically solve the time-dependent Schrödinger equation, propagating from the present to the future. In spite of the obvious practical difficulties in applying such a program to many-body problems, there is in principle no reason why this cannot be done. Indeed, current methods enable the numerical solution of the time-dependent Schrödinger equation of many (Kosloff, 1988, 1994; Hammerich *et al.*, 1994; Zhang and Miller, 1989; Manolopoulos *et al.* 1991) few- (three- and four-) particle systems. Although a buildup of integration errors with propagation time does occur (Leforestier *et al.*, 1991), the errors are not expected to grow at a faster-than-polynomial rate. This fact is in sharp contradistinction, for example, to the situation in classical mechanics in the chaotic region. In that case, the exponential growth of integration error prevents the numerical determination of the state of the system to acceptable accuracy after the elapse of a sufficiently long time unless the initial phase-space coordinates are known to infinite accuracy.

Given then that the integration of the Schrödinger equation is possible, and that given the present we are able to predict the future probabilities, a more ambitious question can be asked: If we know the initial wavefunction, what dynamics (e.g., what Hamiltonian) guarantees a desirable outcome ("objective") in the future? This question constitutes the essence of the field now called *quantum control.*

In practice, one can modify the Hamiltonian by introducing external fields (e.g., laser light) to alter the dynamics. It is then possible to answer the above question in a "trial-and-error" fashion; we guess a Hamiltonian, propagate the initial wavefunction into the future, compare the result with the desirable objective, and correct the guess for the Hamiltonian until satisfactory agreement with the objective is reached. Indeed, a systematic way of executing this procedure is the subfield called *optimal control* (Gordon and Rice, 1997; Tannor and Rice, 1985; Tannor *et al.*, 1986; Tannor and Rice, 1988; Kosloff *et al.*, 1989; Shi *et al.*, 1988; Shi and Rabitz, 1989; Peirce *et al.*, 1991; Jakubetz *et al.*, 1990; Warren *et al.*, 1993; Yan *et al.*, 1993; Krause *et al.*, 1993; Kohler *et al.*, 1995).

This trial-and-error method is very time-consuming, requiring the repeated solution of the time-dependent Schrödinger equation. Further, by its very nature it often leads to solutions that provide little physical insight. When the explicit time-dependent terms in the Hamiltonian serve only to prepare a state that then evolves in the absence of an external field, or when its explicit time dependence can be treated adiabatically, there exists a more elegant method, called *coherent control* (CC) (Brumer and Shapiro, 1986; Shapiro and Brumer, 1987; Brumer and Shapiro, 1992; Shapiro and Brumer, 1993, 1997; Bandrauk *et al.*, 1992; Ivanov *et al.*, 1995; Muller *et al.*, 1990; Potvliege and Smith, 1992; Schafer and Kulander, 1992; Charron *et al.*, 1993), which requires the solution of the (time-independent) Schrödinger equation only once. Moreover, in that case, the CC solution allows for the simultaneous exploration of other possible future outcomes (and not just a single "desirable" objective), which results from different preparations of the initial wavefunction, provides physical insight into the nature of the control solution and provides analytic formulas for control that are useful experimentally. The coherent control method is the subject of the present review.

This review is organized as follows: Section II describes the basic principles behind the preparation and subsequent dynamics of a state excited by laser irradiation to the dissociative continuum. Section III then extends this approach to the excitation of a bound superposition state to show that quantum interference allows for control over dissociative dynamics. This idea, the principle of coherent control, is summarized in Section IV. Section V then describes a number of weak-field coherent control scenarios, including the demonstration that coherent control can be used to break symmetry and to generate chirality. In Section VI we introduce control methods in the strong-field limit, resulting in a powerful method (incoherent interference control) for the control of unimolecular processes. Section VII addresses the application of coherent control to collisional processes, and Section VIII provides a brief summary.

II. Preparation and Dynamics of a Continuum State

The desire to attain control over natural processes is of greatest significance if the control objectives involve *permanent* changes. Transitory objectives, which, once reached, exist only over a fleeting moment in time, are of academic interest but are of very little practical use. Thus, the types of systems we shall review here are those where events, such as bond breaking (dissociation), ionization, or particle exchange, take place over a small region in configuration space (the "interaction zone"). As the system departs from the interaction zone, its constituents decouple from one another and cease to change thereafter.

Under the above circumstances one is invariably dealing with *continuous* energy spectra. This is so because for bound states, which give rise to discrete spectra, decoupling at the end of the process is not possible. By its very definition, the constituents of a bound system remain close together at all times. Therefore, these constituents rarely reach a configuration where they decouple and cease to interact with one another.

Given that we are dealing with continuous spectra, the CC method utilizes some of the formal properties of the solutions of the multichannel scattering problem. In order to understand how and why these properties work, we first review the theory of the *coherent preparation* of an initial state composed of a continuum of scattering eigenfunctions.

Consider the case in which we prepare a wavepacket consisting of a superposition of scattering eigenstates $|E, \mathbf{m}^{\pm}\rangle$ of the material Hamiltonian, H_M, where

$$[E - H_M]|\, E, \mathbf{m}^{\pm}\rangle = 0 \tag{1}$$

subject to the normalization

$$\langle E', \mathbf{m}^{\pm}\,|E, \mathbf{n}^{\pm}\rangle = \delta(E - E')\delta_{\mathbf{m},\mathbf{n}} \tag{2}$$

Here E is the (continuous) energy and $\mathbf{m}$ designates all additional quantum numbers of relevance, e.g., the identity of the collision partners after the collision and all of the internal quantum numbers associated with each partner. The $\pm$ notation differentiates between *outgoing* (+) and *incoming* (−) boundary conditions (Levine, 1969), as explained in detail below.

As a specific method of preparation, we consider excitation of an initial bound state $|E_1\rangle$ by a laser pulse of the form

$$\epsilon(t) = \hat{\epsilon}\,\varepsilon(t) = \hat{\epsilon}\int_{-\infty}^{\infty} d\omega\,\bar{\varepsilon}(\omega)\exp(-i\omega t) \tag{3}$$

where $\epsilon(t)$ is the pulse's electric field vector, $\hat{\epsilon}$ is the polarization direction, and $\bar{\varepsilon}(\omega)$ is the Fourier transform of $\varepsilon(t)$ at angular frequency ω.

We wish to solve the time-dependent Schrödinger equation,

$$i\hbar\frac{d\Psi}{dt} = H\Psi \tag{4}$$

where H is the total Hamiltonian in the presence of the laser field,

$$H = H_M - \mathbf{d}\cdot\hat{\epsilon}\,\varepsilon(t) \tag{5}$$

with $\mathbf{d}$ being the transition-dipole operator and $\mathbf{d}\cdot\hat{\epsilon}$ its projection on the light's polarization direction. Assuming that the radiation-free eigenstates that predominate are the initial state $|E_1\rangle$ and a set of continuum states $|E, \mathbf{m}^{\pm}\rangle$,

we expand Ψ as

$$\begin{aligned}|\,\Psi(t)\rangle &= b_1(t)|\,E_1\rangle\exp(-iE_1t/\hbar) + \sum_{\mathbf{n}=1}^{N}\int dE b_{E,\mathbf{n}}(t)|\,E, \mathbf{n}^{\pm}\rangle\exp(-iEt/\hbar)\\ &\equiv b_1(t)|\,E_1\rangle\exp(-iE_1t/\hbar) + |\,\Psi_e(t)\rangle\end{aligned} \tag{6}$$

where $|\,\Psi_e(t)\rangle$, defined by Eq. (6), is the excited portion of the wavefunction (the "excited wavepacket").

In order to calculate b_1 and $b_{E,\mathbf{n}}$ we substitute Eq. (6) in Eq. (4) to obtain a set of coupled first-order differential equations,

$$\begin{aligned}\frac{db_1(t)}{dt} &= (i/\hbar)\sum_{\mathbf{n}}\int dE b_{E,\mathbf{n}}(t)\exp(-i\omega_{E,1}t)\varepsilon(t)\langle E_1|\mathbf{d}\cdot\hat{\epsilon}|\,E, \mathbf{n}^{\pm}\rangle\\ \frac{db_{E,\mathbf{m}}(t)}{dt} &= (i/\hbar)b_1(t)\exp(i\omega_{E,1}t)\varepsilon(t)\langle E, \mathbf{m}^{\pm}|\mathbf{d}\cdot\hat{\epsilon}|\,E_1\rangle\end{aligned} \tag{7}$$

where $\omega_{E,1} \equiv (E - E_1)/\hbar$. In the presence of a sufficiently weak pulse, we can use first-order perturbation theory, according to which $b_1(t) \approx b_1(t = 0) = 1$, and $b_{E,\mathbf{n}}$ at the end of the pulse Eq. (7) is (Shapiro, 1993)

$$b_{E,\mathbf{n}} = (2\pi i/\hbar)\bar{\varepsilon}(\omega_{E,1})\langle E, \mathbf{n}^{\pm}|\mathbf{d}\cdot\hat{\epsilon}|\,E_1\rangle \tag{8}$$

After the pulse is over, the excited wavepacket is therefore given as

$$|\,\Psi_e(t)\rangle = (2\pi i/\hbar)\sum_{\mathbf{n}}\int dE\,\bar{\varepsilon}(\omega_{E,1})\langle E, \mathbf{n}^{\pm}|\mathbf{d}\cdot\hat{\epsilon}|\,E_1\rangle|\,E, \mathbf{n}^{\pm}\rangle\exp(-iEt/\hbar) \tag{9}$$

We wish now to investigate the long-time properties of Eq. (9). To do so we need to relate the eigenstates of H_M to the eigenstates that describe the freely moving fragments at the end of the process. As an example, consider a triatomic molecule ABC, which breaks apart at the end of the process to yield the $A + BC$ channel (denoted $q = 1$) or the $B + AC$ channel (denoted $q = 2$). Below we explicitly discuss the formalism for the $A + BC$ product. However, the structure is the same for the $B + AC$ channel, with obvious substitutions in the equations.

The Hamiltonian H_M can be written as composed of three parts:

$$H_M = K_{\mathbf{R}} + K_{\mathbf{r}} + W(\mathbf{R}, \mathbf{r}) \tag{10}$$

Here $\mathbf{R}$ is the radius vector between A and the $B-C$ center of mass, $\mathbf{r}$ is the $B-C$ separation, $W(\mathbf{R},\mathbf{r})$ is the total potential energy of A, B, and C, and

$$K_{\mathbf{R}} = \frac{-\hbar^2}{2\mu}\nabla_{\mathbf{R}}^2 \qquad K_{\mathbf{r}} = \frac{-\hbar^2}{2m}\nabla_{\mathbf{r}}^2 \tag{11}$$

are the kinetic energy operators in $\mathbf{R}$ and $\mathbf{r}$, and μ and m are the reduced masses,

$$\mu = m_A(m_B+m_C)/(m_A+m_B+m_C), \qquad m = m_B m_C/(m_B+m_C) \tag{12}$$

If $v(r)$ denotes the asymptotic limit of $W(\mathbf{R},\mathbf{r})$ as A departs from $B-C$,

$$v(r) = \lim_{R\to\infty} W(\mathbf{R},\mathbf{r}) \tag{13}$$

it is clear that the $A-BC$ *interaction potential*, defined as

$$V(\mathbf{R},\mathbf{r}) \equiv W(\mathbf{R},\mathbf{r}) - v(r) \tag{14}$$

vanishes as $R\to\infty$, i.e., $\lim_{R\to\infty} V(\mathbf{R},\mathbf{r}) = 0$. Defining the $B-C$ Hamiltonian as

$$h_{\mathbf{r}} \equiv K_{\mathbf{r}} + v(r) \tag{15}$$

the triatomic Hamiltonian of Eq. (10) can now be rewritten, using Eq. (14), as

$$H_M = K_{\mathbf{R}} + h_{\mathbf{r}} + V(\mathbf{R},\mathbf{r}) \tag{16}$$

We see that it is the interaction potential $V(\mathbf{R},\mathbf{r})$ that couples the motion of the A atom to the motion of the BC diatomic. In its absence, the two free fragments A and BC described by the free Hamiltonian

$$H_0 \equiv K_{\mathbf{R}} + h_{\mathbf{r}} \tag{17}$$

move independently of one another. Because H_0 is a sum of two independent terms, its eigenstates, $|E,\mathbf{m};0\rangle$,

$$[E-H_0]|E,\mathbf{m};0\rangle = 0 \tag{18}$$

are given as products

$$|E,\mathbf{m};0\rangle = |e_{\mathbf{m}}\rangle|\mathbf{k}_{\mathbf{m}}\rangle \tag{19}$$

where

$$[e_{\mathbf{m}} - h_{\mathbf{r}}]|e_{\mathbf{m}}\rangle = 0 \tag{20}$$

with $e_{\mathbf{m}}$ being the *internal* (electronic, vibrational, rotational) energy of the $B-C$ diatomic and with $|\mathbf{k}_{\mathbf{m}}\rangle$ satisfying

$$[E - e_{\mathbf{m}} - K_{\mathbf{R}}]|\mathbf{k}_{\mathbf{m}}\rangle = 0 \tag{21}$$

describing the free (translational) motion of A relative to BC.

The solution of Eq. (21), written in the coordinate representation

$$\left[E - e_{\mathbf{m}} + \frac{\hbar^2}{2\mu}\nabla_{\mathbf{R}}^2\right]\langle\mathbf{R}|\mathbf{k}_{\mathbf{m}}\rangle = 0 \tag{22}$$

describes an energy-normalized plane wave of kinetic energy $E-e_{\mathbf{m}}$,

$$\langle\mathbf{R}|\mathbf{k}_{\mathbf{m}}\rangle = \left[\frac{m k_{\mathbf{m}}}{\hbar^2(2\pi)^3}\right]^{1/2}\exp(i\mathbf{k}_{\mathbf{m}}\cdot\mathbf{R}) \tag{23}$$

where

$$k_m = \{2\mu(E-e_{\mathbf{m}})\}^{1/2}/\hbar \tag{24}$$

is the wavevector of the free motion of A relative to the BC center of mass. Because the free solutions assume the same continuous energy spectrum as do the full solutions $|E,\mathbf{n}^{\pm}\rangle$, they too satisfy the continuous spectrum normalization,

$$\langle E',\mathbf{m};0|E,\mathbf{n};0\rangle = \delta(E-E')\delta_{\mathbf{m},\mathbf{n}} \tag{25}$$

The eigenstates, $|E,\mathbf{n}^{\pm}\rangle$, of the fully interacting Hamiltonian H_M are related to $|E,\mathbf{n};0\rangle$ via the Lippmann-Schwinger equation (Taylor, 1972)

$$|E,\mathbf{n}^{\pm}\rangle = |E,\mathbf{n};0\rangle + \lim_{\epsilon\to 0}[E\pm i\epsilon - H_0]^{-1}V|E,\mathbf{n}^{\pm}\rangle \tag{26}$$

where the plus solution is known as the *outgoing* solution and the minus solution as the *incoming* solution. Each solution is an independent (though not mutually orthogonal) eigenstate of the full Schrödinger equation [Eq. (1)].

We now use the Lippmann-Schwinger equation to explore the long-time behavior of the wavepacket $\Psi_e(t)$ created with the laser pulse. Either the outgoing or the incoming set of solutions can be used as the basis set for expanding $\Psi_e(t)$. In what follows we shall see which type of solution is best for which purpose. Substituting Eq. (26) in Eq. (9), we obtain that

$$|\Psi_e(t)\rangle = (2\pi i/\hbar)\sum_{\mathbf{n}}\int dE \exp(-iEt/\hbar)\bar{\varepsilon}(\omega_{E,1})\langle E,\mathbf{n}^{\pm}|\mathbf{d}\cdot\hat{\epsilon}|E_1\rangle \{|E,\mathbf{n};0\rangle + [E\pm i\epsilon - H_0]^{-1}V|E,\mathbf{n}^{\pm}\rangle\} \tag{27}$$

Using the spectral resolution of $[E\pm i\epsilon - H_0]^{-1}$, we have from Eq. (27) that the probability amplitude of finding a free state $|E',\mathbf{m};0\rangle$ at time t is given as

$$\langle E',\mathbf{m};0|\Psi_e(t)\rangle = (2\pi i/\hbar)\sum_{\mathbf{n}}\int dE \exp(-iEt/\hbar)\bar{\varepsilon}(\omega_{E,1})\langle E,\mathbf{n}^{\pm}|\mathbf{d}\cdot\hat{\epsilon}|E_1\rangle \{\langle E'\mathbf{m};0|E,\mathbf{n};0\rangle + [E\pm i\epsilon - E']^{-1}\langle E'\mathbf{m};0|V|E,\mathbf{n}^{\pm}\rangle\} \tag{28}$$

Using the normalization of the free states [Eq. (25)], we have that

$$\langle E',\mathbf{m};0|\Psi_e(t)\rangle = (2\pi i/\hbar)\exp(-iE't/\hbar)\{\bar{\varepsilon}(\omega_{E',1})\langle E',\mathbf{m}^{\pm}|\mathbf{d}\cdot\hat{\epsilon}|E_1\rangle + \sum_{\mathbf{n}}\int dE \exp(-iEt/\hbar)\bar{\varepsilon}(\omega_{E,1})\langle E,\mathbf{n}^{\pm}|\mathbf{d}\cdot\hat{\epsilon}|E_1\rangle \times [E\pm i\epsilon - E']^{-1}\langle E'\mathbf{m};0|V|E,\mathbf{n}^{\pm}\rangle\} \tag{29}$$

In the $t\to\infty$ limit the integration over E can be performed analytically by contour integration. Note first that in that limit, the integrand on a large semicircle of radius R in the lower part of the complex E plane is zero, because when $E = Re^{i\theta}$, with $\theta < 0$,

$$\exp(-iEt/\hbar) = \exp(-iRe^{i\theta}t/\hbar) = \exp(-iR\cos\theta t/\hbar)\exp(R\sin\theta t/\hbar)_{t\to\infty}\to 0 \tag{30}$$

Thus, the result of the real E integration remains unchanged by supplementing it with integration along a large semicircle in the lower half E-plane. Because in the $-i\epsilon$ case, the integrand has a pole at $E = E' + i\epsilon$ that is outside the closed contour, the whole integral is zero. We obtain that

$$\lim_{t\to\infty}\langle E',\mathbf{m};0|\Psi_e(t)\rangle = (2\pi i/\hbar)\bar{\varepsilon}(\omega_{E',1})\exp(-iE't/\hbar)\langle E',\mathbf{m}^{-}|\mathbf{d}\cdot\hat{\epsilon}|E_1\rangle \tag{31}$$

Hence the coefficients of expansion of the full wavepacket of Eq. (9), in terms of the $|E,\mathbf{m}^{-}\rangle$ states give the probability of observing states $|E,\mathbf{m};0\rangle$ in the distant future.

If instead of the incoming states we use the outgoing states, the closed-contour integration encircles a pole at $E = E' - i\epsilon$. Hence the integration yields

$$\lim_{t\to\infty}\langle E',\mathbf{m};0|\Psi_e(t)\rangle = (2\pi i/\hbar)\exp(-iE't/\hbar)\bar{\varepsilon}(\omega_{E',1}) \times\sum_{\mathbf{n}}S_{\mathbf{n},\mathbf{m}}(E')\langle E',\mathbf{n}^{+}|\mathbf{d}\cdot\hat{\epsilon}|E_1\rangle \tag{32}$$

where the $S_{\mathbf{n},\mathbf{m}}(E')$ matrix,

$$S_{\mathbf{n},\mathbf{m}}(E') \equiv \delta_{\mathbf{n},\mathbf{m}} - 2\pi i\langle E'\mathbf{m};0|V|E',\mathbf{n}^{+}\rangle \tag{33}$$

is known as the S-matrix or scattering matrix.

The form of Eq. (32) appears more complicated than that of Eq. (31) because each $\langle E,\mathbf{m};0|\Psi_e(t)\rangle$ component appears to be made up of contributions from all degenerate $|E,\mathbf{n};0\rangle$ states. Why use it at all then? The reason is that in ordinary scattering events, we want to use states whose past is well known to us. These are the outgoing states because when $t\to-\infty$, it is the contour on the semicircle in the upper half of the complex E-plane that vanishes. Supplementing the real-E integration by such a contour keeps the $E = E' - i\epsilon$ pole out of the contour, and we obtain that

$$\lim_{t\to-\infty}\langle E',\mathbf{m};0|\Psi_e(t)\rangle = (2\pi i/\hbar)\bar{\varepsilon}(\omega_{E',1})\exp(-iE't/\hbar)\langle E',\mathbf{m}^{+}|\mathbf{d}\cdot\hat{\epsilon}|E_1\rangle \tag{34}$$

In contrast, the $t\to-\infty$ limit appears more complicated with the incoming-states expansion because now the $E = E' + i\epsilon$ pole is enclosed by the contour, and we obtain that

$$\lim_{t\to-\infty}\langle E',\mathbf{m};0|\Psi_e(t)\rangle = (2\pi i/\hbar)\exp(-iE't/\hbar)\bar{\varepsilon}(\omega_{E',1}) \times\sum_{\mathbf{n}}S^{-}_{\mathbf{n},\mathbf{m}}(E')\langle E',\mathbf{n}^{-}|\mathbf{d}\cdot\hat{\epsilon}|E_1\rangle \tag{35}$$

where the $S^{-}_{\mathbf{n},\mathbf{m}}(E')$ matrix is defined as

$$S^{-}_{\mathbf{n},\mathbf{m}}(E') \equiv \delta_{\mathbf{n},\mathbf{m}} + 2\pi i \langle E'\mathbf{m}; 0 | V | E', \mathbf{n}^{-} \rangle \tag{36}$$

In the case of the optical pulse excitation, we use the incoming solutions because the origin of the system in the remote past is known to be $|E_1\rangle$ and our interest is in the fate of the system in the distant future.

III. Bichromatic Control of a Superposition State

Consider now how the laser field can be made to modify the outcome of the photo-dissociation process. As seen above, the probability of populating a "free" state $|e_{\mathbf{m}}\rangle|\mathbf{k}_{\mathbf{m}}\rangle$ at any given time is

$$P_{\mathbf{m}}(E)(t) = |\langle e_{\mathbf{m}} | \langle \mathbf{k}_{\mathbf{m}} | \Psi(t) \rangle|^2 \tag{37}$$

Using the expansion of $|\Psi(t)\rangle$ [Eq. (6)], we have that

$$\begin{aligned}\langle e_{\mathbf{m}} | \langle \mathbf{k}_{\mathbf{m}} | \Psi(t) \rangle &= b_1(t) \langle e_{\mathbf{m}} | \langle \mathbf{k}_{\mathbf{m}} | E_1 \rangle \exp(-iE_1 t/\hbar) \\ &\quad + \sum_{n} \int dE b_{E,\mathbf{n}}(t) \langle e_{\mathbf{m}} | \langle \mathbf{k}_{\mathbf{m}} | E, \mathbf{n}^{-} \rangle \exp(-iEt/\hbar)\end{aligned} \tag{38}$$

Assuming that $\langle e_{\mathbf{m}} | E_1 \rangle = 0$, (e.g., the two states belong to different electronic states), it follows from Eq. (38) that in the long-time limit,

$$P_{\mathbf{m}}(E) = |\langle e_{\mathbf{m}} | \langle \mathbf{k}_{\mathbf{m}} | \Psi_e(t \to \infty) \rangle|^2 = |b_{E,\mathbf{m}}(t \to \infty)|^2 \tag{39}$$

Because

$$b_{E,\mathbf{n}}(t \to \infty) = \frac{i}{\hbar} \langle E, \mathbf{n}^{-} | \mathbf{d} \cdot \hat{\epsilon} | E_1 \rangle \int_{-\infty}^{\infty} dt' \varepsilon(t') \exp(-i\omega_{E,1} t) b_1(t') \tag{40}$$

it follows that

$$\frac{P_{\mathbf{n}}(E)}{P_{\mathbf{m}}(E)} = \left| \frac{b_{E,\mathbf{n}}(\infty)}{b_{E,\mathbf{m}}(\infty)} \right|^2 = \left| \frac{\langle E, \mathbf{n}^{-} | \mathbf{d} \cdot \hat{\epsilon} | E_1 \rangle}{\langle E, \mathbf{m}^{-} | \mathbf{d} \cdot \hat{\epsilon} | E_1 \rangle} \right|^2 \tag{41}$$

We see that the relative probabilities of populating different asymptotic states at a fixed energy E are *independent of the laser power and pulse shape*. This result, which coincides with that of perturbation theory, holds true irrespective of the laser power, provided that only *one* initial state $|E_1\rangle$ is coupled to the continuum.

In order to affect the long-time outcome, we must therefore extend the treatment beyond the use of a single initial bound state. For example, starting from a linear superposition of two initial states

$$\Phi(t) = b_1 | E_1 \rangle \exp(-iE_1 t/\hbar) + b_2 | E_2 \rangle \exp(-iE_2 t/\hbar) \tag{42}$$

we have that

$$\begin{aligned}b_{E,\mathbf{n}}(t \to \infty) = \frac{i}{\hbar} \Bigg\{ &\langle E, \mathbf{n}^{-} | \mathbf{d} \cdot \hat{\epsilon} | E_1 \rangle \int_{-\infty}^{\infty} dt' \varepsilon(t') \exp(-i\omega_{E,1} t') b_1(t') \\ &+ \langle E, \mathbf{n}^{-} | \mathbf{d} \cdot \hat{\epsilon} | E_2 \rangle \int_{-\infty}^{\infty} dt' \varepsilon(t') \exp(-i\omega_{E,2} t') b_2(t') \Bigg\}\end{aligned} \tag{43}$$

In first-order perturbation theory, $b_1(t)$ and $b_2(t)$ are constant, so in the weak-field regime,

$$\begin{aligned}b_{E,\mathbf{n}}(t \to \infty) \approx \frac{2\pi i}{\hbar} \{ &\langle E, \mathbf{n}^{-} | \mathbf{d} \cdot \hat{\epsilon} | E_1 \rangle \bar{\epsilon}(\omega_{E,1}) b_1 \\ &+ \langle E, \mathbf{n}^{-} | \mathbf{d} \cdot \hat{\epsilon} | E_2 \rangle \bar{\epsilon}(\omega_{E,2}) b_2 \}\end{aligned} \tag{44}$$

Recognizing that $\bar{\epsilon}(\omega)$ is complex, we can write

$$\bar{\epsilon}(\omega_{E,j}) = |\bar{\epsilon}(\omega_{E,j})| e^{-i\theta(\omega_{E,j})}, \quad (j = 1, 2) \tag{45}$$

and transform Eq. (44) into

$$\begin{aligned}b_{E,\mathbf{n}}(\infty) = \frac{2\pi i}{\hbar} \{ &\langle E, \mathbf{n}^{-} | \mathbf{d} \cdot \hat{\epsilon} | E_1 \rangle |\bar{\epsilon}(\omega_{E,1})| e^{-i\theta(\omega_{E,1})} b_1 \\ &+ \langle E, \mathbf{n}^{-} | \mathbf{d} \cdot \hat{\epsilon} | E_2 \rangle |\bar{\epsilon}(\omega_{E,2})| e^{-i\theta(\omega_{E,2})} b_2 \}\end{aligned} \tag{46}$$

Then, the probability of observing product state $\mathbf{n}$ at infinite time is given as,

$$\begin{aligned}P_{\mathbf{n}}(E) = \frac{4\pi^2}{\hbar^2} |&\langle E, \mathbf{n}^{-} | \mathbf{d} \cdot \hat{\epsilon} | E_1 \rangle |\bar{\epsilon}(\omega_{E,1})| e^{-i\theta(\omega_{E,1})} b_1 \\ &+ \langle E, \mathbf{n}^{-} | \mathbf{d} \cdot \hat{\epsilon} | E_2 \rangle |\bar{\epsilon}(\omega_{E,2})| e^{-i\theta(\omega_{E,2})} b_2 |^2\end{aligned} \tag{47}$$

We see that the pulse attributes have been "imprinted" onto the material matrix elements. As a result, by changing the pulse attributes, we *can* change the branching ratios into different product channels.

The properties we wish to control are often the branching ratios to different chemical products. Note, however, that the approach advocated below, and indeed any CC scenario, can be readily modified to control probabilities of populating individual product states. Realizing that any chemical process such as

$$A + BC(\mathbf{n}) \overset{q=1}{\longleftarrow} ABC \overset{q=2}{\longrightarrow} AB(\mathbf{n}) + C \tag{48}$$

involves a multitude of internal fragment states ($|e_{\mathbf{n}}\rangle$) in each chemical channel, we calculate the total probability to produce products in one of the q channels as

$$P^{(q)}(E) = \sum_{\mathbf{n}} P^{(q)}_{\mathbf{n}}(E) = \sum_{\mathbf{n}} \frac{4\pi^2}{\hbar^2} |\langle E, q, \mathbf{n}^- | \mathrm{d}\cdot\hat{\epsilon}| E_1\rangle|\bar{\epsilon}(\omega_{E,1})|e^{-i\theta(\omega_{E,1})}b_1 + \langle E, q, \mathbf{n}^- | \mathrm{d}\cdot\hat{\epsilon}| E_2\rangle|\bar{\epsilon}(\omega_{E,2})|e^{-i\theta(\omega_{E,1})}b_2|^2 \tag{49}$$

Here we have modified our notation so that $\mathbf{n}$ denotes all quantum numbers other than the arrangement channel label q. By expanding the square, the above expression transforms to

$$P^{(q)}(E) = P^{(q)}_{11}(E) + P^{(q)}_{22}(E) + P^{(q)}_{12}(E) \tag{50}$$

where

$$P^{(q)}_{jj}(E) = \frac{4\pi^2}{\hbar^2}\mu^{(q)}_{jj}|\bar{\epsilon}(\omega_{E,j}|^2 b_j^2 \quad (j = 1,2)$$
$$P^{(q)}_{12}(E) = \frac{4\pi^2}{\hbar^2}|\bar{\epsilon}(\omega_{E,1})||\bar{\epsilon}(\omega_{E,2})|2\mathcal{R}_e\{\mu^{(q)}_{12}e^{-i\theta_{12}}b_1^* b_2\} \tag{51}$$

where

$$\mu^{(q)}_{jj} \equiv \sum_{\mathbf{n}} |\langle E, q, \mathbf{n}^- | \mathrm{d}\cdot\hat{\epsilon}| E_j\rangle|^2, \quad (j = 1,2)$$
$$\mu^{(q)}_{12} = \sum_{\mathbf{n}} \langle E_1 | \mathrm{d}\cdot\hat{\epsilon}| E, q, \mathbf{n}^-\rangle\langle E, q, \mathbf{n}^- | \mathrm{d}\cdot\hat{\epsilon}| E_2\rangle \tag{52}$$

and $\theta_{12} \equiv \theta(\omega_{E,2}) - \theta(\omega_{E,1})$.

The $P^{(q)}_{11}(E)$ and $P^{(q)}_{22}(E)$ terms are the probabilities of photo-dissociating levels $|E_1\rangle$ and $|E_2\rangle$, respectively. The $P^{(q)}_{12}(E)$ is the interference term. It is the only term influenced by the relative phase θ_{12} between the $\bar{\epsilon}(\omega_{E,1})$ and $\bar{\epsilon}(\omega_{E,2})$ field modes.

In order to make the structure of the probability expression Eq. (51) clearer, we write the complex amplitude $\mu^{(q)}_{12}$ as

$$\mu^{(q)}_{12} = |\mu^{(q)}_{12}|e^{i\phi^{(q)}_{12}} \tag{53}$$

where $\phi^{(q)}_{12}$ is the so-called "molecular" or "material" phase, and define the phase α_{12} via

$$b_1^* b_2 = |b_1 b_2|e^{-i\alpha_{12}} \tag{54}$$

With these definitions, the interference term assumes the form

$$P^{(q)}_{12}(E) = \frac{8\pi^2}{\hbar^2}|\bar{\epsilon}(\omega_{E,1})\bar{\epsilon}(\omega_{E,2})\mu^{(q)}_{12}b_1 b_2|\cos[\phi^{(q)}_{12} - \alpha_{12} - \theta_{12}] \tag{55}$$

Because of the dependence of $\phi^{(q)}_{12}$ on q, this term can be positive ("constructive interference") or negative ("destructive interference") with respect to one q channel and the opposite with respect to the other. Hence, by tuning the external phases α_{12} or θ_{12}, we can make the sign of this term negative with respect to one q chemical channel and positive with respect to another. In this way, by changing an external phase factor that is indifferent to the final channels, we attain selectivity (discrimination) between the final channels. The magnitude of this effect can be enhanced by varying the ratio

$$x \equiv \frac{|\bar{\epsilon}(\omega_{E,1})b_1|}{|\bar{\epsilon}(\omega_{E,2})b_2|}$$

The method of controlling the final outcome of a process in this way is at the heart of coherent control.

The structure of the CC equations is most transparent when we write Eq. (50) and Eq. (51) as

$$P^{(q)}(E) = \frac{4\pi^2}{\hbar^2}|\bar{\epsilon}(\omega_{E,1})b_1|^2\{\mu^{(q)}_{11} + x^2\mu^{(q)}_{22} + 2x|\mu^{(q)}_{12}|\cos[\phi^{(q)}_{12} - \alpha_{12} - \theta_{12}]\} \tag{56}$$

In order to attain maximum control over $R_{q'q}$, we can set $P^{(q)}(E) = 0$ for one of the q channels. Both $P^{(q)}(E)$ and $\mu_{11}^{(q)} + x^2\mu_{22}^{(q)}$ of Eq. (56) are positive, so the only way we can minimize $P^{(q)}(E)$ is by making the interference term $2x|\mu_{12}^{(q)}|\cos[\phi_{12}^{(q)} - \alpha_{12} - \theta_{12}]$ as negative as possible, which means setting the external phases such that

$$\alpha_{12} + \theta_{12} = \pi - \phi_{12}^{(q)} \tag{57}$$

Under these circumstances, $\cos[\phi_{12}^{(q)} - \alpha_{12} - \theta_{12}] = -1$ and Eq. (56) becomes

$$P^{(q)}(E) = \frac{4\pi^2}{\hbar^2}|\bar{\epsilon}(\omega_{E,1})b_1|^2\{\mu_{11}^{(q)} + x^2\mu_{22}^{(q)} - 2x|\mu_{12}^{(q)}|\} = 0 \tag{58}$$

This is a quadratic equation in x that has a solution $x = |\mu_{12}^{(q)}|/\mu_{22}^{(q)}$, if and only if $|\mu_{12}^{(q)}|^2 = \mu_{11}^{(q)}\mu_{22}^{(q)}$.

In order to see the circumstances under which this condition is fulfilled we write,

$$\begin{aligned}
\mu_{11}^{(q)} &= \sum_{\mathbf{n}}\langle E_1|\mathrm{d}\cdot\hat{\epsilon}|E,q,\mathbf{n}^-\rangle\langle E,q,\mathbf{n}^-|\mathrm{d}\cdot\hat{\epsilon}|E_1\rangle \\
&= \langle E_1|\mathrm{d}\cdot\hat{\epsilon}\left\{\sum_{\mathbf{n}}|E,q,\mathbf{n}^-\rangle\langle E,q,\mathbf{n}^-|\right\}\mathrm{d}\cdot\hat{\epsilon}|E_1\rangle = \langle E_1\mathrm{d}\cdot\hat{\epsilon}P|P\mathrm{d}\cdot\hat{\epsilon}E_1\rangle \\
\mu_{22}^{(q)} &= \sum_{\mathbf{n}}\langle E_2|\mathrm{d}\cdot\hat{\epsilon}|E,q,\mathbf{n}^-\rangle\langle E,q,\mathbf{n}^-|\mathrm{d}\cdot\hat{\epsilon}|E_2\rangle = \langle E_2\mathrm{d}\cdot\hat{\epsilon}P|P\mathrm{d}\cdot\hat{\epsilon}E_2\rangle \\
|\mu_{12}^{(q)}| &= \left|\sum_{\mathbf{n}}\langle E_1|\mathrm{d}\cdot\hat{\epsilon}|E,q,\mathbf{n}^-\rangle\langle E,q,\mathbf{n}^-|\mathrm{d}\cdot\hat{\epsilon}|E_2\rangle\right| = |\langle E_1\mathrm{d}\cdot\hat{\epsilon}P|P\mathrm{d}\cdot\hat{\epsilon}E_2\rangle|
\end{aligned} \tag{59}$$

where

$$P \equiv \sum_{\mathbf{n}}|E,q,\mathbf{n}^-\rangle\langle E,q,\mathbf{n}^-| \tag{60}$$

and we have used the fact that the projection operator P satisfies $PP = P$. Hence the $\mu_{11}^{(q)}$, $\mu_{22}^{(q)}$, and $|\mu_{12}^{(q)}|$ matrix elements are related as scalar products of the $|E_1\mathrm{d}\cdot\hat{\epsilon}P\rangle$ and $|P\mathrm{d}\cdot\hat{\epsilon}E_2\rangle$ state vectors. By the Schwarz inequality,

$$|\langle E_1\mathrm{d}\cdot\hat{\epsilon}P|P\mathrm{d}\cdot\hat{\epsilon}E_2\rangle|^2 \le \langle E_1\mathrm{d}\cdot\hat{\epsilon}P|P\mathrm{d}\cdot\hat{\epsilon}E_1\rangle\langle E_2\mathrm{d}\cdot\hat{\epsilon}P|P\mathrm{d}\cdot\hat{\epsilon}E_2\rangle \tag{61}$$

with the equality holding only when $|E_1\mathrm{d}\cdot\hat{\epsilon}P\rangle$ and $|P\mathrm{d}\cdot\hat{\epsilon}E_2\rangle$ are parallel to one another. If P is a projection onto a single state — i.e., no $\mathbf{n}$ summation need be performed — then the equality in Eq. (61) holds. That is, by definition, the case, because by definition,

$$\begin{aligned}
&|\langle E_1\mathrm{d}\cdot\hat{\epsilon}|E,q^-\rangle\langle E,q^-|\mathrm{d}\cdot\hat{\epsilon}E_2\rangle|^2 \\
&\quad = \langle E_1\mathrm{d}\cdot\hat{\epsilon}|E,q^-\rangle\langle E,q,^-|\mathrm{d}\cdot\hat{\epsilon}E_1\rangle\langle E_2\mathrm{d}\cdot\hat{\epsilon}|E,q^-\rangle\langle E,q^-|\mathrm{d}\cdot\hat{\epsilon}E_2\rangle
\end{aligned}$$

In all other cases, because of the existence of many $\mathbf{n}$ internal states, the strict inequality holds and the solution of Eq. (58) can never be realized. Nevertheless, numerous computational studies, some discussed below, show that control is extensive.

In general, experiments measure energy-averaged quantities such as the probability P_q of forming product in channel q, and the ratio $R_{q,q'}$ of product in each channel:

$$\begin{aligned}
P_q &= \int dE\, P_q(E) \\
R_{q,q'} &= P_q/P_{q'}
\end{aligned} \tag{62}$$

because products are not distinguished on the basis of total energy. For the case considered above, the photo-dissociation of a superposition state, $P_q(E)$ is nonzero at three energies: $E = E_1 + \hbar\omega_{E,1} = E_2 + \hbar\omega_{E,2}$, $E = E_1 + \hbar\omega_{E,2}$, and $E = E_2 + \hbar\omega_{E,1}$. The contribution from the first of these energies, $P_q(E = E_1 + \hbar\omega_{E,1})$, is given in Eq. (49), where the remaining contributions are

$$\begin{aligned}
P_q(E = E_1 + \hbar\omega_{E,2}) &= \left(\frac{2\pi}{\hbar}\right)^2|b_1\bar{\epsilon}(\omega_{E,2})|^2\mu_q(11) \\
P_q(E = E_2 + \hbar\omega_{E,1}) &= \left(\frac{2\pi}{\hbar}\right)^2|b_2\bar{\epsilon}(\omega_{E,1})|^2\mu_q(22)
\end{aligned} \tag{63}$$

Thus, the overall P_q for $N = 2$ is given by

$$P_q = P_q(E = E_1 + \hbar\omega_{E,1}) + P_q(E = E_1 + \hbar\omega_{E,2}) + P_q(E = E_2 + \hbar\omega_{E,1}) \tag{64}$$

The latter two terms correspond to traditional photo-dissociation terms without associated interference contributions and provide *uncontrollable* photo-dissociation terms that we call "satellites." In this and all coherent

control scenarios discussed below, it is important to attempt to reduce the relative magnitude of the satellite terms in order to increase overall controllability.

As the first example of coherent control, consider the bichromatic control of the photo-dissociation of methyl iodide in the A band (near 266 nm):

$$CH_3 + I^*(^2P_{1/2}) \leftarrow CH_3I \rightarrow CH_3 + I(^2P_{3/2}) \tag{65}$$

The control objective is the formation of ground-state iodine [$I(^2P_{3/2})$, denoted I] versus excited-state iodine [$I(^2P_{1/2})$, denoted I*]. The computation considered a rotating collinear model in which the H_3 center of mass, the C, and the I groups are assumed to lie on a line (Shapiro and Brumer, 1987). All satellite terms are included. The bound states $|E_i\rangle$ are characterized in this case by v, J, and M_J, the vibrational, rotational, and magnetic quantum numbers. Figure 1 shows contour plots of the yield of $CH_3 + I^*$ (i.e., the fraction of product that is $CH_3 + I^*$), as a function of θ_{12} and $s = x^2/[1 + x^2]$ in the photo-dissociation of CH_3I out of an equal superposition of the $|v_1 = 0, J_1 = 2\rangle$ and $|v_2 = 1, J_2 = 2\rangle$ states at two different frequencies, $\omega_{E,1} = 39{,}639\,\text{cm}^{-1}$ and $\omega_{E,1} = 42{,}367\,\text{cm}^{-1}$. The M_J magnetic quantum number is averaged over, and all satellite terms are included. Clearly, control is extensive, ranging from 0.3 to 0.75 as the control parameters are varied. Note also that a comparison of Figs. 1(a) and 1(b), which correspond to results at different excitation frequencies, shows that there is considerable dependence of the control contour topology on frequency.

This bichromatic scenario has been extended theoretically in a number of ways. For example, we have considered (Shapiro and Brumer, 1992) the extension of this scenario to a superposition of N bound states excited by N laser frequencies and demonstrated total control over the dynamics under certain conditions. We have also considered the two-level approach in the condensed phase (Shapiro and Brumer, 1989) in order to examine the effect of collisions and dephasing on control. In particular, the CC scenario described above was extended in the following way. The initial superposition state [Eq. (42)] was assumed prepared by two-photon absorption in the presence of collisions, modeled by a Bloch equation with appropriate T_1, T_2 relaxation times. This transition was assumed saturated, establishing a time-independent density matrix describing this two-level system. This superposition was then pumped to dissociation by a pulsed laser whose width exceeds the spacing between the pair of bound levels. Thus, the pump laser contains both frequencies $\omega_{E,1}, \omega_{E,2}$ necessary to excite the superposition to the same continuum energy E. The resultant branching in CH_3I [Eq. (65)] was examined, and control was found to survive over a substantial temperature range. This model computation motivates applications of CC in the condensed phase, as do the experiments discussed in Section VIII.

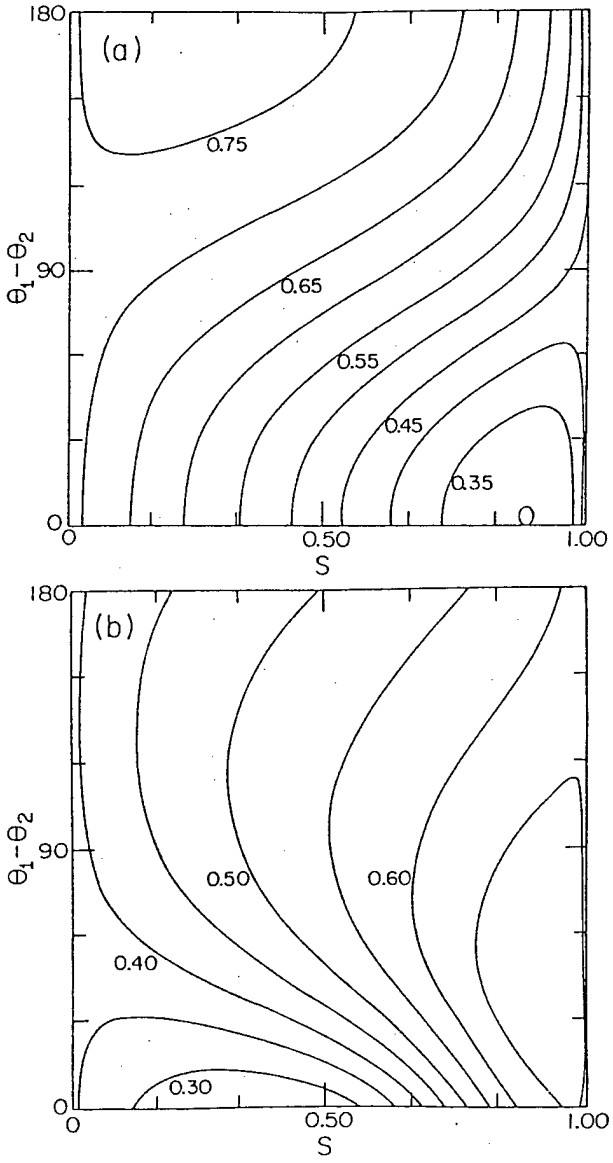

FIG. 1. Contour plot of the yield of I* (i.e., fraction of I* as product) in the bichromatically controlled photo-dissociation of CH_3I starting from an M-averaged initial state. (a) $\omega_{E,1} = 39{,}639\,\text{cm}^{-1}$, (b) $\omega_{E,1} = 42{,}367\,\text{cm}^{-1}$. (From Shapiro and Brumer, 1987.)

IV. The Coherent Control Principle

Photo-dissociation of a superposition state, the scenario described above, will be seen to be just one particular implementation of a general principle of coherent control, i.e., that *coherently driving a state with phase coherence through multiple optical excitation routes to the same final state allows for the possibility of control.* This procedure has a well-known analogy: the interference between paths as a beam of either particles or light passes through a double slit. In that case, interference between two coherent beams leads to spatial patterns of enhanced or reduced probabilities on an observation screen. In the case of coherent control, the overall coherence of a pure state plus laser source allows for the constructive or destructive manipulation of probabilities in product channels. Active control results because the excitation process explicitly imparts experimentally controllable phase and amplitude information to the molecule.

It is important to note that, in general, quantum-interference-based control occurs only between energetically degenerate states. To see this, note that if the excitation creates product states of energy E and E', then the interference term [e.g., Eq. (55)] would carry the phase $\exp[i(E-E')t/\hbar]$. Thus, this term, as well as the interference term, would average to zero over a small time interval, and control would be lost.

Further, it is worth noting that CC scenarios often lead to simple analytic expressions for reaction probabilities in terms of a few molecular parameters and a few control parameters. Hence, the entire dependence of product probabilities on the control parameters can be easily generated experimentally once the molecular terms are determined from a fit of the control expression to a small number of experimentally determined yields.

Numerous scenarios can be designed that rely on the essential coherent control principle. Several are discussed in the following sections.

V. Weak-Field Coherent Control: Unimolecular Processes

A. Interference Between N-Photon and M-Photon Routes

Rather than starting with a nonstationary superposition state, as above, we can achieve CC by photo-dissociating a *single* stationary state via two optical paths (Shapiro *et al.*, 1988). Such paths can consist, for example, of an N-photon process and an M-photon process satisfying $N\omega_N = M\omega_M$, with ω_N and ω_M being the optical frequencies of each path. The numbers N and M can be of the same parity or of opposite parity. It turns out that the latter allows for control over the photo-dissociation differential cross sections, whereas the former

allows for control over both the integral and the differential cross sections. For simplicity we focus here on the three lowest-order cases $(N,M)=(1,3)$, $(N,M)=(1,2)$, and $(N,M)=(2,2)$. Other cases, such as the $(N,M)=(2,4)$ case (Bandrauk *et al.*, 1992; Chelkowski and Bandrauk, 1991), and strong-field extensions (Charron *et al.*, 1995; Szöke *et al.*, 1991; Zuo and Bandrauk, 1996) have been discussed in the literature.

1. *One-Photon versus Three-Photon Interference*

We consider (Shapiro *et al.*, 1988) a molecule, initially in state $|g\rangle|E_i\rangle$, where $|g\rangle$ denotes the ground electronic state, subjected to two co-propagating CW fields of frequencies ω_1 and ω_3 with $\omega_3 = 3\omega_1$. The total Hamiltonian is given by

$$H = H_M - 2\mathbf{d}\cdot\mathcal{R}_e[\hat{\epsilon}_3\bar{\epsilon}_3\exp(-i\omega_3 t) + \hat{\epsilon}_1\bar{\epsilon}_1\exp(-i\omega_1 t)] \tag{66}$$

where $\bar{\epsilon}_i \equiv \bar{\epsilon}(\omega_i)$.

We assume the following physics: (a) dipole transitions within electronic states are negligible compared to those between electronic states; (b) the fields are sufficiently weak to allow the use of perturbation theory; and (c) $E_i + 2\hbar\omega_1$ is below the dissociation threshold, with dissociation occurring in the $|e\rangle$-excited electronic manifold.

Given the above assumptions, the lowest-order expression for the one-photon or three-photon dissociation amplitude $A_{q,\mathbf{m}}(E = E_i + \hbar\omega_1)$ is

$$A_{q,\mathbf{m}}(E = E_i + \hbar\omega_1) = \left(\frac{2\pi i}{\hbar}\right)[\delta(\omega_3 - \omega_{E,i})\bar{\epsilon}_3\langle E,q,\mathbf{m}^-|\,\mathrm{d}_{e,g}\,|E_i\rangle + \delta(3\omega_1 - \omega_{E,i})\bar{\epsilon}_1^3\langle E,q,\mathbf{m}^-|\,T\,|E_i\rangle] \tag{67}$$

where $\mathrm{d}_{e,g} \equiv \langle e|\mathrm{d}\cdot\hat{\epsilon}|g\rangle$ and T denotes the three-photon transition operator, given in third-order perturbation theory as

$$T = \mathrm{d}_{e,g}(E_i - H_g + 2\hbar\omega_1)^{-1}\mathrm{d}_{g,e}(E_i - H_e + \hbar\omega_1)^{-1}\mathrm{d}_{e,g} \tag{68}$$

Because all light sources have a finite frequency width, we can integrate over this width to obtain

$$P_q(E) = \sum_{\mathbf{m}}\left|\int d\omega_3 A_{q,\mathbf{m}}(E = E_i + \hbar\omega_1)\right|^2 = P_q^{(1)}(E) + P_q^{(3)}(E) + P_q^{(13)}(E) \tag{69}$$

where the one-photon photodissociation probability is

$$P_q^{(1)}(E) = \left(\frac{2\pi}{\hbar}\right)^2 |\bar{\epsilon}_3|^2 \sum_{\mathbf{m}} |\langle E, q, \mathbf{m}^- \,|\, \mathrm{d}_{e,g} \,|\, E_i\rangle|^2 \tag{70}$$

the three-photon photodissociation probability is

$$P_q^{(3)}(E) = \left(\frac{2\pi}{\hbar}\right)^2 |\bar{\epsilon}_1|^6 \sum_{\mathbf{m}} |\langle E, q, \mathbf{m}^- \,|\, T \,|\, E_i\rangle|^2 \tag{71}$$

and the one-photon/three-photon interference term is

$$P_q^{(13)}(E) = \left(\frac{2\pi}{\hbar}\right)^2 \left[\bar{\epsilon}_3 \bar{\epsilon}_1^3 \sum_{\mathbf{m}} \langle E_i \,|\, T \,|\, E, q, \mathbf{m}^-\rangle \langle E, q, \mathbf{m}^- \,|\, \mathrm{d}_{e,g} \,|\, E_i\rangle + c.c.\right] \tag{72}$$

As in our discussion of the photo-dissociation of a superposition state, we define a "molecular" interference-amplitude $|F_q^{(13)}|$ and a "molecular" phase $\delta_q^{(13)}$ as

$$|F_q^{(13)}| \exp\left(i\delta_q^{(13)}\right) \equiv \sum_{\mathbf{m}} \langle E_i \,|\, T \,|\, E, q, \mathbf{m}^-\rangle \langle E, q, \mathbf{m}^- \,|\, \mathrm{d}_{e,g} \,|\, E_i\rangle \tag{73}$$

Recognizing that $\bar{\epsilon}_i$ may be complex, $\bar{\epsilon}_i = |\bar{\epsilon}_i| e^{i\phi_i}$, we can write the above interference term as

$$P_q^{(13)}(E) = -2\left(\frac{2\pi}{\hbar}\right)^2 |\bar{\epsilon}_3 \bar{\epsilon}_1^3| \cos(\phi_3 - 3\phi_1 + \delta_q^{(13)}) |F_q^{(13)}| \tag{74}$$

The branching ratio $R_{qq'}(E)$ for channels q and q' can then be written as

$$R_{qq'}(E) = \frac{F_q^{(1)} - 2x\cos(\phi_3 - 3\phi_1 + \delta_q^{(13)})\epsilon_0^2 |F_q^{(13)}| + x^2 \epsilon_0^4 F_q^{(3)}}{F_{q'}^{(1)} - 2x\cos(\phi_3 - 3\phi_1 + \delta_{q'}^{(13)})\epsilon_0^2 |F_{q'}^{(13)}| + x^2 \epsilon_0^4 F_{q'}^{(3)}} \tag{75}$$

where

$$F_q^{(1)} = \left(\frac{\hbar}{\pi|\bar{\epsilon}_3|}\right)^2 P_q^{(1)}(E); \quad F_q^{(3)} = \left(\frac{\hbar}{\pi|\bar{\epsilon}_1|^3}\right)^2 P_q^{(3)}(E) \tag{76}$$

and

$$x = \frac{|\bar{\epsilon}_1|^3}{\epsilon_0^2 |\bar{\epsilon}_3|} \tag{77}$$

where ϵ_0 is defined as a single unit of electric field. x is therefore a dimensionless parameter.

The numerator and denominator of Eq. (75) both display the canonical form for coherent control, i.e., a form similar to Eq. (50) in which there are independent contributions from more than one route, modulated by an interference term. Because the interference term is controllable through variation of laboratory parameters, so too is the product ratio $R_{qq'}(E)$. Thus, the principle on which this control scenario is based is the same as that in Section III, but the interference is introduced in an entirely different way.

With the qualitative principle of interfering pathways exposed, we demonstrate the quantitative extent to which the one-photon versus three-photon scenario alters the yield ratio in a realistic system by considering the photodissociation of IBr:

$$\mathrm{I} + \mathrm{Br} \leftarrow \mathrm{IBr} \rightarrow \mathrm{I} + \mathrm{Br}^* \tag{78}$$

where $\mathrm{Br} = \mathrm{Br}(^2P_{3/2})$ and $\mathrm{Br}^* = \mathrm{Br}(^2P_{1/2})$. Reliable IBr potential curves were used throughout the calculation.

Computational results on this system were obtained (Chan *et al.*, 1991) for two different cases: excitation from states of fixed M_i (the projection of the diatomic angular momentum J_i along the z-axis) and for the average over initial M_i. Results, in the form of a contour plot of the Br^* yield for excitation from $v = 0, J_i = 1, M_i = 0$, and $J_i = 42$ (M_i averaged) are shown in Figs. 2 and 3 as a function of $s = x^2/(1 + x^2)$ and of the relative laser phase $(\phi_3 - 3\phi_1)$. The range of control in each case is impressive, with essentially no loss of control due to M averaging.

The three-photon versus one-photon scenario has been experimentally realized in atoms (Chen *et al.*, 1990) and by Gordon and coworkers (Park *et al.*, 1991; Lu *et al.*, 1992; Kleiman *et al.*, 1995; Zhu *et al.*, 1995, 1997) in a series of experiments on HCl, H_2S, and CO. In the case of HCl, the molecule was excited to an intermediate $^3\Sigma^-(\Omega^+)$ vib-rotational resonance, using a combination of three ω_1 ($\lambda_1 = 336$ nm) photons and one ω_3 ($\lambda_3 = 112$ nm) photon. The ω_3 beam was generated from an ω_1 beam by tripling in a Kr gas cell. Ionization of the intermediate state takes place by absorption of one additional ω_1 photon. Similar demonstrations in ammonia, trimethylamine, triethylamine, cyclooctatetraene, and 1,1-dimethylhydrazine have been reported by Bersohn and coworkers (Wang *et al.*, 1996b) and in Na by Cavalieri *et al.* (1997). Later

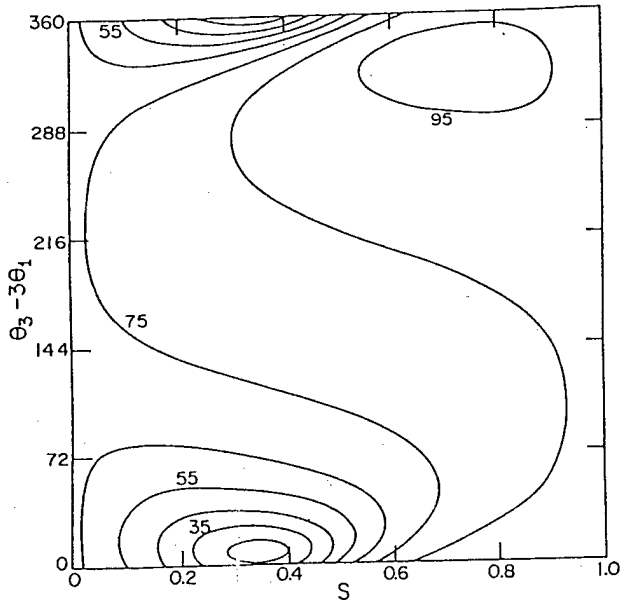

FIG. 2. Contour plot of the yield of Br^* (percentage of Br^* as product) in the photo-dissociation of IBr by the one-photon versus three-photon scenario. The abscissa is the amplitude parameter $s = x^2/(1+x^2)$, and the ordinate is $\theta_3 - 3\theta_1$. Here $\omega_1 = 6657.5\,\text{cm}^{-1}$. (From Chan *et al.*, 1991).

studies (Zhu *et al.*, 1995, 1997) demonstrated control over the production of different channels, specifically the HI^+ versus the H + I channels, in the photo-excitation of HI. This result is highly significant, showing the ability to control the *relative* yield of products in photo-dissociation.

In all of these experiments, control over $R_{qq'}(E)$ was obtained by varying the phase difference $(\phi_3 - 3\phi_1)$ and the parameter x. In doing so, the experiments used co-propagating ω_1 and ω_3 beams with wavevectors suitably "phase-matched" so that Eq. (75) no longer contains the spatial coordinate z, and the interference term is independent of the position in space.

It is also possible to use the one-photon versus three-photon (indeed any N-photon versus M-photon) control scenario to control differential cross sections. To see this, consider rewriting Eqs. (70) through (73) so that they apply to the probability of observing the product in channel q, but at a fixed scattering angle. Then the sum on $\mathbf{m}$ no longer includes an integral over scattering angle. Then the sum on $\mathbf{m}$ no longer includes an integral over scattering angles. The resultant interference term $P_q^{(13)}$ is nonzero, so varying the properties of the lasers will indeed alter the differential cross section into channel q.

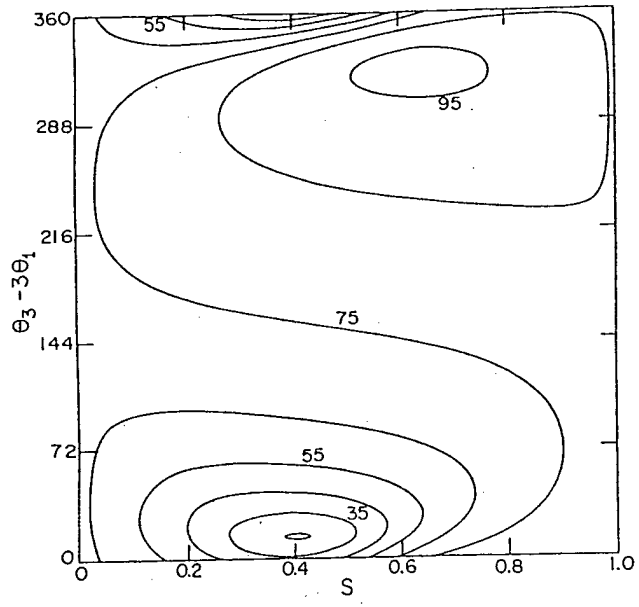

FIG. 3. As in Fig. 2 but for $v = 0$, $J_i = 42$, $\omega_1 = 6635.0\,\text{cm}^{-1}$ with an average over initial M_J. (From Chan *et al.*, 1991.)

2. *One-Photon versus Two-Photon Interference*

Although scenarios for simultaneous absorption of N plus M photons, where N, M are of the same parity, allow for control over both the differential and integral photo-dissociation cross sections, this is not the case when N, M are of different parity. In this case, only control over the differential cross section is possible. To see this, we consider the case of simultaneous one-photon versus two-photon absorption.

The Hamiltonian for a molecule irradiated with two frequencies ω_1 and ω_2, with $\omega_2 = 2\omega_1$, is

$$H = H_M - 2\mathbf{d} \cdot \mathcal{R}_e[\hat{\epsilon}_2 \bar{\epsilon}_2 \exp(-i\omega_2 t) + \hat{\epsilon}_1 \bar{\epsilon}_1 \exp(-i\omega_1 t)] \tag{79}$$

Assuming that $E_i + \hbar\omega_1$ is below the threshold for photo-dissociation and that absorption of ω_1 is via an intermediate electronic state that is dipole accessible, we obtain, in complete analogy to the one-photon versus three-photon case, that the probability $P_q(E, \hat{\mathbf{k}})$ of photo-dissociation into channel q at recoil angles $\hat{\mathbf{k}} \equiv (\theta_k, \phi_k)$ is given by

$$P_q(E, \hat{\mathbf{k}}) = P_q^{(1)}(E, \hat{\mathbf{k}}) + P_q^{(12)}(E, \hat{\mathbf{k}}) + P_q^{(2)}(E, \hat{\mathbf{k}}) \tag{80}$$

where

$$P_q^{(1)}(E,\hat{\mathbf{k}}) = \left(\frac{2\pi}{\hbar}\right)^2 |\bar{\epsilon}_2|^2 |\langle E,\hat{\mathbf{k}},q^- \,|\, \mathrm{d}_{e,g} \,|\, E_i\rangle|^2 \tag{81}$$

$$P_q^{(2)}(E,\hat{\mathbf{k}}) = \left(\frac{2\pi}{\hbar}\right)^2 |\bar{\epsilon}_1|^4 |\langle E_1,\hat{\mathbf{k}},q^- \,|\, D \,|\, E_i\rangle|^2 \tag{82}$$

$$P_q^{(12)}(E,\hat{\mathbf{k}}) = -2\left(\frac{2\pi}{\hbar}\right)^2 |\bar{\epsilon}_2 \bar{\epsilon}_1^2| \cos[\phi_2 - 3\phi_1 + \delta_q^{(12)}(\hat{\mathbf{k}})] |F_q^{(12)}(\hat{\mathbf{k}})| \tag{83}$$

Here, all channel indices $\mathbf{m}$ (which can be readily included) other than the final direction $\hat{\mathbf{k}}$ have been suppressed for clarity. The interference-amplitude $|F_q^{(12)}(\hat{\mathbf{k}})|$ and molecular-phase $\delta_q^{(12)}(\hat{\mathbf{k}})$ are defined by

$$|F_q^{(12)}(\hat{\mathbf{k}})| \exp\left(i\delta_q^{(12)}(\hat{\mathbf{k}})\right) = \langle E_i \,|\, D \,|\, E,\hat{\mathbf{k}},q^-\rangle \langle E,\hat{\mathbf{k}},q^- \,|\, \mathrm{d}_{e,g} \,|\, E_i\rangle \tag{84}$$

where D is the two-photon transition operator, given in lowest-order perturbation theory as

$$D = \sum_{e'} \mathrm{d}_{e,e'} (E_i - H_{e'} + \hbar\omega_1)^{-1} \mathrm{d}_{e',g} \tag{85}$$

The interference term $P_q^{(12)}(E,\hat{\mathbf{k}})$ is generally nonzero, so control over the differential cross section is possible.

Consider, however, the integral cross section into channel q,

$$P_q(E) = \int d\hat{\mathbf{k}}\, P_q(E,\hat{\mathbf{k}}) \tag{86}$$

and focus explicitly on the contribution from $P_q^{(12)}(E,\hat{\mathbf{k}})$. That is, consider

$$\begin{aligned} P_q^{(12)}(E) &= \int d\hat{\mathbf{k}} |F_q^{(12)}(\hat{\mathbf{k}})| \exp\left(i\delta_q^{(12)}(\hat{\mathbf{k}})\right) \\ &= \int d\hat{\mathbf{k}} \langle E_i,J_i,M_i \,|\, D \,|\, E,\hat{\mathbf{k}},q^-\rangle \langle E,\hat{\mathbf{k}},q^- \,|\, \mathrm{d}_{e,g} \,|\, E_i,J_i,M_i\rangle \end{aligned} \tag{87}$$

where we have explicitly inserted the angular momentum characteristics of the initial state, which is of energy E_i, angular momentum J_i, and projection M_i. Using the definition of D [Eq. (85)] and inserting unity in terms of the states $|E_j,J_j,M_j\rangle$ of the intermediate electronic state we get,

$$\begin{aligned} P_q^{(12)}(E) = \sum_j \int d\hat{\mathbf{k}} [\hbar\omega_1 + E_i - E_j]^{-1} &\langle E_i,J_i,M_i \,|\, \mathrm{d}_{g,e'} \,|\, E_j,J_j,M_j\rangle \\ \times \langle E_j,J_j,M_j \,|\, \mathrm{d}_{e',e} \,|\, E,\hat{\mathbf{k}},q^-\rangle &\langle E,\hat{\mathbf{k}},q^- \,|\, \mathrm{d}_{e,g} \,|\, E_i,J_i,M_i\rangle \end{aligned} \tag{88}$$

The above expression must be zero because it embodies two contradictory requirements: Dipole selection rules as applied to $\langle E_i,J_i,M_i \,|\, \mathrm{d}_{g,e'} \,|\, E_j,J_j,M_j\rangle$ require that $J_j - J_i = \pm 1$, whereas by the same rules, $\langle E_j,J_j,M_j|\mathrm{d}_{e',e}|E,\hat{\mathbf{k}},q^-\rangle \times \langle E,\hat{\mathbf{k}},q^- \,|\mathrm{d}_{e,g}\,|E_i,J_i,M_i\rangle$ is nonzero only if $J_j - J_i = \pm 2, 0$. Hence $P_q^{(12)}(E)$ is zero; that is, coherent control over integral cross sections is not possible using the one-photon versus two-photon scenario. However, as noted above, control over the differential cross section is possible. A similar conclusion obtains for any N-photon versus M-photon process where N and M are of different parities.

Experimental implementations of the one-plus-two photon absorption scenario have taken a variety of forms (Baranova *et al.*, 1990; Yin *et al.*, 1992, 1995; Dupont, 1995; Sheeny *et al.*, 1995). For example, Corkum and coworkers (Dupont *et al.*, 1995) have carried out one-photon versus two-photon absorption in crafted quantum wells to demonstrate control over the directional motion of the excited electron. Sipe, van Driel, and coworkers (Hache *et al.*, 1997) have extended this work to the complex case of bulk semiconductors. Following the theoretical work of Charron *et al.* (1995), Sheeny *et al.* (1995) have used this scenario to control product directionality in HD^+ dissociation to $H + D^+$ and $H^+ + D$.

3. *Two-Photon versus Two-Photon Interference*

Here we show that by considering (resonantly enhanced) two-photon versus two-photon dissociation, it is possible to maintain control in a molecular system in thermal equilibrium. The resonant character of the excitations is important because in this way only one state, out of the ensemble of thermally populated molecular states, participates in the photo-dissociation. As shown below, it is also possible in this way to overcome phase jitter in the laser sources.

Consider first photo-dissociation due to the absorption of two photons, of frequency ω_1 and ω_2, where the first photon is assumed resonant with an intermediate bound level. In this process a molecule, initially in a state $|E_i,J_i,M_i\rangle$, is photo-dissociated because of a combination of two CW fields,

$$\epsilon(t) = 2\mathcal{R}_e[\hat{\epsilon}_2 \bar{\epsilon}_2 \exp(-i\omega_2 t) + \hat{\epsilon}_1 \bar{\epsilon}_1 \exp(-i\omega_1 t)] \tag{89}$$

to yield a number of different product channels labeled by q. The near-resonance condition means that absorption of the first photon, of frequency

ω_1, lifts the system to a region close to an intermediate bound state $|E_m J_m M_m\rangle$. The second photon, of frequency ω_2, further excites the system to a dissociating state $|E, \mathbf{k}, q^-\rangle$. The probability-amplitude $D_{\mathbf{kq}}(E, E_i J_i M_i, \omega_2, \omega_1)$ for resonant two-photon $(\omega_1 + \omega_2)$ dissociation is given by (Chen *et al.*, 1993b)

$$D_{\mathbf{kq}}(E, E_i J_i M_i, \omega_2, \omega_1) = \bar{\epsilon}_2 \bar{\epsilon}_1 \sum_{e' E_m, J_m} \frac{\langle E, \mathbf{k}q^-|\mathrm{d}_{e,e'}|E_m J_m M_i\rangle \langle E_m J_m M_i|d_{e',g}|E_i J_i M_i\rangle}{E_i + \hbar\omega_1 - E_m - \Delta_m + i\Gamma_m/2} \tag{90}$$

Here $E = E_i + (\omega_1 + \omega_2)\hbar$, and Δ_m and Γ_m are respectively the radiative shift and width of the intermediate state.

As a consequence of the form of the denominator in Eq. (90), the photo-dissociation probability, given by the square of $D_{\mathbf{kq}}$, is greatly enhanced by the inverse square of the detuning $\Delta = E_i + \hbar\omega_1 - E_m - \Delta_m + i\Gamma_m/2$. Hence, only the levels closest to the resonance $\Delta = 0$ contribute significantly to the dissociation probability. Ideally, this allows us selectively to photo-dissociate a single state from a thermal bath. This holds true as long as the line width Γ_m is less than Δ and the spacings between neighboring transitions are smaller than the laser bandwidth.

Consider now the simultaneous excitation by *two* resonant two-photon routes using three interrelated frequencies, $\omega_0, \omega_+, \omega_-$ with associated field amplitudes and phases denoted as $\bar{\epsilon}_0, \bar{\epsilon}_+, \bar{\epsilon}_-$, and $\theta_0, \theta_+, \theta_-$, respectively, where ω_0 and ω_+ are chosen resonant with intermediate bound-state levels. Choosing the three frequencies such that $2\omega_0 = \omega_+ + \omega_-$, we can make the absorption of $2\omega_0$ photons (pathway "a") interfere with the absorption of an ω_+ and an ω_- photon (pathway "b"), because $E_i + 2\omega_0 = E_i + (\omega_+ + \omega_-) = E$. The probability of photo-dissociation at energy E into arrangement channel q is therefore given as the square of the sum of the two-photon amplitude of pathway "a" and the two-photon amplitude of pathway "b":

$$\begin{aligned} P_q(E, E_i J_i M_i; \omega_0, \omega_+, \omega_-) &\equiv \int d\,\mathbf{k} |D_{\mathbf{kq}}(E, E_i J_i M_i, \omega_0, \omega_0) + D_{\mathbf{kq}}(E, E_i J_i M_i, \omega_+, \omega_-)|^2 \\ &\equiv P_q(a) + P_q(b) + P_q(ab) \end{aligned} \tag{91}$$

Here $P_q(a)$ and $P_q(b)$ are the independent photo-dissociation probabilities associated with routes a and b respectively and $P_q(ab)$ is the interference term between them,

$$P_q(ab) = 2|F_q(ab)| \cos(\delta_q^a - \delta_q^b + 2\theta_0 - \theta_+ - \theta_-) \tag{92}$$

where the interference-amplitude $|F_q(ab)|$ and the molecular phase difference $(\delta_q^a - \delta_q^b)$ are defined via the equation

$$|F_q(ab)| \exp[i(\delta_q^a - \delta_q^b)] = D_{\mathbf{kq}}(E, E_i J_i M_i, \omega_0, \omega_0) D^*_{\mathbf{kq}}(E, E_i J_i M_i, \omega_+, \omega_-) \tag{93}$$

We see that control over the the quantity of interest, the channel branching ratio $R_{qq'}$, can be attained, as in previous scenarios, by varying such quantities as the $(2\theta_0 - \theta_+ - \theta_-)$ phase difference and the $(x = |\bar{\epsilon}_+ \bar{\epsilon}_- / \bar{\epsilon}_0^2|)$ amplitude ratio. Besides the ability to work in a thermal environment, the great advantage of this control scenario is that the $(2\theta_0 - \theta_+ - \theta_-)$ relative phase term allows for the cancellation of individual phase jitters arising in each laser source. For example, one can generate the ω_+ and ω_- frequencies by frequency summing $\omega_+ = \omega_0 + \delta$ and frequency differencing $\omega_- = \omega_0 - \delta$ with a third source of frequency δ. Because ω_+ and ω_- are generated in this way, the phase difference $2\theta_0 - \theta_+ - \theta_-$ between path (a) and path (b) vanishes (Schubert and Wilhelmi, 1986). Thus, fluctuations in θ_0 or δ cancel and have no effect on the interference term.

To demonstrate the range of control afforded by this scheme, consider the photo-dissociation of the Na_2 molecule in $v_i = J_i = 0$ [Fig. 4] to form the $Na(3s) + Na(3p)$ and $Na(3s) + Na(4s)$ products. As the $|E_m J_m M_m\rangle$ intermediate resonance we choose vib-rotational states belonging to the spin-orbit coupled $A^1\Sigma_u^+$ and $b^3\Pi_u$ electronic manifolds (Chen *et al.*, 1993b). Despite the multitude of electronic states involved in the process, the predominant contributions to the products $Na(3s) + Na(3p)$ and $Na(3s) + Na(4s)$ are found to come (Chen *et al.*, 1993b) from the $^3\Pi_g$ and $^3\Sigma_g^+$ states.

Typical control results are shown in Fig. 5, which shows a contour plot of the $Na(3s) + Na(4s)$ yield as a function of the ratio of the laser amplitudes x, and of the relative laser phase $\delta\theta = 2\theta_0 - \theta_+ - \theta_-$. We show the results of photo-dissociation with wavelengths $\lambda_0 = 594.505$ nm, $\lambda_+ = 582.057$ nm, and $\lambda_- = 607.498$ nm (corresponding to ω_0, ω_+, and ω_-) excited via the $^1\Sigma_u^+ v_m = 13$ and 18, $J_m = 1$ intermediate states. The range of control is considerable, with the $Na(4s)$ yield varying from 10% to 51% as $\delta\theta$ is varied.

Experimental demonstrations of this scenario for the ionization of atomic Ba (Wang *et al.*, 1996b) and NO (Pratt, 1996) have been reported.

4. *Polarization Control of Differential Cross Sections*

Rather than attempting coherent control with two different frequencies, it would seem that the use of two different polarizations of the same frequency would be much easier to implement experimentally. It turns out that this

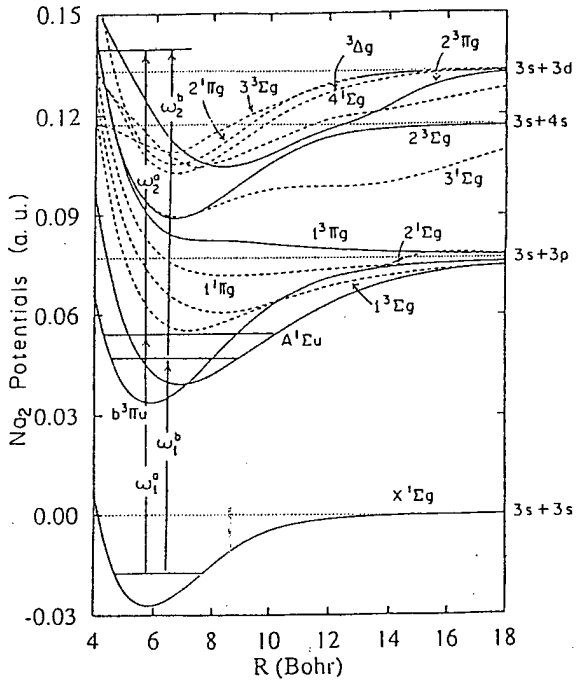

FIG. 4. Na_2 potential energy surfaces relevant to the two-photon versus two-photon control scenario. The arrows indicate the resonant two-photon versus two-photon pathways included in the computation discussed here. (From Chen *et al.*, 1993a.)

scenario is akin to the one-photon versus two-photon control in the sense that integral control is not possible. Further, though differential cross sections can be controlled (Asaro *et al.*, 1988), there is no breaking of the forward-backward symmetry in this case.

In order to see this, we consider the photo-dissociation of a *single* bound state $|E_1\rangle$ by a single CW source of the type

$$\epsilon = \epsilon_1 \exp(i\alpha_1)\hat{\epsilon}_1 + \epsilon_2 \exp(i\alpha_2)\hat{\epsilon}_2$$

where $\hat{\epsilon}_1$ and $\hat{\epsilon}_2$ are two orthonormal vectors.

We can regard the two components $\hat{\epsilon}_1$ and $\hat{\epsilon}_2$ as inducing two independent excitation routes. Choosing $\hat{\epsilon}_1$ and $\hat{\epsilon}_2$ parallel and perpendicular to the quantization (z) axis, respectively, the differential cross section is composed of three terms; one corresponds to photo-dissociation of $|E_1\rangle$ by the $\hat{\epsilon}_1$ component, one corresponds to photo-dissociation of $|E_1\rangle$ by the $\hat{\epsilon}_2$ component, and one is the cross term between these two contributions. Excitation by the parallel

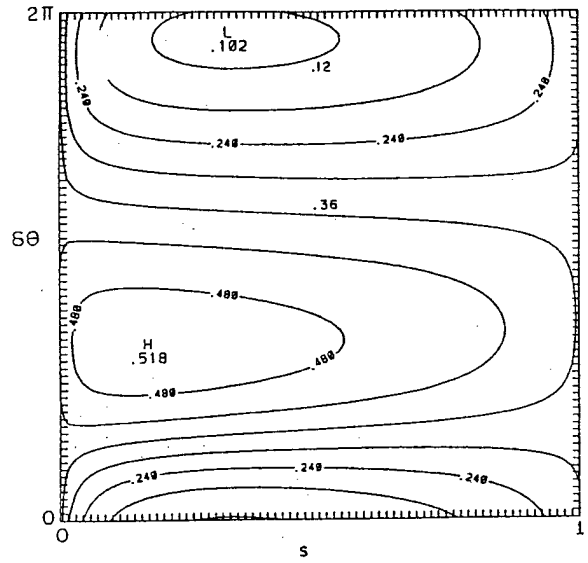

FIG. 5. Contours of equal Na(4s) yield in the controlled photo-dissociation of Na_2, initially in vibrational state $v = 10$. The ordinate is the relative laser phase, and the abscissa is the field intensity ratio s. (From Chen *et al.*, 1993a.)

component allows $\Delta M_J = 0$ transitions, whereas excitation by the perpendicular $\hat{\epsilon}_2$ component allows $\Delta M_J = \pm 1$ transitions. The interference term is therefore comprised of a product of two bound-continuum matrix elements, where the two continua differ in M_J by ± 1. If this cross term is nonzero, then control over the differential cross section is possible. However, producing the integral cross section necessitates integrating the differential cross section over $\hat{\mathbf{k}}$, and under these circumstances, the cross term vanishes. Contrary to the one-photon versus two-photon case, the states comprising the $|E, \hat{\mathbf{k}}^-\rangle$ state are of the same parity. Thus the backward-forward symmetry is not broken. The control manifests itself in our ability to sharpen or broaden the angular distribution about a given recoil direction.

Polarization control in intense fields has been proposed as a means of generating subfemtosecond pulses (Ivanov *et al.*, 1995), but it has yet to be demonstrated experimentally.

B. Pump-Dump Control: Two-Level Excitation

Control of the dynamics via a pump-dump scenario was first introduced by Tannor and Rice (1985). These authors emphasized the localized wavepacket aspects of pump-dump control, entailing the excitation of, and interference

between, many levels. In this section, we consider excitation of only two levels. It can be regarded as the pulsed analog of the bichromatic control with a superposition state outlined in Section III.

Consider a molecule, initially ($t = 0$) in an eigenstate $|E_1\rangle$ of the molecular Hamiltonian H_M, which is subjected to two transform-limited light pulses. The electric field $\epsilon(t)$ consists of two temporally separated pulses

$$\epsilon(t) = \epsilon_x(t) + \epsilon_d(t) \tag{94}$$

The pump pulse $\epsilon_x(t)$ induces a transition to a linear combination of the eigenstates $|E_i\rangle$ of the excited electronic state. Though the pump pulse may be chosen to encompass any number of states, here we choose it sufficiently narrow to excite only a superposition of two states $|E_2\rangle$ and $|E_3\rangle$. The dump pulse $\epsilon_d(t)$ dissociates the molecule by further exciting this superposition state to the continuous part of the spectrum. Both fields are chosen sufficiently weak for perturbation theory to be valid.

For convenience we use Gaussian pulses that peak at $t = t_x$ and t_d, respectively. In particular, the excitation pulse is of the form

$$\varepsilon_x(t) = (\epsilon_x/\tau_x)\exp[-i(\omega_x t + \delta_x)]\exp[-(t - t_x)^2/\tau_x^2] \tag{95}$$

The associated frequency profile is given by

$$\bar{\epsilon}_x(\omega) = (\sqrt{\pi}/2)\epsilon_x\tau_x\exp[-i(\omega_x - \omega)t_x]\exp[-\tau_x^2(\omega_x - \omega)^2/4]\exp(-i\delta_x) \tag{96}$$

By writing $\bar{\epsilon}_x(\omega) = |\bar{\epsilon}_x(\omega)|e^{i\phi(\omega)}$, we see that $\phi(\omega) = (\omega - \omega_x)t_x - \delta_x$. The analogous quantities $\epsilon_d(t)$ and $\bar{\epsilon}_d(\omega)$ are defined similarly, with the parameters t_d and ω_d replacing t_x and ω_x, etc.

Because the two pulses are temporally distinct, it is convenient to deal with each of their effects independently. The superposition state prepared after the $\epsilon_x(t)$ pulse is over is given in first-order perturbation theory as

$$|\phi(t)\rangle = |E_1\rangle e^{-iE_1t/\hbar} + b_2|E_2\rangle e^{-iE_2t/\hbar} + b_3|E_3\rangle e^{-iE_3t/\hbar} \tag{97}$$

where [Eq. (8)]

$$b_k = (2\pi i/\hbar)\langle E_k|\mathrm{d}\cdot\hat{\epsilon}|E_1\rangle\bar{\epsilon}_x(\omega_{k,1}),\ k = 2,3 \tag{98}$$

with $\omega_{k,1} \equiv (E_k - E_1)/\hbar$.

After a delay time of $\tau \equiv t_d - t_x$, the system is subjected to the $\epsilon_d(t)$ pulse. It follows from Eq. (97) that at that time, each preparation coefficient has

picked up an extra phase factor of $e^{-iE_k\tau/\hbar}$, $k = 2,3$. Hence, the phase of b_2 relative to b_3 at that time increases by $[-(E_2 - E_3)\tau/\hbar = \omega_{3,2}\tau]$. Thus the natural two-state time evolution controls the relative phase of the two terms, replacing the externally controlled relative laser phase of the bichromatic control scenario of Section III.

After the conclusion of the $\epsilon_d(t)$ pulse, the system wavefunction is given as

$$|\psi(t)\rangle = |\phi(t)\rangle + \sum_{q,\mathbf{m}}\int dE\, b_{E,q,\mathbf{m}}(t)|E,q,\mathbf{m}^-\rangle e^{-iEt/\hbar} \tag{99}$$

The probability of observing the q product at total energy E in the remote future is therefore given by

$$\begin{aligned} P_q(E) &= \sum_{\mathbf{m}}|b_{E,q,\mathbf{m}}(t=\infty)|^2 \\ &= (2\pi/\hbar^2)\sum_{\mathbf{m}}\left|\sum_{k=2,3} b_k\exp(-iE_k\tau/\hbar)\langle E,q,\mathbf{m}^-|\mathrm{d}_{e,e'}|E_k\rangle\bar{\epsilon}_d(\omega_{EE_k})\right|^2 \end{aligned} \tag{100}$$

where $\omega_{EE_k} = (E - E_k)/\hbar$, b_k is given by Eq. (98), and $\bar{\epsilon}_d(\omega_{EE_K})$ is given via an expression analogous to Eq. (96).

Expanding the square gives

$$\begin{aligned} P_q(E) = \left(\frac{2\pi}{\hbar^2}\right)&[|b_2|^2\mu_q(22)\bar{\epsilon}_2^2 + |b_3|^2\mu_q(33)\bar{\epsilon}_3^2 \\ &+ 2|b_2b_3^*\bar{\epsilon}_2\bar{\epsilon}_3^*\mu_q(23)|\cos(\omega_{32}\tau + \alpha_q(23) + \chi)] \end{aligned} \tag{101}$$

where $\bar{\epsilon}_i = |\bar{\epsilon}_d(\omega_{EE_i})|e^{i\phi(\omega_{EE_i}}$, $\omega_{32} = (E_3 - E_2)/\hbar$, and the phases $\chi, \alpha_q(23)$ are defined via

$$\begin{aligned} \langle E_1|d_{e',g}|E_g\rangle\langle E_g|\mathrm{d}_{g,e'}|E_2\rangle &\equiv |\langle E_1|\mathrm{d}_{e',g}|E_g\rangle\langle E_g|\mathrm{d}_{g,e'}|E_2\rangle|e^{i\chi} \\ \mu_q(ik) \equiv |\mu_q(ik)|e^{i\alpha_q(ik)} &= \sum_{\mathbf{m}}\langle E,q,\mathbf{m}^-|\mathrm{d}_{e,e'}|E_i\rangle\langle E_k|\mathrm{d}_{e',e}|E,q,\mathbf{m}^-\rangle \end{aligned} \tag{102}$$

Integrating Eq. (101) over E to encompass the full width of the second pulse yields the final expressions for the quantities we wish to control: P_q, the probability of forming channel q, and $R_{q,q'}$, the ratio of product probabilities into q versus q'.

Examination of Eq. (101) makes clear that $R_{q,q'}$ can be varied by changing the delay time $\tau = (t_d - t_x)$ or the ratio $x = |b_2/b_3|$; the latter is most conveniently done by detuning the initial excitation pulse. Note that once again, as in the scenarios above, the z dependence of P_q vanishes because of cancellation between the excitation and dump steps. In addition, the phases δ_x, δ_d do not appear in the final result, so the relative phases of the two pulses do not affect the result.

To gain insight into the control afforded by this scenario, we initially applied (Seideman *et al.*, 1989) it to a model collinear branching photo-dissociation reaction with masses of D and H, i.e.,

$$H + HD \leftarrow DH_2 \rightarrow D + H_2 \tag{103}$$

in which one uses the first pulse to excite a pair of states in an electronic state supporting bound states and the second pulse to dissociate the system by de-exciting it back to the ground state, above the dissociation threshold.

Typical control results (Seideman *et al.*, 1989) are displayed in Fig. 6, which shows contours of equal DH yield as a function of $E_x - E_{AV}$ and τ. Here $(E_x - E_{AV})$ measures the deviation of the central excitation energy of the pump pulse from the average energy E_{AV} of the pair of bound states it excites. The DH yield is shown to vary significantly, from 16% to 72%, as the control parameters are varied. This is an extreme range of control, especially if one considers that the product channels differ by only a mass factor.

It is highly instructive to examine the nature of the superposition state prepared in the initial excitation, [Eq. (97)] and its time evolution during the delay between pulses. An example is shown in Fig. 7, where we plot the wavefunction for a collinear model of DH_2 photo-dissociation [Eq. (103)]. Specifically, the axes are the H + HD reaction coordinate S and its orthogonal conjugate x. The wavefunction is shown evolving over half of its total possible period. An examination of Fig. 6 in conjunction with Fig. 7 shows that de-exciting this superposition state at the time of panel (b) would result in a substantially different product yield than de-exciting at the time of panel (e). However, Fig. 7 shows that there is clearly no particular preference of the wavefunction for either large positive or large negative S at these particular times, which would be the case if the reaction control were a result of some spatial characteristics of the wavefunction. Rather, the results make clear that the essential control characteristics of the wavefunction are encrypted in the quantum amplitude and phase of the created superposition state.

The pump-dump scheme has also been applied (Abrashkevich *et al.*, 1998b) (computationally) to the photo-dissociation of a fully realistic representation of Li_2 to control the cross sections for production of Li(2s) + Li(2p), Li(2s) + Li(3p) and Li(2s) + Li(3s). In particular, a CW laser was

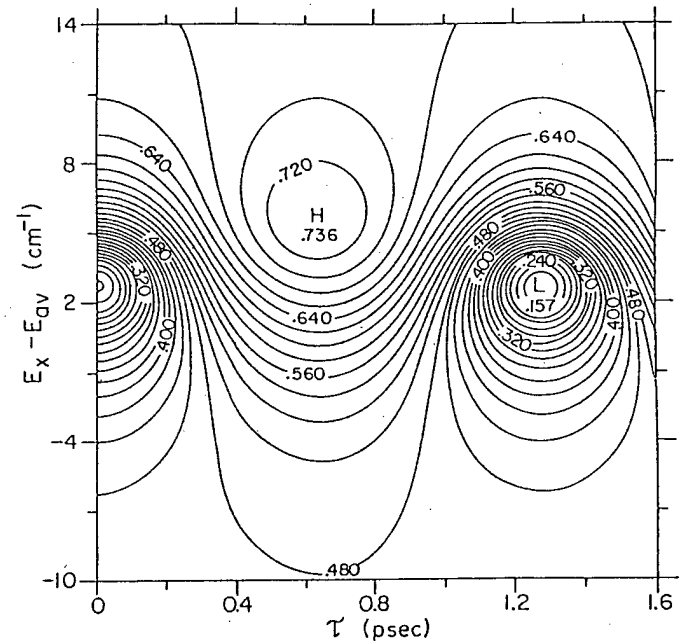

FIG. 6. Contour plot of the DH yield as a function of the detuning of the exciting pulse $E_x - E_{av}$ and the delay variable τ. In this case the time between pulse centers is $\Delta T = (8.44 + 2.11n)ps + \tau$, ensuring nonoverlapping pulses and allowing for arbitrary positive integer n. Here the initially created superposition state is between levels 56 and 57 ($E_1 = 0.323\,849$ a.u., $E_2 = 0.323\,968$ a.u.) of the G1 surface. The letters H and L denote the positions of the absolute maxima and minima, whose magnitudes are explicitly shown. (From Seideman *et al.*, 1989.)

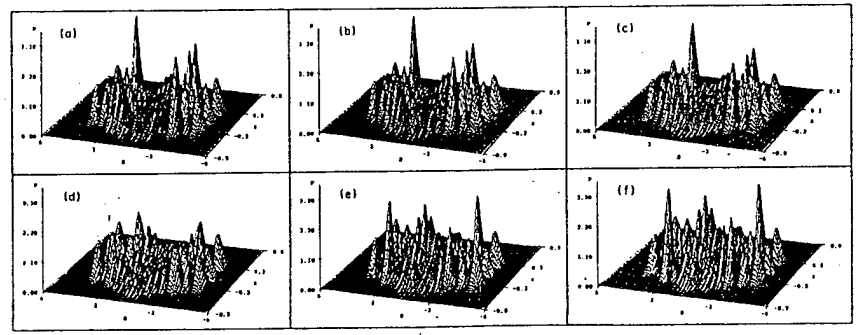

FIG. 7. Time evolution of the square of the wavefunction for a superposition state comprised of levels 56 and 57. The probability is shown as a function of S and its orthogonal coordinate x at times (a) 0, (b) 0.0825 ps, (c) 0.165 ps, (d) 0.33 ps, (e) 0.495 ps, and (f) 0.66 ps, which correspond to equal fractions of one half of the period $2\pi/\omega_{2,1}$. (From Seideman *et al.*, 1989.)

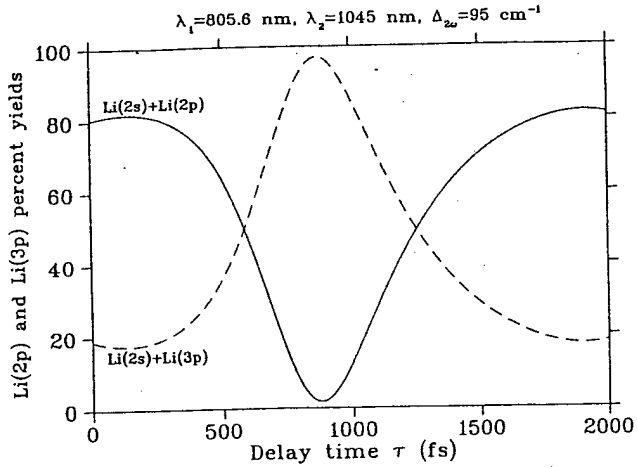

FIG. 8. Li(2p) and Li(3p) yields in the pump-dump controlled photo-dissociation of Li_2 as a function of the delay between pulses. Wavelengths of the two pulses, as well as the frequency width of the second pulse, are indicated. (From Abrashkevich *et al.*, 1998b.)

used to prepare a single rovibrational state of the $A^1\Sigma_u^+$ electronically excited state. Subsequent pump-dump excitation allowed extensive control over product yields with, for instance, Li(2s) + Li(2p) ranging from 2% to 82% as the time delay between pulses is varied over 1 ps. Simultaneously, as seen in Fig. 8, the Li(2s) + Li(3p) product is exactly out of phase so that we have almost total control over the Li(3p) to Li(2p) ratio. Computations have also been done on the control of the polyatomic system:

$$D + OH \leftarrow HOD \rightarrow H + OD$$

via the B-state of HOD (Shapiro and Brumer, 1993).

Note, finally, that control is sensitive to the degree of laser coherence. If the pump laser is only partially coherent (Jiang and Brumer, 1991), then control can be significantly degraded (Jiang *et al.*, 1996). This is not the case for the dump pulse, where a significant degree of laser incoherence can be tolerated.

Experimental studies of pump-dump control fall into two categories: (a) the large number of pump-dump experiments where the dump pulse is used as a probe of the previously prepared dynamics (Potter *et al.*, 1992; Baumert *et al.*, 1991) but that can be interpreted as demonstrations of pump-dump control; and (b) those expressly designed to demonstrate coherent control. The latter category includes work by Wilson (Bardeen *et al.*, 1997), Silberberg (Yelin *et al.*, 1997), and Gerber (Assion *et al.*, 1998). For example, Gerber *et al.* controlled the ratio of $CpFeCOCl^+/FeCl^+$ products in the photo-fragmentation

of $CpFe(CO)_2Cl$ using pulsed and chirped femtosecond sources, opening the way for laser control of large molecular systems.

C. Symmetry Breaking and the Generation of Chirality

Symmetry breaking occurs in nature whenever a system undergoes a (spontaneous or forced) transition to a *nonsymmetric* eigenstate (i.e., states that do not belong to any of the representations of the symmetry group) of the Hamiltonian. Such nonsymmetric eigenstates occur if there exist several degenerate eigenstates, each belonging to a different irreducible symmetry representation, because a linear combination of eigenstates of different symmetry will in general be nonsymmetric.

Nonsymmetric eigenstates of a symmetric Hamiltonian occur naturally in the continuous spectrum of a *BAB* type molecule. It is clear that the $|E, \mathbf{m}, R^-\rangle$ state, which correlates asymptotically with the dissociation of the right *B* group, must be degenerate with the $|E, \mathbf{m}, L^-\rangle$ state, which correlates with the departure of the *B* group on the left-hand side. Hence, any experiment performed in the asymptotic $B + AB$ or $BA + B$ regions must, by necessity, measure the probability of populating a nonsymmetric state. It is also possible to form *symmetric* $|E, \mathbf{m}, s^-\rangle$ and *antisymmetric* $|E, \mathbf{m}, a^-\rangle$ eigenstates of the same Hamiltonian by taking the plus and minus combinations of nonsymmetric states. However, symmetric and antisymmetric states are not directly observable in the asymptotic regime.

We may say that the very act of observation of the dissociated molecule entails the collapse of the system to one of the nonsymmetric states. Because the probability of collapse to the $|E, \mathbf{m}, R^-\rangle$ state is equal to the probability of collapse to the $|E, \mathbf{m}, L^-\rangle$ state, the collapse to a nonsymmetric state does not lead to a preference of *R* over *L* in an *ensemble* of molecules. The above collapse is due to (random) factors that are not in our control. Coherent control techniques do not change this "*spontaneous symmetry breaking*" aspect of quantum mechanics. Rather, as we show below, it allows us to bias the *a priori* probability of producing the *R* or the *L* form.

One of the most important cases of symmetry breaking arises when the two *B* groups (now denoted as *B* and *B'*) are not identical but are enantiomers of each other. (Two molecules are said to be enantiomers of each other if one is the mirror image of the other. If these groups are also "chiral", i.e., if they lack a center of inversion symmetry, then the two enantiomers are distinguishable and can be detected through the distinctive direction of rotation of linearly polarized light).

The existence and role of enantiomers are recognized as one of the fundamental broken symmetries in nature (Barron, 1982; Woolley, 1975; Walker, 1979). It has motivated a long-standing interest in asymmetric synthesis, i.e.,

processes that preferentially produce specific chiral species. Contrary to the prevailing belief (Barron, 1986) that asymmetric synthesis must involve either chiral reactants or chiral external system conditions such as chiral crystalline surfaces, we have shown (Shapiro and Brumer, 1991) (and review below) that preferential production of a chiral photofragment can occur even though the parent molecule is not chiral. In particular, two results have been demonstrated (Shapiro and Brumer, 1991): (1) ordinary photo-dissociation, using linearly polarized light, of a BAB' "pro-chiral" molecule can yield different cross sections for the production of right-handed (B) and left-handed (B') products if the projection of the angular momentum (m_j) of the products is selected; and (2) this natural symmetry breaking may be enhanced and controlled using coherent control.

To treat this problem, consider the pump-dump scenario described in Section V.B, with attention focused on control of the relative yield of two product arrangement channels, where the product angular momentum projection m_j is fixed. That is, we consider $P_q(E; m_j)$ with q labeling either the right- ($q = R$) or the left- ($q = L$) handed product.

As above, the product ratio $R_{qq'} = P_R(E; m_j)/P_L(E; m_j)$ is a function of the delay time $\tau = (t_d - t_x)$ and the ratio $x = |c_1/c_2|$, the latter by varying the energy of the initial excitation pulse. Active control over the products $B + AB'$ versus $B' + AB$, i.e., a variation of $R_{qq'}$ with τ and x, and hence control over left- versus right-handed products, will result only if $P_R(E; m_j)$ and $P_L(E; m_j)$ have different functional dependences on the control parameters x and τ.

To show that $P_R(E; m_j)$ may differ from $P_L(E; m_j)$ for the $B'AB$ case, note first that this molecule belongs to the C_s point group. This group possesses only one plane of symmetry, denoted σ, which is defined as the collection of points satisfying the requirement that the $B - A$ distance equals the $A - B'$ distance. Furthermore, we shall focus upon transitions between electronic states of the same representations, e.g., A' to A' or A'' to A'' (where A' denotes the symmetric representation and A'' the antisymmetric representation of the C_s group). We further assume that the ground vibronic state belongs to the A' representation.

To obtain control, we wish to choose the intermediate state $|E_3\rangle$ to be *symmetric* and the intermediate state $|E_2\rangle$ to be *antisymmetric* with respect to reflection in the σ-plane. Hence we first demonstrate that it is possible optically to excite, simultaneously, both the symmetric $|E_3\rangle$ and the antisymmetric $|E_2\rangle$ states. Using Eq. (98) we see that this requires the existence of both a dipole component that is symmetric, denoted $d^s_{e',g}$, and a component that is antisymmetric, denoted $d^a_{e',g}$, because by the symmetry properties of $|E_3\rangle$ and $|E_2\rangle$,

$$\langle E_3|d_{e',g}|E_1\rangle = \langle E_3|d^s_{e',g}|E_1\rangle, \langle E_2|d_{e',g}|E_1\rangle = \langle E_2|d^a_{e',g}|E_1\rangle \quad (104)$$

Both dipole-moment components do occur in $A' \rightarrow A'$ electronic transitions whenever a bent $B' - -A - -B$ molecule deviates considerably from the equal-distance C_{2v} geometries (where $d^a = 0$). The effect is non–Franck-Condon in nature because the dipole moment must vary with the nuclear configurations. In the terminology of the theory of vibronic transitions, both symmetric and antisymmetric components can be nonzero because of a Herzberg-Teller intensity borrowing (Hollas, 1982) mechanism. It is therefore the case that the excitation pulse can create a $|E_3\rangle, |E_2\rangle$ superposition consisting of two states of different reflection symmetry, a state that is therefore nonsymmetric.

We now show that the nonsymmetry created by this excitation of *nondegenerate* bound states translates to a nonsymmetry in the probability of populating the *degenerate* $|E, \mathbf{m}, R^-\rangle, |E, \mathbf{m}, L^-\rangle$ continuum states. To do so we examine the properties of the bound-free transition matrix elements $\langle E, q, \mathbf{m}^-|\mathrm{d}_{e,e'}|E_k\rangle$ that enter into the probability of dissociation [Eq. (100)]. Note first that although the continuum states $|E, q, \mathbf{m}^-\rangle$ are nonsymmetric, we can define symmetric and antisymmetric continuum eigenfunctions $|E, \mathbf{m}, s^-\rangle$ and $|E, \mathbf{m}, a^-\rangle$ via the relations

$$|E, \mathbf{m}, R^-\rangle \equiv [|E, \mathbf{m}, s^-\rangle + |E, \mathbf{m}, a^-\rangle]/\sqrt{2} \quad (105)$$

$$|E, \mathbf{m}, L^-\rangle \equiv [|E, \mathbf{m}, s^-\rangle - |E, \mathbf{m}, a^-\rangle]/\sqrt{2} \quad (106)$$

Note that $\sigma|E, \mathbf{m}, R^-\rangle = |E, \mathbf{m}, L^-\rangle$. Using the fact that $|E_3\rangle$ is symmetric and $|E_2\rangle$ is antisymmetric, and adopting the notation $a_{s2} \equiv \langle E, \mathbf{m}, \mathrm{s}^-|d^a_{e',g}|E_2\rangle$, $s_{a3} \equiv \langle E, \mathbf{m}, a^-|\mathrm{d}^s_{e,e'}|E_3\rangle$, etc., we have [see Eq. (102)],

$$\mu_q(33) = \sum_{\mathbf{m}} [|s_{s3}|^2 + |a_{a3}|^2 \pm 2\mathcal{R}_e(a_{a3}\, s^*_{s3})] \quad (107)$$

$$\mu_q(22) = \sum_{\mathbf{m}} [|a_{s2}|^2 + |s_{a2}|^2 \pm 2\mathcal{R}_e(a_{s2}\, s^*_{a2})] \quad (108)$$

$$\mu_q(32) = \sum_{\mathbf{m}} [s_{s3}\, a^*_{s2} + a_{a3}\, s^*_{a2} \pm s_{s3}\, s^*_{a2} \pm a_{a3}\, a^*_{s2}] \quad (109)$$

where the plus sign applies for $q = R$, the minus sign applies for $q = L$, and $\mu_q(23) = \mu^*_q(32)$. Equation (109) displays two noteworthy features:

1. $\mu_L(kk) \neq \mu_R(kk), k = 2, 3$. That is, the system displays *natural symmetry breaking* in photo-dissociation from state $|E_3\rangle$ or state $|E_2\rangle$, with right- and left-handed product probabilities differing by

$4\Sigma_m \mathcal{R}_e(s^*_{s3}a_{a3})$ for excitation from $|E_3\rangle$ and by $4\Sigma_m \mathcal{R}_e(a_{s2}s^*_{a2})$ for excitation from $|E_2\rangle$. Note that these symmetry-breaking terms exist only if the transition dipole operator possesses both a symmetric and an antisymmetric component, which can occur only if the Franck-Condon approximation breaks down.

2. $\mu_L(23) \neq \mu_R(23)$. If the Franck-Condon approximation holds, there is no "natural" symmetry breaking of the type discussed above. However, even when the FC approximation holds, $\mu_L(23) \neq \mu_R(23)$ and laser-controlled symmetry breaking according to Eq. (101) is possible.

To demonstrate the range of expected control, we consider a model of enantiomer selectivity (Shapiro and Brumer, 1991), i.e., HOH photo-dissociation in three dimensions, where the two hydrogens are assumed distinguishable:

$$HO + H \leftarrow HOH \rightarrow H + OH$$

The computation of $R_{qq'}$, the HO + H (as distinct from the H + OH) product for polarized OH fragments, was done using the formulation and computational methodology of Segev and Shapiro (1982) and Balint-Kurti and Shapiro (1981). Figure 9 shows the result of first exciting the superposition of symmetric plus antisymmetric vibrational modes $[(1, 0, 0) + (0, 0, 1)]$ with rotational quantum numbers $J_i = J_k = 0$ in the ground electronic state,

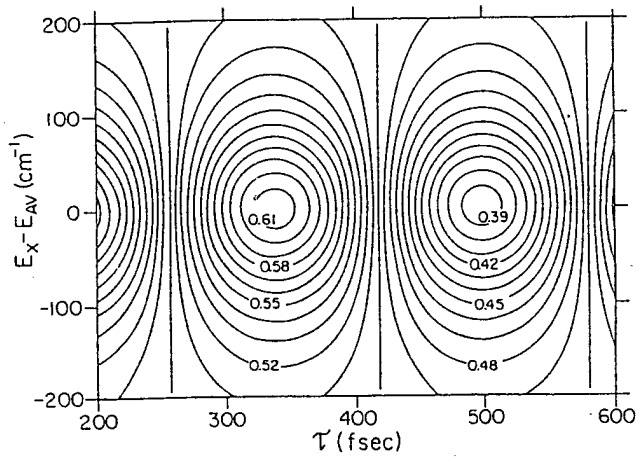

FIG. 9. Contour plot of percent HO + H (as distinct from H + OH) in HOH photodissociation. The ordinate is the detuning from $E_{av} = (E_2 - E_1)/2$, and the abscissa is the time delay between pulses. (From Shapiro and Brumer, 1991.)

followed by dissociation at 70,700 cm^{-1} to the B state using a pulse width of 200 cm^{-1}. Results show that varying the time delay between pulses allows for controlled variation of $R_{qq'}$ from 61% to 39%!

Finally, we discuss symmetry breaking and chirality control with *unpolarized* OH fragments where a summation over the magnetic quantum number m_j is performed. It can be shown that summing over m_j eliminates all contributions to Eq. (109) that involve both $|E, \mathbf{m}, a^-\rangle$ and $|E, \mathbf{m}, s^-\rangle$, and as a result,

$$\mu_L(kk) = \mu_R(kk) = \sum_i [|s_{si}|^2 + |a_{ai}|^2] \tag{110}$$

$$\mu_L(23) = \mu_R(23) = \sum_{i,j} [s_{si}a^*_{sj} + a_{ai}s^*_{aj}] \tag{111}$$

That is, natural symmetry breaking is lost upon m_j summation, both channels $q = R$ and $q = L$ having equal photo-dissociation probabilities, and control over the enantiomer ratio is lost because the interference terms, which still exist, no longer distinguish the $q = R$ and $q = L$ channels.

VI. Strong-Field Incoherent Interference Control

In this section we discuss both the theory and an experiment of an elegant strong-field laser control scenario. As we saw above, the quantum nature of weak-field CC manifests itself in the sensitivity of the outcome to a change in an external *phase*. In contrast, under some strong-field situations, the interference term may become independent of the phase of the light sources involved, which therefore no longer need be coherent. Instead of the phase, the interference term now becomes sensitive to the relative *frequency* between the two light sources. We call the resulting control scenario "incoherent interference control" (IIC) (Chen *et al.*, 1995). The above two features are very favorable from the experimental point of view because one can use conventional non-transform-limited lasers and molecules in thermal environments. Indeed, an experimental realization of IIC has already been reported (Shnitman *et al.*, 1996).

In general terms, the IIC scenario operates as follows: Consider a molecule in an initial bound state $|E_i\rangle$ that absorbs two photons of frequency ω_1 and, in doing so, is excited to a continuum state $|E, q, \mathbf{m}^-\rangle$ via a resonant intermediate state $|E_{j_1}\rangle$. The outcome of this photo-dissociation process can be controlled by applying a "control laser" ω_2 that couples initially unpopulated bound states $|E_{j_2}\rangle$ to the same continuum. With both lasers on, dissociation to $|E, q, \mathbf{m}^-\rangle$ occurs via numerous dissociation pathways. To lowest order,

these are the routes $|E_i\rangle \rightarrow |E_{j_1}\rangle \rightarrow |E,q,\mathbf{m}^-\rangle$ as well as $|E_i\rangle \rightarrow |E_{j_1}\rangle \rightarrow |E',q',\mathbf{m}'^-\rangle \rightarrow |E_{j_2}\rangle \rightarrow |E,q,\mathbf{m}^-\rangle$, etc. Contributions from these multiple pathways to the product in a given channel q at energy E interfere (either constructively or destructively) with one another. Varying the frequency and intensity of the control laser alters the interference and hence the dissociation line shape and the yield of product into a given channel.

The IIC scenario may be viewed as the multichannel extension of the "laser-induced continuum structure" (LICS) phenomenon (see, for example, Knight *et al.*, 1990; Faucher *et al.*, 1993; Cavalieri *et al.*, 1998; and references therein). According to this view, the excitation by the ω_2 photon embeds an unpopulated bound state, $|E_{j_1}\rangle$, in the $|E,q,\mathbf{m}^-\rangle$ continuum. As a result, the continuum becomes structured while the $|E_{j_1}\rangle$ state becomes an unstable resonance. The structured continuum then interferes with the two-ω_1-photon dissociation of the populated state $|E_i\rangle$. The main new feature of the IIC theory presented below is the discovery that this interference effect may be of a different nature for different final channels.

A. Theory of Incoherent Interference Control

The equations governing the IIC scenario are most easily derived by treating both the light and the matter quantum-mechanically. The molecule, whose Hamiltonian is denoted by H_M, interacts with a quantized radiation field with radiative Hamiltonian H_R through the dipolar interaction term H_{MR}. The total Hamiltonian H is then given by

$$H = H_M + H_R + H_{MR} \equiv H_0 + H_{MR} \tag{112}$$

The photo-dissociation process is characterized, as for classical light, by a transition from $|E_i\rangle$, a bound eigenstate of H_M, to $|E,q,\mathbf{m}^-\rangle$, a continuum eigenstate of the same Hamiltonian, which, as in the classical field case, correlates in the infinite future with the noninteracting $|\epsilon_{\mathbf{m},q}\rangle|E-\epsilon_{\mathbf{m},q}\rangle$ product state.

When describing the radiation pulse, it is convenient to work with (multimode) number states $|N_k\rangle$, defined as the eigenstates of H_R,

$$H_R|N_k\rangle \equiv H_R|n_1^{(k)},n_2^{(k)},\ldots\rangle = \hbar\sum_l n_l^{(k)}\omega_l|N_k\rangle \equiv E_{N_k}|N_k\rangle \tag{113}$$

where E_{N_k} is the total radiation energy. The letters $k = i$ and f are used to label the initial and final states, respectively. The eigenstates of $H_0 \equiv H_M + H_R$ are a direct product of the molecular and photon states; e.g., $|(E,q,\mathbf{m}^-)N_f\rangle \equiv |E,q,\mathbf{m}^-\rangle|N_f\rangle$. We call these states "partially" interacting because they encompass interaction via the material part of the Hamiltonian only.

The molecule-radiation interaction H_{MR} is given in the dipole approximation (Cohen-Tannoudji *et al.*, 1992) as

$$H_{MR} = -\mathbf{d}\cdot\epsilon, \quad \text{with} \quad \epsilon = i\sum_l \epsilon_l(\hat{\epsilon}_l a_l - \hat{\epsilon}_l^* a_l^\dagger) \tag{114}$$

where $\mathbf{d}$ is the electric dipole operator, ϵ is the amplitude of the radiation electric field, $\epsilon_l = (2\pi\hbar\omega_l/L^3)^{1/2}$, $\hat{\epsilon}_l$, ω_l are the polarization vector and angular frequency of mode l, respectively, and a_l, $a_l^\dagger$ are photon annihilation and creation operators.

The dynamics of photo-dissociation is completely described by the fully interacting state $|(E,q,\mathbf{m}^-),N_k^-\rangle$, which is an eigenstate of the total Hamiltonian H,

$$H|(E,q,\mathbf{m}^-),N_k^-\rangle = (E+E_{N_k})|(E,q,\mathbf{m}^-),N_k^-\rangle \tag{115}$$

The additional minus superscript on N_k indicates that the state $|(E,q,\mathbf{m}^-)N_k^-\rangle$ becomes the partially interacting state $|(E,q,\mathbf{m}^-)N_k\rangle$ when the radiative interaction H_{MR} is switched off. The $|(E,q,\mathbf{m}^-)N_k^-\rangle$ states satisfy an augmented Lippmann-Schwinger equation [whose purely material analogue is Eq. (26)] of the form

$$|(E,q,\mathbf{m}^-),N_k^-\rangle = |(E,q,\mathbf{m}^-),N_k\rangle + G(E^-+E_{N_k})H_{MR}|(E,q,\mathbf{m}^-)N_k\rangle \tag{116}$$

where the resolvent $G(z) \equiv 1/(z-H)$.

If the system is initially in the partially interacting bound state $|E_i,N_i\rangle \equiv |E_i\rangle|N_i\rangle$, and the radiation-matter interaction is switched on suddenly, then the photo-dissociation amplitude to form the partially interacting state $|E,q,\mathbf{m}^-\rangle|N_f\rangle$ is given by $\langle(E,q,\mathbf{m}^-)N_f^-|E_i,N_i\rangle$. Because $\langle(E,q,\mathbf{m}^-)N_f|E_i,N_i\rangle = 0$, it follows from Eq. (116) that

$$\langle(E,q,\mathbf{m}^-),N_f^-|E_i,N_i\rangle = \langle(E,q,\mathbf{m}^-)N_f|H_{MR}G(E^+ + E_{N_f})|E_i,N_i\rangle \tag{117}$$

Two quantities, derived from the $\langle(E,q,\mathbf{m}^-)N_f|H_{MR}G(E^+ + E_{N_f})|E_i,N_i\rangle$ matrix elements, which can be computed numerically by a variety of techniques (Chen *et al.*, 1994, 1995; Shapiro and Bony, 1985; Balint-Kurti, 1986; Brumer and Shapiro, 1986b. Bandrauk *et al.*, 1989), are of interest: $P(E,q,N_f|E_i,N_i)$, the probability to obtain products in channel q at a given photon number state

distribution $\{N_f\}$ and total material energy E,

$$P(E,q,N_f|E_i,N_i) = \sum_{\mathbf{m}} |\langle (E,q,\mathbf{m}^-),N_f^-|H_{MR}G(E^+ + E_{N_f})|E_i,N_i\rangle|^2 \quad (118)$$

and the total dissociation probability to channel q,

$$P(q) = \sum_{N_f} \int dE\, P(E,q,N_f|E_i,N_i) \quad (119)$$

Focusing on the case of a molecule in the presence of just two field modes, of electric field vectors ϵ_1 and ϵ_2 and frequencies ω_1 and ω_2, we can write the initial state as $|E_i,N_i\rangle = |E_i,n_1,n_2\rangle$, where n_1 and n_2 are the initial occupation numbers of the two field modes, and the molecule-radiation interaction H_{MR} as

$$H_{MR} = -\mathbf{d}\cdot\epsilon_1 - \mathbf{d}\cdot\epsilon_2 \quad (120)$$

The two frequencies are chosen such that $\hbar\omega_1 \approx E_{j_1} - E_i$, i.e., ω_1 is in resonance with the excitation frequency to state $|E_{j_1}\rangle$. ω_2 is chosen such that $E_i + 2\hbar\omega_1 \approx E_{j_2} + \hbar\omega_2$, which means that $2\hbar\omega_1 - \hbar\omega_2$ is in (2-1) resonance with the transition from $|E_i\rangle$ to $|E_{j_2}\rangle$ (see Fig. 1 for the application to Na_2).

Performing a perturbative expansion of Eq. (117) with H_{MR} as given in Eq. (120), and retaining the two lowest-order terms, we obtain that

$$\langle (E,q,\mathbf{m}^-),n_1-2,n_2|H_{MR}G(E^+ + E_{N_f})|E_i,n_1,n_2\rangle = A + B + \cdots \quad (121)$$

$$A = \sum_{j_1\neq i} \frac{\langle (E,q,\mathbf{m}^-),n_1-2|\mathbf{d}\cdot\epsilon_1|E_{j_1},n_1-1\rangle\langle E_{j_1},n_1-1|\mathbf{d}\cdot\epsilon_1|E_i,n_1\rangle}{(E^+ - E_{j_1} - \hbar\omega_1 - r_{j_1,j_1})(E^+ - E_i - 2\hbar\omega_1 - r_{i,i})} \quad (122)$$

$$B = \sum_{j_1,j_2(j_1\neq j_2\neq i)} \frac{\langle (E,q,\mathbf{m}^-),n_2|\mathbf{d}\cdot\epsilon_2|E_{j_2},n_2+1\rangle r_{j_2,j_1}\langle E_{j_1},n_1-1|\mathbf{d}\cdot\epsilon_1|E_i,n_1\rangle}{(E^+ - E_{j_2} - \hbar\omega_2 - r_{j_2,j_2})(E^+ - E_{j_1} - \hbar\omega_1 - r_{j_1,j_1})(E^+ - E_i - 2\hbar\omega_1 - r_{i,i})} \quad (123)$$

The r_{j_2,j_1} terms in Eq. (135), given by

$$r_{j_2,j_1} = \sum_{q',\mathbf{m}'} \int dE' \frac{\langle E_{j_2},n_2+1|\mathbf{d}\cdot\epsilon_2|(E',q',\mathbf{m}'^-),n_2\rangle\langle (E',q',\mathbf{m}'^-),n_1-2|\mathbf{d}\cdot\epsilon_1|E_{j_1},n_1-1\rangle}{E^+ - E'} \quad (124)$$

describe transitions between $|E_{j_1}\rangle$ and $|E_{j_2}\rangle$, accompanied by the absorption of one ω_1 photon and the stimulated emission of an ω_2 photon. Other sequential absorption and emission terms result from the higher-order contributions to Eq. (117).

The term A in Eq. (122) describes the direct resonant two-photon dissociation path $|E_i\rangle \rightarrow |E,q,\mathbf{m}^-\rangle$ via the intermediate states $|E_{j_1}\rangle$ (path A). The term B describes the dissociation path $|E_i\rangle \rightarrow |E',q',\mathbf{m}'^-\rangle \rightarrow |E_{j_2}\rangle \rightarrow |E,q,\mathbf{m}^-\rangle$ induced by ω_1 plus ω_2 (path B). It is important to note that the relative sign of the terms A and B depends on the frequency ω_2, resulting in a sensitivity of the final probability to the frequency of the control laser.

Equation (121) describes the photon fields by number states. However, a complete analysis of interference between the A and B paths necessitates an understanding of the role of the photon phase. Hence we sketch the same argument using multimode coherent states $|\alpha\rangle \equiv |\alpha_1\rangle \oplus |\alpha_2\rangle$, where $|\alpha_1\rangle$ and $|\alpha_2\rangle$ are coherent states of the ω_1 and ω_2 modes:

$$|\alpha_i\rangle = \sum_{n_i} \frac{\alpha_i^{n_i}\exp(-|\alpha_i|^2/2)}{\sqrt{n_i!}}|n_i\rangle, \quad i = 1,2 \quad (125)$$

The quantity α_i is related to the average photon number $\bar{n}_i$ and to the phase ϕ_i of the ω_i laser as $\alpha_i = \sqrt{\bar{n}_i}\exp(i\phi_i)$.

Replacing Eq. (121) by $\langle\alpha|\langle E,\mathbf{m}^-|H_{MR}G(E^+ + E_{N_f})|E_i\rangle|\alpha\rangle$ gives, within the rotating wave approximation,

$$\begin{aligned}\langle\alpha|\langle E,\mathbf{m}^-|H_{MR}G(E^+ + E_{N_f})|E_i\rangle|\alpha\rangle &= e^{2i\phi_1}\bar{A} + e^{i\phi_2}e^{i(2\phi_1-\phi_2)}\bar{B} + \cdots \\ &= e^{2i\phi_1}[\bar{A} + \bar{B} + \cdots] \end{aligned} \quad (126)$$

where $\bar{A}$ and $\bar{B}$ are of the same form as A and B in Eq. (121) but with the photon numbers n_1 and n_2 replaced by the average photon numbers $\bar{n}_1$ and $\bar{n}_2$. Hence, the leading terms in the dissociation probability $|\langle\alpha|\langle E,\mathbf{m}^-|H_{MR}G(E)|E_i\rangle|\alpha\rangle|^2$ can be obtained from Eq. (121) by replacing the photon numbers n_i by the average photon number $\bar{n}_i$. Most significantly, we see that the photodissociation probability is independent of the laser phase. Examination of the higher-order terms in the perturbative expansion of Eq. (117) (within the rotating wave approximation) shows a similar cancellation of the laser phase. Thus, the interference between path A and path B exists even for incoherent light.

Extensive control of the detailed and total probability to form a given q channel using this approach is demonstrated in the next subsection, where computations and experiments pertaining to Na_2 photo-dissociation are discussed. We note that in the actual calculations, it was in fact easier

to compute $\langle (E, q, \mathrm{m}^-), n_1 - 2, n_2 | H_{MR} G(E^+ + E_{N_f}) | E_i, n_1, n_2 \rangle$ [Eq. (117)] directly, using such methods as the high-field extension of the artificial channel method (Bandrauk and Atabek, 1989; Chen *et al.*, 1995; Shapiro and Bony, 1985) rather than the H_{MR} perturbative expansion. Note also that an alternative, complementary perspective on IIC has been advanced by Kobrak and Rice (1998a), based on photoselective adiabatic passage (Kobrak and Rice, 1998b). Their approach provides useful insights into incoherent interference control in the high-intensity limit and successfully reproduces the Na_2 results described below.

B. Computational and Experimental Demonstration

Incoherent interference control has been demonstrated both computationally and experimentally for the case of the two-photon dissociation of the Na_2 molecule. The photo-dissociation process we have examined is,

$$Na_2 \longrightarrow \begin{cases} Na(3s) + Na(3p) \\ Na(3s) + Na(4s) \\ Na(3s) + Na(3d) \end{cases} \tag{127}$$

The control objective is to produce preferentially the Na(3d) or Na(3p) product. In the IIC scenario this is done by varying one of the frequencies, either ω_1 or ω_2.

In the IIC experiment (Shnitman *et al.*, 1996) (see Fig. 10), two dye lasers pumped by a frequency-doubled Nd-Yag laser were used. One dye laser, whose frequency $\omega_2$was tuned between 13,312 cm^{-1} and 13,328 cm^{-1}, was used to dress the continuum with a $|E_{j_2}\rangle$ vib-rotational state of the $A^1\Sigma_u/^3\Pi_u$ electronic manifold (Chen *et al.*, 1993a). The other dye laser, whose frequency $\omega_1$was fixed at 17,474.12 cm^{-1}, was used to induce a two-photon dissociation of the $|E_{v=5,J=37}\rangle$ ground state of Na_2, through intermediate resonances (assigned as $v = 35$, $J = 38$ and $v = 35$, $J = 36$) of the $A^1\Sigma_u/^3\Pi_u$ manifold. The ω_1 and ω_2 pulses, both about 5 ns in duration with the stronger of them (ω_2) having an energy of ~3.5 mJ, were made to overlap in a heat pipe containing Na vapor at 370–410°C. Spontaneous emission from the excited Na atoms [Na(3d) → Na(3p) and Na(3p) → Na(3s)] resulting from the Na_2 photo-dissociation, was detected and dispersed in a spectrometer and a detector with a narrow-bandpass filter.

Figures 11 and 12 display the observed and computed Na(3d) and Na(3p) emission signal as a function of ω_2 at a fixed ω_1. We see that the computed and experimental results are in excellent agreement. Clearly, as the Na(3d) yield dips, the Na(3p) yield peaks, in accordance with theoretical calculations (Chen *et al.*, 1995). The controlled modulation of the Na(3p)/Na(3d)

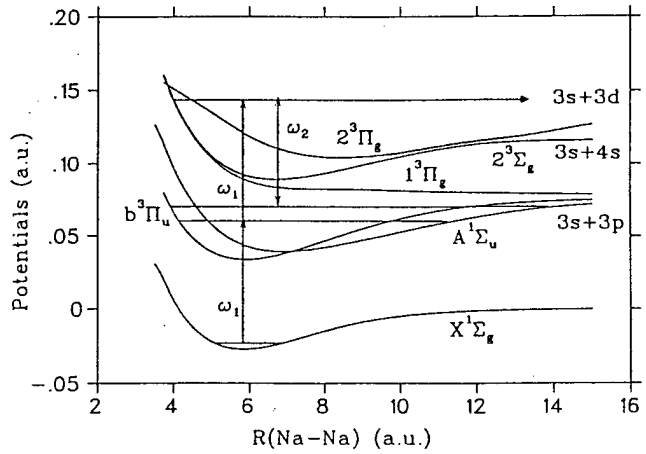

FIG. 10. Incoherent interference control (IIC) scheme and potential energy curves for Na_2. In this scheme a two-ω_1-photon excitation interferes with an ω_2 photon. The two-photon process proceeds from an initial state, assigned here as ($v = 5$, $J = 37$), via the $v = 35$, $J = 36, 38$ levels, belonging to the interacting $A^1\Sigma_u/^3\Pi_u$ electronic states, acting as intermediate resonances. The ω_2 photon dresses the continuum with the (initially unpopulated) $v = 93$, $J = 36$ and $v = 93$, $J = 38$ levels of the $A^1\Sigma_u/^3\Pi_u$ electronic states.

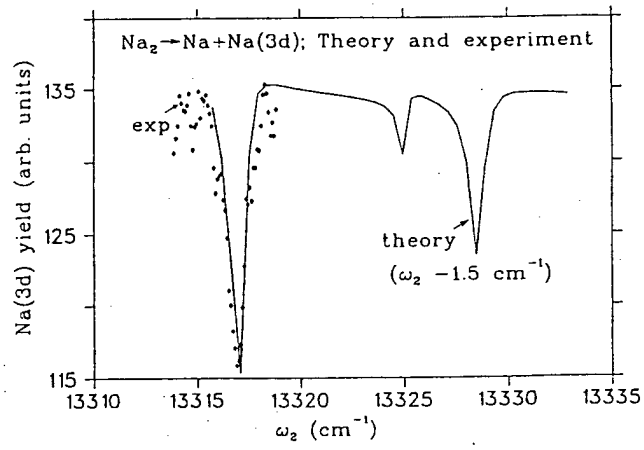

FIG. 11. Comparison of the experimental and theoretical $Na_2 \rightarrow Na(3s) + Na(3d)$ yields as a function of ω_2. In the calculation, an intermediate $v = 33$, $J = 31, 33$ resonance is used, and ω_1 is fixed at 17,720.7 cm^{-1}. The intensities of the two laser fields are $I(\omega_1) = 1.72 \times 10^8$ W/cm^2 and $I(\omega_2) = 2.84 \times 10^8$ W/cm^2. The ω_2 frequency axis of the calculated results was shifted by −1.5 cm^{-1} so that we could better compare the predicted and measured lineshapes.

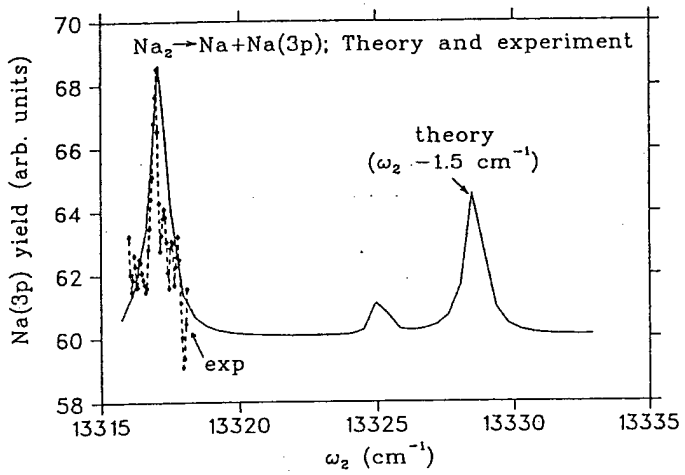

FIG. 12. Comparison of the experimental and theoretical $Na_2 \rightarrow Na(3s) + Na(3p)$ yields as a function of ω_2, with parameters as in Fig. 11.

branching ratio is seen to exceed 30%. It is important to note that this degree of experimental control was attained in a rather hostile environment, i.e., a heat pipe with ongoing molecular collisions, and using lasers with only partially coherent light.

VII. Coherent Control of Bimolecular Processes

The results discussed above deal with control of unimolecular processes, i.e., processes that begin with a single molecule that subsequently undergoes excitation and dynamics. Control has been described in two interlinked stages: (a) the use of multiple excitation routes to create controllable superposition states in the continuum and (b) the effect of the controllable interference term on the final outcome of the process. In this section we generalize coherent control to bimolecular collision processes, i.e., collisions of the type

$$A + D \rightarrow F + G \tag{128}$$

where A, D, F, G are, in general, molecules. Here F and G can be identical to A and D (nonreactive scattering) or different from A and D (reactive scattering). Unlike unimolecular processes, we first demonstrate that coherent control is possible in bimolecular scattering if one creates a superposition of energetically

degenerate scattering states; then we discuss methods for experimentally preparing such states.

Consider then Eq. (128), where we label $A + D$ as arrangement q and $F + G$ as arrangement q'. Below we focus on atom (A) plus diatom ($D = B - C$) scattering, although the results are easily generalized to polyatomic scattering. Eigenfunctions of the asymptotic Hamiltonian, where $A + D$ are widely separated are given, in accordance with Eq. (18), by $|E, q, \mathbf{m}; 0\rangle$, where we have made the channel label q explicit. States of the product are similarly denoted $|E, q', \mathbf{n}; 0\rangle$, and $|E, q', \mathbf{n}^-\rangle$ denotes the incoming solutions associated with product in $|E, q', \mathbf{n}; 0\rangle$. The probability $P_E(\mathbf{n}, q'; \mathbf{m}, q)$ of forming $|E, q', \mathbf{n}; 0\rangle$, having initiated the scattering in $|E, q, \mathbf{m}; 0\rangle$, is given by (Taylor, 1972) as

$$P_E(\mathbf{n}, q'; \mathbf{m}, q) = |\langle E, q', \mathbf{n}; 0 | S | E, q, \mathbf{m}; 0\rangle|^2 \tag{129}$$

where S is the scattering matrix. In analogy with Eq. (36), one can rewrite the probability in terms of $\langle E, q, \mathbf{n}^- | V_q | E, q, \mathbf{m}; 0\rangle$, where V_q is defined, in analogy with Eq. (14), as the component of the total potential that vanishes as the distance A to D becomes arbitrarily large. It is traditional in scattering theory, however, to compute the cross section, given by

$$\sigma_E(\mathbf{n}, q'; \mathbf{m}, q) = |\langle E, q', \mathbf{n}^- | V_q | E, q, \mathbf{m}; 0\rangle|^2 \tag{130}$$

rather than the probability. In addition to the above state-to-state cross section, the cross section of forming product in arrangement q' independent of the internal state $\mathbf{n}$,

$$\sigma_E(q'; \mathbf{m}, q) = \sum_{\mathbf{n}} |\langle E, q', \mathbf{n}^- | V_q | E, q, \mathbf{m}; 0\rangle|^2 \tag{131}$$

is also of interest. Assorted other cross sections may be defined, depending upon which of the elements of $\mathbf{n}$ are summed over. Of relevance below are (a) $\sigma_E(q', \theta, \phi; \mathbf{m}, q)$, corresponding to scattering into the q' product channel and into scattering angles (θ, ϕ), and (b) the traditional differential cross section $\sigma_E(q', \theta; \mathbf{m}, q) = \int d\phi\, \sigma_E(q', \theta, \phi; \mathbf{m}, q)$.

In order to control bimolecular cross sections, we now consider scattering from an initial *superposition* state $|E, q, \{c_{\mathbf{m}}\}\rangle$ comprised of N energetically degenerate states $|E, q, \mathbf{m}; 0\rangle$:

$$|E, q, \{c_{\mathbf{m}}\}\rangle = \sum_{\mathbf{m}=1}^{N} c_{\mathbf{m}} |E, q, \mathbf{m}; 0\rangle \tag{132}$$

The cross section associated with using Eq. (132) as the initial state, obtained by substituting Eq. (132) in Eq. (130), is

$$\begin{aligned}\sigma_E(\mathbf{n}, q'; \{c_m\}, q) &= |\langle E, q', \mathbf{n}^- | V_q \sum_m c_m | E, q, \mathbf{m}; 0\rangle|^2 \\ &= \sum_m |c_m|^2 \langle E, q', \mathbf{n}^- | V_q | E, q, \mathbf{m}; 0\rangle|^2 \\ &\quad + \sum_{m'} \sum_{m \neq m'} c_m c_{m'}^* \langle E, q', \mathbf{n}^- | V_q | E, q, \mathbf{m}; 0\rangle \\ &\quad \times \langle E, q, \mathbf{m}'; 0 | V_q | E, q', \mathbf{n}^-\rangle \\ &\equiv \sum_m |c_m|^2 \sigma(\mathbf{n}, q'; \mathbf{m}, q) + \sum_{m'} \sum_{m \neq m'} c_m c_{m'}^* \sigma(\mathbf{n}, q'; \mathbf{m}', \mathbf{m}, q)\end{aligned} \tag{133}$$

where $\sigma(\mathbf{n}, q'; \mathbf{m}', \mathbf{m}, q)$ is defined via Eq. (133). The total cross section is given by

$$\sigma_E(q'; \{c_m\}, q) = \sum_n \sigma_E(\mathbf{n}, q'; \{c_m\}, q) \tag{134}$$

Note that Eq. (133) and hence Eq. (134) are now of the standard coherent control form, i.e., direct contributions from each member of the superposition, proportional to $|c_m|^2$, plus interference terms that are proportional to $c_m c_{m'}^*$. Hence, by controlling the c_m, we can control the scattering cross section. Note also that both the direct and the interference amplitudes are composed of the same amplitudes. As such, we can even expect control to be effective far from the onset of reaction at reaction thresholds, a feature that overcomes the limitations of previously proposed bimolecular control methods (Krause *et al.*, 1990).

A. Degenerate e_M Superpositions

The easiest way of implementing bimolecular control in the lab is to start with a superposition of scattering states having the same incoming translational wave function $|\mathbf{k}_m\rangle$. This means, however, by Eq. (132), that in order to maintain the degeneracy of the total continuum energy E, we must build the superposition state from degenerate internal states $|e_m\rangle$:

$$|E, q, \{c_m\}\rangle = \sum_m c_m |E, q, \mathbf{m}; 0\rangle \equiv |\mathbf{k}_m\rangle \sum_m c_m |e_m\rangle \tag{135}$$

In atom-diatom scattering, the most obvious candidate for degenerate $|e_m\rangle$ are the $|J, M_J\rangle$ states associated with fixed diatomic rotational angular momentum J. However, in this case the interference terms $\sigma(\mathbf{n}, q'; \mathbf{m}', \mathbf{m}, q)$ contain the cylindrically asymmetric $\exp[i(M_J - M_J')\phi]$ factors (Abrashkevich *et al.*, 1999), which average out upon integration over the azimuthal angle ϕ. As a result, although control over the fully differential $\sigma_E(q', \theta, \phi; \{c_m\}, q)$ cross section is possible, control over the ϕ-averaged differential cross section $\sigma_E(q', \theta; \{c_m\}, q)$ and the total cross section $\sigma_E(q'; \{c_m\}, q)$ cannot be achieved in this way.

To examine the extent of control afforded in this way, we performed detailed computations on one of the most widely studied prototype exchange reactions, that of

$$D + H_2 \rightarrow H + HD$$

Our computations were carried out for $E = 1.25$ eV and H_2 in the $v = 0, J = 2$ vib-rotational state. Both the reactive and the nonreactive differential cross sections $a + \phi = 0$ [denoted $\sigma^R(\theta)$ and $\sigma^{NR}(\theta)$] were examined. Figure 13 shows $\sigma^R(\theta)/\sigma^{NR}(\theta)$ for the linear superposition $c_1|E, J, \kappa_1 = 2\rangle + c_2|E, J, \kappa_2 = 0\rangle$ for various values of $s = |c_1|^2/[|c_1|^2 + |c_2|^2]$ with $\phi_{12} = \arg(a_2/a_1) = 157°$. Here $s = 0$ corresponds to scattering out of the initial state $v = 0, J = 2, \kappa = 2$; and $s = 1$ corresponds to scattering from $v = 0, J = 2, \kappa = 0$. The ratio of controlled differential cross sections is seen to be considerably different from the uncontrolled ratio. For example, the controlled $\sigma^R(\theta)/\sigma^{NR}(\theta)$ at $\theta = 91°$ at $s = 0.748$ is approximately twice as large as the uncontrolled ratios. Analysis of Fig. 13 shows that the maxima and minima of the controlled ratio in the region between 50° and 120° are positioned at the corresponding minima and maxima of the uncontrolled ratios. Exactly the opposite behavior is seen in the outer regions of θ. Hence, coherent control changes both the magnitude and the structure of the differential cross section.

Results for the ratio of the reactive versus nonreactive cross sections at a fixed 0, J value are shown in Fig. 14 for scattering from $c_1|v = 0, J = 2, \kappa = 2\rangle + c_2|v = 0, J = 2, \kappa = 1\rangle$, as a function of the control parameters ϕ_{12} and s. The ratio is seen to vary from 0.032 to 0.113, showing maxima and minima that are well outside the range of results for scattering from a single κ state.

This approach can be extended to include all available energetically degenerate κ_i states ($\kappa_i = -J, -J+1, \ldots, J$), with concomitant improvement in the ratio of reactive to nonreactive product. In addition, one can optimize this ratio (Abrashkevich *et al.*, 1999) as a function of the coefficients c_m. For the $J = 2$ case, the maximum $\sigma^R/\sigma^{NR} = 0.143$, a 20% improvement over the results for a superposed pair of κ_i states.

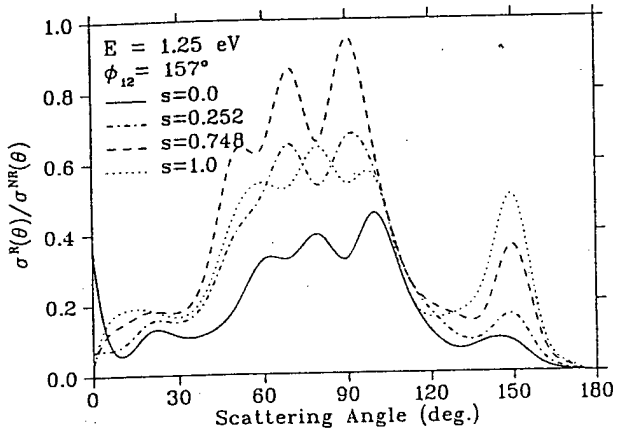

FIG. 13. Dependence of the ratio of the reactive to nonreactive differential cross section $\sigma^R(\theta)/\sigma^{NR}(\theta)$ in controlled $D + H_2$ on the scattering angle θ at $\phi_{12} = 157°$ for four values of s: $s = 0, 1.0.252$, and 0.748. (From Abrashkevich *et al.*, 1998a.)

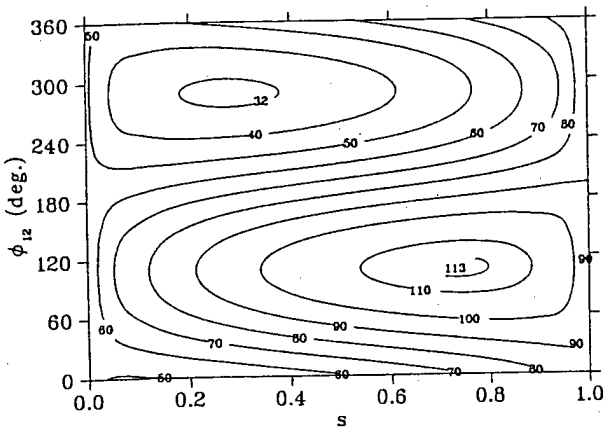

FIG. 14. Contour plot of the ratio of reactive to nonreactive cross section σ^R/σ^{NR} ($\times 10^3$) in controlled $D + H_2$ as a function of ϕ_{12} and s, at a fixed 0, J value.

It remains to ask how such a superposition of helicity states may be prepared. One possibility is a precursor step consisting of the coherently controlled photo-dissociation of a molecule to produce a diatomic product in a controlled superposition of κ states relative to an incoming partner. For example, in the $D + H_2$ case we can subject H_2S to a coherently controlled photo-dissociation step to produce H_2 in a superposition such that aiming the

D atom exactly antiparallel to the direction of the H_2 motion will produce the desired initial $|E, q, \{c_m\}\rangle$.

B. Sculpted Imploding Waves

Rather than using a superposition of internal states $|e_m\rangle$, as in the above discussion, it is possible to effect bimolecular control by using a superposition of translational wavefunctions $|\mathbf{k}_m\rangle$ (Frishman *et al.*, 1999). In order to examine a superposition of incident plane waves, we first perform a partial-wave decomposition of each of the plane waves, assumed directed along the Z-axis:

$$\langle \mathbf{R}|\mathbf{k}_m\rangle = \exp(i\mathbf{k}_m \cdot \mathbf{R}) = \exp(ik_m Z) = \exp(ik_m R\cos\theta)$$
$$= \sum_l c_l j_l(k_m R) P_l(\cos\theta) \tag{136}$$

where $c_l = i^l(2l+1)$ and $j_l(k_m R)$, $P_l(\cos\theta)$ are the spherical Bessel function and Legendre polynomial, respectively. We see that each incoming plane wave is in fact a superposition of energetically degenerate states with fixed coefficients c_l. This suggests the possibility of altering the c_l to produce modified states $\langle \mathbf{R}|\mathbf{k}_{mod}\rangle$ that will display different quantum interferences, hence altering the product cross sections. Thus, in this instance, the initial $|E, q, \{c_m\}\rangle$ is given by $|E, q, \{c_m\}\rangle = |e_m\rangle|\mathbf{k}_{mod}\rangle$, where $|\mathbf{k}_{mod}\rangle$, a "sculpted incoming wavepacket," is parametrized by coefficients $\{c_l\}$.

The effect of changing the structure of the incident wavepacket cannot, however, be measured using the standard definition of the cross section, because that definition relies on a constant flux from one direction (Taylor, 1972). Rather, we consider the magnitude of $F_{q'}$, the outgoing flux into the product channel, as a function of the $|c_l|$, with the constraint that the incident wavefunction is normalized to the usual Dirac delta function (for alternative choices of constraints, see Frishman *et al.*, 1999).

As an example of the control afforded by this approach, consider rotational excitation in a model of the $Ar + H_2(J, M_J) \rightarrow Ar + H_2(J'M_{J'})$ collision. Optimizing the phases χ_l of $c_l = |c_l|\exp(i\chi_l)$ allows a direct study of the effect of varying the interferences between partial-wave components on $F_{q'}$. Typically, altering χ_l allowed for considerable control. For example, with $J = 2, M_J = 0, J' = 0$, it was possible to change $F_{q'}$ by two orders of magnitude, from 5.1×10^{-4} to 3.8×10^{-2}, just by varying the χ_l. These values are to be compared to $F_{q'} = 1 \times 10^{-2}$ associated with scattering from an incident plane wave. Real and imaginary parts of the incident wave functions leading to these maximum and minimum values of the outgoing flux are

shown in Fig. 15. They are distinctly different from one another and from a plane wave.

It remains to establish viable methods to prepare such sculpted imploding matter waves experimentally. Once again, we anticipate doing so via a

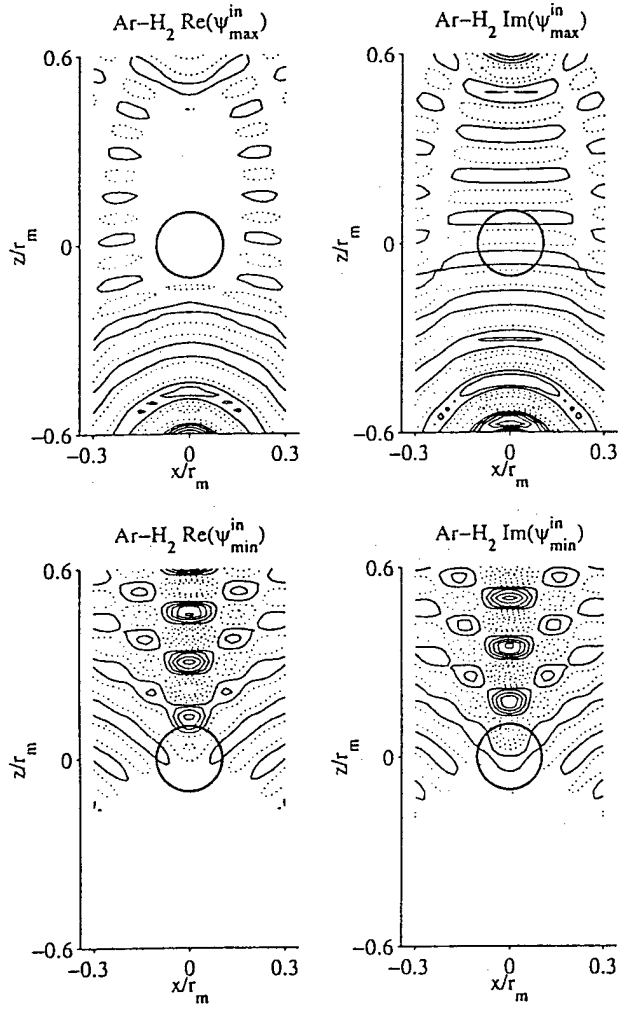

FIG. 15. Real and imaginary parts of the incident wave function leading to maximum and minimum outgoing flux for $Ar + H_2(v = 0,\ j = 2,\ m_j = 0)$. (From Frishman *et al.*, in preparation.)

pre-reactive photo-dissociation step, possibly in conjunction with matter interferometry techniques.

C. Optimized Bimolecular Scattering: Enhancement and Total Suppression

We now extend the treatment of Section VII.A to the case of a superposition composed of more than two states. On the basis of Eqs. (130) and (131), we introduce in this subsection a scheme that optimizes $\sigma(q';\{c_m\},q)$ or $\sigma(q',\mathbf{n};\{c_m\},q)$ as a function of c_m for an arbitrary number of states. One of the most interesting outcomes of this procedure is that it leads to a strong analytic result: if the number of initial open states in the reactant space exceeds the number of open states in the product space, it is possible to find a particular set of $\{c_m\}$ such that one can totally *suppress* reactive scattering. This result is proven below and applied to display the total suppression of tunneling (Frishman *et al.*, 1998).

Consider scattering from incident state $|E,q,\mathbf{n};0\rangle$ to final state $|E,q',\mathbf{m};0\rangle$. To simplify the notation, we specialize the treatment to the case where the $\mathbf{m}$ and $\mathbf{n}$ labels pertain to just a single quantum number, denoted i and f, with associated free states $|E,q,i;0\rangle$ and $|E,q',f;0\rangle$. In accordance with Eq. (129), the probability $P(f,q';i,q)$ of producing product in final state $|f,E,q'\rangle$, having started in the initial state $|i,E,q\rangle$, is

$$P(f,q';i,q) = |S_{fi}|^2 \tag{137}$$

where $S_{fi} = \langle E,f,q'|S|E,i,q\rangle$ and where S is the scattering matrix for the process. The total probability $P(q';i,q)$ of scattering into arrangement channel q', assuming m open product states, is given by

$$P(q';i,q) = \sum_{f=1}^{m} |S_{fi}|^2 \tag{138}$$

To simplify the notation, we have not carried an E label in the probabilities: fixed energy E is understood.

If we now consider scattering from an initial state $|E,q,\{c_i\}\rangle$ comprised of a linear superposition of k states, [i.e., Eq. (146) with $N = k$]. Then the probability of forming $|E,q',f\rangle$ from this initial state is

$$P(f,q';\mathbf{c},q) = \left|\sum_{i=1}^{k} c_i S_{fi}\right|^2 \tag{139}$$

and the total reactive scattering probability into channel q', $P(q';\mathbf{c},q)$, is

$$P(q';\mathbf{c},q)=\sum_{f=1}^{m}\left|\sum_{i=1}^{k}c_iS_{fi}\right|^2 \tag{140}$$

To simplify the notation, we introduce the matrix $\sigma=\mathbf{S}_{q'}^{\dagger}\mathbf{S}_{q'}$ with elements $\sigma_{ij}=\sum_{f=1}^{m}S_{fj}^{*}S_{fi}$, which allows us to rewrite Eq. (140) as

$$P(q';\mathbf{c},q)=\mathbf{c}^{\dagger}\sigma\mathbf{c} \tag{141}$$

Here $\dagger$ denotes the Hermitean conjugate, and the q' subscript on the S indicates that we are dealing with the submatrix of the S matrix associated with scattering into product channel q'.

One can optimize scattering into arrangement channel q', with the normalization constraint $\sum_{i=1}^{k}|c_i|^2=1$, by requiring

$$\frac{\partial}{\partial c_k^{*}}\left[P(q';\mathbf{c},q)-\lambda\sum_{i=1}^{k}|c_i|^2\right]=\frac{\partial}{\partial c_k^{*}}[\mathbf{c}^{\dagger}\sigma\mathbf{c}-\lambda\mathbf{c}^{\dagger}\mathbf{c}]=0 \tag{142}$$

where λ is a Lagrange multiplier. Explicitly taking the derivative gives the result that the optimized coefficients $\mathbf{c}_\lambda$ satisfy the eigenvalue equation

$$\sigma\mathbf{c}_\lambda=\lambda\mathbf{c}_\lambda \tag{143}$$

Additional labels may be necessary to account for degeneracies of the eigenvectors $\mathbf{c}_\lambda$.

We first note that if $\lambda=0$ is an eigenvalue of Eq. (143) with eigenfunctions $\mathbf{c}_0$, then by inserting Eq. (143), into Eq. (141) we have that $P(q';\mathbf{c}_0,q)=0$. That is, if $\lambda=0$ is a solution to Eq. (143), then the coefficients $\mathbf{c}_0$ completely suppress reaction into arrangement channel q'.

Clearly, $\lambda=0$ is a solution if

$$\det(\sigma)=\det(\mathbf{S}_q'^{\dagger}\mathbf{S}_q')=0 \tag{144}$$

which is the case if the number of initial states k participating in the initial superposition is greater than the number m of open product states, a situation that invariably occurs for endoergic processes. To see this result, note that under these circumstances, σ is a matrix of order $k\times k$ and $\mathbf{S}_{q'}$ is of order $k\times m$. If $k>m$, we can construct a $k\times k$-order matrix $\mathbf{A}_q'$ by adding a submatrix of

$(k-m)$ rows of zeros to the lower part of $\mathbf{S}_{q'}$. Then

$$\det(\sigma)=\det(\mathbf{S}_{q'}^{\dagger}\mathbf{S}_{q'})=\det(\mathbf{A}_{q'}^{\dagger}\mathbf{A}_{q'})=\det(\mathbf{A}_{q'}^{\dagger})\det(\mathbf{A}_{q'})=0 \tag{145}$$

The last equality holds because the determinants of $\mathbf{A}_{q'}$ and $\mathbf{A}_{q'}^{\dagger}$ are zero.

As an example of the kind of results that are possible, consider the optimization of a barrier penetration problem modeled by a set of multichannel Schrödinger equations of the type

$$\Psi''(r)=-\frac{2\mu}{\hbar^2}(\mathbf{E}-\mathbf{V})\Psi(r) \tag{146}$$

where μ is the relevant mass, V is the potential matrix, E is a diagonal matrix with elements $E-e_i$, and k is the total number of open channels in arrangement q. Sample scattering results for $k=4$ using a potential matrix constructed from Eckart potentials, i.e.,

$$V_{i\ell}(r)=-\frac{a_{i\ell}\xi}{1-\xi}-\frac{b_{i\ell}\xi}{(1-\xi)^2}+c_{i\ell},\quad i,\ell=1,\ldots,4 \tag{147}$$

where $\xi=-\exp(2\pi r/t)$, with t a distance potential parameter, are shown in Fig. 16. Reactivity is shown as a function of energy for the case where the number of populated initial states j is less than k; here $j=3$. The curves labeled P_i correspond to the standard $P(q';i,q)$, i.e., total reaction probability from each of the individual initial states. The quantities P_1 and P_3, which are open asymptotically at all energies, show a gradual rise with increasing energy, whereas P_2, which is closed on the product side until $E_{th}(3)=0.008$ a.u., stays rather small until $E=E_{th}(3)$, where it displays a very rapid rise to near unity. Total reaction probability reaches unity above $E_{th}(4)=0.010$ a.u., the threshold for the opening of the fourth channel.

Of particular relevance here are the solid curves in Fig. 16, which show the maximum and minimum reactivity obtained from the optimal solutions to Eq. (143). The maximum reactivity is seen to be substantially larger than any of the individual P_i and to reach unity at significantly lower energies than any of these solutions. Minimal reactivity, as predicted by the argument presented above, is seen to be zero for $E<E_{th}(3)$ because the total number of states $(j=3)$ in the superposition exceeds the number of open product states $(m=2)$. At $E>E_{th}(3)$ a third product channel opens so that $j=m$ and the minimal solution is no longer zero.

Note also that the minimum reactivity curve in Fig. 16 reflects a variety of different interesting behaviors, depending on the particular energy. Specifically, below the maximum of V_{11} at 0.005 a.u., the zero minimum corresponds

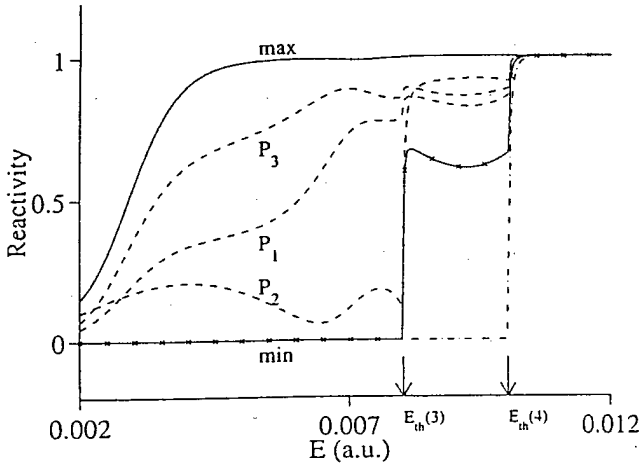

FIG. 16. Reactivity shown as a function of energy in a model system. Dashed curves labeled P_i correspond to the total reactivity from each of the three individual initial states in the prepared superposition. Solid curves with crosses denote the reactivity obtained by solving Eq. (143) for the optimal solutions. The two arrows indicate the threshold energies for opening of the third and fourth channels. The dot-dash curve shows the minimum reactivity resulting from a separate computation that includes four states in the initial superposition.

to suppression of tunneling through that barrier. Above 0.005 a.u., the zero minimum corresponds to suppression of the reactive scattering that occurs *above* the barrier.

Thus it is clear that the ability to superimpose degenerate scattering states has great potential for the control of scattering processes. Note also that, as an obvious extension, similar results hold for tunneling in bound systems if the total number of initial degenerate states at the energy of interest exceeds the number of accessible final states at that energy.

VIII. Summary

Coherent control has been demonstrated formally, computationally, and experimentally to be a viable method for controlling the outcome of isolated atomic molecular and electronic processes that form products in the continuum. It is a method that takes advantage of the quantum nature both of matter and of the incident light to encode quantum interference information into the molecular dynamics. That is, molecular reaction dynamics is intimately linked to the wavefunction phases that are controllable through coherent optical phase excitation. The result is a powerful method to control the dynamics of atomic, molecular, and electronic processes.

IX. Acknowledgments

We are grateful to the U.S. Office of Naval Research for support of the vast majority of this research.

X. References

Abrashkevich, A., Brumer, P., and Shapiro, M. (1999). In preparation.
Abrashkevich, A., Shapiro, M., and Brumer, P. (1998a). *Phys. Rev. Lett.* 81, 3789.
Abrashkevich, D., Shapiro, M., and Brumer, P. (1998b). *J. Chem. Phys.* 108, 3585.
Asaro, C., Brumer, P., and Shapiro, M. (1988). *Phys. Rev. Lett.* 60, 1634.
Assion, T., Baumert, T., Bergt, M., Brixner, T., Kiefer, B., Seyfried, V., Strehle, M., and Gerber, G. (1998). *Science* 282, 919.
Balint-Kurti, G. G., and Shapiro, M. (1981). *Chem. Phys.* 61, 137.
Balint-Kurti, G. G., and Shapiro, M. (1986). *Adv. Chem. Phys.* 60, 403.
Bandrauk, A. D., and Atabek, O. (1989). *Adv. Chem. Phys.* 73, 823.
Bandrauk, A. D., Gauthier, J.-M., and McCann, J. F. (1992). *Chem. Phys. Lett.* 200, 399.
Baranova, B. A., Chudinov, A. N., and Ya Zel'dovitch, B. (1990). *Opt. Comm.* 79, 116.
Bardeen, C. J., Yakovlev, V. V., Wilson, K. R., Carpenter, S. D., Weber, P. M., and Warren, W. S. (1997). *Chem. Phys. Lett.* 280, 151.
Barron, L. D. (1982). *Molecular light scattering and optical activity*. Cambridge University Press (Cambridge, UK).
Barron, L. D. (1986). *Chem. Soc. Rev.* 15, 189.
Baumert, T., Grosser, M., Thalweiser, R., and Gerber, G. (1991). *Phys. Rev. Lett.* 67, 3753.
Brumer, P., and Shapiro, M. (1986a). *Chem. Phys. Lett.* 126, 541.
Brumer, P., and Shapiro, M. (1986b). *Adv. Chem. Phys.* 60, 371.
Brumer, P., and Shapiro, M. (1992). *Ann. Rev. Phys. Chem.* 43, 257.
Cavalieri, S., Eramo, R., and Fini, L. (1997). *Phys. Rev. A* 55, 2941.
Cavalieri, S., Eramo, R., Fini, L., Materazzi, M., Faucher, O., and Charalambidis, D. (1998). *Phys. Rev. A* 57, 2915.
Chan, C. K., Brumer, P., and Shapiro, M. (1991). *J. Chem. Phys.* 94, 2688.
Charron, E., Guisti-Suzor, A., and Mies, F. H. (1993). *Phys. Rev. Lett.* 71, 692.
Charron, E., Giusti-Suzor, A., and Mies, F. H. (1995). *Phys. Rev. Lett.* 75, 2815.
Chelkowski, S., and Bandrauk, A. D. (1991). *Chem. Phys. Lett.* 186, 284.
Chen, C., Yin, Y.-Y., and Elliott, D. S. (1990). *Phys. Rev. Lett.* 64, 507; *Phys. Rev. Lett.* 65, 1737.
Chen, Z., Shapiro, M., and Brumer, P. (1993a). *J. Chem. Phys.* 98, 6843.
Chen, Z., Shapiro, M., and Brumer, P. (1993b). *J. Chem. Phys.* 98, 8647.
Chen, Z., Shapiro, M., and Brumer, P. (1994). *Chem. Phys. Lett.* 228, 289.
Chen, Z., Shapiro, M., and Brumer, P. (1995). *J. Chem. Phys.* 102, 5683.
Cohen-Tannoudji, C., J. Dupont-Roc, J., and G. Grynberg, G. (1992). *Atom-photon interactions*. Wiley (New York).
Dupont, E., Corkum, P. B., Liu, H. C., Buchanan, M., and Wasilewski, Z. R. (1995). *Phys. Rev. Lett.* 74, 3596.
Faucher, O., Charalambidis, D., Fotakis, C., Zhang, J., and Lambropoulos, P. (1993). *Phys. Rev. Lett.* 70, 3004.
Frishman, E., Shapiro, M., and Brumer, P. (1998). *J. Chem. Phys.* In press.
Frishman, E., Shapiro, M., and Brumer, P. (1999). In preparation.
Gordon, R. J., and Rice, S. A. (1997). 48, 595.

Hache, A., Kostoulas, Y., Atanasov, R., Hughes, J. L. P., Sipe, J. E., and van Driel, H.M. (1997). *Phys. Rev. Lett.* 78, 306.
Hammerich, A. D., Manthe, U., Kosloff, R., Meyer, H. D., and Cederbaum, L. S. (1994). *J. Chem. Phys.* 101, 5623.
Hollas, J. M. (1982). *High resolution spectroscopy*. Butterworths (London).
Ivanov, M. Y., Corkum, P. B., and Dietrich, P. (1993). *Laser Physics* 3, 375.
Ivanov, M., Corkum, P. B., Zuo, T., and Bandrauk, A. (1995). *Phys. Rev. Lett.* 74, 2933.
Jakubetz, W., Manz, J., and Schreier, H. J. (1990). *Chem. Phys. Lett.* 165, 100.
Jiang, X.-P., and Brumer, P. (1991). *J. Chem. Phys.* 94, 5833; *Chem. Phys. Lett.* 180, 222.
Jiang, X.-P., Shapiro, M., and Brumer, P. (1996). *J. Chem. Phys.* 104, 607.
Kleiman, V. D., Zhu, L., Li, X., and Gordon, R. J. (1995). *J. Chem. Phys.* 102, 5863.
See, for example, Knight, P. L., Lauder, M. A., and Dalton, B. J. (1990). *Phys. Rep.* 190, 1.
Kobrak, M. N., and Rice, S. A. (1998a). *J. Chem. Phys.* 109, 1.
Kobrak, M. N., and Rice, S. A. (1998b). *Phys. Rev. A* 57, 2885.
Kohler, B., Krause, J. L., Raski, F., Wilson, K. R., Yakovlev, V. V., Whitnell, R.M., and Yan, Y. (1995). *Acct. Chem. Res.* 28, 133.
Kosloff, R. (1988). *J. Phys. Chem.* 92, 2087.
Kosloff, R. (1994). *Ann. Rev. Phys. Chem.* 45, 145.
Kosloff, R., Rice, S. A., Gaspard, P., Tersigni, S., Tannor, and D. J. (1989). *Chem. Phys.* 139, 201.
Kosloff, R., Rice, S. A., Gaspard, P., Tersigni, S., Tannor, and D. J. (1989). *Chem. Phys.* 139, 201.
Krause, J., Shapiro, M., and Brumer, P. (1990) *J. Chem. Phys.* 92, 1126.
Krause, J. L., Whitnell, R. M., Wilson, K. R., Yan, Y., and Mukamel, S. (1993). *J. Chem. Phys.* 99, 6562.
Leforestier, C., Bisseling, R., Cerjan, C., Feit, M., Friesner, R., Guldberg, A., Hammerich, A. D., Julicard, G., Karrlein, W., Dieter Meyer, H., Lipkin, N., Roncero, O., and Kosloff, R. (1991). *J. Comp. Phys.* 94, 59.
Levine, R. D. (1969). *Quantum mechanics of molecular rate processes*. Clarendon (Oxford, UK).
Lu, S.-P., Park, S. M., Xie, Y., and Gordon, R. J. (1992). *J. Chem. Phys.* 96, 6613.
Manolopoulos, D. E., D'Mello, M., and Wyatt, R. E. (1991). *J. Chem. Phys.* 93, 403.
Muller, H. G., Bucksbaum, P. H., Schumacher, D. W., and Zavriyev, A. (1990). *J. Phys. B* 23, 2761.
Park, S. M., Lu, S.-P., and Gordon, R. J. (1991). *J. Chem. Phys.* 94, 8622.
Peirce, A. P., Dahleh, M. A., and Rabitz, H. (1988). *Phys. Rev. A* 37, 4950; *ibid.* (1990). 42, 1065, Shi, S., and Rabitz, H. (1991). *Comp. Phys. Comm.* 63, 71.
Potter, E. D., Herek, J. L., Pedersen, S., Liu, Q., and Zewail, A. H. (1992). *Nature* 355, 66.
Potvliege, R. M., and Smith, P. H. G. (1992). *J. Phys. B* 25, 2501.
Pratt, S. T. (1996). *J. Chem. Phys.* 104, 5776.
Schafer, K. J., and Kulander, K. C. (1992). *Phys. Rev. A* 45, 8026.
Schmidt, I. (1987). Ph.D. Thesis, Kaiserslautern University.
Schubert, M., and Wilhelmi, B. (1986). *Nonlinear optics and quantum electronics*. Wiley (New York).
Segev, E., and Shapiro, M. (1982). *J. Chem. Phys.* 77, 5604.
Seideman, T., Shapiro, M., and Brumer, P. (1989). *J. Chem. Phys.* 90, 7132.
Shapiro, M. (1993). *J. Phys. Chem.* 97, 7396.
Shapiro, M., and Bony, H. (1985). *J. Chem. Phys.* 83, 1588.
Shapiro, M., and Brumer, P. (1987). *Faraday Disc. Chem. Soc.* 82, 177.
Shapiro, M., and Brumer, P. (1989). *J. Chem. Phys.* 90, 6179.
Shapiro, M., and Brumer, P. (1991). *J. Chem. Phys.* 95, 8658.
Shapiro, M., and Brumer, P. (1992). *J. Chem. Phys.* 97, 6259.
Shapiro, M., and Brumer, P. (1993). *Chem. Phys. Lett.* 208, 193.
Shapiro, M., and Brumer, P. (1993). *J. Chem. Phys.* 98, 201.

Shapiro, M., and Brumer, P. (1997). *Trans. Farad. Soc.* 93, 1263.
Shapiro, M., Hepburn, J. W., and Brumer, P. (1988). *Chem. Phys. Lett.* 149, 451.
Sheeny, B., Walker, R. B., and DiMauro, L. F. (1995). *Phys. Rev. Lett.* 74, 4799.
Shi, S., Woody, A., and Rabitz, H. (1988). *J. Chem. Phys.* 88, 6870.
Shi, S., and Rabitz, H. (1989). *Chem. Phys.* 139, 185.
Shnitman, A., Sofer, I., Golub, I., Yogev, A., Shapiro, M., Chen, Z., and Brumer, P. (1996). *Phys. Rev. Lett.* 76, 2886.
Szöke, A., Kulander, K. C., and Bardsley, J. N. (1991). *J. Phys. B.* 24, 3165.
Tannor, D., and Rice, S. A. (1985). *J. Chem. Phys.* 83, 5013.
Tannor, D., Kosloff, R., and Rice, S. A. (1986). *J. Chem. Phys.* 85, 5805.
Tannor, D. J., and Rice, S. A. (1988). *Adv. Chem. Phys.* 70, 441.
Taylor, J. R. (1972). *Scattering theory*. Wiley (New York).
Walker, D. C., ed. (1979). *Origins of optical activity in nature*. Elsevier (Amsterdam).
Wang, F., Chen, C., and Elliott, D. S. (1996). *Phys. Rev. Lett.* 77, 2416.
Wang, X., Bersohn, R., Takahashi, K., Kawasaki, M., and Kim, H. L. (1996). *J. Chem. Phys.* 105, 2992.
Warren, W. S., Rabitz, H., and Dahleh, M. (1993). *Science* 259, 1581.
Yan, Y., Gillilan, R. E., Whitnell, R. M., and Wilson, K. R. (1993). *J. Phys. Chem.* 97, 2320.
Woolley, R. G. (1975). *Adv. Phys.* 25, 27.
Yelin, D., Meshulach, D., and Silberberg, Y. (1997). *Opt. Lett.* 22, 1793.
Yin, Y.-Y., Chen, C., Elliott, D. S., and Smith, A. V. (1992). *Phys. Rev. Lett.* 69, 2353.
Yin, Y.-Y., Shehadeh, R., Elliott, D., and Grant, E. (1995). *Chem. Phys. Lett.* 241, 591.
Zhang, J. Z. H., and Miller, W. H. (1989). *J. Chem. Phys.* 91, 1528.
Zhu, L., Kleiman, V. D., Li, X., Lu, S., Trentelman, K., and Gordon, R.J. (1995). *Science* 270, 77.
Zhu, L., Suto, K., Fiss, J. A., Wada, R., Seideman, T., and Gordon, R. J. (1997). *Phys. Rev. Lett.* 79, 4108.
Zuo, T., and Bandrauk, A. D. (1996). *Phys. Rev. A* 54, 3254.

J. Phys. Chem. A **1999,** *103,* 10333−10342

Optimized Imploding Waves in the Coherent Control of Bimolecular Processes: Atom−Rotor Scattering

Einat Frishman and Moshe Shapiro*

Chemical Physics Department, The Weizmann Institute of Science, Rehovot, Israel

Paul Brumer

Photonics Research Ontario and Chemical Physics Theory Group, University of Toronto, Toronto, Canada M5S 3H6

Received: July 2, 1999; In Final Form: September 3, 1999

Sculpting the incoming wave in bimolecular scattering by varying its partial wave content is shown to provide an effective means of controlling the cross sections for bimolecular collisions. Applications to Ar + H_2 and Ar + HD, treated as atom−rigid rotor scattering, show enhancement factors of the outgoing flux for a selected rotational transition of more than an order of magnitude.

1. Introduction

Considerable work, over the past three decades, has gone into the study of atom−molecule inelastic collisions, including the development of extensive formalism and the calculation of cross sections for rotational, vibrational, and electronic excitations. All of these studies are designed to analyze the natural outcome of the inelastic scattering of atoms and molecules. By contrast, current interest lies in the ability to *control* the outcome of atomic and molecular processes. In particular, modern efforts in coherent control[1−12] have aimed at using lasers to introduce controllable quantum interference terms into the cross sections of atomic and molecular processes. As a consequence, varying specific laser parameters induce changes in these quantum interference terms which, in turn, significantly alter the natural yields and cross sections. Both detailed[1] and elementary[2] reviews of this coherent control approach are available.

Examining the coherent-control literature shows that the vast majority of controlled processes previously considered are unimolecular in nature, e.g., the photodissociation or photoionization of isolated molecules. Only recently have we shown[3−6] that the essential principle of coherent control can be used effectively to alter cross sections for scattering processes. That is, we demonstrated that if one collides two molecules in a superposition of *energetically degenerate* scattering states, then the resultant scattering cross section contains controllable interference terms.

For a general bimolecular collision of the type

$$A + BC(vj) \rightarrow A' + B'C'(v'j')$$

where v and j are vibrational and rotational quantum numbers, the requirement that the total energy be the same means that we must choose all the interfering paths contributing to the process so that they are at energy

$$E = \epsilon_{vj} + \hbar^2k^2/2\mu = \epsilon_{v'j'} + \hbar^2k'^2/2\mu \qquad (1)$$

Here ϵ_{vj} denotes the internal state of the BC molecule with vibrational quantum number v and rotational quantum number j, and $\hbar^2k^2/2\mu$ is the $A-BC$ relative kinetic energy. Similar definitions hold for the primed symbols. Thus, if we attempt bimolecular control by colliding an initial superposition state Φ made up of, for example, two vib−rotational states,

$$\Phi = c_1|v_1j_1\rangle + c_2|v_2j_2\rangle \qquad (2)$$

then we must simultaneously correlate each component of the superposition state with a translational wavefunction whose **k** wave-vector satisfies eq 1, that is

$$\hbar^2k^2_{v_1j_1}/2\mu = E - \epsilon_{v_1j_1}, \quad \hbar^2k^2_{v_2j_2}/2\mu = E - \epsilon_{v_2j_2} \qquad (3)$$

That is, we must construct wavefunctions of the form

$$\Phi = c_1|v_1j_1\rangle|\mathbf{k}_{v_1j_1}\rangle + c_2|v_2j_2\rangle|\mathbf{k}_{v_2j_2}\rangle \qquad (4)$$

which satisfy eq 3. When $\epsilon_{v_1j_1} \neq \epsilon_{v_2j_2}$ this is not an easy task to achieve experimentally, although we have provided some suggested scenarios.[3,6] If, however, the internal states used in the initial superposition state Φ are degenerate, the condition (eq 3) on the relative momenta can be achieved automatically with a single translational energy.

In ref 4 we followed the latter approach by considering an initial superposition state comprised of degenerate m_j magnetic sublevels. The resultant scenario, while allowing control over the angular differential cross section, did not allow for control over the integral cross section. In this paper, we explore the possibility of using another combination of degenerate asymptotic states, that is, different orbital angular momentum partial waves l. In doing so, we deviate from the normal scattering experiment in which two plane waves representing two molecular beams are allowed to collide. Instead, by controlling the l components of the incoming wave, we create a *sculpted imploding wave* and explore its effect on specific quantum transitions.

Although this approach is applicable to any bimolecular collision, we apply it here to rotational excitation (and de-excitation), obtaining optimally constructed imploding waves.

* To whom correspondence should be addressed.

10.1021/jp9922920 CCC: $18.00 © 1999 American Chemical Society
Published on Web 11/17/1999

We show that sculpting the incoming wave can lead to a considerable enhancement of integral cross sections for specific transitions.

The structure of this paper is as follows. In section 2, we summarize the usual theory of rotational excitation by collisions using plane wave beams of structureless atoms and rigid molecular rotors. In section 3, we develop the theory of scattering, and in particular rotational excitation, for the collision between two nonspherical imploding waves. In section 4, we show how to maximize the scattered flux associated with a specific transition by sculpting such nonspherical imploding waves. Finally, in section 5 we demonstrate the utility of our approach via two sample rotational excitation cases, the collision of an Ar atom with H_2 and with HD.

2. Rotational Inelastic Transitions with Incoming Plane-Waves

Here, we summarize the theory of rotational transitions for ordinary inelastic collisions, as formulated by Arthurs and Dalgarno.[13,14] Our purpose is not to repeat this well-know theory, but rather to establish the notation used in this paper and to emphasize the differences between a process occurring with ordinary plane-waves and with sculptured imploding waves.

Consider, then, an atomic projectile colliding with a rigid-rotor target whose coordinates are specified by two angles, θ and ϕ, which comprise the unit vector $\hat{\mathrm{r}} = (\theta, \phi)$. The coordinates of the projectile relative to the rotor center of mass are denoted $\mathrm{R} \equiv (R, \hat{\mathrm{R}})$, with $\hat{\mathrm{R}} \equiv (\Theta, \Phi)$ being a unit direction-vector. With the target Hamiltonian written as

$$H_{rot} = \frac{\hbar^2}{2I} j(j+1) \tag{5}$$

where I is the rotor's moment of inertia and j is the rotor's (internal) angular momentum operator, the total Hamiltonian is given as

$$H = H_{rot} - \frac{\hbar^2}{2\mu}\nabla^2_R + V(R, \mathrm{R}\cdot\hat{\mathrm{r}}) \tag{6}$$

Here, μ is the reduced mass of the atom-rotor system and $V(R,\mathrm{R}\cdot\hat{\mathrm{r}})$ is the atom−rotor interaction potential. It is convenient to introduce the functions $\Psi^{JM}_{jl}(\mathrm{R}, \hat{\mathrm{r}})$, which are the common eigenfunctions of H; the total angular momentum, J; and its projection on a space-fixed Z-axis, M, having entrance-channel internal and orbital angular momenta quantum numbers j and l, respectively. These functions satisfy the Schrödinger equation:

$$H\Psi^{JM}_{jl}(\mathrm{R}, \hat{\mathrm{r}}) = E\Psi^{JM}_{jl}(\mathrm{R}, \hat{\mathrm{r}}) \tag{7}$$

The total energy, E, is comprised of translational and internal rotational energies:

$$E = \frac{k_j^2}{2\mu} + \frac{\hbar^2}{2I} j(j+1) \tag{8}$$

with k_j being the channel wavenumber, given by eq 8 as

$$k_j^2 = \frac{2\mu}{\hbar^2}\left[E - \frac{\hbar^2}{2I} j(j+1)\right] \tag{9}$$

The Schrödinger equation can be solved[13] by expanding $\Psi^{JM}_{jl}(\mathrm{R}, \hat{\mathrm{r}})$ in bispherical harmonics:

$$\Psi^{JM}_{jl}(\mathrm{R}, \hat{\mathrm{r}}) = \sum_{j',l'} \frac{1}{R} u^J_{j'l'\leftarrow jl}(R)\, y^{JM}_{j'l'}(\hat{\mathrm{R}}, \hat{\mathrm{r}}) \tag{10}$$

where $y^{JM}_{jl}(\hat{\mathrm{R}}, \hat{\mathrm{r}})$, the bispherical harmonics, are defined as

$$y^{JM}_{jl}(\hat{\mathrm{R}}, \hat{\mathrm{r}}) = \sum_{m_l=-l}^{l} \sum_{m_j=-j}^{j} (jlm_jm_l; JM) Y_{lm_l}(\hat{\mathrm{R}}) Y_{jm_j}(\hat{\mathrm{r}}) \tag{11}$$

and are eigenfunctions of J, M, j, and l. Substituting eqs 5, 6, and 10 into eq 7 we obtain a set of coupled channel equations for the radial expansion coefficients $u^J_{j'l'\leftarrow jl}(R)$:

$$\frac{\hbar^2}{2\mu}\left[-\frac{\mathrm{d}^2}{\mathrm{d}R^2} + \frac{l'(l'+1)}{R^2} - k_{j'}^2\right] u^J_{j'l'\leftarrow jl}(R) + \sum_{j''}\sum_{l''} V^J_{j'l',j''l''}(R) u^J_{j''l''\leftarrow jl}(R) = 0 \tag{12}$$

where

$$V^J_{j''l'',j'l'}(R) \equiv \int\int y^{JM}_{j''l''}(\hat{\mathrm{R}}, \hat{\mathrm{r}}) V(\mathrm{R}, \hat{\mathrm{r}}) y^{JM}_{j'l'}(\hat{\mathrm{R}}, \hat{\mathrm{r}})\, \mathrm{d}\hat{\mathrm{R}}\, \mathrm{d}\hat{\mathrm{r}} \tag{13}$$

Equations 12 are solved numerically, subject to the boundary conditions,

$$u^J_{j'l'\leftarrow jl}(0) = 0,$$

$$\lim_{R\to\infty} u^J_{j'l'\leftarrow jl}(R) \sim -2i\delta_{jj'}\delta_{ll'} \sin(k_jR - l\pi/2) + \left(\frac{k_j}{k_{j'}}\right)^{1/2} T^J_{j'l'\leftarrow jl} e^{+i(k_{j'}R - l'\pi/2)} = \delta_{jj'}\delta_{ll'} e^{-i(k_jR - l\pi/2)} - \left(\frac{k_j}{k_{j'}}\right)^{1/2} S^J_{j'l'\leftarrow jl} e^{+i(k_{j'}R - l'\pi/2)} \tag{14}$$

where $S^J_{j'l'\leftarrow jl}$, an element of the S matrix, is given in terms of $T^J_{j'l'\leftarrow jl}$ of eq 14 as

$$S^J_{j'l'\leftarrow jl} = \delta_{jj'}\delta_{ll'} - T^J_{j'l'\leftarrow jl} \tag{15}$$

The asymptotic behavior of the wavefunction can be written as

$$\lim_{R\to\infty} \Psi^{JM}_{jl}(\mathrm{R}, \hat{\mathrm{r}}) = \Psi^{in}(\mathrm{R}, \hat{\mathrm{r}}) + \Psi^{sc}(\mathrm{R}, \hat{\mathrm{r}}) \tag{16}$$

where the second term represents a scattered wave, and the first term represents either a plane-wave (whose partial wave components are given in the second line of eq 14) or an *imploding spherical wave* (with partial wave components given in the last time of eq 14).

Given the S matrix, the probability of observing a rotational transition from state jl to state $j'l'$ for fixed J is given as

$$P^J_{j'l'\leftarrow jl} = |S^J_{j'l'\leftarrow jl}|^2 \tag{17}$$

3. Scattering of Sculpted Imploding Waves

We now generalize the treatment of section 2 to include a collision with nonspherical imploding waves. Use of such imploding waves offers a powerful method to control the outcome of the collision and to alter the rotational transition probabilities.

Nonspherical imploding waves are formally obtained by considering superpositions of $\Psi_{jl}^{JM}(R, \hat{r})$ with arbitrary complex coefficients $\{c_{jl}^{JM}\}$

$$\psi_j(R, \hat{r}) = \frac{i}{k_j} \sum_{J=0}^{\infty} \sum_{M=-J}^{J} \sum_{l=|J-j|}^{J+j} c_{jl}^{JM} \Psi_{jl}^{JM}(R, \hat{r}) \quad (18)$$

However, since our interest is control via changes in m_j and m_l rather than J and M, it is more convenient to specify the superposition state via m_j- and m_l-dependent coefficients, denoted as $d_{jl}^{m_j m_l}$, which are related to the c_{jl}^{JM} coefficients by a unitary transformation of the form

$$c_{jl}^{JM} = \sum_{m_j=-j}^{j} \sum_{m_l=-l}^{l} (jlm_j m_l; JM)\, d_{jl}^{m_j m_l} \quad (19)$$

Comparing eqs 19 and 18 with eq 10, we see that for an incoming plane-wave, $d_{jl}^{m_j m_l}(plane) = i^l \sqrt{\pi}\sqrt{2l+1}\delta_{m_j m^0}\delta_{m_l 0}$ where m^0 is the specification for the initial j projection.

By analogy to eq 16, we can break the asymptotic expansion of ψ_j into incoming and scattered parts:

$$\lim_{R\to\infty} \psi_j(R, \hat{r}) = \psi_j^{in}(R, \hat{r}) + \psi_j^{sc}(R, \hat{r}) \quad (20)$$

where

$$\psi_j^{in}(R, \hat{r}) = 2 \sum_{JMl} c_{jl}^{JM} j_l(k_j R) y_{jl}^{JM}(R, \hat{r}) \quad (21)$$

and

$$\psi_j^{sc}(R, \hat{r}) = \frac{i}{k_j R} \sum_{JMl} c_{jl}^{JM} \sum_{j'l'} \left(\frac{k_j}{k_{j'}}\right)^{1/2} T_{j'l'-jl}^{J} e^{+i(k_{j'}r - l'\pi/2)} y_{j'l'}^{JM}(\hat{R}, \hat{r}) \quad (22)$$

Substituting eqs 11 and 19 in eq 21 and using the orthogonality property of the Clebsch-Gordan coefficients[15] allows us to express the incoming wavefunction in terms of $\{d_{jl}^{m_j m_l}\}$ as

$$\psi_j^{in}(R, \hat{r}) = 2 \sum_{l} \sum_{m_j m_l} d_{jl}^{m_j m_l} j_l(k_j R)\, Y_{lm_l}(\hat{R}) Y_{jm_j}(\hat{r}) \quad (23)$$

For cylindrically symmetric potentials, the k_j vector can be chosen in the z direction, and the summation over m_l reduces to the single term $m_l = 0$. As a result, $\psi_j^{in}(R, \hat{r})$ depends on the angle θ between k_j and R but is independent of the azimuthal angle ϕ.

Defining a *generalized* scattering amplitude as

$$f_{j'm_{j'}-jm_j}(\hat{R}) = \sum_{lm_l} d^{m_j m_l}{}_{jl} \sum_{l'm_{l'}} i^{-l'} Y_{l'm_{l'}}(\hat{R}) \sum_{JM} (jlm_j m_l; JM) \times (j'l'm_{j'} m_{l'}; JM) T_{j'l'-jl}^{J} \quad (24)$$

we can write $\psi_j^{sc}(R, \hat{r})$ as

$$\psi_j^{sc}(R, \hat{r}) = \frac{i}{k_j R} \sum_{j'm_{j'}} \sum_{m_j} f_{j'm_{j'}-jm_j}(\hat{R}) \left(\frac{k_j}{k_{j'}}\right)^{1/2} e^{+ik_{j'}R} Y_{j'm_{j'}}(\hat{r}) \quad (25)$$

We now proceed to derive expressions for the incoming and scattered fluxes associated with a general incoming wave. We concentrate on fluxes, rather than cross sections, for the following reason. Plane-waves have a uniform incoming flux coming from *a single* direction and allow for the definition of a cross section as the ratio between the scattered flux and the incoming flux per unit area. However, an arbitrary incoming wave has multidirectional and nonspherical incoming and scattered fluxes. Hence the term "incoming flux per unit area" is meaningless, and a cross section cannot be defined. We therefore adopt the strategy of working separately with the incoming (or imploding) and scattered fluxes and show below (see section 4) how to choose the $\{d_{jl}^{m_j m_l}\}$ coefficients to maximize the scattered flux into a given rotor state j'.

The imploding part of the wavefunction in the $R \to \infty$ limit:

$$\psi^{imp}{}_j(R, \hat{r}) \sim \frac{-2e^{-ik_j R}}{ik_j R} \sum_{l} \sum_{m_j m_l} i^l d_{jl}^{m_j m_l} Y_{lm_l}(\hat{R}) Y_{jm_j}(\hat{r}) \quad (26)$$

has an associated flux

$$F_j^{imp}(R, \hat{r}) = -\frac{i\hbar}{2\mu}\left[\psi_j^{imp*}(R, \hat{r}) \frac{\partial \psi_j^{imp}(R, \hat{r})}{\partial R} - \psi_j^{imp}(R, \hat{r}) \frac{\partial \psi_j^{imp*}(R, \hat{r})}{\partial R}\right] \hat{n} \quad (27)$$

where $\hat{n}$ is a radial unit vector. Using the fact that as $R \to \infty$, $\partial \psi_j^{imp}(R,\hat{r})/\partial R \sim -ik_j \psi_j^{imp}(R, \hat{r})$, we integrate $F_j^{imp}(R, \hat{r})$ over $\hat{R}$ (at radius R) and over $\hat{r}$ to obtain the total flux of $\psi_j^{imp}(R, \hat{r})$ entering a sphere of radius R:

$$F_j^{imp} = \frac{\hbar}{\mu} \mathrm{Im}\left[R^2 \int\int d\hat{r}\, d\hat{R}\, \psi_j^{imp*}(R, \hat{r}) \frac{\partial \psi_j^{imp}(R, \hat{r})}{\partial R}\right] = -\frac{\hbar k_j}{\mu} R^2 \int\int d\hat{r}\, d\hat{R} |\psi_j^{imp}(R, \hat{r})|^2 = -\frac{4\hbar}{\mu k_j} \sum_{l} \sum_{m_j m_l} |d_{jl}^{m_j m_l}|^2 \quad (28)$$

We see that the imploding flux is proportional to the total population of all $\{l, m_l, m_j\}$-states in the incoming wave. Any unitary transformation on $d_{jl}^{m_j m_l}$ conserves this quantity.

For a plane-wave, $d_{jl}^{m_j m_l}(plane) = i^l \sqrt{\pi} 2l + 21\delta_{m_j m^0}\delta_{m_l 0}$. Therefore,

$$\sum_{l} \sum_{m_j m_l} |d_{jl}^{m_j m_l}(plane)|^2 = \pi \sum_{l} (2l + 1) \quad (29)$$

This sum, and hence F_j^{imp} for the plane-wave, are infinite. In order to be able to compare the effectiveness of rotational transitions using a general imploding wave to that of a plane-wave, we consider only a finite portion of both waves by introducing a cutoff angular momentum l_f, chosen to be the highest angular momentum which contributes effectively to the scattering process.

Using a similar calculation as for $\psi_j^{imp}(R, \hat{r})$, the scattered flux of $\psi_j^{sc}(R, \hat{r})$ into j', m_j' is given by

$$F_{j'm_{j'}-j,m_j}^{scat} = \frac{\hbar}{\mu k_j} \int d\hat{R} |f_{j'm_{j'}-jm_j}(\hat{R})|^2 \quad (30)$$

Related, m_j- and/or $m_{j'}$-summed fluxes are given as

$$F_{j'm_{j'}-j}^{scat} = \sum_{m_j} F_{j'm_{j'}-j,m_j}^{scat};\ F_{j'-j,m_j}^{scat} = \sum_{m_{j'}} F_{j'm_{j'}-j,m_j}^{scat};\ F_{j'-j}^{scat} = \sum_{m_j,m_{j'}} F_{j'm_{j'}-j,m_j}^{scat} \quad (31)$$

After some algebra, it is possible to show that

$$F^{scat}_{j'm_{j'}\leftarrow j} = \frac{\hbar}{\mu k_{jl'm_{l'}}} \sum |\sum_{JMl} c^{JM}_{jl}(j'l'm_{j'}m_{l'}; JM) T^{J}_{j'l'\leftarrow jl}|^2 \quad (32)$$

[if $j = j'$, $m_j = m_{j'}$, an additional (infinite) scattered flux exists from the *incoming* wavefunction $\psi^{in}_j(R, \hat{r})$] and that

$$F^{scat}_{j'\leftarrow j,m_j} = \frac{\hbar}{\mu k_{jJMl'}} \sum |\sum_{lm_l} d^{m_jm_l}_{jl}(jlm_jm_l; JM) T^{J}_{j'l'\leftarrow jl}|^2 \quad (33)$$

In a similar fashion we can show that

$$F^{scat}_{j'\leftarrow j} = \frac{\hbar}{\mu k_{jJMl'l''}} \sum c^{JM}_{jl}\, c^{*JM}_{jl''}\, T^{J}_{j'l'\leftarrow jl}\, T^{*J}_{j'l''\leftarrow jl''}\, \delta(j'l'J) = \frac{\hbar}{\mu k_j} \sum_{JMl'} |\sum_{l} c^{JM}_{jl}\, T^{J}_{j'l'\leftarrow jl}|^2 \quad (34)$$

4. Maximization of the Scattered Flux

Consider now maximizing the scattered flux into a given j' state, subject to various constraints. The control parameters are the $d^{m_jm_l}_{jl}$ coefficients, which shape the input wavefunction $\psi^{in}_j(R, \hat{r})$. Our strategy is to formulate the problem as a linear optimization problem in these coefficients.

Note first that if we average on m_j, then control is possible only if the $d^{m_jm_l}_{jl}$ coefficients depend upon m_j. That is, if $d^{m_jm_l}_{jl}$ are independent of m_j, that is, if $d^{m_jm_l}_{jl} = d^{m_l}_{jl}$, then no phase control over the rotational transitions is possible. In order to see this, consider the nonpolarized flux, given (in the absence of m_j dependence), by

$$F^{scat}_{j'\leftarrow j} = \frac{\hbar}{\mu k_j} \frac{1}{(2j+1)} \sum_{lm_l} \sum_{l'm_{l'}} d^{m_l}_{jl}\, d^{*m_{l'}}_{jl''} \sum_{JMmjl'} (jlm_jm_l; JM) \times (jl''m_jm_{l'}; JM) T^{J}_{j'l'\leftarrow jl}\, T^{*J}_{j'l''\leftarrow jl''} \quad (35)$$

Using the orthogonality of the Clebsch-Gordan coefficients,[15] we obtain

$$F^{scat}_{j'\leftarrow j} = \frac{\hbar}{\mu k_j} \frac{1}{(2j+1)} \sum_{Jl'} \sum_{lm_l} \left(\frac{2J+1}{2l+1}\right) |d^{m_l}_{jl}|^2 |T^{J}_{j'l'\leftarrow jl}|^2 \quad (36)$$

That is, the flux no longer depends upon the phase of the $d^{m_jm_l}_{jl}$ coefficients. This loss of control by incoherent averaging over m_j is reminiscent of similar results obtained for m_j control over collision processes.[4]

Consider next maximizing the scattered flux to a given j' manifold for an incoming wave comprised of only one m_j state. For this case we have, using eq 33,

$$F^{scat}_{j'\leftarrow j,m_j} = \frac{\hbar}{\mu k_j} \sum_{ll''} \sum_{m_lm_{l''}} d^{m_jm_l}_{jl}\, d^{*m_jm_{l''}}_{jl''}\, B^{jj'm_j}_{l''lm_l''m_l} \quad (37)$$

where

$$B^{jj'm_j}_{l''lm_l''m_l} \equiv \sum_{JMl'} (jlm_jm_l; JM)(jl''m_jm_{l''}; JM) T^{J}_{j'l'\leftarrow jl}\, T^{*J}_{j'l''\leftarrow jl''} \quad (38)$$

It is easy to show that the $B^{jj'm_j}$ matrices are Hermitian.

Two strategies for control over F^{scat} are in principle possible: the first is "classical", in which we essentially choose favorable values of l and m_l, for which the $B^{jj'm_j}$ matrix elements are largest. The other is quantum mechanical: we allow interference between all the amplitudes comprising the incoming wave. The latter is more general and is utilized here.

Within the framework of the quantum strategies, it is possible to optimize the $d^{m_jm_l}_{jl}$ coefficients, subject to the constraint that either the total incoming flux is the same as that of a plane wave or that the normalization of the incoming wavefunction is the same as that of a plane wave:

$$\int dR d\hat{r} \psi^{*in(1)}_{j1}(R,\hat{r}) \psi^{in(2)}_{j2}(R,\hat{r}) = \delta_{j1j2} \delta(k^{(1)}_{j1} - k^{(2)}_{j2}) \quad (39)$$

Both constraints are considered below. In particular, details of the constraints are discussed in section 4.1 and 4.2, and results are presented in section 5.

4.1. Optimization Subject to Incoming Flux Constraint. In order to equate the incoming flux, given in eq 28 with its plane-wave value, we introduce a Lagrange multiplier $\lambda_{j'}$:

$$F^{\lambda}_{j'\leftarrow j,m_j} = \frac{\hbar}{\mu k_j} [\sum_{lm_l} \sum_{l''m_{l''}} d^{m_jm_l}_{jl}\, d^{*m_jm_{l''}}_{jl''}\, B^{ljm_j}_{l''lm_l''m_l} - \lambda_{j'} \sum_{lm_l} (|d^{m_jm_l}_{jl}|^2 - |d^{m_jm_l}_{jl}(plane)|^2)] \quad (40)$$

Differentiating with respect to $d^{*m_jm_{l''}}_{jl''}$ to obtain the extremum points of $F^{\lambda}_{j'\leftarrow j,m_j}$, we obtain the condition

$$\sum_{m_l} \sum_{l} d^{m_jm_l}_{jl}\, B^{jj'm_j}_{l''lm_l''m_l} = \lambda_{j'} d^{m_jm_l}_{jl''} \qquad l'' = 0, 1, \ldots \quad (41)$$

Defining a $d_{j,m_j} \equiv \{d^{m_jm_l}_{jl}\}$ eigenvector, whose dimension is the number of possible initial l-states, we can write eq 41 in matrix form as

$$B^{jj'm_j} \cdot d_{j,m_j} = d_{j,mj} \cdot \lambda_{j'} \quad (42)$$

where $\lambda_{j'}$ is a diagonal matrix of eigenvalues.

The flux associated with each eigenvector is proportional to the value of the corresponding eigenvalue $\lambda_{j'}$, since by eqs 40 and 42

$$F^{\lambda}_{j'\leftarrow j,m_j} = \frac{\hbar}{\mu k_j} [d^{\dagger}_{j,m_j} \cdot B^{jj,m_j} \cdot d_{j,m_j} - \lambda_{j'} (d^{\dagger}_{j,m_j} \cdot d_{j,m_j} - d^{\dagger}(plane) \cdot d(plane))]$$

$$= \frac{\hbar}{\mu k_j} [\lambda_{j'} d^{\dagger}(plane) \cdot d(plane)] = \frac{\hbar}{\mu k_j} \pi \lambda_{j'} \sum_{l=0}^{l_f} (2l+1) = \frac{\hbar}{\mu k_j} \pi \lambda_{j'} (l_f + 1)^2 \quad (43)$$

Thus, the scattered flux associated with the $j' \leftarrow j, m_j$ transition is $\lambda_{j'}$ times the l_f-truncated sum of the partial-waves weights associated with an incoming plane-wave. In particular, the maximal eigenvalue yields the maximal flux. Since the optimal $\lambda_{j'}$ for one $j' \leftarrow j$ transition will not necessarily enhance the flux associated with any other transition, this control scenario provides a great degree of selectivity of one rotational transition over another.

4.1.1. The Cutoff Angular Momentum l_f. For a plane wave, $F^{scat}_{j'\leftarrow j,m_j} = (\hbar/\mu k_j) d^{\dagger}(plane) \cdot B \cdot d(plane)$. For high l's, $|B^{jj'm_j\,\prime}_{l''lm_{l'}\,m_l}| \rightarrow 0$ faster than $1/(d^{m_jm_l}_{jl}\, d^{\prime\prime *m_jm_{l'}}_{j_{l'}})$, and therefore F^{scat} is finite, even if $d^{\dagger}d$ is infinite. By contrast, according to eq 43, the optimal solution does not contain $|B^{jj'm_j\,\prime}_{l''lm_{l'}\,m_l}|$, and $F^{\lambda}_{j'\leftarrow j,m_j}$ is only

limited by the choice of l_f. As we increase l_f in the construction of the optimal imploding wave we can achieve larger and larger scattered flux into the target j' manifold. Nonetheless, choosing l_f arbitrarily large may not be the best practical approach to increasing the cross section, since the difficulty of preparing the imploding wave in the laboratory is expected to increase with increasing l_f.

In order to decide what type of optimization problem we want to solve, we choose the cutoff parameter l_f according to the following procedure: we calculate the diagonal contribution $(\hbar/\mu k_j)\pi(2l+1)B^{jj'0}_{l''l00}$ of the l-components of a plane-wave (for $m_j = 0$) to the scattered flux (see eq 37) and truncate the sum when this value dips below a preset fraction (1%) of its maximal value.

We emphasize again that for a nonuniform imploding wave, each choice of l_f corresponds to a different scattered flux and hence to a different optimization problem. The above choice of l_f corresponds to optimizing the imploding wave for the first l_f partial wave and setting the weights of the remaining $l > l_f$ partial waves to the values for a plane-wave. These partial waves no longer contribute to the inelastic process of interest.

4.2. Optimization Subject to Incoming Wavefunction Normalization Constraint. If we require the incoming wavefunction $\psi_j^{in}(\mathrm{R}, \hat{\mathrm{r}})$ to satisfy a $\delta_{j_1j_2}\delta(k_{j_1}^{(1)} - k_{j_2}^{(2)})$ normalization condition (eq 39), the coefficients which make up the imploding wave must satisfy (see Appendix) the constraint

$$\sum_{m_j} d^{*m_jm_{l1}}_{j_1l'} d^{m_jm_{l2}}_{j_1l'} = \pi(2l+1)\delta_{m_{l1}0}\delta_{m_{l2}0} \qquad (44)$$

for every l, m_{l_1}, and m_{l_2}.

In the cylindrically symmetric case $m_l = 0$, and if we consider one m_j value, then

$$d^{m_j0}_{jl} = i^l\sqrt{\pi}\sqrt{2l+1}\, e^{i\theta^{m_j0}_{jl}} \qquad (45)$$

That is, the magnitude for each l component is the same as in the plane-wave, and the only free parameters that can be optimized are the phases $\{\theta^{m_j0}_{jl}\}$. The scattered flux of $\psi_j^{sc}(\mathrm{R}, \hat{\mathrm{r}})$ is now given by

$$F^{scat}_{j'\leftarrow j,m_j} = \frac{\hbar}{\mu k_j}\sum_{ll''}\pi(2l+1)^{1/2} (2l''+1)^{1/2} i^{l-1''} e^{i(\theta^{m_j0}_{jl}-\theta^{m_j0}_{j''l''})} B^{jj'm_j}_{l''lm_l''m_l} \qquad (46)$$

The optimization is performed by a nonlinear search routine in the $\{\theta^{m_j0}_{jl}\}$ space of phases.

5. Computational Results

5.1. The Model. To demonstrate the possible control afforded by sculpting the imploding wave, we consider a rotational excitation problem, studied in refs 16 and 17, and compare the imploding wave results to those obtained with plane waves. Following refs 16 and 17, we expand $V(R, \hat{\mathrm{R}}\cdot\hat{\mathrm{r}})$, the projectile–rotor interaction potential, in a series of Legendre polynomials[18] and truncate the expansion, as appropriate for a weakly anisotropic system, after the first three terms:

$$V(R, \hat{\mathrm{R}}\cdot\hat{\mathrm{r}}) = V_0(R) + V_1(R)P_1(\hat{\mathrm{R}}\cdot\hat{\mathrm{r}}) + V_2(R)P_2(\hat{\mathrm{R}}\cdot\hat{\mathrm{r}}) \qquad (47)$$

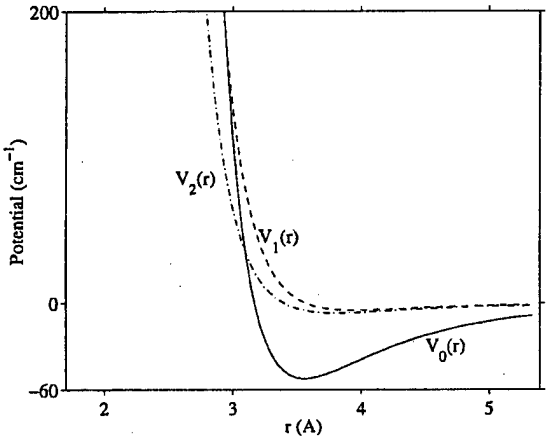

Figure 1. Isotropic potential $V_0(R)$ and leading anisotropic potentials for the Ar–HD and Ar–H_2 systems.

The terms $V_0(R)$ and $V_2(R)$ are parametrized by Lennard-Jones potentials:[19,20,22]

$$V_0(R) = \epsilon_0[(R_0^e/R)^{12} - 2(R_0^e/R)^6] \qquad (48)$$

$$V_2(R) = \epsilon_2[(R_2^e/R)^{12} - 2(R_2^e/R)^6] = a_2\epsilon_0[q(R_0^e/R)^{12} - 2(R_0^e/R)^6] \qquad (49)$$

where

$$q \equiv (R_2^e/R_0^e)^6 \quad \text{and} \quad a_2 \equiv (\epsilon_2/\epsilon_0)q$$

For a heteronuclear diatom composed of two isotopes (such as HD), we can compute $V_1(R)$ as[23]

$$V_1(R) = -\delta\left[\frac{dV_0(R)}{dR} + 0.4\frac{dV_2(R)}{dR} + \frac{1.2}{R}V_2(R)\right]$$

where δ is the displacement of the center of mass of the diatom from the center of force. The potentials $V_0(R)$, $V_1(R)$ (for Ar–HD), and $V_2(R)$ are shown in Figure 1.

By defining a dimensionless variable $x \equiv R/R_m$ and a dimensionless potential $V^* = V/\epsilon$, where $R_m = R_0^e$ and $\epsilon = \epsilon_0$, the Coupled Channels equations (eq 12) assume the form

$$\left[-\frac{\mathrm{d}^2}{\mathrm{d}x^2} + \frac{l'(l'+1)}{x^2} - K_{j'}^2\right]u^J_{j'l'\leftarrow jl}(x) + B\sum_{j''}\sum_{l''}V^J_{j'l'j''l''}(x)u^J_{j''l''\leftarrow jl}(x) = 0 \qquad (50)$$

where

$$B = \frac{2\mu\epsilon R_m^2}{\hbar^2} \quad \text{and} \quad K_j^2 = k_j^2 R_m^2 = \frac{2\mu R_m^2}{\hbar^2}\left[E - \frac{\hbar^2}{2I}j(j+1)\right] \qquad (51)$$

The dynamics is seen to be determined by three dimensionless parameters: B, BE/ϵ, $\mu R_m^2/I$, and by the form of the potential chosen.

We consider the Ar–H_2 system as an example of a homonuclear molecule and the Ar–HD systems as an example of a heteronuclear molecule. The effect of δ on V_0 and on V_2 is of the order of δ^2 and is therefore ignored, and we take V_0 and V_2

TABLE 1: Scattered Flux Associated with All the $j' \leftarrow j = 2$, $m_j = 0$ Transitions when the $j' = 4$ State Is Optimized[a]

(a) Ar−HD System

j'	plane-wave	maximum (flux norm)	$\times 10^3/\pi(l_f+1)^2$	maximum (wfn norm)	minimum (wfn norm)
4	16.3	55.5	7.4	22.0	13.9
			Other Transitions		
0	6.2	0.6	0.1	5.8	15.0
1	37.9	19.8	2.6	49.8	18.0
2	137.2	43.9	5.8	112.9	148.5
3	38.2	31.4	4.2	45.0	40.4
5	2.0	12.8	1.7	2.3	2.0
6	0.1	0.1	0.0	0.1	0.1

(b) Ar−H_2 System

j'	plane-wave	maximum (flux norm)	$\times 10^3/\pi(l_f+1)^2$	maximum (wfn norm)	minimum (wfn norm)
4	1.6	7.4	1.7	2.0	1.0
			Other Transitions		
0	10.5	50.8	11.8	24.4	7.7
2	420.9	112.2	26.1	406.7	424.4

[a] All values have been multiplied by a factor of 1000.

TABLE 2: Scattered Flux Associated with All the $j' \leftarrow j = 2$, $m_j = 0$ Transitions when the $j' = 0$ State Is Optimized[a]

(a) Ar−HD System

j'	plane-wave	maximum (flux norm)	$\times 10^3/\pi(l_f+1)^2$	maximum (wfn norm)	minimum (wfn norm)
0	6.2	66.3	6.7	37.7	0.9
			Other Transitions		
1	37.9	38.4	3.9	33.2	47.3
2	137.2	34.4	3.5	117.4	124.2
3	38.2	54.7	5.5	32.0	44.5
4	16.3	20.2	2.1	15.0	18.9
5	2.0	0.4	0.0	2.1	2.0
6	0.1	0.0	0.0	0.5	0.1

(b) Ar−H_2 System

j'	plane-wave	maximum (flux norm)	$\times 10^3/\pi(l_f+1)^2$	maximum (wfn norm)	minimum (wfn norm)
0	10.5	92.4	13.3	34.8	0.6
			Other Transitions		
2	420.9	171.5	24.7	396.3	431.3
4	1.6	11.0	1.6	2.0	1.3

[a] All values have been multiplied by a factor of 1000.

to be the same for both Ar−H_2 and Ar−HD. For V_1, the leading term is proportional to δ, and the next term, neglected here, is proportional to δ^3.

The potential parameters chosen to model these systems are $\epsilon_0 = 52.21$ cm^{-1}, $R_0^e = 3.5573$ Å, $\epsilon_2 = 6.78$ cm^{-1}, $R_2^e = 3.814$ Å, δ(Ar−HD) = 0.1276 Å.[21,22] Therefore, $a_1 = 0.0359$, $a_2 = 0.198$, and $q = 1.52$. $\mu_{Ar-H_2} = 1.9188$ amu, $\mu_{Ar-HD} = 2.8099$ amu. The H_2 and HD rotational constants are $B_e = 60.80$ and 45.655 cm^{-1}, respectively.[24]

We obtain the $S^J_{j'l'\leftarrow jl}$ matrix elements by propagating the Coupled Channels equations [eq 50] using Gordon's method[25] until we reach the asymptotic region, where the appropriate boundary conditions [eq 14] are imposed. In this case, there are seven open channels ($j = 0, ..., 6$) for Ar−HD at $E_{tot} = 2000$ cm^{-1} and three open channels ($j = 0, 2, 4$) for Ar−H_2 at the same energy. Fixing j_{max}, the maximal j quantum number, to 6, results in (at most) 16 channels for each J. The calculation was repeated for each J value, whose maximal value is given as $J_{max} = j_{max} + l_f$.

The properties of the $\int\int y^{JM}_{j'l'}(\hat{R}, \hat{r})^*\, P_l(\hat{R}\cdot\hat{r})\, y^{JM}_{j'l'}(\hat{R},\hat{r})\, d\hat{R}\, d\hat{r}$ matrix elements[20] ensure that the $V_2(R)P_2(\hat{R}\cdot\hat{r})$ term can only couple j quantum number values of the same parity. The same holds for the l quantum numbers. Therefore, $B^{jj'm_j}_{l'l''m_l m_l}$ vanishes if either of $j - j'$ or $l'' - l$ are odd. This is also the case if there is a $V_1(R)$ potential, but $m_j = 0$ (due to the fact that one of the Clebsch-Gordon coefficients in eq 38 is zero). Hence, the $\mathbf{B}^{jj'}_{m_j m_l}$ matrix factors into an odd-l block and an even-l block, which are diagonalized separately. The overall maximal eigenvalue, therefore, corresponds to a d_{j,m_j} vector with only odd or only even components. The optimized wavefunction is therefore parity-adapted, $\psi_j(R, \hat{r}) = (-1)^p\psi_j(-R, \hat{r})$, where p is the parity of the l states in the expansion.

Below, we discuss the optimization results for four cases: the $j' = 4 \leftarrow j = 2$ and the $j' = 0 \leftarrow j = 2$ transitions for Ar colliding with HD and for Ar colliding with H_2, at a collision energy of $E = 2000$ cm^{-1}. We focus on the case of initial $m_j = 0$.

5.2. Optimization Constrained by the Incoming Flux. Tables 1 and 2 show, in column 3, the flux into all final j', having optimized the results for $j' = 4 \leftarrow j = 2$, $m_j = 0$ or $j' = 0 \leftarrow j = 2$, $m_j = 0$ for both Ar + H_2 and Ar + HD.

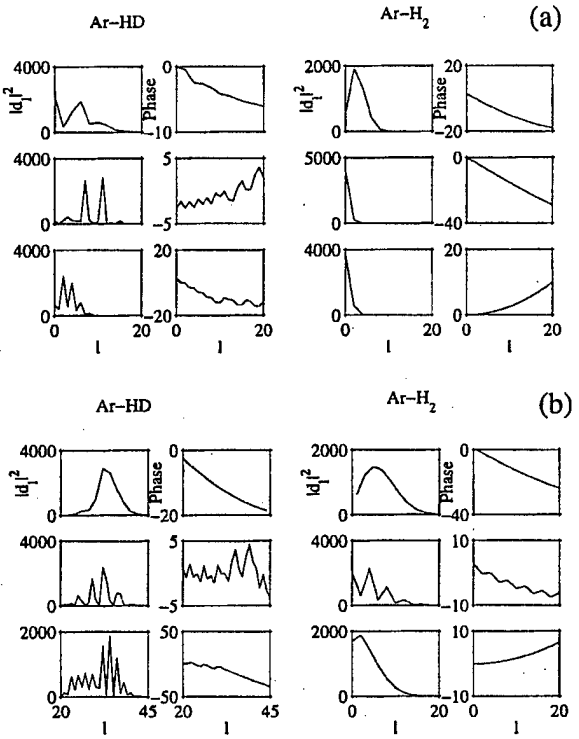

Figure 2. l-Components of the d_{j,m_j} eigenvector (left, absolute square; right, phase) leading to a maximal flux for the Ar−HD and Ar−H_2 systems: (a) $j' = 4 \leftarrow j = 2$, $m_j = 0, 1, 2$; (b) $j' = 0 \leftarrow j = 2$, $m_j = 0, 1, 2$; using the flux-normalization condition. For $m_j = 0$, only even or only odd l-values have nonzero d_l components; hence, only those are shown.

For example, the maximum flux for rotational excitation into $j' = 4$ for Ar + HD is 0.055, as compared to the partial wave result (column 2) of 0.016. Note also that the optimization into $j' = 4$, for example, does not necessarily decrease (or increase) the flux into $j' \neq 4$. That is, each optimization is selective to the particular product channel optimized.

The l-components of the eigenvector d_{j,m_j} leading to a maximal flux for the $j' = 4 \leftarrow j = 2$ and the $j' = 0 \leftarrow j = 2$ transitions are shown in Figure 2. Clearly, as can be seen, lower angular momenta contribute to the Ar−H_2 scattering than to Ar−HD.

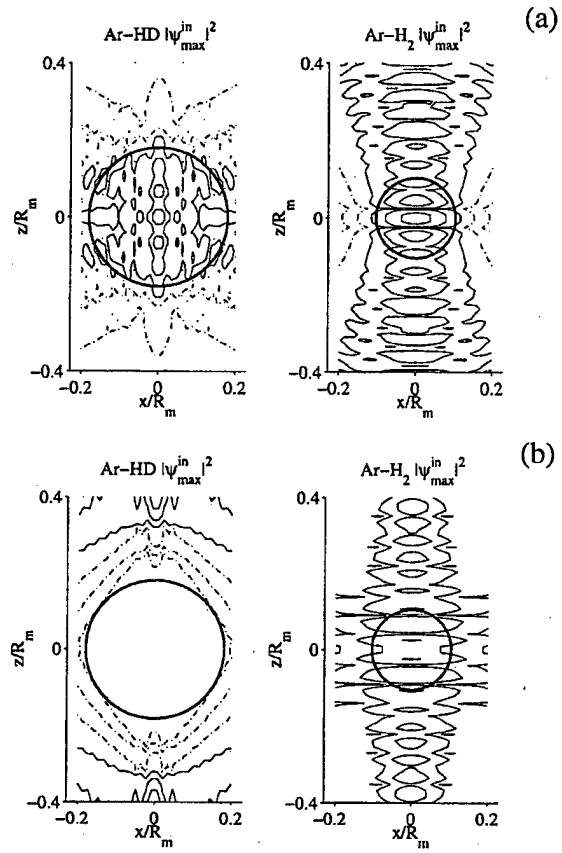

Figure 3. Square of the absolute value of the incoming wavefunction leading to maximum outgoing flux for the Ar−HD and Ar−H_2 systems using flux-normalization condition. The circle depicts the size of the diatomic: (a) $j' = 4 \leftarrow j = 2$, $m_j = 0$ optimization, maximum values of $|\psi^{in}_{max}|^2$ are 520 for Ar−HD and 163 for Ar−H_2; (b) $j' = 0 \leftarrow j = 2$, $m_j = 0$ optimization, maximum values of $|\psi^{in}_{max}|^2$ are 235 for Ar−HD and 125 for Ar−H_2. Solid line contours correspond to 0.5, 0.1, and 0.01 of the maximum value; dashed contours are for 10^{-3}, 10^{-4}, and 10^{-5} of the maximum.

Similarly, lower angular momenta contribute more to the optimized excitation process ($j' = 4 \leftarrow j = 2$) than to the optimized de-excitation ($j' = 0 \leftarrow j = 2$) process.

The cutoff values for the angular momentum are $l_f = 48$ and 36 for Ar−HD and Ar−H_2, respectively, for the $j' = 4 \leftarrow j = 2$, $m_j = 0$ case (Table 1) and 55 and 46 for the $j' = 0 \leftarrow j = 2$, $m_j = 0$ case (Table 2). In order to be able to compare those results, we also give the maximal flux divided by the normalization factor of $\pi(l_f + 1)^2$.

The absolute square value of the incoming wavefunction corresponding to the maximal flux are shown in Figure 3. These should be compared to an incoming plane-wave, whose absolute value is unity. Values for the maximal flux for these cases are provided in the figure captions, from which it is clear that the Ar + HD wavefunctions are less dispersed than those for Ar + H_2. Note that the incoming wavefunctions for the four cases shown in Figure 3 are remarkably different from one another in topology. For example, $|\psi^{in}_{max}|^2$ for Ar + HD $j' = 0 \leftarrow j = 2$ de-excitation is dominant at large values of z, whereas the Ar + HD $|\psi^{in}_{max}|^2$ for excitation $j' = 4 \leftarrow j' = 2$ is heavily concentrated at small z. A similar difference is not seen for the Ar + H_2 case.

The differential cross section is shown, for initial $m_j = 0$ values (summed over all final $m_{j'}$ values), in Figure 4. Interestingly, the optimized cross sections are symmetric about $\theta =$

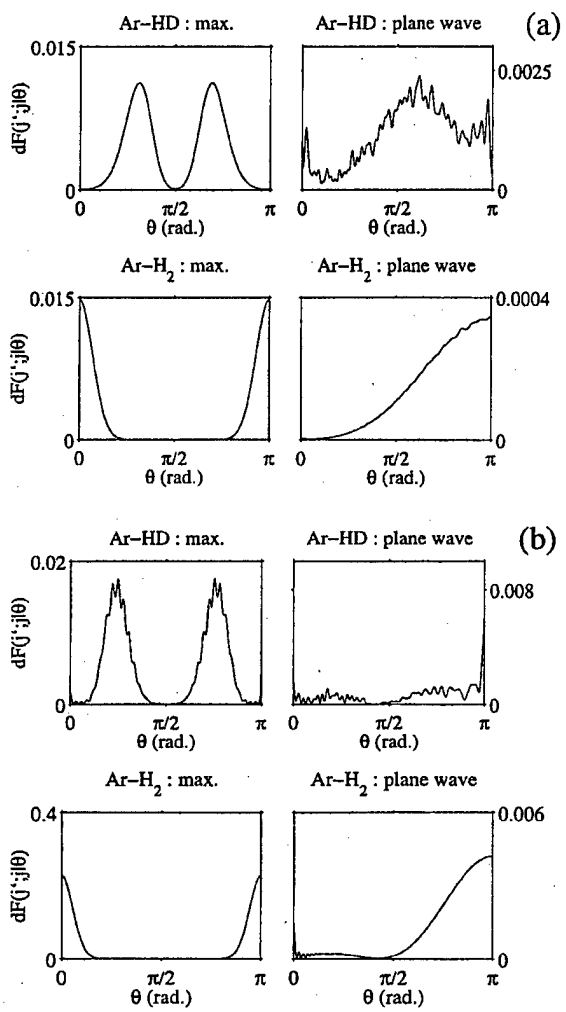

Figure 4. Differential outgoing flux for the case of maximal flux (left) and for a plane-wave (right), for the Ar−HD system (top) and the Ar−H_2 system (bottom). Results are for optimization using the flux-normalization condition: (a) $j' = 4 \leftarrow j = 2$, $m_j = 0$ optimization; (b) $j' = 0 \leftarrow j = 2$, $m_j = 0$ optimization. The plotted flux is a sum over all final m_f values.

90°, whereas the plane-wave result tends to peak near $\theta = 180°$. This is because (for $m_j = 0$) only l values of the same parity contribute to the final result, a consequence of the fact that the $\boldsymbol{B}$ matrix does not couple l values of different parity.

5.3. Optimization Constrained by the Normalization of the Incoming Wave. In the second approach, we require that the incoming wavefunction be normalized as

$$\int d\mathbf{R}d\hat{\mathbf{r}}\psi^{in,(1)*}_{j_1}(\mathbf{R}, \hat{\mathbf{r}})\psi^{in,(2)}_{j_2}(\mathbf{R}, \hat{\mathbf{r}}) = \delta_{j_1 j_2}\delta(k^{(1)}_{j_1} - k^{(2)}_{j_2}) \qquad (52)$$

As in eq 45, the coefficients $d^{m_j m_l}_{jl}$ are given by

$$d^{m_j m_l}_{jl} = i^l \sqrt{\pi}\sqrt{2l+1}e^{i\theta^{m_j 0}_{jl}}\delta_{m_j m_0}\delta m_{l0} \qquad (53)$$

The extrema are obtained at θ values which satisfy the condition

$$\frac{\partial F^{scat}(\theta^{m_j 0}_{j0}, \theta^{m_j 0}_{j1}, ..., \theta^{m_j 0}_{jl}, ...)}{\partial \theta^{m_j 0}_{jl}} = 0 \qquad l = 0, 1, 2, ... \qquad (54)$$

Equation 54 leads to a system of nonlinear equations, which may have many solutions, corresponding to local minima/maxima. To find the absolute minimum/maximum with high

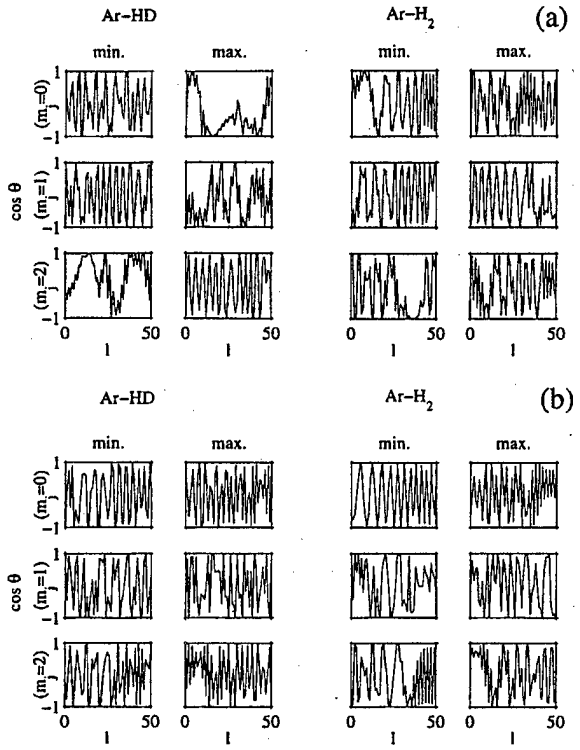

Figure 5. l-components of the d_{j,m_j} eigenvector leading to a minimal (left) and a maximal (right) flux for Ar−HD and Ar−H_2: (a) $j' = 4 \leftarrow j = 2$, $m_j = 0, 1, 2$ optimizations; (b) $j' = 4 \leftarrow j = 2$, $m_j = 0, 1, 2$ optimizations. Wavefunction-normalization conditions were used.

probability, we use a simulated annealing algorithm[26] with variables $\theta_{jl}^{m_j 0}$ for $l = 0$ to l_f, where l_f is estimated in section 4.1.

The maximal and minimal fluxes for the $j' = 4 \leftarrow j = 2$, $m_j = 0$ transition are shown in Tables 1 and 2 (columns 4 and 5), along with the fluxes into other final channels. For the case of Ar + HD, for example, the range of results into $j' = 4$ obtained with incoming plane-wave normalization is 0.0139 to 0.0220, compared to the flux associated with an incoming plane-wave of 0.0163. The less-constrained maximization associated with the flux norm yielded the considerably larger value of 0.0553. Note, however, that even though the $j' = 4 \leftarrow j = 2$, $m_j = 0$ flux has been maximized, it often still remains small compared to the elastic scattering ($j = j' = 2$).

The phase $\theta_{jl}^{m_j 0}$ leading to a minimal and to a maximal flux for the $j' = 4 \leftarrow j = 2$, $m_j = 0, 1, 2$ and for the $j' = 0 \leftarrow j = 2$, $m_j = 0, 1, 2$ transitions are shown in Figure 5. They show remarkably little uniformity, reflecting the individuality of each optimization. This case-dependence is also evident in the absolute squares of the incoming eigenfunctions leading to maximum and to minimum scattered fluxes, shown, for Ar + HD, in Figure 6. The corresponding differential fluxes for $m_j = 0$ (summed over all possible $m_{j'}$) are shown in Figure 7. Note the significantly different angular distributions associated with the optimized vs plane-wave results (Figure 4). Analogous results were obtained for Ar + H_2, but space limitations prevent their consideration here.[27]

Additional studies were carried out to assess the stability of the extrema. For example, the phase of each θ contributing to $d_{jl}^{m_j m_l}$ was varied by π to determine the effect of such changes on the yield. Results showed that the yield was strongly affected by variations in some angles and totally insensitive to changes in others. An alternate study involved random changes in the values of the phases from their values at the extremum, over a range of −0.3 to 0.3 radians. The flux was found to be sensitive to some of these variations, but a wide variety of phases in this range produced similar flux values.

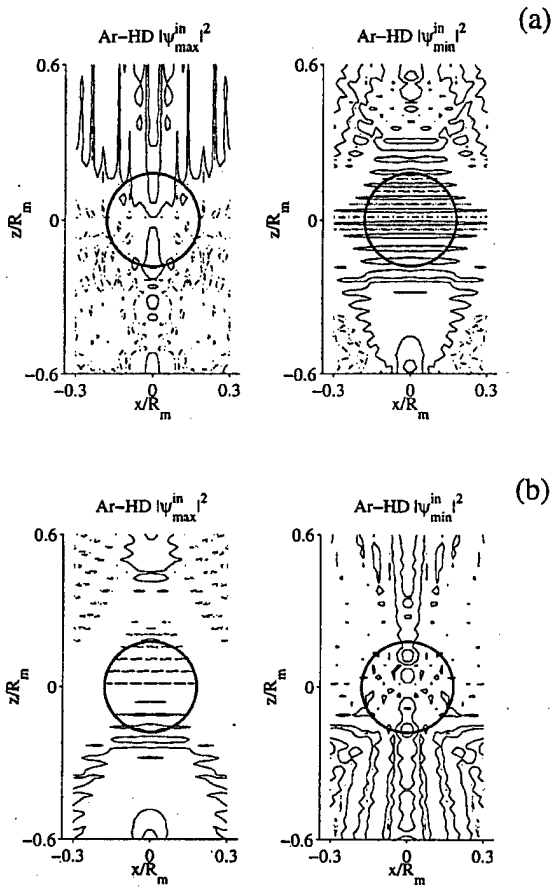

Figure 6. Square of the absolute value of the incoming wavefunctions leading to maximum and minimum outgoing flux for the Ar−HD system using the wavefunction-normalization condition. (a) $j' = 4 \leftarrow j = 2$, $m_j = 0$ optimization, maximum values are 169 for $|\psi^{in}_{max}|^2$ and 138 for $|\psi^{in}_{min}|^2$; (b) $j' = 0 \leftarrow j = 2$, $m_j = 0$ optimization, maximum values are 193 for $|\psi^{in}_{max}|^2$ and 30 for $|\psi^{in}_{min}|^2$. Contour values are as in Figure 3.

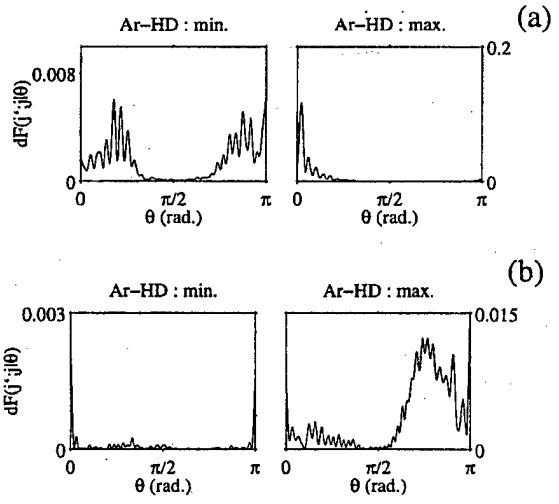

Figure 7. Differential outgoing flux for wavefunctions leading to a minimal flux (left) and a maximal flux (right) for Ar−HD using the wavefunction-normalization condition: (a) $j' = 4 \leftarrow j = 2$, $m_j = 0$ optimization; (b) $j' = 0 \leftarrow j = 2$, $m_j = 0$ optimization.

6. Summary

We have shown that it is possible to significantly alter the nature of the incoming scattering wave in a bimolecular process so as to optimize the scattering into a given product channel. From the viewpoint of coherent control, this is yet another example of how one can superimpose eigenstates in the continuum to produce controllable quantum interferences that affectg the flux into particular channels.

It remains a challenge to produce these modified incoming waves in the laboratory. One possible approach would be to focus the projectile beam or the target beam (or both) with an optical standing wave specifically designed for the purpose.

Acknowledgment. M.S. and P.B. have been greatly influenced through many encounters over the years by the generous spirit of Professor Kent Wilson, a true pioneer in the field of laser chemistry. Support for this research was provided by the U.S. Office of Naval Research, by Photonics Research Ontario, and by the Israel Science Foundation.

Appendix: Orthonormality of General Incoming Waves

In this appendix, we prove the orthogonality properties of (cylindrically asymmetric) incoming waves with arbitrary $d_{jl}^{m_j m_l}$. We also derive the conditions satisfied by $d_{jl}^{m_j m_l}$ when a general incoming wave is constrained to have the normalization of a reference plane-wave.

Orthogonality between plane-waves implies, amongst other things, that two waves propagating along different directions, $\hat{k}^{(1)}$ and $\hat{k}^{(2)}$, are orthogonal to one another. If we insist that the sculpted incoming wavefunctions have this orthogonality property, we must characterize each incoming wavefunction with a $\hat{k}$ vector. However, in contrast to plane-waves, a $\hat{k}$ vector cannot signify the propagation direction of the wavefunction, since a general incoming wavefunctiuon does not have a well-defined propagation direction. The $\hat{k}$ vector should therefore be thought of as a quantum number which helps differentiate one general incoming function from another.

We begin by writing a partial wave expansion, valid over the whole space (and not just in the asymptotic region, as in eq 23), for two incoming wavefunctions, as

$$\psi_{j_1}^{(1)}(\mathrm{R}_1, \hat{\mathrm{r}}) = 2\sum_l \sum_{m_j m_l} d_{jl}^{m_j m_l} j_l(k_{j_1}^{(1)} R_1) Y_{lm_l}(\hat{\mathrm{R}}_1) Y_{jm_j}(\hat{\mathrm{r}}) \qquad \text{(A.1)}$$

$$\psi_{j_2}^{(2)}(\mathrm{R}_2, \hat{\mathrm{r}}) = 2\sum_l \sum_{m_j m_l} d_{jl}^{m_j m_l} j_l(k_{j_2}^{(2)} R_2) Y_{lm_l}(\hat{\mathrm{R}}_2) Y_{jm_j}(\hat{\mathrm{r}}) \qquad \text{(A.2)}$$

Since in the above expansion, $\hat{\mathrm{R}}_1 \equiv (\theta_1, \phi_1)$ and $\hat{\mathrm{R}}_2 \equiv (\theta_2, \phi_2)$ are expressed relative to the directions of $\boldsymbol{k}_{j_1}^{(1)}$ and $\boldsymbol{k}_{j_2}^{(2)}$, respectively, we first need to express both wavefunctions with respect to the same z axis, which can be chosen as the direction of $\boldsymbol{k}_{j_1}^{(1)}$. Rotating the $\boldsymbol{k}_{j_2}^{(2)}$ vector to coincide with the z axis via three Euler angles $(\alpha\ \beta,\ \gamma)$, we can write $\psi_j^{(2)}(\mathrm{R}_2, \hat{\mathrm{r}})$ in the common coordinate system as

$$\psi_j^{(2)}(\mathrm{R}_2, \hat{\mathrm{r}}) = 2\sum_l \sum_{m_j m_l} d_{jl}^{m_j m_l} j_l(k_j R) \sum_{m''_l} D_{m_l m''_l}^{(l_2)}(\alpha, \beta, \gamma) Y_{lm''_l}(\hat{\mathrm{R}}_1)(-1)^{m''_l - m_l} Y_{jm_j}(\hat{\mathrm{r}})$$

where $D_{m_j m''_l}^{(l_2)}(\alpha, \beta, \gamma)$ are Wigner rotation matrices.[15] Integration yields

$$\int \mathrm{dR}_1 d\hat{\mathrm{r}} \psi_{j_1}^{*(1)}(\mathrm{R}_1, \hat{\mathrm{r}}) \psi_{j_2}^{(2)}(\mathrm{R}_2, \hat{\mathrm{r}}) = 4\sum_{l_1 l_2} \sum_{m_{l_1} m_{l_2} m_{j_1} m_{j_2}} d_{j_1 l_1}^{* m_{j_1} m_{l_1}} d_{j_2 l_2}^{m_{j_2} m_{l_2}} \int R^2 \mathrm{d}R j_{l_1}(k_{j_1}^{(1)} R) j_{l_2}(k_{j_2}^{(2)} R) \times$$
$$\int \mathrm{d}\hat{\mathrm{R}}\ Y_{l_1 m_{l_1}}^*(\hat{\mathrm{R}}) \sum_{m''_{l_2}} D_{m l_2 m''_{l_2}}^{(l_2)}(\alpha, \beta, \gamma) Y_{l_2 m''_{l_2}}(\hat{\mathrm{R}}) \times$$
$$(-1)^{m''_{l_2} - m_{l_2}} \int \mathrm{d}\hat{\mathrm{r}}\ Y_{j_1 m_{j_1}}^*(\hat{\mathrm{r}}) Y_{j_2 m_{j_2}}(\hat{\mathrm{r}}) \qquad \text{(A.3)}$$

Using orthonormality relations of the spherical harmonic functions, we obtain

$$\int \mathrm{dR}_1 \mathrm{d}\hat{\mathrm{r}} \psi_{j_1}^{*(1)}(\mathrm{R}_1, \hat{\mathrm{r}}) \psi_{j_2}^{(2)}(\mathrm{R}_2, \hat{\mathrm{r}}) = 4\sum_l \sum_{m_{l_1} m_{l_2}} \sum_{m_j} d_{j_1 l}^{* m_j m_{l_1}} d_{j_1 l}^{m_j m_{l_2}} \times$$
$$\int R^2 \mathrm{d}R\ j_l(k_{j_1}^{(1)} R)\ j_l(k j_2^{(2)} R) \times D_{m_{l_1} m_{l_2}}^{(l)}(\alpha, \beta, \gamma)(-1)^{m_{l_1} - m_{l_2}} \delta_{j_1 j_2}$$

After imposing the Bessel functions orthonormality conditions, we obtain

$$\int \mathrm{dR}_1 \mathrm{d}\hat{\mathrm{r}} \psi_{j_1}^{*(1)}(\mathrm{R}_1, \hat{\mathrm{r}}) \psi_{j_2}^{(2)}(\mathrm{R}_2, \hat{\mathrm{r}}) = 4\sum_l \sum_{m_{l_1} m_{l_2}} \sum_{m_j} \mathrm{d}_{j_1 l}^{* m_j m_{l_1}} \mathrm{d}_{j_1 l}^{m_j m_{l_2}} \times$$
$$\int R^2 \mathrm{d}R\ j_l(k_{j_1}^{(1)} R)\ j_l(k_{j_2}^{(2)} R) \times D_{m_{l_2} m_{l_1}}^{(l)}(\alpha, \beta, \gamma)(-1)^{m_{l_1} - m_{l_2}} \delta_{j_1 j_2}$$

Therefore, the angular normalization requirement is

$$\delta(\hat{k}_{j_1}^{(1)} - \hat{k}_{j_2}^{(2)}) = \frac{1}{4\pi^2} \sum_l \sum_{m_{l_1} m_{l_2}} \sum_{m_j} d_{j_1 l}^{* m_j m_{l_1}} d_{j_1 l}^{m_j m_{l_2}} D_{m_{l_2} m_{l_1}}^{(l)}(\alpha, \beta, \gamma)(-1)^{m_{l_1} - m_{l_2}}$$

Using the identities

$$\delta(\hat{k}_{j_1}^{(1)} - \hat{k}_{j_2}^{(2)}) = \sum_l \sum_{m_2} Y_{lm_2}^*(\hat{k}_{j_1}^{(1)}) Y_{lm_2}(\hat{k}_{j_2}^{(2)}) \qquad \text{(A.4)}$$

$$Y_{lm}(\hat{k}_{j_2}^{(2)}) = \sum_{m''} D_{mm''}^{(l)}(\alpha, \beta, \gamma) Y_{lm''}(\hat{k}_{j_1}^{(1)})(-1)^{m'' - m} \qquad \text{(A.5)}$$

we obtain

$$\delta(\hat{k}_{j_1}^{(1)} - \hat{k}_{j_2}^{(2)}) = \sum_l \sum_{m_{l_2}} Y_{lm_{l2}}^*(\hat{k}_{j_1}^{(1)}) \sum_{m_{l_1}} D_{m_{l2} m_{l_1}}^{(l)}(\alpha, \beta, \gamma) Y_{lm_{l_1}}(\hat{k}_{j_1}^{(1)})(-1)^{m_{l_1} - m_{l2}}$$

$$0 = \sum_l \sum_{m_{l_1}} \sum_{m_{l_2}} \left[\sum_{m_j} \frac{1}{4\pi^2} d_{j_1 l}^{m_j m_{l_1}} d_{j_1 l}^{m_j m_{l2}} - Y_{lm_{l_1}}(\hat{k}_{j_1}^{(1)}) Y_{lm_{l2}}(\hat{k}_{j_2}^{(2)}) \right] \times$$
$$D_{m_{l2} m_{l_1}}^{(l)}(\alpha, \beta, \gamma)(-1)^{m_{l_1} - m_{l2}} \qquad \text{(A.6)}$$

Using the orthogonality and normalization of the rotation matrices (see ref 15, eq 4.6.1)

$$\frac{1}{8\pi^2} \int_0^{2\pi} \int_0^{\pi} \int_0^{2\pi} D_{m'_1 m_1}^{(l_1)}(\alpha, \beta, \gamma) D_{m'_2 m_2}^{(l_2)}(\alpha, \beta, \gamma) \mathrm{d}\alpha \sin\beta d\beta d\gamma =$$
$$\delta_{m'_1 m_1} \delta_{m'_2 m_2} \delta_{l_1 l_2} \frac{1}{2l_1 + 1} \qquad \text{(A.7)}$$

we obtain, my multiplying eq A.6 by $D_{m'_{l2} m'_{l1}}^{(l')}(\alpha, \beta, \gamma)$ and integrating,

$$0 = \sum_{m_j} \frac{1}{4\pi^2} d_{j_1 l}^{*m_j m_{l_1}} d_{j_1 l}^{m_j m_{l_2}} - Y_{l m_{l_1}}(\hat{k}_{j_1}^{(1)}) Y_{l m_{l_2}}(\hat{k}_{j_2}^{(2)}) \quad \text{(A.8)}$$

Finally, choosing $\hat{k}_{j_1}^{(1)} = (0, 0)$, we obtain the normalization condition on the $d_{jl}^{m_j m_{l_1}}$ coefficients as

$$\sum_{m_j} d_{j_1 l}^{*m_j m_{l_1}} d_{j_1 l}^{m_j m_{l_2}} = \pi(2l+1)\delta_{m_{l_1} 0}\delta_{m_{l_2} 0} \quad \text{(A.9)}$$

for every l, m_{l_1}, and m_{l_2}.

References and Notes

(1) For recent reviews, see: Shapiro, M.; Brumer, P. *J. Chem. Soc., Faraday Trans. 2* **1997**, *93*, 1263. Gordon, R. J.; Rice, S. A. *Annu. Rev. Phys. Chem.* **1997**, *48*, 595.

(2) Brumer, P.; Shapiro, M. *Sci. Am.* **1995**, *272*, 56.

(3) Shapiro, M.; Brumer, P. *Phys. Rev. Lett.* **1996**, *77*, 2574. Holmes, D.; Shapiro, M.; Brumer, P. *J. Chem. Phys.* **1996**, *105*, 9162.

(4) Abrashkevich, A. G.; Shapiro, M.; Brumer, P. *Phys. Rev. Lett.* **1998**, *81*, 3789. Errata: *Phys. Rev. Lett.* **1999**, *82*, 3002.

(5) Frishman, E.; Shapiro, M.; Brumer, P. *J. Chem. Phys.* **1999**, *110*, 9.

(6) Brumer, P.; Abrashkevich, A. G., Shapiro, M. *Far. Discuss. Chem. Soc.*, in press.

(7) Tannor, D. J.; Rice, S. A. *Adv. Chem. Phys.* **1988**, *70*, 441. Tannor, D. J.; Rice, S. A. *J. Chem. Phys.* **1985**, *83*, 5013. Tannor, D. J.; Kosloff, R.; Rice, S. A. *J. Chem. Phys.* **1986**, *85*, 5805.

(8) Seideman, T.; Shapiro, M.; Brumer, P. *J. Chem. Phys.* **1989**, *90*, 7132.

(9) Yan, Y.; Gillilan, R. E.; Whitnell, R. M.; Wilson, K. R. *J. Phys. Chem.* **1993**, *97*, 2320. Krause, J. L.; Whitnell, R. M.; Wilson, K. R.; Yan, Y.; Mukamel, S. *J. Chem. Phys.* **1993**, *99*, 6562.

(10) Warren, W. S.; Rabitz, H.; Dahleh, M. *Science* **1993**, *259*, 1581.

(11) Bardeen, C. J.; Yakovlev, V. V.; Wilson, K. R.; Carpenter, S. D.; Weber, P. M.; Warren, W. S. *Chem. Phys. Lett.* **1997**, *280*, 151.

(12) Assion, T.; Baumert, T.; Bergt, M.; Brixner, T.; Kiefer, B.; Seyfried, V.; Strehle, M.; Ferber, G. *Science* **1988**, *282*, 919.

(13) Arthurs, A. M.; Dalgarno, A. *Proc. R. Soc. London* **1960**, *256*, 540.

(14) *Atom–Molecule Collision Theory*; Bernstein, R. B., Ed.; Plenum Press: New York, 1979; Chapters 6, 8, 9, 10.

(15) Edmonds, A. R. *Angular Momentum in Quantum Mechanics*; Princeton University Press: Princeton, NJ, 1960; Chapter 3 (Section 5, eqs 3, 4, and 16).

(16) Johnson, B. R.; Secrest, D.; Lester, W. A.; Bernstein, R. B. *Chem. Phys. Lett.* **1967**, *1*, 396.

(17) Lester, W. A.; Bernstein, R. B. *Chem. Phys. Lett.* **1967**, *1*, 207.

(18) Dewangan, D. P.; Flower, D. R. *J. Phys. B* **1981**, *14*, 2179.

(19) Sun, Y.; Yudson, R. S.; Kouri, D. J. *J. Chem. Phys.* **1989**, *90*, 241.

(20) Bernstein, R. B.; Dalgarno, A.; Massey, H.; Percival, I. C. *Proc. R. Soc. London*, **1963**, *274A*, 427.

(21) Kreek, H.; Le Roy, R. J. *J. Chem. Phys.* **1975**, *63*, 338.

(22) Chu, S. I.; Datta, K. *J. Chem. Phys.* **1982**, *76*, 5307.

(23) Le Roy, R. J.; van Kranendonk, J. *J. Chem. Phys.* **1974**, *61*, 4750.

(24) Herzberg, G.; Huber, K. P. *Molecular Spectra and Molecular Structure*, Part IV; Van Nostrand: New York, 1979.

(25) Gordon, R. G. *J. Chem. Phys.* **1969**, *51*, 14.

(26) (a) Corana, A.; Marchesi, M.; Martini, C.; Ridella, S. *ACM Transactions on Mathematical Software* **1987**, *13*, 262. (b) Goffe, W. L.; Ferrier, G. D.; Rogers, J. *Journal of Econometrics* **1994**, *60*, 65. Fortran source code by Goffe, W. L.

(27) Frishman, E. To appear in Ph.D. dissertation, Weizmann Institute of Science, Rehovot, Israel.

Laboratory conditions in the coherent control of reactive scattering

Paul Brumer,* Alexander Abrashkevich and Moshe Shapiro†

Chemical Physics Theory Group, University of Toronto, and Photonics Research Ontario, Toronto, Canada M5S 3H6

Received 18th March 1999

The essential requirements for preparing a bimolecular collisional superposition state in the laboratory, allowing for control over reactive scattering, are described. Specific applications to isotopic variants of $H + H_2$ scattering are used to demonstrate the range of control for superposition states built from degenerate diatomic states.

I. Introduction

The principle of controlling atomic and molecular processes *via* quantum interference, *i.e.* coherent control, is now well established.[1,2] In particular, one arranges to arrive at a final state through two or more independent coherent routes whose features can be varied *via* experimentally controllable parameters. Having done so, the multiple routes, and the interference between them, can be controlled by changing the relevant laboratory parameters. Numerous computational and experimental studies show that the interference contribution is a function of the particular product so that one can alter the ratio of products by manipulating the interference contributions through laboratory variables. Further, this control is often found to be extensive.

This principle has been established formally and computationally for both unimolecular and bimolecular processes and shown experimentally for unimolecular processes.[3–5] A review of this work makes clear, however, that the control of bimolecular processes is still in its infancy. In particular, we have presented the rudiments of a general formalism for control of bimolecular collisions,[6–8] studied control for one-dimensional reactive scattering[9] and demonstrated control of the differential cross section[7,8] for isotopic variants of $H + H_2$ in a particular implementation discussed further, below. In this paper we systematically describe the specific requirements for bimolecular control and discuss methods for implementing control in the laboratory. In their most general form they invoke the manipulation of matter as waves, an area overlapping with matter interferometry[10] and laser cooling.[11] We then consider one simple scenario to examine the extent of possible control.

Consider then the general collision processes

$$A + D \rightarrow F + G \tag{1}$$

where A, D, F, G are, in general, molecules of mass M_A, M_D, M_F and M_G. Here F and G can be identical to A and D (nonreactive scattering) or different from A and D (reactive scattering). We

† Permanent address: Department of Chemical Physics, The Weizmann Institute of Science, 76100, Rehovot, Israel.

This journal is © The Royal Society of Chemistry 1999

label A + D as arrangement q and F + G as arrangement q'. Eigenfunctions of the asymptotic reactant Hamiltonian at energy E, where A + D are widely separated, are denoted $|E, q, \boldsymbol{m}; 0\rangle$. Here $\boldsymbol{m}$ includes all quantum number which describe the state, other than the energy E and the arrangement q. Asymptotic product states of F + G are similarly denoted $|E, q', \boldsymbol{n}; 0\rangle$, and $|E, q', \boldsymbol{n}^+\rangle$ denotes the outgoing scattering solutions[12] associated with product in state $|E, q', \boldsymbol{n}; 0\rangle$. The probability $P_E(\boldsymbol{n}, q'; \boldsymbol{m}, q)$ of forming the product $|E, q', \boldsymbol{n}; 0\rangle$, having initiated the scattering in $|E, q, \boldsymbol{m}; 0\rangle$ is given by

$$P_E(\boldsymbol{n}, q'; \boldsymbol{m}, q) = |\langle E, q', \boldsymbol{n}; 0|S|E, q, \boldsymbol{m}; 0\rangle|^2 \tag{2}$$

where S is the scattering matrix. Alternatively, the cross section $\sigma_E(\boldsymbol{n}, q'; \boldsymbol{m}, q)$ for forming $|E, q', \boldsymbol{n}; 0\rangle$ having initiated the scattering in $|E, q, \boldsymbol{m}; 0\rangle$ is:

$$\sigma_E(\boldsymbol{n}, q'; \boldsymbol{m}, q) = |\langle E, q', \boldsymbol{n}^+|V_q|E, q, \boldsymbol{m}; 0\rangle|^2. \tag{3}$$

Here V_q is the component of the total potential that vanishes as the A to D distance becomes arbitrarily large. The cross section for scattering into arrangement q', independent of the product internal state $\boldsymbol{n}$, is

$$\sigma_E(q'; \boldsymbol{m}, q) = \sum_{\boldsymbol{n}} |\langle E, q', \boldsymbol{n}^+|V_q|E, q, \boldsymbol{m}; 0\rangle|^2. \tag{4}$$

Assorted other cross sections may be defined, depending upon which of the elements of $\boldsymbol{n}$ are summed over. Of relevance below are (a) $\sigma_E(q', \theta, \phi; \boldsymbol{m}, q)$, corresponding to scattering into the q' product channel and into scattering angles (θ, ϕ) and (b) the traditional differential cross section $\sigma_E(q', \theta; \boldsymbol{m}, q) = \int_0^{2\pi} \mathrm{d}\phi\, \sigma_E(q', \theta, \phi; \boldsymbol{m}, q)$.

Note that eqns. (2)–(4) arise in scattering theory after separating out the motion of the center of mass of A–D, a feature discussed in greater detail in Section II.

To control bimolecular collisions we construct an initial state $|E, q, \{c_{\boldsymbol{m}}\}\rangle$ consisting of a superposition of N energetically degenerate asymptotic states $|E, q, \boldsymbol{m}; 0\rangle$:

$$|E, q, \{c_{\boldsymbol{m}}\}\rangle = \sum_{\boldsymbol{m}} c_{\boldsymbol{m}}|E, q, \boldsymbol{m}; 0\rangle. \tag{5}$$

The cross section associated with using eqn. (5) as the initial state, obtained by replacing $|E, q, \boldsymbol{m}; 0\rangle$ by eqn. (5) in eqn. (3), is

$$\begin{aligned}
\sigma_E(\boldsymbol{n}, q'; \{c_{\boldsymbol{m}}\}, q) &= |\langle E, q', \boldsymbol{n}^+|V_q \sum_{\boldsymbol{m}} c_{\boldsymbol{m}}|E, q, \boldsymbol{m}; 0\rangle|^2 \\
&= \sum_{\boldsymbol{m}} |c_{\boldsymbol{m}}|^2 |\langle E, q', \boldsymbol{n}^+|V_q|E, q, \boldsymbol{m}; 0\rangle|^2 \\
&\quad + \sum_{\boldsymbol{m}'} \sum_{\boldsymbol{m} \neq \boldsymbol{m}'} c_{\boldsymbol{m}} c_{\boldsymbol{m}'}^* \langle E, q', \boldsymbol{n}^+|V_q|E, q, \boldsymbol{m}; 0\rangle\langle E, q, \boldsymbol{m}'; 0|V_q|E, q', \boldsymbol{n}^+\rangle \\
&\equiv \sum_{\boldsymbol{m}} |c_{\boldsymbol{m}}|^2 \sigma(\boldsymbol{n}, q'; \boldsymbol{m}, q) + \sum_{\boldsymbol{m}'} \sum_{\boldsymbol{m} \neq \boldsymbol{m}'} c_{\boldsymbol{m}} c_{\boldsymbol{m}'}^* \sigma(\boldsymbol{n}, q'; \boldsymbol{m}', \boldsymbol{m}, q)
\end{aligned} \tag{6}$$

where $\sigma(\boldsymbol{n}, q'; \boldsymbol{m}', \boldsymbol{m}, q)$ is defined *via* eqn. (6). The total cross section into arrangement q' is given by

$$\sigma_E(q'; \{c_{\boldsymbol{m}}\}, q) = \sum_{\boldsymbol{n}} \sigma_E(\boldsymbol{n}, q'; \{c_{\boldsymbol{m}}\}, q) \tag{7}$$

Note that eqn. (6), and hence eqn. (7), are now of a standard coherent control form, *i.e.* direct contributions from each member of the superposition, proportional to $|c_{\boldsymbol{m}}|^2$, plus interference terms which are proportional to $c_{\boldsymbol{m}} c_{\boldsymbol{m}'}^*$. This form has three significant features. First, it is clear that if we control the $c_{\boldsymbol{m}}$, through assorted preparation methods, then we can control the interference term, and hence the scattering cross section. Second, it provides a specific functional form for control so that the experimentalist needs only determine a small number of terms (the σs) in order to generate the entire control map, *i.e.* control as a function of $c_{\boldsymbol{m}}$. Third, it arises from eqn. (5), which includes only energetically degenerate terms. In particular, if eqn. (5) were to contain states of different energies E and E' then the interference term would carry a factor of $\exp[\mathrm{i}(E - E')t/\hbar]$ which would average to zero over a period $\hbar/(E - E')$ and control would vanish.[13] This degener-

acy requirement, which is standard in all coherent control scenarios, proves somewhat demanding in collisional processes.

II. Preparation of the scattering superposition

To see how the required superposition state [eqn. (5)] can be constructed in the laboratory requires some introductory remarks. Note first that eqns. (2)–(7) and the $|E, q, m; 0\rangle$ are expressed in the center of mass coordinate system and describe the relative translational as well as the internal state of A and D. In typical A–D scattering the removal of the center of mass motion comes about in a straightforward way. That is, let r_A and r_D denote the laboratory position of A and D and $\hbar k^A$, $\hbar k^D$ denote their laboratory momenta. The relative momentum k, relative coordinate r, center of mass momentum K and position R are defined as

$$K = k^A + k^D; \quad R = (M_A r_A + M_D r_D)/(M_A + M_D)$$
$$k = (M_D k^A - M_A k^D)/(M_A + M_D); \quad r = r_A - r_D. \tag{8}$$

In the case where A and D are initially in internal states $|\phi_A(i)\rangle$ and $|\phi_D(j)\rangle$, of energies $E_A(i)$ and $E_D(j)$, and the initial A and D translational motions are described by plane waves of momenta k_i^A and k_j^D then the incident wavefunction ψ_{in} is

$$\psi_{in} = |\phi_A(i)\rangle|\phi_D(j)\rangle\exp(ik_i^A \cdot r_A)\exp(ik_j^D \cdot r_D)$$
$$= |\phi_A(i)\rangle|\phi_D(j)\rangle\exp(ik \cdot r)\exp(iK \cdot R). \tag{9}$$

The second equality follows from eqns. (8). Since the interaction potential V_q between A and D depends solely upon the A–D relative coordinates, the center of mass momentum is conserved in the collision, allowing us to separate out the center of mass motion and to describe the dynamics in the center of mass coordinate system, *i.e.*, in terms of $|E, q, m; 0\rangle$.

Scattering may also occur from a state composed of different values of center of mass momenta K. For example,

$$|\psi_{in}\rangle = \sum_{lm} d_{lm}|E, q, m; 0\rangle|K_l\rangle \quad (K_{l'} \neq K_l). \tag{10}$$

Since the center of mass momentum is conserved, and since it can be measured at the end of the collision, the cross section for scattering into $|E, q', n; 0\rangle$ in this case is given by

$$\sigma_E(n, q'; \{d_{lm}\}, q) = \sum_l \left| \langle E, q', n^+ | V_q \sum_m d_{lm} | E, q, m; 0\rangle \right|^2. \tag{11}$$

That is, components of the wavefunction with different values of $|K_l\rangle$ contribute independently to the reaction cross section and do not interfere with one another.

Consider now preparation of the generalized superposition states [eqn. (5)] where, for simplicity, we limit consideration to the preparation of a superposition of two states. To do so we examine the scattering of A and D, each in a previously prepared superposition state. The wavefunctions ψ_A and ψ_D in the laboratory system are chosen to be of the general form:

$$\psi_A = a_1|\phi_A(1)\rangle\exp(ik_1^A \cdot r_A) + a_2|\phi_A(2)\rangle\exp(ik_2^A \cdot r_A) \tag{12}$$

$$\psi_D = a_3|\phi_D(3)\rangle\exp(ik_3^D \cdot r_D) + a_4|\phi_D(4)\rangle\exp(ik_4^D \cdot r_D). \tag{13}$$

Since A and D are initially noninteracting, the incident wavefunction is

$$\psi_{in} = \psi_A\psi_D = [a_1|\phi_A(1)\rangle\exp(ik_1^A \cdot r_A) + a_2|\phi_A(2)\rangle\exp(ik_2^A \cdot r_A)]$$
$$\times [a_3|\phi_D(3)\rangle\exp(ik_3^D \cdot r_D) + a_4|\phi_D(4)\rangle\exp(ik_4^D \cdot r_D)]$$
$$= \sum_{i=1}^{2}\sum_{j=3}^{4} A_{ij}\exp(ik_{ij} \cdot r)\exp(iK_{ij} \cdot R) \tag{14}$$

where $A_{ij} = a_i a_j|\phi_A(i)\rangle|\phi_D(j)\rangle$, $k_{ij} = (M_D k_i^A - M_A k_j^D)/(M_A + M_D)$, and $K_{ij} = k_i^A + k_j^D$ with $(i = 1, 2; j = 3, 4)$.

As constructed, eqn. (14) is composed of four independent noninterfering incident wavepackets since each has a different center of mass wavevector $\boldsymbol{K}_{ij}$. However, we can set conditions so that interference, and hence control, is indeed achieved. That is, we require the equality of the center of mass motion of two components, plus energy degeneracy:

$$\boldsymbol{K}_{13} = \boldsymbol{K}_{24}$$

$$\hbar^2 k_{13}^2/2\mu + e_{\mathrm{A}}(1) + e_{\mathrm{D}}(3) = \hbar^2 k_{24}^2/2\mu + e_{\mathrm{A}}(2) + e_{\mathrm{D}}(4), \tag{15}$$

with $\mu = M_{\mathrm{A}} M_{\mathrm{D}}/(M_{\mathrm{A}} + M_{\mathrm{D}})$. Eqn. (14) then becomes

$$\psi_{\mathrm{in}} = [A_{13} \exp(\mathrm{i}\boldsymbol{k}_{13} \cdot \boldsymbol{r}) + A_{24} \exp(\mathrm{i}\boldsymbol{k}_{24} \cdot \boldsymbol{r})]\exp(\mathrm{i}\boldsymbol{K}_{13} \cdot \boldsymbol{R})$$
$$+ A_{23} \exp(\mathrm{i}\boldsymbol{k}_{23} \cdot \boldsymbol{r})\exp(\mathrm{i}\boldsymbol{K}_{23} \cdot \boldsymbol{R}) + A_{14} \exp(\mathrm{i}\boldsymbol{k}_{14} \cdot \boldsymbol{r})\exp(\mathrm{i}\boldsymbol{K}_{14} \cdot \boldsymbol{R}), \tag{16}$$

where the term in the first bracket, due to eqn. (15), is a linear superposition of two degenerate states. In accord with eqns. (10) and (11) we expect that the scattering cross section will be composed of noninterfering contributions from three components with different $\boldsymbol{K}_{ij}$, but where the first term allows for control *via* the interference between the A_{13} and A_{24} terms. The two remaining terms, proportional to A_{23} and A_{14}, are uncontrolled satellite contributions.

For example, if we set $\boldsymbol{k}_1^{\mathrm{A}} = -\boldsymbol{k}_3^{\mathrm{D}}$ and $\boldsymbol{k}_2^{\mathrm{A}} = -\boldsymbol{k}_4^{\mathrm{D}}$ then $\boldsymbol{K}_{13} = \boldsymbol{K}_{24} = 0$. In addition, $\boldsymbol{k}_{13} = \boldsymbol{k}_1^{\mathrm{A}}$, $\boldsymbol{k}_{24} = \boldsymbol{k}_2^{\mathrm{A}}$ so that eqn. (15) becomes

$$\hbar^2[(k_1^{\mathrm{A}})^2 - (k_2^{\mathrm{A}})^2] = (2M_{\mathrm{D}} M_{\mathrm{A}})[e_{\mathrm{A}}(2) + e_{\mathrm{D}}(4) - e_{\mathrm{A}}(1) - e_{\mathrm{D}}(3)]/(M_{\mathrm{D}} - M_{\mathrm{A}}) \tag{17}$$

Note also that we can implement eqn. (17) for the case of atom–diatom scattering by setting $|\phi_{\mathrm{A}}(1)\rangle = |\phi_{\mathrm{A}}(2)\rangle = |\phi_{\mathrm{A}}(\mathrm{g})\rangle$, where $|\phi_{\mathrm{A}}(\mathrm{g})\rangle$ is the ground electronic state of atom A. Eqn. (17) then becomes

$$\hbar^2[(k_1^{\mathrm{A}})^2 - (k_2^{\mathrm{A}})^2] = (2M_{\mathrm{D}} M_{\mathrm{A}})[e_{\mathrm{D}}(4) - e_{\mathrm{D}}(3)]/(M_{\mathrm{D}} - M_{\mathrm{A}}) \tag{18}$$

Finally, in the specific case where we superpose degenerate states of the molecule D, eqn. (18) becomes $(k_1^{\mathrm{A}})^2 = (k_2^{\mathrm{A}})^2$. Indeed, in this case we can choose $\boldsymbol{k}_1^{\mathrm{A}} = \boldsymbol{k}_2^{\mathrm{A}} = -\boldsymbol{k}_3^{\mathrm{D}} = -\boldsymbol{k}_4^{\mathrm{D}}$ so that all of the $\boldsymbol{K}_{ij}$ are equal and all of the four terms in eqn. (14) are energetically degenerate in the center of mass coordinate system. Hence in this case, which corresponds to the scattering of an atom off a molecule in a superposition of degenerate molecular states, there are no extraneous uncontrollable satellite contributions. Results for this case are considered below for the case of atom–diatom scattering.

III. *M* Superpositions

It is clear that the easiest way of implementing bimolecular control in the laboratory is to start with a superposition of degenerate states of the fragments. In atom–diatom scattering, to which we restrict attention, we utilize the $(2j + 1)$ diatomic rotational states $|j, m\rangle$, where m is the projection of diatomic angular momentum j along a space fixed axis. In this case (and in the case of the helicity, *i.e.* the projection of the angular momentum along the relative velocity vector,[7,8] as well) we show below that control over the differential cross section is possible but control over the total cross section is not.

Consider first superimposing two m states of the diatomic in atom–diatom scattering. For this case eqn. (5) assumes the form:

$$|n, q\rangle = \sum_{i=1,2} c_i |qvjm_i\rangle |E_q^{\mathrm{kin}}\rangle, \tag{19}$$

where $|qvjm_i\rangle$ is an eigenket of the diatomic of energy ϵ_{qvj}, with v denoting the diatom vibrational quantum number. $|E_q^{\mathrm{kin}}\rangle$ is a plane wave of energy $E_q^{\mathrm{kin}} = E - \epsilon_{qvj}$, describing the free motion of the atom relative to the diatom in the q arrangement.

The differential cross section into scattering angles θ, φ is given by

$$\sigma(q'v'j'k' \leftarrow q, v, j, m_1, m_2 | \theta, \varphi) = \left| \sum_{i=1,2} c_i f_{q'v'j'k' \leftarrow qvjm_i}(\pi - \theta, \varphi) \right|^2. \tag{20}$$

Table 4 Optimal control coefficients c_i, for the H + H'D collisions at $E = 1.25$ eV[a]

		$v = 0, j = 1$		$v = 0, j = 2$		$v = 0, j = 4$		$v = 0, j = 6$	
q	m_i	$\lvert c_i\rvert$	$\arg(c_i)$	$\lvert c_i\rvert$	$\arg(c_i)$	$\lvert c_i\rvert$	$\arg(c_i)$	$\lvert c_i\rvert$	$\arg(c_i)$
2	0	0.914	0.429	0.592	1.958	0.576	−2.250	0.542	−0.756
2	1	0.287	0.0[+0]	0.540	0.476[−π]	0.494	2.539[−π]	0.478	−2.273[+π]
2	2			0.183	0.0[+0]	0.278	1.341[−π]	0.312	2.624[+0]
2	3					0.112	0.381[−π]	0.155	1.393[−π]
2	4					0.028	0.0[+0]	0.052	0.385[+0]
2	5							0.014	−0.212[+π]
2	6							0.003	0.0[+0]
3	0	0.890	−2.973	0.535	0.984	0.498	−0.834	0.500	0.117
3	1	0.322	−π[+π]	0.561	0.194[−π]	0.468	−2.061[+π]	0.453	−1.256[+π]
3	2			0.206	0.0[+0]	0.333	−2.775[+0]	0.328	−2.232[+0]
3	3					0.205	−3.104[+π]	0.213	−2.877[+π]
3	4					0.063	−π[+0]	0.118	3.005[+0]
3	5							0.052	2.882[−π]
3	6							0.012	−π[+0]

[a] $q = 2$ corresponds to the final H' + HD arrangement and $q = 3$ corresponds to the final D + HH' arrangement. Here $c_i = c_{m_i}$ where $-j \leqslant m_i \leqslant j$. Values of $\lvert c_i\rvert$ are found to be a function of $\lvert m_i\rvert$ and $\arg(c_i)$ for $\lvert m_i\rvert$ are shown. In order to get $\arg(c_i)$ for $-\lvert m_i\rvert$, one should add the numbers in square brackets to the value of $\arg(c_i)$ for $\lvert m_i\rvert$. [*e.g.* $\arg(c_i) = 0$ for $q = 3, m_i = -1, v = 0, j = 1$].

nation of the results showed that this is not the case. Thus, optimal control results from quantum interference effects and not from a simple classical reorientation of the angular momentum vector.

IV. Summary

Our general treatment of laboratory conditions for bimolecular control has identified two distinctly different classes of control. In the first, one prepares a superposition of degenerate internal reactant states which is subsequently used as a reagent in the collision. In this case there are no undesirable uncontrolled satellite contributions. However, in examining the most natural case, *i.e.* superposing diatomic m states in collisions with atoms, we have found that (a) one can control differential, but not total integral, cross sections and (b) control, although evident in general, only becomes extensive with the inclusion of many initial m states. An examination of Table 1 shows that this is because the σ_{12} interference contributions are small when compared to the σ_{ii}.

The second control class requires the creation of the desired superposition state [eqn. (5)] from non-degenerate internal states of the reactants. In this instance we require special conditions in the laboratory in which the relative motion of the atom and internal energy are correlated within a laboratory superposition state. Although similar correlations have been established in laser cooling of atoms[11] these techniques have yet to be extended to molecules. Given these conditions controllable superpositions result, but they are accompanied by uncontrolled satellite terms [*e.g.* eqn. (16)]. Nonetheless, previous studies on model collinear scattering[9] suggest the possibility of extensive control under these circumstances due to large relative values of σ_{12}. These studies motivate the further work which is currently underway[24] on three-dimensional atom–diatom scattering using non-degenerate internal states in the initial superposition state.

Acknowledgements

We thank Professors R. Wyatt and B. Ramachandran for providing us with the REACT scattering code and for useful comments on its use. This work was supported in part by the U.S. Office of Naval Research, Photonics Research Ontario and by a grant of HPC time on the CRAY C-90 and the SGI Origin 2000 from the DoD ASC MSRC Center, and the CRAY T-90 and the SGI PCA from the DoD NAVOCEANO MSRC Center.

Here

$$f_{q'v'j'k'\leftarrow qvjm_l}(\theta, \varphi) = \frac{i^{j-j'+1}\, e^{im_l\varphi}}{2k_{qvj}} \sum_J (2J+1) d^J_{k'm_l}(\theta) T_{q'v'j'k',qvjm_l} \tag{21}$$

is the scattering amplitude,[14] $T^J_{q'v'j'k',qvjm_l} = S^J_{q'v'j'k',qvjm_l} - \delta_{q'q}\delta_{v'v}\delta_{j'j}\delta_{k'm_l}$, and $S^J_{q'v'j'k',qvjm_l}$ are the elements of the scattering S-matrix in the helicity representation.[15] Here k' is the helicity of the product diatom (*i.e.* the projection of the product diatom angular momentum onto the final relative translational velocity vector), and $k_{qvj} = \sqrt{2\mu_q(E - \epsilon_{qvj})}/\hbar$, with μ_q being the atom–diatom reduced mass in the q channel. Note that the use of $(\pi - \theta)$ in eqn. (20), rather than θ, is discussed in ref. 16.

Expanding the square in eqn. (20) gives the reactive differential scattering cross section as (where we drop the initial state labels for convenience)

$$\sigma^R(v'j'k' \mid \theta, \varphi) = |c_1|^2\sigma^R_{11}(v'j'k' \mid \theta) + |c_2|^2\sigma^R_{22}(v'j'k' \mid \theta) + 2\,\mathrm{Re}\{c_1^* c_2\, \sigma^R_{12}(v'j'k' \mid \theta, \varphi)\}, \tag{22}$$

where

$$\begin{aligned}\sigma^R_{ii}(v'j'k' \mid \theta) &= |f_{q'v'j'k'\leftarrow qvjm_l}(\pi - \theta, \varphi)|^2 \\ &= (4k^2_{qvj})^{-1} \sum_{J,J'} (2J+1)(2J'+1) d^J_{k'm_l}(\pi - \theta) d^{J'}_{k'm_l}(\pi - \theta) \\ &\quad \times S^J_{q'v'j'k',qvjm_l}[S^{J'}_{q'v'j'k',qvjm_l}]^*, \quad q \neq q', \quad i = 1, 2,\end{aligned} \tag{23}$$

and

$$\begin{aligned}\sigma^R_{12}(v'j'k' \mid \theta, \varphi) &= f_{q'v'j'k'\leftarrow qvjm_l}(\pi - \theta, \varphi) f^*_{q'v'j'k'\leftarrow qvjm_l}(\pi - \theta, \varphi) \\ &= \frac{e^{i(m_1 - m_2)\varphi}}{4k^2_{qvj}} \sum_{J,J'} (2J+1)(2J'+1) \\ &\quad \times d^J_{k'm_1}(\pi - \theta) d^{J'}_{k'm_2}(\pi - \theta) S^J_{q'v'j'k',qvjm_1}[S^{J'}_{q'v'j'k',qvjm_2}]^*, \quad q \neq q'.\end{aligned} \tag{24}$$

Here, the superscript R denotes reactive scattering into a specific final arrangement channel $q' \neq q$. The total differential cross section, $\sigma^R(\theta, \varphi)$, for reaction out of a state in eqn. (19) is given by the sum over final states at energy E as

$$\sigma^R(\theta, \varphi) = \sum_{v',j',k'} \sigma^R(v'j'k' \mid \theta, \varphi). \tag{25}$$

Note that the φ dependence of the measurable cross sections is due solely to the interference term. Integration of eqn. (22) or (25) over angles $\theta \in [0, \pi]$ and $\varphi \in [0, 2\pi]$ gives the state-resolved integral reactive cross section $\sigma^R(v'j'k')$. However, the integral of $\sigma^R_{12}(v'j'k' \mid \theta, \varphi)$ over φ is zero so that the interference term, and hence control over the total cross section disappears. Indeed, the integral over $0 < \varphi < \pi$ exactly cancels the integral over $\pi < \varphi < 2\pi$. For this reason we consider control over scattering into the hemisphere $0 < \varphi < \pi$, giving the state resolved integral cross section denoted $\sigma^R(v'j'k'; \varphi \leqslant \pi)$. This can also be written as three terms, as in eqn. (22), but with the σ^R_{ij} replaced by $\sigma^R_{ij}(v'j'k'; \varphi \leqslant \pi)$, $(i, j = 1, 2)$, where

$$\sigma^R_{ii}(v'j'k'; \varphi \leqslant \pi) = \frac{\pi}{2k^2_{qvj}} \sum_J (2J+1) |S^J_{q'v'j'k',qvjm_l}|^2, \quad i = 1, 2, \tag{26}$$

$$\begin{aligned}\sigma^R_{12}(v'j'k'; \varphi \leqslant \pi) &= (4k^2_{qvj})^{-1} \sum_{J,J'} (2J+1)(2J'+1) S^J_{q'v'j'k',qvjm_1}[S^{J'}_{q'v'j'k',qvjm_2}]^* \\ &\quad \times I(m_1, m_2) \int_0^\pi d\theta \sin\theta\, d^J_{k'm_1}(\pi - \theta) d^{J'}_{k'm_2}(\pi - \theta), \quad q \neq q',\end{aligned} \tag{27}$$

with

$$I(m_1, m_2) = \int_0^\pi d\varphi e^{i(m_1 - m_2)\varphi} = \begin{cases} \dfrac{2i}{m_1 - m_2}, & \text{if } m_1 - m_2 \text{ is odd,} \\ 0, & \text{if } m_1 - m_2 \text{ is even.} \end{cases}$$

Summing over the final v', j', k' at energy E, gives the total integral cross section into the hemisphere as

$$\sigma^{R}(\varphi \leqslant \pi) = \sum_{v',j',k';\varphi \leqslant \pi} \sigma^{R}(v', j', k'). \tag{28}$$

It is important to stress that state-to-state cross sections $\sigma_{ii}^{R}(v'j'k' \mid \theta)$ and $\sigma_{ii}^{R}(v'j'k';\ \varphi \leqslant \pi)$ in eqns. (23) and (26), as well as the corresponding total cross sections $\sigma_{ii}^{R}(\theta)$ and σ_{ii}^{R}, appear in standard scattering theory (see, *e.g.*, ref. 17), while $\sigma_{12}^{R}(v'j'k' \mid \theta, \varphi)$ and $\sigma_{12}^{R}(v'j'k';\ \varphi \leqslant \pi)$ in eqns. (24) and (27) are new types of interference terms which allow for control, through the c_i, over the atom–diatom collision process. Note that significant control requires substantial σ_{12}^{R} which follows from the Schwartz inequality $[|\sigma_{12}^{R}| \leqslant \sqrt{\sigma_{11}^{R}\,\sigma_{22}^{R}}]$, *i.e.* large σ_{12}^{R} requires also large σ_{11}^{R} and σ_{22}^{R}. Therefore, extensive control is not limited to regions near the reactive threshold.[18]

To examine the extent of control over the reaction it is convenient to rewrite the reactive cross section in the form (where we refer to scattering into a hemisphere, but drop the notation "$\varphi \leqslant \pi$" for convenience),

$$\sigma^{R} = [\sigma_{11}^{R} + x^2\sigma_{22}^{R} + 2x|\sigma_{12}^{R}|\cos(\delta_{12}^{R} + \phi_{12})]/(1 + x^2), \tag{29}$$

where $x = |c_2/c_1|$, $\phi_{12} = \arg(c_2/c_1)$, and $\delta_{12}^{R} = \arg(\sigma_{12}^{R})$. In many cases, of greatest interest is control over branching ratio between the reactive and nonreactive total cross sections which is given by

$$\frac{\sigma^{R}}{\sigma^{NR}} = \frac{\sigma_{11}^{R} + x^2\sigma_{22}^{R} + 2x|\sigma_{12}^{R}|\cos(\delta_{12}^{R} + \phi_{12})}{\sigma_{11}^{NR} + x^2\sigma_{22}^{NR} + 2x|\sigma_{12}^{NR}|\cos(\delta_{12}^{NR} + \phi_{12})}. \tag{30}$$

Here NR refers to nonreactive scattering; definitions of the nonreactive cross sections are analogous to their reactive counterparts.

It follows from eqns. (29) and (30) that by varying the c_i coefficients (*i.e.* varying either the relative magnitude, x or the relative phase, ϕ_{12}) in eqn. (19) through the initial preparation step, we can directly alter the interference term σ_{12}^{R} (and/or σ_{12}^{NR}) and hence control the scattering cross sections. Such a preparation might be carried out, for example, by a suitably devised molecular beam experiment where the diatomic is excited, with elliptically polarized light to a collection of well-defined m states.

Note that the above approach can be readily extended to the case of N interfering superposition states, as discussed in Section IIIB below.

A. Computational results

We have considered control over the reactions $D + H_2$, $H + D_2$, and H + H'D (H and H' denote hydrogen atoms which are deemed distinguishable) using this approach and present a few typical results in this section. Control over reaction products is achieved by preparing superpositions of two initial degenerate interfering diatomic states (v, j, m_1) and (v, j, m_2). In our three-dimensional quantum-mechanical calculations, the $A + B_2$ symmetry has been exploited for the first two reactions, while the last one has been considered as an atom–heteronuclear diatom reaction of the general A + BC type. The cross sections reported below are obtained *via* the symmetrization procedure described in ref. 16. Since only initial states of H_2 and D_2 with even j were considered, only the "plus" molecular parity block was computed for each partial wave. The LSTH[19] potential surface was used and scattering calculations were done with the log-derivative version of the Kohn variational principle[20] using a basis set contraction procedure.[21] Scattering calculations were carried out for total angular momentum up to $J = 31$ with $j_{max} = 14$ and $E_{max} = 2.5$ eV for the $D + H_2$ and $H + D_2$ reactions, and up to $J = 46$, $j_{max} = 15$ and $E_{max} = 2.6$ eV for the H + H'D reaction, ensuring fully converged cross sections for the chosen energies. Here, E_{max} and j_{max} are, respectively, the maximum (cutoff) energy and maximum diatomic rotational quantum number of all asymptotic channels and internal basis functions included in the calculation.

Consider, as an example, the results for scattering from a superposition state consisting of the $(v = 1, j = 2, m_1 = 1, m_2 = 0)$, as shown in Fig. 1. Results are reported as contour plots of cross section ratios *vs.* the phase ϕ_{12} and the parameter $s = x^2/(1 + x^2)$. The value $s = 0$ corresponds to scattering from the state with $m_1 = 1$ and $s = 1$ corresponds to scattering from the state with

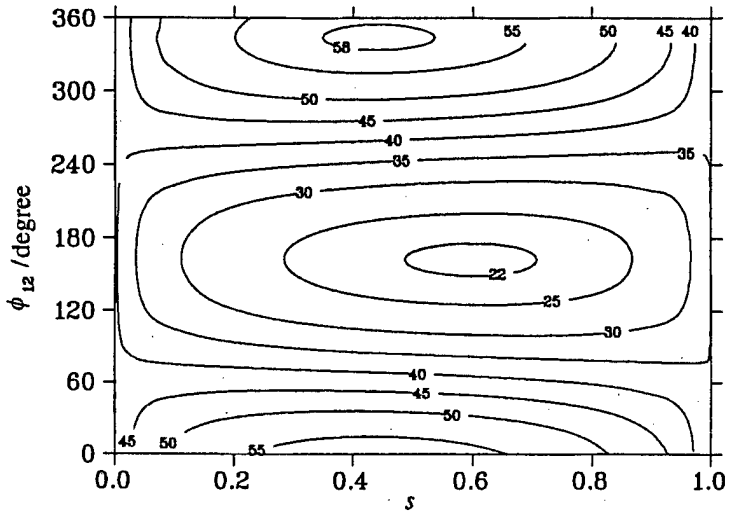

Fig. 1 Contour plot of the $\sigma^{R}(\theta; \varphi \leqslant \pi)/\sigma^{NR}(\theta; \varphi \leqslant \pi)(\times 10^2)$ ratio for $D + H_2$ as a function of ϕ_{12} and s at $\theta = 60°$, with $E = 1.25$ eV. The initial state is a superposition state with $v = 1, j = 2, m_1 = 1, m_2 = 0$.

$m_2 = 0$. Fig. 1 shows $\sigma^{R}(\theta; \varphi \leqslant \pi)/\sigma^{NR}(\varphi \leqslant \pi)(\theta)$, which is seen to vary from 0.22 to 0.58 as ϕ_{12} is changed from 157° to 342° at $s \approx 0.51$. This range should be compared with the uncontrolled ratios of ~ 0.36 at $s = 1$ and ~ 0.40 at $s = 0$. Note further that Fig. 1 is of the familiar form,[1,2] resulting from the interference between two states. Thus, varying the coefficients c_i allows one to either increase or decrease the ratio of differential cross sections, in comparison to the uncontrolled ratio, by a factor of ~ 1.5. Less extensive control was observed, for example, for scattering from the $(v = 0, j = 2, m_1 = 2, m_2 = 1)$ initial state (not shown).

Similar ranges of control are observed for control over the cross section into the hemisphere, *i.e.* $\sigma^{R}(\varphi \leqslant \pi)/\sigma^{NR}(\varphi \leqslant \pi)$, shown in Figs. 2 and 3. The results shown in Fig. 2 correspond to $D + H_2 \rightarrow H + HD$ at $E = 0.93$ eV, with scattering from an initial superposition of $(v = 0, j = 2, m_1 = 1, m_2 = 0)$. The ratio of cross sections is seen to vary from 0.05 to 0.079, showing maximum and minimum that are well outside (up to factor 1.22 and 1.26 respectively) of the range of results

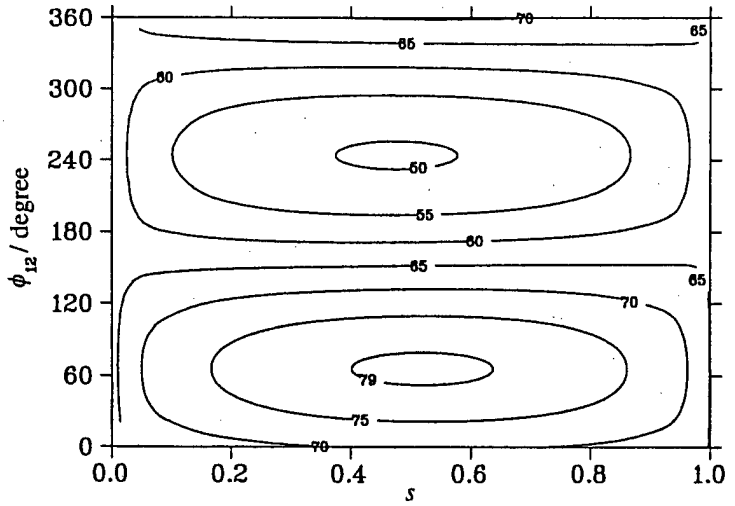

Fig. 2 Contour plot of the ratio $\sigma^{R}(\varphi \leqslant \pi)/\sigma^{NR}(\varphi \leqslant \pi)(\times 10^3)$ for $D + H_2$ at $E = 0.93$ eV as a function of ϕ_{12} and s. The initial state is a superposition of $v = 0, j = 2, m_1 = 1, m_2 = 0$.

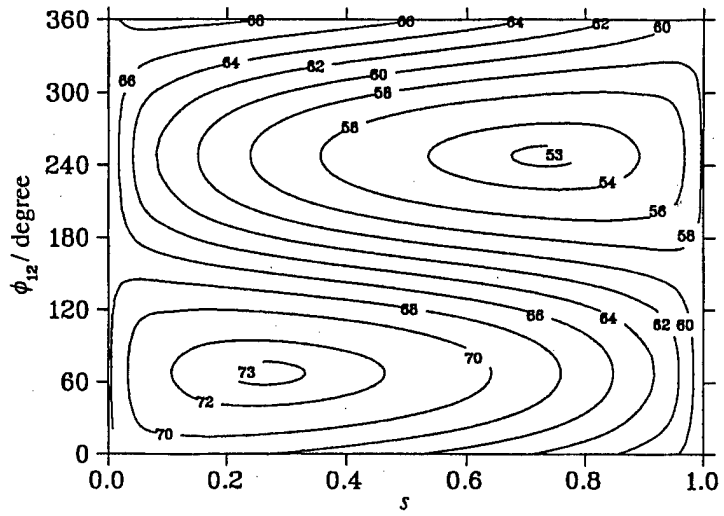

Fig. 3 Contour plot of the ratio $\sigma^{R}(\varphi \leqslant \pi)/\sigma^{NR}(\varphi \leqslant \pi)(\times 10^3)$ for $D + H_2$ at $E = 1.25$ eV as a function of ϕ_{12} and s. The initial state is a superposition of $v = 1, j = 2, m_1 = 1, m_2 = 0$.

for scattering from a single m_i state. Thus, the ratio of cross sections can be increased or decreased by $\approx 20\%$ through coherent control effects. Somewhat better control is observed at higher energies ($E = 1.25$ eV), further from the reaction threshold (Fig. 3) where a superposition of ($v = 1$, $j = 2$, $m_1 = 1$, $m_2 = 0$) initial superposition states shows the ratio of cross sections varying from 0.053 to 0.073 as both ϕ_{12} and s are varied.

In essence, superposing two m levels provides some degree of control over the differential cross sections. Nonetheless, control is far from extensive. The origin of this behavior is evident from the sample results shown in Table 1, which shows the contributions σ_{ii} and σ_{12} for reactive and nonreactive scattering from several initial superposition states at $E = 1.25$ eV. The interference contributions σ_{12} are seen to be, for both the reactive and nonreactive terms, approximately one order of magnitude smaller than the diagonal terms. As a consequence, the extent of control is rather limited. Two alternatives for improved control suggest themselves. The first is to seek alternate linear superpositions, *e.g.* composed from nondegenerate molecular states,[9] whose resultant interference terms are closer in magnitude to the diagonal elements. The second is to examine the extent of control resulting from the inclusion of more than two degenerate reactant states in the initial superposition, as discussed below.

B. Optimized bimolecular scattering

The treatment above can be readily extended to superpositions composed of more than two states. In particular, we adopt a previously devised scheme to optimize the reactive cross section as a function of c_m for an arbitrary number of states.[22]

Consider scattering from incident state $|E, q, n; 0\rangle$ to final state $|E, q', m; 0\rangle$. To simplify the notation we identify the m and n labels with a single quantum number, denoted i and f, with

Table 1 Integral cross sections $\sigma_{ij}^{NR,R}(\varphi \leqslant \pi)$, $i \leqslant j = 1, 2$, for $D + H_2$ at $E = 1.25$ eV[a]

v	j	m_1	m_2	σ_{11}^{NR}	σ_{22}^{NR}	σ_{12}^{NR}	σ_{11}^{R}	σ_{22}^{R}	σ_{12}^{R}
0	2	1	0	2.312(+1)	2.305(+1)	4.294(−1)	3.337(+0)	3.364(+1)	3.578(−1)
0	2	2	1	2.466(+1)	2.312(+1)	8.854(−1)	2.051(+0)	3.337(+0)	8.347(−1)
1	2	1	0	6.051(+1)	6.083(+1)	2.265(−1)	4.092(+0)	3.549(+0)	3.152(−1)
1	2	2	1	6.295(+1)	6.051(+1)	1.014(+0)	1.841(+0)	4.092(+0)	1.077(+0)

[a] Numbers in parentheses denote the power of ten by which the tabulated value should be multiplied.

associated free states $|E, q, i; 0\rangle$ and $|E, q', f; 0\rangle$. The result is, however, completely general. In accord with eqn. (2), the probability $P(f, q'; i, q)$ of producing product in final state $|f, E, q'\rangle$ having started in the initial state $|i, E, q\rangle$ is

$$P(f, q'; i, q) = |S_{fi}|^2 \tag{31}$$

where $S_{fi} = \langle E, f, q'|S|E, i, q\rangle$ and where S is the scattering matrix for the process. The total probability $P(q'; i, q)$ of scattering into arrangement channel q', assuming m open product states, is given by

$$P(q'; i, q) = \sum_{f=1}^{m} |S_{fi}|^2. \tag{32}$$

To simplify the notation we have not carried an E label in the probabilities: fixed energy E is understood.

If we now consider scattering from an initial state $|E, q, \{c_i\}\rangle$ composed of a linear superposition of k states [*i.e.*, eqn. (5) with $N = k$] then the probability of forming $|E, q', f\rangle$ from this initial state is

$$P(f, q'; \boldsymbol{c}, q) = \left|\sum_{i=1} c_i S_{fi}\right|^2. \tag{33}$$

and the total reactive scattering probability into channel q', $P(q'; \boldsymbol{c}, q)$ is

$$P(q'; \boldsymbol{c}, q) = \sum_{f=1}^{m} \left|\sum_{i=1}^{k} c_i S_{fi}\right|^2. \tag{34}$$

To simplify the notation we introduce the matrix $\boldsymbol{A} = \boldsymbol{S}_{q'}^{\dagger}\boldsymbol{S}_{q'}$ with elements $A_{ij} = \sum_{f=1}^{m} S_{fj}^{*} S_{fi}$ which allows us to rewrite eqn. (34) as

$$P(q'; \boldsymbol{c}, q) = \boldsymbol{c}^{\dagger}\boldsymbol{A}\boldsymbol{c}. \tag{35}$$

Here $\dagger$ denotes the Hermitian conjugate and the q' subscript on the $\boldsymbol{S}$ indicates that we are dealing with the submatrix of the $\boldsymbol{S}$ matrix associated with scattering into product channel q'.

One can optimize scattering into arrangement channel q', with the normalization constraint $\sum_{i=1}^{k} |c_i|^2 = 1$, by requiring

$$\frac{\partial}{\partial c_k^{*}}\left[P(q'; \boldsymbol{c}, q) - \lambda \sum_{i=1}^{k} |c_i|^2\right] = \frac{\partial}{\partial c_k^{*}}\left[\boldsymbol{c}^{\dagger}\boldsymbol{A}\boldsymbol{c} - \lambda \boldsymbol{c}^{\dagger}\boldsymbol{c}\right] = 0 \tag{36}$$

where λ is a Lagrange multiplier. Explicitly taking the derivative gives the result that the optimized coefficients $\boldsymbol{c}_{\lambda}$ satisfy the eigenvalue equation

$$\boldsymbol{A}\boldsymbol{c}_{\lambda} = \lambda \boldsymbol{c}_{\lambda}. \tag{37}$$

Additional labels may be necessary to account for degeneracies of the eigenvectors $\boldsymbol{c}_{\lambda}$. Hence, optimization is equivalent to solving eqn. (37).

We have applied this approach to obtain optimal $\boldsymbol{c}_{\lambda}$ for all $H + H_2$ isotopic variants. Typical results are those shown here for H + H'D at $E = 1.25$ eV, where scattering is optimized in each of the two product channels. In each case, we considered optimization of both σ^{NR} and of σ^{R} as a means of maximizing (or minimizing) σ^{R}/σ^{NR}. In all cases, optimization of σ^{R} was found to provide superior results.

Results for the maximum of σ^{R}/σ^{NR} into both product arrangements are shown in columns 5 of Table 2 for a set of even j, along with the corresponding nonreactive and reactive cross sections. Results were similar for odd values of j. Also shown, for comparison purposes, are the maximum uncontrolled ratio, denoted $\sigma_u^{R}/\sigma_u^{NR}$, along with σ_u^{R} and σ_u^{NR}. Optimal control results for the same collision processes, but where we minimize σ^{R}, are presented in Table 3. Examination of Tables 2 and 3 shows a large range of possible control. For example, scattering into $q = 2$ from $j = 2$ ranges over a factor of two, from a maximum of 2.63×10^{-2} to a minimum of 1.15×10^{-2}. A much greater range of control (1.98×10^{-2} to 1.51×10^{-4}) is evident for scattering into $q = 3$ with initial $j = 10$. Indeed the range of control increases with j, a manifestation of the increasing

Table 2 Controlled, $\sigma^{R,NR}(\varphi \leqslant \pi)$, and uncontrolled, $\sigma_u^{R,NR}(\varphi \leqslant \pi)$, integral cross sections for the H + H'D collisions at $E = 1.25$ eV[a] (results of σ^R maximization)

q	j	σ^R	σ^{NR}	σ^R/σ^{NR}	σ_u^R	σ_u^{NR}	σ_u^R/σ_u^{NR}
2	2	1.70(+0)	6.49(+1)	2.63(−2)	1.41(+0)	6.25(+1)	2.26(−2)
2	4	1.96(+0)	6.92(+1)	2.83(−2)	1.39(+0)	6.32(+1)	2.20(−2)
2	6	2.10(+0)	7.53(+1)	2.79(−2)	1.30(+0)	6.47(+1)	2.01(−2)
2	8	1.89(+0)	8.37(+1)	2.26(−2)	1.02(+0)	6.71(+1)	1.52(−2)
2	10	6.08(−1)	9.67(+1)	6.29(−3)	3.12(−1)	7.12(+1)	4.39(−3)
3	2	1.35(+0)	6.39(+1)	2.11(−2)	1.10(+0)	6.25(+1)	1.76(−2)
3	4	1.58(+0)	6.78(+1)	2.34(−2)	1.19(+0)	6.32(+1)	1.88(−2)
3	6	1.86(+0)	7.37(+1)	2.52(−2)	1.28(+0)	6.47(+1)	1.98(−2)
3	8	2.06(+0)	8.25(+1)	2.50(−2)	1.29(+0)	6.71(+1)	1.93(−2)
3	10	1.92(+0)	9.70(+1)	1.98(−2)	1.06(+0)	7.12(+1)	1.49(−2)

[a] In all cases the initial $v = 0$. For each case shown, coefficients c_i were obtained to maximize σ^R. The $q = 2$ arrangement corresponds to H' + HD and $q = 3$ corresponds to D + HH'. Numbers in parentheses denote the power of ten by which the tabulated value should be multiplied.

ability so suppress reactive scattering as the number of initial states increases.[22] We were unable, however, to significantly suppress nonreactive scattering as a means of enhancing the maximal σ^R/σ^{NR} ratio. Nonetheless, in some instances (*e.g.* $q = 2, j = 10$), the optimized σ^R was close to the theoretical maximum of twice the unoptimized σ_u^R.

Optimal control coefficients c_i resulting from the optimization procedure are shown in Table 4 for a number of the cases in Table 2. The case of $j = 1$ has been added to allow the simple verification of the argument below.

Of considerable interest is the question of whether the optimized c_i coefficients merely define a new vector $|j, m; R\rangle$ which is simply a ket vector in a rotated coordinate system. If so this would indicate that the optimum solution corresponds to a simple classical reorientation of the diatomic angular momentum vector. Examination of the results indicate that this is not the case. Specifically, a vector $|j, m; R\rangle$ rotated by Euler angles α, β, γ is given by[23]

$$|j, m; R\rangle = \sum_{m'} \langle j, m' | j, m; R\rangle |j, m'\rangle = \sum_{m'} D^{(j)}_{m'm}(\alpha, \beta, \gamma) |j, m'\rangle. \tag{38}$$

Thus, if the result of the optimal control procedure were merely to affect a rotation of the j vector, then the coefficients c_i should equal (to within an overall phase) $D^{(j)}_{m'm}(\alpha, \beta, \gamma)$. A careful exami-

Table 3 Controlled, $\sigma^{R,NR}(\varphi \leqslant \pi)$, and uncontrolled, $\sigma_u^{R,NR}(\varphi \leqslant \pi)$, integral cross sections for the H + H'D collisions at $E = 1.25$ eV[a] (results of σ^R minimization)

q	j	σ^R	σ^{NR}	σ^R/σ^{NR}	σ_u^R	σ_u^{NR}	σ_u^R/σ_u^{NR}
2	2	7.23(−1)	6.26(+1)	1.15(−2)	8.62(−1)	6.33(+1)	1.36(−2)
2	4	4.70(−1)	6.28(+1)	7.49(−3)	6.64(−1)	6.45(+1)	1.03(−2)
2	6	2.21(−1)	6.31(+1)	3.50(−3)	4.07(−1)	6.62(+1)	6.15(−3)
2	8	3.59(−2)	6.36(+1)	5.65(−4)	1.07(−1)	6.85(+1)	1.56(−3)
2	10	1.18(−3)	6.40(+1)	1.85(−5)	5.60(−3)	7.16(+1)	7.82(−5)
3	2	3.58(−1)	6.34(+1)	5.65(−3)	5.35(−1)	6.33(+1)	8.45(−3)
3	4	2.22(−1)	6.41(+1)	3.46(−3)	4.06(−1)	6.45(+1)	6.29(−3)
3	6	1.22(−1)	6.52(+1)	1.87(−3)	2.87(−1)	6.62(+1)	4.34(−3)
3	8	4.89(−2)	6.67(+1)	7.22(−4)	1.51(−1)	6.85(+1)	2.20(−3)
3	10	1.03(−2)	6.84(+1)	1.51(−4)	4.27(−2)	7.16(+1)	5.96(−4)

[a] In all cases the initial $v = 0$. For each case shown, coefficients c_i were obtained to minimize σ^R. The $q = 2$ arrangement corresponds to H' + HD and $q = 3$ corresponds to D + HH'. Numbers in parentheses denote the power of ten by which the tabulated value should be multiplied.

References

1 M. Shapiro and P. Brumer, *J. Chem. Soc., Faraday Trans.*, 1997, **93**, 1263; P. Brumer and M. Shapiro, *Annu. Rev. Phys. Chem.*, 1992, **43**, 257.
2 B. Kohler, J. L. Krause, F. Raski, K. R. Wilson, V. V. Yakovler, R. M. Whitnell and Y. Yan, *Acc. Chem. Res.*, 1995, **28**, 133; W. S. Warren, H. Rabitz and M. Dahleh, *Science*, 1993, **259**, 1581; S. A. Rice, *ibid.*, 1992, **258**, 412.
3 See, *e.g.*, L. Zhu, V. Kleiman, X. Li, S-P. Liu, K. Trentelman and R. J. Gordon, *Science*, 1995, **270**, 77, and references therein.
4 E. Dupont, P. B. Corkum, H. C. Liu, M. Buchanan and Z. R. Wasilewski, *Phys. Rev. Lett.*, 1995, **74**, 3596.
5 A. Shnitman, I. Sofer, I. Golub, A. Yogev, M. Shapiro, Z. Chen and P. Brumer, *Phys. Rev. Lett.*, 1996, **76**, 2886.
6 M. Shapiro and P. Brumer, *Phys. Rev. Lett.*, 1996, **77**, 2574.
7 A. Abrashkevich, M. Shapiro and P. Brumer, *Phys. Rev. Lett.*, 1998, **81**, 3789.
8 An erratum (A. Abrashkevich, M. Shapiro and P. Brumer, *Phys. Rev. Lett.*, 1999, **82**, 3002) clarifies that the results shown in ref. 7 are valid at $\phi = 0$ and that control over the total cross section is not possible when building the initial superposition from helicity states.
9 D. Holmes, M. Shapiro and P. Brumer, *J. Chem. Phys.*, 1996, **105**, 9162.
10 *Atom Interferometry*, ed. P. Berman, Academic Press, San Diego, 1997.
11 J. Lawall, F. Bardou, K. Shimizu, M. Ledue, A. Aspect and C. Cohen-Tannoudji, *Phys. Rev. Lett.*, 1994, **73**, 1915.
12 J. R. Taylor, *Scattering Theory*, Wiley, New York, 1972.
13 This is not to say that the oscillatory interference term cannot be put to good use. See, for example, our proposal for generating THz radiation: P. Brumer and M. Shapiro, in *Coherent Control in Atoms, Molecules and Semiconductors*, ed. W. Pötz and W. A. Schroeder, Kluwer, Dordrecht, 1999.
14 G. C. Schatz and A. Kuppermann, *J. Chem. Phys.*, 1976, **65**, 4642; eqn. (21) of our paper corrects a typographical error in the seminal Schatz–Kuppermann paper (specifically, m_i should appear in the exponent and not k').
15 R. T. Pack and G. A. Parker, *J. Chem. Phys.*, 1987, **87**, 3888.
16 J. Z. H. Zhang and W. H. Miller, *J. Chem. Phys.*, 1989, **91**, 1528.
17 W. H. Miller, *J. Chem. Phys.*, 1969, **50**, 407.
18 J. L. Krause, M. Shapiro and P. Brumer, *J. Chem. Phys.*, 1990, **92**, 1126.
19 P. Siegbahn and B. Liu, *J. Chem. Phys.*, 1978, **68**, 2457; D. G. Truhlar and C. J. Horowitz, *ibid.*, 1978, **68**, 2466; 1979, **71**, 1514.
20 D. E. Manolopoulos and R. E. Wyatt, *Chem. Phys. Lett.*, 1988, **152**, 23.
21 D. E. Manolopoulos, M. D'Mello and R. E. Wyatt, *J. Chem. Phys.*, 1990, **93**, 403.
22 E. Frishman, M. Shapiro and P. Brumer, *J. Chem. Phys.*, 1999, **110**, 9.
23 A. R. Edmonds, *Angular Momentum in Quantum Mechanics*, Princeton University Press, Princeton, 1960.
24 A. Abrashkevich, M. Shapiro and P. Brumer, work in progress.

Paper 9/02135C

PHYSICAL REVIEW E VOLUME 60, NUMBER 2 AUGUST 1999

Decoherence and correspondence in conservative chaotic dynamics

Jiangbin Gong and Paul Brumer
Chemical Physics Theory Group, University of Toronto, Toronto, Canada M5S 3H6
(Received 3 November 1998; revised manuscript received 19 March 1999)

The quantum and classical dynamics of a conservative nonlinear Hamiltonian system in the chaotic regime are compared in the absence and presence of decoherence effects. Results show marked improvement in classical-quantum correspondence with the introduction of decoherence, even though the initial quantum dynamics is far from the semiclassical limit. [S1063-651X(99)09208-9]

PACS number(s): 05.45.−a, 03.65.Bz, 03.65.Sq, 05.40.−a

I. INTRODUCTION

The means by which quantum mechanics approximates classical mechanics for macroscopic systems remains a subject of considerable interest. Traditional, often heuristic, approaches argue that the equations of classical mechanics emerge naturally as the de Broglie wavelength becomes small. Strong mathematical support for this approach, but with the necessary inclusion of infinitesimal averaging over energy, has recently been given [1]. By contrast, others argue that classical mechanics is not a limiting case of quantum mechanics, but rather that decoherence, i.e., loss of coherence due to coupling to other degrees of freedom, is necessary to ensure the validity of the correspondence principle [2–4]. This proposal, however, is the topic of considerable controversy, with many arguing that the relationship between decoherence and correspondence is tenuous [5].

In this paper we examine a nonlinear oscillator system in the chaotic regime and show that decoherence does indeed lead to substantially improved agreement between classical and quantum mechanics. This constitutes a major extension of previous work on the effect of decoherence, which was limited to one-dimensional driven chaotic systems [6–11]. In particular, our extension is to the broad class of conservative nonlinear Hamiltonian systems, and into the domain where the system is far from the semiclassical regime. In addition, we develop a quantum state diffusion-split operator method that provides a generally useful and efficient method for studying decoherence and gives interesting insights into the origins of decoherence in conservative systems.

To consider the effects of decoherence we adopt the model of Caldeira and Leggett and of Uhruh and Zurek [12] in which the system interacts with a harmonic bath in the weak coupling and high temperature limit. Extending this model to a system with two degrees of freedom gives the time evolution of the density matrix $\hat{\rho}$ in the Wigner representation as [12]

$$\frac{\partial \rho^W}{\partial t}=\{H,\rho^W\}+\sum_{(l_1+l_2)\ \text{odd}}\frac{(\hbar/2i)^{(l_1+l_2-1)}}{l_1!l_2!}\frac{\partial^{(l_1+l_2)}V(x,y)}{\partial x^{l_1}\partial y^{l_2}}\times\frac{\partial^{(l_1+l_2)}\rho_W}{\partial p_x^{l_1}\partial p_y^{l_2}}+D\left(\frac{\partial^2\rho^W}{\partial p_x^2}+\frac{\partial^2\rho^W}{\partial p_y^2}\right). \tag{1}$$

Here (p_x,p_y,x,y) are the system momenta and coordinates, $V(x,y)$ is the potential contribution to the Hamiltonian H, and $\rho^W=\rho^W(p_x,p_y,x,y;t)$ is the Wigner representation of the density matrix $\hat{\rho}$. The first term on the right hand side of Eq. (1) is the classical Poisson bracket which generates classical dynamics, the second term is responsible for quantum/classical differences, and the third term induces decoherence. By using Eq. (1), and by imposing restrictions on the derivatives of the potential to ensure the second term is small relative to the Poisson bracket term, Zurek and Paz [2] (and independently, Kolovsky [13]) derived the following condition for the quantum transition to classical behavior in chaotic systems:

$$\sqrt{\frac{2D}{\lambda}}\chi>\hbar, \tag{2}$$

where λ is the Lyapunov exponent of the classical dynamics, and χ is a characteristic potential length, defined, for the one degree of freedom system that they examined, as the average value of $\sqrt{|\partial_x V/\partial_x^3 V|}$. Below we use this criterion to establish the range of relevant parameters in our numerical studies.

Note that Eq. (1) ignores the back action of the system on the environment. As such, one can show [14] that the system absorbs energy from the environment at a D-dependent rate. Thus, since D is required to be sufficiently large to satisfy Eq. (2), then observable energy absorption is a necessary characteristic of decoherence (without dissipation) in the quantum regime of non-negligible $\hbar$. In the case chosen below the rate is D/m [14] per degree of freedom, where m is the mass, a theoretical prediction which we use to confirm the energy absorption observed computationally.

II. QUANTUM STATE DIFFUSION-SPLIT OPERATOR APPROACH

Solving Eq. (1) is quite complicated for a typical two degree of freedom chaotic system. A useful numerical technique for carrying this out, as well as the specific example of interest, is described in this section.

The particular case we examine is given by the nonlinear oscillator Hamiltonian [16]

$$H=\frac{1}{2}(p_x^2+p_y^2+\alpha x^2y^2)+\frac{\beta}{4}(x^4+y^4), \tag{3}$$

with $\beta=0.01$, $\alpha=1.0$, a regime where the system is fully chaotic [16] with $\lambda\approx 0.5$. Results were also obtained for $\alpha=0.1$ where the system is still chaotic but where the

 © 1999 The American Physical Society

Lyapunov exponent is approximately two times smaller. This system is particularly useful for decoherence studies because (a) it has the simple energy scaling property that all trajectories can be scaled onto one Poincaré surface of section, ensuring that the dynamics is essentially the same even if the system energy changes due to system-environment interaction; (b) the dynamics of this system at $\alpha=1.0$ is very chaotic, enhancing the classical-quantum discrepancy for the closed system and allowing for a study in the quantum regime; (c) the potential has no simple harmonic terms. Thus, any observed agreement between classical and quantum behavior cannot be attributed to the similarity of classical and quantum harmonic oscillator dynamics.

To solve Eq. (1) we adapt the quantum state diffusion (QSD) approach [15] based on the stochastic differential equation for the state vector into a usable scheme for nonlinear oscillator systems. In this approach we solve for the dynamics of the system wave function in the presence of a random potential, to obtain a single realization $|\psi(\xi_m(t),t)\rangle$. Specifically, we consider [15]

$$|d\psi\rangle=\frac{-i}{\hbar}H|\psi\rangle dt + \sum_m (2\langle L_m^\dagger\rangle_{|\psi\rangle}L_m - L_m^\dagger L_m - \langle L_m^\dagger\rangle_{|\psi\rangle}\langle L_m\rangle_{|\psi\rangle})|\psi\rangle dt + \sum_m (L_m-\langle L_m\rangle_{|\psi\rangle})|\psi\rangle d\xi_m, \quad (4)$$

where the operators L_m represent the coupling between the system and environment, and $\langle L_m\rangle_{|\psi\rangle}=\langle\psi|L_m|\psi\rangle/\langle\psi|\psi\rangle$ and where $d\xi_m$ are independent complex differential random variables of a complex normalized Wiener process, with well defined mean properties [15]. Averaging over these realizations by selecting different $d\xi_m$ gives $\rho(t)=(1/S)\Sigma_{\xi_m}|\psi(\xi_m(t),t)\rangle\langle\psi(\xi_m(t),t)|$, with S being the total number of realizations of the time-dependent stochastic variables ξ_m. Note that the $\rho(t)$ is the sum of projection operators computed from individual realizations so that one can regard each contribution $|\psi(\xi_m(t),t)\rangle\langle\psi(\xi_m(t),t)|$ as representing a single laboratory experiment for a quantum open system. Below we utilize this viewpoint to gain insight into the effects of decoherence on the evolution of individual wave packets.

Our specific implementation of the QSD method takes the operators L_i as $L_1=(\sqrt{D}/\hbar)\hat{x}$ and $L_2=(\sqrt{D}/\hbar)\hat{y}$ and uses the first-order Euler method, shown to be accurate for statistical expectation values [17], to integrate Eq. (4). That is, we solve

$$|\psi(t+\delta t)\rangle=\exp(-iH\delta t/\hbar)|\psi(t)\rangle + \frac{D}{\hbar^2}(2\langle x\rangle x-x^2-\langle x\rangle^2)|\psi(t)\rangle + \frac{\sqrt{D}}{\hbar}(x-\langle x\rangle)|\psi(t)\rangle W_1+\frac{D}{\hbar^2}(2\langle y\rangle y-y^2-\langle y\rangle^2)|\psi(t)\rangle + \frac{\sqrt{D}}{\hbar}(y-\langle y\rangle)|\psi(t)\rangle W_2, \quad (5)$$

where δt is the integration time step, and where W_1, W_2 are two ordinary independent complex random variables with (where M denotes the mean) $M((\mathrm{Re}\,W_1)^2)=M((\mathrm{Im}\,W_1)^2)=M((\mathrm{Re}\,W_2)^2)=M((\mathrm{Im}\,W_2)^2)=\delta t$; $M(W_1)=M(W_2)=0$. The Hamiltonian dynamics is carried out via the split operator fast Fourer transform (FFT) technique [18]. Thus, combining the FFT approach and the Euler integration scheme gives a general systematic approach to the wave packet dynamics in the quantum state diffusion picture for nonlinear oscillator systems, even far from the semiclassical limit.

Below we compare these results to classical mechanics by obtaining the classical phase space density $\rho_t(x,y,p_x,p_y)$ which satisfies the Fokker-Planck equation:

$$\frac{\partial}{\partial t}\rho_t(x,y,p_x,p_y) = \{H,\rho_t(x,y,p_x,p_y)\} + D\left(\frac{\partial^2}{\partial p_x^2}\rho_t(x,y,p_x,p_y)+\frac{\partial^2}{\partial p_y^2}\rho_t(x,y,p_x,p_y)\right). \quad (6)$$

In the closed system case ($D=0$) we do this by solving Hamilton's equations to obtain the classical trajectories; 5×10^4 trajectories were found sufficient for convergence. Similarly, in the open system case ($D\neq0$) ρ is obtained by integrating the Langevin-Itô equations for each sample trajectory:

$$dx=\frac{\partial H}{\partial p_x}dt,\quad dy=\frac{\partial H}{\partial p_y}dt,$$
$$dp_x=-\frac{\partial H}{\partial x}dt+\sqrt{2D}\,\eta_1,\quad dp_y=-\frac{\partial H}{\partial y}dt+\sqrt{2D}\,\eta_2. \quad (7)$$

Here $\eta_i, i=1,2$ are independent real differential stochastic variables satisfying $M(\eta_1)=M(\eta_2)=0$, $M(\eta_1^2)=M(\eta_2^2)=dt$. Once again, Monte Carlo sampling from the initial distribution and Euler integration of Eq. (7) gave converged results for ρ with $(2-4)\times10^4$ sample trajectories and a total of 30 to 50 realizations of η_1 and η_2 for each sample trajectory.

III. COMPUTATIONAL RESULTS

As a specific example we chose to examine quantum-classical correspondence using an initial $\psi(x,y,0)$ given as a two-dimensional coherent state with Wigner function,

$$\rho_0(x,y,p_x,p_y)=\left(\frac{1}{\pi^2}\right)\exp\left(-\frac{(x-\bar{x})^2}{\hbar}-\frac{(y-\bar{y}^2)}{\hbar}-\frac{(p_x-\bar{p}_x)^2}{\hbar}-\frac{(p_y-\bar{p}_y)^2}{\hbar}\right), \quad (8)$$

where $\bar{x}$, $\bar{y}$, $\bar{p}_x$, and $\bar{p}_y$ are mean positions and momenta, respectively. In the computations reported below [19] $\hbar=0.1$, $\Delta t=0.002$, $D=6\times10^{-4}$, $\bar{x}=0.40$, $\bar{y}=0.60$, $\bar{p}_x=0.50$, $\bar{p}_y=0.414$ with a spatial grid spacing of $\Delta x=\Delta y$

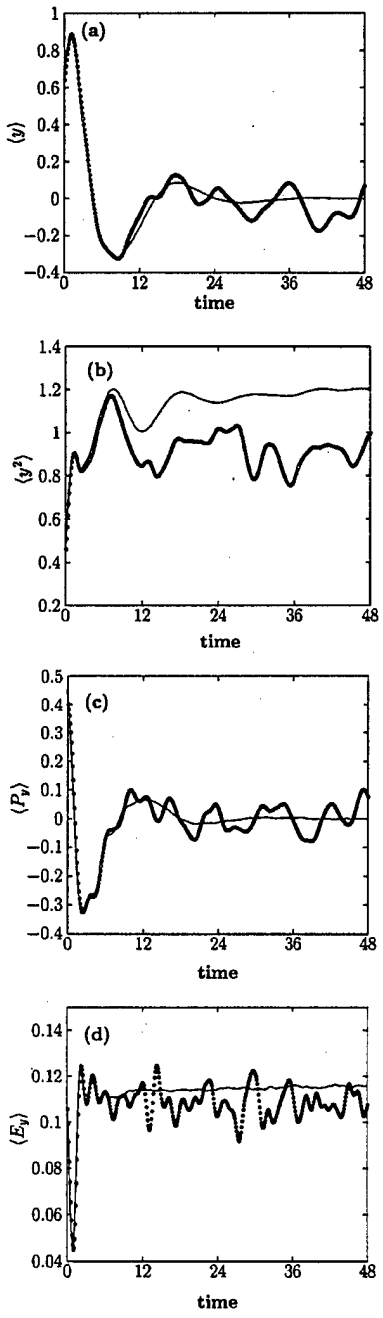

FIG. 1. Time dependence of four statistical moments ($\langle y\rangle$, $\langle y^2\rangle$, $\langle P_y\rangle$, and $\langle E_y\rangle$) for the closed chaotic system case. Dark dots denote quantum results, thin solid lines are classical results. All variables are in dimensionless units [19].

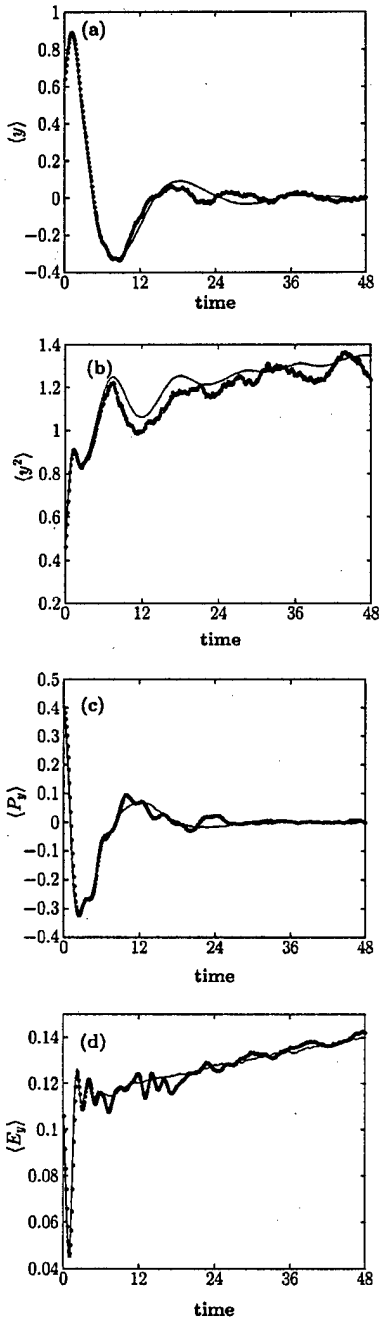

FIG. 2. Same as Fig. 1, but for the open chaotic system case.

$=0.16$. Convergence was checked by decreasing the time steps, enlarging the grid size, and by increasing S, with $S=1000$ found sufficient to obtain convergent results. In addition, energy absorption was in accord with the theoretical prediction cited above.

Note first that our choice of D lies close to the border of the quantum-classical transition predicted by Eq. (2). That is, this two-dimensional system has three characteristic potential lengths χ, $\sqrt{|\partial_x V/\partial_x^3 V|}$, $\sqrt{|\partial_x V/\partial_x^2\partial_y V|}$, and $\sqrt{|\partial_x V/\partial_x\partial_y^2 V|}$. For the energy region of interest their average values are 8, 1.5, and 1, respectively. With $\lambda\approx 0.5$ for $\alpha=1.0$ and approximately two times smaller for $\alpha=0.1$, the inequality (2) is satisfied for at least one of these lengths.

We consider first a comparison of classical and quantum mechanics for the closed (i.e., $D=0$) system, as shown through expectation values of coordinates and momenta and "energy in a zeroth-order mode," e.g., for y, $\langle E_y\rangle=\langle p_y^2/2+(\beta/4)y^4\rangle$. Figure 1 shows the classical and quantum expectation values for four moments associated with y. Analogous results were obtained in the x variable. All figures show qualitatively similar behavior, i.e., after an initial period of classical/quantum agreement the quantum results continue to oscillate while the classical results show smooth relaxation [20]. Computational results in the less chaotic regime ($\alpha=0.1$) showed similar results except that the deviation be-

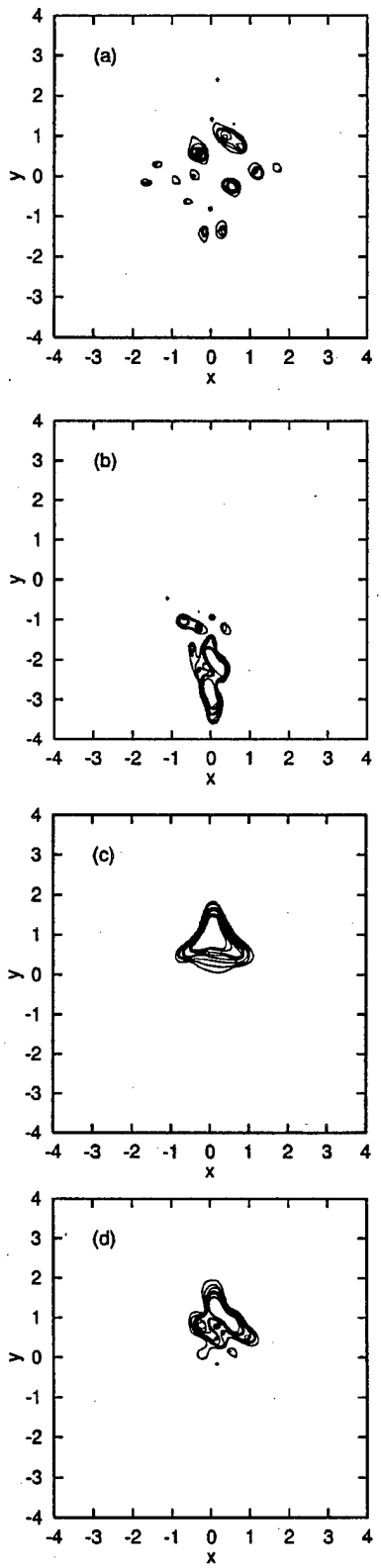

FIG. 3. Contours of constant wave function intensity at $t=25$ for propagation, for the chaotic case, from the same initial state: (a) shows results for the closed system ($D=0$); (b), (c), and (d) show results for different realizations with nonzero D. All variables are in dimensionless units [19].

tween the classical and quantum is significantly less in the $\alpha=0.1$ case, and the classical-quantum discrepancy begins at a later time. Note also that the quantum results do not always simply oscillate about the classical (e.g., see results for $\langle y^2\rangle$) and that the quantum fluctuations about the mean are substantial (e.g., 30% in the case of $\langle E_y\rangle$).

Results for the same moments, after introducing decoherence, are shown in Fig. 2. A comparison of Figs. 1 and 2 shows substantially improved classical-quantum correspondence upon introducing decoherence. In particular, Fig. 2(a) and Fig. 2(c) show that quantum oscillations in the first-order moments are strongly suppressed by decoherence. More remarkable is the observed correspondence for the case of $\langle y^2\rangle$ [see Fig. 2(b)], in which the long term quantum average in the closed system deviated significantly from the long term classical average. This indicates decoherence delocalizes quantum distribution functions within the energy shell, a conservative-system analog of the noise-induced delocalization seen in one-dimensional quantum chaotic systems [6,7,9]. Finally, the correspondence in $\langle E_y\rangle$ is shown in Fig. 2(d), suggesting that the energy transfer between different degrees is also strongly affected by decoherence effects. We also note that similar improved agreement was obtained for moments of x and for the $\alpha=0.1$ case.

Further insight into the effect of decoherence results from examining individual realizations within the QSD approach. For example, Fig. 3 shows four quantum wave functions at $t=25$, each emerging from the same time zero initial wave function. Figure 3(a) shows the result of propagation in the absence of decoherence and Figs. 3(b)–3(d) show three different $|\psi(\xi_m(t),t)\rangle$ at $t=25$, a time by which decoherence appears to have restored considerable correspondence (see Fig. 2). A comparison of Figs. 3(b)–3(d) with Fig. 3(a) shows that the former has far less structure than the latter; indeed Fig. 3(c) shows that decoherence has changed the complex structure in Fig. 3(a) into a single peak. In essence, the competition between the Hamiltonian chaos (which tends to exponentially [21] increase the wave packet structure) and the stronger decoherence effect (which tends to suppress the wave packet structure) is vividly demonstrated here.

Note, finally, that since the parameters chosen above lie in the range expected of a typical molecule, our results suggest the possibility of experimentally observing these effects in the vibrational motion of excited polyatomics. To see this, note that a convenient dimensionless unit to compare systems is the fraction $F(t)$ of energy absorbed per degree of freedom from the bath per vibrational oscillatory period $2\pi/\omega$, relative to the level spacing $\hbar\omega$, where ω is the vibrational period. That is, $F(t)=(D/m)(2\pi/\omega)(1/\hbar\omega)$. From Eq. (2) we have

$$F(t)=2\pi D/(m\hbar\omega^2)>\pi\hbar\lambda/(m\chi^2\omega^2)\approx\pi\hbar/(\chi^2 m\omega), \tag{9}$$

where we have assumed [22] $\lambda\approx\omega$. Typical sizes of the right hand side of the equation for a small molecule are on the order of 10^{-3}, in the same range as that obtained for the model adopted in this paper. With the right hand side of Eq. (9) being the ratio of $\hbar$ to a typical system action, the small molecule is seen to be of the same order of "quantumness" as the adopted model.

IV. SUMMARY

We have shown for a generic conservative chaotic Hamiltonian system that decoherence does indeed lead to significant improvement in classical-quantum correspondence. That is, the tendency for the evolving phase space distribution in chaotic dynamics to fragment exponentially fast is compensated by the smoothing effect of the externally induced decoherence and classical-quantum agreement is significantly improved. Indeed, the stronger the chaos, and hence the fragmentation, the more effective is the decoherence [23], so the balance between them is expected to be retained over a wide range of λ. This is the case even though our studies are in the quantum regime so that the required magnitude of the decoherence leads to substantial difference between the classical results in the presence and absence of decoherence. Nonetheless, correspondence is much improved by the decoherence effects, i.e., *quantum mechanics plus decoherence effects* is in far better agreement with the *classical mechanics plus decoherence effects* than is the analogous comparison in the absence of decoherence. This agreement is expected to improve even further as one approaches the classical limit.

ACKNOWLEDGMENTS

We thank the Natural Sciences and Engineering Research Council of Canada and the U.S. Office of Naval Research for support of this research.

[1] J. Wilkie and P. Brumer, Phys. Rev. A **55**, 27 (1997); **55**, 43 (1997).

[2] W.H. Zurek and J.P. Paz, Phys. Rev. Lett. **72**, 2508 (1994); **75**, 351 (1995).

[3] W.H. Zurek, http://xxx.lanl.gov, e-print quant-ph/9802054.

[4] D. Giulini, E. Joos, C. Kiefer, J. Kupsch, I.O. Stamatescu, and H.D. Zeh, *Decoherence and the Appearance of a Classical World in Quantum Theory* (Springer, Berlin, 1996).

[5] See Letters to the Editor in Phys. Today **46** (4), 81 (1993).

[6] E. Ott, T.M. Antonsen, Jr., and J.D. Hanson, Phys. Rev. Lett. **53**, 2187 (1984).

[7] D. Cohen, Phys. Rev. A **43**, 639 (1991); **44**, 2292 (1991).

[8] K. Shiokawa and B.L. Hu, Phys. Rev. E **52**, 2497 (1995).

[9] R. Graham and S. Miyazaki, Phys. Rev. A **53**, 2683 (1996); P. Goetsch and R. Graham, *ibid.* **54**, 5345 (1996).

[10] L. Bonci, P. Grigolini, A. Laux, and R. Roncaglia, Phys. Rev. A **54**, 112 (1996).

[11] S. Habib, K. Shizume, and W. Zurek, Phys. Rev. Lett. **80**, 4361 (1998).

[12] A.O. Caldeira and A.J. Leggett, Physica A **121**, 587 (1983); W.G. Unruh and W.H. Zurek, Phys. Rev. D **40**, 1071 (1989); B.L. Hu, J.P. Paz, and Y. Zhang, *ibid.* **45**, 2843 (1992); **47**, 1576 (1993).

[13] A.R. Kolovsky, Europhys. Lett. **27**, 79 (1994); Phys. Rev. Lett. **76**, 340 (1996).

[14] J.C. Flores, Europhys. Lett. **29**, 653 (1995).

[15] N. Gisin and I. Percival, J. Phys. A **25**, 5677 (1992), and references therein.

[16] See, e.g., B. Eckhardt, G. Hose, and E. Pollak, Phys. Rev. A **39**, 3776 (1989).

[17] G.N. Milstein, *Numerical Integration of Stochastic Differential Equations* (Kluwer, Dordrecht, 1995).

[18] M.D. Feit, J.A. Fleck, and A. Steiger, J. Comput. Phys. **47**, 412 (1982).

[19] Note that we begin with a dimensionless scaled Hamiltonian [Eq. (3)]. As a result, all relevant variables are understood to be dimensionless and scaled. The relation between the scaled variables and unscaled variables is, however, crucial for retrieving specific units when necessary. For a general Hamiltonian $\tilde{H}=\tilde{p}_x^2/2m_1+\tilde{p}_y^2/2m_2+\tilde{V}(\tilde{x},\tilde{y})$ with all variables with tildes denoting ordinary unscaled variables, we can define the dimensionless scaled variables $x\equiv\sqrt{m_1\omega/\ell}\,\tilde{x}$, $p_x\equiv\sqrt{1/m_1\omega\ell}\,\tilde{p}_x$, $y\equiv\sqrt{m_2\omega/\ell}\,\tilde{y}$, and $p_y\equiv\sqrt{1/m_2\omega\ell}\,\tilde{p}_y$. Here ℓ has units of action, and m_i and ω are ordinary constants with units of mass and frequency. Typically, ω is taken as the average frequency of this system and ℓ is taken to scale the true Planck constant; that is, $\hbar=\tilde{\hbar}/\ell$, where $\tilde{\hbar}$ is the ordinary Planck constant and $\hbar$ is the dimensionless scaled Planck constant. The scaled variables satisfy the canonical equations of motion for the scaled time $t=\omega\tilde{t}$ and the scaled Hamiltonian $H=\tilde{H}/\ell\omega$. For quantum descriptions one can verify that $[x,p_x]=i\hbar$, $[y,p_y]=i\hbar$.

[20] Analogous results were observed previously for the stadium billiard. See K.M. Christoffel and P. Brumer, Phys. Rev. A **33**, 1309 (1985).

[21] J. Gong and P. Brumer (unpublished).

[22] P. Brumer and M. Shapiro, Adv. Chem. Phys. **70**, 365 (1988).

[23] A.K. Pattanayak and P. Brumer, Phys. Rev. Lett. **79**, 4131 (1997).

JOURNAL OF CHEMICAL PHYSICS VOLUME 110, NUMBER 1 1 JANUARY 1999

Coherent enhancement and suppression of reactive scattering and tunneling

Einat Frishman and Moshe Shapiro[a)]
Chemical Physics Department, The Weizmann Institute of Science, Rehovot, Israel 76100

Paul Brumer
Chemical Physics Theory Group, Department of Chemistry, University of Toronto, Toronto, Canada, M5S 3H6

(Received 4 September 1998; accepted 27 October 1998)

An optimization approach to coherent control of scattering is introduced and used to show that one can totally suppress reaction at energy E if the number of populated initial states exceeds the number of open product states (as in endoergic reactions). Numerical results on a multichannel system are presented. © *1999 American Institute of Physics.* [S0021-9606(99)04601-2]

Processes arising from collisions between atoms or molecules are ubiquitous in Physics and Chemistry. Recently[1,2] we showed that it is possible to use coherent control,[3] a quantum-interference based method of controlling atomic and molecular processes, to alter the outcome of such processes. This constitutes a major advance in the range of applicability of quantum control techniques which have traditionally been applicable only to processes involving single species (e.g., molecular photodissociation).[4]

In this letter we describe an optimization procedure for reactive scattering and demonstrate an important general result in the control of collision processes. That is, we show that if the number of open reactive product states is less than the number of open reactant states, then one can use quantum interference to completely suppress reactive scattering. The particular example of suppression of tunneling is computationally demonstrated below.

Consider reactive scattering (e.g., $A+B\rightarrow C+D$) from the initial arrangement channel α described by asymptotic channel Hamiltonians H_α^0 to the product arrangement channel β described by asymptotic channel Hamiltonians H_β^0. (The generalization to multiple product arrangement channels is straightforward.) We wish to control the outcome of this scattering process and note that it suffices to focus attention on scattering at fixed energy E since each energy contributes independently to the final product cross sections.[5]

We denote the eigenstates of H_α^0 and H_β^0 at energy E by $|i,E,\alpha\rangle$ and $|f,E,\beta\rangle$, respectively. Standard scattering theory,[6] gives the probability $p(f,\beta;i,\alpha)$ of producing product in final state $|f,E,\beta\rangle$ having started in the initial state $|i,E,\alpha\rangle$ as

$$p(f,\beta;i,\alpha)=|S_{fi}|^2, \tag{1}$$

where $S_{fi}=\langle f,E,\beta|S|i,E,\alpha\rangle$ and where S is the scattering matrix for the process. The total probability $P(\beta;i,\alpha)$ of scattering into arrangement channel β, assuming m open product states, is given by

$$P(\beta;i,\alpha)=\sum_{f=1}^{m}|S_{fi}|^2. \tag{2}$$

To simplify the notation we have not carried an E label in the probabilities: Fixed energy E is understood.

Consider now, instead, scattering from an initial state $|\mathbf{c},E,\alpha\rangle$ comprised of a linear superposition of k energetically degenerate scattering states, i.e.,

$$|\mathbf{c},E,\alpha\rangle=\sum_{i=1}^{k}c_i|i,E,\alpha\rangle. \tag{3}$$

The probability of forming $|f,E,\beta\rangle$ from this initial state is

$$p(f,\beta;\mathbf{c},\alpha)=\left|\sum_{i=1}^{k}c_iS_{fi}\right|^2, \tag{4}$$

and the total reactive scattering probability into channel β, $P(\beta;\mathbf{c},\alpha)$, is

$$P(\beta;\mathbf{c},\alpha)=\sum_{f=1}^{m}\left|\sum_{i=1}^{k}c_iS_{fi}\right|^2. \tag{5}$$

Note, in Eq. (5), the distinctly different character of the two sums: i.e., the incoherent sum over probabilities to product states and the coherent sum over amplitudes from initial states. The latter sum will, as shown below, allow control over the reactive scattering.

To simplify the notation below we introduce the matrix $\boldsymbol{\sigma}=\mathbf{S}_\beta^\dagger\mathbf{S}_\beta$ with elements $\sigma_{ij}=\Sigma_{f=1}^{m}S_{fj}^*S_{fi}$ which allows us to rewrite Eq. (5) as

$$P(\beta;\mathbf{c},\alpha)=\mathbf{c}^\dagger\boldsymbol{\sigma}\mathbf{c}. \tag{6}$$

Here the daggers denote the Hermitian conjugate and the β subscript on the $\mathbf{S}$ indicates that we are dealing with the submatrix of the S matrix associated with scattering into product channel β.

We now optimize scattering into arrangement channel β, with the normalization constraint $\Sigma_{i=1}^{k}|c_i|^2=1$, by requiring

a)Electronic mail: cfshapir@weizmann.weizmann.ac.il

 © 1999 American Institute of Physics

Downloaded 03 Oct 2001 to 142.150.224.5. Redistribution subject to AIP license or copyright, see http://ojps.aip.org/jcpo/jcpcr.jsp

$$\frac{\partial}{\partial c_k^*}\left[P(\beta;\mathbf{c},\alpha)-\lambda\sum_{i=1}^{k}|c_i|^2\right]=\frac{\partial}{\partial c_k^*}[\mathbf{c}^\dagger\boldsymbol{\sigma}\mathbf{c}-\lambda\mathbf{c}^\dagger\mathbf{c}]=0, \tag{7}$$

where λ is a Lagrange multiplier. Explicitly taking the derivative gives the result that the optimized coefficients $\mathbf{c}_\lambda$ satisfy the eigenvalue equation

$$\boldsymbol{\sigma}\mathbf{c}_\lambda=\lambda\mathbf{c}_\lambda. \tag{8}$$

Additional labels may be necessary to account for degeneracies of the eigenvectors $\mathbf{c}_\lambda$. Note also that Eq. (8) also results from taking derivatives in Eq. (7) with respect to c_k, since $\boldsymbol{\sigma}$ is Hermitian.

Below we examine a model case to obtain the maximum and minimum tunneling possible as a function of energy. Here, however, we focus on the fact that if $\lambda=0$ is an eigenvalue of Eq. (8) with eigenfunctions $\mathbf{c}_0$ then by inserting Eq. (8) into Eq. (6) we have that $P(\beta;\mathbf{c}_0,\alpha)=0$. That is, if $\lambda=0$ is a solution to Eq. (8) then the coefficients $\mathbf{c}_0$ completely suppress reaction into arrangement channel β.

Clearly, $\lambda=0$ is a solution if

$$\det(\boldsymbol{\sigma})=\det(\mathbf{S}_\beta^\dagger\mathbf{S}_\beta)=0, \tag{9}$$

which is the case if the number of initial levels k participating in the initial superposition [Eq. (3)] is greater than the number m of open product states, a situation which invariably occurs for endoergic processes. To see this result note that, under these circumstances, $\boldsymbol{\sigma}$ is a matrix of order $k\times k$ and $\mathbf{S}_\beta$ is of order $k\times m$. If $k>m$ then we can construct a $k\times k$ order matrix $\mathbf{A}_\beta$ by adding a submatrix of $(k-m)$ rows of zeroes to the lower part of $\mathbf{S}_\beta$. Then

$$\det(\boldsymbol{\sigma})=\det(\mathbf{S}_\beta^\dagger\mathbf{S}_\beta)=\det(\mathbf{A}_\beta^\dagger\mathbf{A}_\beta)=\det(\mathbf{A}_\beta^\dagger)\det(\mathbf{A}_\beta)=0. \tag{10}$$

The last equality holds because the determinants of $\mathbf{A}_\beta$ and $\mathbf{A}_\beta^\dagger$ are zero.

Consider now the particular case of tunneling in one dimension where the system has N open incident channels, both as an example of the optimization procedure and of the total control achievable under the conditions described above. Here arrangement α corresponds to particles incident on the barriers through which they tunnel, and arrangement β corresponds to the particles after tunneling. The dynamics is described by the N coupled channel Schrödinger equations

$$\Psi''(r)=-\frac{2\mu}{\hbar^2}(\mathbf{E}-\mathbf{V})\Psi(r), \tag{11}$$

where μ is the relevant mass, $\mathbf{V}$ is the potential matrix, $\mathbf{E}$ is a diagonal matrix with elements E, and N is the total number of open channels in arrangement α.

As a computational example consider an $N=4$. We choose a potential matrix described by Eckart potentials of the form

$$V_{k\ell}(r)=-\frac{\alpha_{k\ell}\xi}{1-\xi}-\frac{b_{k\ell}\xi}{(1-\xi)^2}+c_{k\ell},\quad (k,\ell=1,\ldots,4), \tag{12}$$

where $\xi=-\exp(2\pi r/t)$, with t a distance potential parameter. The matrix elements are shown in Fig. 1. The S matrix elements for this problem are computed by direct numerical propagation of Eq. (11) and the solutions to Eq. (8) are determined to obtain the optimal coefficients.

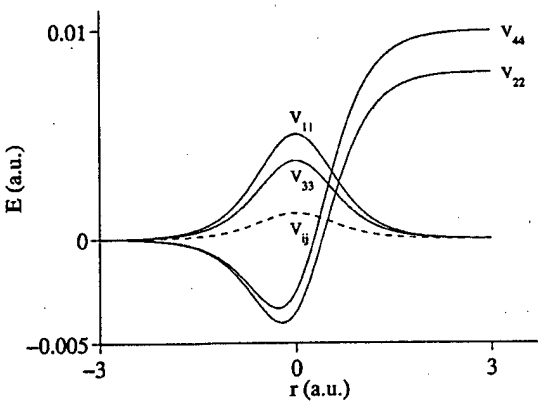

FIG. 1. Elements of the potential matrix for the model scattering problem. V_{ij} denotes the three off diagonal matrix elements $i\neq j$, which are all equal. The nonzero a_{ij},b_{ij},c_{ij} elements [Eq. (12)] are given (in a.u.) by $b_{11}=0.02$, $a_{22}=0.008$, $b_{22}=-0.03$, $b_{33}=0.015$, $a_{44}=0.01$, $b_{44}=-0.03$, $b_{ij}=0.005$, $i\neq j$ with $t=2.5$, and $\mu=0.6666$ a.m.u.

Reactivity is shown as a function of energy in Fig. 2 for the case where the number of populated initial states k is less than N: Here $k=3$. The curves labeled P_i correspond to the standard $P(\beta;i,\alpha)$, i.e., total reaction probability from each of the individual initial states. The quantities P_1 and P_3, which are open asymptotically at all energies, show a gradual rise with increasing energy, whereas P_2, which is closed on the product side until $E_{\text{th}}(3)=0.008$ a.u., stays rather small until $E=E_{\text{th}}(3)$, where it displays a very rapid rise to near unity. Total reaction probability reaches unity above $E_{\text{th}}(4)=0.010$ a.u., the threshold for the opening of the fourth channel.

The main computational results, shown as solid curves in Fig. 2, are the maximum and minimum reactivity obtained

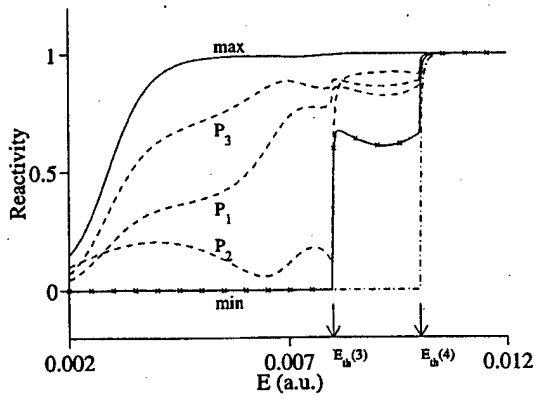

FIG. 2. Reactivity shown as a function of energy. Dashed curves labeled P_i correspond to the total reactivity $P(\beta;i\alpha)$ from each of the three individual initial states in the prepared superposition. Solid curves with crosses denote the reactivity obtained by solving Eq. (8) for the optimal solutions. The two arrows indicate the threshold energies for opening of the third and fourth channels (see Fig. 1). The dot–dash curve shows the minimum reactivity resulting from a separate computation which includes four states in the initial superposition.

Downloaded 03 Oct 2001 to 142.150.224.5. Redistribution subject to AIP license or copyright, see http://ojps.aip.org/jcpo/jcpcr.jsp

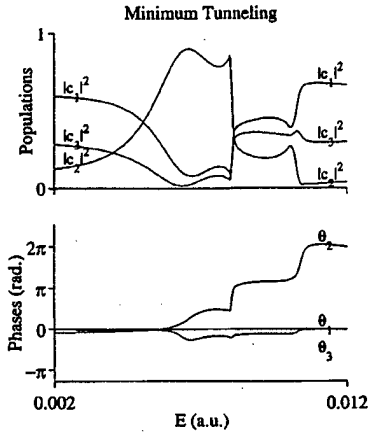

FIG. 3. Optimal coefficients associated with the minimal solutions shown in Fig. 2.

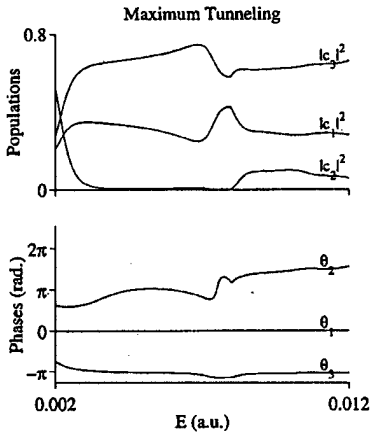

FIG. 4. As in Fig. 3 but for the maximal solutions.

from the optimal solutions to Eq. (8). The maximum reactivity is seen to be substantially larger than any of the individual P_i and to reach unity at significantly lower energies than any of these solutions. Minimal reactivity, as predicted by the argument presented above, is seen to be zero for $E < E_{\text{th}}(3)$ since the total number of states ($k=3$) in the superposition exceeds the number of open product states ($m=2$). At $E > E_{\text{th}}(3)$ a third product channel opens so that $k=m$ and the minimal solution is no longer zero. Nevertheless, it remains smaller than the reactivity for each of the individual states P_i. Note, however, that it is still possible to zero the tunneling over the energy region 0.008 a.u.$< E <$0.010 a.u. by adding an additional state to the initial superposition and re-solving Eq. (8). In this energy regime $k=4 > m=3$ so that total suppression of tunneling continues to be possible. This result is shown as a dot–dashed curve in Fig. 2.

Note that the minimum reactivity curve in Fig. 2 reflects a variety of different interesting behaviors, depending on the particular energy. Specifically, below the maximum of V_{11} at 0.005 a.u. the zero minimum corresponds to suppression of tunneling through that barrier. Above 0.005 a.u. the zero minimum corresponds to suppression of the reactive scattering that occurs *above* the barrier.

The $c_j = |c_j| \exp(i\theta_i)$ associated with the maximal and minimal solutions are shown in Figs. 3 and 4. The $|c_i|$ are seen to follow, except at channel thresholds, a natural trend. That is, the states with higher P_i are weighted more heavily in the case of maximal tunneling and vice versa for the minimal solution, except in some intermediate energy regions. The large weight attributed to the closed channel ($i=2$) in the minimal reactivity case is worth noting. That is, this channel is used as a lever to eliminate the reaction via destructive interference with the open channels, despite the fact that it itself is zero on the product side. The phases θ_2 and θ_3, shown relative to θ_1, are in phase with θ_1 in the minimum tunneling case and generally out of phase with θ_1 in the maximum tunneling case. Additional studies show that the optimal solutions are very sensitive to the values of the phases.

Finally, we note that the experimental realization of this general scenario requires the controlled preparation of superpositions of energetically degenerate scattering states. Preliminary suggestions for preparing such states have been given elsewhere.[1] For example, the simplest of such superpositions would entail superposing degenerate states of one of the reactants (e.g., m_j states of B) and colliding it with A. Alternatively, appropriate states may be prepared by an earlier coherently controlled photodissociation step.[1]

In summary, we have introduced a simple linear optimization scheme for reactive scattering and have analytically demonstrated that total suppression of reactive scattering is guaranteed when the number of product states is less than that of the number of initial reactant states included in a prepared scattering superposition state. As an obvious extension, a similar result holds for tunneling in bound systems, if the total number of initial degenerate states at the energy of interest exceeds the number of accessible final states at that energy.

Support for this work by the U.S. Office of Naval Research is gratefully acknowledged.

[1] M. Shapiro and P. Brumer, Phys. Rev. Lett. **77**, 2574 (1996).
[2] A. Abrashkevich, M. Shapiro, and P. Brumer, Phys. Rev. Lett. (in press).
[3] See, e.g., M. Shapiro and P. Brumer, J. Chem. Soc., Faraday Trans. **93**, 1263 (1997).
[4] See, e.g., R. G. Gordon and S. A. Rice, Annu. Rev. Phys. Chem. **48**, 595 (1997); D. J. Tannor, in *Molecules in Laser Fields*, edited by A. Bandrauk (Marcel Dekker, New York, 1994).
[5] The proof follows as in M. Shapiro and P. Brumer, J. Chem. Phys. **84**, 540 (1986).
[6] J. R. Taylor, *Scattering Theory* (Wiley, New York, 1972).

Downloaded 03 Oct 2001 to 142.150.224.5. Redistribution subject to AIP license or copyright, see http://ojps.aip.org/jcpo/jcpcr.jsp

24

Coherent Control of Reactive Scattering

Alexander Abrashkevich, Moshe Shapiro,* and Paul Brumer

Chemical Physics Theory Group, University of Toronto, and Photonics Research Ontario, Toronto, Canada M5S 3H6

(Received 11 December 1997)

Coherent control of bimolecular reactions is demonstrated for 3D atom-diatom reactive scattering. In particular, a superposition of initial degenerate (vjk) diatomic states is used to control reactive integral and differential cross sections in $D + H_2(vjk) \rightarrow H + HD$, where v and j are the vibrational and rotational quantum numbers of a diatom and k is the projection quantum number of the diatom angular momentum onto the initial relative translational velocity vector. Control over the ratio of reactive to nonreactive scattering is extensive. [S0031-9007(98)07470-5]

PACS numbers: 82.40.Dm, 34.50.Lf, 34.50.Rk

Controlling the dynamics of atoms and molecules has been a long-standing goal in physics. A recent approach, called coherent control, offers a systematic route to reaching this goal. Specifically, in coherent control one uses the quantum properties of light and matter to introduce quantum interference terms into the system dynamics; these terms, and hence the dynamical outcome, can be altered by manipulating laboratory parameters. This approach has proven successful, both theoretically and experimentally, in controlling the outcome of unimolecular processes such as photodissociation (see, e.g., [1–4]). By contrast, control over collisional processes has presented a much greater challenge [5].

In this paper we show that extensive control over quantum reactive scattering can indeed be attained by scattering from an initially prepared superposition of degenerate diatomic states, demonstrating the essence of coherent control in a fundamental collisional process. This constitutes a major extension of the range of possible applications of coherent control. In particular, we show, using the results of three-dimensional calculations for $D + H_2 \rightarrow H + HD$ on a realistic potential surface, that reactive vs nonreactive cross sections (both differential and integral) can be extensively controlled by varying phases and amplitudes in the initially prepared superposition state. Furthermore, the proposed approach is easily extended to any nonrelativistic scattering problem (e.g., atom-atom scattering, low energy nuclear scattering, etc.).

Consider the reaction $A + BC \rightarrow B + AC$ or $C + AB$, where we label the three possible arrangement channels by the symbol $\alpha = (A + BC)$, $b(B + AC)$, or $c(C + AB)$. We consider the simplest method of introducing interference effects into dynamics by examining scattering from an asymptotic state $|\mathbf{n}, \alpha\rangle$ which is an energetically degenerate superposition of scattering states composed of two degenerate states of the diatom. The extension to include more states is straightforward. Consider then

$$|\mathbf{n}, \alpha\rangle = \sum_{i=1,2} a_i |\alpha v j k_i\rangle |E_\alpha^{\mathrm{kin}}(i)\rangle |E_{\mathrm{cm}}(i)\rangle, \quad (1)$$

where $\mathbf{n}$ encapsulates all the state labels other than α, $|E_\alpha^{\mathrm{kin}}(i)\rangle$ are plane waves describing the free motion of the atom relative to the diatom for the α arrangement and $|E_{\mathrm{cm}}(i)\rangle$ describes the motion of the atom-diatom center of mass. The superposition state $|\mathbf{n}, \alpha\rangle$, assumed normalized, is therefore composed of two degenerate eigenstates $|\alpha v j k_i\rangle |E_\alpha^{\mathrm{kin}}(i)\rangle$ of the asymptotic α-channel Hamiltonian, where the quantum numbers v, j, and k_i denote the vibrational, rotational, and angular momentum projection quantum numbers of the diatomic. The latter, k_i, is taken as the helicity, i.e., the angular momentum projection along the relative initial translational velocity vector, and the diatom states $|\alpha v j k_i\rangle$ are of energy $\epsilon_{\alpha v j}$.

Traditional time independent scattering theory deals with asymptotic states where one of the $a_i = 0$, so that scattering correlates with one asymptotic state. The equations below are a direct, but significant, extension of these traditional results. In particular, the differential cross section for forming the α' arrangement at scattering angle θ, having started from the $|\mathbf{n}, \alpha\rangle$ superposition state [Eq. (1)], is given by

$$\sigma^R(\theta) = \sum_{v', j', k'} \left| \sum_{m=1,2} \left\langle E_{\mathrm{cm}}(m) \left| \sum_{i=1,2} a_i f_{\alpha' v' j' k' \leftarrow \alpha v j k_i}(\pi - \theta) \right| E_{\mathrm{cm}}(i) \right\rangle \right|^2, \quad (2)$$

where the superscript R denotes reactive scattering into a specific final arrangement channel $\alpha' \neq \alpha$ and where the scattering amplitude is

$$f_{\alpha' v' j' k' \leftarrow \alpha v j k_i}(\theta) = (2 i \mathrm{k}_{\alpha v j})^{-1} \sum_J (2J + 1) d^J_{k' k_i}(\theta) \times [S^J_{\alpha' v' j' k', \alpha v j k_i} - \delta_{\alpha' \alpha} \delta_{v' v} \delta_{j' j} \delta_{k' k_i}]. \quad (3)$$

Here $S^J_{\alpha' v' j' k', \alpha v j k_i}$ are the elements of scattering S matrix in the helicity representation, J is the total angular momentum, k' is the helicity of the product diatom (i.e., the projection of the diatom angular momentum onto the final relative translational velocity vector), $d^J_{k' k_i}(\theta)$ are the reduced rotation matrices [6], and $\mathrm{k}_{\alpha v j} = \sqrt{2\mu_\alpha (E - \epsilon_{\alpha v j})}/\hbar$, with μ_α being the

 © 1998 The American Physical Society

atom-diatom reduced mass in the α channel. Expanding the square in Eq. (2) gives the reactive differential scattering cross section as

$$\sigma^R(\theta) = |a_1|^2\sigma_{11}^R(\theta) + |a_2|^2\sigma_{22}^R(\theta) + 2\,\mathrm{Re}\{a_1^* a_2 \sigma_{12}^R(\theta)\}, \tag{4}$$

where

$$\sigma_{ii}^R(\theta) = \sum_{v',j',k'} |f_{\alpha' v' j' k' \leftarrow \alpha v j k_i}(\pi - \theta)|^2, \qquad i = 1,2, \tag{5}$$

$$\sigma_{12}^R(\theta) = \sum_{v',j',k'} \langle E_{\mathrm{cm}}(1) \mid E_{\mathrm{cm}}(2)\rangle_V f_{\alpha' v' j' k' \leftarrow \alpha v j k_1}(\pi - \theta) \times f^*_{\alpha' v' j' k' \leftarrow \alpha v j k_2}(\pi - \theta). \tag{6}$$

In the cases considered here, i.e., a superposition of degenerate diatomic states, the overlap $\langle E_{\mathrm{cm}}(1) \mid E_{\mathrm{cm}}(2)\rangle_V$ of the center of mass wave functions over the scattering volume V, which appears in Eq. (6), is unity.

Integration of Eq. (4) over angle θ gives the integral reactive cross section σ^R. This can also be written as three terms, as in Eq. (4), but with $\sigma_{ij}^R(\theta)$ replaced by σ_{ij}^R where

$$\sigma_{ii}^R = \frac{\pi}{k_{\alpha v j}^2} \sum_{v',j',k'} \sum_J (2J+1)\,|S^J_{\alpha' v' j' k', \alpha v j k_i}|^2, \qquad i = 1,2, \tag{7}$$

$$\sigma_{12}^R = \frac{\pi}{2k_{\alpha v j}^2} \langle E_{\mathrm{cm}}(1) \mid E_{\mathrm{cm}}(2)\rangle_V \sum_{v',j',k'} \sum_{J,J'} (2J+1)(2J'+1) S^J_{\alpha' v' j' k', \alpha v j k_1} [S^{J'}_{\alpha' v' j' k', \alpha v j k_2}]^* \times \int_0^\pi d\theta \sin\theta\, d^J_{k' k_1}(\pi - \theta) d^{J'}_{k' k_2}(\pi - \theta), \qquad \alpha \neq \alpha'. \tag{8}$$

Note that $\sigma_{ii}^R(\theta)$ and σ_{ii}^R in Eqs. (5) and (7) are the differential and integral cross sections that appear in standard scattering theory, while $\sigma_{12}^R(\theta)$ and σ_{12}^R in Eqs. (6) and (8) are new types of interference terms which allow for control through the a_i over the atom-diatom collision process. Note further that significant control requires substantial σ_{12}^R and, by the Schwartz inequality $[|\sigma_{12}^R| \leq \sqrt{\sigma_{11}^R \sigma_{22}^R}\,]$, large σ_{11}^R and σ_{22}^R. Significantly then, extensive control is not limited to regions near the reactive threshold [7]. Further, although Eqs. (4), (7), and (8) indicate that the differential and total reactive cross sections are controllable, removing the sums over v', j', and k' shows that detailed cross sections to product states $|\alpha', v', j', k'\rangle$ can also be controlled.

Thus, by varying the coefficients a_i in Eq. (1) through an initial preparation step, we can directly alter the interference term σ_{12}^R and hence control the scattering cross sections. Such a preparation might be carried out, for example, by a suitably devised molecular beam experiment where the diatomic is excited, via elliptically polarized light to a collection of well defined m_j states. Alternatively, the prereactive step may consist of coherently controlling the photodissociation of a polyatomic molecule [1] to produce the diatom in a controlled superposition of k states relative to an incoming scattering partner. For example, in the D + H_2 case considered below we can subject H_2S to a coherently controlled preparatory step producing H_2. Aiming the D atom exactly antiparallel to the direction of motion of the H_2 will then produce the desired scattering of a k superposition.

To examine the extent of control it is useful to rewrite the total reactive cross section in the form

$$\sigma^R = [\sigma_{11}^R + x^2\sigma_{22}^R + 2x|\sigma_{12}^R| \times \cos(\delta_{12}^R + \phi_{12})]/(1 + x^2), \tag{9}$$

where $x = |a_2/a_1|$, $\phi_{12} = \arg(a_2/a_1)$, and $\delta_{12}^R = \arg(\sigma_{12}^R)$. Of greatest interest is control over the reactive to nonreactive cross section branching ratio which is given by

$$\frac{\sigma^R}{\sigma^{\mathrm{NR}}} = \frac{\sigma_{11}^R + x^2\sigma_{22}^R + 2x|\sigma_{12}^R|\cos(\delta_{12}^R + \phi_{12})}{\sigma_{11}^{\mathrm{NR}} + x^2\sigma_{22}^{\mathrm{NR}} + 2x|\sigma_{12}^{\mathrm{NR}}|\cos(\delta_{12}^{\mathrm{NR}} + \phi_{12})}, \tag{10}$$

where the nonreactive terms are denoted NR and have definitions analogous to their reactive counterparts (i.e., α' is replaced by α in the defining equations for the cross sections). A formula similar to Eq. (10) holds for the ratio of reactive to nonreactive differential cross sections with total cross section terms replaced by differential cross section terms; that is, with σ_{mn}^R replaced by $\sigma_{mn}^R(\theta)$, etc.

In this Letter we apply this approach to D + H_2 → H + HD at $E = 1.25$ eV. In particular, we expose the dependence of the cross sections on a_i. Scattering calculations were done with the log-derivative version of the Kohn variational principle [8] using a basis set contraction approach [9], and cross sections were obtained via the symmetrization procedure described in Ref. [10]. Calculations were carried out using the accurate LSTH (Liu-Siegbahn-Truhlar-Horowitz) [11] potential energy surface for total angular momentum from $J = 0$ to 31 with $j_{\max} = 14$, ensuring fully converged cross sections for the chosen energy. It is worth noting that these calculations are CPU intensive, requiring in excess of 35 hours of CRAY T-90 time. Calculation of scattering amplitudes for all possible transitions took about 90 hours of the SGI PCA CPU time.

Control results for a specific initial vibrotational state ($v = 0, j = 2$) of diatom H_2 at scattering energy $E = 1.25$ eV are discussed below. (Qualitatively similar results were obtained for other initial states and for D + H_2 → H + HD and H + D_2 → D + HD [12].) This energy, rather far from the reaction threshold, allows us

to demonstrate substantial control in the presence of a significant natural reactive cross section.

Consider first the range of coherent control over the differential cross sections. Initial numerical tests showed that the best control over the $\sigma^R(\theta)/\sigma^{NR}(\theta)$ differential cross section ratio for transitions from initial states with $v = 0, j = 2$, and k_1, k_2 in the range $-2, -1, \ldots, 2$ occurred at $\theta \sim 60°$. Figure 1a shows results for this ratio and scattering angle as a function of relative phase ϕ_{12} and the amplitude parameter $s = x^2/(1 + x^2)$, for $k_1 = 1, k_2 = 0$. Varying s from zero to one corresponds to changing the initial superposition from scattering out of state one ($s = 0$, corresponding to $a_1 = 1, a_2 = 0$) to scattering out of the second state ($s = 1$ corresponding to $a_1 = 0, a_2 = 1$). The results clearly show substantial control over $\sigma^R(\theta)/\sigma^{NR}(\theta)$. That is, varying s and ϕ_{12} allows a change in the ratio from 0.23 to 1.01, compared with the uncontrolled ratio of ~0.55. Similarly, for example, the $\sigma^R(\theta)/\sigma^{NR}(\theta)$ ratio can be increased by a factor of 4.4 just by changing the phase angle ϕ_{12} from 260° to 67° at $s = 0.49$.

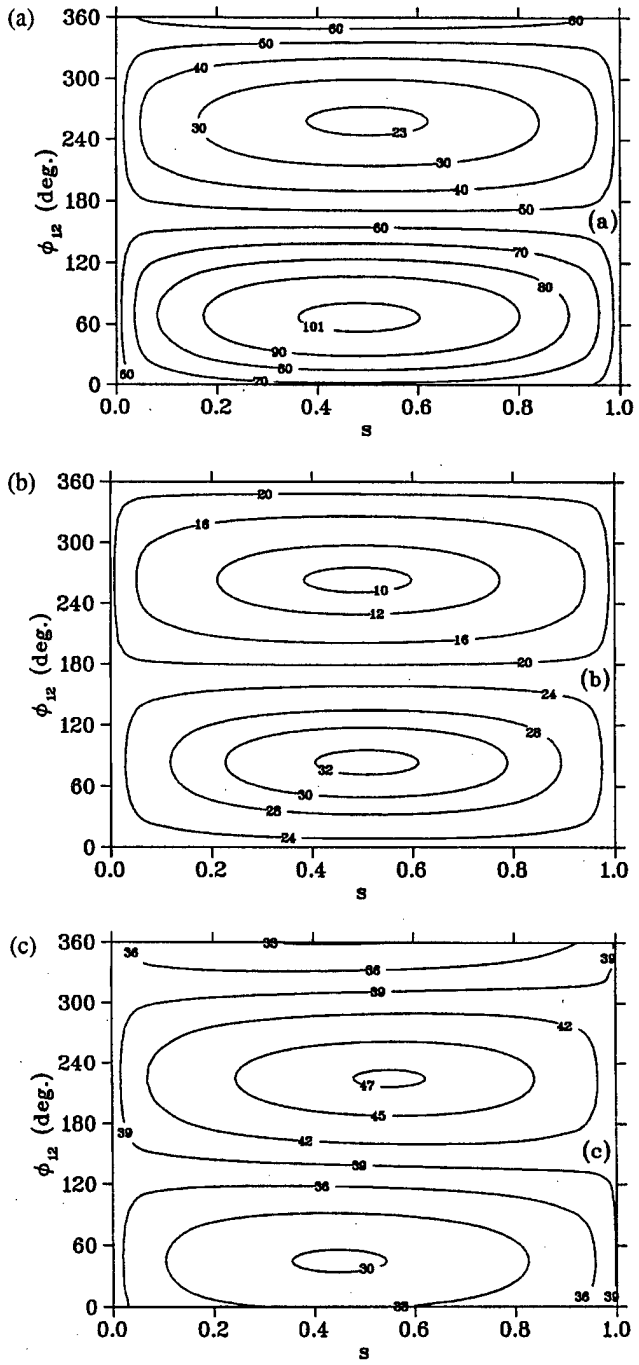

FIG. 1. Contour plot of the differential cross section as a function of ϕ_{12} and s, for a transition from an initial superposition state with $v = 0, j = 2, k_1 = 1, k_2 = 0$ at scattering angle $\theta = 60°$ and total energy $E = 1.25$ eV: (a) Reactive to nonreactive ratio $\sigma^R(\theta)/\sigma^{NR}(\theta)$, (b) reactive $\sigma^R(\theta)$, and (c) nonreactive $\sigma^{NR}(\theta)$. Contour values in (a), (b), and (c) report values of $\sigma \times 10^2$.

Figures 1b and 1c show the σ^R and σ^{NR} corresponding to Fig. 1a. Control over both $\sigma^R(\theta = 60°)$ and $\sigma^{NR}(\theta = 60°)$ is clearly seen, with σ^R ranging from $0.10a_0^2$ sr^{-1} to $0.32a_0^2$ sr^{-1} as s and ϕ_{12} are varied. This compares, for example, to the uncontrolled values of $\sigma_{11}^R(\theta) = 0.21$ sr^{-1} and $\sigma_{22}^R(\theta) = 0.22a_0^2$ sr^{-1} at $s = 0$ and $s = 1$. Similar control can be seen in σ^{NR}. Indeed, both the constructive enhancement of σ^R and the destructive depletion of σ^{NR} are seen to be responsible for the controlled σ^R/σ^{NR} maximum.

Also of interest is the θ dependence of $\sigma^R(\theta)/\sigma^{NR}(\theta)$ as a function of s and ϕ_{12}. Figure 2 shows the θ dependence of this ratio, for scattering from a superposition state composed of $v = 0, j = 2, k_1 = 2, k_2 = 0$ at $\phi_{12} = 157°$ and at four different values of s. [Note that these results also show, for limits $s = 0$ and $s = 1$, the dependence of the ratio on the initial k state, the first such data of its kind. That is, $s = 0$ corresponds to scattering out of the initial state ($v = 0, j = 2, k = 2$), and $s = 1$ corresponds to scattering from ($v = 0, j = 2$,

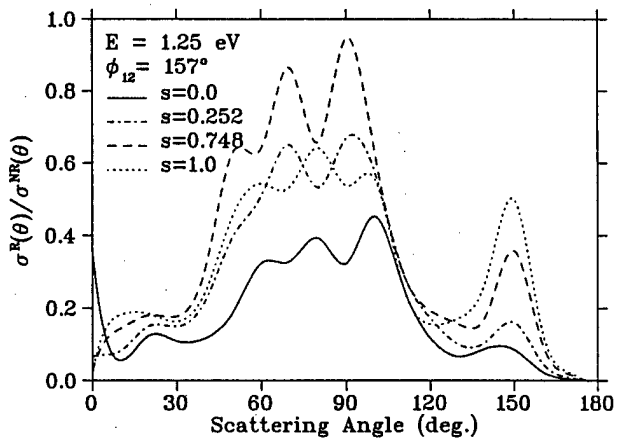

FIG. 2. Dependence of the $\sigma^R(\theta)/\sigma^{NR}(\theta)$ ratio on the scattering angle θ at $\phi_{12}^{max} = 157°$ and at four values of s: $s = 0$, $s = 1$, $s = 0.252$, and $s = 0.748$ for the case of $v = 0$, $j = 2, k_1 = 2, k_2 = 0$.

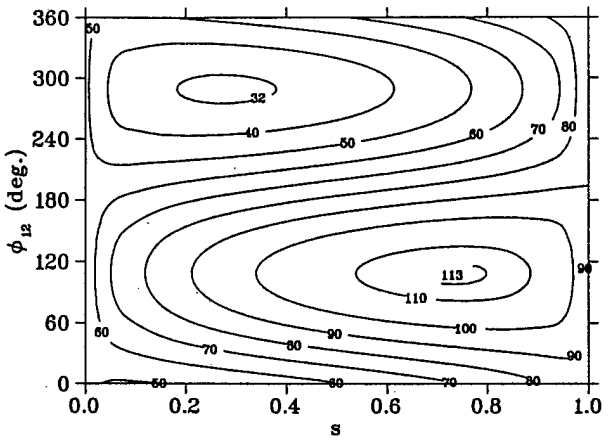

FIG. 3. Contour plot of the σ^R/σ^{NR} ($\times 10^3$) integral cross section ratio as a function of ϕ_{12} and s; for the case of $v = 0, j = 2, k_1 = 2, k_2 = 1$.

$k = 0$).] For this transition the controlled ratio of differential cross sections is seen to be considerably different from the uncontrolled ratio. For example, the controlled $\sigma^R(\theta)/\sigma^{NR}(\theta)$ for $s = 0.748$ is about twice as large as the uncontrolled ratios at $\theta = 91°$. Analysis of Fig. 2 shows that maxima and minima of the controlled σ^R/σ^{NR} ratio in the region between 50° and 120° are achieved at the corresponding minima and maxima of uncontrolled ratios. That is, quantum interference leads to constructive enhancement of the σ^R/σ^{NR} ratio at minima of uncontrolled ratios and to destructive depletion of controlled ratios at their maxima. Exactly the opposite behavior is observed in the outer θ regions. Hence coherent control changes both the magnitude and the structure of the differential cross section. Note also that the maxima of the controlled differential cross sections far exceed those for $s = 0$ and $s = 1$, confirming that the changes are due to quantum interference effects, as opposed to an interpolation between the $s = 0$ and $s = 1$ curves.

Of great interest as well is the extent of control over the integral cross sections. Figure 3 shows a contour plot of the ratio of integral cross sections σ^R/σ^{NR} for scattering from $v = 0, j = 2, k_1 = 2, k_2 = 1$ as a function of the control parameters ϕ_{12} and s. The ratio is seen to vary from 0.032 to 0.113, showing maxima and minima that are well outside the range of the results for scattering from a single k_i state. Greater control is anticipated at higher energies where the uncontrolled σ^R and σ^{NR} become comparable.

In this Letter we have demonstrated that one may obtain considerable control over differential and integral cross sections branching ratios for realistic atom-diatom reactive scattering by preparing, and varying the characteristics of, a superposition of degenerate scattering states. Further, although not explored here, we expect similar control over detailed cross sections to specific product states.

Since the results of molecular beam experiments are well represented by time independent scattering theory and since our computations are state of the art, we anticipate that observed results will be in accord with our computations. Further, additional computations suggest that the control is not very sensitive to small changes in total energy so that one would anticipate little effect due to velocity distributions, etc. However, control is always sensitive to dephasing effects, e.g., external collisions, a feature to be examined in future papers.

This study opens a vast new area of application for coherent control. Work currently underway will extend studies to atom-heteronuclear diatom scattering to results at higher collision energies [12] and will incorporate specific scenarios to prepare the initial superposition state.

We thank Dr. B. Ramachandran for providing us with the REACT scattering code and for useful comments on its use. This work was supported in part by the U.S. Office of Naval Research, Photonics Research Ontario and by a grant of HPC time on the CRAY C-90 and the SGI Origin 2000 from the DoD ASC MSRC Center, and the CRAY T-90 and the SGI PCA from the DoD NAVOCEANO MSRC Center.

*Permanent address: Department of Chemical Physics, The Weizmann Institute of Science, 76100, Rehovot, Israel.

[1] M. Shapiro and P. Brumer, Trans. Faraday Soc. **93**, 1263 (1997); P. Brumer and M. Shapiro, Annu. Rev. Phys. Chem. **43**, 257 (1992); A. Shnitman, I. Sofer, I. Golub, A. Yogev, M. Shapiro, Z. Chen, and P. Brumer, Phys. Rev. Lett. **76**, 2886 (1996).

[2] B. Kohler, J.L. Krause, F. Raski, K.R. Wilson, V.V. Yakovler, R.M. Whitnell, and Y. Yan, Acc. Chem. Res. **28**, 133 (1995); W.S. Warren, H. Rabitz, and M. Dahleh, Science **259**, 1581 (1993); S.A. Rice, *ibid.* **258**, 412 (1992).

[3] B. Sheeny, B. Walker, and L.F. DiMauro, Phys. Rev. Lett. **74**, 4799 (1995).

[4] E. Dupont, P.B. Corkum, H.C. Liu, M. Buchanan, and Z.R. Wasilewski, Phys. Rev. Lett. **74**, 3596 (1995).

[5] M. Shapiro and P. Brumer, Phys. Rev. Lett. **77**, 2574 (1996); D. Holmes, M. Shapiro, and P. Brumer, J. Chem. Phys. **105**, 9162 (1996).

[6] W.H. Miller, J. Chem. Phys. **50**, 407 (1969).

[7] J.L. Krause, M. Shapiro, and P. Brumer, J. Chem. Phys. **92**, 1126 (1990).

[8] D.E. Manolopoulos and R.E. Wyatt, Chem. Phys. Lett. **152**, 23 (1988).

[9] D.E. Manolopoulos, M. D'Mello, and R.E. Wyatt, J. Chem. Phys. **93**, 403 (1990).

[10] J.Z.H. Zhang and W.H. Miller, J. Chem. Phys. **91**, 1528 (1989).

[11] P. Siegbahn and B. Liu, J. Chem. Phys. **68**, 2457 (1978); D.G. Truhlar and C.J. Horowitz, *ibid.* **68**, 2466 (1978); **71**, 1514 (1979).

[12] A. Abrashkevich, M. Shapiro, and P. Brumer (to be published).

Erratum: Coherent Control of Reactive Scattering [Phys. Rev. Lett. 81, 3789 (1998)]

Alexander Abrashkevich, Moshe Shapiro, and Paul Brumer

[S0031-9007(99)08828-6]

Equation (2) of our Letter derives from Eq. (5.31) of Ref. [1], where the dependence of the scattering amplitude on the helicity is stated to be of the form $\exp(ik'\phi)$, with ϕ being the azimuthal scattering angle and k' being the final helicity [2]. This exponential factor does not appear in the cross section, our Eq. (2), since it is the absolute square of the amplitude for fixed k' [although this factor should have appeared in Eq. (3)]. However, we have recently determined that Eq. (5.31) of Ref. [1] contains a typographical error; the ϕ dependence of the scattering amplitude should read $\exp(ik_i\phi)$, where k_i is the initial helicity. Since our Eq. (2) contains contributions from several different k_i values, the resultant corrected cross section is no longer ϕ dependent. Indeed, there is no control of the cross section when integrated over all ϕ. Hence, the general discussion of control in our Letter applies only to ϕ-dependent cross sections, and the particular results shown in Figs. 1–3 of our Letter correspond to observations at $\phi = 0$.

We thank Jiangbin Gong, University of Toronto, for deriving this result and Professor George Schatz, Northwestern University, for confirming the typographical error.

[1] G. Schatz and A. Kuppermann, J. Chem. Phys. **65**, 4642 (1976).
[2] We adopt the alternative θ dependence of J. Z. H. Zhang and W. H. Miller, J. Chem. Phys. **91**, 1528 (1989).

 0031-9007/99/82(14)/3002(1)$15.00 © 1999 The American Physical Society

JOURNAL OF CHEMICAL PHYSICS VOLUME 109, NUMBER 8 22 AUGUST 1998

Semiclassical initial value approach for chaotic long-lived dynamics

G. Campolieti and Paul Brumer
Chemical Physics Theory Group, Department of Chemistry, University of Toronto, Toronto M5S 3H6 Canada

(Received 24 February 1998; accepted 22 May 1998)

A time-dependent initial value semiclassical propagator approach is developed and applied to the propagation of a two-dimensional quantum system whose classical counterpart is highly chaotic. The energy spectrum of a quartic oscillator, obtained from the propagated wavefunction, is shown to be accurately and simply computed by application of stationary-phase Monte Carlo integration. Chaotic trajectories are handled naturally, without giving rise to the singularities seen in other methods. © *1998 American Institute of Physics.* [S0021-9606(98)00932-5]

I. INTRODUCTION

Semiclassical techniques promise a means of carrying out complex quantum computations by using input solely from classical dynamics. Recently, attention has been directed towards utilizing semiclassical initial value representation (IVR) methods for wave function propagation. These methods, which are based on integrals over initial phase space regions,[1–5] provide a direct propagation technique for a wide variety of problems. For example, we recently derived and numerically implemented an IVR approach to three-dimensional molecular photodissociation[4] utilizing stationary-phase Monte Carlo methods.[6] The results provide encouragement for future applications.

Chaotic systems do, however, provide a serious challenge to the implementation of IVR methods. In particular, several years ago Kay[7] extended the Herman–Kluk-type initial value approach[8] and noted that long-lived chaotic trajectories led to highly singular trajectory contributions due to rapidly growing stability matrices. Kay's suggestion was to simply discard these trajectory contributions within a simple Monte Carlo integration method, relying on the expectation that chaotic trajectory phase space regions contribute oscillatory contributions which cancel out. This approach, successfully demonstrated on two-dimensional chaotic systems, is nonetheless unsatisfying since it relies on an *ad hoc* procedure for treating chaotic contributions. Further motivation for the work below is the study of Manolopoulos[3] where a combination of the Herman–Kluk IVR with a cellular dynamics approach[9] allowed an accurate computation of energy spectra without the need to specifically eliminate chaotic trajectories.

In this paper we show that a stationary phase Monte Carlo method (SPMC) within an IVR form provides a natural means for handling long-lived chaotic trajectory contributions to wave function propagation. In particular, we demonstrate that the weighting function introduced in the SPMC procedure damps out chaotic trajectory contributions through an exponential dependence on exactly those stability matrices which were responsible for previously observed singular contributions to the integrand. To demonstrate the utility of the approach we apply it to the quartic oscillator studied by Kay, obtaining a set of semiclassical energy levels in very good agreement with quantum mechanics. The result is a natural, effective, and useful means of computing wave function dynamics in cases where dynamics is either chaotic or nonchaotic.

This paper is organized as follows. Section II contains the IVR integral formulae for wave function propagation and for the evaluation of the semiclassical correlation function. The application of the SPMC is also discussed. Section III describes an application to the quartic oscillator system studied by Kay. Results are presented in Sec. III and comments are provided in the conclusion.

II. IVR WAVE FUNCTION PROPAGATION, CORRELATION FUNCTIONS, AND ENERGY SPECTRA

Several IVR formulae for semiclassical wave function propagation were given in recent papers. Here we consider the form which we previously derived[4] for wave function propagation in the coordinate representation:

$$\Psi(\mathbf{q}_1,t)\sim(2\pi i\hbar)^{-N/2}\int d\mathbf{p}_1|\det J(t)|^{1/2}e^{-i(\pi/2)\nu[\mathbf{p}_1;t]} \times\exp\left[\frac{i}{\hbar}\bar{\phi}(\mathbf{q}_1,\mathbf{p}_1;t)\right]\Psi(\mathbf{q}(t),0). \quad (1)$$

The notation used throughout is that of Ref. 4. That is, $\Psi(\mathbf{q},t)$ is the coordinate wave function at time t, $J(t)=\partial\mathbf{q}(t)/\partial\mathbf{p}_1$ is a classical stability matrix, $\bar{\phi}(\mathbf{q}_1,\mathbf{p}_1;t)=\int_0^t dt'[\mathbf{p}(t')\cdot\dot{\mathbf{q}}(t')-H(\mathbf{q}(t'),\mathbf{p}(t'))]$ is the classical action, and $\nu[\mathbf{p}_1,t]$ is a Maslov index. The latter has been carefully worked out in Refs. 10 and 11. All classical quantities (trajectories, stability matrices, Maslov indices, and action integrals) at time t are obtained from trajectories $\mathbf{q}(t)$, $\mathbf{p}(t)$ which begin at $\mathbf{q}_1$, $\mathbf{p}_1$ at time zero and which evolve via Hamilton's equations with Hamiltonian H; e.g., $\mathbf{q}(t)=\mathbf{q}(\mathbf{q}_1,\mathbf{p}_1;t)$. Contributions to the integrand in Eq. (1) are due to classical trajectories which are used to evaluate both the phase (action+Maslov phase index) and amplitude (determinant of a stability matrix). Note that the integrand is

 © 1998 American Institute of Physics

Downloaded 03 Oct 2001 to 142.150.224.5. Redistribution subject to AIP license or copyright, see http://ojps.aip.org/jcpo/jcpcr.jsp

highly oscillatory due to variations in $\bar{\phi}/\hbar$; the major contributions to the integral in Eq. (1) will therefore come from regions of stationary phase.

To test the utility of the procedure described below we follow Kay[7] and compute symmetry adapted energy levels. Two methods suggest themselves, either (a) Fourier transforming the wave function autocorrelation or (b) analyzing the spectral density. In the first approach we introduce an IVR autocorrelation function, obtained by inserting Eq. (1) into

$$C(t)=\langle\Psi(0)|\Psi(t)\rangle=\int d\mathbf{q}_1\Psi(\mathbf{q}_1,0)^*\Psi(\mathbf{q}_1,t) \tag{2}$$

giving

$$C(t)^{sc}\sim(2\pi i\hbar)^{-N/2}\int d\mathbf{q}_1\Psi(\mathbf{q}_1,0)^*\int d\mathbf{p}_1|\det J(t)|^{1/2}$$
$$\times e^{-i(\pi/2)\nu}\exp\left[\frac{i}{\hbar}\bar{\phi}(\mathbf{q}_1,\mathbf{p}_1;t)\right]\Psi(\mathbf{q}(t),0). \tag{3}$$

Energy eigenstates can be obtained from the peaks of the spectral intensity $I(E)$, i.e., the Fourier transform of the autocorrelation function. An IVR semiclassical expression for spectral intensities then obtains as:

$$I(E)^{sc}=\mathrm{Re}\int_0^T dt\, e^{iEt/\hbar}C(t)^{sc}. \tag{4}$$

Here $C(t)^{sc}$ is given by Eq. (3), the time T is taken sufficiently large, and Re denotes the real part of the quantity which follows. In the case where symmetries of the Hamiltonian exist, then one can also generate energy spectra for each individual symmetry. Following Kay[7] we write the symmetry-adapted, semiclassical spectral intensity as:

$$I_\Gamma(E)=\mathrm{Re}\int_0^T dt\, e^{iEt/\hbar}\langle\hat{P}_\Gamma\Psi(0)|\Psi(t)\rangle. \tag{5}$$

Here $\hat{P}_\Gamma$ is a projection operator[12] for the irreducible representation Γ which can be written as a linear combination of symmetry operators. The symmetry-adapted correlation function within the integral in Eq. (5) is given by Eq. (3) with the initial wave function $\Psi(\mathbf{q}_1,0)$ replaced by the symmetry adapted[13] $\Psi_\Gamma(\mathbf{q}_1,0)=\hat{P}_\Gamma\Psi(0)$. Below we consider the propagation of a Gaussian wave function,

$$\Psi(\mathbf{q},0)=(2\alpha/\pi)^{1/2}\exp(-\alpha|\mathbf{q}-\mathbf{q}^0|^2), \tag{6}$$

and choose to project out (in accord with Kay) states of A_1 symmetry. Although here $\Psi(\mathbf{q},0)$ is chosen to be smooth, oscillatory wave functions can be readily treated.

Another well known method of obtaining energy spectra uses the density of states approach. Here the energy spectrum is obtained by noting the formula for the state density $\mathrm{Tr}[\delta(E-H)]$ in the form:

$$\rho(E)=\frac{1}{\pi\hbar}\mathrm{Re}\int_0^T dt\, e^{iEt/\hbar}\int d\mathbf{q}_1\langle\mathbf{q}_1|e^{-i\hat{H}t/\hbar}|\mathbf{q}_1\rangle. \tag{7}$$

By making use of the mixed representation propagator,[11] which was used to derive Eq. (1), we can express the diagonal coordinate matrix element of the propagator as

$$\langle\mathbf{q}_1|e^{-i\hat{H}t/\hbar}|\mathbf{q}_1\rangle^{sc}$$
$$\sim\frac{(2\pi i\hbar)^{-N/2}}{(2\pi\hbar)^N}\int d\mathbf{p}_2 e^{i\mathbf{q}_1\cdot\mathbf{p}_2/\hbar}\int d\mathbf{p}_1|\det J(t)|^{1/2}$$
$$\times e^{-i(\pi/2)\nu}e^{i\bar{\phi}(\mathbf{q}_1,\mathbf{p}_1;t)/\hbar}e^{-i\mathbf{q}(t)\cdot\mathbf{p}_2/\hbar}\sim(2\pi i\hbar)^{-N/2}$$
$$\times\int d\mathbf{p}_1|\det J(t)|^{1/2}e^{-i(\pi/2)\nu}e^{i\bar{\phi}(\mathbf{q}_1,\mathbf{p}_1;t)/\hbar}\delta(\mathbf{q}_1-\mathbf{q}(t)). \tag{8}$$

Inserting this into Eq. (7) gives

$$\rho(E)^{sc}$$
$$=\frac{(2\pi i\hbar)^{-N/2}}{\pi\hbar}\mathrm{Re}\int_0^T dt\, e^{iEt/\hbar}\int d\mathbf{q}_1\int d\mathbf{p}_1|\det J(t)|^{1/2}$$
$$\times e^{-i(\pi/2)\nu}e^{i\bar{\phi}(\mathbf{q}_1,\mathbf{p}_1;t)/\hbar}\delta(\mathbf{q}_1-\mathbf{q}(t)). \tag{9}$$

The highly oscillatory nature of the integrands in Eqs. (5) and (9) will generally render a primitive MC approach useless. In such an approach, only amplitude terms play a role in importance sampling distributions. Here we introduce stationary-phase Monte Carlo sampling (SPMC)[6] to compute the desired integrals. The SPMC procedure, which can be done on a subspace of the integrand, or over all phase space, isolates regions of stationary phase by incorporating filtering functions into the MC sampling. To provide a sampling over all phase space we introduce:

$$D_{0,\epsilon}(\mathbf{x};E)=\exp\left\{-\frac{\epsilon}{2}\partial_{\mathbf{x}}\bar{\phi}\cdot\boldsymbol{\Delta}\cdot\partial_{\mathbf{x}}\bar{\phi}\right\}, \tag{10}$$

where $\mathbf{x}\equiv(\mathbf{q}_1,\mathbf{p}_1)$, and where $\partial_{\mathbf{x}}\bar{\phi}$ denotes the vector of partial derivatives with respect to the $\mathbf{q}_1$ and $\mathbf{p}_1$ components. The derivatives of the phase with respect to $\mathbf{q}_1$ are given by $\mathbf{v}(t)\equiv L(t)^\dagger\cdot\mathbf{p}(t)-\mathbf{p}_1$ with $L(t)=\partial\mathbf{q}(t)/\partial\mathbf{q}_1$ and those with respect to $\mathbf{p}_1$ by $J(t)^\dagger\cdot\mathbf{p}(t)$, where $\dagger$ is transpose. Incorporating the damping function in Eq. (10) into either Eq. (5) or (9) gives us the working formulae to compute the spectra. Here these spectra are used as a means of testing the quality of the wave packet propagation.

The $D_{0,\epsilon}$ function involves gradients of the phase in a negative exponential, which emphasize regions of stationary phase when used as a sampling distribution. The factor ϵ is an overall damping parameter, and elements in the diagonal matrix $\boldsymbol{\Delta}_i$ characterize the sampling widths in each integration variable. In the case of the calculations that follow in the next section, we simply choose $\boldsymbol{\Delta}_i=1$ for all i.

Incorporating all components gives the symmetry-adapted spectral intensity [Eq. (5)] gives, as a computationally tractable expression:

Downloaded 03 Oct 2001 to 142.150.224.5. Redistribution subject to AIP license or copyright, see http://ojps.aip.org/jcpo/jcpcr.jsp

$$I_\Gamma(E)^{sc}=\mathrm{Re}\Big\{(2\pi i\hbar)^{-N/2}\int_0^T dt\, e^{iEt/\hbar}\int_{P_\Gamma} d\mathbf{q}_1\Psi(\mathbf{q}_1,0)^* \times\int d\mathbf{p}_1|\det J(t)|^{1/2}\Psi(\mathbf{q}(t),0)e^{-i(\pi/2)\nu} \times\exp\Big[\frac{i}{\hbar}\bar{\phi}(\mathbf{q}_1,\mathbf{p}_1;t)\Big] \times\exp\Big[-\frac{\epsilon}{2}\mathbf{p}(t)^\dagger\cdot J(t)J(t)^\dagger\cdot\mathbf{p}(t)\Big] \times\exp\Big[-\frac{\epsilon}{2}\mathbf{v}(t)^\dagger\cdot\mathbf{v}(t)\Big]\Big\}. \quad (11)$$

Here the subscript P_Γ indicates that the initial points $\mathbf{q}_1$ are to be chosen in accord with A_1 symmetry.[13] Similarly, Eq. (9) becomes:

$$\rho(E)^{sc}\sim\frac{1}{\pi}\mathrm{Re}\Big\{\Big(\frac{\alpha/\pi}{2\pi i\hbar}\Big)^{N/2}\int_0^T dt\, e^{iEt/\hbar}\int_{P_\Gamma} d\mathbf{q}_1 \times\int d\mathbf{p}_1|\det J(t)|^{1/2}e^{-i(\pi/2)\nu}e^{i\bar{\phi}/\hbar}e^{(-\alpha|\mathbf{q}_1-\mathbf{q}(t)|^2)} \times\exp\Big[-\frac{\epsilon}{2}\mathbf{p}(t)^\dagger\cdot J(t)J(t)^\dagger\cdot\mathbf{p}(t)\Big] \times\exp\Big[-\frac{\epsilon}{2}\mathbf{v}(t)^\dagger\cdot\mathbf{v}(t)\Big]\Big\}. \quad (12)$$

Here we have replaced the delta function in Eq. (9) by a narrow Gaussian of the form $\delta(\mathbf{q}_1-\mathbf{q}(t))\simeq(\alpha/\pi)^{N/2}\times\exp(-\alpha|\mathbf{q}_1-\mathbf{q}(t)|^2)$, inserted the SPMC damping function and have taken the appropriate symmetry projection.[7]

One can readily show that the approach taken by using Eq. (11) and integrating out over the center (i.e., $\mathbf{q}_0$) of the initial wave packet is the same as Eq. (12), in the large α limit.

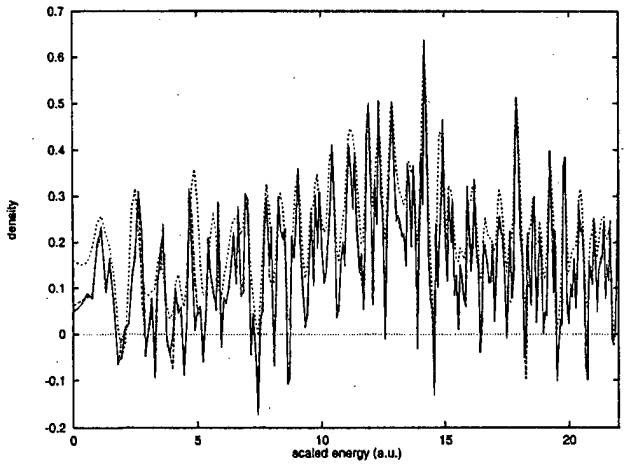

FIG. 1. Effect of ϵ damping parameter on semiclassical density of states for A_1 symmetry of quartic oscillator. Here the density $\rho(E)^{sc}$ is plotted versus the scaled energy $\bar{E}=(2E)^{3/4}$. Results are shown for $\epsilon=10^{-2}$ (dashed), $\epsilon=10^{-3}$ (dotted), and $\epsilon=10^{-5}$ (solid).

Note that previous studies of systems with chaotic trajectories experienced difficulties due to the blowup of the $[\det J(t)]$ for long-lived chaotic trajectories. Here this growth is naturally damped by the first J-dependent exponential term in the SPMC damping function in the integrand.

Equations (11) and (12) both provide approaches to computing the energy spectrum. Our numerical studies indicate that Eq. (12) is more convenient to use numerically, providing good results for small values of α and hence resulting in fewer wasted trajectories. Application of Eq. (12) is demonstrated below.

III. APPLICATIONS TO CHAOTIC QUARTIC OSCILLATOR

We test the applicability of our IVR approach by considering the same case explored by Kay,[7] i.e., the highly chaotic quartic oscillator with Hamiltonian

$$H=(p_x^2+p_y^2)/2+x^2y^2/2+\beta(x^4+y^4)/4, \quad (13)$$

with $\beta=0.01$. In particular, we implement Eq. (12) to compute the symmetry-adapted semiclassical density of states. We choose $\alpha=2$ and project onto A_1 symmetry. The integrals in Eq. (12) are computed by a two-step procedure: first we compute the full phase space integral in $\mathbf{q},\mathbf{p}$, and then we Fourier transform the result to compute the time integral. In accordance with previous studies[7] we choose the maximum propagation time as $T=50.0$ (atomic units are used throughout).

The phase space integrals in Eq. (12) are computed by a relatively simple "inactive" SPMC procedure as follows. The initial momenta and coordinates are sampled uniformly and randomly within a range for which the corresponding classical energies do not exceed $E_{\max}\sim40.0$. Since the potential is positive definite, the corresponding momentum range is the rectangle $p_{x,1}\times p_{y,1}=[-10,10]\times[-10,10]$. Allowed coordinate space points are restricted to a rectangle $x_1\times y_1=[-12,12]\times[-12,12]$. The Monte Carlo sums are then accumulated at equally spaced intermediate time intervals $\Delta T=0.1$. The final time integral is computed by Fourier transforming the data, i.e., using the 500 points between $T=0$ and $T=50.0$. The trajectories are computed using a variable step size predictor–corrector algorithm with controlled local relative and absolute error. In order to compare our semiclassical results with those of Kay[7] we did not introduce a time windowing procedure, although we found that results varied insignificantly if a window function of the form $\exp(-(t/\tau)^2$ was used in the final Fourier transform with $\tau\geqslant37.5$.

The only remaining parameter is the damping ϵ. Its choice is an important aspect of the SPMC procedure,[1,4,14] having a dramatic effect on the convergence and feasibility of SPMC integration. For the case reported here, we found that attaining acceptable convergence and suppressing the divergence due to chaotic trajectories required $\epsilon\geqslant10^{-5}$. Further, maintaining detailed narrow peaks in the energy spectrum necessitated $\epsilon\leqslant10^{-2}$.

The effect of ϵ damping on the density of states of A_1 symmetry is shown in Fig. 1. Here we see that good agreement is obtained over a substantial range of $\epsilon=10^{-3}$ to

Downloaded 03 Oct 2001 to 142.150.224.5. Redistribution subject to AIP license or copyright, see http://ojps.aip.org/jcpo/jcpcr.jsp

TABLE I. Scaled semiclassical energy values, $\bar{E}=(2E)^{3/4}$, for A_1 symmetry of quadric oscillator. Values are estimated from the density of states in Fig. 1. QM are quantum results, SC IVR are our results, and SC are Kay's[7] results. Numbers followed by a superscript "a" denotes our estimate from Kay's Fig. 9.

Peak No.	QM	SC IVR	SC
1	1.09	1.12	1.19
2		1.50	1.8[a]
3	2.71	2.70	2.71
4		3.17	3.0[a]
5	3.70	3.67	3.72
6		4.13	4.0[a]
7	4.63	4.69	4.66
			5.0[a]
8	5.48	5.44	5.65
9	5.84	5.85	5.96
10		6.45	6.0[a]
11	6.62	6.65	6.57
12		6.95	7.1[a]
13	7.55	7.75	7.56
14	7.93	7.94	7.94
15	8.52	8.53	8.50
16	8.96	9.06	9.05
17	9.52	9.54	9.50
18		9.76	9.8[a]
19	9.92	9.93	9.94
20	10.47	10.45	10.46
21	10.82	10.86	10.80
22	11.38	11.35	11.39
23	11.61	11.61	11.64
24	12.37	12.35	12.38
25	12.64		
26	12.82	12.84	12.71
27	13.35	13.35	13.35
28	13.47	13.50	13.51
29		13.73	
30	14.03	14.04	14.06
31	14.32	14.23	14.29
32	14.68	14.65	14.68
33	15.02	14.95	14.99
34		15.16	
35	15.29	15.29	15.29
36	15.85	15.90	
37	16.02	15.98	15.97
38	16.26	16.20	16.27
39	16.59	16.59	16.64
40	17.04	16.92	16.93
41	17.22	17.21	17.15
42	17.35	17.35	17.37
43	17.81	17.90	17.88
44	18.08	18.06	18.09
45	18.24	18.34	18.31
46	18.61	18.61	18.74
47	18.93	18.85	18.88
48	19.13	19.20	19.09
49	19.43	19.44	19.44
50	19.66	19.80	19.86
51	19.97	20.05	19.99
52	20.14	20.19	20.21
53	20.52	20.53	20.62

10^{-5}; significantly larger values, such as $\epsilon=10^{-1}$ broaden the peaks substantially. Results shown are for 500 000 trajectories, but results using 100 000 trajectories were accurate to within 10%. (Far fewer trajectories are expected to be required if $D_{0,\epsilon}(\mathbf{x};E)$ were actively included in the importance sampling). In the absence of ϵ damping the integral was dominated, as in Kay's case, by divergent contributions from long-lived chaotic trajectories.

Our best results for the semiclassical density of states of A_1 symmetry are shown as the solid curve in Fig. 1. It is to be compared to Fig. 9 of Ref. 7. The plots of the densities are similar; broader peaks occur within the $\bar{E}=0-5$ range and progressively sharper peaks dominate the rest of the energy region. In addition, there are a few extra peaks when results are compared to the quantum A_1 energies. They are similar in character to the extra peaks observed by Kay,[7] being more prevalent at lower energies. Their origin is unclear but Kay notes that similar spurious peaks are evident in applications of Gutzwiller's trace formula. Note also that the computed density of states is not everywhere positive, reflecting the fact that Eq. (7) is not guaranteed positive for approximate expressions for the propagator. Nonetheless, the peaks depicting the position of the states are clear, rising up well above this background.

The peak positions, which give the semiclassically computed energies, are reported in Table I where they are compared to the quantum results. They are seen to be in good agreement, with all semiclassical energies within 5% of the quantum results, and many energies being accurate to within 1%. The same sort of agreement exists between our results and those of Kay.

IV. CONCLUSIONS

We have applied an initial value integral representation (IVR) semiclassical propagator approach to the study of energy spectra of a highly chaotic system. The method relies on stationary-phase Monte Carlo (SPMC) methods to integrate the highly oscillatory IVR integrals in the full phase space and to eliminate divergent contributions from long-lived chaotic trajectories. Further, our approach shares the simplicity of previous methods insofar as it does not require that one incorporate special dynamical properties of the system into the calculations, requiring rather simple Monte Carlo simulations. For the two-dimensional quartic oscillator system studied, the method gives energy spectra in good agreement with quantum values, while providing a natural means for handling chaos.

The extension of this method to higher dimensions is clearly important. In this case we would advocate using Monte Carlo importance sampling in a more active manner, which would reduce the number of required trajectories. Such applications are currently under study.

ACKNOWLEDGMENTS

This work was supported by the U.S. Office of Naval Research and by the Natural Sciences and Engineering Council of Canada.

[1] B. W. Spath and W. H. Miller, Chem. Phys. Lett. **262**, 486 (1996).
[2] K. G. Kay, J. Chem. Phys. **100**, 4377 (1994); , 4432 (1994).
[3] A. R. Walton and D. E. Manolopoulos, Mol. Phys. **87**, 961 (1996); Chem. Phys. Lett. **244**, 448 (1995).
[4] G. Campolieti and P. Brumer, J. Chem. Phys. **107**, 791 (1997).
[5] D. Provost and P. Brumer, Phys. Rev. Lett. **74**, 250 (1995).

Downloaded 03 Oct 2001 to 142.150.224.5. Redistribution subject to AIP license or copyright, see http://ojps.aip.org/jcpo/jcpcr.jsp

[6] J. D. Doll, D. L. Freeman, and M. J. Gillan, Chem. Phys. Lett. **143**, 277 (1988); J. D. Doll, T. L. Beck, and D. L. Freeman, J. Chem. Phys. **89**, 5753 (1988); N. Makri and W. H. Miller, Chem. Phys. Lett. **139**, 10 (1987).
[7] K. G. Kay, J. Chem. Phys. **101**, 2250 (1994).
[8] M. F. Herman and E. Kluk, Chem. Phys. **91**, 27 (1984).
[9] E. J. Heller, J. Chem. Phys. **94**, 2723 (1991).
[10] G. Campolieti and P. Brumer, Phys. Rev. A **50**, 997 (1994).
[11] G. Campolieti and P. Brumer, Phys. Rev. A **43**, 1 (1996).
[12] F. A. Cotton, *Chemical Applications of Group Theory* (Wiley-Interscience, New York, 1971).
[13] For the A_1 symmetry of interest below, $\hat{P}_\Gamma f(x,y)=0.25[f(x,y)+f(x,-y)+f(y,-x)+f(y,x)]$.
[14] See also J. Cao and Gregory A. Voth, J. Chem. Phys. **104**, 273 (1996).

Downloaded 03 Oct 2001 to 142.150.224.5. Redistribution subject to AIP license or copyright, see http://ojps.aip.org/jcpo/jcpcr.jsp

In the above, A, B, C are either atoms, groups of atoms, electrons, or photons, m, m' denote the internal (vibrational, rotational, photon occupation) quantum numbers of the reactants or products.

Given $\Psi(t=0)$, the system wave function at an initial time, the evolution of the system is determined by the time-dependent material Schrödinger equation,

$$H_M \Psi(t) = i\hbar \partial \Psi(t)/\partial t \,, \tag{3}$$

where H_M is the system Hamiltonian. The long-term behavior of $\Psi(t)$ is intimately connected with the nature of the time-independent continuum energy eigenstates. For every continuum energy value E, each of the possible outcomes observed in the product region is represented by an independent wave function. This "boundary" condition is expressed more precisely by denoting the different possible chemical products of the breakup of ABC in Eq. (1) by an index q (e.g., $q=1$ denotes the $A+BC$ products) and all additional identifying state labels by m. The set of continuum eigenfunctions of the material Hamiltonian,

$$H_M |\, E, m, q^- \,\rangle = E |\, E, m, q^- \,\rangle, \tag{4}$$

is now defined via the requirement that asymptotically every $|\, E, m, q^- \,\rangle$ state goes over to a state of the separated products, denoted by $|\, E, m, q^0 \,\rangle$ [40] that is of energy E, chemical identity q, and remaining quantum numbers m.

The description of the system in terms of $|\, E, m, q^- \,\rangle$ has an important advantage: Expressing the state of the system in the present in terms of these states, i.e., writing an initial continuum state as

$$\Psi(t=0) = \sum_{q,m} \int dE c_{q,m}(E) |\, E, m, q^- \,\rangle, \tag{5}$$

means that we know the fate of the system in the future. Since each of the $|\, E, m, q^- \,\rangle$ states correlates with a *single* product state, the probability of observing each $|\, E, m, q^0 \,\rangle$ product state is simply given by $|c_{q,m}(E)|^2$, the *preparation* probabilities. The probability of producing a chemical product q in the future is therefore given as

$$P_q = \sum_m \int dE |c_{q,m}(E)|^2. \tag{6}$$

Below we demonstrate that the key to laser control is to change one $c_{q,m}(E)$ coefficient relative to another $c_{q',m}(E)$ coefficient *at the same energy*. In order to understand how this can be done we discuss now the process of preparation.

1.2 Perturbation Theory, System Preparation, and Coherence

Consider the effect of an electric field $\epsilon(t)$ on an initially bound eigenstate $|\, E_g \,\rangle$ of the radiation-free Hamiltonian H_M. The overall Hamiltonian is then given by

$$H = H_M - \mathrm{d}[\bar{\epsilon}(t) + \bar{\epsilon}^*(t)], \tag{7}$$

where d is the component of the dipole moment along the electric field.

If the impinging photon is energetic enough to dissociate the molecule, it is then necessary to expand $|\, \Psi(t) \,\rangle$ in the bound and scattering eigenstates of the radiation-free Hamiltonian,

$$|\, \Psi(t) \,\rangle = \sum_i c_i(t) |\, E_i \,\rangle \exp(-iE_i t/\hbar) + \sum_{m,q} \int dE c_{E,m,q}(t) |\, E, m, q^- \,\rangle \exp(-iEt/\hbar). \tag{8}$$

Insertion of Eq. (8) into the time dependent Schrödinger equation results in a set of first-order differential equations for the $c_\nu(t)$ coefficients, where ν represents either the bound (i) or scattering (E, m, q) indices.

For weak fields, the use of first-order perturbation theory gives, for the post-pulse preparation coefficient,

$$c_{E,m,q}(t \gg \Gamma) = (\sqrt{2\pi}/i\hbar)\epsilon(\omega_{E,E_g}) \langle E, m, q^- | \mathrm{d} | E_g \rangle \tag{9}$$

where Γ is the pulse duration and

$$\epsilon(\omega) = \frac{1}{\sqrt{2\pi}} \int_{-\infty}^{\infty} \exp(i\omega t)\, \bar{\epsilon}(t)\, dt. \tag{10}$$

It follows from Eq. (6) and Eq. (9) that the probability $P(E,q)$ of forming an asymptotic product in arrangement q is

$$P(E,q) = \sum_m |c_{E,m,q}(t \gg \Gamma)|^2 = (2\pi/\hbar^2) \sum_m |\epsilon(\omega_{E,E_g}) \langle E_g | \mathrm{d} | E, m, q^- \rangle|^2 \tag{11}$$

and that the branching ratio $R(1,2;E)$ between the $q=1$ products and the $q=2$ products at energy E is given by

$$R(1,2;E) = \frac{\sum_m |\langle\, E_g \,|\mathrm{d}|\, E, m, 1^- \,\rangle|^2}{\sum_m |\langle\, E_g \,|\mathrm{d}|\, E, m, 2^- \,\rangle|^2}. \tag{12}$$

1.3 Coherent Control of Chemical Reactions

We now address the issue of how to alter the above yield ratio $R(1,2;E)$ in a *systematic* fashion. Equation (12) makes clear that (at least in the weak field regime) this can not be achieved by altering the laser intensity, since the field strength cancels out in the expression for R. Quantum interference phenomena can, however, alter the numerator or denominator of R in an independent and controlled way. This can be achieved by accessing the final continuum state via two or more interfering pathways. One of the first examples that we studied [1] involves preparing a molecule in a superposition $c_1 |\, \phi_1 \,\rangle + c_2 |\, \phi_2 \,\rangle$ state and exciting the two components to the same final continuum energy E by using two CW sources. The field employed is of the form

$$\bar{\epsilon}(t) = \epsilon_1 e^{-i\omega_1 t + i\chi_1} + \epsilon_2 e^{-i\omega_2 t + i\chi_2}, \tag{13}$$

where $\hbar\omega_i = E - E_i$. A straightforward computation [1] yields that

$$R(1,2;E) = \frac{\sum_m |\langle \tilde{\epsilon}_1 c_1 \phi_1 + \tilde{\epsilon}_2 c_2 \phi_2 | \mathrm{d} | E, m, 1^- \rangle|^2}{\sum_m |\langle \tilde{\epsilon}_1 c_1 \phi_1 + \tilde{\epsilon}_2 c_2 \phi_2 | \mathrm{d} | E, m, 2^- \rangle|^2}, \tag{14}$$

where $\tilde{\epsilon}_i = \epsilon_i \exp(i\chi_i)$. Expanding the square gives

$$R(1,2;E) =$$

$$\frac{\sum_m [|\tilde{\epsilon}_1 c_1 \langle \phi_1 | \mathrm{d} | E, m, 1^- \rangle|^2 + |\tilde{\epsilon}_2 c_2 \langle \phi_2 | \mathrm{d} | E, m, 1^- \rangle|^2 + 2Re[c_1 c_2^* \tilde{\epsilon}_1 \tilde{\epsilon}_2^* \langle \phi_1 | \mathrm{d} | E, m, 1^- \rangle]}{\sum_m [|\tilde{\epsilon}_1 c_1 \langle \phi_1 | \mathrm{d} | E, m, 2^- \rangle|^2 + |\tilde{\epsilon}_2 c_2 \langle \phi_2 | \mathrm{d} | E, m, 2^- \rangle|^2 + 2Re[c_1 c_2^* \tilde{\epsilon}_1 \tilde{\epsilon}_2^* \langle \phi_1 | \mathrm{d} | E, m, 2^- \rangle]} \tag{15}$$

The structure of the numerator and denominator of Eq. (15) is of the type desired: i.e., each has a term associated with the excitation of the $|\phi_1\rangle$ state, a term associated with the excitation of the $|\phi_2\rangle$ state, and a term corresponding to the interference between the two excitation routes. The interference term, which can be either constructive or destructive, is in general different for the two product channels. What makes Eq. (15) so important *in practice* is that the interference term has coefficients whose magnitude and sign depend upon *experimentally controllable* parameters. In the case of Eq. (15), the experimental parameters that alter the yield [1] are contained in the complex quantity $A = \tilde{\epsilon}_2 c_2 / \tilde{\epsilon}_1 c_1$. Both $x \equiv |A|$ and $\theta_1 - \theta_2 \equiv arg(A)$ can be controlled separately in the experiment.

The "real time" analogue of the above two CW frequencies scenario, in which the superposition state preparation is affected by a single broadband pulse and the dissociation by a second pulse, is discussed in detail in Sect. 2.2 below.

2 Representative Control Scenarios

The two-step approach is but one particular implementation of coherent control; numerous other scenarios may be designed. They all rely upon the same "coherent control principle," that *in order to achieve control one must drive a state through multiple independent optical excitation routes to the same final state.*

It would seem that laser incoherence would lead to loss of control, since incoherence implies that the phases of $\tilde{\epsilon}_1$ and $\tilde{\epsilon}_2$ in Eq. (15) are random. An ensemble average of these phases is expected to lead to the disappearance of the interference term. This is true, however, only in the fully chaotic limit. Control can persist in the presence of some laser incoherence [16], or when the initial state is described by a *mixed*, as distinct from *pure*, state [7]. Most surprising is the fact, described below, that by utilizing strong laser fields one can attain quantum interference control with completely *incoherent* sources [41].

We now describe in more detail three control scenarios.

2.1 1-Photon, 3-Photon Interference

So far, we have exploited quantum interference phenomena by dissociating a superposition of several energy eigenstates with a single type (one photon absorption) process. It is possible instead to start with a *single* energy eigenstate and employ interference between optical routes of *different* types. Such is the interference between two multiphoton processes of different multiplicities. In order to satisfy the coherent control principle, which requires that we reach the same final energy E, we must use photons of commensurate frequencies, i.e., frequencies that satisfy an $m\omega_1 = n\omega_2$ relation, with integer m and n. Selection rules dictate the acceptable n, m pairs.

As the simplest example, we examine a one photon process interfering with a three photon process ("3 vs. 1" control). Let H_g and H_e be the nuclear Hamiltonians for a ground and an excited electronic state. H_g is assumed to have a discrete spectrum and H_e to possess a continuous spectrum. The molecule, initially in an eigenstate $|E_i\rangle$ of H_g, is subjected to two electric fields given by

$$\epsilon(t) = \epsilon_1 \cos(\omega_1 t + \mathbf{k}_1 \cdot \mathbf{R} + \theta_1) + \epsilon_3 \cos(\omega_3 t + \mathbf{k}_3 \cdot \mathbf{R} + \theta_3). \tag{16}$$

Here $\omega_3 = 3\omega_1$, $\epsilon_l = \epsilon_l \hat{\epsilon}_l$, $l = 1, 3$; ϵ_l is the magnitude and $\hat{\epsilon}_l$ is the polarization of the electric fields, $\mathbf{k}_i$ are the wavevectors. The two fields are chosen parallel, with $\mathbf{k}_3 = 3\mathbf{k}_1$.

The probability $P(E, q; E_i)$ of producing product with energy E in arrangement q from a state $|E_i\rangle$ is given by

$$P(E, q; E_i) = P_3(E, q; E_i) + P_{13}(E, q; E_i) + P_1(E, q; E_i), \tag{17}$$

where $P_1(E, q; E_i)$ and $P_3(E, q; E_i)$ are the probabilities of dissociation due to the ω_1 and ω_3 excitation, and $P_{13}(E, q; E_i)$ is the term due to interference between the two excitation routes.

In the weak field limit, $P_3(E, q; E_i)$ is given by

$$P_3(E, q; E_i) = (\frac{\pi}{\hbar})^2 \epsilon_3^2 F_3^{(q)}, \tag{18}$$

where

$$F_3^{(q)} = \sum_n |\langle E, n, q^- | (\hat{\epsilon}_3 \cdot \mathrm{d})_{e,g} | E_i \rangle|^2 , \tag{19}$$

d is the electric dipole operator, and

$$(\hat{\epsilon}_3 \cdot \mathrm{d})_{e,g} = \langle e | \hat{\epsilon}_3 \cdot \mathrm{d} | g \rangle , \tag{20}$$

with $|g\rangle$ and $|e\rangle$ denoting the ground and excited electronic states, respectively. $P_1(E, q; E_i)$ is given in third-order perturbation theory by [6]

$$P_1(E, q; E_i) = (\frac{\pi}{\hbar})^2 \epsilon_1^6 F_1^{(q)}, \tag{21}$$

where

$$F_1^{(q)} = \sum_n |\langle E, n, q^- | T | E_i \rangle|^2 , \tag{22}$$

with

$$T = (\hat{\epsilon}_1 \cdot \mathrm{d})_{e,g}(E_i - H_g + 2\hbar\omega_1)^{-1}(\hat{\epsilon}_1 \cdot \mathrm{d})_{g,e}(E_i - H_e + \hbar\omega_1)^{-1}(\hat{\epsilon}_1 \cdot \mathrm{d})_{e,g} \ . \quad (23)$$

We assumed that $E_i + 2\hbar\omega_1$ is below the dissociation threshold and that dissociation occurs from the excited electronic state only.

A similar derivation [6] gives the cross term in Eq. (17) as

$$P_{13}(E, q; E_i) = -2(\frac{\pi}{\hbar})^2 \epsilon_3 \epsilon_1^3 \cos(\theta_3 - 3\theta_1 + \delta_{13}^{(q)})|F_{13}^{(q)}| \quad (24)$$

with the amplitude $|F_{13}^{(q)}|$ and phase $\delta_{13}^{(q)}$ defined by

$$|F_{13}^{(q)}| \exp(i\delta_{13}^{(q)}) = \sum_n \langle E_i \,|\, T \,|\, E, n, q^- \rangle \langle E, n, q^- \,|\, (\hat{\epsilon}_3 \cdot \mathrm{d})_{e,g} \,|\, E_i \rangle \ . \quad (25)$$

The branching ratio $R_{qq'}$ between the q and q' products can then be written as

$$R_{qq'} = \frac{F_3^{(q)} - 2x\cos(\theta_3 - 3\theta_1 + \delta_{13}^{(q)})|F_{13}^{(q)}| + x^2 F_1^{(q)}}{F_3^{(q')} - 2x\cos(\theta_3 - 3\theta_1 + \delta_{13}^{(q')})|F_{13}^{(q')}| + x^2 F_1^{(q')}} \quad (26)$$

, where x is defined as

$$x = \epsilon_1^3/\epsilon_3. \quad (27)$$

The numerator and denominator of Eq. (26) contain contributions from two independent routes and an interference term. Since the interference term is controllable through variation of laboratory parameters, so too is the product ratio $R_{qq'}$. Thus the principle upon which this control scenario is based is the same as in the first example above, although the interference is introduced in an entirely different way.

Experimental control over $R_{qq'}$ is obtained by varying the difference $(\theta_3 - 3\theta_1)$ and the parameter x. The former is the phase difference between the ω_3 and the ω_1 laser fields, and the latter, via Eq. (27), incorporates the ratio of the two lasers' amplitudes. Experimentally, one envisions using "tripling" to produce ω_3 from ω_1; the subsequent variation of the phase of one of these beams provides a straightforward method of altering $\theta_3 - 3\theta_1$. Indeed, generating ω_3 from ω_1 allows for compensation of any phase jumps in the two laser sources. Thus the relative phase $\omega_3 - 3\omega$ is well-defined.

As pointed out above, "3 vs. 1" is not necessarily the only viable control scenario in the "*nvs.m*" family. It has the advantage that one may generate one of the frequencies (the tripled photon) from the other. This is indeed the reason why the "3 vs. 1" route was the first control scenario to be implemented experimentally (see the discussion below).

Control of *integral* (in contrast to *differential*) cross-sections requires that the $|\, E, n, q^- \,\rangle$ continuum states be made up of equal parity $|\, J, M \,\rangle$ angular momentum states. This means that in the "*mvs.n*" control scheme, the integer n must have the same parity as the integer m. Thus, studies of a "2 vs. 2" scheme for the control of the Na_2 photodissociation [15, 42] (discussed in detail in Sect. 2.3) and of a "2 vs. 4" scenario for the control of the Cl_2 photodissociation [43], have been published. In addition, studies of "3 vs. 1" control with strong fields, have also appeared [44, 45, 46]. These studies and others [47] have verified that "*nvs.m*" control is viable even when strong fields are used, although the dependence on the x amplitude and the $\theta_n - 3\theta_m$ phase factors is no longer as transparent as in the weak field case, discussed above.

The weak field "3 vs. 1" scenario has now been experimentally implemented in part in REMPI type experiments. The experiments demonstrated control of the total ionization rate, first in Hg [28], and then in HCl and CO [29]. In the case of HCl [29], the molecule was excited to an intermediate $^3\Sigma^-(\Omega^+)$ vib-rotational resonance, using a combination of three ω_1 ($\lambda_1 = 336$ nm) photons and one ω_3 ($\lambda_3 = 112$ nm) photon. The ω_3 beam was generated from an ω_1 beam by tripling in a Kr gas cell. Ionization of the intermediate state takes place by absorption of one additional ω_1 photon.

The relative phase of the light fields was varied by passing the ω_1 and ω_2 beams through a second Ar or H_2 ("tuning") gas cell of variable pressure. The HCl REMPI experiments verified the prediction of a sinusoidal dependence of the ionization rates on the relative phase of the two exciting lasers of Eq. (26). The HCl experiment also verified the prediction of Eq. (26) of the dependence of the strength of the sinusoidal modulation of the ionization current on the x amplitude factor. More recently, control over branching processes such as dissociation vs. ionization in HI was demonstrated by Gordon et al. [30].

If one is content with controlling angular distributions, one can lift the equal parity restriction. Absorption of two photons of perpendicular polarizations [5, 8], or of two photons interfering with their second-harmonic photon ("2 vs. 1" scenario) [8, 33, 34], result in states of different parities. Though such processes do not lead to control of integral quantities, they do allow for control of differential cross-sections. The "1 vs. 2" scenario (discussed in Sect. 4) has been implemented experimentally for the control of photo-current directionality in semiconductors using no bias voltage [33, 35] and for the control of the orientation of the HD^+ photodissociation [36].

2.2 The Pump-Dump Scheme

An alternative version of the scenario outlined in Sect. 1.3 is a "pump-dump" scheme [18, 19], in which an initial superposition of bound states is prepared with one laser pulse and subsequently dissociated with another. The pump and dump steps are assumed to be temporally separated by a time delay τ. The analysis below shows that under these circumstances the control parameters are the central frequency of the pump pulse and the time delay between the two pulses.

Consider a molecule, initially ($t = 0$) in eigenstate $|\, E_g \,\rangle$ of Hamiltonian H_M, subjected to two transform limited light pulses. The field $\bar{\epsilon}(t)$ consists of two temporally separated pulses $\bar{\epsilon}(t) = \bar{\epsilon}_x(t) + \bar{\epsilon}_d(t)$, with the Fourier transform of $\bar{\epsilon}_x(t)$ denoted by $\epsilon_x(\omega)$, etc. For convenience, we have chosen Gaussian pulses peaking at $t = t_x$ and t_d respectively. As discussed in Sect. 1.2, the $\bar{\epsilon}_x(t)$ pulse induces a transition to a linear combination of two excited bound electronic state

with nuclear eigenfunctions $|E_1\rangle$ and $|E_2\rangle$, and the $\bar{\epsilon}_d(t)$ pulse dissociates the molecule by further exciting it to the continuous part of the spectrum. Both fields are chosen sufficiently weak for perturbation theory to be valid [48].

The superposition state prepared by the $\bar{\epsilon}_x(t)$ pulse, whose width is chosen to encompass just the two E_1 and E_2 levels, is given in first-order perturbation theory as

$$|\phi(t)\rangle = |E_g\rangle e^{-iE_g t/\hbar} + c_1|E_1\rangle e^{-iE_1 t/\hbar} + c_2|E_2\rangle e^{-iE_2 t/\hbar}, \tag{28}$$

where

$$c_k = (\sqrt{2\pi}/i\hbar)\langle E_k|\mathrm{d}|E_g\rangle \epsilon_x(\omega_{kg}),\ k = 1, 2, \tag{29}$$

with $\omega_{kg} \equiv (E_k - E_g)/\hbar$.

After a delay time of $\tau \equiv t_d - t_x$ the system is subjected to the $\bar{\epsilon}_d(t)$ pulse. It follows from Eq. (28) that after this delay time, each preparation coefficient has picked up an extra phase factor of $e^{-iE_k\tau/\hbar}$, $k = 1, 2$. Hence, the phase of c_1 relative to c_2 at that time increases by $[-(E_1 - E_2)\tau/\hbar = \omega_{2,1}\tau]$. Thus the natural two-state time evolution replaces the relative laser phase of the two-frequency control scenario of Sect. 1.3.

After the decay of the $\bar{\epsilon}_d(t)$ pulse, the system wave function is given as

$$|\psi(t)\rangle = |\phi(t)\rangle + \sum_{n,q}\int dE B(E, n, q|t)|E, n, q^-\rangle e^{-iEt/\hbar}. \tag{30}$$

The probability of observing the q fragments at total energy E in the remote future is therefore given as

$$P(E, q) = \sum_n |B(E, n, q|t = \infty)|^2$$

$$= (2\pi/\hbar^2)\sum_n |\sum_{k=1,2} c_k \langle E, n, q^-|\mathrm{d}|E_k\rangle \epsilon_d(\omega_{EE_k})|^2, \tag{31}$$

where $\omega_{EE_k} = (E - E_k)/\hbar$, and c_k is given by Eq. (29).

Expanding the square and using the Gaussian pulse shape gives

$$P(E, q) = (2\pi/\hbar^2)[|c_1|^2 \mathrm{d}_{1,1}^{(q)}\epsilon_1^2 + |c_2|^2 \mathrm{d}_{2,2}^{(q)}\epsilon_2^2$$
$$+2|c_1 c_2^* \epsilon_1 \epsilon_2 \mathrm{d}_{1,2}^{(q)}| \cos(\omega_{2,1}(t_d - t_x) + \alpha_{1,2}^{(q)}(E) + \phi)], \tag{32}$$

where $\epsilon_i = |\epsilon_d(\omega_{EE_i})|$, $\omega_{2,1} = (E_2 - E_1)/\hbar$, and the phases ϕ, $\alpha_{1,2}^{(q)}(E)$ are defined by

$$\langle E_1|\mathrm{d}|E_g\rangle\langle E_g|\mathrm{d}|E_2\rangle \equiv |\langle E_1|\mathrm{d}|E_g\rangle\langle E_g|\mathrm{d}|E_2\rangle| e^{i\phi}$$

$$\mathrm{d}_{i,k}^{(q)}(E) \equiv |\mathrm{d}_{i,k}^{(q)}(E)| e^{i\alpha_{i,k}^{(q)}(E)} = \sum_n \langle E, n, q^-|\mathrm{d}|E_i\rangle\langle E_k|\mathrm{d}|E, n, q^-\rangle. \tag{33}$$

Integrating over E to encompass the full width of the second pulse and forming the ratio $Y = P(q)/[\sum_q P(q)]$ gives the ratio of products in each of the two arrangement channels, i.e. the quantity we wish to control. Once again it is the sum of two direct photodissociation contributions plus an interference term.

Examination of Eq. (32) makes clear that the product ratio Y can be varied by changing the delay time $\tau = (t_d - t_x)$ or ratio $x = |c_1/c_2|$; the latter is most conveniently done by detuning the initial excitation pulse.

An example of this type of pump-dump control [11] is provided by the example of IBr photodissociation. Specifically, we showed computationally that it is possible to control the Br* vs. Br yield in this process, using two conveniently chosen picosecond pulses. The first pulse was chosen to prepare a linear superposition of two bound states that arise from mixing of the X and A states. A subsequent pulse pumps this superposition to dissociation where the relative yields of Br and Br* are examined. The results show the vast range of control that is possible with this relatively simple experimental setup.

Theoretical work on similar pump-dump scenarios for the control of the

$$\mathrm{D} + \mathrm{OH} \leftarrow \mathrm{HOD} \rightarrow \mathrm{H} + \mathrm{OD}$$

dissociation via the B-state [49] of HOD and the A-state [50] of HOD have recently been published. Work on pump-dump control of Li_2 photodissociation is in progress [51]

2.3 Resonantly Enhanced "2 vs. 2" Control of a Thermal Ensemble

In practice, there are a number of sources of incoherence that tend to diminish control. Prominent amongst these are effects due to an initial thermal distribution of states and effects due to partial coherence of the laser source. Below we describe one approach, based upon a resonant "2 vs. 2" scenario, that deals effectively with both problems. An alternative method, in which coherence is retained in the presence of collisions, is discussed elsewhere [7].

The specific scheme we advocate is the particular case of Na_2 photodissociation . Here the molecule is lifted from an initial bound state $|E_i, J_i, M_i\rangle$ to energy E via two independent two photon routes. To introduce notation, first consider a single such two-photon route. Absorption of the first photon of frequency ω_1 lifts the system to a region close to an intermediate bound state $|E_m J_m M_m\rangle$, and a second photon of frequency ω_2 carries the system to the dissociating states $|E, \hat{\mathbf{k}}, q^-\rangle$, where the scattering angles are specified by $\hat{\mathbf{k}} = (\theta_k, \phi_k)$. Here the J's are the angular momentum, the M's are their projections along the z-axis, and the values of energy, E_i and E_m, include specification of the vibrational quantum numbers. Specifically, if we denote the phases of the coherent states by ϕ_1 and ϕ_2, the wavevectors by $\mathbf{k}_1$ and $\mathbf{k}_2$ with overall phases $\theta_i = \mathbf{k}_i \cdot \mathbf{R} + \phi_i$ $(i = 1, 2)$, and the electric field amplitudes by ϵ_1 and ϵ_2, then the probability amplitude for resonant two-photon $(\omega_1 + \omega_2)$ photodissociation is given [15, 42] by

$$T_{\hat{\mathbf{k}}q,i}(E, E_i J_i M_i, \omega_2, \omega_1) =$$

$$\sum_{E_m,J_m} \frac{\langle E,\hat{\mathbf{k}},q^-|\mathrm{d}_2\epsilon_2|E_mJ_mM_i\rangle\langle E_mJ_mM_i|\mathrm{d}_1\epsilon_1|E_iJ_iM_i\rangle}{\omega_1-(E_m+\delta_m-E_i)+i\Gamma_m}\exp[i(\theta_1+\theta_2)] =$$

$$\frac{\sqrt{2\mathrm{m}k_q}}{h}\sum_{J,p,\lambda\geq 0}\sum_{E_m,J_m}\sqrt{2J+1}\begin{pmatrix} J & 1 & J_m \\ -M_i & 0 & M_i\end{pmatrix}\begin{pmatrix} J_m & 1 & J_i \\ -M_i & 0 & M_i\end{pmatrix}$$

$$\cdot D^{Jp}_{\lambda,M_i}(\theta_k,\phi_k,0)t(E,E_iJ_i,\omega_2,\omega_1,q|Jp\lambda,E_mJ_m)\exp[i(\theta_1+\theta_2)] \qquad (34)$$

Here d_i is the component of the dipole moment along the electric-field vector of the ith laser mode, $E=E_i+(\omega_1+\omega_2)$, δ_m and Γ_m are respectively the radiative shift and width of the intermediate state, m is the reduced mass, and k_q is the relative momentum of the dissociated product in the q-channel. The D^{Jp}_{λ,M_i} is the parity-adapted rotation matrix [52] with λ the magnitude of the projection on the internuclear axis of the electronic angular momentum and $(-1)^Jp$ the parity of the rotation matrix. We have set $\hbar\equiv 1$ and assumed for simplicity lasers that are linearly polarized and with parallel electric-field vectors. Note that the T-matrix element in Eq. (34) is a complex quantity, whose phase is the sum of the laser phase $\theta_1+\theta_2$ and the molecular phase, i.e., the phase of t matrix.

Because the t-matrix element contains a factor of $[\omega_1-(E_m+\delta_m-E_i)+i\Gamma_m]^{-1}$ the probability is greatly enhanced by the approximate inverse square of the detuning $\Delta=\omega_1-(E_m+\delta_m-E_i)$ as long as the line width Γ_m is less than Δ. Hence only the levels closest to the resonance $\Delta=0$ contribute significantly to the dissociation probability. *This allows us to photodissociate only a select number of states (preferably one) from a thermal bath.*

Consider then the following coherent control scenario. A molecule is irradiated with three interrelated frequencies $\omega_0,\omega_+,\omega_-$ where photodissociation occurs at $E=E_i+2\omega_0=E_i+(\omega_++\omega_-)$ and where ω_0 and ω_+ are chosen resonant with intermediate bound state levels. The probability of photodissociation at energy E into arrangement channel q is then given by the square of the sum of the T matrix elements from pathway "a" $(\omega_0+\omega_0)$ and pathway "b" $(\omega_++\omega_-)$. That is, the probability into channel q is given by

$$P_q(E,E_iJ_iM_i;\omega_0,\omega_+,\omega_-)\equiv$$
$$\int d\hat{\mathbf{k}}\left|T_{\hat{\mathbf{k}}q,i}(E,E_iJ_iM_i,\omega_0,\omega_0)+T_{\hat{\mathbf{k}}q,i}(E,E_iJ_iM_i,\omega_+,\omega_-)\right|^2$$
$$\equiv P^{(q)}(a)+P^{(q)}(b)+P^{(q)}(ab). \qquad (35)$$

Here $P^{(q)}(a)$ and $P^{(q)}(b)$ are the independent photodissociation probabilities associated with routes a and b respectively, and $P^{(q)}(ab)$ is the interference term between them, discussed below. Note that the two T matrix elements in Eq. (35) are associated with different lasers and as such contain different laser phases. Specifically, the overall phases of the three laser fields are $\theta_0=\mathbf{k}_0\cdot\mathbf{R}+\phi_0,\theta_+=\mathbf{k}_+\cdot\mathbf{R}+\phi_+$, and $\theta_-=\mathbf{k}_-\cdot\mathbf{R}+\phi_-$, where ϕ_0, ϕ_+, and ϕ_- are the photon phases, and $\mathbf{k}_0$, $\mathbf{k}_+$, and $\mathbf{k}_-$ are the wavevectors of the laser modes ω_0, ω_+, and ω_-, whose electric field strengths are $\epsilon_0,\epsilon_+,\epsilon_-$ and intensities I_0,I_+,I_-.

The optical path-path interference term $P^{(q)}(ab)$ is given by

$$P^{(q)}(ab)=2\epsilon_0^2\epsilon_+\epsilon_-|\mu^{(q)}_{ab}|\exp[i(\delta^q_a-\delta^q_b)]\cos(\alpha^q_a-\alpha^q_b) \qquad (36)$$

with relative phase

$$\alpha^q_a-\alpha^q_b=(\delta^q_a-\delta^q_b)+(2\theta_0-\theta_+-\theta_-), \qquad (37)$$

where the amplitude $|\mu^{(q)}_{ab}|$ and the molecular phase difference $(\delta^q_a-\delta^q_b)$ are defined by

$$\epsilon_0^2\epsilon_+\epsilon_-|\mu^{(q)}_{ab}|\exp[i(\delta^q_a-\delta^q_b)]=\frac{8\pi\mathrm{m}k_q}{h^2}\sum_{J,p,\lambda\geq 0}\sum_{E_m,J_m;E'_m,J'_m}$$
$$\begin{pmatrix} J & 1 & J_m \\ -M_i & 0 & M_i\end{pmatrix}\begin{pmatrix} J_m & 1 & J_i \\ -M_i & 0 & M_i\end{pmatrix}\begin{pmatrix} J & 1 & J'_m \\ -M_i & 0 & M_i\end{pmatrix}\begin{pmatrix} J'_m & 1 & J_i \\ -M_i & 0 & M_i\end{pmatrix}$$
$$\cdot t(E,E_iJ_i,\omega_0,\omega_0,q|Jp\lambda,E_mJ_m)t^*(E,E_iJ_i,\omega_-,\omega_+,q|Jp\lambda,E'_mJ'_m). \qquad (38)$$

Consider now the quantity of interest $R_{qq'}$, the branching ratio of the product in the q-channel to that in the q'-channel. Noting that in the weak field case $P^{(q)}(a)$ is proportional to ϵ_0^4, $P^{(q)}(b)$ to $\epsilon_+^2\epsilon_-^2$, and $P^{(q)}(ab)$ to $\epsilon_0^2\epsilon_+\epsilon_-$, we can write

$$R_{qq'}=\frac{\mu^{(q)}_{aa}+x^2\mu^{(q)}_{bb}+2x|\mu^{(q)}_{ab}|\cos(\alpha^q_a-\alpha^q_b)+(B^{(q)}/\epsilon_0^4)}{\mu^{(q')}_{aa}+x^2\mu^{(q')}_{bb}+2x|\mu^{(q')}_{ab}|\cos(\alpha^{q'}_a-\alpha^{q'}_b)+(B^{(q')}/\epsilon_0^4)}, \qquad (39)$$

where $\mu^{(q)}_{aa}=P^{(q)}(a)/\epsilon_0^4$, $\mu^{(q)}_{bb}=P^{(q)}(b)/(\epsilon_+^2\epsilon_-^2)$, and $x=\epsilon_+\epsilon_-/\epsilon_0^2=\sqrt{I_+I_-}/I_0$. The terms with $B^{(q)},B^{(q')}$, described below, correspond to resonant photodissociation routes to energies other than $E=E_i+2\hbar\omega_0$, and hence [4] to terms that do not coherently interfere with the a and b pathways. Minimization of these terms, due to absorption of $(\omega_0+\omega_-)$, $(\omega_0+\omega_+)$, $(\omega_++\omega_0)$, or $(\omega_++\omega_+)$, is discussed elsewhere [15, 42]. Here we just emphasize that the product ratio in Eq. (39) depends upon both the laser intensities and relative laser phase. Hence manipulating these laboratory parameters allows for control over the relative cross section between channels.

The proposed scenario, embodied in Eq. (39), also provides a means by which control can be improved by eliminating effects due to laser jitter. Specifically, the term $2\phi_0-\phi_+-\phi_-$ contained in the relative phase $\alpha^q_a-\alpha^q_b$ can be subject to the phase fluctuations arising from laser instabilities. If such fluctuations are sufficiently large, then the interference term in Eq. (39), and hence control, disappears [16]. We can eliminate this problem by generating ω_+ as $\omega_+=2\omega_0-\omega_-$ via frequency doubling of ω_0 and frequency differencing of ω_- from the resulting beam. It is easy to see that in this case the quantity $2\phi_0-\phi_+-\phi_-$ vanishes, irrespective of the phase jitter and drift of either source! Control is then attained by introducing an extra, perfectly controlled phase, χ, through the addition of a delay line in, say, the ω_- beam.

Typical computational results for Na_2 are provided elsewhere [15, 42]. Note also that control is not limited to two-product channels, such as those discussed above. Recent computations [42] on higher energy Na_2 photodissociation , where more product arrangement channels are available, show equally large ranges of control for the three-channel case.

3 Control of Symmetry Breaking

Weak field phase interference has one remarkable property; it can lead to controlled *symmetry breaking* [12]. Below we show that the pump–dump scheme described above (Sect. 2.2) can lead to symmetry breaking in systems with three-dimensional spherical symmetry and to the generation of chirality, provided that magnetic quantum state selection is performed. Other mechanisms for collinear symmetry breaking in *strong* fields have recently been proposed [53, 54]. There, for example, it was shown that one can generate *even* high harmonics by exciting a symmetric double quantum-well. However, in contrast to the symmetry breaking scenario described below, the generation of even harmonics is not expected to exist in systems with three dimensional spherical symmetry.

In general, symmetry breaking occurs whenever a system executes a transition to a *nonsymmetric* eigenstate of the Hamiltonian. Strictly speaking, nonsymmetric eigenstates (i.e., states that do not belong to any of the symmetry group representations) can occur if there exist several degenerate eigenstates, each belonging to a different irreducible representation. Any linear combination of such eigenstates is nonsymmetric.

Nonsymmetric eigenstates of a symmetric Hamiltonian also occur in the continuous spectrum of a BAB type molecule. It is clear that the $|\, E, n, R^- \,\rangle$ state, which correlates asymptotically with the dissociation of the right B group, must be degenerate with the $|\, E, n, L^- \,\rangle$ state, giving rise to the departure of the left B group. It is also possible to form a *symmetric* $|\, E, n, s^- \,\rangle$ and an *antisymmetric* $|\, E, n, a^- \,\rangle$ eigenstate of the same Hamiltonian by taking the $\pm$ combination of these states. There is an important physical distinction between the nonsymmetric states and states that are symmetric/antisymmetric: Any experiment performed in the asymptotic $B - -AB$ or $BA - -B$ regions must, by necessity, measure the probability of populating a nonsymmetric state. This follows because when the $B - -AB$ distance or the $BA - -B$ distance is large, a given group B is either far away from *or* close to group A. Thus symmetric and antisymmetric states are not directly observable in the asymptotic regime.

We conclude that the very act of observation of the dissociated molecule entails the collapse of the system to one of the nonsymmetric states. As long as the probability of collapse to the $|\, E, n, R^- \,\rangle$ state is equal to the probability of collapse to the $|\, E, n, L^- \,\rangle$ state, the collapse to a nonsymmetric state does not lead to a preference of R over L in an *ensemble* of molecules. This is the case when the above collapse is *spontaneous*, i.e., occurring due to some (random) factors not in our control. Coherent control techniques allow us to influence these probabilities. In this case, symmetry breaking is stimulated rather than spontaneous. This has far-reaching physical and practical significance.

One of the most important cases of symmetry breaking arises when the two B groups (now denoted by B and B') are not identical, but are enantiomers of one another. (Two groups of atoms are said to be enantiomers of one another if one is the mirror image of the other. If these groups are also "chiral," i.e., they lack a center of inversion symmetry, then the two enantiomers are distinguishable and can be detected through the distinctive direction of rotation of linearly polarized light.)

The existence and role of enantiomers is recognized as one of the fundamental broken symmetries in nature [55]. It has motivated a long-standing interest in asymmetric synthesis, i.e., a process that preferentially produces a specific chiral species. Contrary to the prevailing belief [56] that asymmetric synthesis must necessarily involve either chiral reactants or chiral external system conditions such as chiral crystalline surfaces, we show below that preferential production of a chiral photofragment can occur even though the parent molecule is not chiral. In particular, two results are demonstrated: (1) Ordinary photodissociation, using linearly polarized light, of a BAB' "pro-chiral" molecule may yield different cross- sections for the production of right-handed (B) and left-handed (B') products, when the direction of the angular momentum (m_j) of the products is selected; and (2) this natural symmetry breaking may be enhanced and controlled using coherent lasers.

To treat this problem we return to the formulation of the pump–dump scenario described above, with attention focused on control of the relative yield of two product arrangement channels, but with angular momentum projection m_j fixed. Explicitly considering the dissociation of BAB' into right- (R) and left- (L) hand products, we have

$$Y = P(L, m_j)/P(L, m_j) + P(R, m_j). \tag{40}$$

As above, the product ratio Y is a function of the delay time $\tau = (t_d - t_x)$ and ratio $x = |c_1/c_2|$, the latter by detuning the initial excitation pulse. Active control over the products $B + AB'$ vs. $B' + AB$, i.e., a variation of Y with τ and x, and hence control over left- vs. right-handed products, will result only if $P(R, m_j)$ and $P(L, m_j)$ have different functional dependences on x and τ.

We first note that this molecule belongs to the C_s point group, which is a group possessing only one symmetry plane. This plane, denoted by σ, is defined as the collection of the C_{2v} points, i.e., points satisfying the $B - -A = A - -B'$ condition, where $B - -A$ designates the distance between the B and A groups. We now show that $P(R, m_j)$ may be different from $P(L, m_j)$ for the $B'AB$ case. In order to do that, we choose the intermediate state $|\, E_1 \,\rangle$ to be *symmetric* and the state $|\, E_2 \,\rangle$ to be *antisymmetric* with respect to reflection in the σ plane. Furthermore, we shall focus upon transitions between electronic states of the same representations, e.g., A' to A' or A'' to A'' (where A' denotes the symmetric representation and A'' the antisymmetric representation of the C_s group). We further assume that the ground vibronic state belongs to the A' representation.

The first thing to demonstrate is that it is possible to excite simultaneously, by optical means, both the symmetric $|E_1\rangle$ and antisymmetric $|E_2\rangle$ states. Using Eq. (29) we see that this requires the existence of both a symmetric d component, denoted by d_s, and an antisymmetric d component, denoted by d_a, because by the symmetry properties of $|E_1\rangle$ and $|E_2\rangle$,

$$\langle E_1|d|E_g\rangle = \langle E_1|d_s|E_g\rangle, \quad \langle E_2|d|E_g\rangle = \langle E_2|d_a|E_g\rangle. \tag{41}$$

The existence of both dipole-moment components occurs in $A' \rightarrow A'$ electronic transitions whenever a bent $B'--A--B$ molecule deviates considerably from the equidistant C_{2v} geometries (where $d_a = 0$). The effect is nonFranck–Condon in nature, because we no longer assume that the dipole moment does not vary with the nuclear configurations. (In the theory of vibronic-transitions terminology the existence of both d_s and d_a is due to a Herzberg–Teller intensity borrowing [57] mechanism).

We conclude that the excitation pulse *can* create a $|E_1\rangle, |E_2\rangle$ superposition consisting of two states of different reflection symmetry, which is therefore nonsymmetric. We now wish to show that this nonsymmetry, established by exciting *nondegenerate bound* states, translates to a nonsymmetry in the probability of populating the two *degenerate* $|E,n,R^-\rangle, |E,n,L^-\rangle$ *continuum* states. We proceed by examining the properties of the bound-free transition matrix elements of Eq. (33) entering the probability expression of Eq. (32).

Although the continuum states of interest $|E,n,q^-\rangle$ are nonsymmetric, they satisfy a closure relation, since $\sigma|E,n,R^-\rangle = |E,n,L^-\rangle$ and vice versa. Working with the symmetric and antisymmetric continuum eigenfunctions

$$|E,n,R^-\rangle \equiv (|E,n,s^-\rangle + |E,n,a^-\rangle)/\sqrt{2}, \tag{42}$$

$$|E,n,L^-\rangle \equiv (|E,n,s^-\rangle - |E,n,a^-\rangle)/\sqrt{2}, \tag{43}$$

using the fact that $|E_1\rangle$ is symmetric and $|E_2\rangle$ antisymmetric, and adopting the notation $A_{s2} \equiv \langle E,n,s^-|d_a|E_2\rangle$, $S_{a1} \equiv \langle E,n,a^-|d_s|E_1\rangle$, etc. we have

$$d_{11}^{(q)} = \sum{}' [|S_{s1}|^2 + |A_{a1}|^2 \pm 2Re(A_{a1}S_{s1}^*)] \tag{44}$$

$$d_{22}^{(q)} = \sum{}' [|A_{s2}|^2 + |S_{a2}|^2 \pm 2Re(A_{s2}S_{a2}^*)] \tag{45}$$

$$d_{12}^{(q)} = \sum{}' [S_{s1}A_{s2}^* + A_{a1}S_{a2}^* \pm S_{s1}S_{a2}^* \pm A_{a1}A_{s2}^*], \tag{46}$$

where the plus sign applies for $q = R$ and the minus sign for $q = L$.

Equation (46) displays two noteworthy features:

(1) $d_{kk}^{(R)} \neq d_{kk}^{(L)}$, $k = 1,2$. That is, the system displays *natural symmetry breaking* in photodissociation from state $|E_1\rangle$ or state $|E_2\rangle$, with right- and left-handed product probabilities differing by $4\sum'$ $\mathrm{Re}(S_{s1}^*A_{a1})$ for excitation from $|E_1\rangle$, and $4\sum'$ $\mathrm{Re}(A_{s2}S_{a2}^*)$ for excitation from $|E_2\rangle$. Note that these symmetry breaking terms may be relatively small, since they rely upon nonFranck–Condon contributions. However, even in the Franck–Condon approximation,

(2) $d_{12}^{(R)} \neq d_{12}^{(L)}$. Thus laser-controlled symmetry breaking, which depends upon $d_{12}^{(q)}$ in accordance with Eq. (32), is therefore possible, allowing enhancement of the enantiomer ratio for the m_j polarized product.

We have demonstrated the extent of expected control, by considering a model symmetry breaking in the HOH photodissociation in three dimensions, where the two hydrogens are assumed distinguishable [12]. The computation was done using the formulation and computational methodology of Segev et al. [58].

4 Control with Intense Laser Fields

We now consider some extensions of CC to strong laser fields. Parallel work involving other strong field scenarios has been done by Bandrauk et al. [43], Corkum et al. [47], Bardsley et al. [44], Lambropoulos et al. [59] and Guisti-Suzor et al. [45]. Here we concentrate on a strong field control scenario in which the dependence on the relative phase between the two laser beams, and hence on laser coherence, disappears. As a result, coherence plays no role in this scenario (save for being intimately linked with the existence of the narrow-band laser sources needed for its execution). Although the unimportance of coherence means that we lose phase control, the effect still depends on quantum interference phenomena. The scenario is therefore called *interference control*.

To illustrate interference control, we look at the control of the electronic states of Na atoms generated by the photodissociation of Na_2, a process treated in the context of weak field CC in Sect. 2.3. We envision a scenario in which we employ two laser sources: One laser (not necessarily intense) with center frequency ω_1 is used to excite a molecule from an initially populated bound state $|E_i\rangle$ to a dissociative state $|E,m,q^-\rangle$. A second laser, with frequency ω_2, is used to couple ("dress") the continuum with some (initially unpopulated) bound states $|E_j\rangle$. With both lasers on, dissociation to $|E,m,q^-\rangle$ occurs via one direct $|E_i\rangle \rightarrow |E,m,q^-\rangle$, and a multitude of indirect, e.g., $|E_i\rangle \rightarrow |E,m,q^-\rangle \rightarrow |E_j\rangle \rightarrow |E,m,q^-\rangle$, pathways. The interference between these pathways to form a given channel q at product energy E can be either constructive or destructive. As we show below, varying the frequencies and intensities of the two excitation lasers strongly affects this interference term, providing a means of controlling the photodissociation line shape, and the branching ratio into different products.

With this scenario in mind, we now briefly discuss the methodology of dealing with strong laser fields and the extension of CC ideas to this domain. We consider the photodissociation of a molecule with Hamiltonian H_M in the presence of a radiation field with Hamiltonian H_R whose eigenstates are the Fock states $|n_k\rangle$ with energy $n_k\hbar\omega_k$. (In the case of several frequencies, the repeated index in $n_k\omega_k$ implies the sum over the modes.)

Strong field dynamics is completely embodied [60] in the fully interacting eigenstates of the total Hamiltonian H, $H = H_M + H_R + V$, where V is the light-matter interaction, denoted by $|(E,m,q^-),n_k^-\rangle$:

$$H|(E,m,q^-),n_k^-\rangle = (E + n_k\hbar\omega_k)|(E,m,q^-),n_k^-\rangle\ . \tag{47}$$

The minus superscript on n_k is used in exactly the same way as in the weak field domain: it is a reminder that each $|(E,m,q^-),n_k^-\rangle$ state correlates to a noninteracting $|(E,m,q^-),n_k\rangle \equiv |E,m,q^-\rangle|n_k\rangle$ state when the light-matter interaction V is switched off.

If the system is initially in the $|E_i,n_i\rangle \equiv |E_i\rangle|n_i\rangle$ state and we suddenly switch on V, the photodissociation amplitude to form in the future the product state $|E,m,q^-\rangle|n_k\rangle$ is given simply [60] as the overlap between the initial state and fully interacting state $\langle(E,m,q^-),n_k^-|E_i,n_i\rangle$. This overlap assumes the convenient form

$$\langle(E,m,q^-),n_k^-|E_i,n_i\rangle = \langle(E,m,q^-),n_k|VG(E^+ + n_k\hbar\omega_k)|E_i,n_i\rangle, \qquad (48)$$

by using the Lippmann–Schwinger equation

$$\langle(E,m,q^-),n_k^-| = \langle(E,m,q^-),n_k| + \langle(E,m,q^-),n_k|VG(E^+ + n_k\hbar\omega_k). \qquad (49)$$

Here $G(\mathcal{E}) = 1/(\mathcal{E}-H)$ and $E^+ = E + i\delta$, with $\delta \to 0^+$ at the end of the computation. Equation (48) is exact and provides a connection between the photodissociation amplitude and the VG matrix element. It is the latter that we compute exactly using a high field extension of the artificial channel method [61, 62].

Two quantities are of interest: the channel specific line shape,

$$A(E,q,n_k|E_i,n_i) = \int d\hat{\mathbf{k}}\,|\langle(E,\hat{\mathbf{k}},q^-),n_k^-|E_i,n_i\rangle|^2, \qquad (50)$$

and the total dissociation probability to channel q,

$$P(q) = \sum_{n_k}\int dE\,A(E,q,n_k|E_i,n_i). \qquad (51)$$

In Eq. (51), the sum is over photons that excite the molecule above the dissociation threshold. In writing (50), diatomic dissociation is assumed, so that $m = \hat{\mathbf{k}}$.

Consider, for example, the photodissociation of Na_2 from the $|E_i\rangle = |v=19,^3\Pi_u\rangle$ initial state, where v denotes the vibrational quantum number in the $^3\Pi_u$ electronic potential [63]. $|E_i\rangle$ is assumed to have been prepared by previous excitation from the ground electronic state. Excitations from $|E_i\rangle$ by ω_1 and mixing of the initially unpopulated $|E_j\rangle$ by ω_2 to the dissociating continua produce Na(3s)+Na(3p) and Na(3s)+Na(4s). Computations were done with ω_1 chosen within the range 15,430 $\text{cm}^{-1} < \omega_1 <$ 15,700 cm^{-1} with intensity $I_1 \sim 10^{10}$ W/cm^2, which is sufficiently energetic to dissociate levels of the $^3\Pi_u$ state with $v \geq 19$ to both Na(3s) + Na(3p) and Na(3s) + Na(4s). The second laser has fixed frequency $\omega_2 = 13,964$ cm^{-1} and intensity $I_2 = 3.2\times10^{11}$ W/cm^2 and can dissociate levels with $v \geq 26$ to both products. Under these circumstances the contribution of above threshold dissociation is found to be negligible. However cognizance must be taken of the possibility of dissociation of $|E_i\rangle$ by ω_2 and of $|E_j\rangle$ by ω_1. These processes do not interfere and cannot be controlled. Hence we must find the range of parameters that minimizes them.

Computational studies [64] show that extensive control over product branching in Na_2 photodissociation is possible. In addition, recent experimental results on this system [38] confirm the theory. Indeed, experimental and theoretical results are in excellent agreement with one another [38, 65].

5 Bimolecular Processes

Until recently, the issue of effectively controlling collisional events was, despite some effort [66], unresolved. The difficulty is that the extension of coherent control scenarios based on the preparation of initial superposition states requires that one optically prepare a coherent superposition of *degenerate* continuum states. This is difficult, but it is required because only states of the same total energy can interfere to alter the reaction products. Quite recently, we demonstrated [67] methods of achieving this goal, as described below.

Consider the collision of a beam of molecules B with a beam of molecules or atoms C, that yields products F and G, i.e.,

$$B + C \to F + G. \qquad (52)$$

F and G can be identical to (nonreactive scattering), or different from (reactive scattering) B and C. We call $B+C$ the β arrangement and $F+G$ the γ arrangement. Traditional time-independent scattering theory proceeds by considering (52) with $B+C$ starting in an eigenstate of the free Hamiltonian H_β^0 in the β arrangement:

$$H_\beta^0 = K_\beta + h_B + h_C, \qquad (53)$$

with K_β being the kinetic energy of the $B-C$ relative motion and h_B, h_C denoting the internal Hamiltonians of B and C.

To attain control over the process, consider then the following superposition, which we show below, can be realized experimentally, as the initial asymptotic state

$$|\,\mathrm{n},\beta\rangle = |\,0,C\rangle\sum_{i=1,2} a_i|\,i,B\rangle|\,E_\beta^{kin}(i)\rangle|\,E_{cm}(i)\rangle, \qquad (54)$$

Here

$$E_\beta^{kin}(i) = E - \varepsilon_C(0) - \varepsilon_B(i). \qquad (55)$$

where $|\,i,X\rangle$ with $X = B,C$ are eigenstates, of energy $\varepsilon_X(i)$, of h_B and h_C,

$$[\varepsilon_X(i) - h_X]|\,i,X\rangle = 0, \quad X = B,C. \qquad (56)$$

The $|\,E_\beta^{kin}(i)\rangle$ and $|\,E_{cm}(i)\rangle$ states are plane waves describing the free motion of B relative to C and the motion of the $B-C$ center of mass, i.e., $\langle\mathbf{r}_{BC}|\,E_\beta^{kin}(i)\rangle = \exp(i\mathbf{k}_i\cdot\mathbf{r}_{BC})$, $\langle\mathbf{R}_{BC}|\,E_{cm}(i)\rangle = \exp(i\mathbf{K}_i\cdot\mathbf{R}_{BC})$, where $|\mathbf{k}_i| = \{2\mu_{BC}E_\beta^{kin}(i)\}^{\frac{1}{2}}/\hbar$, $\mu_{BC} = m_Bm_C/(m_B+m_C)$ is the reduced mass of the BC

pair, and $\mathbf{K}_i$ is the BC center of mass momentum. Here $\mathbf{R}_{BC}, \mathbf{r}_{BC}$ are the position of the BC center of mass and the $B-C$ relative vector, respectively.

The superposition state $|\,\mathrm{n},\beta\,\rangle$ is composed of degenerate eigenstates of H^0_β,

$$[E - H^0_\beta]|\,0,C\,\rangle|\,i,B\,\rangle|\,E - \varepsilon_C(0) - \varepsilon_B(i)\,\rangle = 0, \tag{57}$$

and center of mass terms. As a result, we can use standard time-independent scattering theory to calculate the cross-section for scattering from this state to any of the γ-arrangement final states. The latter states, of the form $|\,j,\gamma\rangle|\,E^{kin}\,\rangle|\,E_{cm}(i)\,\rangle$, have a component in the center of mass system that satisfies the free Schrödinger equation in the product space,

$$[E - H^0_\gamma]|\,j,\gamma\rangle|\,E - \varepsilon_\gamma(j)\,\rangle = 0, \tag{58}$$

where $|\,j,\gamma\,\rangle$ are the eigenstates of the $F+G$ internal Hamiltonians,

$$[\varepsilon_\gamma(j) - h_F - h_G]|\,j,\gamma\,\rangle = 0, \tag{59}$$

and $H^0_\gamma = K_\gamma + h_F + h_G$ is analogous to (53), describing the product in arrangement γ.

The cross-section for forming one of the γ-arrangement final states, having started from the $|\,\mathrm{n},\beta\,\rangle$ superposition state, is given by

$$\sigma(j,\gamma \leftarrow \mathrm{n},\beta|E) = |\sum_{l=1,2}\langle\, E_{cm}(l)\,|\langle\, E,j,\gamma^-\,|V_\beta|\,\mathrm{n},\beta\,\rangle|^2 \tag{60}$$

Here $V_\beta = H - H^0_\beta$ is the (reactive or nonreactive) interaction potential, with H being the Hamiltonian in the center of mass system. The $|\,E,j,\gamma^-\,\rangle$ are incoming eigenstates of H,

$$[E - H]|\,E,j,\gamma^-\,\rangle = 0, \tag{61}$$

which go over in the asymptotic limit to a specific free state of the $F+G$ products,

$$\exp(-iEt/\hbar)|\,E,j,\gamma^-\,\rangle \overset{t\to\infty}{\to} \exp(-iEt/\hbar)|\,E-\varepsilon_\gamma(j)\,\rangle|\,j,\gamma\,\rangle. \tag{62}$$

Substituting Eq. (54) in Eq. (60) gives, for the reactive cross-section,

$$\sigma(j,\gamma \leftarrow \mathrm{n},\beta|E) =$$

$$|\sum_{l=1,2}\langle\, E_{cm}(l)\,|\sum_{i=1,2} a_i\langle\, E,j,\gamma^-\,|V_\beta|\,0,C\,\rangle|\,i,B\,\rangle|\,E^{kin}_\beta(i)\,\rangle|\,E_{cm}(i)\,\rangle|^2 =$$

$$|a_1|^2\sigma^R_{11}(j) + |a_2|^2\sigma^R_{22}(j) + 2\mathrm{R_e}a_1^*a_2\sigma^R_{12}(j), \quad \gamma \neq \beta \tag{63}$$

where

$$\sigma^R_{ii}(j) = |\langle\, E,j,\gamma^-\,|V_\beta|\,0,C\,\rangle|\,i,B\,\rangle|\,E^{kin}_\beta(i)\,\rangle|^2, \; i=1,2,$$

$$\sigma^R_{12}(j) = \langle\, E^{kin}_\beta(1)\,|\langle\, 1,B\,|\langle\, 0,C\,|V_\beta|\,E,j,\gamma^-\,\rangle\langle\, E,j,\gamma^-\,|V_\beta|\,0,C\,\rangle|\,2,B\,\rangle|\,E^{kin}_\beta(2)\,\rangle$$
$$\times\langle E_{cm}(1)|\,E_{cm}(2)\,\rangle, \quad \gamma \neq \beta. \tag{64}$$

Although the matrix element $\langle E_{cm}(1)|\,E_{cm}(2)\,\rangle = \int d\mathbf{R}_{BC}\exp[i(\mathbf{K}_2 - \mathbf{K}_1)\cdot \mathbf{R}_{BC}]$ integrated over all space is zero, the proper region of integration in this case is the intersection volume of the B and C beams. Hence if $(\mathbf{K}_2 - \mathbf{K}_1)$ is made sufficiently small, then the integral over this region can be made nonzero, and control over the cross-section is possible. An experimental means of achieving this result is discussed below.

Although (64) indicates that one can control detailed cross sections, often we only want to control the total reactive vs. the total nonreactive cross-section. In that case, the reactive to nonreactive branching ratio is given as

$$\frac{\sigma^R}{\sigma^{NR}} = \frac{\sum_j \sigma(j,\gamma\neq\beta \leftarrow \mathrm{n},\beta|E)}{\sum_j \sigma(j,\beta \leftarrow \mathrm{n},\beta|E)} =$$

$$\frac{\sigma^R_{11} + x^2\sigma^R_{22} + 2x|\sigma^R_{12}|\cos(\delta^R_{12}+\theta_{12})}{\sigma^{NR}_{11} + x^2\sigma^{NR}_{22} + 2x|\sigma^{NR}_{12}|\cos(\delta^{NR}_{12}+\theta_{12})}, \tag{65}$$

where $x = |a_2/a_1|$, $\theta_{12} = arg(a_2/a_1)$, $\sigma^R_{ik} = \sum_j \sigma^R_{ik}(j)$, $i,k = 1,2$, with similar definitions holding for σ^{NR}_{ik}, and $\delta^R_{12} = arg(\sigma^R_{12})$, $\delta^{NR}_{12} = arg(\sigma^{NR}_{12})$. Thus, the reactive vs. nonreactive cross-section ratio can be controlled by varying the relative magnitude, x, and the relative phase, θ_{12}, of the a_1 and a_2 coefficients.

Control over the a_i can be attained by a number of routes. One approach prepares the $B-C$ superposition by exciting B to a superposition state and colliding the result with C. Specifically, consider preparing $|\,\mathrm{n},\beta\,\rangle$ by first irradiating $|\,1,B\,\rangle|\,E^{kin}_B(1)\,\rangle$ to produce

$$|\,\mathrm{n},B\,\rangle = \sum_{i=1,2} a_i|\,i,B\,\rangle|\,E^{kin}_B(1)\,\rangle, \tag{66}$$

where $|\,E^{kin}_B(1)\,\rangle$ describes the motion of the center of mass of B. Passing this superposition through a hexapole field or using laser cooling techniques allows us to alter the velocities of $|\,1,B\,\rangle$ and $|\,2,B\,\rangle$, giving

$$|\,\mathrm{n},B\,\rangle = \sum_{i=1,2} a_i|\,i,B\,\rangle|\,E^{kin}_B(i)\,\rangle, \tag{67}$$

where $\langle\,\mathbf{r}_B\,|E^{kin}_B(i)\rangle = \exp(i\mathbf{k}^B_i\cdot\mathbf{r}_B)$, $\mathbf{k}^B_1 \neq \mathbf{k}^B_2$, and where $\mathbf{r}_B$ is the lab position of B. Colliding the $|\,\mathrm{n},B\,\rangle$ superposition state with particle C, of momentum $\mathbf{k}^C$, gives the $B-C$ superposition state

$$|\,\psi\,\rangle = |\,0,C\,\rangle\sum_{i=1,2} a_i|\,i,B\,\rangle|\,E^{kin}_B(i)\,\rangle|\,E^{kin}_C\,\rangle|\,E_{cm}(i)\,\rangle, \tag{68}$$

To produce (54), however, requires that the degeneracy condition (55), be satisfied, i.e., that

$$E^{kin}_\beta(1) - E^{kin}_\beta(2) = \varepsilon_B(2) - \varepsilon_B(1). \tag{69}$$

That is, with $\mathbf{K}_i = \mathbf{k}^B_i + \mathbf{k}_C$ and with the $B-C$ relative center of mass momentum given by $\mathbf{k}_i = (m_C\mathbf{k}^B_i - m_B\mathbf{k}_C)/(m_B+m_C)$, (68) becomes

$$(\hbar^2/2\mu_{BC})(k_1^2 - k_2^2) = \varepsilon_B(2) - \varepsilon_B(1), \tag{70}$$

or

$$\{\hbar^2/[2(m_B+m_C)]\}[(m_C/m_B)((k_1^B)^2-(k_2^B)^2)-2\mathbf{k}_C\cdot(\mathbf{k}_1^B-\mathbf{k}_2^B)] = \varepsilon_B(2)-\varepsilon_B(1). \quad (71)$$

Thus, to achieve control requires that $\mathbf{k}_i^B, \mathbf{k}_C$ be chosen to satisfy the degeneracy condition imposed by (71). Further, $\langle E_{cm}(1)|\, E_{cm}(2)\,\rangle$ must be nonzero. Since by virtue of the definition of $\mathbf{K}_i$, $\int d\mathbf{R}_{BC}\exp[i(\mathbf{K}_1-\mathbf{K}_2)\cdot\mathbf{R}_{BC}] = \int d\mathbf{R}_{BC}\exp[i(\mathbf{k}_1^B-\mathbf{k}_2^B)\cdot\mathbf{R}_{BC}]$, if $(\mathbf{k}_1^B-\mathbf{k}_2^B)$ is made sufficiently small then $\langle E_{cm}(1)|\, E_{cm}(2)\,\rangle$ is nonzero when integrated over the volume of intersection of the B and C beams. Under these circumstances, (55) becomes

$$\{\hbar^2/(m_B+m_C)\}[\mathbf{k}_C\cdot(\mathbf{k}_1^B-\mathbf{k}_2^B)] \approx \varepsilon_B(1)-\varepsilon_B(2), \quad (72)$$

so that large $\mathbf{k}_C$ may be required to satisfy this condition. With such a $\mathbf{k}_C$, bimolecular control, regulated by the amplitude and phases of the a_i, is established.

Alternative methods of preparing the superposition in (54) and maintaining a nonzero $\langle E_{cm}(1)|\, E_{cm}(2)\,\rangle$ can be envisioned. The most obvious deals with superposing degenerate states of B. The energy degeneracy requirement is then automatically satisfied, and since $\mathbf{K}_1 = \mathbf{K}_2$, then $\langle E_{cm}(1)|\, E_{cm}(2)\,\rangle$ is trivially nonzero. Examples include collisions such as $H(2s)+D$ in a superposition with $H(2p)+D$, where D is a molecule and where $H(2s), H(2p)$ result from a

rior coherently controlled photolysis of H_2. Similarly, one can envision using elliptically polarized light to prepare a superposition of m_j states, where m_j is the z-projection of the rotational angular momentum of a diatomic B, and then colliding the result with C. Once again, the degeneracy of the states ensures that control is possible and that the center of mass overlap matrix element is nonzero[68].

Finally, note that the above *formalism* can be readily extended to general superposition states of the form

$$|\,\mathrm{n},\beta\,\rangle = \sum_{i,l} a_{il}|\,i,B\,\rangle|\,l,C\,\rangle|\,E_\beta^{kin}(i,l)\,\rangle|\,E_{cm}(i,l)\,\rangle, \quad (73)$$

with $E_\beta^{kin}(i,l) = E-\varepsilon_C(l)-\varepsilon_B(i)$. Here, the $|\,E_\beta^{kin}(i,l)\,\rangle$ states are plane waves describing the free motion of B relative to C, ($\langle\mathbf{R}|\,E_\beta^{kin}(i,l)\,\rangle \equiv \exp(i\mathbf{k}_{il}\cdot\mathbf{R})$), where $|\mathbf{k}_{il}| = [2\mu_{BC}E_\beta^{kin}(i,l)]^{\frac{1}{2}}/\hbar$. That is, we can show that such a superposition leads to interference if the $\langle E_{cm}(j,k)|\, E_{cm}(i,l)\,\rangle$ are nonzero, and hence to the possibility of control over the reaction cross-sections. We are currently examining possible methods for experimentally realizing such states.

The possibility of successfully applying coherent control techniques to bimolecular processes opens up a vast new area of control research.

6 Conclusions

Our discussion makes clear that the characteristic features that we invoke in order to control chemical reactions are purely quantum in nature. There is, for example, little classical about the time-dependent picture where the ultimate outcome of the deexcitation, i.e., product H + HD or H_2 + D, depends entirely upon the phase and amplitude characteristics of the wave function. Indeed, as repeatedly emphasized above, if, e.g., collisional effects are sufficiently strong so as to randomize the phases, then reaction control is lost. Hence reaction dynamics are intimately linked to the wave function phases, which are controllable through coherent optical phase excitation.

These results must be viewed in light of the history of molecular reaction dynamics over the past two decades. Possibly the most useful result of the reaction dynamics research effort has been the recognition that the vast majority of qualitatively important phenomena in reaction dynamics are well described by classical mechanics. Quantum and semiclassical mechanics were viewed as necessary only insofar as they correct quantitative failures of classical mechanics for unusual circumstances and/or for the dynamics of very light particles. Considering reaction dynamics in traditional chemistry to be essentially classical in character therefore appeared to be essentially correct for the vast majority of naturally occurring molecular processes. Coherence played no role. The coherent control approach makes clear, however, that coherence phenomena have great potential for application. The quantum phase is always present and can be used to our advantage, even though it is irrelevant to traditional chemistry. By calling attention to the extreme importance of coherence phenomena to controlled chemistry we herald the introduction of a new focus in atomic and molecular science, i.e., introducing coherence in controlled environments to modify molecular processes, thus defining the area of coherence chemistry.

Acknowledgments

. We acknowledge support for this research by the U.S. Office of Naval Research.

References

1. P. Brumer and M. Shapiro, Chem. Phys. Lett. **126**, 541 (1986).
2. M. Shapiro and P. Brumer, J. Chem. Phys. **84**, 4103 (1986).
3. P. Brumer and M. Shapiro, Faraday Disc. Chem. Soc. **82**, 177 (1986).
4. M. Shapiro and P. Brumer, J. Chem. Phys. **84**, 4103 (1986).
5. C. Asaro, P. Brumer, and M. Shapiro, Phys. Rev. Lett. **60**, 1634 (1988).
6. M. Shapiro, J. Hepburn, and P. Brumer, Chem. Phys. Lett. **149**, 451 (1988).
7. P. Brumer and M. Shapiro, J. Chem. Phys. **90**, 6179 (1989).
8. G. Kurizki, M. Shapiro, and P. Brumer, Phys. Rev. B, **39**, 3435 (1989).
9. T. Seideman, M. Shapiro, and P. Brumer, J. Chem. Phys. **90**, 7136 (1989).
10. J. Krause, M. Shapiro, and P. Brumer, J. Chem. Phys. **92**, 1126 (1990).
11. I. Levy, M. Shapiro, and P. Brumer, J. Chem. Phys., **93**, 2493 (1990).
12. M. Shapiro and P. Brumer, J. Chem. Phys. **95**, 8658 (1991).
13. P. Brumer and M. Shapiro, Ann. Rev. Phys. Chem. **43**, 257 (1992).
14. M. Shapiro and P. Brumer, J. Chem. Phys. **97**, 6259 (1992).
15. Z. Chen, P. Brumer, and M. Shapiro, Chem. Phys. Lett. **198**, 498 (1992).

16. X.-P. Jiang, P. Brumer, and M. Shapiro, J. Chem. Phys. **104**, 607 (1996).
17. J. Dods, P. Brumer, and M. Shapiro, Can. J. Chem **72**, (Polanyi Honor Issue) 958 (1994).
18. D. J. Tannor and S. A. Rice, J. Chem. Phys. **83**, 5013 (1985); D. J. Tannor, R. Kosloff, and S. A. Rice, J. Chem. Phys. **85**, 5805 (1986).
19. S. A. Rice, D. J. Tannor, and R. Kosloff, J. Chem. Soc. Faraday Trans. **82**, 2423 (1986).
20. D. J. Tannor and S. A. Rice, Adv. Chem. Phys. **70**, 441 (1988).
21. R. Kosloff, S. A. Rice, P. Gaspard, S. Tersigni, and D. J. Tannor, Chem. Phys. **139**, 201 (1989).
22. S. Tersigni, P. Gaspard, and S. A. Rice, J. Chem. Phys. **93**, 1670 (1990).
23. S. Shi, A. Woody, and H. Rabitz, J. Chem. Phys. **88**, 6870 (1988); S. Shi and H. Rabitz, Chem. Phys. **139**, 185 (1989).
24. A. P. Peirce, M. Dahleh, and H. Rabitz, Phys. Rev. A **37**, 4950 (1988).
25. S. Shi and H. Rabitz, J. Chem. Phys. **92**, 364 (1990).
26. J. L. Krause, R. M. Whitnell, K. R. Wilson, Y. Yan, and S. Mukamel, J. Chem. Phys. **99**, 6562 (1993).
27. W. Jakubetz, B. Just, J. Manz, and H.-J. Schreier, J. Phys. Chem. **94**, 2294 (1990).
28. C. Chen, Y.-Y. Yin, and D. S. Elliott, Phys. Rev. Lett. **64**, 507 (1990) ; *ibid* **65**, 1737.
29. S. M. Park, S.-P. Lu, and R. J. Gordon, J. Chem. Phys. **94**, 8622 (1991); S.-P. Liu, S. M. Park, Y. Xie, and R. J. Gordon, J. Chem. Phys. **96**, 6613 (1992).
30. L. Zhu, U. Kleiman, X. Li, S.-P. Lu, K. Trentelman, and R. J. Gordon, Science **270**, 77 (1995).
31. N. F. Scherer, A. J. Ruggiero, M. Du, and G. R. Fleming J. Chem. Phys. **93**, 856 (1990).
32. K. J. Boller, A. Imamoglu, and S. E. Harris, Phys. Rev. Lett. **66**, 2593 (1991).
33. B. A. Baranova, A. N. Chudinov, and B. Ya. Zel'dovitch, Opt. Comm. **79**, 116 (1990).
34. Y.-Y. Yin, C, Chen, D. S. Elliott, and A. V. Smith, Phys. Rev. Lett. **69**, 2353 1992.
35. E. Dupont, P. B. Corkum, H. C. Liu, M. Buchanan, and Z. R. Wasilewski, Phys. Rev. Lett. **74**, 3596 (1995).
36. B. Sheeny, B. Walker, and L. F.Dimauro, Phys. Rev. Lett. **74**, 4799 (1995).
37. Y.-Y. Yin, R. Shehadeh, D. Elliott, and E. Grant, Chem. Phys. Lett. **241**, 591 (1995).
38. A. Shnitman, I. Sofer, I. Golub, A. Yogev, M. Shapiro, Z. Chen, and P. Brumer, Phys. Rev. Lett. **76**, 2886 (1996).
39. For a discussion see, e.g., J. D. Macomber *The Dynamics of Spectroscopic Transitions* (Wiley, N.Y., 1976)
40. This is the asymptotic condition of scattering theory; see J. R. Taylor, *Scattering Theory* (Wiley, N.Y., 1972).
41. Z. Chen, M. Shapiro and P. Brumer, Chem. Phys. Lett. **228**, 289 (1994).
42. Z. Chen, P. Brumer and M. Shapiro, J. Chem. Phys. **98**, 6843 (1993).
43. S. Chelkowski and A. D. Bandrauk, Chem. Phys. Lett. **186**, 284 (1991); A. D. Bandrauk, J. M. Gauthier, and J. F. McCann, Chem. Phys. Lett. **200**, 399 (1992).
44. A. Szöke, K. C. Kulander, and J. N. Bardsley, J. Phys. B **24**, 3165 (1991) ; R. M. Potvliege and P. H. G. Smith, J. Phys. B **25**, 2501 (1992).
45. E. Charron, A. Guisti-Suzor and F. H. Mies, Phys. Rev. Lett. **71**, 692 (1993).
46. R. Blank and M. Shapiro, Phys. Rev. A **52**, 4278 (1995).
47. S. Chelkowski, A. D. Bandrauk, and P. B. Corkum, Phys. Rev. Lett. **65**, 2355 (1990).
48. The use of perturbation theory does not necessarily imply small total yields. Computational results (P. Brumer and M. Shapiro – to be published) indicate that perturbation theory is quantitatively correct for dissociation probabilities as large as 0.20.
49. M. Shapiro and P. Brumer, J. Chem. Phys. **98**, 201 (1993).
50. N. E.Henriksen and B. Amstrup, Chem. Phys. Lett. **213**, 65 (1993) ; *J. Chem. Phys.* **97** 8285
51. D. Abrashkevich, M. Shapiro, and P. Brumer (to be published).
52. I. Levy I and M. Shapiro, J. Chem. Phys. **89**, 2900 (1988).
53. R. Bavli and H. Metiu, Phys. Rev. Lett. **69**, 1986 (1992).
54. M. Yu. Ivanov, P. B. Corkum, and P. Dietrich, Laser Physics **3**, 375 (1993).
55. L. D. Barron, 1982 *Molecular Light Scattering and Optical Activity* (Cambridge Univ. Press, Cambridge, 1982); R. G. Woolley,Adv. Phys. **25**, 27 (1975) ; *Origins of Optical Activity in Nature*, ed., D. C. Walker (Elsevier, Amsterdam, 1979).
56. For a discussion see L. D. Barron, Chem. Soc. Rev. **15**, 189 (1986).
57. J. M. Hollas,*High Resolution Spectroscopy* (Butterworths, London, 1972).
58. E. Segev E and M. Shapiro, J. Chem. Phys. **77**, 5604 (1982).
59. T. Nakajima and P. Lambropoulos, Phys. Rev. Lett. **70**, 1081 (1993).
60. P. Brumer and M. Shapiro,*Adv. Chem. Phys.* **60**, 371, ed. K. P. Lawley (Wiley-Interscience, N.Y., 1986).
61. M. Shapiro and H. Bony, J. Chem. Phys. **83**, 1588 (1985); G..G. Balint-Kurti and M. Shapiro, *Adv. Chem. Phys.* **60**, 403, ed. K. P. Lawley (Wiley-Interscience, N.Y., 1986).
62. A. D. Bandrauk and O. Atabek, *Adv. Chem. Phys.* **73**, 823 (1989).
63. The potential curves and the relevant electronic dipole moments are taken from I. Schmidt, in Ph.D. Thesis, Kaiserslautern University, 1987.
64. Z. Chen, M. Shapiro, and P. Brumer,,J. Chem. Phys. **102**, 5683 (1995) ; Z. Chen, M. Shapiro, and P. Brumer, Phys. Rev. A **52**, 2225 (1995) ; M. Shapiro, Z. Chen, and P. Brumer, Chem. Phys. (in press)
65. A. Shnitman, I. Sofer, I. Golub, A. Yogev, M. Shapiro, Z. Chen, and P. Brumer (manuscript in preparation).
66. J. Krause M. Shapiro, and P. Brumer, J. Chem. Phys. **92**, 1126 (1990).
67. M. Shapiro and P. Brumer, Phys. Rev. Lett. **177**, 2574 (1996)
68. A. Abrashkevich, M. Shapiro, and P. Brumer (to be published)

This article was processed using the LaTeX macro package with LLNCS style

COHERENT CONTROL IN ATOMS, MOLECULES
AND SEMICONDUCTORS
Editors: W. Potz and W. A. Schroeder
Kluwer Academic Publishers
Dordrecht, 1999

Proceedings of an International Workshop
held in Chicago, USA, 19-22 May 1998

SCENARIOS IN COHERENT CONTROL

PAUL BRUMER
Chemical Physics Theory Group and
Photonics Research Ontario
University of Toronto
Toronto M5S 3H6 Canada

AND

MOSHE SHAPIRO
Chemical Physics Department,
Weizmann Institute of Science
Rehovot, Israel 76100

Abstract. Coherent control of molecular processes provides a means of controlling the dynamics of molecules, and of molecular processes, via laser induced quantum interference. We briefly review this approach, with a focus on scenarios useful for controlled currents in semiconductors and on alternate new control scenarios.

1. Introduction

Since 1986, efforts to control molecular motion and molecular processes have turned to the use of quantum interference as a means of directing molecules towards desired goals. Below we provide a brief sketch of the ideas which underlay the coherent control approach and call attention to the two scenarios which have either been proposed or utilized to control photocurrents in semiconductors. In addition we mention recent new directions in this area. Both comprehensive (Shapiro & Brumer 1997) and elementary reviews (Brumer & Shapiro 1995) are available elsewhere. Alternate methods of addressing the molecular control problem have also been recently reviewed by Gordon and Rice (1997).

Many of the proposed coherent control scenarios rely upon a simple way of achieving active control over the prepared and final state of the system.

27

Specifically, active control over the final state is achieved by driving an initially pure molecular state through two or more independent coherent optical excitation routes. [Both the requirement for an initially pure molecular state and purely coherent excitation sources can be relaxed considerably. All that is really required is that some degree of molecular coherence be established in the molecular state prepared by the multiple excitation routes. See Shapiro & Brumer (1989); Jiang *et al.* (1996).] The final state of the system displays interference terms between these multiple routes, and its magnitude and sign depend upon laboratory parameters. As a consequence, final state characteristics can be manipulated directly in the laboratory.

This approach has a well-known analogy, the interference between paths as a beam of either particles or of light passes through a double slit. In that instance a source coherence leads to either constructive or destructive interference, manifest as patterns of enhanced or reduced probabilities on an observation screen. In the case of coherent control the overall coherence of a pure state plus laser source allows for the constructive or destructive manipulation of final state properties of molecules. The principles upon which this approach rests are similar to those relied upon in recent Quantum Optics developments including Electromagnetically Induced Transparency, Lasers Without Inversion, population trapping, etc. (Scully & Zubairy 1997). Interest in Chemical Physics, however, often focuses on complex multilevel multidimensional systems excited to coupled continua where molecular rearrangement can occur.

Recognition that the essential feature of coherent control is the generation of quantum interference through independent coherent excitation pathways allows for the development of numerous control scenarios based upon this principle. In the case of the control of photocurrents in semiconductors, an application particularly relevant to this workshop, two of these many (Shapiro & Brumer 1997) scenarios have been considered. We address these specifically below.

1.1. PHOTOIONIZATION OF A SUPERPOSITION STATE

Properties of a photocurrent generated in a semiconductor are usually controlled by a bias voltage (Seeger, 1973). The role of this voltage is to give *thermodynamic* preference to the flow of photoelectrons in one direction (the forward or backward direction in a $p-n$ junction.) In a p-type or n-type semiconductor the probability of carrier photoemission (from a single impurity) without an external voltage is anisotropic only inasmuch as the crystal possesses mass or dielectric constant anisotropies, but the probabilities of emission backward and forward along a given crystal axis are equal. Although photocurrents are commonly produced by laser illumination, the laser coherence does not affect the process.

Here we review our coherent control scheme (Kurizki, Shapiro & Brumer), proposed originally in 1988, for generating and controlling photocurrents without bias voltage, relying instead on the coherence of the illuminating source. Specifically, a superposition of two bound donor (or exciton) states is photoionized by two mutually phase-locked lasers at slightly different frequencies with the same polarization axis. The result is a current along the direction of polarization. The realization of the scheme is discussed for shallow-level donors in semiconductors.

Consider a semiconductor doped with shallow-level donors. The bound state wavefunction of such a donor is successfully described by the hydrogenic effective-mass theory (Pantelides, 1978) with wavefunction:

$$\chi_{\mathbf{n}}(\mathbf{r}) = \langle \mathbf{r}|\mathbf{n}\rangle = V^{-1/2}\int_{-\infty}^{\infty} B_{\mathbf{n},\mathbf{k}} u_{\mathbf{k}}(\mathbf{r}) e^{i\mathbf{k}\cdot\mathbf{r}} d\mathbf{k} \qquad (1)$$

Here $u_{\mathbf{k}}(\mathbf{r})$ is the conduction band Bloch state correlated to the asymptotic free-electron momentum $\hbar\mathbf{k}$, V is the normalization volume and $B_{\mathbf{n},\mathbf{k}}$ is the corresponding Fourier component of the hydrogenic wavefunction envelope $\chi_{\mathbf{n}}$. For semiconductors with effective-mass anisotropy, the $\chi_{\mathbf{n}}$ are evaluated variationally (Faulkner, 1969; Kasami, 1968; Baldereschi & Diaz, 1970; Kohn & Luttinger 1955; Ridley. 1980) Although the theory described below holds for any superposition of bound donor states, a superposition of $|\,1s\,\rangle$ and $|\,2p_o\,\rangle$ states will be considered explicitly. For these cases a simple variational procedure (Kohn & Luttinger, 1955), whose results agree reasonably well with those of more refined procedures, yields

$$\begin{aligned} \chi_{1s} &= \pi^{1/3}\exp\{-[(x^2+y^2)/a^2+z^2/b^2]^{1/2}\} \\ \chi_{2p_o} &= \sqrt{2}\pi^{3/4}b^{-1}z\exp\{-[(x^2+y^2)/a^2+z^2/b^2]^{1/2}\}. \end{aligned} \qquad (2)$$

Here the coordinates [normalized to the effective Bohr radius $a^* = \hbar^2/(m_\perp e^2)$] coincide with the main axes of the cubic crystal. Depending on the ratio $\gamma = m_\perp/m_{||}$ (the parallel direction coinciding with z), the a and b parameters vary between $a = b = 1$ for nearly isotropic materials with $\gamma = 1$ (e.g. GaAs, GaSb, InAs) and $a \approx 4/3\pi$; $b \approx (1/3)(4/\pi)^{2/3}\gamma^{1/3}$ for highly anisotropic materials (e.g. Si or Ge) with $\gamma << 1$.

Let a superposition of the $|\,1s\,\rangle$ and $|\,2p_o\,\rangle$ states be prepared by some coherent process. As pointed out before, this can be achieved by a short coherent laser pulse or various other means. It is possible to discriminate against the excitation of the $|\,2p_{\pm1}\,\rangle$ states either by frequency tuning, (e.g., the $2p_{\pm1} - 2p_o$ splitting is $\sim 5meV$ in Si), or by linearly polarizing the laser along the z-axis. Consider now the simultaneous excitation of this

superposition state to a kinetic energy level E_k in the conduction band continuum by two z-polarized infrared or visible lasers with frequencies $\omega_{1s}, \omega_{2p_o}$; the former lifts the $|1s\rangle$ state to E_k and the latter lifts the $|2p_o\rangle$ state to E_k. These excitations involve the energy conservation relation:

$$E_k = \frac{\hbar^2 k_\perp^2}{2m_\perp} + \frac{\hbar^2 k_z^2}{2m_{||}} = \hbar\omega_n - |E_n| - \sum_p p\hbar\omega \tag{3}$$

Here the n-state energy is measured from the conduction-band edge and the last term accounts for the emission ($p > 0$) or absorption ($p < 0$) of p phonons of frequency ω. For the sake of simplicity, we shall use the zero phonon-frequency line; hence, $\hbar\omega_{1s} = E_k + |E_{1s}|, \hbar\omega_{2p_o} = E_k + |E_{2p_o}|$.

In what follows we consider only electric-dipole induced optical transitions with the electric field along the z axis. The electric dipole transition amplitudes from an impurity state $|\mathrm{n}\rangle$ to the asymptotic (far from impurity) plane wave $\langle \mathbf{r}|\mathbf{k}\rangle = V^{-1/2} e^{i\mathbf{k}\cdot\mathbf{r}} u_{\mathbf{k}}(\mathbf{r})$ is

$$\langle \mathbf{k}|\mu_z|\,\mathrm{n}\,\rangle = \frac{-ie\hbar}{m_{||}(E_\mathbf{k} + |E_\mathrm{n}|)} \langle \mathbf{k}|(-i\hbar\partial/\partial z)|\,\mathrm{n}\,\rangle \tag{4}$$

The last factor is, using Eq. (1), simply given as

$$\langle \mathbf{k}| - i\hbar\partial/\partial z|\,\mathrm{n}\,\rangle = \hbar \mathbf{k}_z \langle \mathbf{k}|\,\mathrm{n}\,\rangle = \hbar \mathbf{k}_z B_{\mathrm{n},\mathbf{k}} \tag{5}$$

We now consider the photoionization of the superposition state,

$$|\,\psi\,\rangle = c_1|\,1\,\rangle + c_2|\,2\,\rangle \tag{6}$$

where 1 denotes the $1s$ state and 2 the $2p_o$ state. We let a z-polarized two-color source, whose electric field is given as,

$$\epsilon_z(t) = \epsilon_1 \cos(\omega_1 t + \phi_1) + \epsilon_2 \cos(\omega_2 t + \phi_2) \tag{7}$$

act on this superposition state. The rate (probability per unit time and unit solid angle) of photoemission to a conduction state with momentum $\hbar\mathbf{k}$ resulting from this action is,

$$P(\cos\theta) = (2\pi/\hbar)\rho(k) |\sum_{n=1,2} e^{-i\phi_n} \epsilon_n c_n \langle \mathbf{k}|\mu_z|\,\mathrm{n}\,\rangle|^2 \tag{8}$$

Here,

$$\begin{aligned} \cos\theta &= k_z/k; \sin\theta = k_\perp/\gamma^{1/2}k, \\ k &= (2m_{||}E_k)^{1/2}/\hbar, \\ \rho(k) &= (m_\perp V/8\pi^3\hbar^2)k \end{aligned} \tag{9}$$

and $\rho(k)$ is the density of final states. The Franck-Condon factor for the zero phonon line has been set here to unity.

Denoting $c_n = |c_n| \exp(i\alpha_n)$ and using Eqs. (4) and (5) in Eq. (8) gives the form:

$$P(\cos\theta) = [A_1|B_{1s,\mathbf{k}}|^2 + A_2|B_{2p_o,\mathbf{k}}|^2 + A_{12}\cos(\alpha_1 - \alpha_2 - \phi_1 + \phi_2 + \alpha_{12})|B_{1s,\mathbf{k}}B_{2p_o,\mathbf{k}}|]\cos^2\theta \tag{10}$$

where

$$\begin{aligned} A_n &= \frac{2\pi e^2\hbar^3 k^2 \rho(k)|\epsilon_n c_n|^2}{m_{||}^2 (E_k + E_n)^2} \quad (n = 1, 2) \\ A_{12} &= \frac{4\pi e^2\hbar^3 k^2 \rho(\kappa)|\epsilon_1\epsilon_2 c_1 c_2|}{m_{||}^2 (E_k + E_1)(E_k + E_2)} \end{aligned} \tag{11}$$

Here α_{12} is defined by $B_{1s,\mathbf{k}}B^*_{2p_o,\mathbf{k}} = |B_{1s,\mathbf{k}}B_{2p_o,\mathbf{k}}| \exp(i\alpha_{12})$ and $E_1 = |E_{1s}|, E_2 = |E_{2po}|$.

The evaluation of $P(\cos\theta)$ requires the Fourier components $B_{\mathrm{n},\mathbf{k}}$. For the present choice of impurity states and z axis these components are obtained from Eq. (2) as

$$\begin{aligned} B_{1s,\mathbf{k}} &= 8\pi^{4/3} a^2 b V^{-1/2}/G^2 \\ B_{2p_o,\mathbf{k}} &= -i\sqrt{2}(32) a^2 b^2 \pi^{7/4} V^{-1/2} a^* k_z / G^3 \end{aligned} \tag{12}$$

with

$$G = G(\cos^2\theta) = [1 + \gamma(a^* a k)^2 + (b^2 - a^2\gamma)(a^* k)^2 \cos^2\theta] \tag{13}$$

It is clear from Eq. (12) that $\alpha_{12} = \pi/2$.

Given the above expression, the net current flowing in the z-direction is given as

$$\begin{aligned} I_z^+ &= (eNV\hbar/m_{||})\tau \times F \int_o^{2\pi} \int_o^{\pi} d\Omega P(\cos\theta) k \cos\theta \\ &= 256(eNV\hbar^4 k^5/m_{||}^3)\tau \times F a^4 b^3 \pi^{25/12} \frac{|\epsilon_1\epsilon_2 c_1 c_2|}{(E_k + E_1)(E_k + E_2)} \\ &\quad \cos(\alpha_1 - \alpha_2 - \phi_1 + \phi_2 + \frac{\pi}{2}) \int_{-1}^{+1} dx \frac{x^4}{[G(x^2)]^5}, \end{aligned} \tag{14}$$

where τ is the free electron collisional relaxation time, N is the donor concentration in cm^{-3}, and F is the x-y cross-sectional area of the sample.

We note that contributions from the diagonal A_1 and A_2 terms are odd in $\cos\theta$ and have vanished, whereas the interference term induces a directional current flow! Thus coherent interference contributions result in a controlled directional current flow.

Several additional remarks are in order: First, the phases ϕ_1 and ϕ_2 of Eq. (7) contain the spatial phase factors $\exp[i\mathbf{k}\cdot\mathbf{R}]$, where $\mathbf{k}$ is the light

wave vector. The difference in the spatial phases can be exactly offset by the phase difference $\alpha_1 - \alpha_2$ in the preparation step (e.g., in a Raman preparation of $|\psi\rangle$), or eliminated by phase matching. Second, there are substantial experimental simplifications associated with applying the photodissociating lasers at the same time as initiating the preparation of the superposition state. Third, two colour light also causes excitation (via ω_{2p_o}) of the $|1s\rangle$ level to the state at $[E_k + |E_{2p_o}| - |E_{1s}|]$ and of the $|2p_o\rangle$ level (via ω_{1s}) to the state at $[E_k + |E_{1s}| - |E_{po}|]$, i.e. the uncontrolled satellite contributions discussed above. In this case, however, these terms contribute to the A_1 and A_2 terms in Eq. (10) and hence do not contribute to degrade the controlled current I_z^+.

The magnitude and sign of the current is controllable for a given host material and superposition state parameters via (a) the optical phase difference $\phi_1 - \phi_2$, (b) the donor number N, and/or (c) the ionizing field strengths ϵ_1 and ϵ_2 and their frequencies ω_1 and ω_2. To estimate a typical current, consider the I_z resulting from the following parameters: $\epsilon_1 = \epsilon_2 =$ 0.1 Volts/cm, $k = 5 \times 10^7 cm^{-1}$, $|c_1 c_2| = 0.25$, and $\tau = 10^{-14}$ to 10^{-13} sec. The latter corresponds to a mean free path ($\hbar k\tau/m$) of 100 to 1000 Angstroms, a typical value for the ballistic electrons at the cited k value. Further $N(Si)V = 10^{18} cm^{-3} V$ where V is the effective interaction volume. For a sample of 0.1 micron × 10 micron × 10 micron, $V = 10^{-11} cm^3$. Utilizing Eq. (14) , and these parameter values, we obtain a current $I_z = 10$ to 100 mA. Thus, sizeable currents may be readily produced, due to the high quantum efficiency of the silicon photoionization.

Equations (11)-(14) apply, evidently, to photoionization of other $|ns\rangle - |n'p_o\rangle$ superpositions, where $|n - n'| = 1$, upon substituting the appropriate Fourier coefficients $B_{ns,\mathbf{k}}$ and $B_{n'p_o,\mathbf{k}}$. It may turn out to be more practical to use other states than those discussed above.

1.2. N VS. M PHOTON ABSORPTION

The above procedure relies upon coherence established in a superposition state and interference generated by simultaneous irradiation with two sources. In the alternate scenario described below interference is established by excitation via two different operators, in particular operators inducing N-photon and M-photon absorption. Here we explicitly consider the case of M=3, N=1 (Shapiro, Hepburn & Brumer, 1988) and describe it in terms of molecular excitation, but the generality of the approach, to e.g. the semiconductor case should be clear. Indeed, this approach was subsequently applied experimentally, for the case of M=2, N=1 to the control of photocurrents in semiconductors (Dupont *et al.* 1995; Hache *et al.* 1997).

Consider a molecule which, when excited to total energy E, dissociates to a number of distinct products. The total Hamiltonian is denoted $H = H_q^0 + V_q$, where H_q^0 is the Hamiltonian of the separated products in the arrangement channel labeled by q, ($q = 1, 2, ...$) and V_q is the interaction between products in arrangement q. For example, $q = 1, 2$ may be the A+BC and AB+C products, respectively, of the photon induced dissociation of a molecule denoted ABC:

$$A + BC \leftarrow ABC \rightarrow AB + C \tag{15}$$

We denote eigenvalues of H_0^q by $|E, n, q^0\rangle$, where n denotes the scattering angles and all quantum numbers other than E. Eigenfunctions of H, which correlate with $|E, n, q^0\rangle$ at large product separation, are labeled $|E, n, q^-\rangle$. By the definition (see, e.g. Taylor 1972) of $|E, n, q^-\rangle$, a state prepared experimentally as a superposition $|\Psi(t = 0)\rangle = \sum_{n,q} c_{n,q} |E, n, q^-\rangle$ has probability $|c_{n,q}|^2$ of forming product in channel q, with quantum numbers n. As a consequence, the probability of forming a product in any asymptotic state is equal to the probability of initially forming the appropriate minus state which correlates with the desired product. The essence of control lies, therefore, in forming the desired linear combination at the time of preparation. The essence of the coherent control is to utilize phase and intensity properties of laser excitation to alter the character of the prepared state so as to enhance production of the desired product.

As a specific example of coherent control, consider unimolecular photoexcitation (Shapiro, Hepburn & Brumer 1988; Chan, Brumer & Shapiro 1991) where a system, initially in pure state $|E_i\rangle$, is excited to energy E, by simultaneous application of a CW field and its third harmonic:

$$\epsilon(t) = \epsilon_3 \underset{\sim}{\hat{\epsilon}}_3 \cos[(\omega_3 + \theta_3)t] + \epsilon_1 \underset{\sim}{\hat{\epsilon}}_1 \cos[(\omega_1 + \theta_1)t], \tag{16}$$

($\omega_3 = 3\omega_1$), providing two independent optically driven routes from $|E_i\rangle$ to $|E, n, q^-\rangle$. Here $\underset{\sim}{\hat{\epsilon}}_i (i = 1, 3)$ denotes a unit vector in the i^{th} field direction.

Straightforward perturbation theory, valid for the weak fields under consideration, gives the probability $P(E, q; E_i)$ of forming product at energy E in arrangement q as:

$$P(E, q; E_i) = P_3(E, q; E_i) + P_1(E, q; E_i) + P_{13}(E, q; E_i) \; . \tag{17}$$

Here $P_3(E, q; E_i)$ is the probability arising from the one photon route,

$$P_3(E, q; E_i) = (\frac{\pi}{\hbar})^2 \epsilon_3^2 \sum_n |\langle E, n, q^- | (\underset{\sim}{\hat{\epsilon}}_3 \cdot \underset{\sim}{\mu})_{e,g} | E_i \rangle|^2 \; . \tag{18}$$

where $\underset{\sim}{\mu}$ is the electric dipole operator, and $(\underset{\sim}{\hat{\epsilon}}_3 \cdot \underset{\sim}{\mu})_{e,g} = \langle e | \underset{\sim}{\hat{\epsilon}}_3 \cdot \underset{\sim}{\mu} | g \rangle$ where $|g\rangle$ and $|e\rangle$ are the ground and excited electronic state wavefunctions, respectively. The second term is the photodissociation contribution

from the three photon route given by:

$$P_1(E,q;E_i) = (\frac{\pi}{\hbar})^2 \epsilon_1^6 \sum_n |\langle E,n,q^- \,|\, T \,|\, E_i \rangle|^2 \,, \tag{19}$$

with

$$T = (\underset{\sim}{\hat{\epsilon}}_1 \cdot \underset{\sim}{\mu})_{e,g} (E_i - H_g + 2\hbar\omega_1)^{-1} (\underset{\sim}{\hat{\epsilon}}_1 \cdot \underset{\sim}{\mu})_{g,e} (E_i - H_e + \hbar\omega_1)^{-1} (\underset{\sim}{\hat{\epsilon}}_1 \cdot \underset{\sim}{\mu})_{e,g} \,. \tag{20}$$

The final and most significant term $P_{13}(E,q;E_i)$ arises from one photon-three photon interference:

$$P_{13}(E,q;E_i) = -2(\pi/\hbar)^2 \epsilon_3 \epsilon_1^3 \cos(\theta_3 - 3\theta_1 + \delta_{13}^{(q)}) |F_{13}^{(q)}| \tag{21}$$

with the amplitude $|F_{13}^{(q)}|$ and phase $\delta_{13}^{(q)}$ defined by

$$|F_{13}^{(q)}| \exp(i\delta_{13}^{(q)}) = \sum_n \langle E_i \,|\, T \,|\, E,n,q^- \rangle \langle E,n,q^- \,|\, (\underset{\sim}{\hat{\epsilon}}_3 \cdot \underset{\sim}{\mu})_{e,g} \,|\, E_i \rangle \,. \tag{22}$$

The branching ratio $R_{qq'}$ for channels q and q', can then be written as

$$R_{qq'} = \frac{P(E,q;E_i)}{P(E,q';E_i)} = \frac{F_3^{(q)} - 2x\cos(\theta_3 - 3\theta_1 + \delta_{13}^{(q)}) \epsilon_0^2 |F_{13}^{(q)}| + x^2 \epsilon_0^4 F_1^{(q)}}{F_3^{(q')} - 2x\cos(\theta_3 - 3\theta_1 + \delta_{13}^{(q')}) \epsilon_0^2 |F_{13}^{(q')}| + x^2 \epsilon_0^4 F_1^{(q')}} \,. \tag{23}$$

where

$$\begin{aligned} F_3^{(q)} &= (\hbar/\pi)^2 \frac{P_3(E,q;E_i)}{\epsilon_3^2} \,, \\ F_1^{(q)} &= (\hbar/\pi)^2 \frac{P_1(E,q;E_i)}{\epsilon_1^6} \,, \end{aligned} \tag{24}$$

with $F_3^{(q')}$ and $F_1^{(q')}$ defined similarly. Here $x = \bar{\epsilon}_1^3/\bar{\epsilon}_3$ with $\epsilon_l = \bar{\epsilon}_l \epsilon_0$; the quantity ϵ_0 essentially carries the unit for the electric field.

The numerator and denominator of Eq.(23) each display what we regard as the canonical form for coherent control: independent contributions from more than one route which are modulated by an interference term. Since the interference term is controllable through variation of laboratory parameters (here the relative intensity and relative phase of the two lasers), so too is the product ratio $R_{qq'}$.

This 1-photon vs. 3-photon scenario has been investigated both computationally (Chan, Brumer & Shapiro 1991) and experimentally (Chen, Yin & Elliott 1990; Chen & Elliott 1990; Park, Lu & Gordon 1991; Zhu *et al.* 1995). Both show that extensive control over product probabilities is possible.

In most cases, n above denotes a set of quantum numbers, e.g. rotational, vibrational, electronic as well as scattering angles of the dissociation product. By summing only over a subset of the set n one can control the probability of forming product in states defined by the remaining quantum numbers. For example, if the sum over n excludes the scattering angle then one can control the probability of scattering into a particular angle (Asaro, Brumer & Shapiro 1988) which, for example, allows for control over photocurrent directionality.

One further note is of interest in the context of this workshop. In the studies above, N-photon and M-photon excitation both lead to the same energy. This is done to ensure that the interference term is time independent so that it does not average to zero over a given time interval. However, it is worth noting that allowing excitation to two different energies E and E', will result in an interference term that oscillates with frequency $\Omega = (E - E')/\hbar$. In the case of electron excitation, simultaneous excitation to $E \neq E'$ may well lead to a useful source of tunable radiation, e.g. in the Terahertz domain. That is, by varying either of the frequencies inducing the M or N photon absorption one can control Ω, and hence the frequency of the emitted radiation.

1.3. OTHER SCENARIOS

Once one appreciates the essence of coherent control, i.e. the simultaneous coherent excitation of the system by multiple routes, numerous scenarios can be devised (Shapiro & Brumer 1997), many of which have been computationally shown to provide highly successful control schemes. For example, quantum interference may be introduced and manipulated through the use of laser pulse sequences. In the simplest such scenario (Seideman, Shapiro & Brumer 1989) an initial transform limited laser pulse excites a superposition of bound molecular Hamiltonian eigenstates and a subsequent transform-limited pulse carries this superposition to the continuum. By varying the characteristics of the pulses, and the time delay between them, one introduces and alters the quantum interference between routes to the continuum. High quality computations on the two-photon dissociation of IBr (Levy *et al.* 1990) and Li_2 (Abrashkevich *et al.* 1998) show that extensive control over the ratio of photodissociation products is possible.

Controlling molecular dynamics by altering the shape and detailed characteristics of laser pulses and laser pulse sequences was pioneered by Tannor and Rice (1986) and subsequently cast as an optimal control problem by Rabitz and coworkers (Shi, Woody & Rabitz 1988). There is sufficient representation at this workshop of this pulsed laser approach to warrant our limiting our remarks to three general observations. They are: (a) in each

of these approaches the essential effect of varying the characteristics of the laser pulses is to control and alter the quantum interferences introduced optically into the molecule whose dynamics we wish to control. The tendency to utilize short pulses implies, however, a large frequency bandwidth and hence the participation of many molecular energy levels; (b) our experience continues to be that CW excitation, or very simple pulse shapes, suffice to give excellent control, at least over product distributions in chemical reactions. It is unclear to us under what circumstances complicated pulse shapes will be required; and (c) optimal control calculations tend to yield many different pulse shapes which all reach the desired goal. As a consequence it is very difficult to extract the physics of the problem from either the optimal control computation or the optimal control result (Paci, Shapiro & Brumer 1998).

Coherent control is a rapidly growing field and there have been numerous new scenarios proposed in the past five years which are worthy of note. We call attention here to two specific advances. First, we note the particularly exciting prospect (Chen, Shapiro & Brumer 1995) in which a bound state of a molecular system is excited to the continuum by a laser of frequency ω which is, in turn, coupled to another (initially empty) bound state by an intense laser of frequency ω'. Varying either ω or ω' can be shown to provide an effective means of controlling the ratio of photodissociation products. This approach, which we call Incoherent Interference Control, is conceptually related to Laser Induced Continuum Structure (Knight, Lauder & Dalton 1990), but the latter has only been used to control the total ionization cross sections in atoms. Clearly, the ability to use this scenario to differentiate between different dissociation products, and to control their relative probabilities, constitutes a huge increase in the utility of this approach. In addition, the method can be shown to be relatively insensitive to both molecular collisions and to the quality of the lasers used. Hence the approach is highly resistant to effects which would normally cause loss of coherence, and hence loss of quantum-interference based control.

Both experimental and theoretical studies of Incoherent Interference Control (Chen, Shapiro & Brumer 1995; Shnitman *et al.* 1996) show it to be a very effective means of controlling photodissociation dynamics. In particular, a recent study of the dissociation of Na_2 to produce different atomic products showed that one could significantly increase the production of Na(3s) + Na(3p) while simultaneously reducing the production of Na(3s) + Na(3d) by varying ω' over 3 cm^{-1}. Experiment and theory were found to be in excellent agreement. Most recently we have examined the possibility of improving control over cross sections in this scenario by varying pulse orderings, intensities and widths in a pulsed laser version of incoherent interference control. Our results showed that excellent control over cross sections is possible for a wide range of laser pulse parameters (Shapiro, Chen & Brumer 1997). Further, complementary work on multilevel adiabatic passage techniques (Kobrak & Rice 1998) suggests a deeper qualitative picture of the origins of quantum interference in this incoherent interference control scenario.

Finally we note that most of the work in coherent control has focused on unimolecular processes, i.e., processes involving excitation of a single molecule, such as that in Eq. (1). However, the vast majority of chemical reactions of interest are bimolecular in nature, i.e., of the type:

$$A + B \rightarrow C + D \tag{25}$$

In a recent series of papers (Shapiro & Brumer 1996; Holmes, Shapiro and Brumer 1996; Abrashkevich, Brumer and Shapiro 1998) we showed how coherent control could be extended to control such processes. In particular, what is required for coherent control of collision processes is that one prepares the desired initial superposition of *degenerate collisional* eigenstates. For example, if one prepares an initial state as a superposition of asymptotic states $|E, n, q^0\rangle$, e.g. as $\sum c_n |E, n, q^0\rangle$, then the overall scattering cross section will display traditional scattering contributions from each of the $|E, n, q^0\rangle$ states, plus additional interference terms dependent upon the amplitude and phases of the c_n. Thus, by controlling these coefficients, i.e. the constitution of the initial superposition state, one also gains control over the outcome of the scattering process.

In summary, numerous scenarios for achieving control have been studied both numerically as well as computationally for simple molecular processes. Of these, many would seem applicable to studies of control in device physics.

Acknowledgment: This work was supported by the US Office of Naval Research.

References

ABRASHKEVICH, A., SHAPIRO, M. & BRUMER, P., 1998 manuscript in preparation.
ABRASHKEVICH, D. G., SHAPIRO, M. & BRUMER, P. 1998 *J. Chem. Phys.* 108 3585.
ASARO, C., BRUMER, P. & SHAPIRO, M. *Phys. Rev. Lett.* 1988 60 1634
BALDERESCHI,A. & DIAZ, M.G., Nuov. Cim. 1970 68B, 217. (1970).
BRUMER, P. & SHAPIRO, M. 1995 *Scientific American* 272, 56.
CHAN, C. K., BRUMER, P. & SHAPIRO, M., 1991 *J. Chem. Phys.* 94 2688.
CHEN C. & ELLIOTT D. S. 1990 *Phys. Rev. Lett.* 65 1737.
CHEN, C., YIN, Y.-Y. & ELLIOTT, D. S. 1990 *Phys. Rev. Lett.* 64 507.
CHEN, Z., SHAPIRO, M. & BRUMER, P. 1995 *Phys. Rev. A* 52 2225.
DUPONT E., CORKUM, P.B., LIU, H.C., BUCHANEN M. & WASILEWSKI, Z.R. 1995 *Phys. Rev. Lett.* 74, 3596
FAULKNER, R.A. *Phys. Rev.* 1969 184, 713.
GORDON, R. J. & RICE, S. A. 1997 *Ann. Rev. Phys. Chem.* 48 601.

HACHE, A., KOSTOULOS, Y., ATANASOV, R., HUGHES, J.L.P., SIPE, J.E. & VAN DRIEL 1997 *Phys. Rev. Lett.* **78** 306.
HOLMES, D., SHAPIRO, M. & BRUMER, P. 1996 *J. Chem. Phys.* **105** 9162;
HUANG, K. & RHYS, A., Proc. Roy. Soc. 1950 **A204**, 406. 3435
JIANG, X.-P., BRUMER, P. & SHAPIRO, M. 1996 *J. Chem. Phys.* **104** 607.
KASAMI, A., J. Phys. Soc. Japan 1968 **24**, 551.
KNIGHT, P. L., LAUDER, M. A. & DALTON, B. J. 1990 *Phys. Rep.* **190** 1.
KOBRAK, M. & RICE, S. A. 1998, in press.
KOHN, W. & LUTTINGER,J.M., Phys. Rev. 1955 **98**, 915.
KURIZKI, G., SHAPIRO, M. & BRUMER, P. 1989 *Phys. Rev. B* **39** 3435.
LEVY, I., SHAPIRO, M. & BRUMER, P. 1990 *J. Chem. Phys.* **93** 2493.
PACI, J., SHAPIRO, M. AND BRUMER, P. 1998 *J. Chem. Phys.* (submitted)
PANTELIDES, S.T. *Rev. Mod. Phys.* 1978 **50**, 797.
PARK, S. M., LU, S.-P. & GORDON, R. J. 1991 *J. Chem. Phys.* **94** 8622.
RIDLEY, B.K., J. Phys. 1980**C13**, 2015.
SCULLY, M. O. & ZUBAIRY, M. S. 1997 *Quantum Optics* (Cambridge Univ. Press, Cambridge), Chap. 7 provides a recent review.
SEEGER K., *Semiconductor Physics* (Springer Verlag, Berlin, 1973).
SEIDEMAN, T., SHAPIRO, M. & BRUMER, P. 1989 *J. Chem. Phys.* **90** 7132.
SHAPIRO, M. & BRUMER, P. 1989 *J. Chem. Phys.* **90** 6179.
SHAPIRO, M. & BRUMER, P. 1996 *Phys. Rev. Lett.* **77** 2574;
SHAPIRO, M. & BRUMER, P. 1997 *Trans. Farad. Soc.* **82** 177
SHAPIRO, M., HEPBURN, J. & BRUMER, P. 1988 *Chem. Phys. Lett.* **149** 451.
SHAPIRO, M., CHEN, Z. & BRUMER, P. 1997 *Chem. Phys.* **217** 325
SHI, S., WOODY, A. & RABITZ, H. 1988 *J. Chem. Phys.* **88** 6870.
SHNITMAN, A., SOFER, I., GOLUB, I., YOGEV, A., SHAPIRO, M., CHEN, Z. & BRUMER, P. 1996 *Phys. Rev. Lett.* **76** 2886.
TANNOR, D. J. & RICE, S. A. 1985 *J. Chem. Phys.* **83** 5013.
TAYLOR, J. R. 1972 *Scattering Theory*, (Wiley, New York)
ZHU, L., KLEIMAN, V., LI, X., LU, S.-P., TRENTELMAN, K. & GORDON, R..J. 1995 *Science* **270** 77.

Laser and Particle Beams (1998), *vol.* 16, *no.* 4, *pp.* 599–603
Printed in the United States of America

Quantum coherence in the control of molecular processes

By PAUL BRUMER* AND MOSHE SHAPIRO**
*Chemical Physics Theory Group and Photonics Research Ontario, University of Toronto, Toronto M5S 3H6, Canada
**Chemical Physics Department, Weizmann Institute of Science, Rehovot, Israel 76100

(Received 3 November 1997; Accepted 1 May 1998)

Coherent control of molecular processes provides a means of controlling the dynamics of molecules, and of molecular processes, *via* laser-induced quantum interference. We briefly review this approach, provide relevant references, and highlight recent advances in the control of molecular processes.

Many papers presented at this "Snowbird Conference" share a common theme in that they describe quantum optics applications that take advantage of coherence properties of matter and radiation. Here we call the attention of the quantum electronics community to an independent parallel development of coherence-based ideas in chemical physics. In particular, since 1986, efforts to control molecular motion and molecular processes have turned to the use of quantum interference as a means of directing molecules toward desired goals. Below we provide a brief sketch of the ideas that underlie this work and call attention to recent new directions in this area. Both comprehensive (Shapiro & Brumer 1997) and elementary reviews (Brumer & Shapiro 1995) are available elsewhere. Alternate methods of addressing the molecular control problem have also been recently reviewed by Gordon and Rice (1997).

Many of the proposed coherent control scenarios rely upon a simple way of achieving active control over the prepared and final state of the system. Specifically, active control over the final state is achieved by driving an initially pure molecular state through two or more independent coherent optical excitation routes. [Both the requirement for an initially pure molecular state and purely coherent excitation sources can be relaxed considerably. All that is really required is that some degree of molecular coherence be established in the molecular state prepared by the multiple excitation routes. See Shapiro & Brumer (1989); Jiang *et al.* (1996).] The final state of the system displays interference terms between these multiple routes, and its magnitude and sign depend upon laboratory parameters. As a consequence, final state characteristics can be manipulated directly in the laboratory.

This approach has a well-known analogy, the interference between paths as a beam of either particles or of light passes through a double slit. In that instance source coherence leads to either constructive or destructive interference, manifest as patterns of enhanced or reduced probabilities on an observation screen. In the case of coherent control the overall coherence of a pure state plus laser source allows for the constructive or destructive manipulation of final state properties of molecules. The principles upon which this approach rests are similar to those relied upon in recent quantum optics developments including electromagnetically induced transparency, lasers without inversion, population trapping, and so on (Scully & Zubiary 1997). Interest in chemical physics, however, often focuses on complex multilevel multidimensional systems excited to coupled continua where molecular rearrangement can occur.

© 1998 Cambridge University Press 0263-0346/98 $12.50

28

To introduce the essence of coherent control consider a molecule that, when excited to total energy E, dissociates to a number of distinct products. The total Hamiltonian is denoted $H = H_q^0 + V_q$, where H_q^0 is the Hamiltonian of the separated products in the arrangement channel labeled by q ($q = 1,2,\ldots$) and V_q is the interaction between products in arrangement q. For example, $q = 1,2$ may be the $A + BC$ and $AB + C$ products, respectively, of the photon-induced dissociation of a molecule denoted ABC:

$$A + BC \leftarrow ABC \rightarrow AB + C. \tag{1}$$

We denote eigenvalues of H_0^q by $|E,n,q^0\rangle$, where n denotes the scattering angles and all quantum numbers other than E. Eigenfunctions of H, which correlate with $|E,n,q^0\rangle$ at large product separation, are labeled $|E,n,q^-\rangle$. By the definition [see, e.g., Taylor (1972)] of $|E,n,q^-\rangle$, a state prepared experimentally as a superposition $|\Psi(t=0)\rangle = \sum_{n,q} c_{n,q}|E,n,q^-\rangle$ has probability $|c_{n,q}|^2$ of forming product in channel q, with quantum numbers n. As a consequence, the probability of forming a product in any asymptotic state is equal to the probability of initially forming the appropriate minus state that correlates with the desired product. The essence of control lies, therefore, in forming the desired linear combination at the time of preparation. The essence of the coherent control approach is to utilize phase and intensity properties of laser excitation to alter the character of the prepared state so as to enhance production of the desired product.

As a specific example of coherent control, consider unimolecular photoexcitation (Shapiro *et al.* 1988; Chan *et al.* 1991) where a system, initially in pure state $|E_i\rangle$, is excited to energy E by simultaneous application of a CW field and its third harmonic:

$$\epsilon(t) = \epsilon_3 \hat{\epsilon}_3 \cos[(\omega_3 + \theta_3)t] + \epsilon_1 \hat{\epsilon} \cos[(\omega_1 + \theta_1)t], \tag{2}$$

($\omega_3 = 3\omega_1$), providing two independent optically driven routes from $|E_i\rangle$ to $|E,n,q^-\rangle$. Here $\hat{\epsilon}_i (i = 1,3)$ denotes a unit vector in the ith field direction.

Straightforward perturbation theory, valid for the weak fields under consideration, gives the probability $P(E,q;E_i)$ of forming product at energy E in arrangement q as

$$P(E,q;E_i) = P_3(E,q;E_i) + P_1(E,q;E_i) + P_{13}(E,q;E_i). \tag{3}$$

Here $P_3(E,q;E_i)$ is the probability arising from the one-photon route,

$$P_3(E,q;E_i) = \left(\frac{\pi}{\hbar}\right)^2 \epsilon_3^2 \sum_n |\langle E,n,q^-|(\hat{\epsilon}_3 \cdot \underline{\mu})_{e,g}|E_i\rangle|^2, \tag{4}$$

where $\underline{\mu}$ is the electric dipole operator, and $(\hat{\epsilon}_3 \cdot \underline{\mu})_{e,g} = \langle e|\hat{\epsilon}_3 \cdot \underline{\mu}|g\rangle$, where $|g\rangle$ and $|e\rangle$ are the ground and excited electronic state wavefunctions, respectively. The second term is the photodissociation contribution from the three-photon route given by

$$P_1(E,q;E_i) = \left(\frac{\pi}{\hbar}\right)^2 \epsilon_1^6 \sum_n |\langle E,n,q^-|T|E_i\rangle|^2, \tag{5}$$

with

$$T = (\hat{\epsilon}_1 \cdot \underline{\mu})_{e,g}(E_i - H_g + 2\hbar\omega_1)^{-1}(\hat{\epsilon}_1 \cdot \underline{\mu})_{g,e}(E_i - H_e + \hbar\omega_1)^{-1}(\hat{\epsilon}_1 \cdot \underline{\mu})_{e,g}. \tag{6}$$

The final and most significant term $P_{13}(E,q;E_i)$ arises from one-photon–three-photon interference:

$$P_{13}(E,q;E_i) = -2(\pi/\hbar)^2 \epsilon_3 \epsilon_1^3 \cos(\theta_3 - 3\theta_1 + \delta_{13}^{(q)})|F_{13}^{(q)}|, \tag{7}$$

with the amplitude $|F_{13}^{(q)}|$ and phase $\delta_{13}^{(q)}$ defined by

$$|F_{13}^{(q)}|\exp(i\delta_{13}^{(q)}) = \sum_n \langle E_i|T|E,n,q^-\rangle\langle E,n,q^-|(\hat{\epsilon}_3 \cdot \underline{\mu})_{e,g}|E_i\rangle. \tag{8}$$

The branching ratio $R_{qq'}$ for channels q and q' can then be written as

$$R_{qq'} = \frac{P(E,q;E_i)}{P(E,q';E_i)} = \frac{F_3^{(q)} - 2x\cos(\theta_3 - 3\theta_1 + \delta_{13}^{(q)})\epsilon_0^2|F_{13}^{(q)}| + x^2\epsilon_0^4 F_1^{(q)}}{F_3^{(q')} - 2x\cos(\theta_3 - 3\theta_1 + \delta_{13}^{(q')})\epsilon_0^2|F_{13}^{(q')}| + x^2\epsilon_0^4 F_1^{(q')}}, \tag{9}$$

where

$$F_3^{(q)} = (\hbar/\pi)^2 \frac{P_3(E,q;E_i)}{\epsilon_3^2},$$

$$F_1^{(q)} = (\hbar/\pi)^2 \frac{P_1(E,q;E_i)}{\epsilon_1^6}, \tag{10}$$

with $F_3^{(q')}$ and $F_1^{(q')}$ defined similarly. Here $x = \bar{\epsilon}_1^3/\bar{\epsilon}_3$ with $\epsilon_i = \bar{\epsilon}_i\epsilon_0$; the quantity ϵ_0 essentially carries the unit for the electric field.

The numerator and denominator of equation (9) each display what we regard as the canonical form for coherent control: independent contributions from more than one route that are modulated by an interference term. Since the interference term is controllable through variation of laboratory parameters (here the relative intensity and relative phase of the two lasers), so too is the product ratio $R_{qq'}$.

This one-photon versus three-photon scenario has been investigated both computationally (Chan *et al.* 1991) and experimentally (Chen *et al.* 1990; Chen & Elliott 1990; Park *et al.* 1991; Zhu *et al.* 1995). Both show that extensive control over product probabilities is possible.

In most cases, n above denotes a set of quantum numbers, for example, rotational, vibrational, electronic, as well as scattering angles of the dissociation product. By summing only over a subset of the set n one can control the probability of forming product in states defined by the remaining quantum numbers. For example, if the sum over n excludes the scattering angle then one can control the probability of scattering into a particular angle (Asaro *et al.* 1988). This has been implemented experimentally, in an approach analogous to the one-photon versus three-photon scenario, where one simultaneously absorbs two photons, ω_1 and $\omega_2 = 2\omega_1$, to control photocurrent directionality in semiconductors (Dupont *et al.* 1995; Hache *et al.* 1997). An earlier scenario to control photocurrent directionality relied on a similar principle but a somewhat different implementation of coherent control (Kurizki *et al.* 1989) in which a superposition state is prepared and subsequently photodissociated by several lasers.

Once one appreciates the essence of coherent control, that is, the simultaneous coherent excitation of the system by multiple routes, numerous scenarios can be devised (Shapiro & Brumer 1997), many of which have been computationally shown to provide highly successful control schemes. For example, quantum interference may be introduced and manipulated through the use of laser-pulse sequences. In the simplest such scenario (Seideman *et al.* 1989) an initial transform limited laser pulse excites a superposition of bound molecular Hamiltonian eigenstates and a subsequent transform limited pulse carries this superposition to the continuum. By varying the characteristics of the pulses, and the time delay between them, one introduces and alters the quantum interference between routes to the continuum. High-quality computations on the two-photon dissociation of IBr (Levy *et al.* 1990) and Li_2 (Abrashkevich *et al.* 1998a) show that extensive control over the ratio of photodissociation products is possible.

Controlling molecular dynamics by altering the shape and detailed characteristics of laser pulses and laser-pulse sequences was pioneered by Tannor and Rice (1985) and subsequently cast as an optimal control problem by Rabitz and coworkers (Shi *et al.* 1988). There is sufficient representation at this Snowbird meeting of this pulsed-laser approach to warrant our limiting our remarks to one general observation. That is, in each of these cases the essential effect of varying the characteristics of the laser pulses is to control and alter the quantum

interferences introduced, optically, into the molecule whose dynamics we wish to control. The tendency to utilize short pulses implies, however, a large frequency bandwidth and hence the participation of many molecular energy levels.

Coherent control is a rapidly growing field, and there have been numerous developments in the past five years that are worthy of note. We call attention here to two specific advances. First, we note the particularly exciting prospect (Chen *et al.* 1995) in which a bound state of a molecular system is excited to the continuum by a laser of frequency ω that is, in turn, coupled to another (initially empty) bound state by an intense laser of frequency ω'. Varying either ω or ω' can be shown to provide an effective means of controlling the ratio of photodissociation products. This approach, which we call incoherent interference control, is conceptually related to laser induced continuum structure (Knight *et al.* 1990), but the latter has only been used to control the total ionization cross sections in atoms. Clearly, the ability to use this scenario to differentiate between different dissociation products, and to control their relative probabilities, constitutes a huge increase in the utility of this approach. In addition, the method can be shown to be relatively insensitive both to molecular collisions and to the quality of the lasers used. Hence the approach is highly resistant to effects that would normally cause loss of coherence, and hence loss of quantum-interference-based control.

Both experimental and theoretical studies of incoherent interference control (Chen *et al.* 1995; Shnitman *et al.* 1996) show it to be a very effective means of controlling photodissociation dynamics. In particular, a recent study of the dissociation of Na_2 to produce different atomic products showed that one could significantly increase the production of $Na(3s) + Na(3p)$ while simultaneously reducing the production of $Na(3s) + Na(3d)$ by varying ω' over 3 cm^{-1}. Experiment and theory were found to be in excellent agreement. Most recently we have examined the possibility of improving control over cross sections in this scenario by varying pulse orderings, intensities, and widths in a pulsed-laser version of incoherent interference control. Our results showed that excellent control over cross sections is possible for a wide range of laser-pulse parameters (Shapiro *et al.* 1997). Further, complementary work on multilevel adiabatic passage techniques (Kobrak & Rice 1998) suggests a deeper qualitative picture of the origins of quantum interference in this incoherent interference control scenario.

Finally we note that most of the work in coherent control has focused on unimolecular processes, that is, processes involving excitation of a single molecule, such as that in equation (1). However, the vast majority of chemical reactions of interest are bimolecular in nature, that is, of the type

$$A + B \rightarrow C + D. \tag{11}$$

In a recent series of papers (Holmes *et al.* 1996; Shapiro & Brumer 1996; Abrashkevich *et al.* 1998b) we showed how coherent control could be extended to control such processes. In particular, what is required for coherent control of collision processes is that one prepares the desired initial superposition of *degenerate collisional* eigenstates. For example, if one prepares an initial state as a superposition of asymptotic states $|E,n,q^0\rangle$, for instance, as $\sum c_n|E,n,q^0\rangle$, then the overall scattering cross section will display traditional scattering contributions from each of the $|E,n,q^0\rangle$ states, plus additional interference terms dependent upon the amplitude and phases of the c_n. Thus, by controlling these coefficients, that is, the constitution of the initial superposition state, one also gains control over the outcome of the scattering process.

Coherent control is a rapidly growing field that takes advantage of quantum-interference effects to control molecular motion. It is joined by matter interferometry, Bose–Einstein condensation, and quantum computing as four developing areas of modern physics that rely on the uniquely quantum nature of matter interference.

Acknowledgment

This work was supported by the U.S. Office of Naval Research.

REFERENCES

Abrashkevich, A. *et al.* 1988a *Phys. Rev. Lett.* (in press).
Abrashkevich, D.G. *et al.* 1998b *J. Chem. Phys.* **108**, 3585.
Asaro, C. *et al.* 1988 *Phys. Rev. Lett.* **60**, 1634.
Brumer, P. & Shapiro, M. 1995 *Sci. Am.* **272**, 56.
Chan, C.K. *et al.* 1991 *J. Chem. Phys.* **94**, 2688.
Chen, C. & Elliott, D.S. 1990 *Phys. Rev. Lett.* **65**, 1737.
Chen, C. *et al.* 1990 *Phys. Rev. Lett.* **64**, 507.
Chen, Z. *et al.* 1995 *Phys. Rev. A* **52**, 2225.
Dupont, E. *et al.* 1995 *Phys. Rev. Lett.* **74**, 3596.
Gordon, R.J. & Rice, S.A. 1997 *Ann. Rev. Phys. Chem.* **48**, 601.
Hache, A. *et al.* 1997 *Phys. Rev. Lett.* **78**, 306.
Holmes, D. *et al.* 1996 *J. Chem. Phys.* **105**, 9162.
Jiang, X.-P. *et al.* 1996 *J. Chem. Phys.* **104**, 607.
Knight, P.L. *et al.* 1990 *Phys. Rep.* **190**, 1.
Kobrak, M. & Rice, S.A. 1998 *J. Chem. Phys.* (in press).
Kurizki, G. *et al.* 1989 *Phys. Rev. B* **39**, 3435.
Levy, I. *et al.* 1990 *J. Chem. Phys.* **93**, 2493.
Park, S.M. *et al.* 1991 *J. Chem. Phys.* **94**, 8622.
Scully, M.O. & Zubairy, M.S. 1997 *Quantum Optics* (Cambridge University Press, Cambridge). Chap. 7 provides a recent review.
Seideman, T. *et al.* 1989 *J. Chem. Phys.* **90**, 7132.
Shapiro, M. & Brumer, P. 1989 *J. Chem. Phys.* **90**, 6179.
Shapiro, M. & Brumer, P. 1996 *Phys. Rev. Lett.* **77**, 2574.
Shapiro, M. & Brumer, P. 1997 *Trans. Faraday Soc.* **82**, 177.
Shapiro, M. *et al.* 1988 *Chem. Phys. Lett.* **149**, 451.
Shapiro, M. *et al.* 1997 *Chem. Phys.* **217**, 325.
Shi, S. *et al.* 1988 *J. Chem. Phys.* **88**, 6870.
Shnitman, A. *et al.* 1996 *Phys. Rev. Lett.* **76**, 2886.
Tannor, D.J. & Rice, S.A. 1985 *J. Chem. Phys.* **83**, 5013.
Taylor, J.R. 1972 *Scattering Theory* (Wiley, New York).
Zhu, L. *et al.* 1995 *Science* **270**, 77.

29

NANOMETRIC SCALE COHERENTLY CONTROLLED DEPOSITION

FIELD OF THE INVENTION

The present invention relates to the field of the controlled deposition of molecules and atoms on surfaces on a nanometric scale.

BACKGROUND OF THE INVENTION

The optical manipulation of atoms in their ground state constituting an atomic beam has been widely studied over the past few years. It has been shown, for instance in the article "Calculation of Atomic Positions in Nanometer-scale Direct-write Optical Lithography with an Optical Standing Wave", by K.K. Berggren et al., published in Journal of the Optical Society of America B, Vol.11, pp. 1166-1176 (1994), and in the references thereto, that an atomic beam can be focused to sub-micron scale dimensions by using the dipole forces exerted on the atoms by an electromagnetic field, such as that present in a standing light wave. One possible application of this phenomenon is in direct-write atomic nanolithography, which offers the possibility of microfabrication applications in the microelectronic industry, at resolutions well below the wavelength of ultra-violet light, as commonly used.

In U.S. Patent 5,360,764 to R. J. Celotta and J. J. McClelland, hereby incorporated by reference in its entirety, there is described the use of a combination of laser cooling techniques and periodic standing wave electromagnetic fields to enable the focusing of atoms and their subsequent deposition on a substrate, on a nanometric scale. However, the technique described therein has a number of disadvantages; firstly, it is limited to the controlled deposition of atoms, and there are many practical chemical processes,

nanometric scale is also a needed technique which is hitherto unavailable.

The disclosures of each of the publications mentioned in this section, and of those in the other sections of this specification, are hereby incorporated by reference, each in its entirety.

SUMMARY OF THE INVENTION

The present invention seeks to provide a new method and apparatus for the optical focusing of atomic or molecular beams, such that the atoms or molecules can be deposited in aperiodic structures, with resolutions of down to 10-15 nanometers. The ability to deposit atoms or molecules on surfaces at a nanometric scale has important applications in the semiconductor industry for the purposes of direct deposition etching and for other lithographic processes. The nature of the pattern formed, including the position and width of the component parts of the pattern, are altered by varying a number of parameters associated with the beam preparation and with the electromagnetic fields to which the beam is subjected.

A beam of atoms or molecules, aimed at the surface on which the deposition is required, is preferably sent through a skimmer to minimize velocity components perpendicular to the direction of the beam. The beam is then preferably further collimated by means of laser cooling or by sympathetic cooling or supersonic expansion, in order to reduce the transverse velocity to minimal levels. The better the collimation, the finer the resolution of the focusing effect achieved. The laser cooling can be performed by any of the methods known in the art. One such method is described in the article co-authored by one of the present applicants, entitled "Complete population transfer to and from a continuum and the radiative association of cold Na atoms to produce translationally cold Na_2 molecules in specific vib-rotational states" published in Optics Express, Vol. 4, pp.91-106 (Jan., 1999), hereby incorporated in its entirety by reference. Other methods are also given in the many references cited therein. Alternatively, for an atomic beam, laser cooling may be achieved by passing the atoms through

optical focusing.

The prepared atomic or molecular beam then preferably passes through two or more standing electromagnetic fields directed parallel to the surface, which too may be produced by means of interacting laser beams. By varying the characteristics of the laser beams, the atomic or molecular properties, the distance of the stationary fields from the surface, and the properties of the stationary electromagnetic fields, the nature of the pattern deposited on the surface can be controlled, including the position, intensity and resolution of the component parts of the pattern. In general, the pattern displays a large background with several relatively low intense peaks when there is no atomic or molecular coherence, whereas the peaks become intense and the background weak when the atomic or molecular coherence is introduced.

In the case of atomic beam deposition, since the superposition may be formed from Rydberg excited states of the atoms, this affords the possibility of much higher polarizabilities, and hence requires much lower laser powers than for molecular beam deposition.

There is thus provided in accordance with a preferred embodiment of the present invention, a method of depositing atoms or molecules in a predetermined pattern onto a surface by means of coherently controlled optical focusing of a beam of the atoms or molecules.

There is further provided in accordance with yet other preferred embodiments of the present invention, a method as described above and consisting of the steps of providing a collimated beam of atoms or molecules to be deposited, directing the beam through a first electromagnetic field, typically produced by a laser beam, operative to produce a superposition of states of the atoms or molecules, and thereafter directing the beam through a second electromagnetic field, typically produced by two or more standing waves, such that the atoms or molecules are focused onto the surface in the predetermined pattern.

In accordance with still another preferred embodiment of the present

In accordance with yet another preferred embodiment of the present invention, there is provided a method of depositing atoms or molecules in a predetermined pattern onto a surface as described above, and wherein the atoms or molecules are operative to perform applications such as nanolithography, micro-etching, the writing of information on a storage medium, the formation of photolithographic masks, the production of doped regions within the surface, the production of high profile tip structures on the surface, or the production of optical grating structures on the surface.

There is further provided in accordance with yet another preferred embodiment of the present invention, a system for the deposition of atoms or molecules in a predetermined pattern onto a surface by means of coherently controlled optical focusing of a beam of the atoms or molecules.

In accordance with still another preferred embodiment of the present invention, there is provided a system for the deposition of atoms or molecules as described above, and consisting of a source emitting a beam of the atoms or molecules, a laser cooling stage for minimizing the transverse velocity components of the molecules of the beam, a first electromagnetic field through which the beam is directed, operative to produce a superposition of states of the atoms or molecules, and a second electromagnetic field, through which the beam is thereafter directed, such that the atoms or molecules are focused onto the surface in the predetermined pattern.

There is provided in accordance with yet a further preferred embodiment of the present invention, a system for the deposition of atoms or molecules as described above and wherein the first electromagnetic field is formed by at least one first laser beam.

There is even further provided in accordance with a preferred embodiment of the present invention, a system for the deposition of atoms or molecules as described above and wherein the second electromagnetic field consists of at least two standing waves formed by laser beams.

of phase between the two standing waves, for the superposition |000> + |020>;

Figs. 10(a) to 10(f) illustrate the variation in the form and intensity of the strongest peak shown in Fig. 9(b) at $z_s = 0.49$, as a function of six different values of the relative phase between the two standing waves;

Figs. 11(a) to 11(f) show the variation in the form and intensity of the strongest peak shown in Fig. 9(b), as a function of the intensity of the two SW fields, for six different values of the field of SW2;

Figs. 12(a) to 12(c) show plots of the density distribution for three different values of the interaction time, T_{int}, for the superposition |000> + |020>;

Figs. 13(a) to 13(d) show the density distribution of deposition as a function of free flight distance, L_{ff} for four different values of L_{ff};

Figs. 14(a) to 14(d) show the width of a typical deposited peak as a function of the rotational temperature of the molecules, for four different values of T_r ; and

Figs. 15(a) to 15(d) are graphs which show the density distribution for the deposition of atomic rubidium for different interaction times, both in the presence of and in the absence of coherent control.

near resonant, CW laser beams 20, 22, positioned above the substrate 24 onto which the molecules are to be deposited. While passing through the SW radiation field, the atoms or molecules experience a dipole force, due to the SW-induced optical potential (OP), which acts as an array of lenses, causing those atoms or molecules in the beam with kinetic energy less than the depth of the OP to focus into predefined patterns 26 as they deposit onto the substrate 24. Those atoms or molecules with kinetic energy greater than the depth of the OP skip over the potential well and are lost to the ordered deposition process.

According to a preferred method of embodiment of the present invention, the kinetic energy of the beam in the x-direction $v_{\|}$ is approximately fixed and is much larger than the magnitude of the OP, such that a majority of the atoms or molecules are indeed focused as desired. In the y-direction, perpendicular to the direction of the two SW's, the focusing region is essentially uniform. The focusing effect is then described by an effective one dimensional OP along the z-direction. The atoms or molecules in the beam execute motion according to the Hamilton's equation:

$$m_{N_2} \ddot{z}_i = p_i \qquad (1)$$

and

$$p_i = \frac{d}{dz} V_{op}|_{zi,pi} \qquad (2)$$

where V_{op} is the optical potential and the subscript i symbolizes the i-th atom or molecule in the beam, treated as a point-like particle. The result of focusing by means of a one-dimensional OP along the z-direction is a pattern of lines of deposited atoms or molecules, of essentially uniform intensity in the y-direction, the lines being spaced in the z-direction and of width and intensity in accordance with the deposition parameters used.

According to another preferred embodiment of the present invention, it is possible to deposit an array of spots rather than an array of lines, by adding another electromagnetic field, preferably produced by another pair of laser beam standing waves, preferably directed orthogonally to the first pair of SW's and in the same plane thereto. The second electromagnetic wave then produces an

superposition state composed of two Hamiltonian eigenstates. An extension to a superposition state involving more than two eigenstates is also possible. The superposition state is given by:

$$|\psi(t)> = c_1|\varphi_1> e^{-iE_1t/h} + c_2|\varphi_2> e^{-iE_2t/h} \qquad (3)$$

where $|\varphi_i>$ represents the Hamiltonian eigenstates of energy E_i. This coherent state is prepared by two-photon absorption using a laser of frequency ω_L and amplitude E_L. Application of perturbation theory methods, such as is known in the art, leads to the evaluation of the population of the upper level as:

$$|c_2|^2 = \frac{|E_L|^4}{h^4} \sum_{m,n} \frac{\mu_{1m}\mu_{m2}\mu_{2n}\mu_{n1}}{(\Omega_{m1} - \omega_L)(\Omega_{n1} - \omega_L)(\Delta_{2\omega L} - i\gamma)(\Delta_{2\omega L} + i\gamma)} \leq 0.2 \qquad (4)$$

where $\Omega_{mn} = (E_m - E_n)/h$ and $\Delta_{2\omega L} = \Omega_{21} - 2\omega_L \equiv (E_2 - E_1)/h - 2\omega_L$ is the detuning of the two-photon absorption from resonance, and γ is the linewidth of the transition between two superposition states where m and n represent the quantum numbers corresponding to the rotational, vibrational and electronic states. Note that within the perturbation regime $|c_2|^2 \leq 0.2$, which restricts the power of the pump laser. Assuming a negligible value of $\Delta_{2\omega L}$, a restriction on two parameters results, viz., $|c_2|^2$ and γ. Table I shows the value of the pump field E_L required as a function of γ, for $|c_2|^2 = 0.2$. The pump laser is set at the frequency ω_L required for a resonant two-photon absorption process between the levels of the ground electronic state $|\varphi_1> = |v=0,J=0,M=0>$ and $|\varphi_2> = |v=0,J=2,M=0>$.

Table 1

γ (Hz)	E_L (V/m)
8.3×10^6	1.0×10^7
1.0×10^9	1.1×10^8

Table 3

ν_1	ν_2	E_L (V/m)	I_L (W/cm^2)	ω_L (Hz)
0	1	4.6×10^{8}	9.18×10^{10}	2.1988×10^{14}
0	2	4.72×10^{8}	1.18×10^{11}	4.3673×10^{14}
0	3	4.74×10^{8}	1.19×10^{11}	6.5077×10^{14}
0	4	7.5×10^{8}	2.98×10^{11}	8.6241×10^{14}

In the next step the beam downstream of the cooler is assumed to have a Gaussian transverse speed distribution, $f(v_\perp) = n\frac{1}{\sqrt{\pi\sigma_{v\perp}}}e^{\frac{-(v_\perp-\bar{v}_\perp)^2}{\sigma_{v\perp}^2}}$, where n is the number of particles used for simulation. The center of the distribution $\bar{v}_\perp$ is zero or very close to zero, and the spread of the distribution is $\sigma_{v\perp}$. Calculations show that the deposition associated with a particular width $\sigma_{v\perp}$ may be approximately calculated by computing the deposition using a zero transverse velocity width and then broadening the computed peaks by $\sqrt{2}\, t_d\, \sigma_{v\perp}$, where t_d is the time it takes for an atom or molecule to get from the collimated source to the deposition surface. The value for the longitudinal speed $\upsilon_{||}$ of the beam is taken to be 600 m/s. This value can be obtained from the expression:

$$\upsilon_{||} = \left(\frac{2K\gamma T_0}{M_{buff}(\gamma-1)}\right)^{1/2}$$

where K is the Boltzmann constant, M_{buff} is the mass of the buffer gas atom used, γ is the specific heat ratio of the buffer gas and T_0 is the initial temperature. This expression is derived in the book "Atomic and Molecular Beam Methods" edited by G. Scoles, published by Oxford University Press, (1988). The effect of as described above aberrations due to the longitudinal speed distribution has been omitted here.

where $E(\omega_i)$ are defined above, $E'(\omega_{21}+\omega_1) = E_1^{(0)}\cos(k_1 z)\exp[(\omega_{21}+\omega_1)t]$, and $E'(\omega_{21}-\omega_2) = E_2^{(0)}\cos(k_2 z+\theta_F)\exp[(\omega_{21}-\omega_2)t]$, and $\mu(-\omega) = \mu(\omega)^*$. The susceptibilities χ above are given by

$$\chi^{in}(\omega_1) = \frac{1}{\hbar}\sum c_1 c_2^*[\frac{\mu_{j1}\mu_{2j}}{\omega_{j1}+\omega_2} + \frac{\mu_{j2}\mu_{1j}}{\omega_{j2}-\omega_2}]\frac{E_2^{(0)}}{E_1^{(0)}}$$

$$\chi^{in}(\omega_2) = \frac{1}{\hbar}\sum c_2 c_1^*[\frac{\mu_{j2}\mu_{1j}}{\omega_{j2}+\omega_1} + \frac{\mu_{j1}\mu_{2j}}{\omega_{j1}-\omega_1}]\frac{E_1^{(0)}}{E_2^{(0)}}$$

$$\begin{aligned}\chi^{ni}(\omega_1) &= \frac{1}{\hbar}\sum |c_1|^2\mu_{j1}\mu_{1j}[\frac{1}{\omega_{j1}+\omega_1} + \frac{1}{\omega_{j1}-\omega_1}] \\ &+\frac{1}{\hbar}\sum |c_2|^2\mu_{j2}\mu_{2j}[\frac{1}{\omega_{j2}+\omega_1} + \frac{1}{\omega_{j2}-\omega_1}]\end{aligned}$$

$$\begin{aligned}\chi^{ni}(\omega_2) &= \frac{1}{\hbar}\sum |c_1|^2\mu_{j1}\mu_{1j}[\frac{1}{\omega_{j1}+\omega_2} + \frac{1}{\omega_{j1}-\omega_2}] \\ &+\frac{1}{\hbar}\sum |c_2|^2\mu_{j2}\mu_{2j}[\frac{1}{\omega_{j2}+\omega_2} + \frac{1}{\omega_{j2}-\omega_2}]\end{aligned}$$

$$\chi^{in}(\omega_{21}+\omega_1) = \frac{1}{\hbar}\sum c_2 c_1^*[\frac{\mu_{j1}\mu_{2j}}{\omega_{j1}+\omega_1} + \frac{\mu_{j2}\mu_{1j}}{\omega_{j2}-\omega_1}]$$

$$\chi^{in}(\omega_{21}-\omega_2) = \frac{1}{\hbar}\sum c_1 c_2^*[\frac{\mu_{j1}\mu_{2j}}{\omega_{j1}-\omega_2} + \frac{\mu_{j2}\mu_{1j}}{\omega_{j2}+\omega_2}]$$

where $\omega_{mn} = (E_m - E_n)/\hbar$, $\mu_{ij} = < \phi_i|\mu.\hat{n}|\phi_j >$, $\hat{n}$ being the unit vector along the direction of polarization of the external field. Since both the SW are linearly polarized along the z axis (Eq.(6)) only the zz component of the polarizability, denoted χ_{zz}, need be considered. Here the superscripts "in" and "ni" refer to the interference and non-interference terms respectively of χ, where the interference terms are the direct consequence of the coherent superposition of the $|\phi_1>$ and $|\phi_2>$ state. Control over $\chi(\omega_i)$ is obtained by changing various parameters, e.g., $|\frac{E_2^{(0)}}{E_1^{(0)}}|$, $|c_1|$, $|c_2|$, θ_M and θ_F, where θ_M is the relative phase of c_1 and c_2.

$$V_{op}^{in} = -[8E_1^{(0)^2}\cos(k_1 z)\cos(k_2 z+\theta_F)\chi_r^{in}(\omega_1) + 8E_2^{(0)^2}\cos(k_1 z)\cos(k_2 z+\theta_F)\chi_r^{in}(\omega_2)] \quad (12)$$

Thus, the optical potential in the absence of molecular coherence consists of two terms each representing the dipole interaction of the field and the induced molecular dipole of the same frequency.

Thus, the molecules experience the above optical potential, which is an oscillating function along the z direction and which acts as an array of lenses. Each minimum of the potential behaves as a focusing center and each maximum behaves as a defocusing center. The results is an inhomogeneous aperiodic distribution of potential minima whose depths vary, depending on z, $E_1^{(0)}$, $E_2^{(0)}$, $|c_1|$, $|c_2|$, θ_M and θ_F. Reference is now made to Figs. 2 and 3 (to be discussed in detail hereinbelow), which show typical results of the molecular density distribution obtained along the z-direction, together with the corresponding optical potential. It is seen that V_{op}^{ni} represents a periodic array of lenses, whereas $V_{op} = V_{op}^{ni} + V_{op}^{in}$ does not. Thus, unlike traditional atomic lithography where the optical potential is purely periodic, different optical potentials can be obtained by altering terms in the potential which enter via quantum interference. This feature of the present invention enables pattern formation not realized in prior art conventional atomic lithographic techniques.

The classical density distribution of molecules on the substrate is now calculated. For an initial uniform spatial distribution of molecules in the beam after the cooling process, $\rho(z,0) = constant$, the classical trajectories can be calculated for every molecule interacting with the optical potential given by Eq.(8) to obtain the spatial distribution of molecule $\rho(z,T)$ at time $T = T_{int} + \frac{L_{II}}{v_{\|}}$, where T_{int} is the actual interaction interaction time between the molecules and the optical potential, and is equal to $L_{int}/v_{\|}$.

The numerical steps in the computation for this molecular density distribution after interacting with the SW-induced OP are as follows :

The deposition density distribution patterns obtained are functions of the parameters used in performing the coherently controlled optical focusing of the molecular beam. Ideally, every minimum of the Optical Potential OP acts as a focusing center, giving rise after a sufficient time of interaction, to a delta function molecular density distribution, and producing a corresponding pattern on the substrate. The deposition pattern formed, $\rho\ (z_s, T)$ can be approximated by the expression:

$$\rho\ (z_s, T) = \sum_m |a(z_s,T)|^2\ f(z,T)\ \delta(z_s-z_m) \qquad (13)$$

where $|a(z_s,T)|^2$ is the intensity of focusing at a given point z_s onto the substrate at time T, and f(z,T) may be chosen as a Lorentzian function. The point z_m is the position of a minimum in the optical potential. The width of f(z,T) together with $|a(z_s,T)|^2$ measures the quality of focusing of the molecules, in terms of the intensity and width of the focused beam particle deposits. The focusing quality of the deposition is dependent on a number of parameters, namely, c_1, c_2, θ_F, $\sigma_{v\perp}$, $|\phi_1>$, $|\phi_2>$, L_{ff}, T_{int}, $E_1^{(0)}$ and $E_2^{(0)}$. As illustrative of the method of the present invention, the effect of these parameters on the nature of the resulting molecular deposit is now described.

(a) The Effect of Molecular Coherence:

The parameters c_1, c_2, θ_M, $|\phi_1>$ and $|\phi_2>$ introduced into the OP are the direct consequence of molecular coherence. As can be seen from the expressions for V_{op} (equations 11 and 12), these parameters do not affect the location of the OP minima. Hence they have no direct effect on changing the position of the deposition onto a substrate. However, they do have a direct effect on the intensity of the deposition resulting from the change in the magnitude of the OP. If there were no molecular coherence, deposition would be due only to $V_{op}^{(ni)}$, i.e., the usual dipolar interaction between the molecule and the coherent electric field.

The effect of molecular coherence on the deposition distribution is shown in Figs. 2(a) to 2(d), which show how the density distribution of deposition

used in the example shown in plotting Figs. 2(a) to (d), the weaker spots appear at intervals of approximately $0.5\lambda_2$, with the brighter spots appearing at larger intervals. By contrast, without molecular coherence, as is seen from Fig. 2(a), there is a uniform array of deposition peaks of lower intensity than the maximum peaks obtained with molecular coherence, appearing at a regular interval of $0.5\lambda_2$.

Figs. 3(a) to 3(d) are plotted under the same conditions as Figs. 2(a) to 2(d), but show an enlarged section in the z_s direction, to better illustrate the differences between the bright and weak deposition spots.

Reference is now made to Figs. 4(a) to 4(d) which show the separate contributions to the molecular density as a function of z_s, due to the first and second SW fields, $E_1^{(0)}$ and $E_2^{(0)}$, taking into account only the non-interference term $V_{op}^{(ni)}$ of the optical potential. The parameters used for this example are identical to those used for calculating the distributions shown in the various plots of Figs. 2 and 3. Fig. 4(a) shows a plot of ρ for the first field, Fig. 4(b) shows the values of $V_{op}^{(ni)}$ for the first field, Fig. 4(c) shows a plot of ρ for the second field, and Fig. 4(d) shows the values of $V_{op}^{(ni)}$ for the second field. It is observed that since $E_2 >> E_1$, the contribution of the SW field of frequency ω_1 is small compared with that of ω_2 . It should also be noted that Fig. 4(c) and Fig. 3(a) are essentially equivalent.

Figs. 5(a) to 5(f) and Figs. 6(a) to 6(f) show the dependence of $\rho(z_s,T_{int})$ on different superpositions of states. Figs. 5(a) to 5(f) show the results using the superposition ($|000> + |\nu 00>$), where ν takes the values 1 to 6 for Figs. 5(a) to 5(f) respectively, while Figs. 6(a) to 6(f) show the results using the superposition ($|000> + |\nu 20>$), where ν takes values of 0 to 5 for Figs. 6(a) to 6(f) respectively. In the calculations used for plotting all parts of Figs. 5 and 6, the values $\gamma = 1\times10^9$ Hz and $|c_2|^2 = 0.2$ are assumed, and the other parameters used are identical to those used in Figs. 2 to 4, except that in fig. 5, $\theta_F = 2.65$ rad.

Figs. 7(a) to 7(f) show the dependence of $\rho(z_s,T_{int})$ on $|c_2|^2$ for six different values of $|c_2|^2$. For Fig. 7(a), $|c_2|^2 = 0.01$, for (b) 0.1, for (c) 0.15, for (d) 0.2, for (e) 0.4 and for (f) 0.5. The superposition used is between the $|000>$ and $|020>$

that the peaks become weaker and broader as θ_F changes from -2.65 to -2.15 radian. In other words, there is an optimum value for θ_F that results in the most intense and highest resolution peak.

Figs. 11(a) to 11(f), using similar calculations, show the variation in the form and intensity of the strongest peak shown in Fig. 9(a), as a function of the intensity of the two SW fields. In Figs. 11, the value of $E_2^{(0)}/E_1^{(0)}$ is set at 1.0×10^4 and $E_2^{(0)}$ = (a) 1.0×10^6, (b) 0.97×10^6, (c) 0.94×10^6, (d) 0.91×10^6, (e) 0.88×10^6, and (f) 0.85×10^6 V/cm. Approximately optimum values of $E_2^{(0)}$ = 1.0×10^6V/cm and $E_2^{(0)}/E_1^{(0)} = 1.0\times10^4$ result in a deposition density distribution peak with maximum intensity and minimum width. As is seen from Figs. 11(b) to 11(f), deviation from these values results in the peak becoming fainter and broader.

(c) Effect of Beam Parameters

The beam parameters, T_{int} , L_{ff} and $\sigma_{v\perp}$ also have an effect on the deposition density distribution. This effect is illustrated in the density plots shown in Figs. 12(a) to 12(c) and Figs. 13(a) to 13(d). Since the SW-induced optical potential is comprised of a series of harmonic-type potential wells of varying depth, the time of interaction T_{int} plays a crucial role in determining the nature of the deposition. In general, if T_{int} is longer than the quarter period of oscillation of the molecule in any of the potential wells, sharp peaks will not be formed in the molecular density distribution. Instead the distribution will have large number of smaller peaks. Expressed mathematically, a single sharp peak in the region of the potential minima will be formed only when $T_{int} \sim (2n+1)T/4$, where T is the period of harmonic oscillation for a particular potential well. When $T_{int} \neq (2n+1)T/4$, every peak formed at every potential minima after a time T/4, or (2n+1) multiples of T/4, splits into many weaker peaks.

This result can be demonstrated by reference to Figs. 12(a) to 12(c), which show plots of the spatial values of $\rho(z_s,T_{int})$ obtained for three different values of

decreases rapidly with increase of L_{ff} , and the peak itself broadens and splits into lower peaks.

The effect of the rotational cooling on the quality of the deposition is illustrated in Figs. 14(a) to 14(d), which show the width of a typical deposited peak as a function of the rotational temperature of the molecules. Fig. 14(a) is shown at a temperature T_r of 298°K, 14(b) at 150°K, 14(c) at 50°K, and 14(d) at 10°K. The graphs show that the deposited peaks becomes wider and more erratic with decrease in the rotational temperature. The effect of rotational cooling is thus opposite to that of the translational cooling.

Finally, Figs. 15(a) to 15(d) are graphs of density distributions obtained, for the deposition of atomic rubidium for different interaction times, both in the presence of and in the absence of coherent control, according to another preferred embodiment of the present invention. The coherent control is achieved using a supersposition of Rydberg states of the atoms, in this case the 8s and 8d states. This preparation can be performed by laser exciting the species from the ground atomic state, preferably where the atoms already have, as a result of preliminary laser cooling, a small transverse velocity distribution. The atoms are passed through two laser fields with wavelengths of 3430.8 nm and 13291.9 nm, respectively, and with intensities of only 1.91×10^{-3} Watt per square cm, and 0.19 Watt per square cm., respectively. Such weak fields are effective because of the high polarizability obtained from Rydberg excited atoms. The results shown in Figs. 15(a) to 15(d) are obtained with the values $\theta_M = 1.5$ rad and $\theta_F = 1.26$ rad, where θ_M and θ_F are defined above and with $|c_1|^2 = 0.8$ and $|c_2|^2 = 0.2$.

In Figs. 15(a) and 15(b) the deposition results atoms pass through the field for 0.26 μsec. In the absence of any interference terms, i.e. where the atoms are only subject to V^{ni} then the resultant deposition is shown in Fig. 15(b). By contrast, when both V^{ni} and V^{in}, are present i.e. where the interference term is included, then the deposition is much improved, as observed in Fig. 15(a). Similar results are shown in Figs. 15(c) and 15(d) for interaction times of 0.36 μsec. It is apparent from the examples shown, that, as in the molecular deposition

CLAIMS

We claim:

1. A method of depositing molecules in a predetermined pattern onto a surface by means of coherently controlled optical focusing of a beam of said molecules.

2. The method according to claim 1 and comprising the steps of:

providing a collimated beam of molecules;

directing said beam through a first electromagnetic field operative to produce a superposition of bound states of said molecules; and

thereafter directing said beam through a second electromagnetic field, such that said molecules are focused onto said surface in said predetermined pattern.

3. The method according to claim 2 and wherein said second electromagnetic field comprises at least two standing waves.

4. The method according to claim 2 and wherein said superposition of bound states of said molecules is formed by means of a two-photon absorption process.

5. The method according to claim 2 and also comprising the step of cooling said beam of molecules before production of said superposition of bound states.

6. The method according to claim 5 and wherein said step of cooling said beam is effected by means of a mechanical cooling process.

7. The method according to claim 6 and wherein said mechanical cooling process is effected by expansion of said beam through a supersonic nozzle.

orthogonally to said second electromagnetic field, and in effectively the same common plane, such that said molecules are focused onto said surface in a predetermined array pattern.

18. The method according to claim 1 and wherein said predetermined pattern has a resolution of less than 50 nanometers.

19. The method according to claim 1 and wherein said predetermined pattern has a resolution of less than 20 nanometers.

20. A method of depositing molecules in a predetermined pattern onto a surface by means of coherently controlled optical focusing of a beam of said molecules, wherein said molecules are operative to perform nanolithography.

21. A method of depositing molecules in a predetermined pattern onto a surface according to claim 1, wherein said surface is a storage medium, and said molecules are operative to write information on said storage medium.

22. A method of depositing molecules in a predetermined pattern onto a surface according to claim 1, wherein said molecules in said predetermined pattern constitute a photolithographic mask.

23. A method of depositing molecules in a predetermined pattern onto a surface according to claim 1, wherein said molecules produce doped regions within said surface.

24. A method of depositing molecules in a predetermined pattern onto a surface according to claim 1, wherein said molecules produce a high profile tip structure on said surface.

wherein said mechanical cooler comprises a device for the expansion of said beam through a supersonic nozzle.

32. A system for the deposition of molecules according to claim 28 and wherein said first electromagnetic field is formed by at least one first laser beam.

33. A system for the deposition of molecules according to claim 28 and wherein said second electromagnetic field comprises at least two standing waves formed by laser beams.

34. A method of depositing atoms in a predetermined pattern onto a surface by means of coherently controlled optical focusing of a beam of said atoms.

35. The method according to claim 34 and comprising the steps of:

providing a collimated beam of atoms;

directing said beam through a first electromagnetic field operative to produce a superposition of excited states of said atoms; and

thereafter directing said beam through a second electromagnetic field, such that said atoms are focused onto said surface in said predetermined pattern.

36. The method according to claim 35 and wherein said excited states are Rydberg states.

37. The method according to claim 35 and wherein said second electromagnetic field comprises at least two standing waves.

38. The method according to claim 35 and also comprising the step of cooling said beam of molecules before production of said superposition of excited states.

orthogonally to said second electromagnetic field, and in effectively the same common plane, such that said atoms are focused onto said surface in a predetermined array pattern.

49. The method according to claim 34 and wherein said predetermined pattern has a resolution of less than 50 nanometers.

50. The method according to claim 34 and wherein said predetermined pattern has a resolution of less than 20 nanometers.

51. A method of depositing atoms in a predetermined pattern onto a surface by means of coherently controlled optical focusing of a beam of said atoms, wherein said atoms are operative to perform nanolithography.

52. A method of depositing atoms in a predetermined pattern onto a surface according to claim 34, wherein said surface is a storage medium, and said atoms are operative to write information on said storage medium.

53. A method of depositing atoms in a predetermined pattern onto a surface according to claim 34, wherein said atoms in said predetermined pattern constitute a photolithographic mask.

54. A method of depositing atoms in a predetermined pattern onto a surface according to claim 34, wherein said atoms produce doped regions within said surface.

55. A method of depositing atoms in a predetermined pattern onto a surface according to claim 34, wherein said atoms produce a high profile tip structure on said surface.

through a supersonic nozzle.

63. A system for the deposition of atoms according to claim 58 and wherein said first electromagnetic field is formed by at least one first laser beam.

64. A system for the deposition of atoms according to claim 58 and wherein said second electromagnetic field comprises at least two standing waves formed by laser beams.

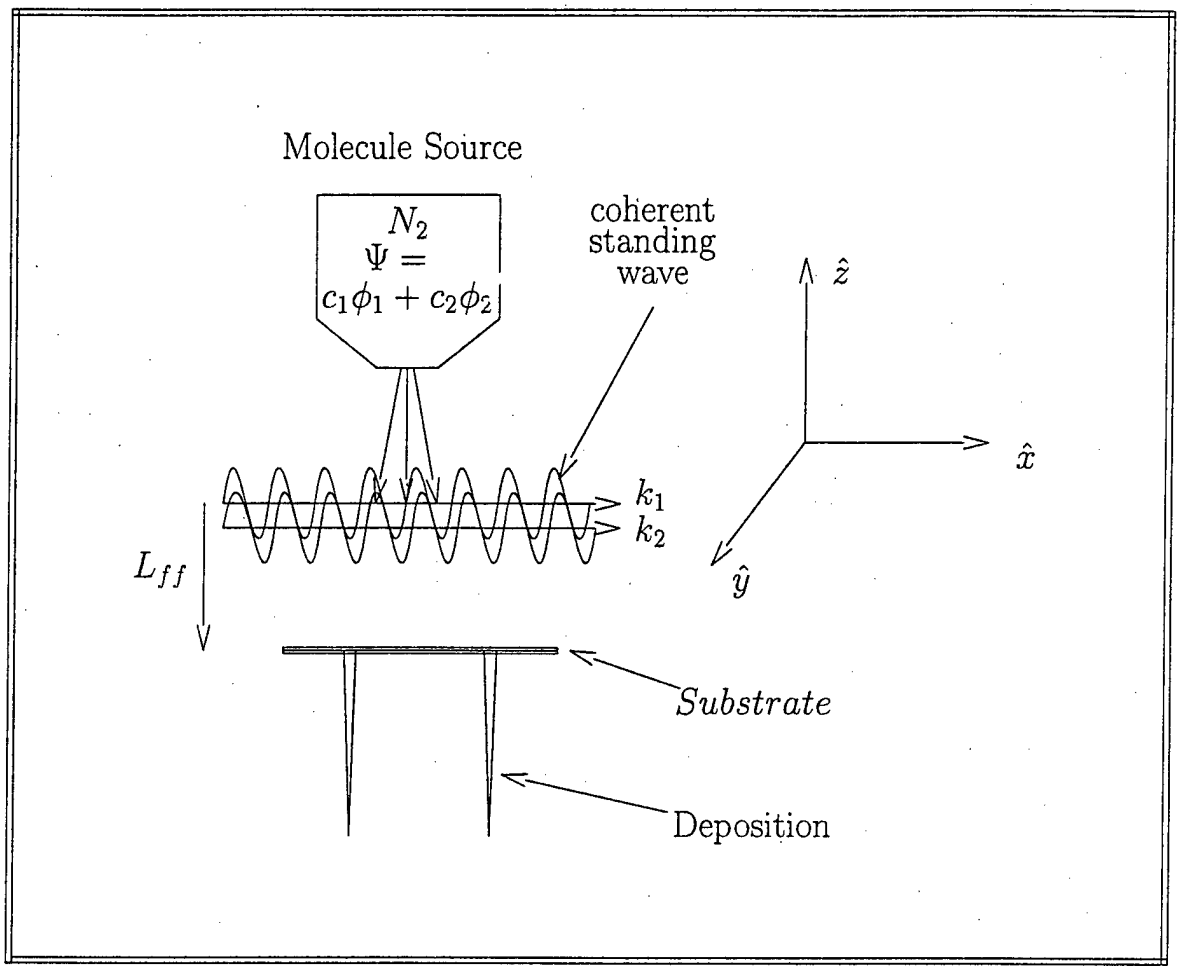
Molecule Source
N_2
$\Psi =$
$c_1\phi_1 + c_2\phi_2$
coherent
standing
wave
$\hat{z}$
$\hat{x}$
$\hat{y}$
k_1
k_2
L_{ff}
Substrate
Deposition

Fig 1

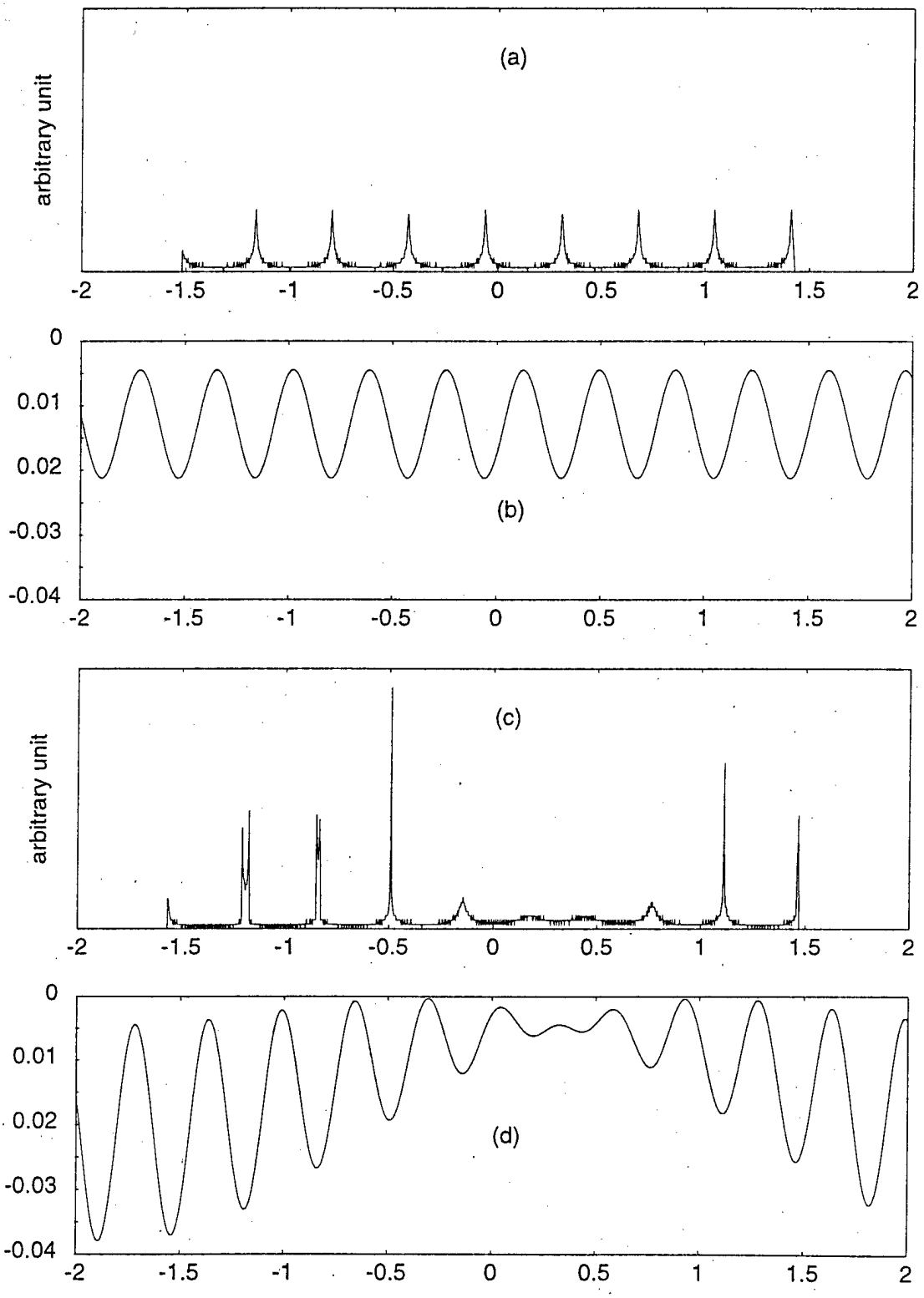
(a)
arbitrary unit
-2
-1.5
-1
-0.5
0
0.5
1
1.5
2
0
0.01
0.02
-0.03
-0.04
(b)
(c)
arbitrary unit
(d)

Fig. 3

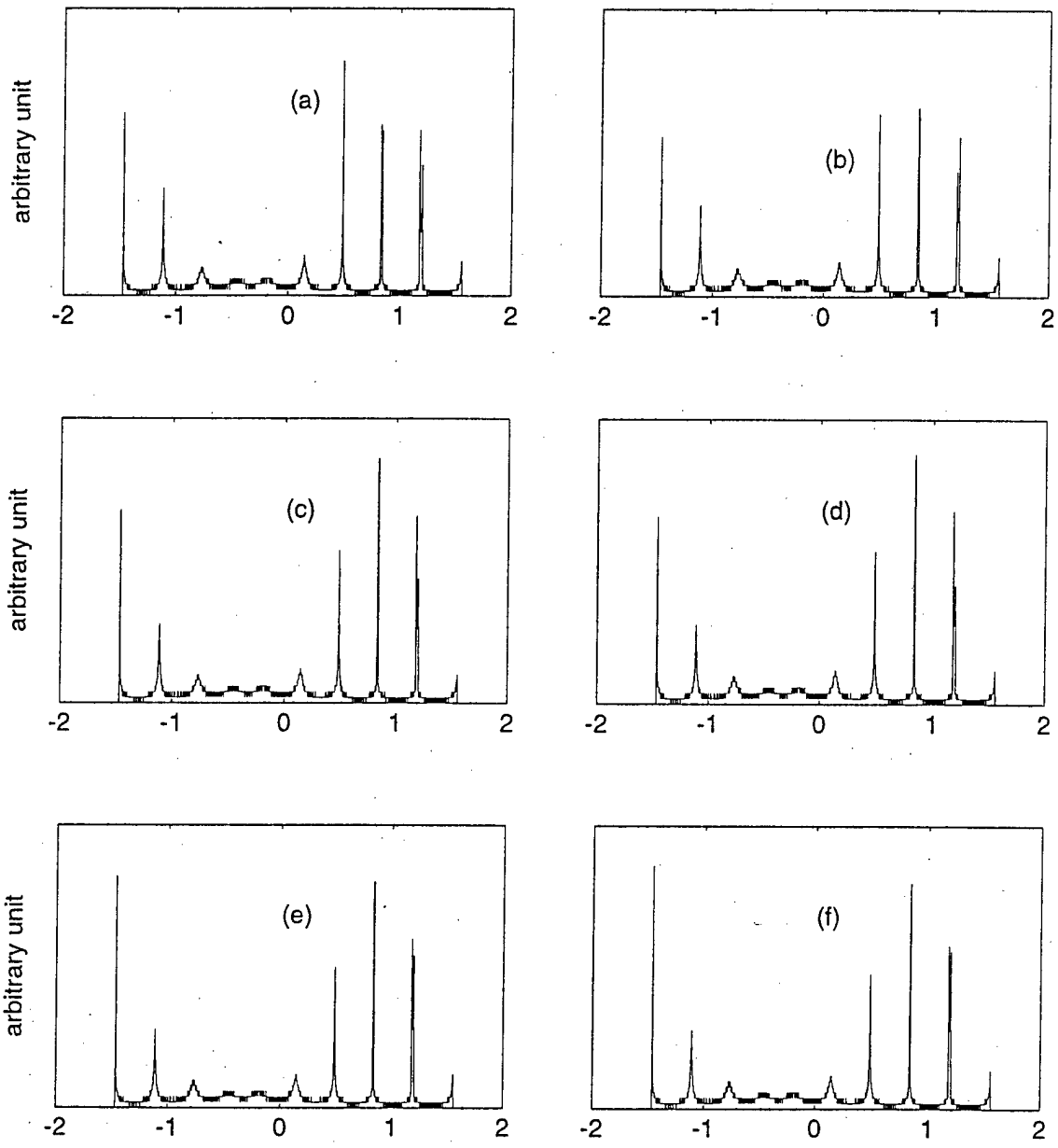

Fig. 5

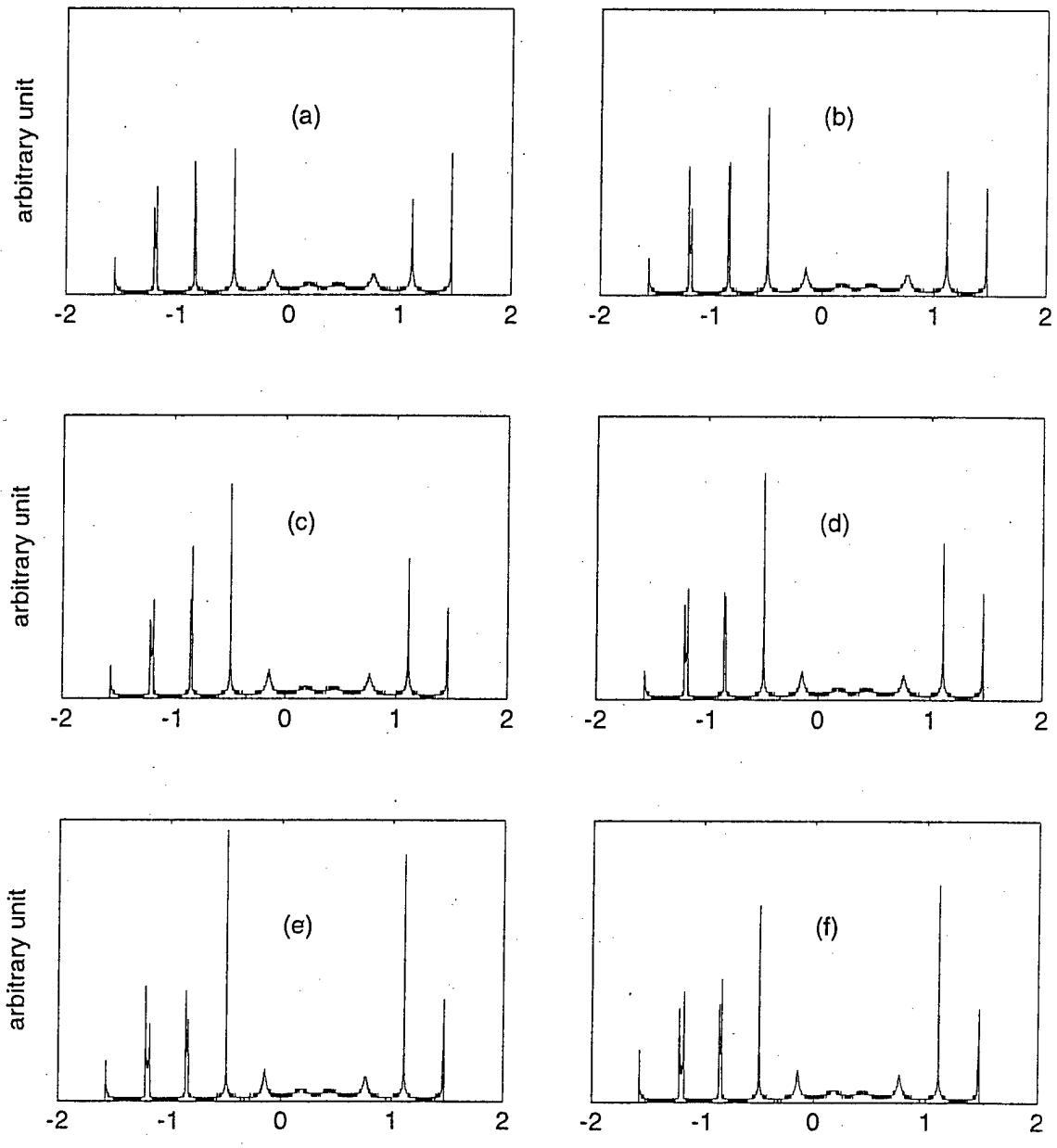

Fig. 7

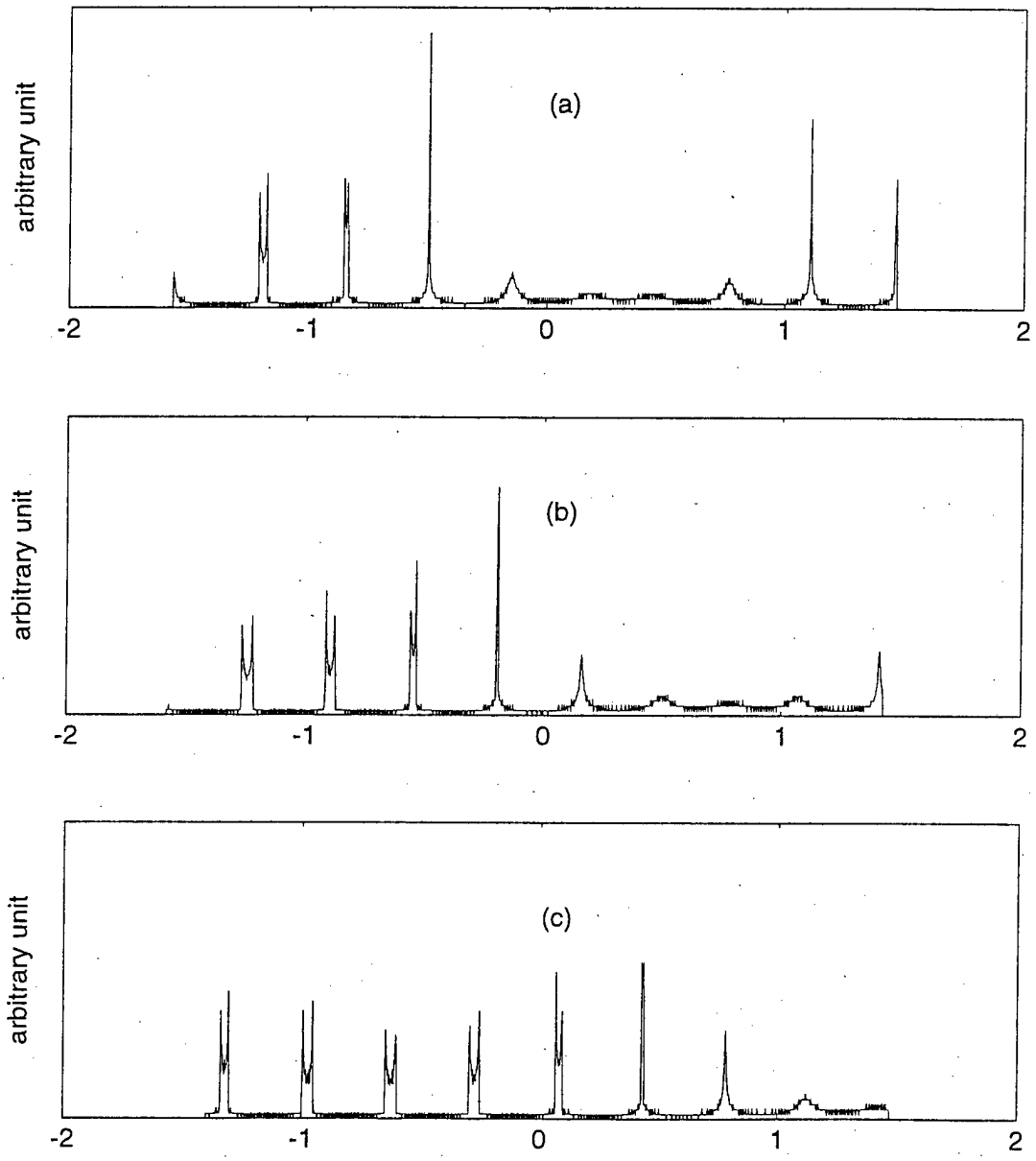
arbitrary unit
(a)
-2
-1
0
1
2
arbitrary unit
(b)
-2
-1
0
1
2
arbitrary unit
(c)
-2
-1
0
1
2

Fig. 9

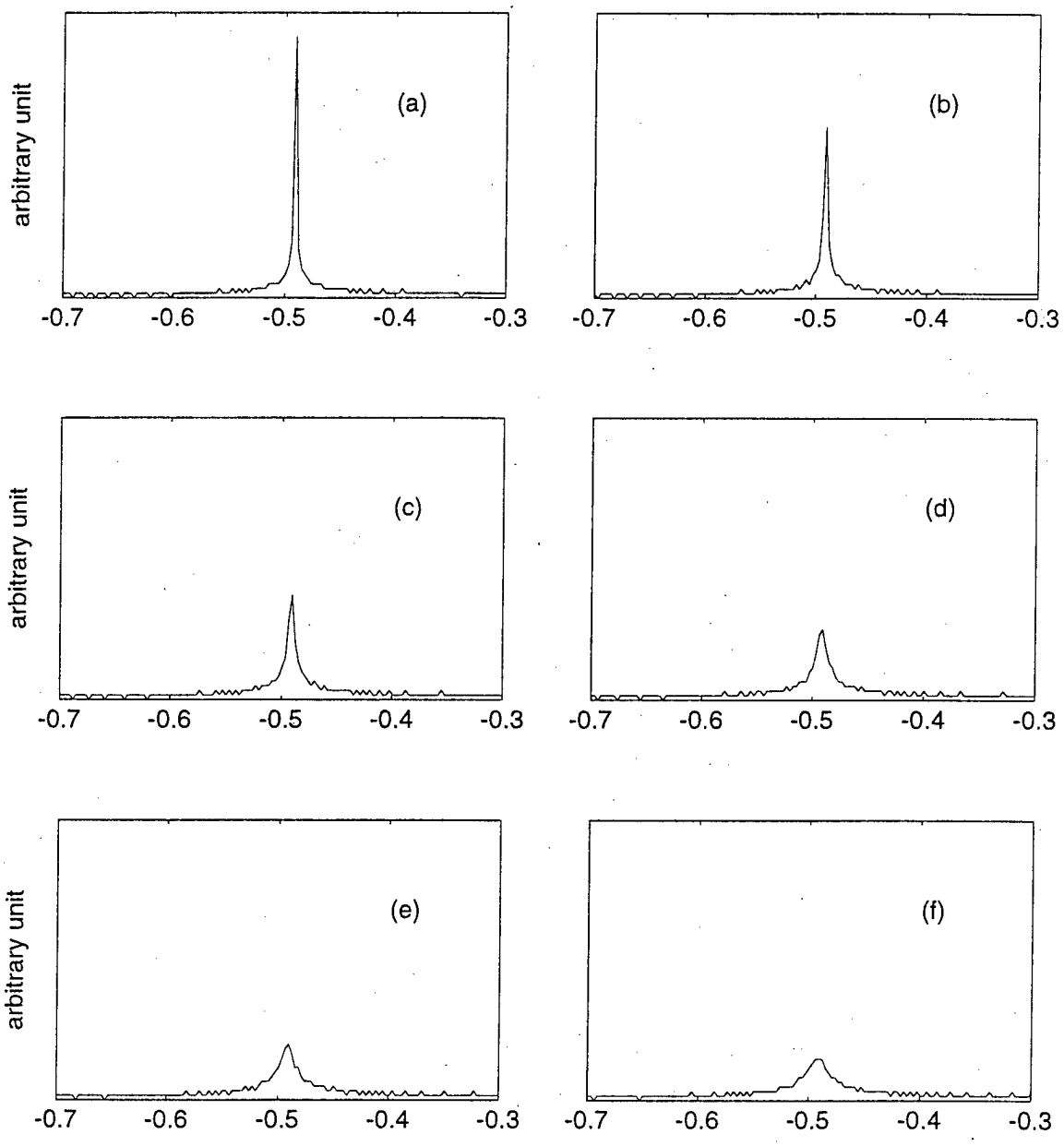

Fig. 11

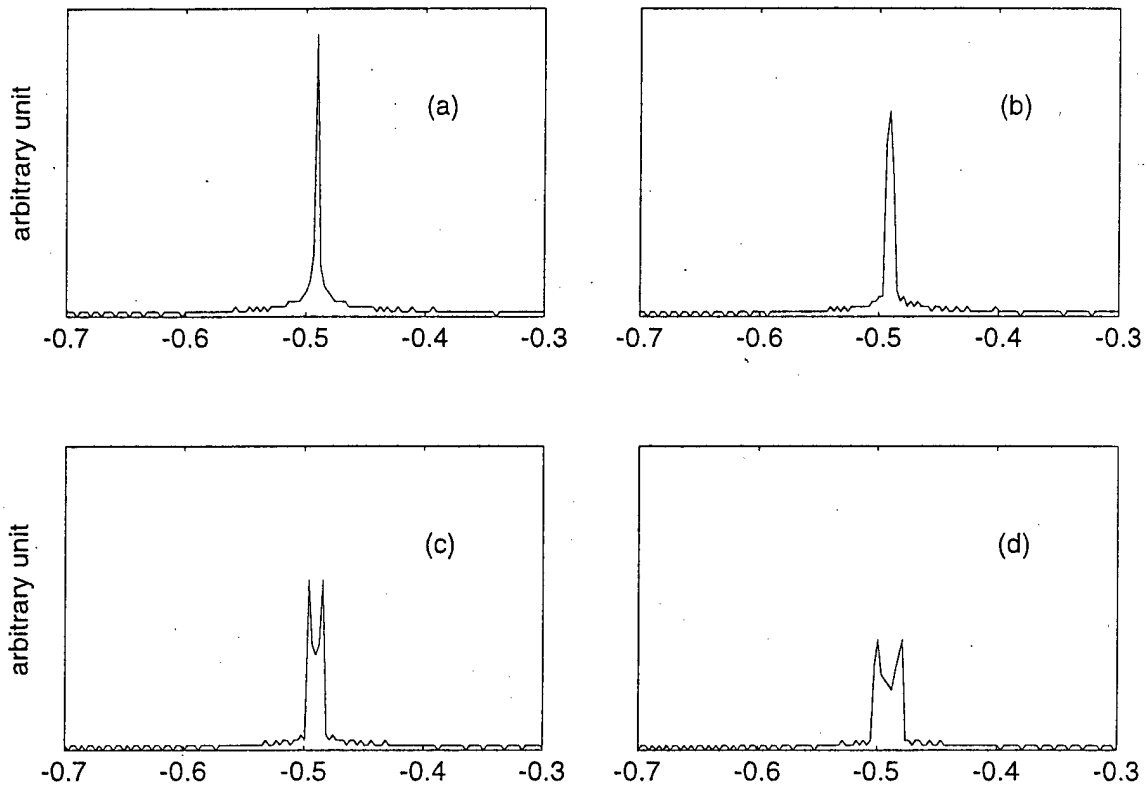

Fig. 13

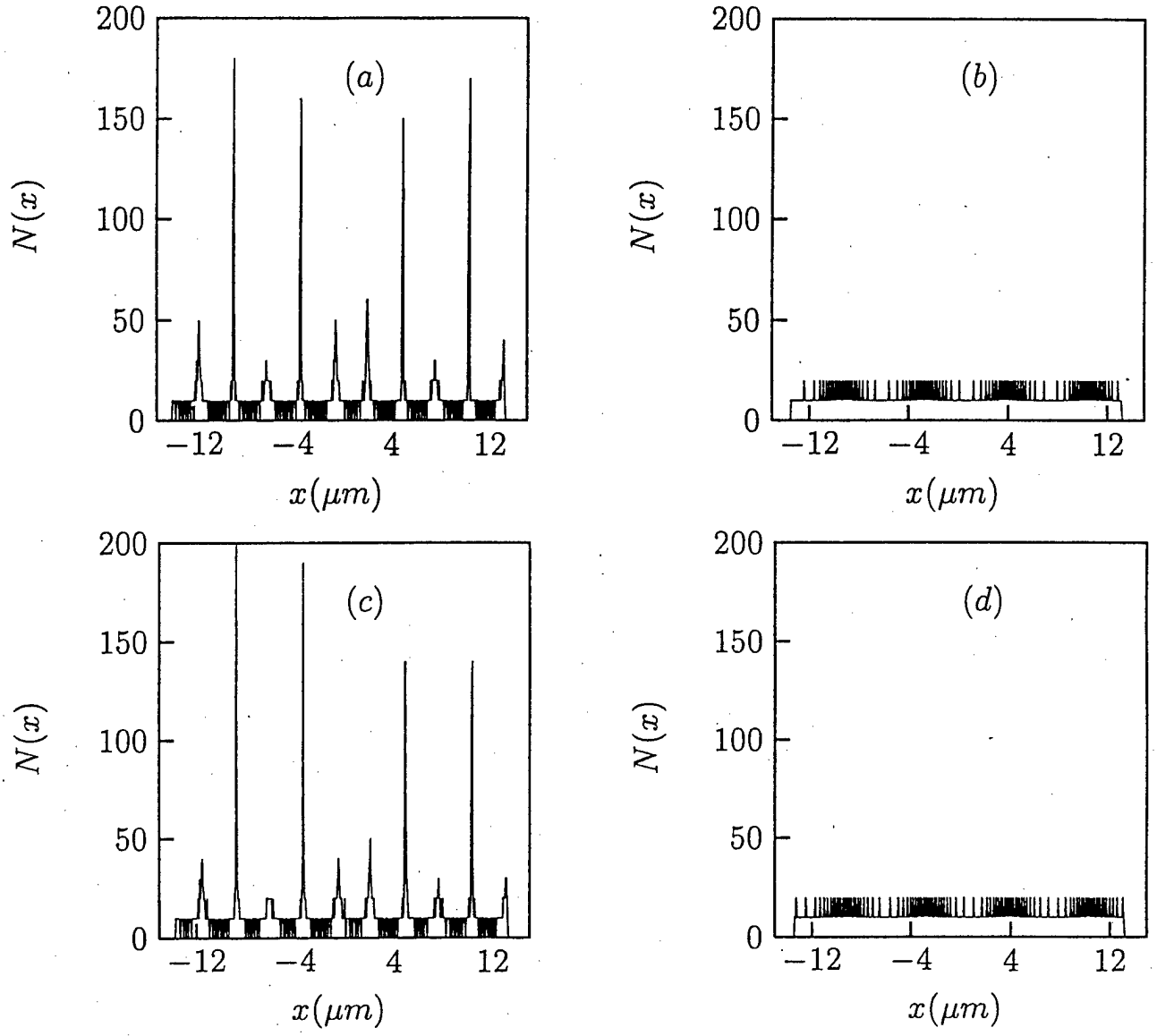

Fig. 15

REPORT DOCUMENTATION PAGE

Form Approved
OMB No. 0704-0188

Public reporting burden for this collection of information is estimated to average 1 hour per response, including the time for reviewing instructions, searching data sources, gathering and maintaining the data needed, and completing and reviewing the collection of information. Send comments regarding this burden estimate or any other aspect of this collection of information, including suggestions for reducing this burden to Washington Headquarters Service, Directorate for Information Operations and Reports, 1215 Jefferson Davis Highway, Suite 1204, Arlington, VA 22202-4302, and to the Office of Management and Budget, Paperwork Reduction Project (0704-0188) Washington, DC 20503.
PLEASE DO NOT RETURN YOUR FORM TO THE ABOVE ADDRESS.

1. REPORT DATE *(DD-MM-YYYY)*	2. REPORT DATE	3. DATES COVERED *(From - To)*
29-10-2001	Final Report	January 1998 - October 2001

4. TITLE AND SUBTITLE

Coherent Control of Chemical Reactions

5a. CONTRACT NUMBER

5b. GRANT NUMBER
N00014-96-1-0433

5c. PROGRAM ELEMENT NUMBER

6. AUTHOR(S)

Brumer, Paul W.

5d. PROJECT NUMBER

5e. TASK NUMBER

5f. WORK UNIT NUMBER

7. PERFORMING ORGANIZATION NAME(S) AND ADDRESS(ES)

Department of Chemistry
University of Toronto
Toronto, ON, CANADA M5S 3H6

8. PERFORMING ORGANIZATION REPORT NUMBER

9. SPONSORING/MONITORING AGENCY NAME(S) AND ADDRESS(ES)

Office of Naval Research
ONR 331
Ballston Center Tower One
800 North Quincy Street
Arlington, Virginia 22217-5660

10. SPONSOR/MONITOR'S ACRONYM(S)

11. SPONSORING/MONITORING AGENCY REPORT NUMBER

12. DISTRIBUTION AVAILABILITY STATEMENT

For public distribution

13. SUPPLEMENTARY NOTES

14. ABSTRACT

Over the past three years we have made significant contributions to the ongoing development of the coherent control of atomic and molecular processes. Specifically, we have contributed to (1) bimolecular reaction dynamics and controlled collision phenomena; (2) control of molecular chirality and asymmetric synthesis; (3) theory, and practical considerations, in the control of the photodissociation of real systems; (4) control in large molecular systems; (5) the continued development of semiclassical mechanics specifically for coherent control applications; and (6) control of molecular nanoscale deposition on surfaces.

15. SUBJECT TERMS

Coherent control, lasers, molecular processes, chemical reactions

16. SECURITY CLASSIFICATION OF:			17. LIMITATION OF ABSTRACT	18. NUMBER OF PAGES	19a. NAME OF RESPONSIBLE PERSON
a. REPORT	b. ABSTRACT	c. THIS PAGE	SAR		19b. TELEPONE NUMBER *(Include area code)*